Université Fédérale

Toulouse Midi-Pyrenees

# THÈSE

En vue de l'obtention du

## DOCTORAT DE L'UNIVERSITE DE TOULOUSE

Délivré par:

IMT - Ecole Nationale Supérieure des Mines d'Albi-Carmaux

Cotutelle internationale avec
INCQS/FIOCRUZ, Brésil

---

Présentée et soutenue par:

Janine BONIATTI

le 30 juin 2021

**Titre:**

# Développement et caractérisation de dispersions solides amorphes de Praziquantel à usage pédiatrique par extrusion à chaud et impression 3D

---

Ecole doctorale et discipline ou spécialité :
ED MEGEP : Génie des procédés et de l'Environnement

Unité de recherche :
Centre RAPSODEE, UMR CNRS 5302, IMT Mines Albi

Directeurs de Thése :
Maria-Inês RÉ, Directrice de Recherche, IMT Mines Albi
Fabio Coelho AMENDOEIRA, Professeur, INCQS/FIOCRUZ

**Jury :**

Jose Carlos Costa da Silva PINTO, Professeur, UFRJ/Brésil, Rapporteur
Eric BEYSSAC, Professeur, Université Clermont Auvergne /France, Rapporteur
Ana Cristina Martins de Almeida NOGUEIRA, Professeure, INCQS/FIOCRUZ, Examinatrice
Gabriel Lima Barros de ARAUJO, Professeur, USP/Brésil, Examinateur

POS GRADUATION PROGRAM IN SANITARY SURVEILLANCE
NATIONAL INSTITUTE FOR HEALTH QUALITY CONTROL
OSWALDO CRUZ FOUNDATION
&
UNIVERSITÉ FÉDÉRALE TOULOUSE MIDI-PYRÉNÉES
ÉCOLE DOCTORALE MÉCANIQUE, ENERGÉTIQUE, GÉNIE CIVIL & PROCÉDÉS
IMT MINES ALBI – ÉCOLE NATIONALE SUPÉRIEURE DES MINES D'ALBI-CARMAUX

**Janine Boniatti**

# DEVELOPMENT AND CHARACTERIZATION OF PRAZIQUANTEL AMORPHOUS SOLID DISPERSIONS FOR PAEDIATRIC USE BY HOT MELT EXTRUSION AND 3D PRINTING

Supervisor in Brazil: Prof. Fábio Coelho Amendoeira
Supervisor in France: Prof. Maria Inês Ré

Rio de Janeiro
2021

JANINE BONIATTI

# DEVELOPMENT AND CHARACTERIZATION OF PRAZIQUANTEL AMORPHOUS SOLID DISPERSIONS FOR PAEDIATRIC USE BY HOT MELT EXTRUSION AND 3D PRINTING

Thesis in international joint supervision submitted in partial fulfilment of the requirements for the degree of Doctor in Sciences (National Institute for Quality Control in Health (INCQS)/Oswaldo Cruz Foundation-FIOCRUZ, Brazil) and degree of Doctor in Environment and Process Engineering (IMT MINES ALBI – ÉCOLE NATIONALE SUPÉRIEURE DES MINES D'ALBI-CARMAUX, Federal University of Toulouse, France).

Supervisor in Brazil: Prof. Fábio Coelho Amendoeira

Co-Supervisor in Brazil: Laís Bastos da Fonseca

Alessandra Lifsitch Viçosa

Supervisor in France: Prof. Maria Inês Ré

Co-Supervisor in France: Ass. Prof. Martial Sauceau

Rio de Janeiro

2021

Janine Boniatti

**DEVELOPMENT AND CHARACTERIZATION OF PRAZIQUANTEL AMORPHOUS SOLID DISPERSIONS FOR PAEDIATRIC USE BY HOT MELT EXTRUSION AND 3D PRINTING**

Thesis in international joint supervision submitted in partial fulfilment of the requirements for the degree of Doctor in Sciences (National Institute for Quality Control in Health (INCQS)/Oswaldo Cruz Foundation (FIOCRUZ), Brazil) and degree of Environment and Process Engineering (IMT MINES ALBI – ÉCOLE NATIONALE SUPÉRIEURE DES MINES D'ALBI-CARMAUX, Federal University of Toulouse, France).

Approved: _____/_____/_____

EXAMINATION BOARD

Ana Cristina Martins de Almeida Nogueira/INCQS - Fiocruz

José Carlos Costa da Silva Pinto/UFRJ

Eric Beyssac/UCA

Fábio Coelho Amendoeira/INCQS – Fiocruz (Brazil)

Maria Inês-Ré/IMT Mines Albi (France)

With all my love, to my daughter Helena,
companion of every adventure in this journey.

## ACKNOWLEDGEMENTS

I am extremely happy to write these thanks. It is gratifying to get here, and many people are co-responsible for this, which makes it even more challenging to mention so much in so little space. Here is what I consider to be one of my “results”: nobody achieves anything alone.

I wanted to start by thanking Katia Miriam Peixoto, she was one of the first people who encouraged, and supported me. Thank you for the conversations and the friendship.

Thanks to the LEES team (Ana, Lucas, Andreça, Sabrina, and Marcos) for being so supportive and loyal, and for replacing me as a great team when I needed to leave. To Rafael Seiceira, my eternal gratitude for the partnership, friendship, teachings and for making happy even the worst days, when challenges seemed insurmountable.

The LabFE team (Ana, Thiago, Deise, Augusto, Italo, Tamires, Marcia and Caroline), thank you for your help with the experiments and for understanding my absence during the period in France.

I thank the direction of Farmanguinhos, Jorge Mendonça and Nubia Boechat, for agreeing with my period abroad and for authorizing my departure to France.

I am grateful to the graduate program of INCQS and Katia Leandro for helping me in the whole process so that this joint thesis was possible.

To my advisor Fabio Amendoeira for the moments of teaching, conversation, support and encouragement.

Thank you, Alessandra Viçosa, for your co-tutorship, friendship, and all the efforts made so that I could complete the stage of my Ph.D. in France. I will always be grateful to you, as you always believed that it would be possible.

Many thanks to my co-advisor, Lais Bastos da Fonseca. I have no words to describe the role she played in this process. Thank you, Lais, for being the first person to welcome me as a student and believe in me ever since. With you, I learned beyond the technician, and you are a model of professionalism and person to me.

Thanks to my advisor Maria Ines for having me in Albi and for allowing me to have wonderful life experiences. I appreciate your patience, encouragement, guidance, teachings, and the precious time you dedicated to me. Thanks for the intense learning, the opportunities, and especially for the support in all "scientific adventures" (be it a new test, or a stay in London for 3D printing). I am so grateful also for the friendship we developed and for the affection you have for my family.

To my co-advisors Martial Sauceau and Romain Sescousse for the moments of teaching, conversation and support.

I thank Clélia Christina Mello-Silva and Érica Tex Paulino for all the exchange of experience and for their help with pharmacokinetic experiments.

I am very grateful to Leticia Vallim and the entire LabSEFAR team for their help with animals and pharmacokinetic experiments.

I thank the entire IMT Mines Albi team (Christine Rolland, Laurent Devriendt, Rachel Calvet, Phillipe Accart, Véronique Nallet, Séverine Patry, Céline Boachon, Manolita Boval, Dolores Liret, Noemie, Thèrese, and Fabienne Espitalier) for welcoming me and always being willing to teach.

J'aimerais également remercier Sylvie Deconfeto pour son aide, sa gentillesse, disponibilité, ainsi que son amabilité avec moi e ma familie.

Thanks to the Gala Platform team (Antoine, Laurene, Katia, Marine, and Angelique), with whom I had the honor and privilege to spend a good part of my days producing more than 30 HME batches and countless pleasant moments. “Un grand merci”!

To Alvaro Goyanes for accepting my ideas and making an effort to have me at FabRx in the middle of a pandemic. Thank you so much for the many conversations, discussions, and your help with all the 3D printing experiments.

I thank Professor Catherine Tuleu for having kindly received me at UCL - School of Pharmacy. Thank you for the teachings, the warm welcome, and the discussions we had.

I am grateful to the friends I built along this journey, especially to Magno, Sibele, Akhil, Maria Theresa, Marine, Bahaa, Felipe, Roger, Barath, Hayfa, Carla, Jennifer. I will always remember our exchange of experiences and our laid-back funny moments.

An enormous thank you to Suenia de Paiva Lacerda, who, from the first day in Albi, has spared no effort to help and encourage me. My eternal gratitude to you for all that was this period and for the great friendship built. I am sure that I have won a friendship for life! I extend my gratitude to Rafaelle for all the moments shared.

To Anne Marie Fontes and Eric for her kindness and all the wonderful moments we shared. J’exprime tous mes remerciements et mon affection à vous.

To Jean-Paul for the kindness with us since day 1 in French lands. Thank you for receiving my family so lovingly and for all the help during this period. Je vous remercie et j'espère que nous pourrons nous rencontrer bientôt !

To my brother Vinícius for the constant encouragement and the help with the figures and projects. Te amo!

To Cassia for being tireless and always willing to help me. Te amo!

My deepest and most sincere thanks to my parents Altair and Jaquelina. Thank you for giving up on your dreams so that I could fulfill mine. Thank you for being Helena's mom and dad when I was gone. Obrigada, amo vocês infinitamente!

Lovely thanks to my husband for his love, affection, patience and, mainly, for facing all the adventures of this life in a joyful way, even when the challenges arose. Love you!

Finally, I thank my greatest encourager, my greatest love, Helena. Thank you, my daughter, for being by my side on this walk. It is true that with you, the challenge was bigger, but it was also immensely more joyful, fun, and pleasurable. Please forgive me for the moments when I was absent for the realization of this thesis. I love you with all my heart.

*Cette thèse a été faite avec beaucoup de dévouement et d'amour. Mais si cela aide et encourage tous ces gens, ce ne serait certainement pas possible. Mes plus sincères remerciements!*

If you’re going to try, go all the
way.
Otherwise, don’t even start.

If you’re going to try, go all the
way.
This could mean losing girlfriends,
wives, relatives, jobs and
maybe your mind.

Go all the way.
it could mean not eating for 3 or 4 days.
It could mean freezing on a
park bench.
It could mean jail,
it could mean derision,
mockery,
isolation.
Isolation is the gift,
all the others are a test of your
endurance, of
how much you really want to
do it.
And you’ll do it
despite rejection and the worst odds
and it will be better than
anything else
you can imagine.

If you’re going to try,
go all the way.
There is no other feeling like
that.
You will be alone with the gods
and the nights will flame with
fire.

*Roll the dice - Charles Bukowski*

## ABSTRACT

Janine Boniatti. Development and characterization of praziquantel amorphous solid dispersions for paediatric use by hot melt extrusion and 3d printing. Rio de Janeiro, 2021. Thesis (Doctor in Sciences), National Institute for Quality Control in Health (INCQS)/Oswaldo Cruz Foundation (FIOCRUZ), Brazil; (Doctor in Process Engineering and Environment), IMT Mines Albi, University of Toulouse, France, 2021.

For the past 40 years, praziquantel (PZQ) has been the standard treatment for schistosomiasis, the neglected parasitic disease that affects more than 250 million people worldwide. However, there is no adequate paediatric formulation on the market, leading to off-label use and the division of commercial tablets for adults. This thesis focused on the development of a PZQ formulation based on solid amorphous dispersion (ASD) to solve physicochemical (low water solubility) and sensory (bitter taste) of PZQ active pharmaceutical ingredient (API) disadvantages. ASD with 35 to 50 w/w% API (binary and ternary systems) were produced by hot-melt extrusion (HME) using vinylpyrrolidone-vinyl acetate copolymer (Kollidon® VA 64) as a polymeric carrier. The binary systems consisted of PZQ and Kollidon® VA 64. To rationally develop ASD highly loaded with PZQ, the first study of this thesis focused on the construction of a PZQ- Kollidon® VA 64 phase diagram, constructed from a thermal study of the recrystallization of a supersaturated ASD (50 % PZQ), generated by spray drying. The ternary systems were formulated with a surfactant as an additional component (5 w/w%), using two different types (Span ™ 20 and Kolliphor® SLS). Several techniques were used to characterize the produced ASD (PZQ content, thermal properties, particle morphology, apparent solubility, dissolution profile, and physical stability). All binary and ternary ASD increased the PZQ apparent solubility, more specifically, 70 % to 90 % more than the equilibrium concentration in water at 37°C. The dissolution kinetics was also improved, for example, 90 % of drug release in one hour for the ternary ASD containing SPAN 20 as a surfactant and 35 wt% of API. The second challenge is to mask the bitter taste of PZQ. Taste masking assessments (in vivo and in vitro) and pharmacokinetics studies were performed with selected formulations. Positive results related to masking the bitter taste for both PZQ load (50 and 35 wt%) could be demonstrated. The third challenge for paediatric PZQ is the need of accurate dose adjustment. As an alternative to overcome the challenge of adjusting the doses of a paediatric medicine based on PZQ for children, the use of 3D printing technology (FDM) with direct feeding of powdered amorphous solid dispersions was proposed. We could demonstrate the feasibility of obtaining printlets with two different doses of PZQ (100 and 150 mg) using ternary ASD. The printlets containing 35 wt% of API load and SPAN 20 showed the best dissolution performance. This work demonstrated the interest of ternary ASD containing PZQ in the form of pellets or powder for compressed 3D printing. The main obstacles in the formulation of PZQ, such as low drug solubility, inappropriate taste, and high and variable dosage requirements, can be overcome using the combination of different technologies (production of ASD by HME and FDM as SD printing technology).



Key words: amorphous solid dispersions, hot-melt extrusion, solubility enhancement, phase diagram, praziquantel, direct powder extrusion 3D printing, printing pharmaceuticals, paediatric treatment.

## RÉSUMÉ

Janine Boniatti. Développement et caractérisation de dispersions solides amorphes de Praziquantel à usage pédiatrique par extrusion à chaud et impression 3D. Rio de Janeiro, 2021. Thèse (Doctorat Sciences), Institut National de Contrôle de Qualité en Santé (INCQS)/Fondation Osvaldo Cruz (FIOCRUZ), Brésil ; (Doctorat en Génie des Procédés et de l'Environnement), IMT Mines Albi, Université de Toulouse, France, 2021.

Depuis 40 ans, le praziquantel (PZQ) est le traitement standard de la schistosomiase, une maladie parasitaire négligée qui touche plus de 250 millions de personnes dans le monde. Cependant, il n'existe pas de formulation pédiatrique adéquate sur le marché, ce qui conduit à une utilisation hors indication et à la division des comprimés commerciaux pour les adultes. Cette thèse s'articule autour du développement d'une dispersion amorphe solide (ASD) pour le PZQ afin d'améliorer certaines caractéristiques physico-chimiques (faible solubilité dans l'eau) et sensoriels (goût amer) de cet API. Des ASD contenant 35 à 50 % en masse d'API (systèmes binaires et ternaires) ont été produites par extrusion à chaud (HME) en utilisant un copolymère vinylpyrrolidone-acétate de vinyle (Kollidon® VA 64) comme support polymère. Les systèmes binaires sont constitués de PZQ et de Kollidon® VA 64. Afin de développer rationnellement des ASD hautement chargées en PZQ, la première étude de cette thèse porte sur la construction d'un diagramme de phase PZQ- Kollidon® VA 64, construit à partir d'une étude thermique de la recristallisation d'une ASD sursaturé (50 % PZQ), générée par séchage par pulvérisation. Les systèmes ternaires ont été formulés avec un tensioactif comme composant supplémentaire (5 % en masse), en utilisant deux types différents (Span ™ 20 et Kolliphor® SLS). Plusieurs techniques ont été utilisées pour caractériser les ASD produites (teneur en PZQ, propriétés thermiques, morphologie des particules, solubilité apparente, profil de dissolution et stabilité physique). Les ASD binaires et ternaires augmentent la solubilité apparente de la PZQ, plus précisément de 70 % à 90 % par rapport à la concentration d'équilibre dans l'eau à 37 °C. La cinétique de dissolution a également été améliorée, par exemple, 90 % de libération du médicament en une heure pour l'ASD ternaire contenant du SPAN 20 comme surfactant et 35 % en masse d'API. Le deuxième défi consiste à masquer le goût amer du PZQ. Des évaluations du masquage du goût (in vivo et in vitro) et des études pharmacocinétiques ont été réalisées avec des formulations sélectionnées. Des résultats positifs liés au masquage du goût amer pour les deux charges de PZQ (50 et 35 % en masse) ont pu être démontrés. Le troisième défi pour le PZQ à usage pédiatrique est le besoin d'un ajustement précis de la dose. Comme alternative pour surmonter le défi de l'ajustement des doses d'un médicament pédiatrique à base de PZQ pour les enfants, l'utilisation de la technologie d'impression 3D (FDM) avec alimentation directe de dispersions solides amorphes en poudre a été proposée. Nous avons pu démontrer la faisabilité d'obtenir des imprimés (printlets) avec deux doses différentes de PZQ (100 et 150 mg) en utilisant la technologie de FDM. Les printlets avec 35 % en masse de PZQ et SPAN 20 ont montré la meilleure performance de dissolution. Ce travail a démontré l'intérêt d'une dispersion solide amorphe ternaire contenant du PZQ sous forme de pellets ou de poudre pour l'impression 3D directe (FDM). Les principaux obstacles à la formulation du PZQ, tels qu'une faible solubilité du médicament, un goût inapproprié et des exigences de dosage élevées et variables, peuvent être surmontés en utilisant la combinaison de différents technologies (production d'ASD par HME et FDM comme technologie d'impression 3D).



Mots clés : dispersions solides amorphes, extrusion à chaud, amélioration de la solubilité, diagramme de phase, praziquantel, impression 3D par extrusion directe de poudre, impression de produits pharmaceutiques, traitement pédiatrique.

## RESUMO

Janine Boniatti. Desenvolvimento e caracterização de dispersões sólidas amorfas de praziquantel para uso pediátrico por *hot melt extrusion* e impressão 3D. Rio de Janeiro, 2021. Tese (Doutorado em Ciências), Instituto Nacional de Controle de Qualidade em Saúde (NCQS)/Fundação Osvaldo Cruz (FIOCRUZ), Brasil; (Doutorado em Engenharia de Processo e Meio Ambiente), IMT Mines Albi, Universidade de Toulouse, France, 2021.

Nos últimos 40 anos, o praziquantel (PZQ) tem sido o tratamento padrão para a esquistossomose, uma doença parasitária negligenciada que afeta mais de 250 milhões de pessoas em todo o mundo. No entanto, não existe uma formulação pediátrica adequada no mercado, levando ao uso *off-label* e à divisão de comprimidos comerciais para adultos. Esta tese se concentrou no desenvolvimento de uma formulação de PZQ baseada em dispersão sólida amorfa (ASD) para resolver as desvantagens físico-químicas (baixa solubilidade em água) e sensoriais (sabor amargo) do PZQ – insumo farmacêutico ativo (IFA). ASD com 35 a 50 % p/p de IFA (sistemas binários e ternários) foram produzidos por extrusão de fusão a quente (HME) usando o copolímero de vinilpirrolidona-acetato de vinila (Kollidon® VA 64) como um carreador polimérico. Os sistemas binários consistiram em PZQ e Kollidon® VA 64. Para desenvolver racionalmente ASD com altas cargas de PZQ, o primeiro estudo desta tese focou na construção de um diagrama de fases PZQ- Kollidon® VA 64, obtido a partir de um estudo térmico de recristalização de uma ASD supersaturada (50 % PZQ), gerado por *spray drying*. Os sistemas ternários foram formulados com um surfactante como componente adicional (5 % p/p) e, utilizou-se dois tipos diferentes (Span ™ 20 e Kolliphor® SLS). Diversas técnicas foram empregadas para caracterizar a ASD produzida (teor de PZQ, propriedades térmicas, morfologia das partículas, solubilidade aparente, perfil de dissolução e estabilidade física). Todas as ASD binárias e ternárias aumentaram a solubilidade aparente do PZQ, mais especificamente, 70 % a 90 % a mais do que a concentração de equilíbrio em água a 37 °C. A cinética de dissolução também foi melhorada, por exemplo, 90 % da liberação do IFA em uma hora para a ASD ternária contendo SPAN 20 como surfactante e 35 % em peso do IFA. O segundo desafio é mascarar o sabor amargo do PZQ. Avaliações de mascaramento de sabor (in vivo e in vitro) e estudos farmacocinéticos foram realizados com formulações selecionadas. Resultados positivos relacionados ao mascaramento do sabor amargo para ambas as cargas de PZQ (50 e 35 % em peso) puderam ser demonstradas. O terceiro desafio para o PZQ pediátrico é a necessidade de um ajuste preciso da dose. Como alternativa para superar a barreira do ajuste de doses de um medicamento pediátrico a base de PZQ para crianças, foi proposta a utilização da tecnologia de impressão 3D (FDM) com alimentação direta dispersões sólidas amorfas em pó. Pudemos demonstrar a viabilidade de obter printlets (comprimidos obtidos por impressão 3D) com duas doses diferentes de PZQ (100 e 150 mg) usando ASD ternária. Os printlets contendo 35 % em peso do IFA e SPAN 20 apresentaram o melhor desempenho de dissolução. Este trabalho demonstrou o interesse de ASD ternária na forma de pellets ou pó para impressão 3D de comprimidos contendo PZQ. Os principais obstáculos para formulação do PZQ, como baixa solubilidade do fármaco, sabor inadequado e requisitos de dosagem alta e variável, puderam ser superados usando a combinação de diferentes tecnologias (produção de ASD por HME e FDM como tecnologia de impressão SD).



Palavras-chave: dispersões sólidas amorfas, *extrusao à quente*, incremento de solubilidade, diagrama de fase, praziquantel, impressão 3D por alimentão extrusão direta de pó, impressão farmacêutica, tratamento pediátrico.

## LIST OF EQUATIONS

## LIST OF TABLES

## LIST OF FIGURES

## ABBREVIATIONS

| | |
|---|---|
| 3D | Three-Dimensional |
| AC | Compressed Air |
| ANVISA | Agência Nacional de Vigilância Sanitária |
| API | Active Pharmaceutical Ingredient |
| ASD | Amorphous Solid Dispersion |
| ATR-FTIR | Attenuated Total Reflectance with Fourier Transform Infrared |
| AUC | Area Under The Curve |
| BATA | Brief-Access Taste |
| BCS | Biopharmaceutical Classification System |
| C-1816 | Sucrose stearate |
| CCDC | Cambridge Crystallographic Data Centre |
| CD | Cyclodextrins |
| $C_{equilibrium}$ | Equilibrium concentration |
| CEUA | Animal Use Ethics Committee |
| CG-MS | Gas Chromatography–Mass Spectrometry |
| Chit | chitosan |
| CK | Couchman-Karasz |
| $C_{max}$ | Maximum concentration |
| CROSP | Crospovidone |
| CV | Coefficient of Variation |
| DoE | Design of Experiments |
| DPE | Direct Powder Extruder |
| DSC | Differential Scanning Calorimetry |
| EFZ | Efavirenz |
| EMA | European Medicines Agency |
| Eudragit® | Polymethacrylate-based copolymers |
| EVA | Ethylene Vinyl Acetate |
| F-127 | Poloxamer |
| FDA | Food And Drug Administration |
| FDM | Fused Deposition Modeling |
| FIOCRUZ | Fundação Oswaldo Cruz |
| FT-IR | Fourier Transform Infrared |
| GIT | Gastrointestinal Tract |
| GMS | Glyceryl monostearate |
| GT | Gordon-Taylor |
| HF | Heat Flow |
| HME | Hot Melt Extrusion |
| HPC | Hydroxypropylcellulose |
| HPH | High-pressure homogenization |
| HPLC | High Performance Liquid Chromatography |
| HPMC | Hydroxypropyl methylcellulose |
| HPMCAS | Hydroxypropyl Methylcellulose Acetate Succinate |
| ICH | International Council for Harmonisation |

| | |
|---|---|
| IDPMA | Interactive Document Mapping plot |
| INM | Indomethacin |
| IOC | Oswaldo Cruz Institute |
| ISO | International Organization for Standardization |
| IUPAC | Pure and Applied Chemistry Union |
| LDH | Layered Double Hydroxide |
| LN | Liquid Nitrogen |
| MC | Methyl Cellulose |
| mDSC | Modulated Differential Scanning Calorimetry |
| MDX | Maltodextrin |
| MeCD | Methyl-β-cyclodextrin |
| MMCS | Make Medicines Child Size |
| MS/MG | Ministério Da Saúde/Minas Gerais |
| MW | Molecular Weight |
| NiTsPc | tetrasulphonated nickel (II) phthalocyanine |
| NMR | Nuclear Magnetic Resonance |
| NMT | Not more than |
| P 188 | Ploxamer 188 |
| PAM | Pressure-Assisted Microsyringe |
| PANI | poly(aniline) |
| PCE | Schistosomiasis Control Program |
| PDCO | Paediatric Committee |
| PECE | Programa Especial de Controle da Esquistossomose |
| PEDOT:PSS | poly(3,4-ethylene dioxythiophene): poly(styrene sulfonate) |
| PEG | Polietilenoglicol |
| PHB | poly (3-hydroxybutyrate) |
| PEI | poly(ethyleneimine) |
| PICU | Paediatric Intensive Care Unit |
| PIPs | Paediatric Investigation Plans |
| PLGA | Poly(Lactic-Co-Glycolic Acid) |
| PM | Physical Mixture |
| PMMA | Polymethacrylates |
| PPy | poly(pyrrole) |
| PSD | Particle Size Distribution |
| PSPs | Paediatric Study Plans |
| PSS | poly(styrene sulfonate) |
| PTFE | Polytetrafluoroethylene |
| PVA | Polyvinyl Alcohol |
| PVP | Polyvinylpyrrolidone |
| PVPVA | Polyvinylpyrrolidone/Vinyl Acetate |
| PXRD | Powder X-Ray Diffraction |
| PZQ | Praziquantel |
| PZQ | Praziquantel |
| RAC-PZQ | Racemic praziquantel |
| RBM | Rebamipide |

| | |
|---|---|
| RDC | Resolução da Diretoria Colegiada |
| RENAME | Relação Nacional De Medicamentos Essenciais |
| Rebamipide | RBM |
| RH | Relative Humidity |
| RT | Room Temperature |
| SANAR | Programa de Enfrentamento às Doenças Negligenciadas do Estado de Pernambuco |
| SD | Standard Deviation |
| SEM | Scanning Electron Microscope |
| SGF | Simulated Gastric Fluid |
| SI | Sink index |
| SLN | Solid Lipid Nanoparticles |
| SLS | Sodium Lauril Sulfate |
| SPAN 20 | Span™ 20 |
| SSE | Semi-Solid Extrusion |
| SSF | Simulated Salivar Fluid |
| SSG | Sodium Starch Glycolate |
| SUS | Sistema Único De Saúde (Brazilian National Health Service) |
| $T_g$ | Glass transition |
| TGA | Thermogravimetric Analysis |
| $T_{gmix}$ | Glass transition of mixture |
| $T_m$ | Melting Temperature |
| $T_{max}$ | Maximum Time |
| $T_{onset}$ | Onset Temperature |
| $T_{peak}$ | Peak Temperature |
| $T_{recrystallization}$ | Recristalization Temperature |
| UFF | Universidade Federal Fluminense |
| UPLC-MS | Ultraperformance Liquid Chromatography-Mass |
| USP | United States Pharmacopeia |
| USP/IFSC | Universidade de São Paulo/Instituto de Física de São Carlos |
| UV | Ultraviolet |
| WHO | World Health Organization |

## CONTENTS

# CHAPTER 1 - GENERAL INTRODUCTION AND THESIS OBJECTIVES

# 1. GENERAL INTRODUCTION

Neglected tropical diseases (NTDs) affect more than 1.4 billion people worldwide, with children making a significant proportion [1]–[3]. The second most frequent is schistosomiasis disease and affects around 28 million preschool-age children (5 to 14 years old) [1]–[6].

Schistosomiasis, also known as bilharzia, is considered one of the NTDs. It is a disease caused by parasitic worm, corresponding to helminths of class Trematoda, family Schistossomatidae and genus *Schistosoma* [1]. The six schistosomes species infecting humans are *S. guineensis, S. hermatobium, S, intercalatum, S. japonicum, S. mansoni, and S. mekongi*, and the three majors are *S. mansoni, S. haematobium* and *S. japonicum* [1], [6].

The parasites that cause schistosomiasis live in certain types of freshwater snails. The infectious form of the parasite, known as cercariae, emerge from the snail into the water. People can become infected when its skin meets contaminated freshwater. In Brazil, it is estimated that 8 to 10 million people are infected by *S. mansoni*, and 30 million live in areas with a high risk of contamination.

Schistosomiasis is second only to malaria as the most devastating parasitic disease, and the major cause of morbidity in the world. Globally, it is estimated that it affects over 250 million people in 78 countries of the world and is responsible for some 280,000 deaths each year [6].

Basic sanitation, potable water access, education for hygiene and snail control are means of schistosomiasis prevention. Besides sanitary measures for disease control, the treatment of schistosomiasis is also a necessary measure to decrease, and eradication of this disease generally linked to poverty [1], [7], [8]. However, this significant public health problem must be monitored and taken care of in the guidelines, such as establishing large-scale preventive treatment programs. These measures may have important consequences for public health due to the change in the biology and immunoepidemiology of *S. mansoni* [7].

Praziquantel (PZQ) is the reference drug in the treatment of schistosomiasis according to World Health Organization (WHO), by reasons like high efficiency, low toxicity, and low costs. All those factors make praziquantel the only commercial drug for the treatment of schistosomiasis, for which, there is no vaccine available.

Still regarding PZQ, there is no appropriate paediatric medicine available in the market. Currently, children's treatment is realized with the adaptation of the adult medicine, by splitting or smashing tablets [9]. For children, the dosage is adjusted to the child bodyweight by

administering in sets of 150 mg (1/4 tablet) [9], [10]. That practice clearly leads to a low adherence to treatment since it highlights the bad taste of the medicine. Also, factors as high corporal variability and tablet splitting into homogeneous parts hamper the drug efficacy [11].

The difficulty in developing a pharmaceutical form based on praziquantel suitable for children lies in three main factors:

a. it is an API class II of the BCS, that means low water solubility, which need to be increased for the sake of good oral bioavailability.
b. there is a need to mask the bitter taste of the API to allow paediatric patients to accept PZQ medicine and adhere to the schistosomiasis treatment.
c. another challenge is the production of formulations with different dosages to allow administration of the accurate dose due to the children's weight contributing to the efficacy of the treatment.

*The first challenge is to improve water solubility.*

Different technical approaches have already been employed to improve bioavailability for praziquantel, the focus being in improving its water solubility or dissolution rate. Among them, modification of crystal form (polymorphs, hydrates, cocrystal) or physical characteristics (reduction of crystal particle size), complexation with cyclodextrins, association of praziquantel with lipids or polymers in a particulate form (nano or microparticles) or as solid dispersions, in which other excipients might also be added such as surfactants.

Techniques that have been used to generate solid forms and increase the solubility of PZQ are milling or co-milling with excipients; preparation of an organic solution or suspension containing praziquantel and excipients, with subsequent evaporation of the solvent; dispersion (or melting) of praziquantel in molten carriers followed by solidification. Among all technical approaches, solid dispersions are highly effective for enhancing the dissolution, absorption, and therapeutic efficacy of different poorly water-soluble drugs. Regarding praziquantel, solid dispersions with a wide variety of excipients have been investigated. For that purpose, preparation methods using a solvent evaporation step are the most used.

Even if a crystalline state provides a highly solid-stable form, the amorphous state of a drug could be preferred due to enhanced apparent solubility, dissolution, and oral bioavailability that they are able to offer. However, maintaining the drug in its amorphous state is one of the great challenges in formulation development. Amorphous solid dispersion (ASD) is one promising approach to increase the physical stability of an amorphous drug. ASD are generally generated

by modifying the crystalline structure (amorphization) of the drug during dispersion in a polymeric matrix.

ASD can be produced by different technologies, among them, melt processes. Hot melt extrusion (HME) is a continuous manufacturing process for which the interest in as a pharmaceutical process continues to grow. Some ASD-based products produced by HME process are already available on the market, for example, Kaletra® (ritonavir/lopinavir), Onmel™ (intraconazole), Norvir® (ritonavir), and NuvaRing® (etonogestrel/ethinylestriol/ ethinyladiol).

An ASD containing praziquantel could represent a promising way to accomplish a paediatric formulation containing the high drug load (50 wt%) required for designing an API dose close to 150 mg. In fact, there are already several studies to obtain ASDs using associations of PZQ with polymeric carriers by techniques such as melting, solvent, or co-grinding. Some of them have demonstrated promising results with solubility enhancement up to 4.6-fold greater than the raw praziquantel, however all have employed a manufacturing process that has been proven to be possible at lab scale, but the step up to industrial-scale production is still rather large.

The use of HME process to produce ASD involves a challenging study from a scientific and technological perspective as there are still gaps that need to be further explored. The first understanding is the maximum concentration of an API capable to be solubilized in the polymer. The praziquantel load in these solid structures is a critical factor, since paediatric formulations will require large API amounts on ASDs to reduce the physical dimension of the final pharmaceutical dosage forms (mini tablets or others).

Still with high drug loads, processability will be the new challenge for achieving optimal parameters such as assessing screw configuration, temperature profile during extrusion, and feed and flow ratios. The extent of API's amorphization, water-solubility, dissolution kinetics and physical stability may provide a photograph of the correlation between process parameters and these ASD product characteristics.

High API load in ASDs can also correspond to supersaturated formulations whose physical stability need to be controlled. One of the biggest challenges to produce ASDs is the physical stability of these systems highly dependent on their composition (API load, polymer carrier) and the environmental conditions.

*The second challenge is to mask the bitter taste of praziquantel.*

Praziquantel has a bitter taste for children and is also very noticeable for oral administration of the adult tablet. Due to crushing, the taste becomes even more pronounced for paediatric treatment. As a result, incomplete treatment, and effectiveness. Currently, some technological strategies are described in the literature to overcome this problem with a focus on liquid and solid oral pharmaceutical forms. For liquids, the API complexation technique in solution is widely explored. The interactions of the molecule with the taste buds are prevented. Cyclodextrins and maltodextrins were explored for paediatric use. Regarding solids, mini-tablets and orodispersible mini-tablets have been proposed, seeking to combine two advantages: dose flexibility and taste masking with the help of different excipients for direct compression and with masking capacity.

Amorphous solid dispersion (ASD) might have an important role in taste masking. The dispersion of the API in the polymer can provide a physical barrier that masks the drug's bitter taste. However, with the amorphous form, it would expect an increase in solubility and, therefore, the evaluation of ASDs in terms of taste is challenging.

Although each of the strategies has barriers to be overcome (e.g., excipients suitable for children), taste assessment represents yet another challenge. The literature is extensive on this subject, as the gold standard for evaluating taste would be the human panel. However, for paediatric products, these experiments with children are very restrictive. The use of adults does not always provide consistent results due to physiological differences in terms of perception and taste preferences. Thus, in vivo (animal) and in vitro (electronic tongue) methods have been increasingly used and discussed to evaluate paediatric products.

*The third challenge for paediatric PZQ is the possibility of accurate dose adjustment*.

The possibility of precise dose adjustment could bring enormous benefits to the efficacy of the schistosomiasis with praziquantel treatment since the children's dosage is based on the dose-to-weight ratio.

3D printing technologies are gaining more and more strength in the pharmaceutical area due to the possibilities that they represent. Currently, the most applied 3D printing technique is Fused Deposition Modeling (FDM). Most of the studies dealing with HME - FDM 3D combination shows the approach of a continuous process starting from feeding the 3D printer with HME filaments. Several APIs have already been described in the literature as a model for printing printlets[1] using this approach. Specifically, 3D printing to paediatric pharmaceutical

[1] Printlets: 3D printed tablets

forms has been presented with benefits that researchers must carefully evaluate and conduct. The possibility of printing any shape makes the childish appeal viable using forms like "bear" viable. Even colour printing to make it attractive for pharmaceuticals medicines should also be evaluated with attention, especially in children.

One of the disadvantages of the HME filaments for 3DP is finding the right combination of excipients to provide appropriate mechanical and physical characteristics for 3DP. The filaments production has been the stage of the highest intellectual dedication of the researchers requires for the API incorporation. Recently, a technology that does not necessarily require the preparation of filaments using HME and could potentially allow the direct extrusion of mixtures of raw API and carriers as powders was proposed. It is known as a direct powder extrusion 3D printing. This technology allows the production of printlets in a single step, adding particulate material to the feeder. It could represent an alternative for accurate dose adjustment and personalized medicines.

However, one of the greatest difficulties today is to achieve success in solving simultaneously the three limitations: low solubility (oral bioavailability), bad sensory (bitter taste) and need to personalize paediatric medicines (children's dosage based on the dose-to-weight ratio).

## 2. THESIS OBJECTIVES

In Brazil, the Oswaldo Cruz Foundation (Fiocruz) is the most prominent Institution of Science and Technology in Health in Latin America. One of its main missions is manufacturing strategic products for the Brazilian Unified Public Health System (SUS) through its *Complexo Tecnológico de Medicamentos*[2] (Farmanguinhos). Fiocruz is the main institution for research on schistosomiasis in Brazil.

This doctoral thesis was undertaken under the framework of an international joint supervision between *Instituto Nacional de Controle de Qualidade em Saúde*[3] (INCQS)/Fiocruz in Brazil (Rio de Janeiro) and *l'École Nationale Supérieure des Mines d'Albi-Carmaux/Institut Mines Telecom* (IMT Mines Albi) in France (Albi). It aimed to contribute with alternatives to assist in a significant public health problem that is schistosomiasis.

[2] N.T.: Technological Medicines Complex (loose translation).
[3] N.T.: National Institute for Quality Control in Health (loose translation).

The work was firstly focused on developing a praziquantel formulation based on ASDs to solve both physicochemical (low solubility) and sensory (bitter) API problems. Secondly, since the children's dosage is based on the dose-to-weight ratio, it aimed to check the possibility of personalizing dosage by using 3D printing technologies.

A previous study conducted by Fiocruz team has identified the polymer of their choice to produce ASDs containing praziquantel. The polymer is polyvidone-vinylacetate 64 (Kollidon® VA 64/PVPVA 64) and it was a fixed formulation parameter in this thesis. It will be called 'PVPVA' in this manuscript.

The work covered the following studies:

- Experimental determination of praziquantel solubility in the polymer (PVPVA) (temperature-composition phase diagram). The phase diagram was considered an early-stage development tool to assist in predicting the stability of PZQ-PVPVA ASDs at different API loadings and under different thermal conditions.

- Experimental studies of ASDs with PZQ load from 35 to 50 wt% produced by hot melt extrusion (HME) process. Binary systems were constituted of PZQ and PVPVA. Ternary systems were formulated with one surfactant as an additional component (5 wt%), and two types were used (Span™ 20 and Kolliphor® SLS Fine). The ternary systems were studied in two different twin-screw extruders (pharma 11, at BASF/BR, and pharma 16, at IMT MINES ALBI/FR). The ASDs generated in these different studies were characterized using a wide range de techniques: API content, thermal properties, morphology, apparent solubility, dissolution profile, and physical stability, taste masking tests (in vivo and in vitro) and pharmacokinetic study (the two later, for selected formulations).

- Use of a recent 3D printing technology based on the direct feed of powdered material for shaping personalized paediatric medicines from selected ASD formulations. The prototypes generated were characterized with respect to their thermal properties, morphology, dissolution profile, physical stability, and taste masking tests (in vitro).

## 3. THESIS OUTLINE

The manuscript is made up of seven Chapters.

Chapter 1 is an introductory Chapter.

Chapter 2 provides background and is divided into four sections. Firstly, section 1 presents an overview of schistosomiasis disease and treatment. Section 2 is focused on PZQ (characteristics, benefits in treating the disease, formulation challenges). Section 3 introduces some challenges and strategies on the pharmaceutical development of paediatric drugs, focusing on acceptance and palatability. The last section covers amorphous solid dispersions and concludes with the presentation of opportunities that 3D printing technology can offer to develop medicines, especially paediatric ones.

Chapter 3 is dedicated to characterization of the raw materials used in this thesis.

Chapter 4 presents the study carried out to evaluate the solubility of API (PZQ) in the polymer (PVPVA) from the recrystallization of a supersaturated solid form produced by spray drying. Unexpected results obtained during the production of supersaturated systems by spray drying are also discussed.

Chapter 5 focuses on the development of binary and ternary ASDs. The Chapter is then divided into four Sub-chapters that address the different studies performed with binary (Sub-Chapter 5.1) or ternary systems produced on different equipment (pharma 11 extruder – Sub-Chapter 5.2 and pharma 16 extruder – Sub-Chapters 5.3 and 5.4).

Chapter 6 presents the 3D printing step to obtain the PZQ prototype units.

Chapter 7 provides an overall summary, conclusions and perspectives of the work presented in this thesis.

The graphic abstract of this thesis is presented in Figure 1.

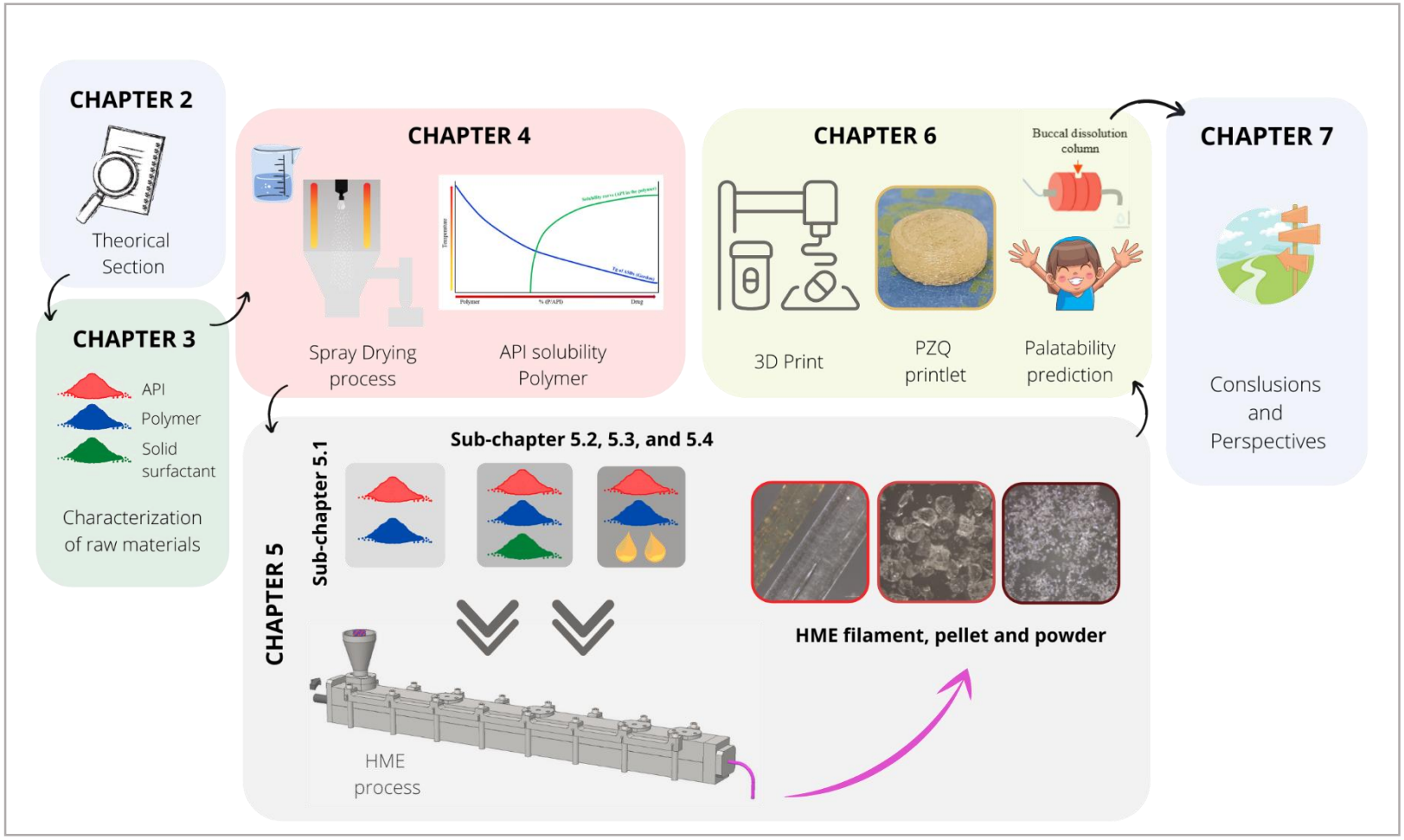


Figure 1. Schematic representation of this thesis.

# CHAPTER 2 - THEORICAL SECTION

# 1. INTRODUCTION

Chapter 2 provides background and is divided into four sections.

Firstly, section 1 presents an overview of schistosomiasis disease and treatment. It shows statistical data and public health impacts in Brazil and the world.

Section 2 is dedicated to the schistosomiasis treatment reference drug praziquantel. The mechanism of action, pharmacokinetics, physicochemical properties, and the commercial medicines are presented.

The following important topic treated in Section 3 deals with the challenges surrounding the lack of appropriate medication for paediatric patients. The target population of the praziquantel-based formulation is intended to be explored in this thesis. The main aspects addressed here are acceptance and palatability. This section also presents the formulation strategies in developing paediatric medicines covering traditional and emerging forms such as tablets, mini-tablets, orodispersible forms, chewable tablets, and 3D printed forms (named printlets). It finalized the section with a special focus on the different approaches that have been proposed for praziquantel medicines, aiming to improve some properties like water solubility, dissolution kinetics, and then oral bioavailability.

The next section focuses on the formulation approach explored in this thesis, the amorphous solid dispersions. Some fundamental aspects are introduced (amorphous state, advantages, and limitations of this category of solid forms, the solubility of the drug in the polymer, manufacturing processes) to conclude with a review of the previous studies employing the same praziquantel formulations approach. Finally, opportunities that 3D printing technology could offer to develop medicines, especially paediatric ones, including regulatory aspects for pharmaceutical use, are addressed.

# 2. SCHISTOSSOMIASIS

Schistosomiasis is caused by helminths of class Trematoda, family Schistossomatidae and genus *Schistosoma* [12]. Six species belonging to that genus are capable to infect humans: *S. guineensis*, *S. hermatobium*, *S. intercalatum*, *S. japonicum*, *S. mansoni*, and *S. mekongi*, from which *S. haematobium* and *S. mansoni* predominate [1].

In Brazil, the species with major prevalence is *S. mansoni*, which was set due to the Atlantic slave trade. Its establishment was caused by both the presence of susceptible

intermediate hosts (snails of genus *Biomphalaria*) and environment conditions in the country, similar to those found on the species' region of origin [12].

The disease transmission begins when human feces contaminated with parasite eggs enter the water. Those eggs liberate a caterpillar named miracidium, that in turn penetrates snails that belong to genus *Biomphalaria* - the intermediate host in which another type of the parasite grows: the cercariae. That new parasite can penetrate human skin or mucosa of exposed members, such as feet and legs when touching contaminated water. Later, the parasite feeds on and grows in the human's intrahepatic portal system, migrating already mated to the inferior mesenteric vein area, where the oviposition happens. The first eggs may be found in the feces of the infected person around forty-two days after the cercariae's penetration (Figure 2) [1], [2], [12], [13].

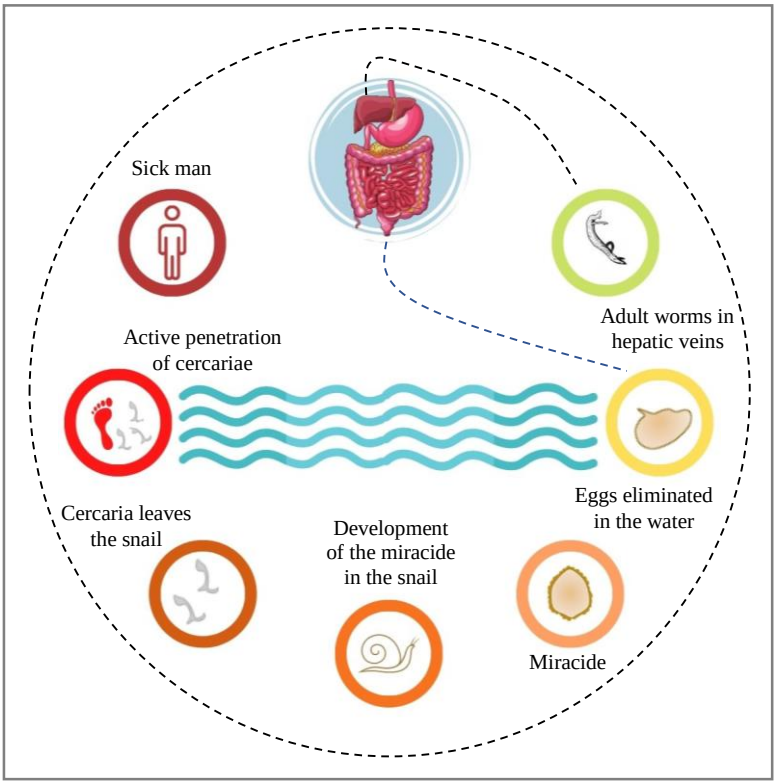


Figure 2. Biological cycle of *S. mansoni*. Source: author.

The disease - schistosomiasis - may be classified as acute or chronic. Its acute phase is characterized by mild symptoms of diarrhea, low-grade fever, headache, sweating, asthenia, anorexia, and weight loss. On the other hand, during the chronic phase, the patient's condition varies from the absence of hemodynamic alterations to several clinical pictures corresponding to portal hypertension, pulmonary hypertension, cyanosis, and glomerulopathies. Different

presentations of the disease may be observed, as pseudotumoral, neural and panvisceral, and schistosomiasis is sometimes associated with chronic septicemic salmonellosis and other morbid conditions. However, the main complication of schistosomiasis is portal hypertension, whose advanced stage causes bleeding, ascites, edema, and severe hepatic insufficiency. It nearly always leads to death despite the treatment, due to the irreversibility of the fibrosis and cirrhosis around the granuloma [14], [15].

Schistosomiasis morbidity rate is related, amongst other factors, with the intensity and length of the infection, as well as with the host's immune response to parasite antigens. Also, the parasite load depends on the intensity of contact with contaminated water, more common where sanitary conditions are precarious. A great part of the affected population lives in poverty, with dreadful sanitary conditions and low economic development [14]–[16].

All these factors are interrelated and responsible for determining the transmission intensity, which varies from place to place. That complex scenario surrounding the transmission of schistosomiasis, disease control depends on several preventive actions, such as early diagnosis and appropriate treatment, surveillance and control of intermediate hosts, health education and sanitation actions, as well as improvements on housing conditions. Those measures also aim to reduce the geographic expansion of schistosomiasis [14] and, according to the Brazilian Health Surveillance Secretariat (2014), should be implemented in an integrated manner, as part of a regular control program. The Federal Ministry of Health determines as well that it is up to municipalities to regularly carry out active search and treatment of carriers, over the long term, on average in biennial cycles, to keep the prevalence low and reduce the onset of the disease.

### 1.1 Epidemiological evidence

In Brazil, it is estimated that 8 to 10 million people are infected by schistosomiasis and the other 30 million live in areas with a high risk of contamination [17], [18]. Recent data released by SANAR – *Programa de Enfrentamento às Doenças Negligenciadas do Estado de Pernambuco* [19] show that this state has the highest level of endemicity for schistosomiasis and presents a historical series of mortality, almost five times higher than the national one. In 2010, 358 deaths were registered, mainly from prioritized municipalities [19].

Worldwide, schistosomiasis affects almost every continent, but Africa is still responsible for the great majority of cases (around 90 %). In Asia, there are close to 900 thousand people infected with the parasite, most of them living in China [1], [18]. According

to information from World Health Organization (WHO) [1], in 2013 the total number of people in need of treatment for schistosomiasis in the world was approximately 260 million, of whom 46 % was school-age children (5 to 14 years old). It is known that younger children are a vulnerable population, but data for that year range are still limited. Moreover, around 779 million people live in endemic areas, which makes schistosomiasis the second on the ranking of neglected tropical diseases in terms of socioeconomic resources and the second most problematic disease for public health in underdeveloped nations. From those, Brazil is the most affected country in South America [1], [2], [20], [21]. Schistosomiasis infects more than 230 to 250 million people annually [2].

The mortality rate for schistosomiasis is close to 280,000 people per year, with the highest percentage of deaths on the African continent [2], [20]. In Brazil, the extensive geographical distribution of schistosomiasis alone scales the magnitude of this public health problem. In addition, the occurrence of severe forms and deaths makes schistosomiasis one of the most transcendent parasites. The morbidity of schistosomiasis represents great damage to the population's health, quality of life, and economic losses [14].

With regard once more to Brazil, according to official statistics published in 2014, *S. mansoni* is present in the states of Ceará, Piauí, and Maranhão, all in the Northeast; Pará, in the northern region; Goiás and Federal District, in the Midwest; Espírito Santo, Sao Paulo, Rio de Janeiro and Minas Gerais in the Southeast; and Paraná, Santa Catarina and Rio Grande do Sul, in the Southern Region. In total, there are 19 Federated Units where transmission is active [14].

### 1.2 Treatment

Basic sanitation, potable water access, education for hygiene and snail control are means of achieving lasting benefits and prevention for the population, not only related to the problem of schistosomiasis, but also of every disease delivered by polluted water, as salmonellosis, hepatitis, giardiasis, etc. [1], [8], [12].

Nonetheless, given the data discussed above, in addition to sanitary measures, which are efficient for disease control, the treatment of schistosomiasis must be brought to attention to contribute to its decrease and eradication. Concerning that, chemotherapy is sometimes needed. The chemotherapy treatment for schistosomiasis has a history of limitations, due to the reduced number of efficient, safe, and well-tolerated medicines available [15], [20], [22].

The drugs that are being widely used to treat schistosomiasis are oxamniquine and praziquantel. Nevertheless, oxamniquine acts only against schistosomiasis and causes side

effects on the central nervous system, besides having carcinogenic effects [12], [20]. Also, oxamniquine is described as having a complex and high-cost production, which led Pfizer to suspend its offering [23]. Praziquantel, on the other hand, is a very effective drug in the treatment of schistosomiasis and of other diseases caused by genus *Schistosoma*; it has milder and few side effects, as well as superior pharmacological activity in comparison to oxamniquine. It also has high efficiency, low toxicity and costs less [21], [24], [25]. All those factors make praziquantel the only commercial drug for the treatment of *Schistosoma sp.*, for which, besides, there is no vaccine available [25]–[27].

In Brazil, praziquantel was introduced in the Schistosomiasis Control Program (PCE in the Portuguese acronym) back in 1996, and remains the drug of choice for schistosomiasis, both in public and clinical campaigns. According to the WHO – Model List Essential Medicines [28], praziquantel is recognized as the primary drug in the treatment of all kinds of *Schistosoma*, besides being indicated for the treatment of taeniasis, cysticercosis [23], [29].

The treatment of schistosomiasis consists of 20 mg/Kg three times a day at intervals of four to six hours; this therapeutic regimen shall then be repeated after four to six weeks [9], [10]. Another option of treatment is a single dose of 40 mg/Kg for just one day (depending on the parasite), usually used as preventive chemotherapy [30]. For children, the dosage is adjusted to the child bodyweight by administering in sets of 150 mg (1/4 tablet) [9], [10]. The efficacy of that treatment can be measured by parasite egg excretion on feces; results showed that 60 - 90 % of the cases are cured (no more eggs in feces) and 80 – 95 % of noncured patients have an average reduction in the number on excreted eggs, depending on the level of infection [23], [31].

### 1.3 Health Policies

In Brazil, campaign initiatives for fighting schistosomiasis began in 1953 by the Federal Government. In 1956 it was created the *Departamento de Endemias Rurais*[4] of the Brazilian Ministry of Health, which was composed of various centers and research cores focusing on treating diseases like schistosomiasis. Only in 1970, it was implemented the *Programa Especial de Controle da Esquistossomose* (PECE)[5], which was renamed *Programa de Controle da Esquistossomose* (PCE) five years later. In 1990, the PCE[6] was placed under the direct

[4] N.T.: Department of Rural Endemic Diseases (loose translation).
[5] N.T.: Special Program for Control of Schistosomiasis (loose translation)
[6] N.T.: Program for Control of Schistosomiasis (loose translation)

responsibility of the *Fundação Nacional de Saúde* and, since 1993, a decentralization of the actions aimed at controlling the disease has been implemented, by putting the control of schistosomiasis in charge of the municipal offices in each territory [16].

Currently, the federal administration is working on encouraging national industrial development, especially in the drugs and medicines field. In this context, the decree MS/GM n. 3.916/1998 approved a National Policy for Medicines, following the prescriptions of the National Health Surveillance System, whose objective is to promote better health conditions for the population through actions as (i) sanitary regulation for medicines; (ii) scientific and technologic development, focusing on the pharmaceutical industry; (iii) promotion of drug manufacturing, first and foremost by official pharmaceutical labs.

Praziquantel is one of the drugs listed on the National Relation of Medicines (RENAME), part of the strategic component on pharmaceutical assistance, destined to guarantee access to medicines and other supplies that prevent, diagnose and treat diseases and their specific complications, covered by strategic health policies from the Brazilian National Health Service (*Sistema Único de Saúde* – SUS) [32]. Now, considering schistosomiasis is a serious public health problem, praziquantel must be improved so that paediatric drugs can respond to children with efficiency, security and quality under the standards and guidelines recommended by the National Health Surveillance System.

## 3. PRAZIQUANTEL

Praziquantel is the result of a collaborative work by two pharmaceutical companies in Germany, Bayer A.G. and E. Merck [33], [34]. The anti-helminthic activity was discovered in 1972 by Bayer and its action against a broad spectrum of pathogenic platyhelminths was confirmed in partnership with Merck (WHO, 1998). Praziquantel was patented in Germany in 1973 and in the United States in 1977. It became available in the European market in 1978 and worldwide in the ’80s. Initially, it was restricted to veterinary use and the registry for its use by humans was granted by the Food and Drug Administration (FDA) in 1982 [35].

Currently, praziquantel is the first-choice drug for the treatment of diseases caused by different species of genus *Schistosoma* and it is also indicated to treat infections by other helminths of the class Trematoda [36]. It is present on the WHO Model List of Essential Drug, with a posology of 150 mg or 600 mg capsules to treat helminthic intestinal infections and of

600 mg capsules to treat schistosomiasis infections and other pathologies caused by trematodes [28].

Furthermore, in regions where schistosomiasis treatment is massive, as in Africa, praziquantel is also used for chemoprophylaxis since 2006. This means that where there are high levels of schistosomiasis endemicity and precariousness of health services, the treatment is administered regardless of previous diagnosis [8], [21].

Additionally, there are studies already showing that praziquantel may increase paclitaxel's anticancer activity, which demonstrates how therapeutic indications of praziquantel may increase over the next few years [37].

### 1.4 Mechanism of action

Praziquantel mechanism of action is not totally elucidated. It is known, however, that the anthelminthic action of the drug is probably due to the inhibition of schistosome $Na^+K^+$ pump, increasing the permeability of the helminth membrane to certain monovalent and divalent cations, mostly calcium, which causes muscles activity intensification, followed by contraction and spastic paralysis. As a consequence, helminths separate from the host's tissues and are quickly dislocated from the mesenteric veins to the liver, whereas intestinal helminths are expelled [24], [38]. Is known that praziquantel can act on various stages of *Schistosoma* and affect adult parasites, miracidia and cercariae, but has little or no effect on the parasite eggs, sporocysts or schistosomula [39].

### 1.5 Pharmacokinetics of praziquantel

The drug currently available for the treatment of schistosomiasis is praziquantel in the form of tablets, as will be further detailed in this section. This product is manufactured with racemic API and, for this, absorption is carried out quickly by the gastrointestinal tract, and the plasma peak is reached about 1 to 3 hours after its oral administration [20], [40].

It is a drug that has an extensive first-pass effect on the liver, broad binding to plasma proteins (about 85 %), half-life around 60 to 90 minutes, and its excretion occurs through urine [41].

Recent studies have confirmed that the (R) - Praziquantel enantiomer is responsible for the pharmacological activity, and (S) - Praziquantel, although it has no anti-schistosomiasis

activity, plays some role in contributing to the extent of the activity performed by (R) – Praziquantel [41]–[46].

In 2018, the Zanolla et al. research group reported the formation of the polymorphic form B of praziquantel by milling [30]. The following year, a study on pharmacokinetics of that new polymorphic form in mouses was published. Although the new crystalline structure has shown an increase in properties such as solubility, dissolution rate, and chemical stability, the general level bloods were lower when compared to the praziquantel formulation based on the racemic form [40].

### 1.6 Commercial medicines of praziquantel

Currently, praziquantel is commercialized at doses of 500 mg and, most commonly, 600 mg worldwide. The reference medicine is produced by Bayer at 600 mg strength, in the form of coated tablets with 22 mm length (Figure 3) commercialized under the name of Biltricide®. Cisticid® 600 mg and Cisticid® 500 mg are commercialized by Merck KGaA for human use [9]. Praziquantel posology is based with the patient's weight, hence one of the existing difficulties for treating children is the administration of the appropriate dosage, to which cutting the tablet is widely used (the reference medicine is commercialized with 3 grooves and can be divided into up to 4 parts). The splitting/smashing practice tablets cause dosage impacts and improve the unpleasant taste by eliminating the product coating. [9].


Figure 3. International reference drug (Biltricide®) produced by the German company Bayer Healthcare Pharmaceutics – praziquantel 600 mg dose. Source: [4] (with permission).

Another issue of praziquantel is that the medicines are produced from the racemic mixture of the API, one being active against the helminth and the other inactive. As the separation of both isomers is a very expensive technique, it is usually not applied, keeping one of the structures with a null effect. That makes a need for increasing the concentration of the drug for each dose, which in turn results in tablets that are quite big and difficult to swallow, mainly for children that represents a high number of infected patients [11].

In Brazil, there is just one praziquantel-based product available (Praziquantel 600 mg), from a public company (Farmanguinhos/Fiocruz) linked to the Ministry of Health (Figure 4) [47].


Figure 4. a) Primary package e; b) Tablet produced by Farmanguinhos/FIOCRUZ – Praziquantel, 600 mg dose. Source: Author.

According to the Cisticid® leaflet, the tablet must be swallowed entirely, with potable water and during meals. Otherwise, when needed, it may be dissolved and administered via nasogastric tube. As for Cestox®, the leaflet indicates that tablets must be swallowed entirely, without chewing [48]. About the medicine produced by Farmanguinhos, the guidance is not to chew tablets, but to split them into two or four parts to permit the administration of individual doses. Due to the bitter taste, according to Farmanguinhos, they should also be swallowed immediately with enough liquid to avoid vomiting [49].

The cure rate using praziquantel is known to approach 80 % for adults and 70 % for children [14]. In a document of Technical Guidelines for Surveillance of Schistosoma mansoni published by the Brazilian Ministry of Health [14], it is highlighted the need for attention to patients who have been treated several times and who have not healed, which must be notified to the PCE. Those guidelines are indicative of concern about the resistance of strains to the use of praziquantel. This may be due to the difficulty of administering the drug with a more accurate dosage for the patient (mainly paediatric) and the lack of adherence to treatment due to palatability.

There are some reports of a commercial praziquantel medicine for children in suspension form, Epiquantel® 120 mg/mL produced by the Egyptian company (Egyptian Pharmaceutical Industries Co). It is known, though, that there is no information regarding the

acceptance of that product by children in the literature and, even though that would be the only paediatric drug available, it was not adopted by WHO [50], [51]. Moreover, when consulting the company's website, there is no description of its availability. The only product categorized as “antiparasitic & schistosomicide” is Distocid® 600 mg in tablet form.

Against this background, the need for a formulation for praziquantel that can be administered to children and overcome the barriers of bioavailability, bitter taste and dosage is clear.

### 1.7 Resistance to praziquantel

In 2017, 100 million people (80 million school-age children) received free preventive treatment (praziquantel) for schistosomiasis [27] and, it is known that the control of schistosomiasis is predominantly dependent on this therapy for millions of people around the world [46].

However, it is important to mention that some studies are being undertaken to verify the heterogeneity in the cure rates with this medication. Currently, there is great concern about the variations in the drug efficacy found in diverse populations, raised by the possibility of praziquantel resistance among parasites. For this reason, different studies are conducted to assess the factors that can result in praziquantel levels in the systemic circulation that potentially contribute to these low and variable cure rates [46], [52].

The main variables that are discussed in this regard are the different formulations and brands, the patient's liver health, medications administered concomitantly and genetic factors [43], [44], [46].

### 1.8 Physical and chemical properties of Praziquantel

Praziquantel (PZQ) is an imidazole derivative, chemically known as: (+)-2cyclohexylcarbonyl-1,2,3,6,7,11b-hexahydro-4H-pyrazine[2,1-a]isoquilonin-4-one [29], [53]. Its molecule weights 312.4 g/mol and contains an oxo group in position 4, which is an important characteristic, since it cannot be modified without suppressing drug activity [34].

PZQ is described as a white to nearly white crystalline powder, it has a low solubility in water and it is soluble in ethanol and in other solvents organics [35], [54]. Other physicochemical characteristics of PZQ are presented in Table 1.

Table 1. Summary of physicochemical characteristics of Praziquantel.

| ***PZQ - Physicochemical characteristics*** | | ***References*** |
|---|---|---|
| Molecular weight | 312.4 g/mol | [53]–[57] |
| Melting point | 136-144 ºC | [53]–[58] |
| Glass Transition temperature | 35.9 -37.7 ºC | [56], [59] |
| Water solubility | 0.14 mg/mL (20 ºC) | [30], [60] |
| | 0.22 mg/mL (25 ºC) | [61] |
| | 0.40 mg/mL (25 ºC) | [4], [57], [62]–[66] |
| | 0.28 mg/mL (37 ºC) | [67] |
| Ethanol solubility | 63 - 97 mg/mL | [57] |
| pKa | 19.38 | [57] |
| LogP | 2.42 | [57] |
| Taste threshold | 0.03 mg/mL | [68] |

Chemically, it is known that PZQ is hydrophobic and a chiral substance (position 11b), obtained mainly from a racemic mixture (1:1 mixture of enantiomers) (Figure 5**Erro! Fonte de referência não encontrada.**). The optical resolution proved that the anthelminthic activity is principally due to the R-(-)-enantiomer (L-PZQ or (-)-PZQ or R-PZQ) while the S-(+)-enantiomer (D-PZQ or (+)-PZQ or S-PZQ) is inactive, presenting higher toxicity and being the main responsible for praziquantel bitter taste [20], [34], [60], [69]. The isomers also have different physicochemical characteristics such as solubility (R-PZQ 1.91 mmol/L, S-PZQ 1.64 mmol/L and Rac-PZQ 0.92 mmol/L) and melting temperature (R-PZQ $T_{onset}$ 109.4 ºC, $T_{peak}$ 122.3 ºC and, $\Delta H$ 77.3 J/g; S-PZQ $T_{onset}$ 109.7, $T_{peak}$ 112.6 ºC and $\Delta H$ 78.2 J/g) [70].

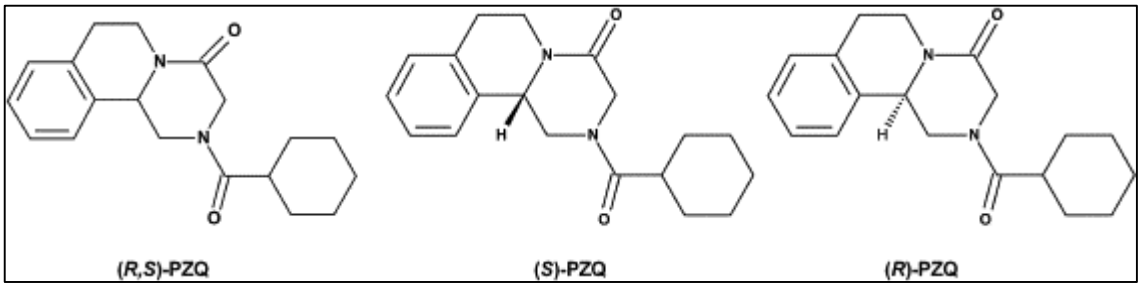


Figure 5. Chemical structure of praziquantel a) (R,S)-praziquantel (racemic), b) (S)-praziquantel and, c) (R)-praziquantel (Reuse from [5] with permission).

There are currently two anhydrous crystalline structures of PZQ described in The Cambridge Crystallographic Data Center (CCDC), which are the commercial racemic compound (TELCEU) [33] and the second crystalline structure (TELCEU01), described in the literature as PZQ polymorph B [10] (Figure 6). Like the commercial crystal structure, form B

is described as a mixture of enantiomers. In addition to these structures, enantiomers hemihydrates (SIBUG and SIBUG01) [42], [71], the enantiomer (R)-praziquantel hydrate (LIVED), and some acid derivate were also observed [72].

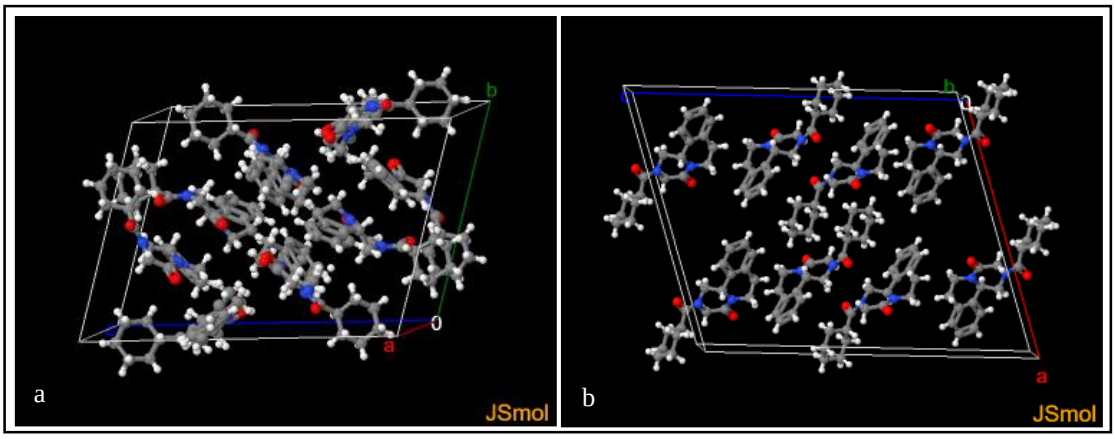


Figure 6. Unit cell of crystal structure of anhydrous PZQ a) commercial racemic compound (TELCEU) and b) praziquantel form B (TELCEU01) (Reuse from [10], [33] CCDC 896767 and 1557658 ).

Some disorders in the position of the atoms can be visualized on the crystalline structure of anhydrous PZQ (Figure 7). In contrast, the crystalline structure of the hemihydrate of the enantiomer R of PZQ (SIGBUG01) [42] is well defined, presenting four praziquantel molecules and three water molecules.

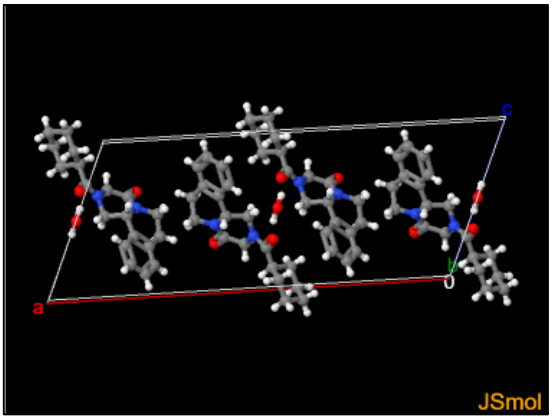


Figure 7. Crystal structure of the hemihydrate of (R)-Praziquantel (SIGBUG01) (Reuse from CCSD 710418 [42].

Figure 8 shows the diffraction patterns published in the CCDC for the racemic form of PZQ, and the enantiomers, respectively.

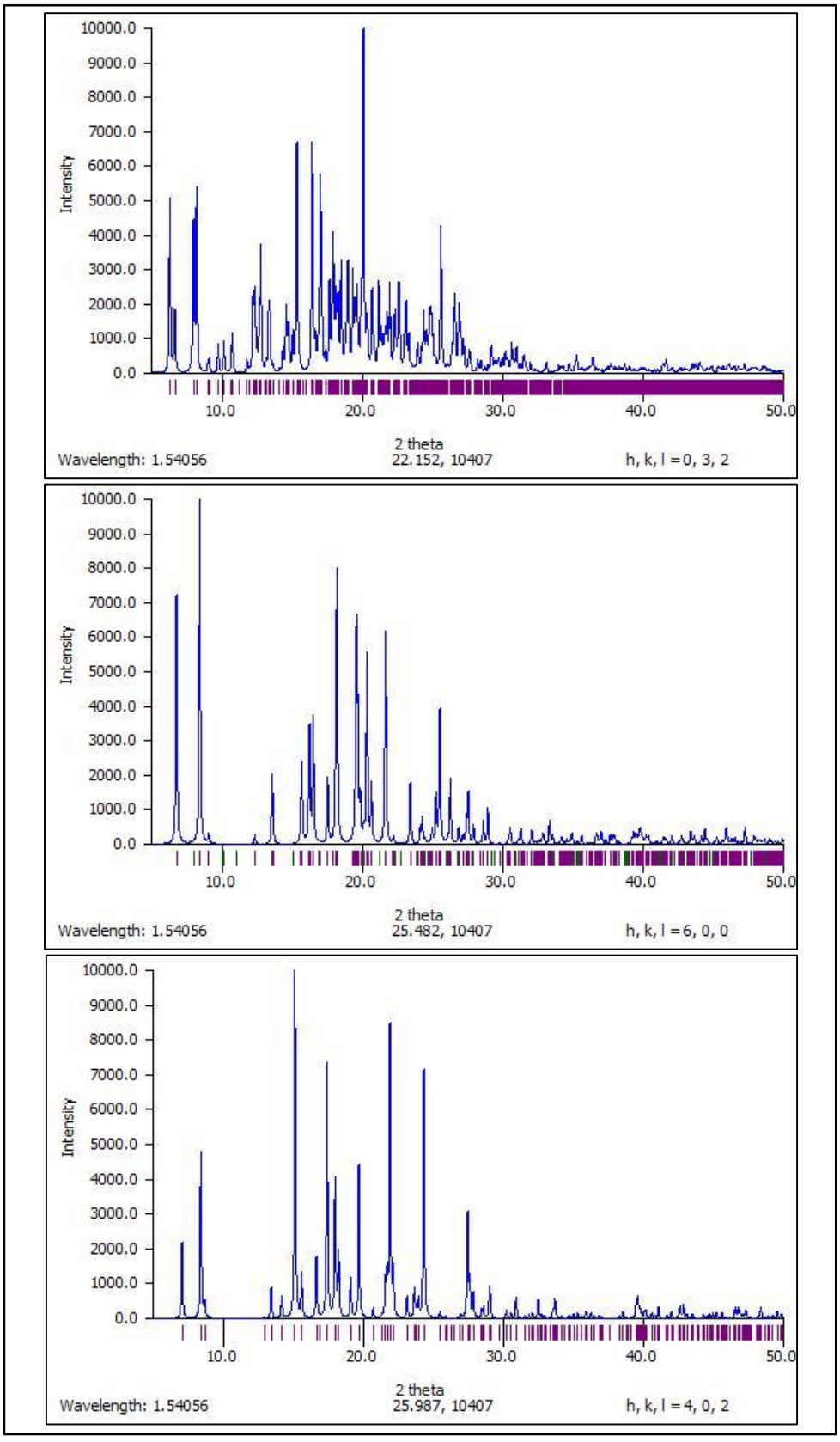


Figure 8. Praziquantel patterns XRPD. a) racemic form - TELCEU [33], b) form B TELCEU01 [30] and, the enantiomer form C – SIBUG and, SIBUG01 [42], [71] (Reuse from CCSD 710418, 896767 and 1557658 ).

The polymorphic form C of PZQ was recently described. It was characterized during a study that used the design of experiments (DoE) approach to evaluate milling conditions of PZQ Form B [73]. This crystalline structure was elucidated thanks to its production from API grinding alone and the association of different solid-state characterization techniques such as Differential Scanning Calorimetry (DSC), Thermogravimetric Analysis (TGA), Synchrotron X-Ray powder diffraction, Nuclear Magnetic Resonance (NMR) measurements and, Fourier-transform infrared spectroscopy (FT-IR). It was verified that forms B and C have very close characteristics. For example, through X-ray diffraction (XRD) results, it was possible to visualize the diffraction patterns' differences between the racemic form, form B and form C (Table 2), while through FT-IR, it was not possible to identify differences between B and C forms (Figure 9) [73].

Table 2. Summary of the main diffraction peaks on powder diffractograms for different PZQ solid forms.

| ***PZQ form*** | ***Angles of 2Θ*** | ***References*** |
|---|---|---|
| Commercial PZQ | 7.08, 8.42, 12.1, 13.2, 14.7, 13.3, 16.3, 17.5, 18.5, 18.8, 19.2, 20.0, 21.1, 21.7, 22.5, 22.9, 24.3, 25.4, 26.5, 28.8, 29.1, 30.1, 31.4 | [74] |
| Form B | 6.83, 8.48, 9.08, 12.35, 13.64, 15.74, 16.28, 16.55, 17.6, 18.23, 19.61, 19.94, 20.39, 20.45, 21.68, 22.34, 23.45, 25.31, 25.58, 26.3, 27.59, 27.95, 28.64, 28.97, 30.53, 31.4, 33.38 | [73] |
| Form C | 6.95, 8.54, 12.68, 13.94, 15.38, 16.1, 16.49, 17.66, 18.05, 18.71, 19.43, 19.76, 20.54, 21.56, 22.13, 22.16, 22.55, 24.29, 25.19, 26.12, 27.59, 28.76, 29.0, 30.92, 31.16, 34.64 | [73] |
| Monohydrate | 12.0, 13.0, 16.2, 17.2, 18.5, 19.1, 20.2, 21.0, 22.7, 24.7, 24.9 26.6, 28.0, 30.7 | [74] |
| Hemihydrate | 6.28, 16.14, 16.50, 17.18, 18.67, 19.12, 20.05, 20.41 and 24.37 | [63] |

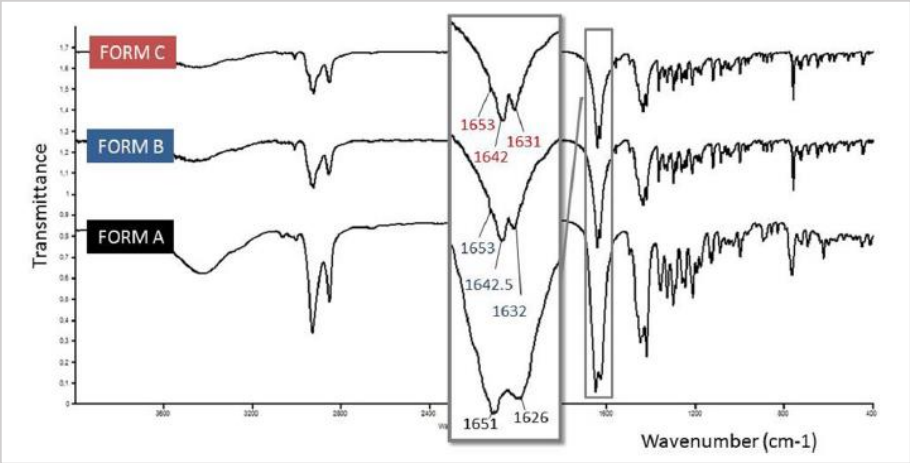


Figure 9. Similarity of the three PZQ polymorphic forms by FT-IR spectra (Reuse from [73] with permission).

The same study [73] has identified the melting points for forms B and C, respectively: 106.84 ºC ($\Delta H$ = 71.06 J/g) and 110.28 ºC ($\Delta H$ = 69.03 J/g), lower than the melting point of the racemic mixture (144 ºC and $\Delta H$ = 104.13 J/g) [74]. It was also demonstrated that Form C provided lower physical stability after two months of storage in a desiccator at 25 ºC protected from light, unlike the one-year stability reported for polymorph B [73]. This stability result was confirmed by the appearance of an endothermic signal in the fusion region of the commercial racemic PZQ. No other parameters have been evaluated for monitoring stability.

It is estimated that one-third of the pharmaceutical molecules can exist as a hydrate [75]. For PZQ, the obtention of the monohydrate and hemihydrate forms was reported in the literature [74], [75].

The hemihydrate form of PZQ was prepared by Zanolla and collaborators [75]. by three different methods: a) starting from the commercial PZQ, b) starting from the PZQ form B, or c) starting from preformed seeds of the hemihydrate form of the PZQ and commercial PZQ [75]. The first option involved three stages: the grinding of the commercial PZQ, adding water, and new grinding. In the second and third methods, water was added to the materials, and the grinding process was done in a single step. The procedure to obtain form B was also carried out with the specific grinding conditions of the pure commercial API [10], [75]. The hemihydrate form of PZQ generated in this work presented a completely different PXRD pattern (shown in Table 2) from the previous structures of PZQ already discussed here (racemic form, forms B and C). DSC analysis revealed a first endothermic event in the region of 68 ºC (61.38 J/g) related to dehydration. TGA confirmed it with a 2.19 % loss of mass - a good correlation with the expected 2.73 % theoretical value for the hemihydrate form. Other characterizations were

carried out like FT-IR, Scanning Electron Microscope (SEM), and Crystal Structure Solution, to complete the characterization of the hemihydrate PZQ solid form. About its physical stability, after three months under room temperature conditions, it started to show diffraction peaks corresponding to form B, until complete transformation to form B at the end of 12 months. The grinding and exposure of the hemihydrate sample at 50 °C for a few hours also resulted in form B. However, none of the cases studied evidenced the transition of the hemihydrate sample to the more stable racemic form and no evidence of form C. The hypothesis is that the preference for migration to form B is like packing arrangement (anti-conformation), unlike commercial PZQ (*syn* conformation). It is believed that to reach this rotation and reach racemic form (commercial) much more energy is needed than the dehydration process [75].

The Biopharmaceutical Classification System (BCS) was established in 1995 [76] to determine water solubility and intestinal permeability characteristics of a drug molecule. Characteristics are divided into four different classes and predict the in vivo/in vitro relationship of the molecule [77] (Figure 10). A drug is considered highly soluble if its highest dosage is capable of solubilizing in a volume less than or equal to 250 mL, with pH between 1.0 and 6.8 and at a temperature of 37 ºC ± 1 ºC. To be considered highly permeable, its higher dose must present an absorption equal to or greater than 85 % (mass balance determination) or comparable to the intravenous reference dose [20], [77]–[79].

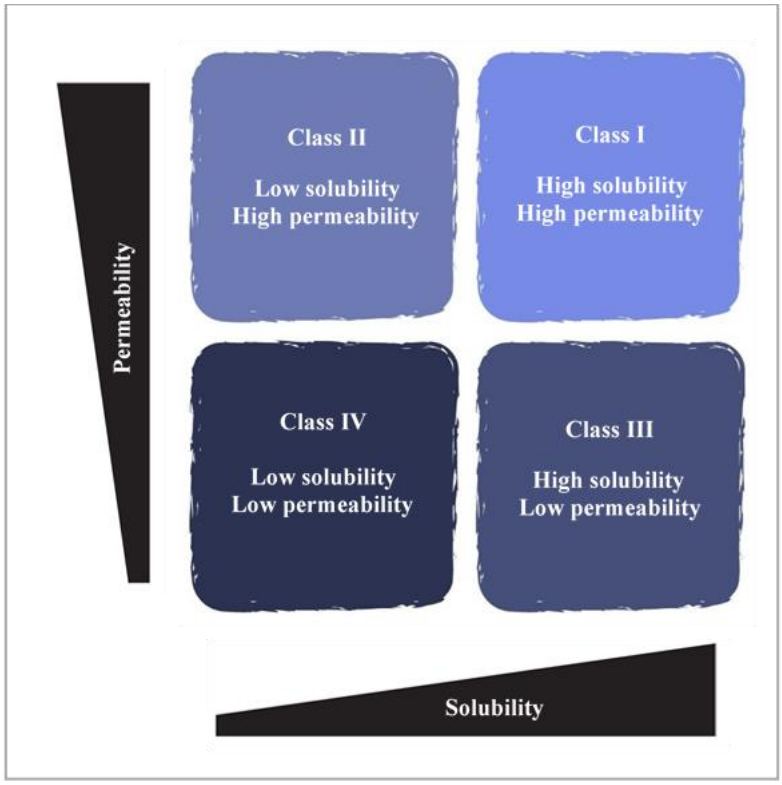


Figure 10. The Biopharmaceutical Classification System (BCS) (Source: Author).

PZQ is a drug in class II according to the BCS classification, which means that it has low water solubility (Table 1) and high permeability. The dissolution rate is a decisive factor to determine the effective concentration of the drug able to reach the parasite tissue, and this is one of the main reasons for high doses [20]. Likewise, permeability is of essential relevance as it is directly related to the processes of absorption, distribution, metabolism, and excretion.

## 4. PHARMACEUTICAL DEVELOPMENT WITH EMPHASIS ON PAEDIATRIC MEDICINES

Increasing efforts have been developed by the European Medicines Agency (EMA) and the Food and Drug Administration (FDA) to encourage responses to the needs of child patients [80]. In 2007, WHO launched the 'make medicines child size' (MMCS) campaign so that specific attention was given to the need for children to receive the correct medicine at the correct dose [81]. In that same year, data indicated that there was still an alarming gap in the number of paediatric drugs officially licensed for paediatric use [82]. About 50 % of the drugs available for use in children are still considered off-license and/or off-label [82], [83]. This panorama is also evident for 90 % of the drugs administered to babies and neonates in the Paediatric Intensive Care Unit (PICU) of the European Union [84]. This means that paediatricians prescribe drugs authorized for adults by only adjusting the dose and format [83]. To satisfy the need for suitable dosage forms for the paediatric group, some practices are usually employed in the administration routine to overcome drug suitability problems, such as mixing the drug with food additives, and crushing/dissolving pills. However, all those practices may bring on technical and clinical risks such as drug degradation, microbial contamination, dosage calculation errors, and the formulation's therapeutic inefficiency [83], [85]. Besides that, the adaptation of pharmaceutical forms for administration to children has a history of even more drastic results as occurred in Ethiopia during a deworming campaign [9]: children under 36 months died from asphyxiation following albendazole administration [9], [84].

In the same year of 2007, the EMA established paediatric regulation, which triggered the development of guidelines for manufacture and prescription of children’s drugs, through the Paediatric Committee (PDCO) [83]. All this work resulted in recognition of paediatric drug development as a specific department within companies. One of the results that came from that initiative was the requirement imposed to EMA and FDA agencies in need to submit paediatric development strategies through Paediatric Investigation Plans (PIPs) and Paediatric Study Plans

(PSPs) of presenting product development strategies [86]. In 10 years of paediatric regulation in the European Union, 260 new medicines for paediatric use (new indications and new market authorizations) have been authorized.

Pharmaceutical technologies, research, and business models have been evolving rapidly in recent years, which favor improving the paediatric medication scenario. However, even after ten years of incentives, guidelines, committees, and, especially, regulations for paediatric drugs, there is still a great need to develop products suitable for this group of patients [87].

Currently, pharmaceutical development is a big challenge: in recent years, about 70% of new drug candidates are classified as poorly water-soluble, which is the factor mostly responsible for their low bioavailability and low therapeutic efficacy [88].

In an attempt to overcome this barrier, numerous formulation strategies have been devised, such as micro and nanoparticles, inclusion complexes, salt formation, cocrystals, polymorphic modification, eutectic mixtures, among others [10], [79], [89]–[92]. However, in the case of paediatric medications, improving the solubility of a drug may not be the solution to all barriers encountered. Besides, the development of these drugs poses the challenge of encompassing a large age group meeting their specific needs with respect to the pharmaceutical forms available for administration [93].

About 80 % of adult medicines are not necessarily suitable for paediatric populations, so they have not yet been developed directly for paediatric patients [85]. This group of patients presents a great diversity in terms of anatomy, physiological and psychological response when compared to adults and, as a result, the therapeutic response is varied. Furthermore, the development of paediatric formulations also has specific challenges related to physicochemical properties such as solubility, permeability, stability, and organoleptic properties of active pharmaceutical ingredients. All those factors may likely be connected to safety, tolerability and efficacy in the developed drug [85].

The issue of palatability is not considered a key problem in developing oral forms for adults, as the coating can disguise unpleasant tastes, and adults have another clarification on the subject. In the child population, dysphagia is a problem, which leads to a significant preference for liquid, orodispersible, or chewable formulae in drugs of choice. Consequently, developing pharmaceutical solutions that beat the challenge of unpleasant taste masking becomes even more complex [94].

This problem has been widely discussed in the last ten years, and the most widely used techniques to mask drug taste are: bitter receptor blockers, sweetening and flavouring systems, modification of API solubility, complexation and coating systems [94]. Although the criteria

for acceptance and quality of a drug for adults may undergo evaluation of parameters such as high dose flexibility, swallowability, palatability, and safety of excipients, the same cannot happen for paediatric formulae, as all these factors are crucial for their acceptance and the efficiency of treatment.

Against this background, WHO strongly recommends that anthelmintic manufacturers responsible for public health programs for preschool children develop appropriate formulations [95]–[97]. The WHO [98] presents a classification in 5 bands for the paediatric patient group: a) new born, premature, lactating; b) new-borns from zero to 28 days; c) babies and children over 28 days to 23 months; d) children from 2 to 12 years old and; e) adolescents from 12 to 16/18 years.

Obtaining a paediatric PZQ formulation should then address three main issues:

a) *increasing PZQ solubility and dissolution*, which is expected to allow de reduction of the dose of the drug to be administered, increasing the absorption efficiency, and reducing side effects and the costs involved in the production process and,
b) *masking the bitter taste of the PZQ molecule* to allow paediatric patients to accept PZQ medicine and adhere to the schistosomiasis treatment.
c) *optimize formulations with different dosages* to allow correct administration of the dose due to the children's weight contributing to the efficacy of the treatment.

### 4.1 Acceptability

According to EMA, the acceptability of a drug is defined by the patient's or caregiver's ability to use the product according to the proposed purpose. This acceptability is determined through the relationship between the patient's characteristics (age, ability, type of disease, social/cultural backgrounds and settings (e.g., home, hospital, or school) and those of the product (palatability, swallowability (size and shape, dosage form), appearance (colour, shape), ease of administration (necessity of modification before administration), required dose (dosing volume, number of tablets, break marks), dose frequency, administration device and packaging [86], [99], [100].

Acceptability must be addressed in full during pharmaceutical development so that all the patients' needs for which the drug is intended can be met. Currently, some drugs for paediatric use on the market are only the reduction of the dosage available for adult patients. Examples of this practice are benznidazole and the artesunate association of mefloquine publicly available in Brazil to treat Chagas disease and Malaria, respectively. The lower dosage

naturally reduced tablet sizes, but other specific criteria for better acceptance of paediatric patients were not considered. Although efforts and support in developing specific and appropriate formulations for children with neglected diseases are challenging, this group of patients cannot be considered small adults [87], [101]. On the other hand, another group of drugs representing more than 80 % of the drugs prescribed and intended for children is classified as off-label. These drugs have not been formally tested in this population and are therefore not labelled for use in neonates, infants, and children [102]. Currently, the use of praziquantel in children is off-label, and its administration requires breaking the pill to fit the body weight [9], [103]–[105].

### 4.2 Palatability

Although palatability is not the only fact that affects drug acceptance, it is still considered the first cause of non-adherence to treatment, especially in children [99], [100], [106]. However, it is important to mention that other patients who do not fall under the category of "standard patient" [107] are equal beneficiaries of an approach considering the importance of it. Although geriatric patients have different characteristics to be considered, pharmacokinetics cannot be framed only by physiological variations in age, as in paediatric patients (neonates, children, infants, and adolescents). The elderly have their pharmacokinetics strongly affected by morbidity, co-morbidity, multiple drug use, or reduced organ function [107]. Given this scenario, paediatric and geriatric patients are groups in which the palatability of a drug can determine treatment adherence and, consequently, therapeutic efficacy.

According to EMA, palatability is defined by an overall appreciation of an (oral) medicine by organoleptic properties such as vision (appearance), smell, taste, aftertaste, and mouthfeel set of organoleptic perceptions (taste, smell, residual taste, dose, volume or size and texture (mouth feel) emitted by a patient and which directly affect his acceptance [86], [99], [101]. The notion that taste is related to the perception of aroma, mouthfeel, and texture is important, while the taste is directly related to the sensations perceived through the taste buds in the tongue epithelium and the oral cavity [86], [101], [108]. All this palatability response will be directly dependent on the excipients, actives and the pharmaceutical form used in the development of the product [109].

For paediatric formulations, palatability is one of the main important features that affect acceptability [99]. The overall appreciation of a drug for organoleptic properties such as smell, taste, texture (mouthfeel) and possibly sight and sound may be crucial for a child to accept the

treatment. That is, palatability is linked to the acceptability of the drug to the indicated patients and is likely to have a significant impact on patient compliance and, consequently, on product safety and efficacy [99], [109].

### 4.2.1 Taste

Taste is one of the senses in which humans and other animals can develop perceptions about the environment in which they live [110]. Taste modalities are basically described as sweetness, sourness, saltiness, bitterness, and umami [111], [112]. When introducing medication into the mouth, the first perceptions of taste come from the taste buds, which are structures composed of about 50 to 100 neuroepithelial cells arranged in groups, resembling the shape of an onion (Figure 11). The main function of taste buds is to transmit a molecule's taste that comes in contact with the tongue to the nervous system [113]. These cells can be classified according to their morphology, protein expression, and signalling characteristics. Each cell type is responsible for transmitting one of the following tastes: type I - probably, salty taste, type II - sweet, umami and bitter, type III - sour, and type IV - basal cells.

The function of taste buds is to transmit information on the taste of the molecule to the central nervous system.

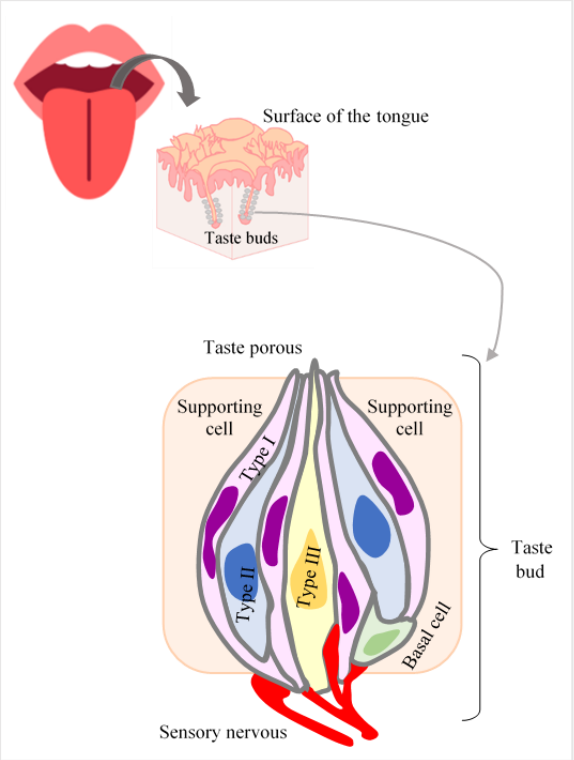


Figure 11. Process of taste perception in the mouth (Source: Author).

When it comes to medicines' taste, this is a key factor in achieving the desired treatment's success, especially when the patient is a child [68], [114]. In a study conducted by Ascent Paediatrics, Inc. (Wilmington, Massachusetts) with 500 parents, 75 % of the unfinished treatments were due to the drug's bad taste [115]. Besides, 90 % of paediatricians report that the taste of the medication and palatability are the major barriers to be overcome for the treatment's adequate conclusion [110].

#### *4.1.4.1 Taste assessment*

Since most APIs have a bitter taste or poor organoleptic properties, the development and validation of methods for taste evaluation is a fundamental requirement for obtaining palatable pharmaceutical formulations, especially for paediatric patients [114], [116], [117]. The sooner the taste screening of the API or formulation is carried out, the greater the chance of development adequacy and the lesser the cost of the tests stage [68], [118].

The test considered the gold standard for assessing the taste of medicines is the human panel. This tool faces ethical and safety difficulties though, especially when it comes to products with limited toxicity data [114], [119]. This scenario becomes even more restrictive with medicines for paediatric use due to technical, practical, regulatory factors, questionnaire design, and reliability of paediatric responses depending on the ability of children to distinguish and express variations in taste and sensations in the mouth [118], [120].

To circumvent this problem, other tools can be used to assess taste. The measures can be classified as direct (when the response is due to the taste itself) and indirect (when the measure is due to the dissolution and/or release of the API and the quantification is related to the taste response) [114]. For the first, in vivo (animal behaviour assessment) and in vitro (electronic tongue) methods can be used. [114].

In a literature review on non-human techniques for the evaluation of taste in pure drugs, evaluation of taste masking and commercial formulations showed that among the most used in vivo techniques, the BATA model stands out and, for the in vitro evaluation, commercial electronic language (Astree and Insent) [114].

As for the latter, the results showed a good correlation with the human panel, but electronic language responses still have some limitations because it is necessary to calibrate the equipment with taste standards or validate the result with the human panel. Nonetheless, it is undeniable that the technique can be a very useful tool in the Early screening of taste of pure APIs and evaluate formulations that have gone through the taste masking stage. Likewise, in

vitro experiments for dissolving or evaluating drug release have shown promising results, even if these experiments depend on previous data determining the API taste threshold (in vivo). In vitro experiments are all relatively simple and can be easily accessed and executed, both for API alone and formulated products, but they must be associated with other assessment tools, such as supporting the interpretation of data obtained through the electronic language.

On the other hand, in vivo methods showed a good correlation with the taste response in humans. The most described method is BATA, and different drugs and products have already been evaluated. It is important to mention that, in addition to BATA, other in vivo experiments are described and are based on the consumption of the solution for the relationship with the taste of the sample. It is important to note, however, that in most in vivo taste assessment methods, rodent liquid deprivation is used before the test experiment. This means that the evaluation of the solutions will report the palatability and not the taste quality of the product under test since deprivation can influence the licks' baseline profile [114].

#### 4.1.4.1.1 In vivo test assessment

##### 4.2.1.1.1.1 Brief-access taste aversion (BATA)

The rodent brief-access taste aversion model (BATA) is one of the most in vivo assessment tools described in studies that analyse APIs, formulated and commercial products in the literature.

The experiment is based on the brief exposure (from around 06 to 10 seconds) of animals kept in water deprivation (to encourage them to drink) to the taste solution to be evaluated. The apparatus used to provide the solution has a system for computing the number of times animals lick, called licking [114]. The result is based on the change in the number of licks; that is, high numbers are interpreted as a pleasant taste, and, conversely, a minimum number of licks reflects the aversion [114]. This type of test can be used to determine a taste threshold for pure APIs, and this theory assumes that taste sensations are dependent on the intensity of the stimuli [121]. Different concentrations are made available to the animals, and a dose-response curve (number of licks) can be drawn, and the tolerability determined (Figure 12). Besides, it is possible to predict a formulation or drug's tolerability by correlating the number of licks obtained with water (a neutral solution).

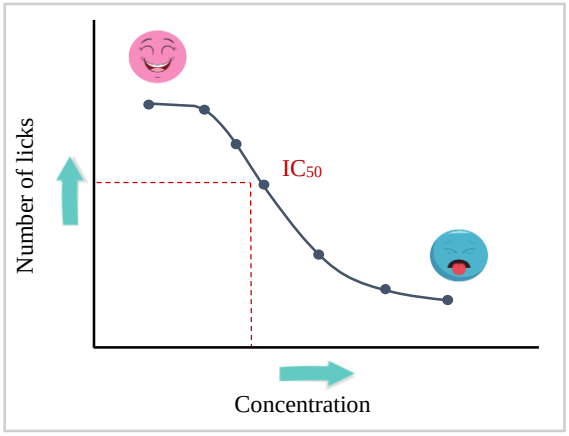


Figure 12. Dose-response curve for BATA model. Source: Author.

#### 4.2.1.1.1.2 Aversion evaluation by volume consumed

The aversion assessment test by measuring the volume consumed is quite like BATA. However, it does not have a sensor for accurate counting of the number of licks; but exposure to the test solution is described in about 30 minutes [107], based on the difference in volume between the initial moment and the final exposure time.

That test is also preferably carried out on rodents that go through the same period of deprivation and water supply. It is assumed that the volume difference is the amount consumed by the animal. Moreover, following the same assessment, the higher the value consumed, the greater the animal's tolerability and acceptance of the test solution.

This type of model was used to evaluate the taste masking of the caffeine from a formulation produced by hot melt extrusion process (HME) and presented promising results because it was possible to discriminate the differences in taste and clearly capture the animals' different expressions [116]. This characteristic of the in vivo experiment is extremely important for evaluations of formulations with a paediatric purpose since the human panel with adults generates questionable results if transposed to children. Still, studies show a good correlation in the pattern of behaviour between rats and primates with human babies, especially in the evaluation of palatability through characteristic expressions such as facial expression (bitter) and protrusion of the tongue (pleasant taste) [116], [122].

#### 4.1.4.1.2 In vitro test assessment

In vitro tests for evaluating medicines' taste have been widely disseminated in the literature, especially for the initial stages of developing medicine where the taste of API and taste masking for formulations in preclinical stages are initially evaluated [114].

#### 4.2.1.1.1.3 Electronic taste sensors

Currently, there are two main commercial equipment for taste evaluation using electronic sensors, which are commonly called electronic tongues. The Japanese model is based on the use of lipid membrane sensors (SA401, SA402/TS-5000z - Insent Inc., Atsugi-chi, Japan), while the French one (α-Astree sensor - Alpha MOS) performs measurements based on the chemical modification of structures [114]. In addition to these, several other electronic languages are characterized by differentiation in the type of receiver, selectivity, necessary sample properties, and operating characteristics [123].

The literature is vast in the publication of evaluations using these electronic sensors for taste evaluation, or taste masking of drugs and formulations [124]–[133] and the results of the majority have reported a good relationship with the human panel [114]. However, a study that evaluated the taste masking of PZQ after the use of cyclodextrins concluded that the use of electronic language (Insent Inc., Atsugi-chi, Japan) did not provide coherent results for none of the tested sensors [68], due to the characteristics of the molecule (non-ionic and poorly water-soluble). Later, another study that used the microencapsulation technique of PZQ in a polymeric matrix also evaluated taste masking through coated sensors, and the principle of detection used was electrical impedance spectroscopy. Then, the electrical response was used to evaluate the taste-masking properties of the formulations. The results were evaluated by interactive document mapping (IDPMA) plot and show the efficiency of taste masking across the different regions where the samples are positioned [134].

Although the results obtained with the electronic language are promising, especially for the early development stages, there are still barriers to be overcome. Unlike in vivo experiments, in electronic language tests, it is necessary to calibrate the equipment to understand the bitter taste. Hence, the use is still somewhat limited and requires the association of the result with other techniques, especially when the molecule has an unknown taste characteristic [114].

#### 4.2.1.1.1.4 In vitro dissolution and drug release for palatability evaluation

This evaluation method can initially be presented in a simple way, but its stages and applications must be evaluated carefully.

To carry out this method, regardless of the analytical detection technique, three main factors must be analysed: the dissolution of the drug (medium, pH characteristics), sample withdrawal, and analytical evaluation. As a calibration, the dissolution of the pure API must be performed, and this step is hardly found in the literature [135].

The UV spectroscopy is one of the most employed tools to determine taste masking by the dissolution method. It can be used in-line with an optical fiber, and several studies have already shown positive results or offline analysis with a spectrophotometer or HPLC with a UV detector.

It is assumed that a drug needs to be dissolved to cause an unpleasant taste and, likewise, the evaluation of the influence of excipients needs to be considered. In these methods, the most critical action is to assume an absolute correlation of the concentration released with the taste of the drug [135].

Other important factors are related to the specifications of the methods, such as adjusting the temperature of the oral cavity, volume of medium, pH, physiological variations depending on age [135], [136]. Many studies have reported the use of 900 ml of dissolution medium, and criticism is related to the correlation to the volume of saliva in the oral cavity (about 1 to 2 ml) [137]. Recently, a study published by Keeley et al. [80], presented a column to assess palatability by the dissolution method where the internal volume mimics 1 or 2 mL. In this work, it was possible to quantify the taste masking of formulations developed with different coating types, unlike the conventional dissolution technique from The United States Pharmacopeia (USP), which provided only the distinction between coating technologies and thicknesses.

# 5 STRATEGIES IN THE DEVELOPMENT OF PAEDIATRIC FORMULATIONS

## 5.1 Traditional and emerging forms

As an initial stage in developing a paediatric pharmaceutical formulation, characteristics such as pharmacokinetics and pharmacodynamics, potential routes of administration, toxicity relationship, and taste preferences should be evaluated due to the children's age [84].

In general, it can be said that from birth to around 16 or 18 years old, individuals are considered paediatric patients [94]. However, when analysing this age group, it is easy to see

big differences in the physiological development of the body and the need for personalized development for different stages of childhood [84].

According to the International Conference of Harmonization (ICH), childhood is divided into 5 age groups related to the development stage (pharmacokinetic and pharmacological). Also, the European Committee for Medicinal Products for Human Use further subdivides the age group “children” into “preschool children”, and “school children” to more precisely reflect the children's ability to accept and use different dosage forms (Figure 13) [84].

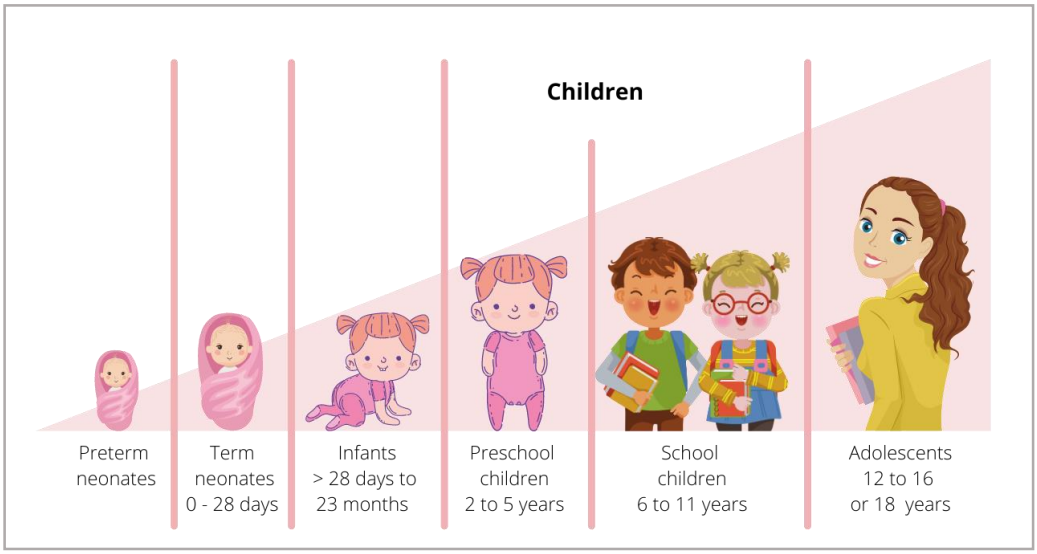


Figure 13. Stages of growth. Source: Author.

Although liquid pharmaceutical forms come to mind as paediatric patients' choice, solid forms have been preferred due to characteristics such as greater stability, longer and easier storage, and ease of transport [84], [101].

Traditional solid dosage forms are associated with pills that are difficult to administer to children due to their size, taste, and acceptability. The lack of choice makes it necessary to manipulate these dosage forms, such as cracking or breaking the tablet for administration. This type of practice, as previously mentioned, portrays the worst scenario for paediatric patients as it results in variation in dosage, problems with adherence to treatment, and, consequently, lack of therapeutic efficacy [87].

New approaches in developing solid paediatric formulations have been discussed according to age and need [101]. One of the most discussed dosage forms considered promising for developing drugs suitable for children is the mini-tablet. Mini-tablets are characterized by

a size ranging from 2 to 3 mm [138]. Their acceptability and swallowing are already described by several studies [138]–[141], moreover, the flexibility of dosage and the traditional process production (compression) make the technology a good alternative for the traditional pharmaceutical industry [139].

Orodispersible dosage forms (films, tablets, mini-tablets, lyophilized powder forms) are another pharmaceutical form widely discussed for paediatric patients as they can quickly disperse or dissolve in the oral cavity [129].

In addition, as a multiparticulate dosage form, we can mention the use of pellets with good acceptability and dosing flexibility [142], [143], which can cover a wide age range, depending on the adaptability of the formulation. Pellets can be administered by mixing them with food, which also provides another advantage to this form [143]. The most widely used technique for the production of this type of formulation is extrusion-spheronization, which offers numerous technological advantages such as a high-throughput process, ease of operation, high drug loading capacity, and particle size with a small variation range [142].

Another pharmaceutical form that has gained visibility is chewable tablets. They are dosage forms that have good acceptability due to characteristics such as disintegration in the mouth through chewing, smooth texture, and not requiring water for administration. The biggest challenge in developing this type of formulation lies in the choice of excipients [144], that must be assertive to guarantee the good disintegration characteristics in the mouth. Also, excipients intended to mask the taste of the API cannot be enough to this end, requiring the combination of different sweeteners or excipients to circumventing this barrier.

### 5.2 3D printed forms

More recently, 3D medicine printing technology has been described as a tool capable of bringing countless benefits, and personalization is one of the most important. The main advantages of the technology are the ability of producing units with specific and precise doses and high reproducibility, and it also allows production on demand, the development of polypill[7] formulation and the modulation of drug release [145]–[147].

Although all these advantages are exciting to developers, the possibility of personalizing the therapy has been one of the factors widely discussed and increasingly sought after. This means saying, for example, that it is possible to make a specific dose adjustment for a patient

[7] Polypill: range of pills that combine many medicines to provide a single solid dosage form that allows the patients to self-administer easily [347].

with specific characteristics (children have different pharmacokinetics and pharmacodynamics), making the treatment more assertive, greater patient compliance with the treatment [146], [148]. Besides, the rationalization of medications is also an important factor as waste is reduced. With these characteristics, the 3D printing of medicines aimed at paediatric patients can add even more advantages, such as the possibility of more palatable and better-accepted drugs with different types of shapes [149].

Several 3D drug printing technologies are available, among them, FDM (Fused Deposition Modeling), which is the most studied to produce pharmaceutical forms [27], [150], [151].

FDM principle is based on the deposition of layer-by-layer from the extrusion of a molten/softened formulation through a nozzle tip and the deposition of the extrudate filament onto a colder substrate (printing table), leaving behind a 3D object when the material has solidified. The printing nozzle moves horizontally and vertically after each layer (Figure 14).

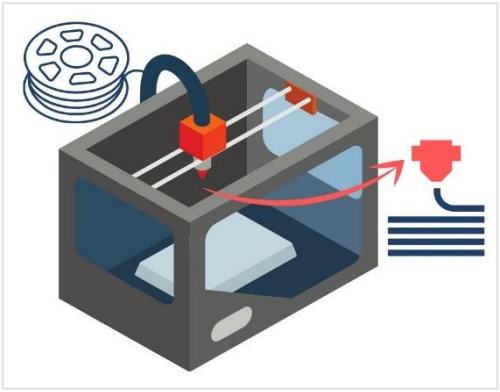

Figure 14. Schematic representation of 3D printing using the FDM technique with filament feed. Source: Author.

One of the first works that demonstrated the ability to print filaments in the pharmaceutical area used Fluorescein sodium salt and PVA as a carrier polymer. Tablets of 10 mm diameter and 3.6 mm height were printed and the different possibilities of infill and the impact on the drug release profile were evaluated [152].

Recently, a work was published describing a technique for the production of double-layer tablets containing rifampicin and isoniazid [153]. The type of polymer, drug loading, filling density, and layers were investigated for drug release in an acid medium, rapid (immediate) for isoniazid, and delayed for rifampicin. The percentage of filling and the number of layers for the adequate drug release rate were seen as crucial steps.

Formulated filaments can be produced by hot melt extrusion process, and then be later printed by FDM [154], [155]. In this case, the first step of HME filament production with optimal printing conditions and adequate API loading is one of the biggest challenges faced by the pharmaceutical industry [156].

## 6. PHARMACEUTICAL DEVELOPMENT WITH EMPHASIS ON PZQ MEDICINES

Different approaches have already been described in the literature to improve bioavailability for praziquantel.

In Table 3, the technical approaches were regrouped by category. The main categories are isomers separation, modification of the crystal form (polymorphs, hydrates, cocrystal) or their physical characteristics (reduction of crystal particle size), complexation with cyclodextrins, lipid-based nano and microparticles, polymeric nano and microparticles and solid dispersions (crystalline and amorphous).

Table 3. Literature reporting improved solubility and/or dissolution obtained through different PZQ formulation approaches.

| ***Technical approach*** | ***API concentration or proportion (wt %, mg or p/p)*** | ***PZQ final form*** | ***Carrier/Surfactant*** | ***Reference*** |
|---|---|---|---|---|
| Isomers separation | - | (+)-PZQ and (-)-PZQ | - | [70] |
| Modification of the crystal form | - | PZQ B fom | - | [10] |
| | - | PZQ C form | - | [73] |
| | - | PZQ Monohydrate form | - | [74] |
| | - | PZQ Hemyhydrate form | - | [75] |
| | 1:1 (PZQ:coformer) | Cocrystals | Coformers (citric, malic, salicilic and tartaric acids) | [37] |
| Modification of physical characteristics of crystals | 1:1 and 1:0.5 | Nanosized particles | Poloxamer 188 (P 188), P-188/Sodium lauril sulfate (SLS), P-188/Maltodextrin (MDX), P-188/polivinilpirrolidona (PVP) | [157] |
| Cyclodextrin (CD) complexation | 1:1 | PZQ-CD complex | Methyl-β-cyclodextrin (MeCD) | [158] |
| | 75, 100 and 75 mg | PZQ-CD complex | CDs (α-, β- and ɤ-) | [159] |
| Lipid-based particles | 1:1 | Nanosuspension | PEG-60 - castor oil hydrogenated | [160] |
| | 20 mg | Nanoparticles | Cetyl palmitate | [161] |
| | 1:1 | Microparticles | Gelucire® 50/13 and PVP K30 | [60] |
| | 3:1, 1:1 and 1:3 | Microparticles | Mannitol, Gelurice® 50/13 and, Gelurice® 50/13 + Mannitol | [63] |
| | 10 % | Microparticles | Gelurice® 50/13 | [58] |
| | 200 mg | Microspheres | poly (3-hydroxybutyrate) and Eudragit® E | [162] |
| Polymer-based particles | 10, 20 and, 30 % | Nanoparticles | Poly(D,L-lactide-coglycolide) (PLGA), DL-lactide glycolide and poly(vinyl alcohol) (PVA) | [163] |
| | 20 % | Nanoparticles | poly (methyl methacrylate) (PMMA) | [164]–[166] |
| | PZQ:EPO - 1:1 ; 1:2<br>PZQ:EPO:GMS - 1:1:0.3 ; 1:2:0.6 | Microparticles | Eudragit® E PO(EPO) and Glyceryl monostearate (GMS) | [61] |
| | 1:1 and 1:2:1 | Microcapsules e microspheres | Eudragit® E100 and Eudragit® L30D55 | [134] |

| | | | | |
|---|---|---|---|---|
| | 20:1, 10:1, 10:2, 10:3 | Microparticles | Poloxamer 407 (F-127), Sucrose stearate | [69] |
| Solid Dispersion (SD) | 10 to 100 % | SD/ASD | PVP K30 | [67] |
| | 1:1, 1:2.4, 1:5, 1:9 | ASD | PVP K12, PVP K17, PVP K25 | [167] |
| | 1:0.25; 1:0.5 and 1:1 | SD | Sodium alginate and Carboxymethylcellulose | [29] |
| | 1:5 | SD | Calcium carbonate | [168] |
| | 1:1, 1:1:1 and 2:1:1 | SD | Poloxamer 237 and PVP K30 | [169] |
| | 1:1, 2:1 and 3:1 | SD | PVP K30 | [65] |
| | 1:1, 1:2, 1:3 (each) | SD/shaped as tablets | Mannitol, Urea, PEG 6000 | [170] |
| | 1:1 | SD | PVP K30 and Crospovidone (CROS) | [59] |
| | 1:1 and 1:2 | ASD | PVP, PVP VA, CROSPVP and, SSG | [66] |
| | 1:1, 1:2 and 2:1 | SD | PEG-60 - castor oil hydrogenated | [171] |

Eudragit® E 100 = cationic polymethacrylate polymer (granules); Eudragit® E PO = the same as Eudragit® E 100 (powder) and Gelurice® 50/13 = stearoyl polyoxyl-32 glycerides (non-ionic water-dispersible surfactant) [60], [61].

*Isomer's separation.* PZQ medicines currently used are produced from the racemic mixture of the API, R- and D-PZQ in different proportions, in which levo-praziquantel (L-PZQ or (-)-PZQ or R-PZQ) is the active principle, while the dextro-praziquantel (D-PZQ or (+)-PZQ or S-PZQ) is not and, furthermore, the latter is bitter than the former. The bitterness difference is one of the driving characteristics of the development of a formulation with only one of the isomers [42]. As the separation of both isomers is a very expensive technique, it is usually not applied [42]. A technical route of interest is the separation of PZQ racemic mixture and several research groups have been working in the isomers separation to obtain L-PZQ and D-PZQ with high purities (higher than 97 %) and larger scales of production (higher than 253 g $kg_{ads}^{-1}$ $day^{-1}$) using chromatographic processes [172]. Unfortunately, current chemical routes are not effective to attend large scale production.

*Modification of the crystal form*. The solid state directly influences properties like solubility and dissolution kinetics of an API [48]. As already discussed, PZQ presents different solid forms, the more used being the racemic mixture, also identified in the literature as commercial form (crystalline) A. New polymorphic forms have been identified more recently, named B and C [30], [73]. They are characterized by different properties among them, the water solubility. Forms B and C appear to be more water-soluble than the racemic form (form C with 2.7-fold > form B 1.4-fold greater of the racemic praziquantel) [23], [56]. Despite a better solubility or dissolution kinetics, the use of new polymorphic forms requires attention because they can be physically less stable, as experimentally demonstrated with Forms B and C [56].

Hydrate forms of PZQ also exists. The generation of hemihydrate PZQ form was demonstrated from two stages of grinding, starting from the racemic mixture (form A). PZQ form A was first milled (30 min at 25 Hz), then secondly milled in the presence of an equimolar amount of water (1 h at 25 Hz) [75]. Like the new PZQ polymorphs recently identified (forms B and C), the resulting hemihydrate form named PZQ-HH appears to be more soluble (1.4-fold greater) than the PZQ racemic form. A monohydrate form of PZQ was produced by Salazar-Rojas et al. from PZQ (form A) [ 67] and characterized with respect to the intrinsic dissolution (2.2 mg $cm^{-2}h^{-1}$), which was also slightly higher than the intrinsic dissolution of the form A (1.6 mg $cm^{-2}h^{-1}$).

*Cocrystals*. Cocrystals are very interesting and useful product for improving different properties such as dissolution rate, melting point, solubility, and chemical stability of an API during the solid-state synthesis. They are solid substances, which consist of molecular complexes of the API with one or more solid components [173]. Pharmaceutical cocrystals are typically composed of an API and a nontoxic guest molecule (cocrystal former) in a stoichiometric ratio. For purposes of comparison, salt formation can improve the solubility sometimes 100- or even 1000-fold, while cocrystals can improve it 4- to 160-fold [174]. To our knowledge, the first cocrystals of PZQ were identified via liquid-assisted grinding of PZQ crystals and coformers. A total of nine 1:1 and 2:1 cocrystals with oxalic acid, malonic acid, succinic acid maleic acid, fumaric acid, glutaric acid, adipic acid, and pimelic acid [33]. Among them, the cocrystals obtained from PZQ and malic acid (1:1) showed the better solubility performance (2.1-fold greater) than the racemic PZQ [37].

*Modification of physical characteristics of crystals.* It is well-established that one of the possible approaches for overcoming dissolution rate and even low water solubility issue is to reduce the drug particle size, leading to the enhancement of the specific surface area, the saturation solubility (below the micrometric range), and, thus, the dissolution rate [175]. The effect of the particle size reduction was another approach used, to improve PZQ dissolution rate. PZQ dispersions have been developed by high-pressure homogenization (HPH), in which PZQ crystals were brought by cavitation, high-shear forces and collision of the particles against each other. The PZQ dispersions were developed using different stabilizers, selected upon PZQ saturation solubility after screening (Poloxamer 188, Poloxamer 188/Sodium lauril sulfate, Poloxamer 188/Maltodextrin, Poloxamer 188/ Polyvinylpyrrolidone PVP). After 60 cycles of HPH, all formulations exhibited a particle size distribution below 2 μm, with highly significant reduction with respect to PZQ raw material ($d_{10}$ 8.24 ± 0.3 μm, $d_{50}$ 18.63 ± 0.8 μm and $d_{90}$ 102.31 ± 29.9 μm). Characterization studies including particle size distribution, crystallinity, morphology, drug content, and in vitro dissolution profiles, were performed over selected formulations. The formulation with the smallest particle size distribution ($d_{10}$ 830.3 ± 131.4 nm, $d_{50}$ 1063.3 ± 193.5 nm and $d_{90}$ 1132.7 ± 205.4 nm) was produced in presence of Poloxamer 188/PVP as stabilizer, corresponding to the better improvement on the dissolution kinetics. In this study, PZQ crystallinity was partially preserved during the HPH process. It is well established in the literature [175], [176] that crystal structure

change or even amorphization can occur during particle size reduction by milling processes.

*Complexation of PZQ and cyclodextrins*. Cyclodextrins (CDs) have been widely investigated as a unique pharmaceutical excipient for past few decades and is still explored for new applications [91]. CDs can be defined as cyclic oligosaccharides assembled of D-(+) glucopyranose units connected by α- (1,4) glucosidic bonds to form torus-like macro rings. Naturally occurring α, β, and γ CDs consist of 6, 7, and 8 glucopyranose units, respectively, and differ in their molecular weight, cavity size, and solubility (Figure 15) [91].

PZQ has already been formulated with β and ɤ - cyclodextrins [159]. Using high-resolution solid-state NMR spectroscopy, the interaction between PZQ and the cyclodextrins and derivatives were deeply investigated. The PZQ presented a tendency to stay in an anti-conformation in the complex, especially in the molar ratio 1: 2 PZQ:CD [177]. Other PZQ:CD complexes were also developed, for example, with methyl-β-cyclodextrin (modified CD with a methoxy group instead of primary hydroxyls) (1:1 stoichiometry), in which PZQ was found to be completely amorphous, with 5.5-fold water solubility increase, suggesting that this PZQ:CD complex may be more bioavailable than the racemic PZQ alone [177].

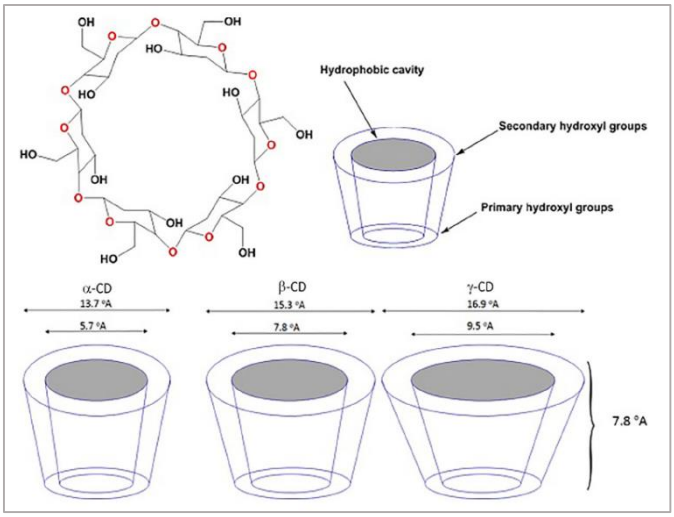


Figure 15. Representation of the chemical structure and the molecular shape of α, β, and γ cyclodextrins. Source: from [91] (with permission).

Hydroxypropyl-β-cyclodextrin was also used to form complex with PZQ cocrystals (PZQ: malic acid coformer) previously described in this section [37]. The cyclodextrin complex formed with the PZQ: malic acid cocrystals (1:1) resulted in 2.2-times the solubility of the racemic raw PZQ crystals, comparable to that of the PZQ cocrystals before complexation (2.1 times the solubility of the racemic raw PZQ crystals).

Furthermore, it appears that all tested systems (cocrystals and cyclodextrins) showed photostability problems, causing degradation of about 7.9 % and 6.8 %, respectively.

*Lipid-based particles.* Micro and nanoparticulate forms constituted by racemic PZQ and lipids are another formulation approach that has been investigated. In this category, it can be found solid lipid nanoparticles (SLN) of PZQ with different lipids, for example, cetyl palmitate [161], and hydrogenated castor oil [160].

Different methods have been employed for this end. The first method consists in elaborating a mixture of PZQ and lipid to produce a clear melting solution, to which an aqueous surfactant solution is added under mechanical agitation (or sonication) to form a hot nanoemulsion. The hot nanoemulsion is then cooled down to obtain a nanoparticle suspension. This method was employed to produce SLN nanosuspension of PZQ and hydrogenated castor oil [160].

Another method is called hot homogenization technique. Here, PZQ is incorporated into the melted lipid. The drug loaded lipidic phase is dispersed in a hot aqueous phase containing surfactants under continuous stirring to form a coarse o/w emulsion. It is then homogenized at the temperature above the melting point of the lipid using high pressure homogenization with piston-gap homogenizers to form o/w nanoemulsion, which is then cooled to room temperature for solidification and formation of solid lipid nanoparticles. The hot homogenization method was employed to produce SLN nanosuspension of PZQ and cetyl palmitate, using Tween® 80 in the aqueous phase [161].

The mentioned PZQ-SLN formulations presented some similar physical characteristics, for example, a nanometric size and low polydispersity index (in the range of 260-300nm for PZQ- hydrogenated castor oil and PZQ-cetyl palmitate SLN, with a polydispersity index less than 0.3). Regarding PZQ-cetyl palmitate SLN, an improved dissolution profile and great parasiticidal properties was demonstrated. For PZQ-hydrogenated castor oil SLN, the pharmacokinetics and therapeutic efficacy of the

suspension were studied in dogs (subcutaneous administration of the suspension). The results demonstrated that SLNs increased the bioavailability of PZQ 5.67-fold and extended the mean residence time of the drug from 56.71 to 280.38 hours.

PZQ nanoparticles with hydrogenated castor oil solid lipid (1:1) were also tested later [178] to other administration routes (oral, intramuscular, and subcutaneous) in rats. The different routes of administration tested (intramuscular, and subcutaneous) were expected to represent alternative ways to overcome the extensive first-pass effect evidenced by the oral route. In this way, the dose reduction for the formulated products could be expected.

PZQ has also been formulated with lipids at the microscopic size scale, with several excipients and by different methods, among them, co-milling or melt granulation. Spray congealing is frequently used as the cooling step. In this process, the molten material is sprayed through nozzles into a chamber containing cool air t produce spherical uniform shaped particles (microspheres).

Gelucire® 50/13 is the lipid most used in the lipid based PZQ microspheres. For Gelucire® 50/13 was used to produce microspheres with different PZQ loads (5, 10, 20, and 30 wt%) by using an ultrasonic spray congealing process [58]. Microspheres with different sizes (75-150 µm, 150-250 µm, and 250-355 µm) were generated. Unlike the microspheres size, the dissolution rate was impacted by the PZQ load in the microspheres, being lowered for loads higher than 15 % PZQ. The PZQ solubility was increased 3-times compared to the solubility of raw PZQ crystals.

Gelucire® 50/13 was also used with other additives such as polyvinylpyrrolidone (PVP) [60] or Mannitol [63] or misture of both [63]. In all cases, PZQ solubility was improved, for example, 2 times for microspheres composed by PZQ and Gelucire® 50/13 (1:1), and 4.6 times when PZQ was firstly co-milled with crospovidone (1:1) [60], [179].

Formulations based on lipids as excipients presents advantages such as solvent-free, rapid, and low expensive manufacturing methods able to increase the dissolution rate of PZQ. Their use presents the challenge for evaluating controlled release of the loaded drug and the long-term physical stability due to polymorphic transformations of lipids than can take place during aging.

*Polymer-based particles.* Another way to improve the dissolution and solubility of poorly water-soluble APIs is by producing microparticles or nanoparticles with polymers.

In general they are produced by an emulsion–solvent evaporation process [163] aiming a controlled PZQ release. Typically, a solution of the polymer in an organic solvent is produced to which PZQ is added. The resulting organic solution containing PZQ and the polymer is poured in an aqueous phase generally containing a surfactant like poly(vinyl alcohol), PVA. The emulsion is then subjected to constant stirring, followed by evaporation of the solvent (by vacuum generally), leading to the entrapment of PZQ into the polymeric micro or nanoparticles formed. The micro or nanoparticles formed can be washed to remove additives, such as surfactants, filtered and dried under appropriate conditions [4].

The technique was used for example to encapsulate PZQ in PLGA nanoparticles containing 10 to 30 wt% PZQ. In all nanoparticles produced, PZQ was found to be amorphous. Throughout characterisation studies, no molecular interactions between PZQ and PLGA have been identified and the physical stability of nanoparticles was confirmed after four months of storage at room temperature [163]. The same process was used to produce PZQ microspheres using poly (3-hydroxybutyrate) (PHB) and mixtures between this biodegradable polymer and Eudragit® E, a cationic copolymer based on dimethylaminoethyl methacrylate, butyl methacrylate, and methyl methacrylate. [162]. It was found, during in vitro dissolution tests, that the mass composition 75:25 (Eudragit® E: PHB) significantly improved the PZQ release compared to the microspheres containing PZQ and PHB alone. The increase in the dissolution kinetics of the drug was related to the high proportion of Eudragit® E present in the formulation that gave them characteristics of greater porosity. In summary, with polymer-based particles the PZQ release kinetics may be modulated by the type of polymer and its content in the particles.

Miniemulsion polymerization has also been used to manufacture of polymer nanoparticles containing PZQ [165], [180]. This technique presents many advantages, including the non-use of toxic solvents and the possibility to perform the encapsulation of chemicals in-situ. Two phases comprise a typical formulation: the aqueous dispersant phase and the emulsified organic phase, which contains monomers and co-stabilizers. The monomer droplets are stabilized by surfactants added to the aqueous phase (which prevents particle coalescence). At least one co-stabilizer is added to the organic phase (which prevents the diffusional degradation of the droplets). Ionic surfactants can be anionic or cationic and form electrical layers around the particles that reduce particle collision rates and coalescence efficiency. Nanoparticles loaded with PZQ were prepared through in situ miniemulsion copolymerization of methyl methacrylate (MMA) with

diethylaminoethyl methacrylate (DEAEMA) or dimethylaminoethyl methacrylate (DMAEMA) as comonomers. Due to the cationic nature of the water-soluble comonomers, the use of different ionic surfactants was also investigated (cetyl trimethyl ammonium bromide (CTAB) as a cationic surfactant or sodium dodecylsufate (SDS) as an anionic surfactant in deionized water). The organic phase was prepared with 0–20 wt% of PZQ, mineral oil, and one wt% of Aazobisisobutyronitrile (AIBN, used as free-radical initiator) MMA. Nanoparticles with narrow particle size distributions, characteristic average diameters ranging from 50 nm to 110 nm, and loaded with 20 wt% of PZQ were manufactured successfully [180]. However, it was possible to observe that PZQ significantly impacted the course of the polymerization and stability of obtained nanoparticles.

Polymer-based particles containing PZQ can also be produced by other techniques like hot-melt extrusion and spray drying [61]. For example, the development of a paediatric PZQ formulation containing Eudragit® and glyceryl monostearate was performed testing the two mentioned techniques. Glyceryl monostearate was added to provide better flow in the physical mixture and as taste masking agent. The final mass proportions studied for PZQ: Eudragit®: glycerol monostearate were: 1:1:0.3 and 1:2:0.6. The mixtures were extruded, and the resulting HME-filaments were ground after the process (particle size - 3 to 400 μm). On the other hand, the same formulations were processed by spray drying. For that, the mixtures were dissolved in absolute ethanol to give a solution that was then spray-dried. Spray-dried powders are smaller (1–16 μm) than those produced by milling of the HME-extrudate. Both systems showed an increase in dissolution (PZQ[8]; 0.2 mg/mL; spray-dryed powders PZQ: E: GMS 27.8 % 0.6 mg/mL, and extrudates[5] PZQ: PEG 27.8 % (70-100 °C) 0.4 mg/mL). Taste masking was more effective for the particles obtained by HME process. However, this result was obtained from in vitro test[9], and an in vivo evaluation would be necessary (PZQ 0.17 mg/mL; physical mixtures with 43.5 % PZQ 1.1 mg/mL; spray-dried powders with 43.5 % PZQ 0.3 mg/mL; ground extrudates with 43.5 % PZQ 0.03 mg/mL; physical mixtures with 27.8 % PZQ 1.3 mg/mL, spray-dried powders with 27.8 % PZQ 0.9 mg/mL, and ground extrudates with 27.8 % 0.03 mg/mL).

[8] non-sink dissolution profiles in Simulated gastric fluid sine pepsin (spSGF)
[9] no sink dissolution in simulated salivary fluid (SSF)

*Solid dispersions*. One promising approach for solubility enhancement is solid dispersion, which has also been investigated for PZQ [92]. A solid dispersion consists of one or more hydrophobic API dispersed in a hydrophilic inert carrier or a mixture of carriers [181], [182]. The classification of solid dispersions as eutectic mixtures, solid solutions and vitreous solutions is based on the physical state of the API and its carrier [183]. Solid dispersions are divided in four generations: the first used crystalline carriers and the API can be crystalline or amorphous; the second generation used amorphous polymeric carriers with crystalline or amorphous APIs, the third used carriers with surface activity or emulsifying properties, which can improve the dissolution properties and finally, the fourth can be referred as controlled release solid dispersions, for which the release kinetics are modulated with soluble or insoluble-water carriers [92], [181], [184], [185].

Perissuti et al [179] shows different types of solid dispersion that have been proposed for PZQ improvement of properties such as water solubility, dissolution kinetics and palatability. Different processes (milling, solvent evaporation) have been employed to produce solid dispersions with PZQ and excipients. A variety of them can be seen in Table 1: water-soluble polymers such as polyvinylpyrrolidone (PVP), polyethylene glycol (PEG) and alginate, insoluble form of polyvinylpyrrolidone (crospovidone, CROS), sugar alcohol (mannitol), cellulose derivatives (carboxymethylcellulose) and other organic (urea) and inorganic (calcium carbonate) compounds.

Solvent evaporation method is the most applied to produce solid dispersions containing praziquantel. In most studies, PZQ and the polymer carrier are dissolved in a common solvent, for example, ethanol [167]. Afterward, the resulting organic solution is subjected to drying, and different drying techniques can be used for this step, such as drying oven under reduced pressure [29], [169] or rotary evaporation [167].

Most studies discuss the types of polymers or surfactants used, the mass proportion between components in a mixture, or the solvent composition on the final solid properties such as physical characteristics and solubility and dissolution performances.

Some examples of partially amorphous solid dispersions of PZQ produced by solvent evaporation are given in Table 1. A first example can be given, in which the final state of PZQ depended on the solvent composition [65]. In this case the polymer was PVPK 30, and different solvents (water, ethanol, and water/ethanol) were used to produce the liquid formulations of PZQ and PVPK 30. Solid dispersions produced from solvents containing water led to the presence of crystalline PZQ in the solid form, whereas an

amorphous form was obtained with pure ethanol. These differences in the solid state of PZQ resulted in differences in the solubility too. SDs prepared with a mixture of water and ethanol presented lower solubility when compared to those obtained only with ethanol.

Another example is related to solid dispersions produced with sodium starch glycolate (SSG) [66]. SSG is an excipient commonly used in oral pharmaceuticals as a disintegrant to promote rapid disintegration and dissolution of immediate release solid dosage forms. PZQ solid dispersion was prepared using co-solubilisation (in ethanol) and solvent evaporation consecutive step. The mass proportions between PZQ and SSG were 2:1, 1:1, 1:2 or 1:3. Traces of crystalline PZQ were found in these solid dispersions, although an amorphous form of PZQ was expected. Despite that, the partially amorphous solid dispersion PZQ:SSG 1:3 could increase the dissolution[10] rate compared to the equivalent physical mixture of constituents, as well PZQ alone (PZQ: SSG 90 %, PM 70 %, and PZQ 60 % dissolved in 120 min) [66].

Solid dispersions of PZQ and three different carriers (mannitol, urea, and PEG 6000) in the mass proportions PZQ: carrier of 1: 1, 1: 2, and 1: 3 were also obtained by solvent (chloroform) evaporation [170]. The better results on dissolution enhancement were obtained with the composition PZQ: PEG 6000 1: 2, which was attributed to the hydrophilic characteristics of PEG 6000 (better wettability and dispersibility abilities). The solid dispersions were used to produce tablets by direct compression. The in vitro PZQ controlled release reached about 82 % in 12 h.

Another parameter affecting solid dispersion properties is the characteristics of the polymer, like its molecular weight. As an example, amorphous solid dispersions of PZQ were prepared in a rotatory evaporator using different types of polyvinylpyrrolidone with molecular weights of 3000 (PVP K12), 11000 (PVP K17), and 34000 PVP K25 g/mol [167]. The best solubility performance (10 times greater than PZQ alone) was obtained with the lower molecular weight polymer, PVP K12, demonstrating the effect of this parameter, which may influence other polymer properties including glass transition temperature, solution, and melt viscosity.

Amorphous solid dispersion is the formulation approach employed in this thesis and will be focused on the next section.

[10] The dissolution test was performed in 900 mL of 0.1 M HCl with 0.2 %w/v of sodium lauryl sulphate, at 37 ± 0.5 °C, rotating at 50 rpm, and for 120 min. PZQ (USP method).

# 7. AMORPHOUS SOLID DISPERSIONS

Amorphous solid dispersions (ASDs) are widely known for their definition: an amorphous API dispersed in an amorphous phase which comprises a polymer, a mixture of polymers, or a mixture of polymers and surfactants [186]. Amorphous solid dispersions are an increasingly important formulation approach to improve the dissolution rate ant the apparent solubility of poorly-water soluble compounds such as PZQ and will be focused on this section.

## 7.1 The amorphous state

Solids can be either amorphous or crystalline. Pharmaceutical companies have focused, in a historic way, on developing crystalline forms of molecules of pharmacological interest and much effort has gone toward discovering and developing the most stable crystalline form of an API. Developing the most stable form will prevent changes in the formulation after manufacture and helps to ensure a reliable API product.

Some main pharmaceutical features of crystalline and amorphous compounds are grouped in Table 4. In the crystalline state the molecules are structured regularly in a lattice formation, while amorphous solids are disordered at the molecular level, with some short-range packing order but lacking the long-range order of a crystalline form.

Van der Waals forces, hydrogen bonding and other intermolecular interactions hold the molecules within the crystal lattice, resulting in lower molecular mobility. Because the molecular interactions in the crystalline state are strong, the compound is usually more stable, but the dissolution rate is slower.

As illustrated in Table 4, amorphous solids have higher dissolution rates than the crystal forms and, when they are dissolved, API concentrations in solution can be higher than the saturated solution of the crystalline form (i.e., they can form a supersaturated solution for which the highest concentration is known as $C_{max}$). The super-saturated state is temporary because the API recrystallises back ($T_{recrystallisation}$) to the saturation concentration equal to that of the crystal form, $C_{equilibrium}$. The temporarily supersaturated API solution creates a time window for enhanced in-vivo absorption. Therefore, maintaining the compound in its amorphous state is one of the great challenges in formulation development.

Tabela 4. Pharmaceutical features of crystalline and amorphous compounds. Source: Author and adapted from [249].

| ***Feature*** | ***Crystalline*** | ***Amorphous*** |
|---|---|---|
| Schematic structure of one powder particle | 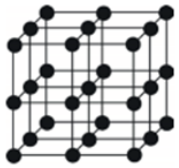 |  |
| | ● = one API molecule, ▬ = crystal bond | |
| Molecular orientation | Regular | Irregular |
| Stability physical structure | Strong | Weak |
| Dissolution | 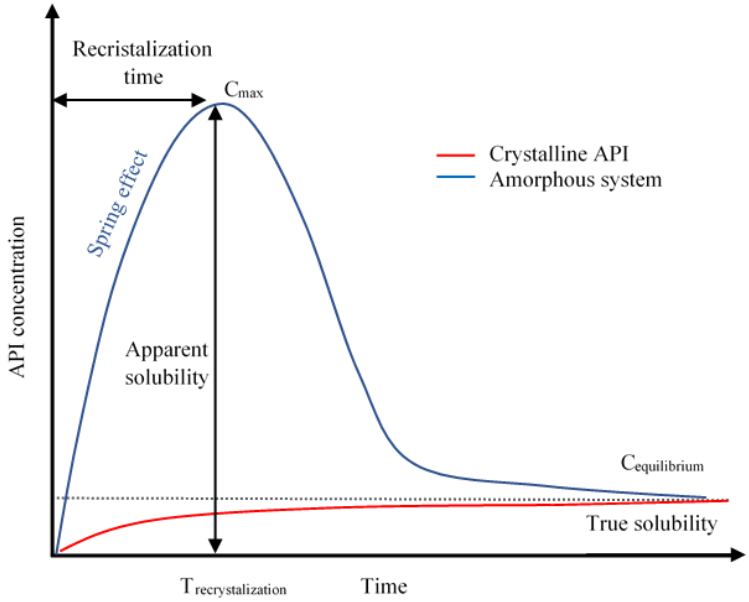 | |



$C_{max}$ = highest apparent solubility

$C_{equilibrium}$ = intrinsic solubility of the API

$T_{recrystallization}$ = time at wich API starts to recristallize after having reached its highest apparent solubility

Figure 16 represents a schematic depiction of the variation of enthalpy (or volume) as a function of temperature for crystalline and amorphous states of a pure compound [78], [187], [188]. When a crystalline compound is heated, it undergoes melting at temperature $T_m$. Then when the molten compound is slowly cooled, the molecules have sufficient time to move from their current location to a thermodynamically stable point on the crystal lattice, regenerating a crystalline structure. If, however, the molten compound is cooled suddenly, it can reach a super-cooled liquid state. If it is cooled further below its $T_m$, the system remains in equilibrium until the glass transition temperature ($T_g$) is reached, below which it enters a nonequilibrium (rubbery) state and converts into the amorphous (glassy) state of the compound.

The glass transition is a second order thermodynamic transition characterized by a step change in the heat capacity which is also associated with changes in other thermodynamic properties such as volume, enthalpy, and entropy [187]. The amorphous state has a higher free energy than the crystalline state and molecules or atoms can convert gradually into the highly ordered crystalline state if they are maintained at a specific temperature for a long time [148], [151]- [156].

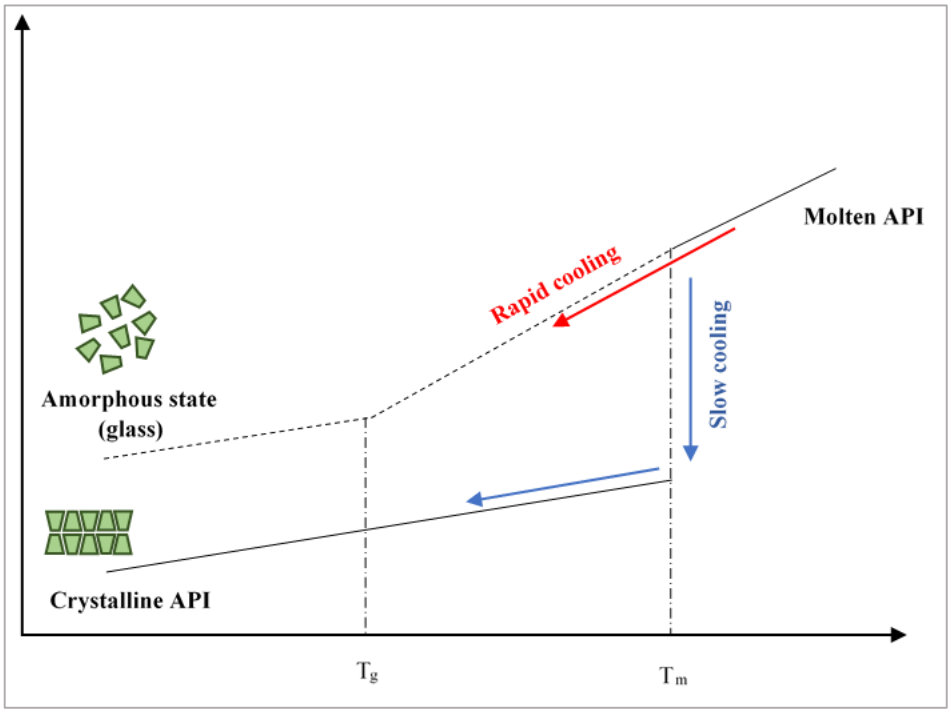


Figure 16. Schematic depiction of the variation of enthalpy (or volume) as a function of temperature for crystalline, amorphous (glassy). Source: Author and adapted from [78].

### 7.1.1 Characteristics of amorphous solid dispersions

#### *7.1.1.1 Parachute effect*

The challenge is in creating concentrations of the API that are many times higher than the thermodynamic solubility concentration and maintaining these high concentrations for an adequate time for the absorption process to take place.

The benefit of supersaturation as a strategy for improving the intestinal absorption and bioavailability of ASDs depends on two essential steps: the generation (the ‘spring’)

and maintenance (the ‘parachute’) of the metastable supersaturated state, as largely described in the literature [193]–[196] and depicted in Figure 17.

The ‘spring’ effect is due to the higher energy form of the amorphous solid form (compared to the crystalline form) and has already been demonstrated for different APIs (e.g.: felodipine, indomethacin, carbamazepine, glibenclamide, hydrochlorotiazide) [197]–[200]. Once supersaturation has been induced, recrystallisation of API molecules will occur through kinetically or thermodynamically controlled processes.

The ‘parachute’ is the temporary inhibition of recrystallisation by interfering with nucleation and/or crystal growth, achieved by the use of other components such as polymers and surfactants [195], [201] [195], [202].

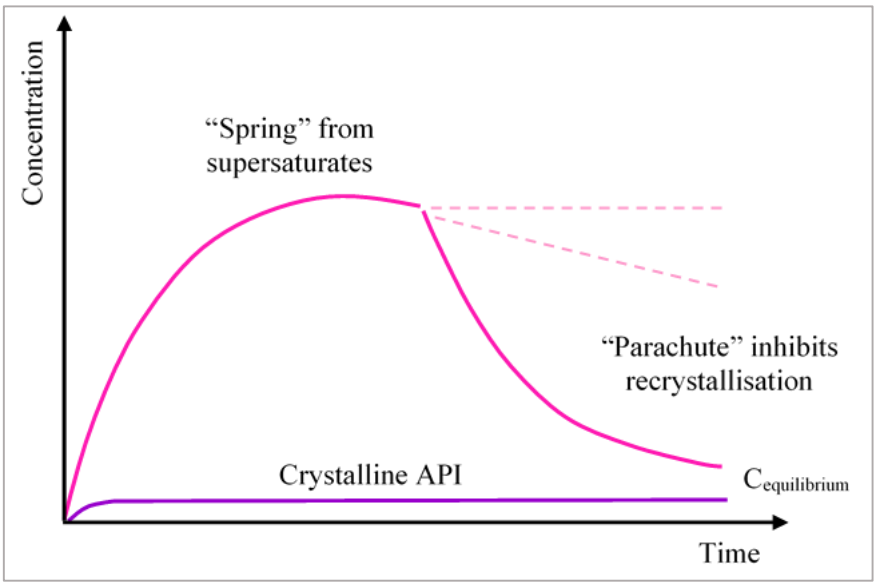


Figure 17. Representation of the "spring" and "parachute" model: high supersaturation (stable form of the API) achieved by the amorphous phase (the spring), while desupersaturation is retarded (the parachute) by the action of recrystallisation inhibitors. Adapted from [196].

### *7.1.1.2 Physical stability*

Besides the parachute effect on the dissolution of the amorphous API, the presence of excipients such as polymers, surfactants, or mixtures of both will also contribute to a better physical stability of the formulation, by decreasing the activation energy for API recrystallization (Figure 18) [186], [203].

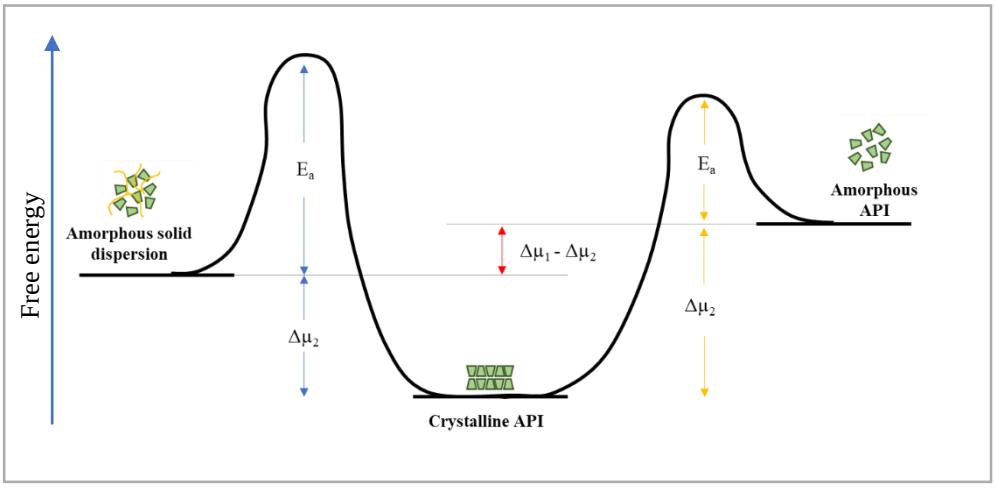


Figure 18. Amorphous API versus ASD in terms of activation energy barrier. Adapted from [186], [207]. Diagram is not scale.

Amorphous materials are very sensitive to their environmental conditions and temperature and humidity can directly affect their stability [204]. Polymer carriers can improve the physical stability of the amorphous compounds by increasing the glass transition temperature ($T_g$) [205] (see more details in 7.1.2.1 Glass transition). However, polymer carriers not only stabilize the dispersed amorphous API but can also increase wettability and, prevent API recrystallisation in the gastrointestinal tract (GIT), as reported in the literature [202], [206] and already said before.

Currently, carriers are categorized as synthetic and natural, and they are selected based on several factors, such as toxicity, cost, physical and chemical properties and processability (melting, solubilization in solvents).

Natural product-based polymers are mainly composed of cellulose derivatives such as hydroxypropyl methylcellulose (HPMC), hydroxypropyl cellulose (HPC), hydroxypropyl methylcellulose acetate succinate (HPMC-AS), hydroxypropyl methyl cellulose phthalate (HPMCP) and ethylcellulose [78], [205], [207].

Polyvinyl pyrrolidone (PVP), polyethylene glycols (PEG), polymethacrylates (PMMA) and, poly-(vinylpyrrolidone-co-vinyl acetate) [78], [206]–[209] are some examples of carries in the group of synthetic polymers.

It has been demonstrated in the literature that the presence of surfactants has the potential to reduce recrystallization by inhibiting nucleation and crystal growth [210]–[213], which depends on factors like the chemical structure of the API and the surfactant, the temperature, and the pH [201]. [214], [215]. For example, different formulations of

efavirenz (API) containing a polymer carrier (HPMC HP 50 and HP 55) and a mixture of two surfactants (sucrose palmitate and polysorbate 80) in different concentrations were used to produce ASD by the hot melt extrusion process [216]. The presence of surfactants in the formulation accelerated the dissolution (probably increasing wettability), without impact on $C_{max}$ measured during dissolution. The surfactants currently used in the production of solid amorphous dispersions are shown in Table 5.

Table 5. Summary of the surfactants generally used in amorphous solid dispersions [217]–[220].

| ***Class*** | ***Surfactants*** | ***Trade name*** | ***$T_m$ (ºC)*** |
|---|---|---|---|
| Non ionic | Poloxamer 188 | Kolliphor® P188 | 52-57 |
| | Poloxamer 237 | Kolliphor® P237 | 49 |
| | Poloxamer 338 | Kolliphor® P338 | 57 |
| | P407 | Kolliphor® P407 | 55 |
| | Polysorbate 20 | Tween™ 20 | - |
| | Polysorbate 80 | Tween™ 80 | - |
| | Sorbitan monolaurate | Span™ 20 | - |
| | d-α-tocopheryl polyethylene glycol 1000 succinate | TPGS 1000® | 37-41 |
| Anionic | Docusate sodium | | 153 -157 |
| | Sodium lauryl sulfate | Kolliphor® SLS | |

### 7.1.2 Evaluation of amorphous solid dispersion properties

As already introduced, amorphous solid dispersions appear to be a suitable formulation for increasing the dissolution and absorption rates of poorly soluble APIs. Key parameters of interest that can influence product performance include the glass transition temperature ($T_g$), miscibility between the API and carrier/excipients and the rate and extent of API recristallisation.

#### *7.1.2.1 Glass Transition*

The first thermal event associated with an amorphous system is the glass transition temperature ($T_g$) which is the temperature at which an amorphous "glass" turns into a metastable "supercooled liquid" [192], as illustrated in Figure 18.

The molecular level mixing of an amorphous API with an amorphous polymer can lead to a binary system considered miscible when only one $T_g$ is observed as also represented in Figure 19 ($T_{gmix}$). More than one $T_g$ indicates more than one amorphous phase.

Assuming that the glass transition temperature of an amorphous solid dispersion is between the temperature of the pure API and that of the pure polymer, the increase of $T_g$ to $T_{gmix}$ might increase physical stability by reducing molecular mobility [221] (Figure 19). The use of polymers with high glass transition temperatures are preferred as they act as anti-plasticizers leading to higher $T_{gmix}$ [222].

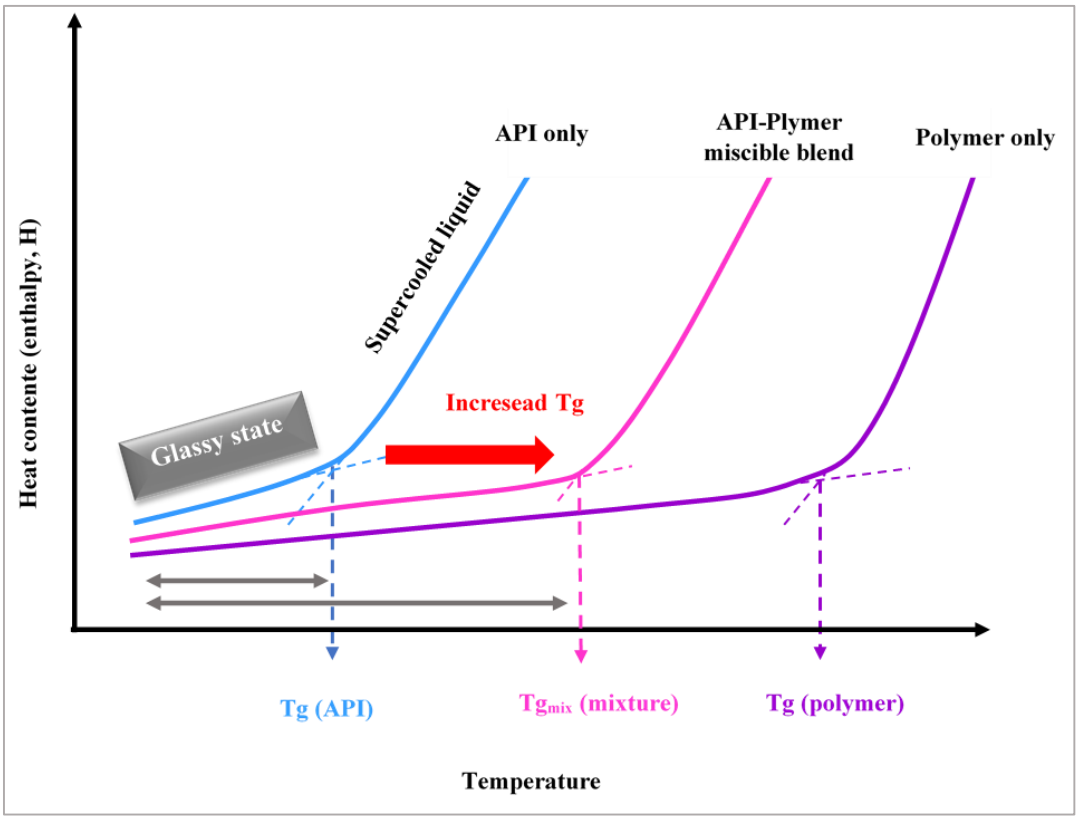


Figure 19. Plot of enthalpy, entropy, or free volume in function of temperature for molecular substances. Adapted from [192], [231].

The relation between the physical stability of ASDs and their composition was demonstrated for example with sildenafil ASDs and two different polymer carriers, PVPVA and PVA [221]. The $T_g$ of the individual constituents were 57.85 ºC, 102.85 ºC and 40.85 ºC for the API, PVPVA and PVA, respectively. The increase on PVPVA concentration resulted in increased $T_{gmix}$ (51.85 ºC with 25 % PVA to 92.85 ºC with 75

% PVPVA), whereas an opposite effect was observed with PVA (68.85 ºC with 25 % PVPVA to 42.85 ºC with 75 % PVA), negatively impacting the physical stability of the resulting PVA- sildenafil ASDs.

Although its low $T_g$, PVA has been successfully used as carrier in other amorphous formulations (ASD) with APIs such as rebamipide (RBM) with a high $T_g$ of 215.4 ºC. For this binary, a formulation with 30 % PVA and a lowered $T_{gmix}$ of 178.4 ºC did not show signs of physical evolution when exposed to stress conditions of humidity (75 % RH) during a stability test performed for 11 days.

Several equations are described to predict the Tg of solid mixtures such as Fox or Couchman-Karasz (CK) or Gordon-Taylor (GT) [222]–[224]. The later has been widely used and reported in scientific publications [78], [88], [188], [225] to predict the $T_{gmix}$ of amorphous mixtures from $T_g$ temperatures of the individual components (API and polymer) assuming an ideal mixture:

Equation 1

$$T_{gmix} = W_1 T_{g1} + \frac{K_g W_2 T_{g2}}{W_1} + K_g W_2$$

This equation assumes that $T_{gmix}$, $T_{g1}$, and $T_{g2}$ are glass transition temperature of the mixture (API-polymer), amorphous API, and polymer. $W_1$ and $W_2$ are the weight fraction of API and polymer, respectively, and *k* is a constant that depends on the level of interaction between the API and the polymer [51], [67], [154]. This constant can be determined using the Equation 2.

Equation 2

$$K = \frac{\Delta C_p^{PZQ}}{\Delta C_p^{Kol}}$$

Where $\Delta C_p^{PZQ}$ and $\Delta C_p^{Kol}$ correspond to the heat capacity step of $T_g$ for the API and polymer, respectively.

Differences between experimental $T_{gmix}$ and theoretical $T_{gmix}$ calculated by the Gordon-Taylor equation (ideal mixture, without interactions) have been attributed to intermolecular interactions between constituents or self-associations [192], [226].

Negative $T_{gmix}$ deviations can occur if molecular forces between API and polymer are weaker than self-associating interactive API-API or polymer-polymer forces [224]. Negative $T_{gmix}$ deviations may also be related to unidentified phase separation, when two amorphous phases are formed by only one of them is detected [192], [226].

Unlike, interactions between components can also result in lower free volume and higher $T_g$ values [224], [227]. The work of Liu and collaborators [228] is mentioned here to illustrate one study case in which higher experimental $T_{gmix}$ was measured for co-amorphous systems. Different co-amorphous (API-API) samples (cimetidine/naproxen, cimetidine/indomethacin, naproxen/indomethacin) were analysed by the association of different analytical techniques (DSC, Raman and terahertz spectroscopies and $^{13}C$ solid state NMR). All co-amorphous mixtures showed a single $T_{gmix}$ (42.3, 59.7 and 22.3 °C) higher than the GT calculated values (9.2, 44.7 and 10.7 °C) and the positive deviation was explained by the authors by interactions de type π – π, salt formation and hydrogen bonds between the respective components.

#### 7.1.2.1.1 Additional factors influencing glass transition

The glass transition is a kinetic event influenced by the presence of additives, the production process (thermal history) but also by the measurement method (heating or cooling rate) [229], [230].

The addition of a plasticizer to the polymer carrier causes the polymer chains to separate and an increase in the free volume [231], [232]. As a result, polymer chains can move more easily, and the more easily this occurs, the lower the temperature required for the polymer to leave the glassy rigid state to enter the rubberized soft. $T_g$ will change according to how easily the polymer chains move. Other factors can influence the movement of the chains, such as the pending groups.

The experimental procedure can also influence the $T_g$ value by changing the cooling rate or the experimental measurement protocol used [231], [233], [234]. As an example, a study performed with sucrose (70 % and 30 wt%) solution [235], evaluating the impact of two cooling rates during DSC analysis (150 ºC/min and 1 ºC/min), is cited.

For the more concentrated sucrose solution (70 wt%), a lower $T_g$ (-66.7 ºC) was measured from the rapid cooling compared to the slow one ($T_g$ -64.6 ºC).

For the more diluted sucrose solution (30 wt%), also a lower $T_g$ (-34.6 ºC) was measured from the rapid cooling compared to the slow one ($T_g$ 33.3 ºC).

These results were related to the amount of frozen water. More water could be frozen in a slower cooling, so higher $T_g$ were obtained [235].

Other factors can also affect $T_g$ as the amorphous sample preparation process. For example, amorphous solid dispersions of nisoldipine (API) and PVP K25 as polymer, containing 30 wt% of nisoldipine were prepared by two different methods involving solubilisation of API and polymer in a common solvent (methanol), which was then evaporated in a subsequent step. The processes used were spray drying and rotary evaporation. The resulting ASDs presented different $T_g$ 85 °C (from spray drying) against 103.5 °C (from rotary evaporation). The lowering of $T_g$ on the sample obtained from spray drying may be due to an incomplete drying of the product during the process, via the plasticization effect of water.

Finally, concerning the impact of the cooling rate during ASDs production, it has been demonstrated that ASDs produced using slower cooling rates have lower $T_{gmix}$ than those quickly cooled [236]. As last example, three different cooling systems were evaluated: a) compressed air (AC) 25 ºC, b) room temperature (RT) and, c) liquid nitrogen (LN) in the production of solid dispersions of indomethacin (INM/30 wt%) with a surfactant (P407/15 wt%) and a mixture of polymers (PVPVA 64 (27.5 wt%) and PL-360 (27.5 wt%) [219]. The $T_{gmix}$ was higher for the rapidly cooled sample (LN/70.19 ºC, RT/69.24 ºC, AC/67.42 ºC). This means that the cooling speed can impact the rate of amorphization and/or recrystallization.

7.1.2.1.1.1 Correlation of solid dispersion stability and $T_g$

The main factors that influence the stability of supersaturated solid amorphous dispersions characterized by an inherent recrystallization tendency are the temperature and moisture because they can dramatically impact the molecular mobility of the system. If a sample is stored below its $T_g$, the risk of devitrification is considerably reduced. Although it is often not feasible for the product, the literature describes the storage temperature rule “50 °C below $T_g$” to reduce molecular mobility [224], [237], [238].

Amorphous solid dispersions can be supersaturated at room temperatures commonly applied for material storage (20 °C to 40 °C) and their physical stability will

be strongly dependent on their demixing kinetics under these temperature conditions [237].

Similarly, the presence of moisture leads to an increase in the free volume due to the formation of hydrogen bonds with polymeric chains increasing the distance between them. This increase in volume leads to a decrease in $T_g$ [236], [239]. This phenomenon has been widely described in the literature. A decrease in $T_g$ with increasing relative humidity is illustrated here for starch materials as an example: wheat starch ($T_g$ 90 ºC at 0.151 % RH; $T_g$ 67 ºC at 0.164 % RH) and pregelatinized wheat starch ($T_g$ 127 ºC at 0.078 % RH; 92 ºC at 0.122 % RH) [231].

*7.1.2.2 Solubility of the API in the polymer matrix*

The solubility of an API in a polymer matrix is a very important parameter that must be considered during polymer selection for an ASD [206].

A phase diagram is very useful to predict the stability of a binary ASD under different temperature conditions. A simplified phase diagram of API/polymer binary mixture is given in Figure 20. Here, the solubility line describes the amount of API that can be dissolved into a polymer without re(crystallization). For a given temperature, the ASD is thermodynamically stable if its composition is left of the solubility line. Below the solubility line, the API tends to recrystallize, which might compromise the bioavailability-improving effect of an ASD.

The curve of API solubility in the polymer (solid curve) is particularly important not only to select the lower limit of the processing temperature to obtain a molecular dispersion by a thermal process like as hot melt extrusion, but also to understand the supersaturation level of such dispersions when they are cooled down (e.g., to the storage temperature).

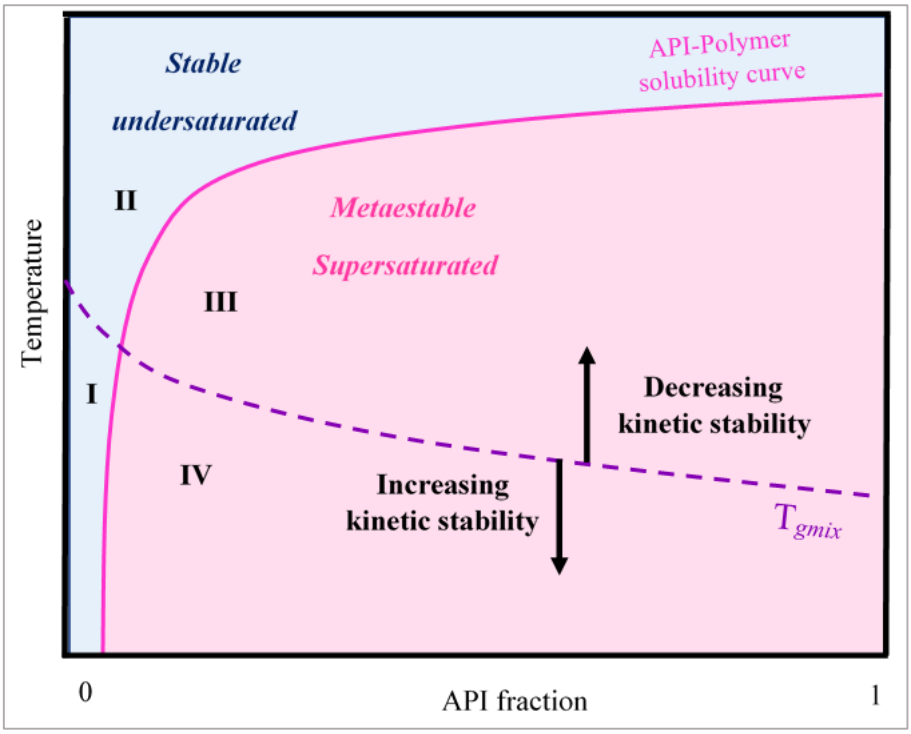


Figure 20. Diagram showing the change in equilibrium concentrations as a function of temperature (in pink) and the change in glass transition temperatures of the mixture (in purple). The intersection of these two curves delimits zones of stability I, II, III and IV.

The glass-transition temperature ($T_{gmix}$) depicts the transition temperature from the super-cooled, glassy state of the formulation to its liquid state. The glass transition temperature $T_g$ curve can be correlated from using empirical approaches, e.g., the Gordon-Taylor-Equation or can be measured experimentally from fused physical mixtures by thermal (DSC) analysis (dotted curve). The glass-transition temperature indicates a change in mobility and viscosity which usually dramatically decreases the rate of crystallization and/or phase separation, a knowledge of which is essential for predicting the storage stability of an ASD [184], [240], [241], mainly when it is supersaturated.

For example, Figure 19 shows two kinetically unstable regions (III and IV – pink region). In region III, above the $T_{gmix}$ dotted curve, API recrystallization has a high probability to occur due to the higher molecular mobility in the supersaturated state. In region IV, below the $T_{gmix}$ dotted curve, there is a reduction in mobility and viscosity which reduces the rate of demixing (phase separation) and API crystallization [184],

[240], [241]. In contrast, in regions I and II (blue region), the binary mixture is undersaturated [240], [241].

Generally, $T_{gmix}$ decreases continuously from that of the pure polymer to that of pure API [242]. Ideally, a molecular dispersion should be kinetically stable at its storage temperature as this is important for its dissolution profile. The potential risks with unstable systems are phase separation or recrystallisation (short-term or long-term) and a negative impact on apparent solubility and dissolution kinetic profiles [242]. Such stability can be achieved by carefully selecting the composition of the binary mixture.

Although the knowledge of the thermodynamic phase behavior is very important, experimental results for these systems are rather limited in the literature. Measuring the API solubility in polymers is still a challenge due to the high polymers viscosity that hampers the solubility equilibrium achievement (equilibrium between a crystalline solute and its solution) and makes difficult the experimental construction of solubility curves in a low time consuming [184]. For this reason, different methods have been developed to determine the solubility of APIs in polymeric carriers, among them, methods based on thermal analysis such as the melting point depression method [243], [244], the dissolution end point [244] and recrystallization methods [223], [245].

Figure 21 shows the schematic time evolutions of $T_{gmix}$ of an API/polymer mixture when reaching its equilibrium solubility upon annealing [246]. The top curve corresponds to a dissolution process (melting point depression, dissolution end point methods) while the bottom curve corresponds to a demixing process (recrystallisation methods). The dissolution process follows the dissolution kinetics of APIs into polymers at under saturated concentration solutions. The demixing process characterizes the recrystallization of the API in excess in a supersaturated homogeneous API-polymer solid solution.

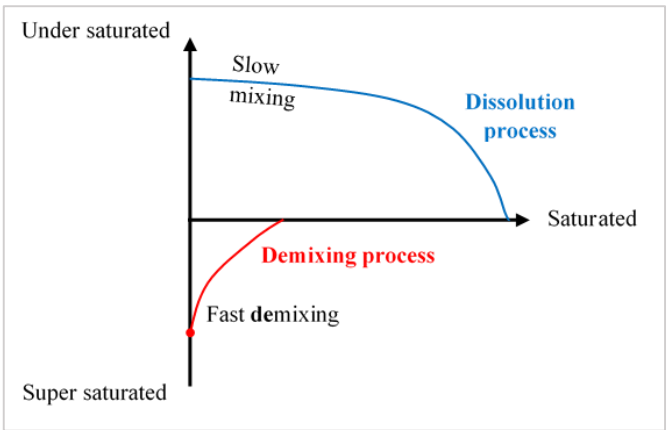

Figure 21. Schematic time and process evolution of the glass transition temperature of an API/polymer mixture when reaching its equilibrium solubility upon annealing. Adapted from [246].

some limitations, such as the long process, standardization, and particle size, affecting the results [247]. The demixing kinetics of APIs from supersaturated systems is expected to be much faster than the dissolution kinetics of APIs into undersaturated systems. This difference arises directly from the molecular mobility in the polymer matrix, which is higher in supersaturated API-polymer solutions than in undersaturated ones.

For the experimental determination of phase diagrams of an API/polymer mixture, the supersaturation of the API into the polymer can be obtained from a physical mixture of crystalline API and polymer carrier by different techniques such as film casting method [243] and comilling [246], [248] that forces the miscibility of the two compounds to reach supersaturation. The supersaturated glass solution is then loaded in a DSC analyser and annealed above its $T_g$ during a sufficient time to complete the demixing process: release the excess of API in the mixture and reach the equilibrium solution concentration at the annealing temperature. The use of spray drying was recently proposed [244] as an alternative to determine API-carrier solubility from demixing, because it is a fast process (some seconds) compared to solvent casting or comilling which are very time-consuming (hours). The binary mixture used for the authors [244] to demonstrate the feasibility of the method was Efavirenz-Soluplus®[11].

In this work the composition-temperature phase diagram for the binary praziquantel and the chosen polymer (that will be presented later) will be determined by following the recrystallization of PZQ from a supersaturated API-polymer solid solution generated by spray drying. The method will be detailed in the experimental section of the Chapter 4.

### *7.1.2.3 Considerations about solubility and dissolution of amorphous solid dispersions*

According to Pure and Applied Chemistry Union (IUPAC), solubility is defined as the solute concentration in the saturated solution, expressed as the portion of the designated solute in the designated solvent [249]. It is a thermodynamic parameter and usually measured according to techniques developed by Higuchi and Connors in which an excessive amount of solute is suspended in a solvent and stirred or rotated for an

[11] Soluplus® is a polyvinylcaprolactam-polyvinyl acetate-polyethylene glycol graft co-polymer [348].

extended period of time (typically 24, 48 or 72 hours) to achieve the concentration equilibrium [250]. When equilibrium is reached, the suspension is filtered and the concentration of the solute in the filtrate is measured using ultraviolet light absorption spectroscopy (UV) or high-performance liquid chromatography (HPLC) and compared to a standard UV or HPLC. Because it is a thermodynamic parameter, the solubility is dependent on the solute (for example, $pKa$, lipophilicity, and intermolecular forces in the solid state) and solvent properties (for example, pH, polarity, and solvent interactions) [251].

During solubility measurements, a crystalline material solubilizes over time, which leads to increasing solute concentration in the filtrate up to reach the maximum concentration which is the equilibrium concentration (solubility of the solute in the solvent at specific conditions of temperature). For amorphous materials, as discussed before, the solubilization profile is different. Higher solute concentrations are reached earlier (spring effect) increasing up to a maximum value ($C_{max}$), represented in Figure 22. Considering a possible recrystallisation of the high solute concentration in the medium, the solute concentration in the filtrate will decrease after the peak of solubilization ($C_{max}$). The API concentration from ASDs at the peak of the solubilization could be used for the determination of apparent (kinetic) solubility ($C_{max}$) as represented in Figure 22.

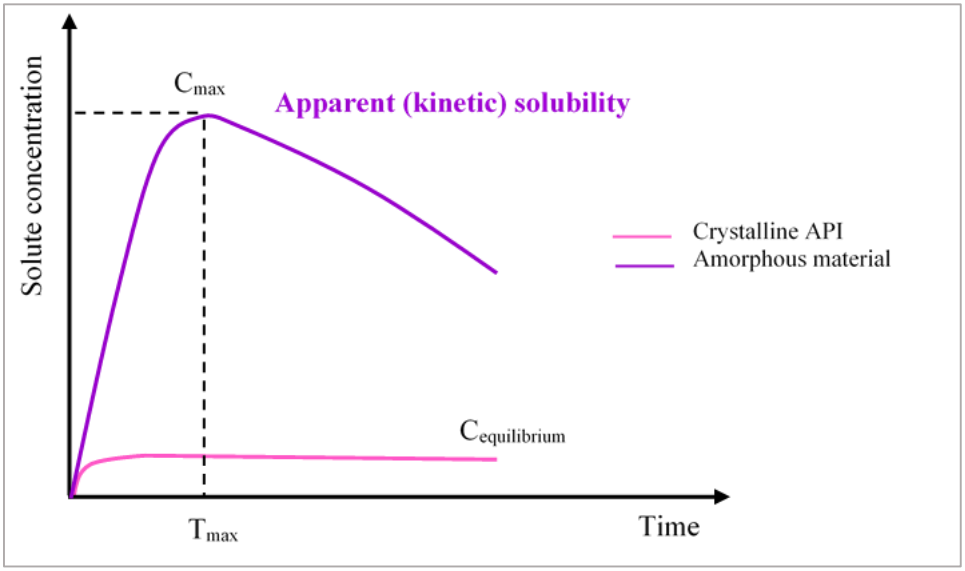


Figure 22. Schematic representation of kinetic solubility for amorphous and crystalline materials. Adapted from [184].

For the increase in solubility to be effectively bioavailable, it is important to determine the longevity of this supersaturation in the amorphous state. The rate at which an API goes into solution (dissolution rate) is then an essential pre-requisite for the absorption process and an important aspect of formulation development of ASDs.

Essentially, the apparent solubility advantage of ASDs determines the probability of success of improving bioavailability in vivo. Typically, the apparent solubility behaviours of ASDs are evaluated by dissolution studies. Not only the point of maximum concentration achieved ($C_{max}$) but also the extent of supersaturation is biorelevant.

The term "dissolution" describes the mixing of the two phases, resulting in a new homogeneous phase: the "solution" [251], [252]. Generally, the solute (API in this thesis context) goes into solution and the rate of its dissolution is a determining step towards absorption. Moreover, a fraction of the dissolved API may recrystallise before absorption as represented in Figure 23 if the available concentration exceeds the API's thermodynamic solubility [251], [252]. In this case, bioavailability may be affected.

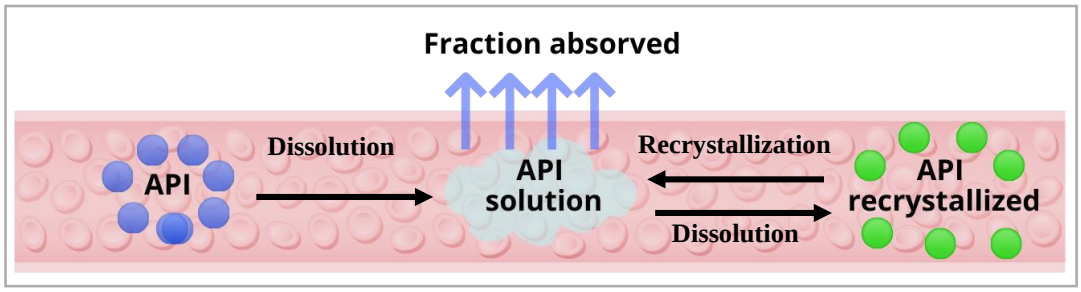


Figure 23. Schematic demonstration of solubility, dissolution, and oral absorption. The drug must be in solution to be absorbed. Dissolution will drive the initial solubilization of the API, and solubility in the gastrointestinal media will drive potential precipitation events. At the same time, there is intrinsic permeability of the compound and absorption. Source: adapted from [251].

The rate of dissolution of a solid can be expressed by using Noyes-Whitney equation:

Equation 3

$$\frac{dX}{dt} = \frac{DA}{h}\left(\boldsymbol{C_s} - \frac{X}{V}\right)$$

where, $\frac{\boldsymbol{dX}}{\boldsymbol{dt}}$ is the dissolution rate, **A** is the surface area available for dissolution, **D** is the diffusion coefficient of the API particle, **h** is the thickness of the diffusion layer

adjacent to the dissolving API particle surface, $\boldsymbol{C_s}$ is the saturation solubility of the API particle in diffusion layer, **X** is the amount of the API particle dissolved at time **t** and **V** is the volume of dissolution medium [251].

As ASD disintegrates, the increased apparent solubility of the amorphous form will yield a higher dissolution rate relative to the corresponding stable (crystalline) form, as well the increased surface area (A) resulting from size reduction of the API particles during solid dispersion process to the molecular or nearly molecular scale.

The dissolution behaviour of ASDs is governed by the degree of supersaturation (C > Cs) [201], [251], [253]. Then, crystallization can take place under supersaturated conditions and the rate of this transformation is affected by the degree of supersaturation besides factors like API physicochemical properties and API-carrier interactions.

The dissolution method during the development of an ASD formulation is usually, if not always, different from a quality control dissolution test that is mainly designed to verify the consistency of a API product as well as the process robustness and long-term stability [201], [251], [252]. Therefore, variations in methodologies can be found, such as the composition of the dissolution medium, presence of surfactant, pH, and agitation [253], [254].

Tests can be performed in sink or non-sink conditions for super-saturating formulation. The sink index (SI) is defined as follows [253]:

Equation 4

$$\boldsymbol{SI} = \frac{C_s}{Dose/_{Volume}}$$

Where $\boldsymbol{C_s}$ is the solubility of crystalline API, V the volume of dissolution medium and Dose is the total amount of API in the test sample to achieve specific SI. is maintained at a constant value, by adjusting the amount of ASD sample in accordance to the measured $\boldsymbol{C_s}$ of API in the dissolution medium. In other words, sink condition is the volume of medium, at least three times greater than necessary to obtain a saturated solution of the drug, so that the concentration gradient is maintained without interfering with the dissolution rate [220], [251]–[253]. The API (dose) will be completely dissolved according to this condition. The dissolution behaviour of amorphous APIs is governed by the degree of supersaturation. Thus, it is natural for dissolution studies to be conducted initially in non-sink conditions when a API load relevant to dose can be more

discriminating since the ability for a formulation to maintain supersaturation can only be tested under this condition [251]–[253], [255].

The sink/non-sink condition is a critical factor for the dissolution method. However, a recent study showed that about 86% of the works do not specify the condition used [251].

## 7.2 Manufacturing processes of amorphous solid dispersions

The choice of a manufacturing technique is dependent upon API and polymer properties and might have an impact on the stability and pharmaceutical performance of amorphous solid dispersions.

Crystal lattice disruption (also called mechanical activation), co-solubilization followed by rapid solvent removal and melting are the most common basic principles involved in the production of ASDs.

### 7.2.1 Crystal lattice disruption

The disruption of the crystal lattice of an API (Figure 24) , also called mechanical activation may be performed by high-intensity milling and has a wide range of applications [256]. Especially for the pharmaceutical industry, with a large part of the APIs with crystalline characteristics and low solubility, this technique can considerably alter the structure of these molecules [239]. As a result, there are changes in API properties such as solubility, dissolution, and hygroscopicity [256], [257].

The use of this technique has been shown to be effective in amorphization of APIs, for example, budesonide [256], indomethacin [256], [257], crystalline anhydrous α-lactose [258], praziquantel [59], naproxen [259], and sulindac [260]. This method has been successful in the creation of co-amorphous systems [245], [260] and more recently, in the creation of amorphous solid dispersions [259]. Some benefits of using milling for the creation of solid dispersions include the non-use of possibly toxic or destabilizing solvents (green synthesis), and its potential for thermolabile compounds [256].

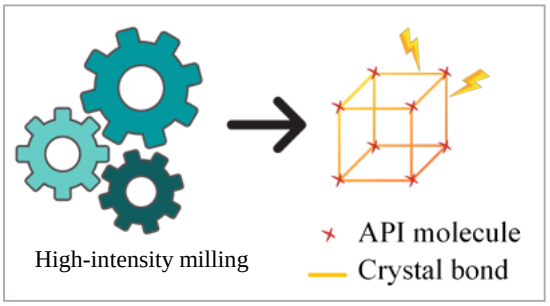


Figure 24. Illustration of the disruption of the crystal lattice by mechanical activation. Source: Author.

Regarding PZQ, a number of papers [33], [37], [59], [69], [75] have demonstrated that the mechanochemical activation of PZQ, via neat grinding or comilling with different polymers (Povidone, Copovidone, Crospovidone and Sodium Starch Glycolate) enabled the transformation of the original PZQ polymorphic form into a new polymorphic variety of racemic PZQ [10], [73] or into a drug amorphous state [75].

In these studies, different parameters have influenced the PZQ solubility, the PZQ structure (degradation) during co-milling and the physical stability of the solid forms obtained. For example, co-milling of crystals of racemic PZQ and polymers (poly (vinylpyrrolidone) (PVP) and crospovidone (CROS)) in a vibrational mill [59] revealed some negative feature related to the degradation of the PZQ. In fact, the use of PVP and CROS led to different levels of API degradation depending on the milling parameters used and the proportion of excipients.

Another example of mechanical activation to modify PZQ bioavailability involved the use of surfactants such as poloxamers and sucrose esters as carriers. As with polymeric systems, it has been demonstrated that grinding and formulation parameters impacted solubility (double for proportions F-127 - 10: 3 and C-1816 - 10:2), dissolution, and content. Unlike the polymer mixture, there was no degradation of the PZQ in the presence of poloxamer (F-127) and sucrose stearate (C-1816) [69] during co-milling. This difference related to degradation may be linked to the different materials (oxide-based zirconium and stainless steel) of the grinding jars and balls used in those studies. Although stainless steel does not offer such a chemically inert environment for the mechanochemical activation as the zirconium oxide does, it did not lead to significant PZQ degradation [69], which was explained by its higher thermal conductivity, thus providing a more efficient distribution of the generated heat.

In summary, the milling process can be a valid alternative to produce amorphous, stable systems with increased solubility of the PZQ when associated with a

recrystallization inhibitor. However, according to the studies carried out, it is verified that it is a methodology dependent on the ideal adjustment of different parameters to guarantee the obtainment of a quality product (frequency, time, and temperature of the grinding process, excipients, grinding ball material). In addition, these are generally lengthy procedures (for example, obtaining the polymorphic form B of the PZQ requires 4 hours of uninterrupted milling [10].

### 7.2.2 Co-solubilisation and rapid solvent evaporation

In this method, API and polymer are dissolved in an organic solvent to give a solution, and the solvent is subsequently removed by evaporation. A well-established technique in this category is spray drying (Figure 25), in which a API-polymer solution is fed through a nozzle and mixed with pressurized gas to form fine droplets (atomization) [261]–[263]. Other nozzle types, employing centrifugal, pressure, kinetic or vibration energy for atomization are available as well. These droplets are further transported and dried along a heated gas flow through a drying chamber and a cyclone, where particles within a desirable size range fall out of the gas stream in a collector [261].

The formulation of solid dispersions through spray drying has been received considerable attention and has already been used in several APIs BCS class II to improve solubility, dissolution, and consequently bioavailability, such as meloxicam [264], curcumin [265], itraconazole [266], indomethacin [261]. The subsequently formed powder can be processed in a wide array of API delivery systems (capsules, tablets, dispersible powders). Spray drying is a suitable method for thermally degradable compounds since the temperature during spray drying reaches lower values compared to that in the melt processes. The presence of residual solvent, which can act as a plasticizer or is potentially toxic, is seen as one of the disadvantages of this technique.

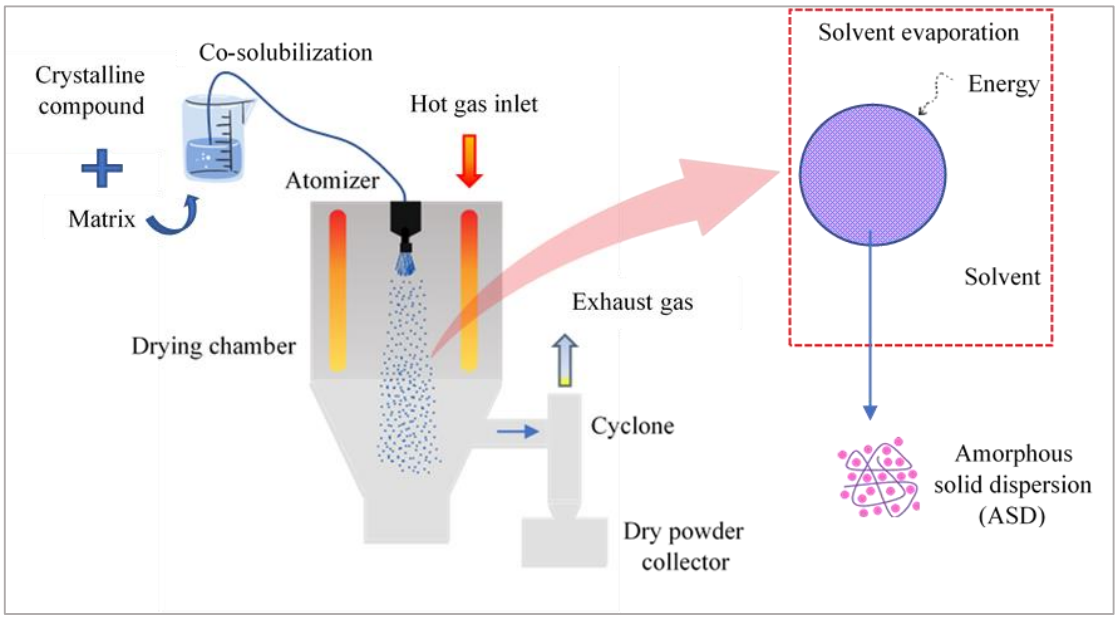


Figure 25. Illustration of the formation of an amorphous solid dispersion by spray drying. Source: Author.

As already described before in this Chapter (item 4), co-solubilisation and rapid solvent evaporation is the most applied technique to produce solid dispersions containing praziquantel. Different carriers and solvents like ethanol [167] or chloroform [170] have been already used. However, most of the scientific studies using this technique have been employed drying techniques other than spray drying to produce ASDs, for example, in an oven [29] or in a rotary evaporator [167].

### 7.2.3 Melting processes

In a laboratory, melting processes can be very simple. For example, a solid dispersion can be obtained by combining the constituents of the formulation in a DSC pan and heating the sample until melting of all ingredients, followed by forced cooling. Moving up in scale, a melt-quenching approach can be employed.

These techniques can be used to produce up to several grams. Hot melt extrusion (HME) has been explored as a scale-up process to produce amorphous solid dispersions by melting process and is the technique of our interest in this work. From our knowledge, there are no reports in the literature on using this technique to produce solid dispersions of PZQ with a focus on increasing solubility, taste masking or in an intermediate solid form (ASD) aiming a final paediatric pharmaceutical dosage form. For this reason, and because of our interest, HME will be described in more details in the next section.

*7.2.3.1 Hot melt extrusion*

The HME technique was first invented by Joseph Brama in the late 18th century for the manufacture of lead pipes and has since been widely spread as a production process for different areas such as rubber, food and plastic [188], [267], [268].

In general, the HME process can be divided into three stages: feeding, conveying, melting, mixing and shaping, and down streaming (Figure 26). Basically, the technology itself involves the application of heat, pressure, and agitation through an extrusion channel to mix materials together, and subsequently forcing them out through a die, which allows to produce extrudates of different shapes and diameters.

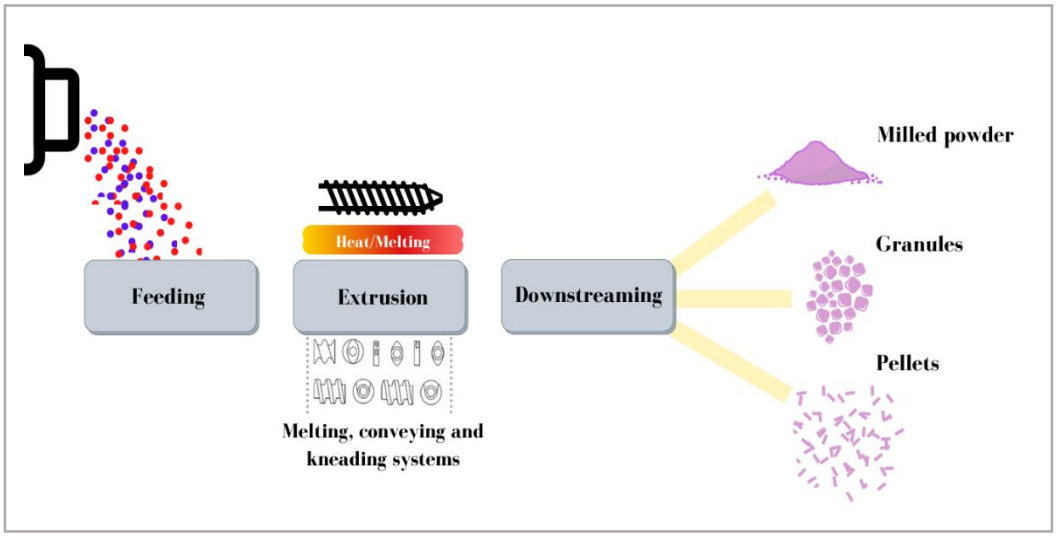


Figure 26. Schematic representation of a hot melt extrusion process. Source: Author based on [184], [188].

The temperature decrease out of the dye allows for solidification. During the melt extrusion process, the dissolution of APIs into the polymer matrix is accelerated under the influence of shear and heat. The barrel temperature, screw speed, screw design and feed rate are process parameters which can influence the quality of the end product [269].

The HME process can be conducted using a single-screw or twin-screws. Although their operation follows the same principle, generally, in the plastics industry, single-screw is used because it is a simpler process [268]. In the pharmaceutical area, the twin-screw is preferred because it has advantages such as higher kneading and dispersing capacities, less tendency to over-heat, and shorter residence times, which prevents degradation of heat-sensitive components [184]. Also, for pharmaceutical processes, the

equipment must meet specific regulatory compliance. For example, all metallurgy parts of the extruder must be inert (physically and chemically), not appear to have any erosion, absorption, or adsorption during the process. It is also necessary to plan quality inspections and to provide cleaning validation protocols according the main regulatory guides [268].

Figure 27 illustrates the representation of the HME process with a twin-screw extruder. Typically, the equipment consists of the feeder (allowing volumetric or gravimetric feeding), the barrel in which the twin-screw is inside, a control unit, torque sensors, heating/cooling device, and die. The process starts by feeding the material, which is then transported along with the two screws through co-rotation using thermal and mechanical energy. These forces will be defined through the following parameters: barrel temperature, feed rate, screw configuration, screw speed, and torque [268], [270], [271].

The heating zones are present along the entire length of the barrel and can be individually controlled according to the physical-chemical characteristics of the product being processed. [271].

The screw configuration can be defined in several different ways using conveying, mixing and distributive flow elements and discharge feed screws [184], [271]. The transport elements have the function of pushing the material forward along the length of the barrel passing from zone to zone and have no capacity to mix the material. In contrast, the mixing elements can be positioned at 0, 30, 60, and 90. The greater the angle used, the lower the transport capacity and the greater the shear [271].

After the material passes through the entire barrel and is extruded, its output is usually made in the form of filament with a diameter adjusted according to a die. Commonly, the filament is cooled and then shaped according to the desired final physical form (pellets, powder, granules).

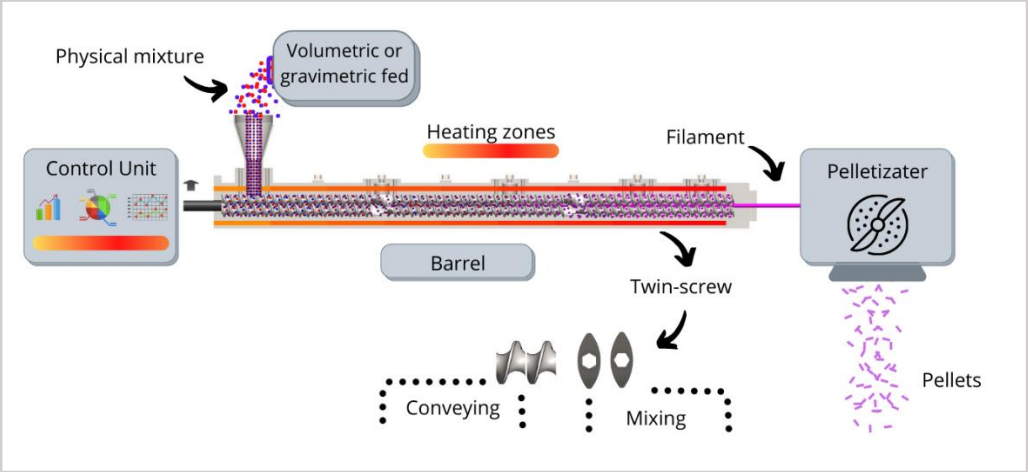


Figure 27. Representation of HME process. Source: Author.

The formation of ASD by the HME process is the result of the combination of mixing and melting. For this to be possible, it is necessary to add energy to the system, and this energy comes from two important parameters: the heating of the barrel and the rotation and configuration of the screw. The first will influence the softening and melting of the material along the path, and the second will increase heating as a result of the shear forces [259], [272], [273].

The main input and dependent variables can be seen in Figure 28.

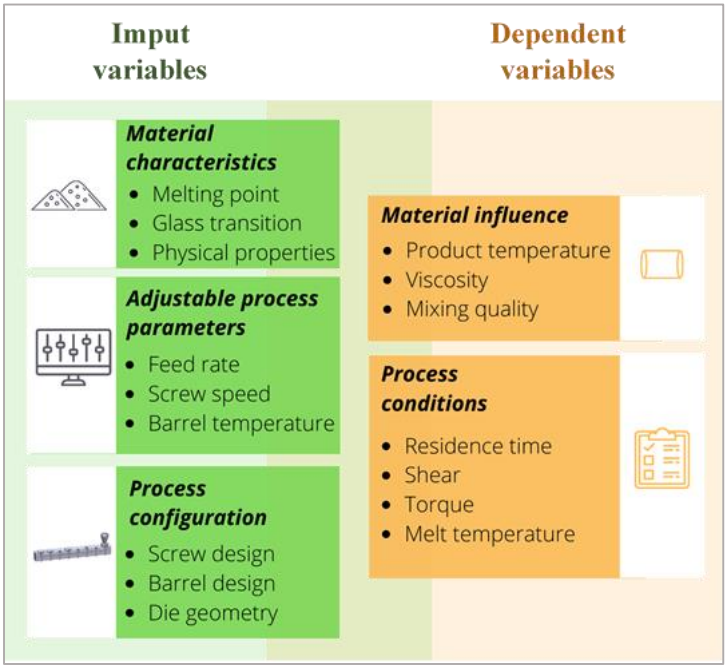


Figure 28. Input and dependent variables in the HME process.

The interest of HME process in the pharmaceutical area has grown rapidly in recent years, as confirmed by the number of scientific publications in the period 2000-2020 (Figure 29) [187], [225].

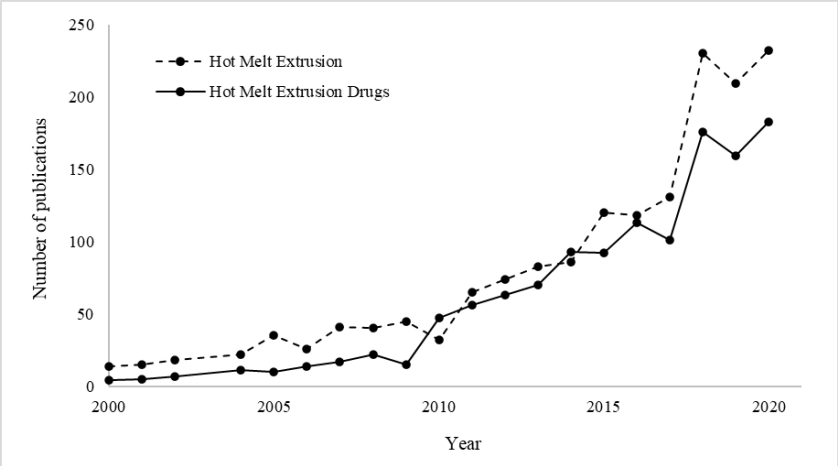


Figure 29. Publications present in the Scopus® database with search using the terms: hot melt extrusion and hot melt extrusion & APIs from 2000 to 2020.

Besides the increasing number of scientific publications, the growth of patents is also verified for granules [274], [275], pellets [276], controlled-release tablets [272], transdermal controlled-release patches, implants, taste-masked oral fast dissolving systems [277]–[279] and other pharmaceutical API delivery systems [225], [280].

Currently, the pharmaceutical market has several products available that make use of HME technology in their production (Table 6) [225], [267], [280].

The reason for the abrupt growth of scientific and technological production in the area is due to some advantages over other methods. It is a process that does not require the presence of solvents, is fast and continuous, has an excellent mixing capacity, high productivity (on a commercial scale it is possible to make more than 500 Kg/h), and has a wide applicability [281].

Regarding ASDs, the FDA approved 19 ASD-based products [282] in the period 2007-2017. This growing interest in the pharmaceutical industry is closely linked to the fact that currently, about 70 % of developing APIs are water-insoluble which makes the ASD approach an increasingly accepted strategy to get around this problem [283].

Despite the advantages mentioned, the HME technique also has some disadvantages. The stability of the API/polymer mixture may be a limiting factor due to the high energy provided in processing by both temperatures rise and shear. The limited number of polymers available with adequate flowability, thermal stability and pharmaceutical properties suitable for their use may make it impossible to achieve a desired quality formulation using HME [125]. The complexity of the influence of process parameters such as temperature, thread design, thread speed, residence time, cooling rate, polymer rheology and the influence of API concentration on the rheological behavior of the polymer are challenges for the more large of the technique for ASDs production [284].

Table 6. Currently marketed HME products. Source: Author and adapted from [225], [267].

| ***Trade name*** | ***Owner*** | ***API*** | ***Polymer*** | ***Terapeutic indication*** | ***Pharmaceutical form*** | ***HME pouporse*** |
|---|---|---|---|---|---|---|
| Lacrisert® | Valeant | without API - implant acts as wetting agent | HPC | Dry eye syndrome | ocular | Shaped (rod) system |
| Ozurdex® | Allergan | dexamethasone | PLGA | Macular edema | | Shaped system |
| Depot-profact® | Sanofi AventisBuserelim | Buserelin acetate | PLGA | Prostate cancer | subcutaneous | Shaped (rod) system |
| Probuphine® | Titan Pharmaceuticals | Buprenorphine | EVA | Opioid dependence | | Shaped (rod) system |
| Zoladex® | AstraZeneca | Gosserelin acetate | PLGA | Prostate cancer | | Shaped (rod) system (different size) |
| Implanon® | Merck | Etonogestrel | EVA | Contraceptive | | Shaped (rod) system |
| Annovera® | Therapeutics MD | Ethinylestradiol/ segesterone acetate | Silicone | Contraceptive | intravaginal | Shaped (ring) and multilayer system |
| NuvaRing® | Merck | Etonogestrel/ Etinilestradiol | EVA | Contraceptive | | Shaped ring |
| Isoptin® SER | Abbott | Verapamil | HPC/HPMC | Hypertension | oral | Shaped system (oral) |
| Rezulin® | Parker-Davis | Troglitazone | PVP | Diabetes | | Amorphous dispersion |
| Cesamet® | Meda Pharmaceuticals | Nabilone | PVP | Aniemetic | | Solid dispersion |
| Adalat SL® | Bayer | Nifedipine | HPMC/PEO | Antianginal agent | | Controlled realease |
| Fenoglide® | Life Cycle Pharma | Fenofibrate | PEG 6000 | Dyslipdemia | | Solid dispersion |
| Noxafil® | Merck | Posaconazole | HPMCAS | Antifungal | | Amorphous dispersion |

| ***Trade name*** | ***Owner*** | ***API*** | ***Polymer*** | ***Terapeutic indication*** | ***Pharmaceutical form*** | ***HME pouporse*** |
|---|---|---|---|---|---|---|
| Belsomra® | Merck | Suvorexant | Copovidone | Insomnia | Oral | Amorphous dispersion |
| Technivie® | Abbvie | Ombitasvir | Copovidone / vitamin E / polyethilene glycol succinate | Hepatitis C virus | | Amorphous dispersion (3 separate ASDs) |
| Venclyxto® | Abbvie | Venetoclax | Copovidone / polysorbate 80 / colloidal silicon dioxide | Chronic lymphocitic leukemia | | Amorphous dispersion |
| Viekira pak® | Abbvie | Ombitasvir/paritaprevir /ritonavir/dasabuvir | Copovidone | Hepatitis C virus | | Amorphous dispersion (3 separate ASDs) |
| Mavyret | Abbvie | Glecaprevir/pibrentasvir | Copovidone / vitamin E / polyethilene glycol succinate | | | Amorphous dispersion |
| Norvir® | Abbott | ritonavir | PEG-glyceride | Viral infection | | Amorphous dispersion |
| Kaletra® | Abbott | lopinavir / ritonavir | Copovidone | Viral infection | | Amorphous dispersion |
| Onmel® | Merz | Itraconazole | HPMC | Onychomycosis | Oral | Amorphous dispersion |
| Gris-PEG® | Pedinol | griseofulvine | PEG | Onychomycosis | | Crystalline dispersion |
| Covera-HS® | Pfizer | verapamil hydrochloride | HPC | Hyperversion and angina pectoris | | Melt granulation |
| Eucreas® | Norvartis | vildagliptin / metformina | HPC | Diabets - type II | | Melt granulation |
| Zithromax® | Pfizer | azithromycin-coated enteric multiparticulate | Pregelatinized starch | Bacterial infection | | Melt granulation |

#### 7.2.3.1.1 Carriers for HME

There is an extensive list of polymers being widely used for HME, and some are listed in Table 7 [268], [272], [285]. Polymers can be amorphous (polyacrylic acid), semicrystalline (poly L-lactic acid), or crystalline (polyethylene glycol). Although amorphous polymers are the most used, the use of semi-crystalline crystals (such as Poloxamer 407) has been used with a strategy to overcome the disadvantages of HME due to its high processing temperatures. In this way, the association with this type of polymer can be interesting for thermosensitive APIs [219]. In addition, some more plasticizers can be added to the system, which contains a semi-crystalline polymer so that less energy is needed for the process and, consequently, lower temperature and lower torque [286]. Their physicochemical properties provide opportunities to overcome processability challenges in HME and make it possible to obtain new pharmaceutical materials [268].

Polymers are the main excipients used for the production of ASDs [184]. Table 8 gives a list of amorphous polymers available for this use. The success of ASD production depends largely on the correct choice of carrier, and it must be based on its main properties such as glass transition temperature, degradation temperature, solubilization capacity, and mechanical characteristics [268]. A prerequisite of the polymer to be used in HME is appropriate thermoplastic behavior. However, the number of such polymers approved for pharmaceutical use is still limited.

Table 7. Summary of the polymers generally used in HME. Source: Author and adapted from [184], [199], [225], [268].

| ***Structure*** | ***Polymer chemical name**** | ***Trade name*** | ***$T_g$ (°C)*** | ***$T_d$ (°C)*** |
|---|---|---|---|---|
| Amorphous | PVP (MW 2000–3000) | Kollidon® 12 PF | 72 | 196 |
| | PVP (MW 7000–11,000) | Kollidon® 17 PF | 140 | 217 |
| | PVP (MW 28,000–34,000) | Kollidon® 25 | 153 | 166 |
| | PVP (MW 44,000–54,000) | Kollidon® 30 | 160 | 171 |
| | PVP (MW 1,000,000–1,500,000) | Kollidon® 90F | 177 | 194 |
| | Vinyl pyrrolidone: vinyl acetate 6:4 (MW 45,000–70,000) | Kollidon® VA64 | 105 | 270 |
| | Poly(vinyl caprolactam-covinylacetateethylene glycol) graft polymer( MW 90,000–140,000) | Soluplus® | 72 | 278 |
| | Methyl Cellulose (MC) (MW 14,000) | Methocel™A | 200 | 247 |
| | Hydroxypropyl cellulose (HPC) (MW 95000) | Klucel® LF | 111 | 227 |
| | Hydroxypropyl methyl cellulose acetate succinate (HPMCAS) | AFFINISOL™ HPMC HME | ~115 | >250 |
| | Butyl methacrylate:Dimethylamino ethyl methacrylate:Methyl methacrylate (1:2:1) (MW – 47,000 Da) | Eudragit® E PO | 52 | 250 |

*MW: molecular weight

## 8. 3D PRINTING TECHNOLOGY FOR MEDICINES

FDM is the most discussed technology for pharmaceuticals medicines, and the related main way is using filaments from HME to direct feed the printer. However, with this approach, researchers have spent most of the time because the material into printable filament and passing the filament through a heated nozzle [287]. It means that filaments must have rheological properties and mechanical strength adequate to ensure proper processability in FDM 3D printing [287]. The high dependency of physical and mechanical properties of the filaments for printing feasibility [156], [288] becomes more critical especially when high-drug loads are required.

One way to get round this problem is to work with the direct powder extruder 3D printer (DPE). This concept was applied for the first time to print itraconazole tablets and different types of HPC as a polymer [156]. Binary physical mixtures were prepared in the mass proportion 35:65 (API: Polymer) to obtain a final dose of 100 mg. Tablets of 10 mm diameter and 3.6 mm height were printed with each of the prepared mixtures. The dissolution rate was found to be dependent on the type of HPC polymer used, which was related to the solid state of ASDs (amorphous or partially amorphous). The faster dissolution kinetics was obtained from the only completely amorphous ASD, formed with the polymer named HPC-UL.

The possibility of directly feeding powdered material into the extruder printer may become a great advance for the pharmaceutical area. Most publications that aim to obtain a pharmaceutical form by 3D FDM printing investigate the critical process and formulation parameters for the obtention of HME filaments with adequate mechanical characteristics for printing (not too soft, not too hard) like the drug load and the type of polymer. So, the possibility of excluding the previous stage of production of HME filament to feed the printer is attractive. However, for 3D printer (DPE), in some cases where a completely amorphous material is desired like an amorphous solid dispersion, caution is necessary, because it may be not completely amorphized during the printing process, as observed with print itraconazole-HPC tablets [156].

In turn, the SSE 3D printing technology is based on the deposition of a material in the form of gel or paste in sequential layers to form the desired 3D object. The printing process is exactly as described for the FDM process, however, the most important difference is in the use of molten filaments for printing, while SSE uses soft materials.

Goyanes et al. [289] made available a list of names to identify SSE 3D printing technology in the pharmaceutical field:

- ✓ pressure-assisted microsyringe (PAM) printing
- ✓ robocasting or robotic material extrusion
- ✓ cold extrusion-based printing
- ✓ hydrogel-forming extrusion
- ✓ melting extrusion
- ✓ thermal extrusion
- ✓ soft-material extrusion
- ✓ melting solidification printing process
- ✓ direct ink writing
- ✓ hot melt ram extrusion
- ✓ pneumatic extrusion hot melt
- ✓ micro-extrusion.

The feeding of this type of printer usually occurs through a syringe, which represents an advantage technique when compared to the others. This characteristic provides greater precision and quality to the product, what is crucial to the pharmaceutical industry [289].

In addition to the already mentioned characteristics of other types of 3D technologies such as medication customization, production on demand, design variability, the possibility of different release profiles, speed, and ease of the process, SSE also relies on low temperatures for print.

For paediatric use, this technology can be even more attractive due to the possibility of printing chewable medicines. In a recent study, chewable printlets of isoleucine in various colours and tastes were prepared to treat a rare metabolic disease that mainly affects children [290]. These drugs were administered to paediatric hospitalized patients that could choose the colour and taste of their preference. The results were very promising, showing no difference in plasma levels of 3D drugs compared to conventional treatment.

## 8.1 Brief approach on regulatory 3D printing aspects

In August 2015, the first drug obtained by 3D printing was approved by the FDA, and this ends up being a milestone for innovation in the pharmaceutical industry's drug production area. Spritam® (levetiracetam) is a drug for seizures that disintegrate in the mouth with a small

amount of water [31]. It is an innovation for patients, including those with difficulties swallowing solid oral dosage forms [31–33].

However, the great appeal of 3D printing in the pharmaceutical area is the personalization of medicines. A topic that has been treated since the nineties with new therapies to meet each patient's characteristics.

Currently, the pharmaceutical industry is accustomed to producing large quantities and "one size fits all" drugs, that is, without flexibilities specific doses for specific individuals. Then, regulatory requirements are defined to assess the quality of this type of approach [32]. Changing production to something personalized requires new regulatory discussions, and the area is under increasing discussion.

Regulation has already been approved to produce medical devices obtained by 3D printing [32]. The specifications of medicine produced by 3D printing must follow the guidelines described in ICH Q6 (for bulk products). However, if 3D production is a conventional dosage form, the current pharmacopeial requirements must be followed. Also, if necessary, specific quality attributes for any product generated by 3D printing can be added. For example, suppose a tablet is produced by 3D printing with its internal porosity increased to obtain a quick release of the drug. In that case, the measure of porosity can be considered as an additional attribute [32]. It is important to be clear that production on-demand or specific characteristics of patients may require specific quality attributes.

Although "Technical Considerations for Additive Manufacturing of Medical Devices" was published in 2017, there are no specific requirements for pharmaceutical drug requirements. To date, there is no clear and specific regulation to differentiate the way of producing personalized medicines obtained by 3D printing in any country [32]. Currently, the European Medicines Agency (EMA) has defined some measures for the approval of medicines using 3D printing as the complete certification of electronic components and a specific master file for submission. Japan also had some similarities [33]. *Agencia Nacional de Vigilância Sanitária* (ANVISA[12]) is developing new regulatory frameworks to facilitate the development of innovative products [33].

## 9. CHAPTER SYNTHESIS

Chapter 2 reviewed the literature about topics of interest for our work: an overview of schistosomiasis disease and treatment, characteristics of the API studied in this thesis (PZQ),

[12] Brazilian Health Regulatory Agency

challenges and strategies on the pharmaceutical development of paediatric medicines and, ways that will be investigated here to propose new directions to formulate praziquantel for paediatric use. Emphasis was given to amorphous solid dispersions and 3D printing technology.

An overview of the literature on amorphous solid dispersions to praziquantel summarized the main results of previous works. The main points to be highlighted are:

- Until now, several solid dispersions have been proposed using different carriers, and only one suggests the partial use of the amorphous dispersion approach, making the correlation between increased solubility and, consequently, increased unpleasant taste perception. None intends to study the increase of solubility by the amorphization of API in a polymer and evaluation of taste perceptions with the paediatric pharmaceutical formulation.
- Hot-melt extrusion can be a promising continuous production method for amorphous solid dispersions of praziquantel. However, it is crucial to select correct excipients and compositions to produce amorphous and stabilized formulations of PZQ.
- Finally, could 3D printing be an adequate technology to produce printed tablets with a suitable dosage for children, from formulated amorphous solid dispersions powders of PZQ?

This thesis will try to answer these questions and technological needs.

# CHAPTER 3 - CHARACTERIZATION OF RAW MATERIALS

# 1. INTRODUCTION

Three formulations were studied in this thesis, constituted of two or three constituents. For the binary system, API (Praziquantel) and polymer (PVPVA, Kollidon® VA 64) were used. For the ternary, a surfactant was added as the third constituent: SPAN 20 and Kolliphor® SLS Fine.

In this Chapter, all active materials, excipients, solvents, reagents, reference standards used are firstly introduced.

Secondly, the characterisation of some properties of the main pure components, of interest for this work, are presented. They are:

- Physical characteristics of the primary particles (morphology, particle size);
- PZQ composition (dosage and determination of impurities);
- PZQ solubility and dissolution profile in different media;
- Thermal properties (glass transition, melting and degradation temperatures);
- Physical stability evaluation of PZQ and the polymer under three controlled conditions (15 to 30 ºC/max 60 % RH, 30 ºC/75 % RH and 40 ºC/7 5% RH).

Figure 30 present the graphic structure of the Chapter 3.

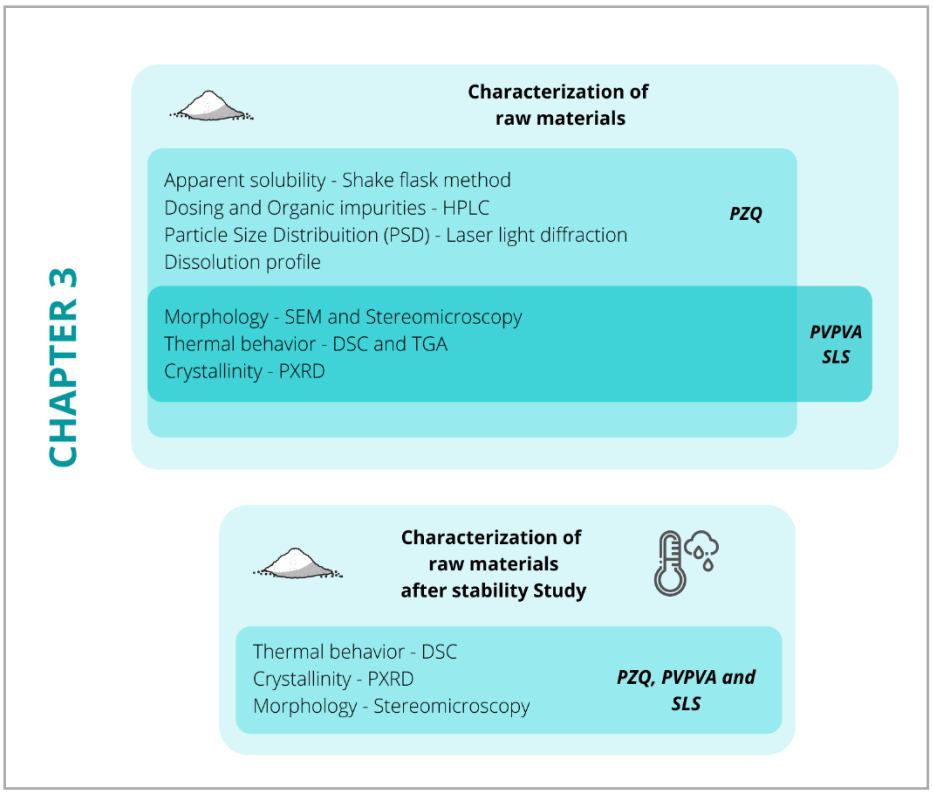


Figure 30. Graphic structure of chapter 4 (Source: Author).

## 2. MATERIALS

The production of the main formulations developed was based on three compositions:

- API: Polymer
- API: Polymer: Solid Surfactant
- API: Polymer: Liquid Surfactant

The materials used for these formulations are shown in Table 8.

The quantitative compositions will be detailed in each of the following Chapters as well as the respective methods of preparation, characterisation results, and assessments of physicochemical sensory, and pharmacokinetic characteristics.

### 2.1 Active Pharmaceutical Ingredient (API)

Racemic praziquantel ($C_{19}H_{24}N_2O_2$), was kindly provided by Farmanguinhos, Fiocruz, Brazil.

### 2.2 Polymer

A vinyl pyrrolidone-vinyl acetate copolymer $(C_6H_9NO)_n$ x $(C_4H_6O_2)_m$) (PVP-VA), Kollidon® VA 64, was provided by BASF corporation (Jacareí, Brazil; Burgbernheim, Germany).

### 2.3 Surfactants

Two surfactants were used as the third component in ternary amorphous solid dispersions produced by hot melt extrusion (HME).

Sorbitan monolaurate ($C_{18}H_{34}O_6$), Span™ 20, was purchased from Croda International Pcl (UK).

Sodium lauryl sulfate, Kolliphor® SLS Fine, was donated by BASF corporation (Jacareí, Brazil; Burgbernheim, Germany).

Polietilenoglicol 4000 (PEG 4000) was purchased from Sigma-Aldrich (Germany) to prepare sample suspensions for animal gavage procedures during pharmacokinetics studies.

## 2.4 Solvents and reagents

Ethanol (99 %) was used as common solvent for racemic praziquantel and the polymer PVPVA to produce spray-dried samples. It was purchased from Carlo ERBA Reagent (Italy).

Acetonitrile and methanol HPLC/Spectro for the HPLC experiments were purchased from Merck (Germany) and Tedia Company (Fairfield, USA).

Distilled and purified water (conductivity of 18.2 MΩ.cm at 23 °C) was produced by the purification system Milli-Q (Purelab DI, MK2, E3lga, UK).

Hydrochloric acid fuming 37 % (Merck KGaA, Darmstadt, Germany), Acetic acid (glacial) (Merck KGaA, Darmstadt, Germany), Sodium Hydroxide 97.0 % PA (Bio Scie, Anápolis/GO, Brazil), Sodium Dodecyl Sulfate 95 % (J. T. Baker, Pennsylvania, EUA), Potassium dihydrogen phosphate (Merck KGaA, Darmstadt, Germany), Sodium acetate trihydrate (Scharlab S.L., Sentmenat, Spain) were used to prepare the aqueous media for the solubility tests.

Sodium Dodecyl Sulfate 95 % (J. T. Baker, Pennsylvania, EUA) was used for dissolution profiles tests.

Formic acid and tert-butyl methyl ether from Scharlau (Spain) and methanol from Tedia (Fairfield, OH, USA) were used for bioanalytical and pharmacokinetic analysis.

Heparin sodium 5.000 IU /mL from B. Braum (Germany) was applied on blood samples during the pharmacokinetic experiments with animals.

Sodium chloride and Potassium phosphate monobasic (Merck®, Germany) and, Sodium phosphate dibasic (Sigma-Aldrich®, St. Louis, USA) was used for in vitro taste masking test evaluation.

## 2.5 Reference standard

The praziquantel reference standard was purchased from USP® (Rockville, MD, USA) for drug content analysis and validation of the bioanalytical and pharmacokinetic methods.

Praziquantel reference compound-related (A, B, and C) standard was purchased from USP® (Rockville, MD, USA) for impurities analysis.

Diazepam reference standard was donated by INCQS (Rio de Janeiro, RJ, Brazil), and caffeine was purchased from USP® (Rockville, MD, USA). They are used with nicotine bitartrate dihydrate as internal standard (IS) to validate the bioanalytical and pharmacokinetic methods.

**2.6 Active materials**

Ketamine and xylazine from USP (USA) were used as a combination of anaesthetics for animals' euthanasia procedures after pharmacokinetic study.

Praziquantel commercial tablets (Farmanguinhos/Fiocruz) were used for the taste masking tests.

Table 8. Main materials used in this thesis to produce binary and ternary ASD systems.

| ***Substance*** | ***Physical form*** | ***Code for this thesis*** | ***Molecule*** | ***Reference*** |
|---|---|---|---|---|
| Praziquantel | powder | PZQ | 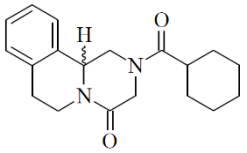 | [291] |
| Vinyl pyrrolidone-vinyl acetate copolymer | powder | PVPVA | 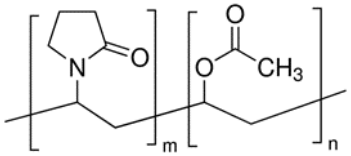 | [292] |
| Sorbitan monolaurate | liquid | SPAN | 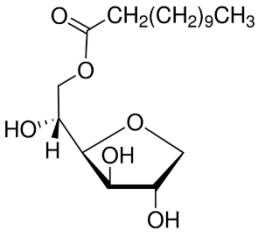 | [217] |
| Sodium lauryl sulfate | powder | SLS | 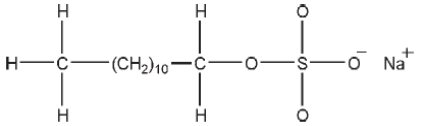 | [217], [293] |

# 3. CHARACTERIZATION OF FORMULATIONS RAW MATERIALS

## 3.1 Methods

### 3.1.1 Dosage of PZQ and related compounds by High-Performance Liquid Chromatography (HPLC)

High-performance liquid chromatography (HPLC) is a technique used to separate molecules based on size and surface charge, among other properties. The incorporation of ultra-violet (UV) spectroscopy with HPLC allows the concentration of molecules to be determined following separation. HPLC-UV was used to quantify PZQ according to the pharmacopeia method [3]. The HPLC system used consisted of two mobile phase delivery pumps (LC-10 ADVP, Shimadzu, Japan), a UV–Vis detector (SPD-10Avp, Shimadzu, Japan), an autosampler (SIL-20A, Shimadzu, Japan), an interface (SCL-10Avp, Shimadzu, Japan) for the acquisition of data through a software Ez-Star and a column Kinetex® C18 100 Å (150×4.60 mm – 5 µm). The mobile phase comprised methanol and water (60:40 V/V), the flow rate was 1.5 ml/min, injection volume was 10 µL, and conducted absorbance readings at a fixed wavelength of 210 nm. The retention time of PZQ was about 1 min and set the run time at 10 min. Quantification was carried out using a fresh stock PZQ standard (Brazilian Pharmacopoeia – batch 1069) solution prepared each time before starting the analysis dissolving 9 mg of PZQ in the mobile phase for a final concentration of 0.18 mg/mL. For each sample, an equivalent of 37.5 mg of PZQ was weighed in duplicate in 25 ml volumetric flasks and added to the mobile phase. The solutions were subjected to ultrasound for 5 minutes. The sample was filtered with a PTFE 0.22 µm filter and diluted to 0.18 mg/mL. After homogenization, a fresh aliquot was filtered (same type of filter) and transferred to a vial. HPLC analysis took place immediately after sample preparation. The results were expressed in the percentage of PZQ recovery.

The quantification of the related compounds in the PZQ sample (namely A, B, and C), was based on recommendations from the American Pharmacopoeia [53].

Initially, individual solutions were prepared with the respective PZQ standard related compounds (USP) (A, B, and C[13] - batches: R01600, R079Q0 and R032B0, respectively). A solution for each impurity standard was prepared in a mobile phase to a final concentration of 0.04 mg/mL). The PZQ sample was also dissolved in the mobile phase to a final concentration of 20 mg/mL.

The solutions were injected in duplicate on the HPLC, and the calculation of each related compound of PZQ was performed by normalization in the function of the relative retention time (RRT) (Table 9).

Table 9. Acceptance criteria for PZQ related compounds [53].

| ***Compound*** | ***Relative Retention Time (RRT)*** | ***Acceptance criteria NMT* (%)*** |
|---|---|---|
| PZQ | 1.0 | 0.2 |
| Praziquantel related compound A | 0.8 | - |
| Praziquantel related compound B** | 1.8 | 0.2 |
| Praziquantel related compound C** | 2.1 | 0.2 |

*NMT = no more than; ** Stored in a refrigerator (2 to 8 ºC).

### 3.1.2 Thermogravimetric Analysis (TGA)

Thermogravimetric analysis or thermal gravimetric analysis (TGA) is a method of thermal analysis in which the mass of a sample is measured over time as the temperature changes. This measurement provides information for example about physical phenomena, such as phase transitions, absorption, adsorption, and desorption. For TGA analysis, the sample (9.5 – 10.5 mg) was carefully weighed in aluminium crucibles. The tests were performed in a Mettler Toledo Thermogravimetric Analyser, model DSC/TGA3+, under a dynamic nitrogen atmosphere with a 50 mL/min flow rate and a heating rate of 10 ºC/min, in the temperature range from 25 to 300 °C. The TGA equipment was previously calibrated with metallic indium and aluminium standards.

### 3.1.3 Differential Scanning Calorimetry (DSC)

[13] Related compound A = 2-Benzoyl-1,2,3,6,7,11b-hexahydro-4H-pyrazino [2,1-a]isoquinolin-4-one; Related compound B = 2-(Cyclohexylcarbonyl)-2,3,6,7-tetrahydro-4H-pyrazino [2,1-a]isoquinolin-4-one, and Related compound C = 2-(N-Formylhexahydrohippuroyl-1,2,3,4-tetrahydroisoquinolin-1-one [53].

Differential Scanning Calorimetry (DSC) is an analytical technique which measures the heat flow into or out of a sample as a function of time and/or temperature. Plots showing differences in heat flow between a sample and reference, as a function of time or temperature, yield information on thermal transitions in a sample due to melting, crystallization, chemical reactions, glass transitions, and other exothermic (heat evolving) and endothermic (heat absorbing) transitions. For DSC analysis, samples with a mass between 3.0 and 3.5 mg were carefully weighed in aluminium crucibles, sealed with aluminium caps. The tests were carried out in a Mettler Toledo model DSC/TGA3+ differential exploratory calorimeter, under a dynamic nitrogen atmosphere with a flow rate of 80 mL/min and a heating rate of 10 °C/min, in the temperature range from 25 to 250 °C. The DSC equipment was previously calibrated with metallic zinc and indium.

### 3.1.4 Powder X-Ray Diffraction (PXRD)

PXRD or Powder X-Ray Diffraction is a method for measuring the X-Rays scattered by a crystalline sample as a function of the scattering angle. Analysis of this distribution gives a lot of information about the microstructure and properties of the sample. X-ray sample diffraction patterns were obtained on a Bruker diffractometer model D8-Advance (at UFF - *Universidade Federal Fluminense*), using CuKα radiation (λ for Kα1 = 1.54060 Å; λ for Kα2 = 1.54438 Å), 40 KV and 40 mA current, with scanning speed of 0.2 °/second in the 2θ range of 3-50 º.

### 3.1.5 Scanning Electronic Microscopy (SEM)

SEM is a class of electron microscopy that uses a high-energy electron beam to scan the samples and provide a high magnification and resolution image. The electron beam from the electron gun interacts with the electrons on the sample surface and produces specific signals about the topography [294]. The SEM images are obtained by analyzing the signals from the secondary and backscattered electrons. Non-conductive samples need to be coated by a layer of a conductive element such as gold or platinum.

The SEM analyses were performed at the Rudolph Barth Electron Microscopy Platform (IOC/Fiocruz), using an electronic microscope Jeol, model JSM6390LV and a sputter coated (Deton Vaccum Desck IV) to apply an ultra-thin coating of platinum (Pt) on the non-conducting samples before analyses.

A small piece of double-sided tape was added over the stub. Then, an aliquot from the vial containing the sample by random selection with the aid of a spatula. It added to the tape attached to the stub. Light strokes were made on the stub to disperse the particles into the tape, and the stub was subjected to 10 mA plating for about 3 minutes and continuous argon flow.

The SEM analysis were performed on the Pt-coated samples. During the analysis, images were obtained from the four representative quadrants of the stub. For this, we used the methodology of dividing the stub into four quadrants, thus contemplating several microphotographs that provide a representative analysis. Schematically, Figure 31 shows the preparation of the stub and its division for the capture of images in different regions to guarantee good sampling.

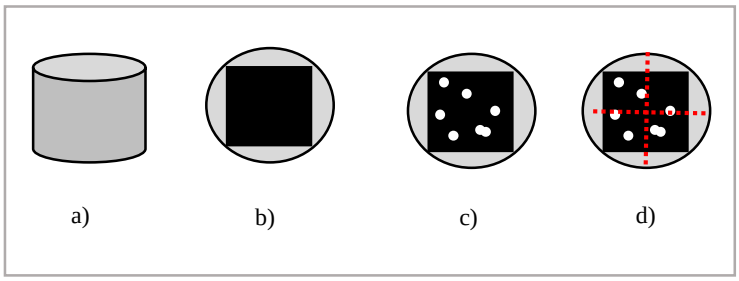


Figure 31 a) Schematic representation of a stub; b) a top view representation of a stub with the presence of the carbon-coated double-sided tape; c) representation of the top view of a stub with the sample already added to the tape surface; d) (imaginary) stub for the purpose of representative images from different parts of the stub. Source: Author.

### 3.1.6 Particle Size Distribution by Laser Diffraction

The laser light diffraction technique used for the determination of particle-size distribution is based on the analysis of the diffraction pattern produced when particles are exposed to a beam of laser light. Sample dispersed at an adequate concentration in a suitable liquid or gas, passed through a laser. The light scattered by the particles at various angles is measured by a multi-element detector. These scattering pattern values are then transformed, using an appropriate optical model and mathematical procedure, to yield the proportion of total volume to a discrete number of size classes, forming a volumetric particle-size distribution. This is one of the most common techniques for particle size analysis on the pharmaceutical industries and a good practice is to develop and validate this method according to official and specifics guidelines such as American pharmacopeia [1] and International Organization for Standardization (ISO) [2].

In this thesis the procedure developed for PSD measurement was based on the assumptions described in ISO 13320 [295] and USP [296]. For the analysis of particle size distribution of the API used in this work, initially, the dispersion medium to be used in the well of the analysis equipment was prepared. About 2 g of praziquantel was added in three liters of purified water and subjected to magnetic stirring for four hours. The saturated solution was filtrated in a 0.45 µm cellulose membrane with a vacuum system. At the same time, 42 mg of surfactant (polysorbate 80) weighed in a glass beaker. Approximately 30 ml of the saturated filtered solution was transferred, and the aid of a spatula stirred vigorously until the complete solubilization of the surfactant. This solution was transferred to the beaker containing all the saturated and previously filtered solutions. The final solution was submitted to magnetic stirring for 5 minutes for complete homogenization.

The mass in the range of 27.5 ± 2.5 mg weighted and then transferred to a plastic test tube with a cap and conical bottom. 10 mL of surfactant-containing saturated praziquantel solution was added and stirred manually (up and down) about five times. The sample was vortexed for 5 minutes (speed 1, continuous mode) and inserted in the ultrasound for 01 min. At the end of the ultrasound time, the prepared suspension was immediately added to the equipment for reading. The saturated solution was also used as a sample dispersion medium and rinsed solution between each measurement. Finally, it was added for further sample addition.

### 3.1.7 Stereomicroscopy

Stereomicroscope is a type of optical microscope that offer lower resolution power where the magnification typically ranges between 6x and 50x while optical microscope have around 40x to 1,000x [294].

An Olympus SZX9 stereomicroscope (Olympus) was used, coupled to a camera of the same brand model Oly-220 to capture the images. The magnification was adjusted according to the characteristics of each sample and the purpose of the analysis.

### 3.1.8 Solubility studies of raw PZQ

Solubility studies of raw PZQ were performed following the standard shake flask method (Incubator Shaker SL 222, Solab) (Figure 32). Table 10 shows the different solvents in which the PZQ solubility will be experimentally determined.

Table 10. Composition of the different media used to evaluate the PZQ solubility.

| Medium | pH | Concentration of SLS (wt%) |
|---|---|---|
| Purified water | 7.2 | - |
| HCl 0,1 N | 1.2 | 0; 0.05; 0.1 and 0.2 |
| Acetate buffer | 4.5 | |
| Phosphate buffer | 6.8 | |

*Preparation of the dissolution media*: HCl 0.1 N medium was prepared according to USP 43 (2020) [3] by diluting HCL 0.1 N with purified water. Likewise, sodium acetate trihydrate was solubilized in purified water and acetic acid (2 N) was added to the solution and the pH was adjusted to 4.5. The third buffer medium, potassium phosphate monobasic, was solubilized in purified water and the pH was adjusted to 6.8 with 0.2 M sodium hydroxide. For the preparation of the respective media containing surfactant, the preparation procedure was the same as described above with the addition of sodium lauryl sulphate in various concentrations: 0.05 %, 0.1 %, and 0.2 % (wt).

*Solubility measurements (Figure 32)***Erro! Fonte de referência não encontrada.**: For that purpose, an excess amount of samples powder was added into 50 mL of each tested medium under magnetic agitation at 37 ± 0.5 °C. The samples of 2 mL were filtered (cellulose acetate filter, 0.22 µm) and collected to the vial at pre-determined time points (0.5 h, 1 h, 24 h or 48 h). The concentration of PZQ in water was measured by an HPLC system equipped with a UV-visible detector (with the same method described before). The experiments were carried out in triplicate and for all samples the final pH of the medium was recorded.

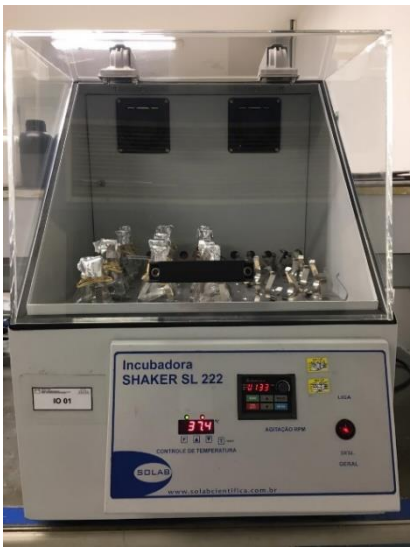


Figure 32. Experimental apparatus for PZQ solubility studies at 37°C ± 0.5°C. Source: Author.

### 3.1.9 Dissolution Profile

Dissolution tests were performed to investigate the PZQ release profile according the dissolution method described in USP for PZQ tablets [297]. Dissolution tests were executed using an USP apparatus 2 (Dissolutor VK7010, Varian) at 50 rpm with 900 mL of dissolution medium (0.1 N HCl with and without 0.2 % by weight of SLS[14]). Samples with the equivalent dose of 150 mg of PZQ was added directly to the dissolution medium at 37 °C. At predetermined time points (5, 10, 15, 30, 60, and 120 min), 5 ml of aliquots were withdrawn and immediately filtered (0.45 µm - PTFE) to the respective vial.

The collected samples were assayed by HPLC-UV, as previously described. All dissolution experiments were conducted at least in triplicate, and the SD (%) was calculated at each time point. Dissolution profile curve (amount of drug dissolved over time) was calculated using a calibration curve.

### 3.1.10 Stability studies

The solid raw materials (PZQ, PVPVA and SLS) were conditioned in glass plates and covered with parchment paper to avoid falling particles or dirt (Figure 33). The

[14] The dissolution profile of the PZQ was evaluated under two different conditions of dissolution medium: with and without the addition of SLS.

samples were stored during 30 days at three different conditions given in Table 11, to evaluate the physical stability of the samples.

The samples were analysed at pre-determined time points (starting point – t0, 15 and 30 days – t10 and t15, respectively). DSC, PXRD, SEM, and stereomicroscopy were performed according to the methodologies described in sections 2.1.3, 2.1.4, 2.1.5, and 2.1.7.

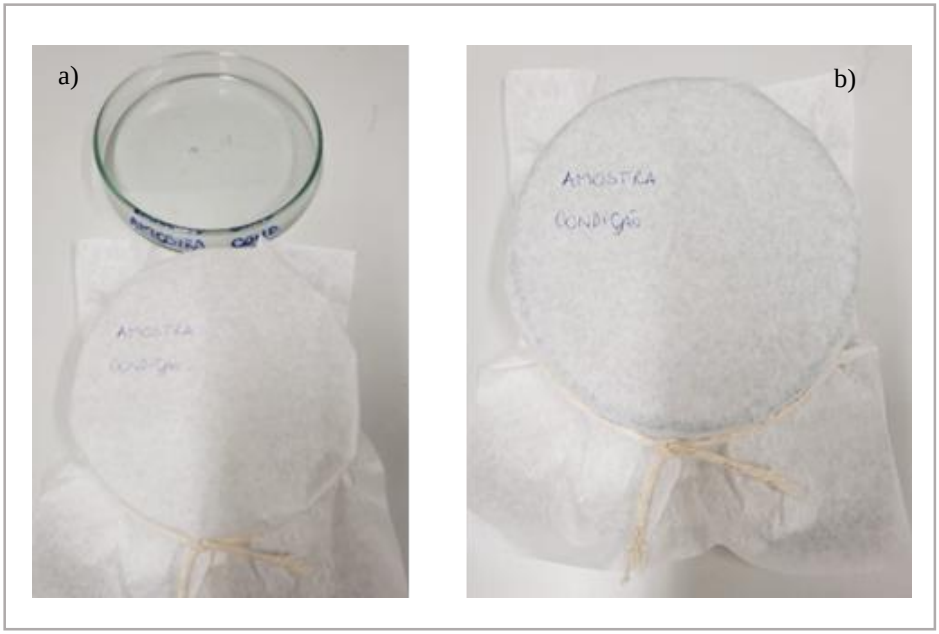


Figure 33. a) Petri dish and paper - recipient to put samples on stability; b) sample ready to climatic chamber for the stability study. Source: Author.

Table 11. Stability study conditions.

| ***Condition name*** | ***Storage condition*** | |
|---|---|---|
| | *Temperature (°C)* | *Relative humidity (%)* |
| Room temperature (RT)[1] | between 15 and 30 | 60 |
| Long-term stability (LT)[2] | 30 ± 2 | 75 ± 5 |
| Accelerated stability (AS)[3] | 40 ± 2 | 75 ± 5 |

[1] in the laboratory; [2,3] in a climatic chamber (Weis Technok /WK13')

# 4. RESULTS

## 4.1 Dosage of PZQ and related compounds

The PZQ used is approved according to the specifications of the American Pharmacopoeia [53], an official compendium recognized by the ANVISA in Brazil and by other regulatory agencies in the world, such as the FDA. It was subjected to dosage (PZQ content and content of organic impurities) by HPLC analysis, according to the experimental procedure described in 3.1.1 section.

Table 12 presents the API content for the raw PZQ sample and the concentration of each related compound. According to the references peak obtained by standards related compounds, it was possible to calculate the correspondent each one for the PZQ sample thanks to the relative retention time. No PZQ related compounds identified were higher than 0.06 wt%, indicating that the sample meets the requirements established by official compendiums for this API (NMT 0.2 % for each one). Also, PZQ was according to the specifications for drug content (100.6 ± 0.8 wt%).

Table 12. PZQ dosage and organic impurities determined by HPLC measurements.

| | ***Measured dosage (wt%)**** | ***Specification*** [53] |
|---|---|---|
| PZQ (raw material) | 100.60 ± 0.8 | 98.5 – 101.0% |
| Related compound A | 0.004 ± 0.0001 | |
| Related compound B | 0.047 ± 0.0005 | Max 0.2% |
| Related compound C | 0.002 ± 0.0003 | |

*Values represent the standard deviation, n = 2

## 4.2 Thermogravimetric Analysis (TGA)

TG analysis can provide a fingerprint of the sample's thermal behaviour and is used as a basis for determining the initial stages of the development of the DSC method such as endpoint run temperature. All percentage results regarding the mass variations of pure compounds are presented in Table 13.

Table 13. Mass variation from TG analysis for pure compounds.

| ***Pure compounds*** | ***Δm (%)*** | | | | | | |
|---|---|---|---|---|---|---|---|
| | ***RT**** | | | ***30 °C / 75 %*** | | ***40 °C / 75 %*** | |
| | ***t0*** | ***t15*** | ***t30*** | ***t15*** | ***t30*** | ***t15*** | ***t30*** |
| PZQ | 0.036 | 0.099 | 0.084 | 0.209 | 0.099 | 0.223 | 0.105 |
| | 0.053 | 0.110 | 0.089 | 0.217 | 0.101 | 0.216 | 0.117 |
| PVPVA | 4.545 | 5.383 | 7.047 | 10.857 | 12.140 | 10.887 | 11.228 |
| | 4.276 | 5.572 | 7.070 | 10.767 | 11.950 | 10.527 | 10.948 |
| SLS | 1.323 | 0.853 | 0.945 | 2.138 | 1.233 | 1.523 | 0.774 |
| | 1.329 | 0.843 | 1.033 | 2.113 | 0.535 | 1.532 | 0.786 |

*RT = room temperature

The results show that praziquantel is anhydrous with a mass loss of less than 0.1 %. The polymer (PVPVA) is hygroscopic and absorbs water over time, depending on the storage condition, unlike surfactant (powder), which does not vary by more than 0.5 wt% at room temperature and about 1 wt% under stress conditions.

### 4.3 Differential Scanning Calorimetry (DSC)

The heat flow (HF) is plotted as a function of temperature and shows the DSC curves obtained for the pure compound, PZQ, PVPVA, and the surfactant SLS which will be used as the third component in some ASD formulations (Figure 34).

The DSC curve for PZQ shows an endothermic signal at 140.77 °C ($T_{peak}$ - mean, n = 2), according to the literature $T_m$ data for the racemic form [298][74][161]. The DSC analysis of the polymer demonstrated a variation at approximately 110 ºC, probably related to the loss of mass that was confirmed by the TG analysis (4.4 %) (4.2 section) [299].

For the surfactant SLS, Figure 34 shows an endothermic event starting at around 90 ºC, followed by the melting of the material around 190 ºC and then degradation from 200°C.

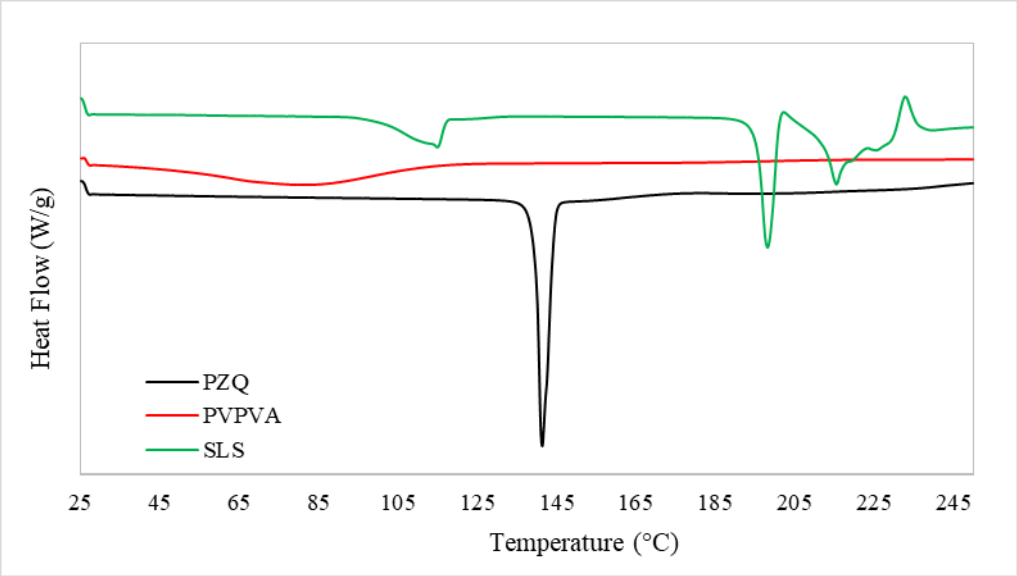


Figure 34. DSC curves of pure compounds: PZQ, PVPVA and SLS.

As explained, all materials were exposed to different environmental conditions for 30 days and they were monitored by different techniques, among them, DSC analysis. Figure 35 shows the DSC curves obtained during the stability study of PZQ at the three pre-fixed analysis points (t0, t15 and t30).

A single endothermic event, characteristic of the praziquantel fusion, was observed for all the studied conditions. Table 14 shows the values of fusion enthalpy ($\Delta H_{fusion}$) and fusion temperature ($T_{onset}$ and $T_{peak}$), respectively.

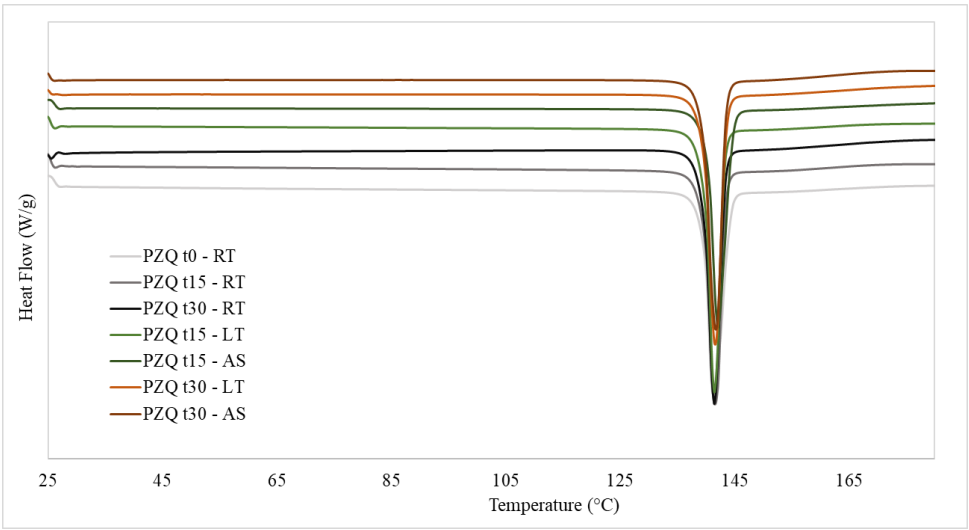


Figure 35. DSC curves of PZQ under different conditions of stability study.

Table 14. PZQ fusion enthalpy ($\Delta H_{fusion}$) and fusion temperature ($T_{onset}$ and $T_{peak}$) under different storage conditions.

| ***Thermal behaviour of PZQ - Stability study for 30 days*** | | | | | | | |
|---|---|---|---|---|---|---|---|
| **$\Delta H_{fusion}$ (J/g)** | | | | | | | |
| | **RT** | | | **LT (30°C/75%)** | | **AS (40°C/75%)** | |
| | **t0** | **t15** | **t30** | **t15** | **t30** | **t15** | **t30** |
| PZQ | 101.47 | 99.29 | 104.93 | 103.49 | 106.67 | 100.40 | 107.67 |
| | 99.37 | 101.36 | 103.85 | 103.54 | 109.67 | 100.43 | 109.99 |
| **Average** | **100.4** | **100.3** | **104.4** | **103.5** | **108.2** | **100.4** | **108.8** |
| SD | 1.48 | 1.46 | 0.76 | 0.04 | 2.12 | 0.02 | 0.14 |
| **$T_{onset}$ (°C)** | | | | | | | |
| | **RT** | | | **LT (30°C/75%)** | | **AS (40°C/75%)** | |
| | **t0** | **t15** | **t30** | **t15** | **t30** | **t15** | **t30** |
| PZQ | 139.24 | 139.31 | 139.28 | 139.34 | 139.28 | 139.29 | 139.21 |
| | 139.18 | 139.25 | 139.30 | 139.19 | 139.29 | 139.89 | 139.34 |
| **Average** | **139.2** | **139.3** | **139.3** | **139.3** | **139.3** | **139.6** | **139.3** |
| SD | **0.04** | **0.04** | **0.01** | **0.11** | **0.01** | **0.42** | **0.09** |
| **$T_{peak}$ (°C)** | | | | | | | |
| | **RT** | | | **LT (30°C/75%)** | | **AS (40°C/75%)** | |
| | **t0** | **t15** | **t30** | **t15** | **t30** | **t15** | **t30** |
| PZQ | 140.66 | 140.42 | 140.79 | 140.53 | 140.89 | 140.64 | 141.10 |
| | 140.87 | 140.63 | 140.83 | 140.69 | 140.70 | 141.43 | 140.95 |
| **Average** | **140.8** | **140.5** | **140.8** | **140.6** | **140.8** | **141.0** | **141.0** |
| SD | **0.15** | **0.15** | **0.03** | **0.11** | **0.13** | **0.56** | **0.11** |

The physical stability of raw PZQ at 30 ºC/40 ºC and 75 % RH in a period of 30 days was confirmed by DSC and TG results:

- any thermal change was detected in the DSC curves, keeping the single endothermic fusion event at around 140 ºC for all storage conditions.
- very small mass loss of approximately 0.1 % detected by TG analysis (Table 14).

This physical stability was expected since a similar behaviour was reported [37] for PZQ exposed to close environment conditions (40 °C/75 % RH) for 90 days.

### 4.4 Powder X-Ray Diffraction (PXRD)

Figure 36 shows the PXRD diffractogram for PZQ, PVPVA and SLS samples, revealing the crystalline nature of PZQ and SLS and the amorphous nature of the polymer.

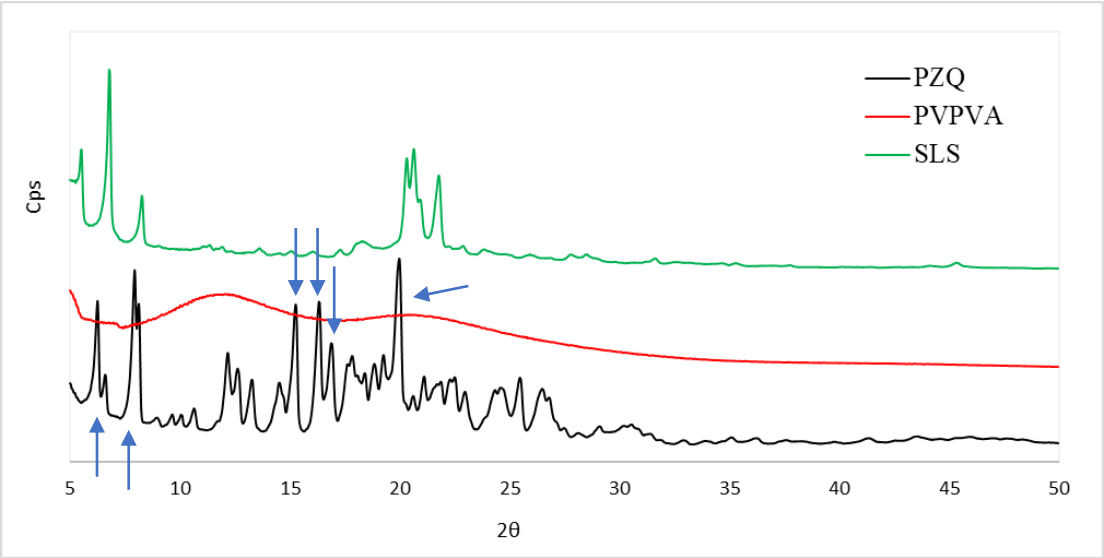


Figure 36. Diffractogram pattern of the pure compounds (PZQ, PVPVA, and SLS) and indication of the characteristic diffraction angles for racemic PZQ.

To complete the analysis of these results, a previous study published by LARA et al. (2013) performed with PZQ cocrystals is mentioned here. During this work, it was necessary to characterize the crystal structure of PZQ using monocrystal X-ray diffraction. As one of the results, the crystalline phase of PZQ (racemate) was elucidated and published in *The Cambridge Crystallographic Data Centre* (CCSD) (see Table 2 - Chapter 2) [10], [33], [73] . Comparing the diffraction pattern of raw PZQ with that in the Chapter 2 (item 3.5), the racemate form of our raw PZQ is confirmed with similar angles of diffraction signals (2θ - 6.3, 6.7, 8.0, 8.18, 15.4, 16.3, 17.5 and 20.1, indicated by blue arrow on Figure 36). The difference in signal intensity is probable related, on one side, to differences in method sensibility (PXRD and monocrystal XRD) and, on the other, to differences on the degree of crystallinity between samples.

Figure 37 shows the diffraction patterns for raw PZQ during the stability test, confirming its unchanged solid state after exposition to the different environment conditions. This result corroborates with the data obtained with DSC analysis.

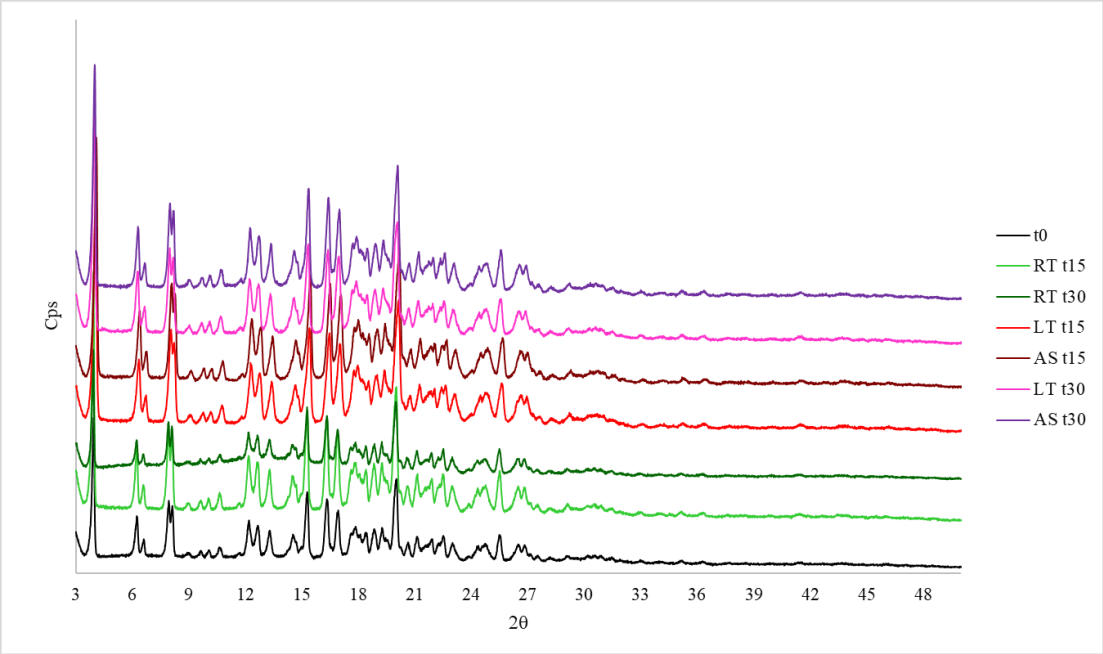


Figure 37. PXRD diffractogram obtained for the PZQ exposed to different environment conditions (RT, LT, and AS) for 30 days.

Similarly, the polymer SLS and the solid surfactant PVPVA exposed to the same stability test were analysed and the PXRD diffractograms obtained are presented in Figure 38 and Figure 39, respectively.

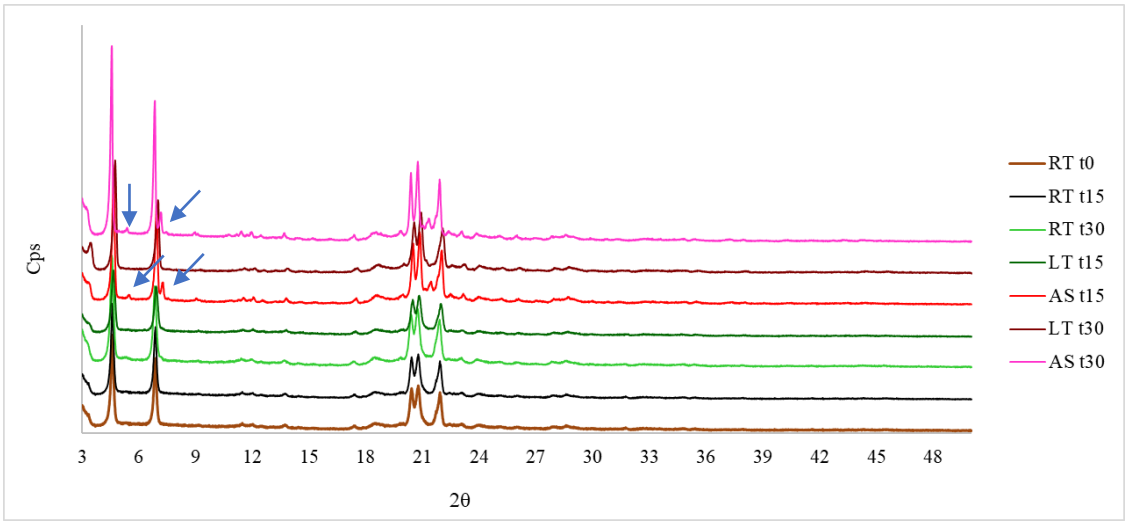


Figure 38. PXRD diffractograms for SLS samples exposed to different environment conditions (RT, LT, and AS) for 30 days.

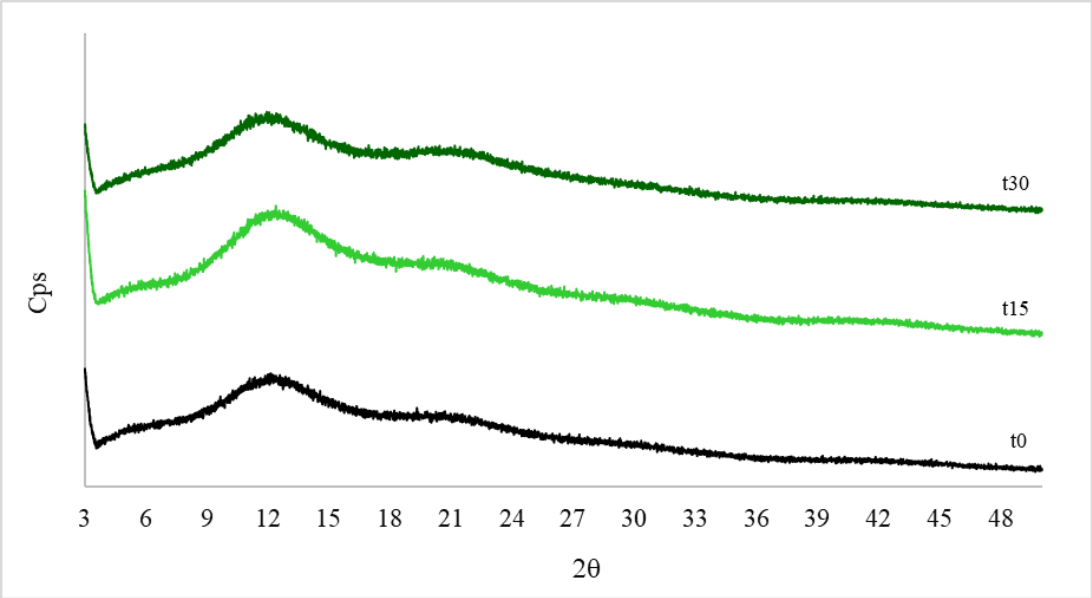


Figure 39. XRD diffractograms for PVPVA samples exposed to room conditions RT for 30 days.

The surfactant SLS showed all characteristics diffraction signals and others two small diffraction peaks (angles at 5.4 and 7.2) for the samples after 15 and 30 days of stability study under AS condition (40 ºC and 75% RH).

The PVPVA polymer samples were analysed only under ambient temperature conditions and remained unchanged (amorphous). At t15, the samples were physically modified (fine powder to agglomerates) when exposed to the humid environment, as will be evidenced by stereomicroscopy in item 3.1.7.

## 4.5 Scanning Electronic Microscopy (SEM)

The SEM microphotographs of the commercial PZQ particles are shown in Figure 40. According to the American pharmacopoeia [300], SEM images show that the predominant morphology in the PZQ sample is columnar. The columnar microstructure resulted from an oriented attachment growth mechanism, in which nuclei precipitating from solution attached along preferred crystallographic facets to form highly oriented, size-quantized columnar grains [301].

Still, with the dimensions of the primary particles, it is possible to say that the material has characteristics of a micronized (milled) sample. This material was probably ground after synthesis. Generally, this type of procedure is adopted to improve the dissolution of pharmaceutical ingredients that are poorly soluble in water.

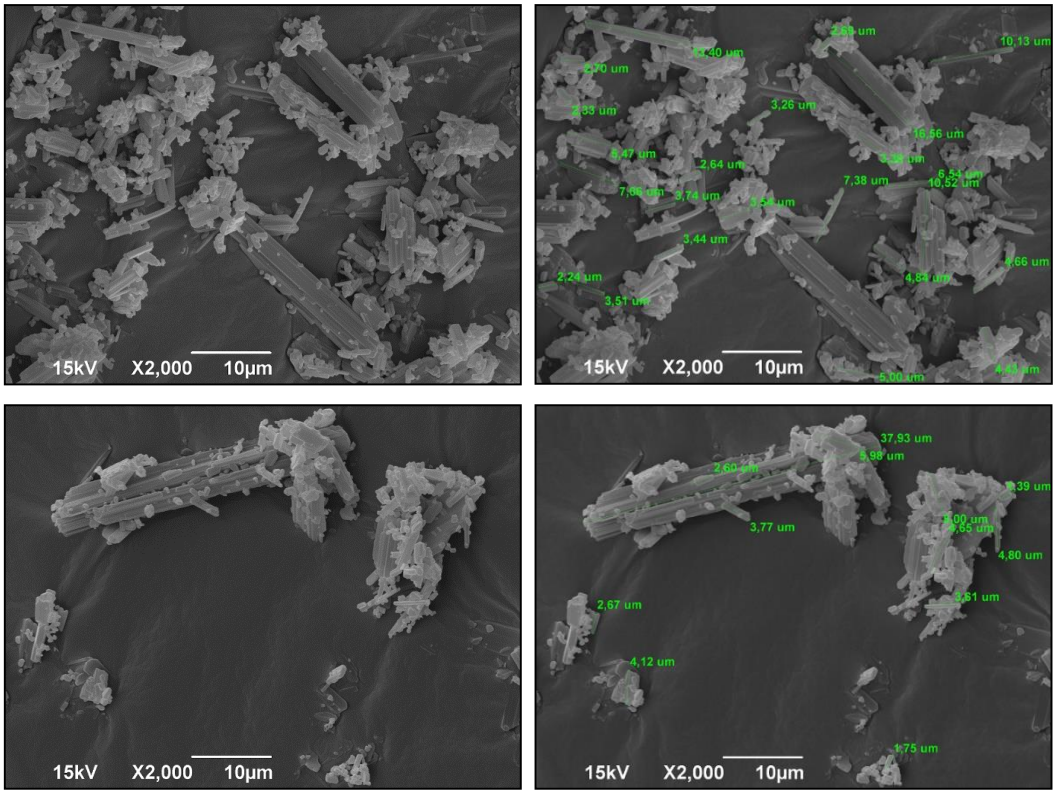


Figure 40. SEM images of the raw PZQ particles.

The SEM images of polymer (PVPVA) and the surfactant (SLS) are shown in Figure 41 and 42. The polymer's primary particles are predominantly spherical in shape, and the surfactant used has a rounded morphology of agglomerated primary particles and are in accordance with that described by the respective technical documents [292], [293].

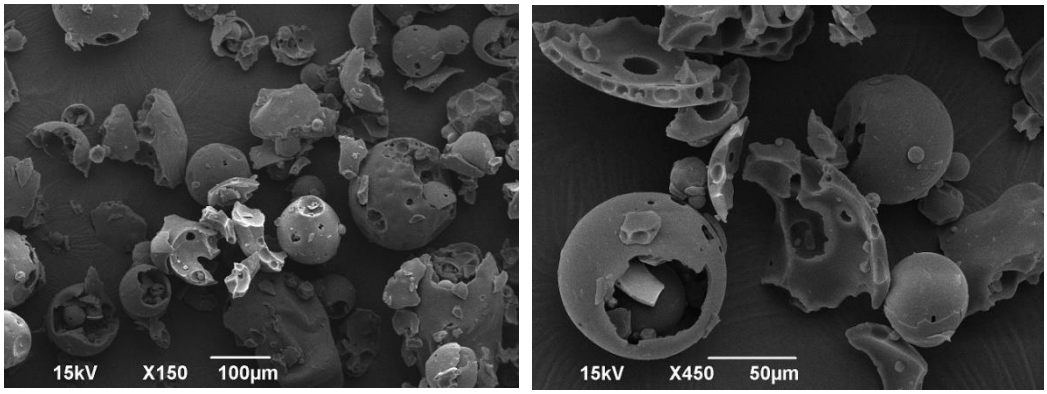


Figure 41. SEM images of raw PVPVA particles.

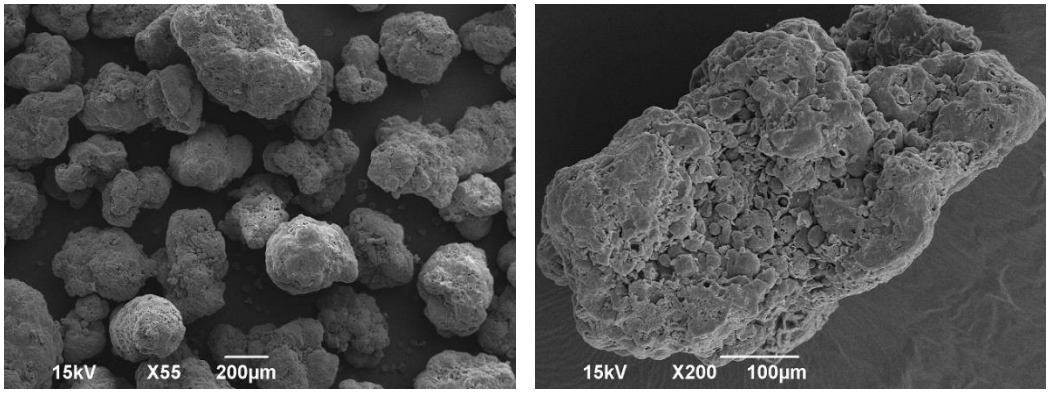


Figure 42. SEM images of raw SLS particles.

## 4.6 Stereomicroscopy

Stereomicroscopic images of the raw materials were obtained to verify their physical aspect behaviour under different storage conditions. Figure 43, 44 and 45 represent the images at different times and conditions of temperature and relative humidity for PVPVA, SLS, and PZQ, respectively.

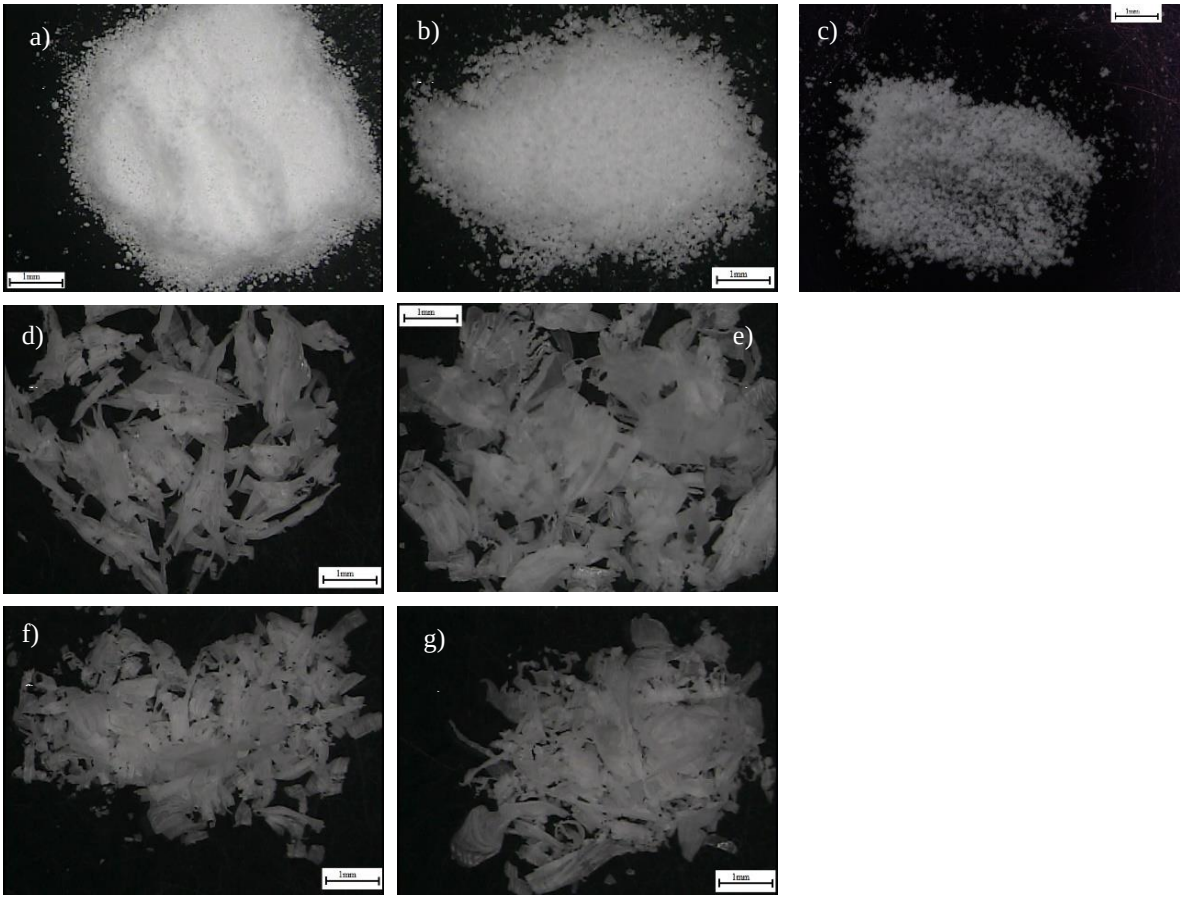


Figure 43. Stereomicroscopy images of PVPVA: a) RT t0; b) RT t15; c) RT t30; d) LT t15; e) AS t15; f) LT t30; AS t30.

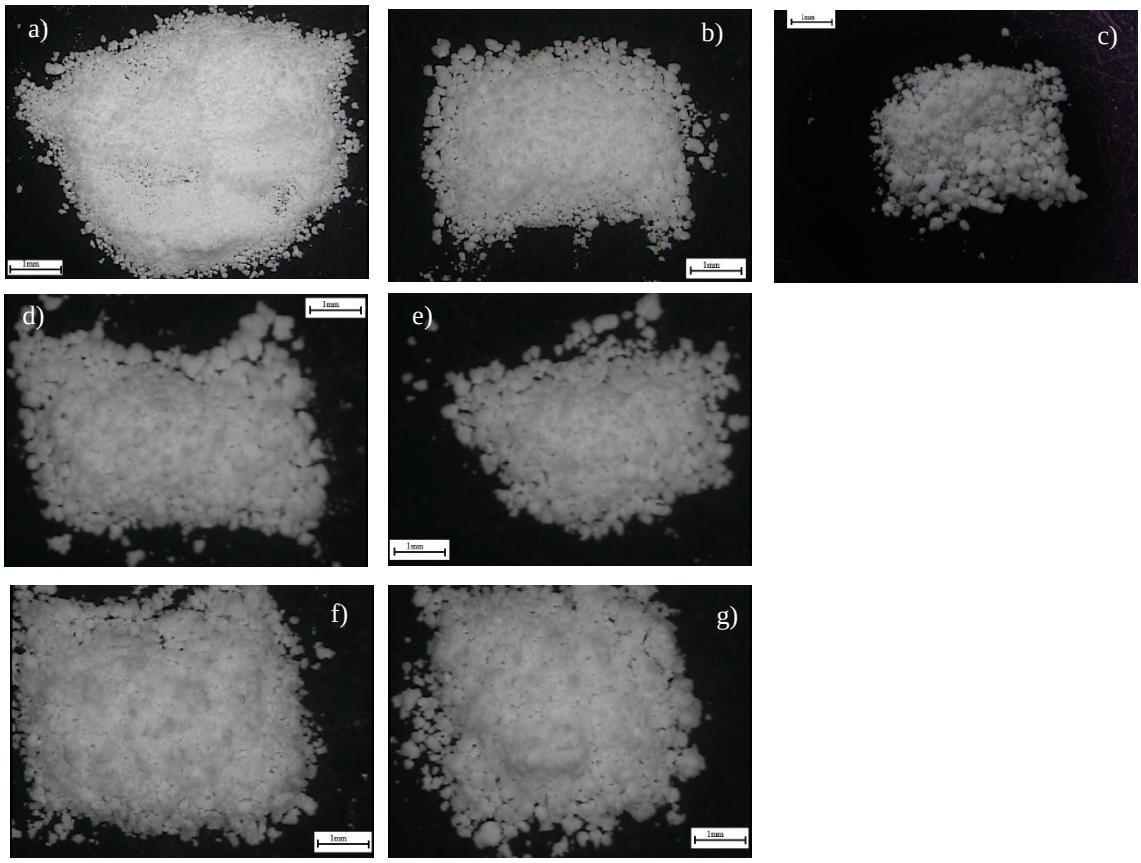


Figure 44. Stereomicroscopy images of SLS: a) RT t0; b) RT t15; c) RT t30; d) LT t15; e) AS t15; f) LT t30; AS t30.

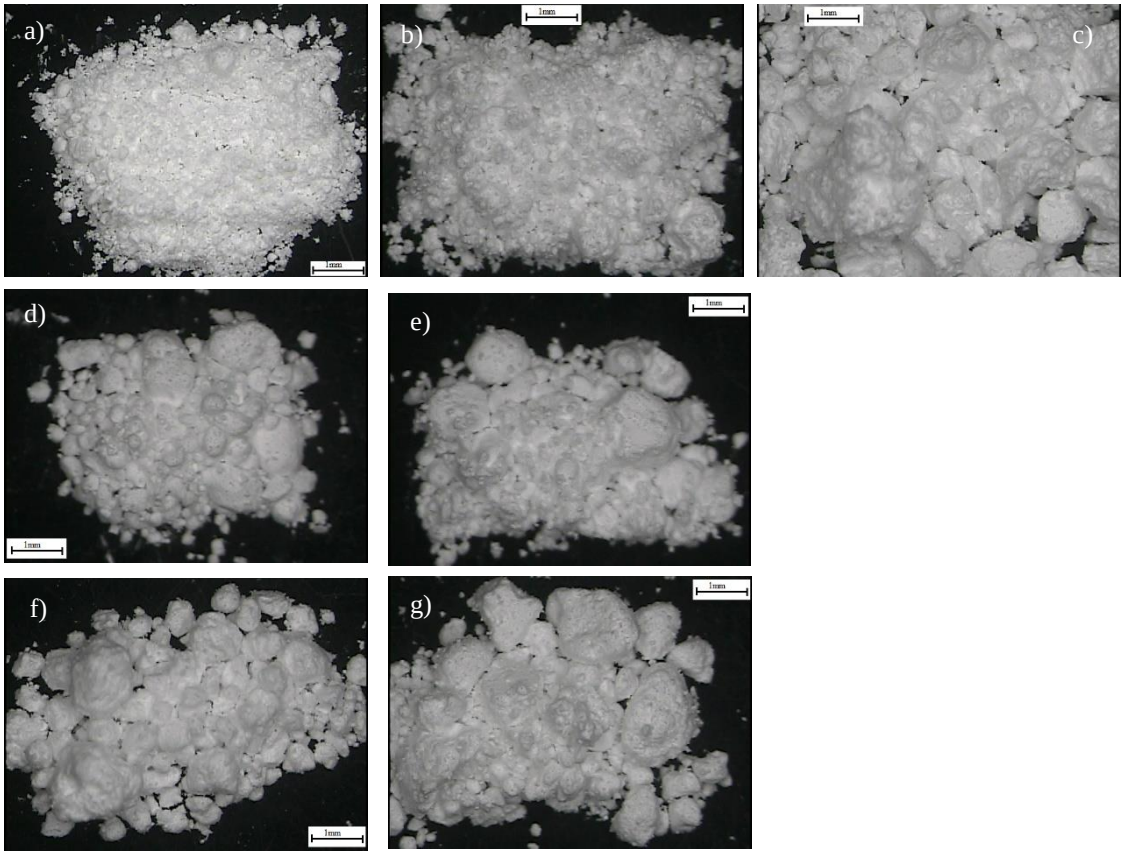


Figure 45. Stereomicroscopy images of PZQ: a) RT t0; b) RT t15; c) RT t30; d) LT t15; e) AS t15; f) LT t30; AS t30.

The images of the commercial polymer (PVPVA) after insertion in the climatic chamber present structures in the form of "splinters". However, this appearance resulted from scraping with a spatula to remove the sample that adhered to the glass plate. The polymer was influenced by environmental conditions, changing its initial physical state (fine powder to agglomerate).

The SLS and PZQ remained similar to the original state and showed no physical changes like the polymer.

## 4.7 Particle size distribution (PSD) by laser light diffraction

The method used to analyse the particle size distribution of PZQ was previously developed and validated. The data were recorded in an official notebook of Farmanguinhos/Fiocruz, and a validation report was generated (08/2017) with all detailed results.

The method validation was carried according to the parameters indicated in the American Pharmacopoeia [296] and ISO 13320-1 [295]. Three PZQ samples were used from different manufacturers[15] to address the variability of characteristics related to dimension during the validation process. The summarized results of the validation are given in Table 15.

Table 15. Summary of the results obtained to validate the process for the PZQ PSD method by laser light diffraction.

| ***PZQ PSD - Validation*** | | | | |
|---|---|---|---|---|
| ***Sample*** | $\mathbf{d_x}^*$ | ***System repeatability (CV%)*** | ***Methodology repetibility (CV%)*** | ***Intermediated precision (CV%)*** |
| PZQ Nº 6 | $d_{10}$ | 0.96 | 5.94 | 4.87 |
| | $d_{50}$ | 2.75 | 11.93 | 9.91 |
| | $d_{90}$ | 1.66 | 8.97 | 7.17 |
| PZQ Nº 7 | $d_{10}$ | 2.93 | 3.82 | 10.02 |
| | $d_{50}$ | 4.13 | 3.62 | 6.37 |
| | $d_{90}$ | 4.46 | 6.31 | 5.02 |
| PZQ Nº 8 | $d_{10}$ | 2.02 | 0.47 | 3.19 |
| | $d_{50}$ | 4.58 | 0.86 | 4.82 |
| | $d_{90}$ | 6.66 | 5.39 | 4.65 |

$* d_x =$ particle diameter corresponding to x % of the cumulative undersize distribution (here by volume)

The PSD analysis of the PZQ used in this work was performed using the developed and validated method. Table 16 shows the results of particle size distribution by scattering laser light obtained for the three samples of the PZQ.

Table 16. PSD of pure PZQ used in this thesis

| | ***PSD (μm)**** | | | | |
|---|---|---|---|---|---|
| | $\boldsymbol{d_{10}}$ | $\boldsymbol{d_{50}}$ | $\boldsymbol{d_{90}}$ | $\boldsymbol{d_{4.3}}$ | ***Span*** |
| PZQ | 1.04 ± 0.01 | 3.14 ± 0.06 | 8.59 ± 0.35 | 4.35 ± 0.21 | 2.40 ± 0.09 |

* Values represent the standard deviation, n = 3

[15] More details about this samples on the official notebook.

Figure 46 shows the cumulative and incremental distribution curves for the mean (n = 3) of PZQ.

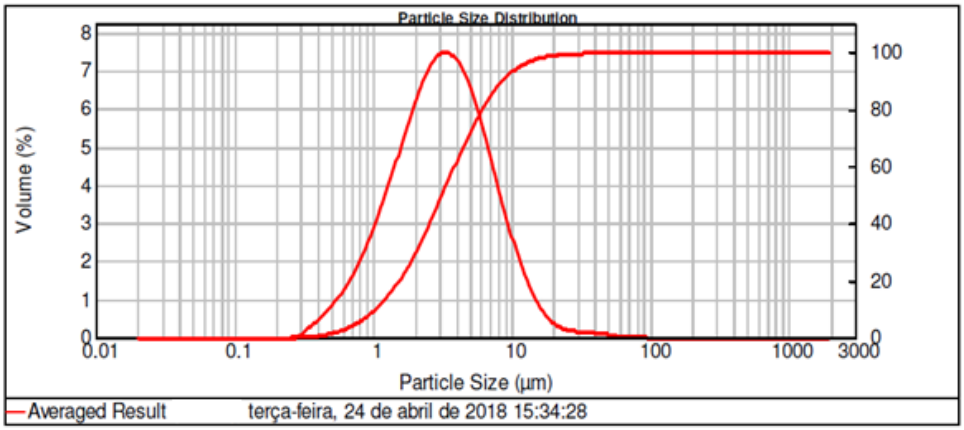


Figure 46. Cumulative and incremental PSD curve of PZQ.

PZQ is in accordance with the nomenclature identification being categorized as micronized. Most of its particles (90 %) have dimensions less than 9 µm. This analysis uses as a premise the approximation of the measurement performed to an equivalent sphere. In contrast, microscopy is a direct analysis and is used to validate the result obtained, especially for PSD by scattering laser light [296]. SEM images obtained for the PZQ corroborate the PSD results obtained by laser diffraction analysis.

## 4.8 PZQ solubility in aqueous media

HCl 0.1 M and, phosphate buffer pH 6.8 are commonly proposed in the literature [37][63] for the evaluation of PZQ solubility in pH 1.2 and pH 6.8, respectively. Here, raw PZQ solubility was evaluated in three media (HCl 0.1 M, acetate buffer pH 4.5 and phosphate buffer pH 6.8) in absence or presence of different concentrations of surfactant (SLS).

The results are grouped in Table 17. From these data, the presence of SLS did not cause a significant variation on the solubility in HCL 0.1M pH 1.2, contrarily to the other two media were the PZQ solubility increased significantly ($p < 0.05$) as the SLS concentration was increased.

Table 17. Raw PZQ solubility in different aqueous media at 37 °C ± 0.5 ºC.

| *Medium* | *Inicial pH* | *Final pH* | *Solubility (mg/mL)* |
|---|---|---|---|
| HCl 0.1 M | 1.09 ± 0.01 | 1.11 ± 0.01 | 0.19 ± 0.05 |
| HCl 0.1 M with 0.05 % SLS | 1.17 ± 0.01 | 1.15 ± 0.01 | 0.23 ± 0.04 |
| HCl 0.1 M with 0.1 % SLS | 1.15 ± 0.01 | 1.20 ± 0.03 | 0.21 ± 0.02 |
| HCl 0.1 M with 0.2 % SLS | 1.17 ± 0.01 | 1.15 ± 0.01 | 0.18 ± 0.02 |
| Acetate buffer pH 4.5 | 4.52 ± 0.01 | 4.52 ± 0.02 | 0.20 ± 0.04 |
| Acetate buffer pH 4.5 with 0.05 % SLS | 4.53 ± 0.01 | 4.54 ± 0.02 | 0.29 ± 0.01 |
| Acetate buffer pH 4.5 with 0.1 % SLS | 4.52 ± 0.01 | 4.52 ± 0.01 | 0.35 ± 0.02 |
| Acetate buffer pH 4.5 with 0.2 % SLS | 4.53 ± 0.00 | 4.53 ± 0.01 | 0.37 ± 0.01 |
| Phosphate buffer pH 6.8 | 6.73 ± 0.00 | 6.75 ± 0.00 | 0.20 ± 0.02 |
| Phosphate buffer pH 6.8 with 0.0 5% SLS | 6.83 ± 0.00 | 6.83 ± 0.01 | 0.32 ± 0.02 |
| Phosphate buffer pH 6.8 with 0.1 % SLS | 6.83 ± 0.01 | 6.82 ± 0.01 | 0.36 ± 0.07 |
| Phosphate buffer pH 6.8 with 0.2 % SLS | 6.82 ± 0.02 | 6.81 ± 0.01 | 0.42 ± 0.03 |

According to Resolution-RDC No. 37/201 [302], a drug is considered highly soluble when its highest dose administered orally (maximum dose per administration described in package insert) is completely solubilized in a volume up to 250 mL of each of the solutions tested within the range of physiological pH at 37 ± 1 ºC. According to the package insert for the PZQ reference drug, Cisticid® 500 mg [48], the highest dose administered is 600 mg of Praziquantel. The measured solubility data confirmed that the API used in this study does not meet the recommended criteria to be considered highly water-soluble, which was expected considering its classification as class II drug, according to the biopharmaceutical classification system [303].

In addition to these data, the water solubility of the PZQ was analysed. For this experiment, measurements were made up to 48 hours, and the results are shown in Table 18.

Table 18. Raw PZQ water solubility at 37 °C ± 0.5 ºC.

| *Time (h)* | *Solubility (mg/mL)** |
|---|---|
| 0.5 | 0.174 ± 0.02 |
| 1 | 0.181 ± 0.15 |
| 24 | 0.184 ± 0.03 |
| 48 | 0.195 ± 0.01 |

* Average value, n = 2

As mentioned before, several studies in the literature explore different tools to improve the solubility of the PZQ and solubility in water. The evaluation method is generally based on the excess addition of API in water and agitation of the suspension for 24 to 72 hours. The difference between the studies is in the temperature used to experiment. Most studies make a physical-chemical assessment using 20 ºC or 25 ºC to conduct the analysis and the results are around 0.14 mg/mL [18], [33], [53], [60], [304]. However, when a biopharmaceutical evaluation is desired, a temperature of 37 ºC is used and our results are similar for the common values reported at lower bath temperature.

### 4.9 Dissolution profile

Some preliminary experiments were carried out by powder dispersion according to the pharmacopeia method proposed for PZQ tablets in acid medium (HCl 0.1 N). However, the presence of surfactant in the medium might have an impact on the powder dispersion, modifying the powder wettability and then the initial dissolution time. For this reason, we have decided to perform dissolution tests without the addition of surfactant too. The difference on the dissolution kinetics obtained under these two different conditions was clearly demonstrated (Figure 47).

The dissolution results in the medium without surfactant revealed a slow and incomplete dissolution profile [24]. A study evaluating how PZQ was mixed with a surfactant to increase dissolution found that PZQ alone had a similar dissolution profile (about 26 % in 90 minutes) [24]. In the same vein, a recent study that evaluated the use of smart excipients, such as layered double hydroxide (LDH) to promote an appropriate delivery system, showed a similar result for pure PZQ [25]. Although the use of surfactant (0.2 wt% SLS) is described in the pharmacopeial method for evaluating praziquantel tablets, its use in the development of new formulations or intermediates may not be favourable to discriminate the differences between samples. We have then concluded that the acid medium without surfactant was the discriminating medium to be used throughout that thesis.

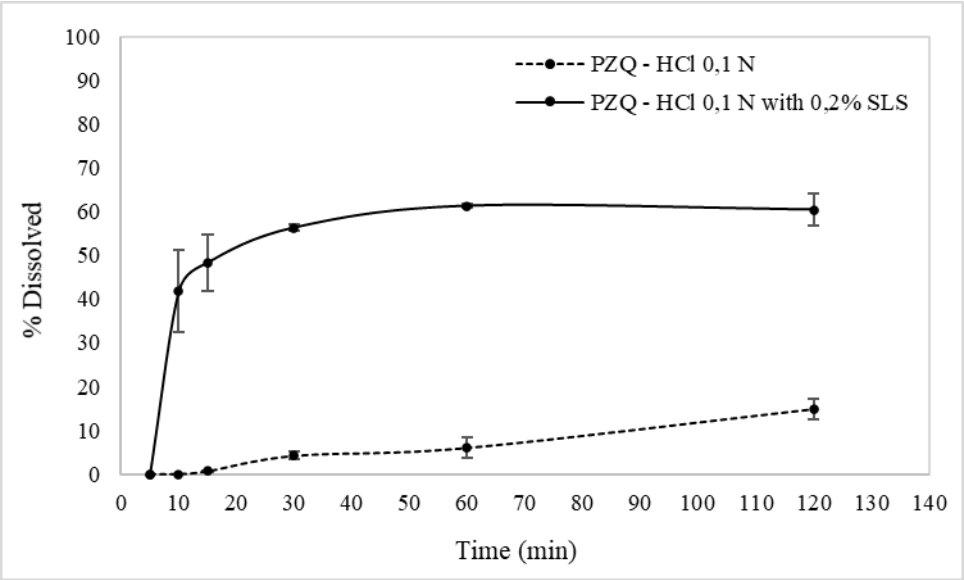


Figure 47. PZQ in vitro dissolution profile in acidic medium added (or not) of 0.2 wt% SLS.

The dissolution results in the medium without surfactant reveals a slow and incomplete dissolution profile [24]. A study evaluating how PZQ was mixed with a surfactant to increase dissolution found that the unprocessed material has a similar dissolution profile (about 26 % in 90 minutes) [24]. In the same vein, a recent study that evaluated the use of smart excipients, such as layered double hydroxide (LDH) to promote an appropriate delivery system, showed a similar result for pure PZQ [25]. Although the use of surfactant (0.2 wt% SLS) is described in the pharmacopeial method for evaluating praziquantel tablets, its use in the development of new formulations or intermediates may not be favourable to discriminate the differences between samples.

## 5. CONCLUSIONS

The most important pure materials were characterized.

The raw API (PZQ) refers to the racemic crystal structure described as commercial in the literature, confirmed by DSC, PXRD and image analysis.

Both, the raw PZQ and the polymer carrier (PVPVA) of interest in this thesis, are physically stable after exposition to different environment conditions for 30 days.

The low PZQ solubility at 37 °C ± 1 ºC. was demonstrated:

- in purified water, in accordance with literature data (0.18 - 0.2 mg/mL),
- in acidic medium (HCl 0.1 N), around 0.2 mg/mL, not influenced by the addition of surfactant (0.2 wt% SLS),
- in phosphate and acetate buffers (pH 4.5 and 6.8, respectively), equivalent to that in acidic medium, but in these media, the addition of 0.2 wt% SLS led to an increase of PZQ solubility (0.37 mg/mL in acetate buffer pH 4.5 and 0.42 mg/mL in phosphate buffer pH 6.8).

The dissolution profile of the raw PZQ was evaluated according to the pharmacopeial method described for praziquantel tablets, evidencing the low dissolution rate (15 wt% in 2h) which was strongly affected by the addition of 0.2 wt% SLS in the medium (60 wt% in 2h). This background can be decisive for the discrimination of the dissolution profiles between different formulations and allowed us to decide not to use surfactant in the dissolution tests in the subsequent studies.

# CHAPTER 4 - DETERMINATION OF PZQ SOLUBILITY IN PVPVA BY RECRYSTALLIZATION FROM SUPERSATURATED SOLID SOLUTION

## 1. INTRODUCTION

It is widely discussed in the literature that, although ASDs have been a technological alternative for poorly water-soluble drugs, a critical point of these systems is their physical stability.

One of the main parameters affecting the physical stability of an ASD is the drug solubility in the carrier, because this value determines the maximal drug load without a risk of phase separation and recrystallization. Phase-diagrams have been experimentally obtained by following the recrystallization of the drug from a supersaturated homogeneous drug-polymer solid solution, commonly produced by processes as solvent casting, comilling or, more recently, spray drying.

In the thesis, a composition-temperature phase diagram Praziquantel (PZQ) - Kollidon® VA 64 (PVPVA) was established and is one of the main subjects treated in this Chapter.

The first part is dedicated to the generation and characterisation of supersaturated solid solutions containing PZQ and the polymer Kollidon® VA 64 (PVPVA) by spray drying process.

Unexpectedly, in some batches of spray-dried powders produced in this study, traces of crystalline forms of PZQ were found, which are different from the initial racemic form. As mentioned before, two polymorphic forms (B and C) of praziquantel have been recently described by researchers. They present different physical and chemical characteristics compared to the racemic PZQ. It will be shown in the end of this part that the traces of crystallinity found in some of the supersaturated solid solutions could correspond to one of these polymorphic forms of PZQ recently reported.

The second part of the Chapter deals with the construction of the temperature-composition PZQ - PVPVA phase diagram, by means of a thermal study of recrystallization with one of the spray-dried supersaturated solid solutions presented in the first part of the Chapter.

For the sake of clarity, the two parts will be presented separately.

# PART 1 - GENERATION AND CHARACTERIZATION OF SUPERSATURATED PZQ SOLUTIONS BY SPRAY DRYING

## 1. METHODS

### 1.1. Generation of supersaturated PZQ solutions by spray drying

Spray drying was the process used to generate supersaturated solutions of PZQ in Kollidon® VA 64 (PVPVA) with 50 wt% and 70 wt% of theoretical loads of PZQ.

A Buchi B-290 mini spray dryer (Buchi Labortechnik AG, Flawil, Switzerland) equipped with Inert Loop B-295 and an integrated two-fluid 0.7 mm nozzle was used (Figure 48). The feeding solution was prepared by dissolving PZQ in a 10 wt% solution of PVPVA in absolute ethanol 99.9 %. The inlet air temperature was set to 80 ± 2°C (dry method 1) or 110 ± 2 °C (dry method 2), aspiration rate of 100 % (i.e., 35 $m^3$/h), compressed nitrogen atomization flow rate set at 600 L/h and liquid feed rate of 2.8 to 7.2 mL/min. The dry powder was recovered in a cyclone. Ethanol in the outlet gas flow was continuously condensed for further disposal.

The formulation and operating conditions used are summarized in Table 19. Different compositions of the binary PZQ: PVPVA system were prepared by spray drying. It aimed to obtain an amorphous solid solution of PZQ to use on the determination of the API-polymer solubility curve by the recrystallization method (DSC).

For purposes of comparison, physical mixtures (PM) of PZQ in PVPVA with 50 w%t and 70 wt% of PZQ were produced by manual mixing (coded PM 50 and PM 70, respectively).

All samples were stored in a glass flask protected from light and inside a desiccator stored at 20°C.

Table 19. Composition, process parameters to produce PZQ spray-dried powders and effective drug content.

| ***Samples*** ***(n = 3)*** | ***Composition*** ***PZQ : PVPVA*** ***(wt%)*** | ***Inlet gas temperature*** ***(°C)*** | ***Dry Method code*** | ***Outlet gas temperature*** ***(°C)*** |
|---|---|---|---|---|
| SD 1 | 50:50 | 80 ± 2 °C | 1 | 48 ± 2 °C |
| SD 2 | 70:30 | | | |
| SD 3 | 50:50 | 110 ± 2 °C | 2 | 68 ± 2 °C |
| SD 4 | 70:30 | | | |

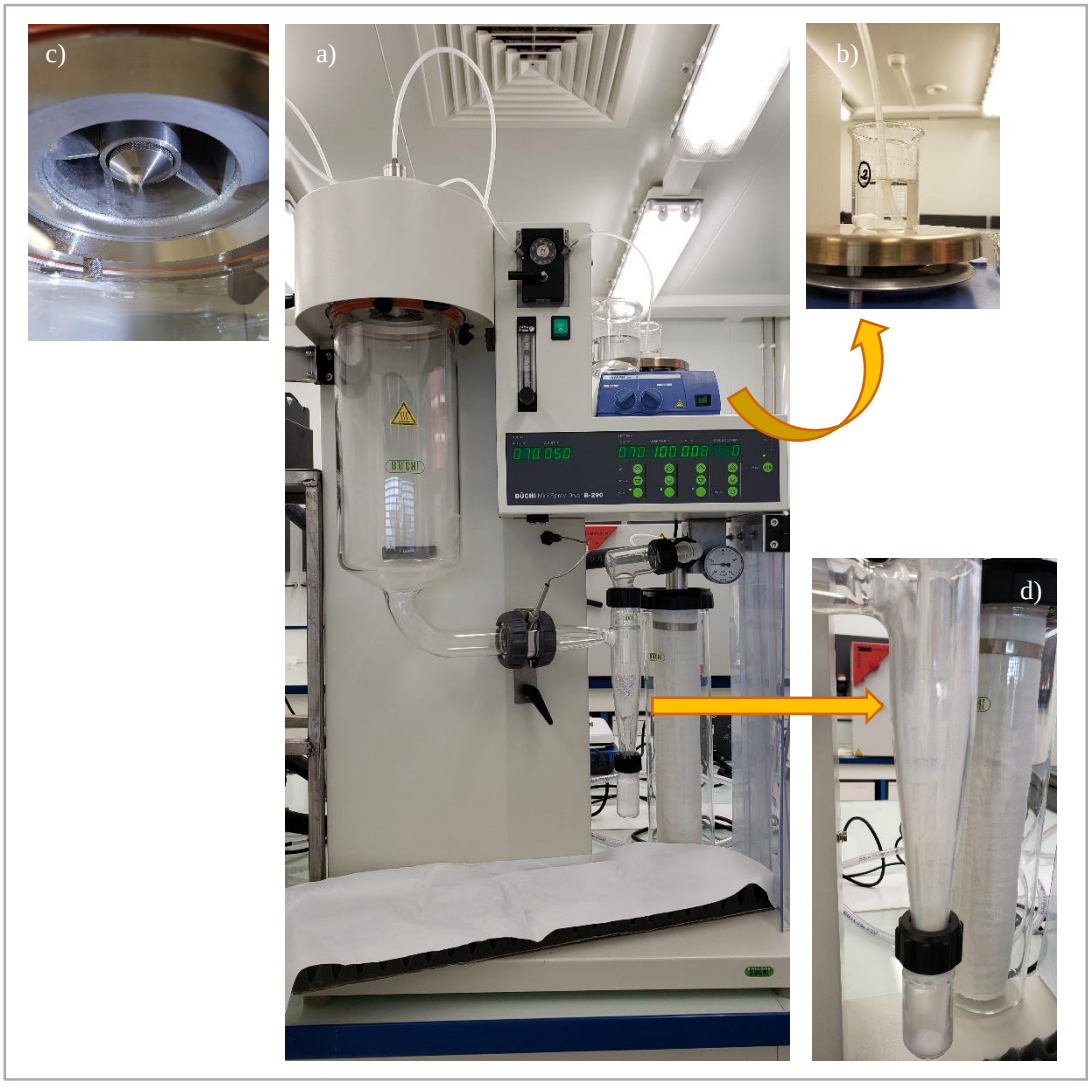


Figure 48. Spray drying used for samples production. a) Buchi B-290 mini spray dryer; b) liquid feed; c) sample spraying; d) cyclone and sample colector.

## 1.2 Characterization of supersaturated PZQ solutions

### 1.2.1 Determination of drug loading

HPLC-UV method [297] was used for PZQ dosage in the spray-dried samples.

The HPLC system used consisted of two mobile phase delivery pumps (LC-10 ADVP, Shimadzu, Japan), a UV–Vis detector (SPD-10Avp, Shimadzu, Japan), an autosampler (SIL-20A, Shimadzu, Japan), an interface (SCL-10Avp, Simadzu, Japan) for the acquisition of data through a software Ez-Star and a column Protosil C18 100 Å (150×4.60 mm - 5 µm, Phenomenex, Bologna, Italy). The mobile phase comprised methanol and water (60:40 V/V), the flow rate was 1.5 ml/min, injection volume was 10µL and absorbance readings were conducted at a fixed wavelength of 210 nm. The retention time of PZQ was about 3 min and the run time was set at 10 min. Quantification was carried out using a fresh stock solution prepared each time before starting the analysis. The standard solution of PZQ was prepared by dissolving 9 mg of PZQ in the mobile phase to obtain a final concentration of 0.18 mg/mL. For each sample, an equivalent of 37.5 mg of PZQ was weighed in duplicate, in 25 ml volumetric flasks, and added to the mobile phase. The solutions were subjected to ultrasound for 5 minutes. The sample was filtered with a PTFE 0.22 µm filter and diluted to 0.18 mg/mL. The flask was homogenized, and a fresh aliquot was filtered (same type of filter) and transferred directly to a vial. HPLC analysis took place immediately after the sample preparation. The results were expressed in the percentage of PZQ recovery.

### 1.2.2 Differential Scanning Calorimetry (DSC)

The analyses were performed by using a DSC Q200 with the base module and mDSC (TA instruments, USA). Nitrogen was used as the purging gas at 50 mL/min, the analysis was made in non-hermetic aluminium pans, indium standards were used for enthalpy and temperature calibration and an empty aluminium pan was used as a blank. As for mDSC, sapphire was used to calibrate in CP. Samples were heated at 2 °C/min. from 10 to 160 °C, with a modulation period of 40 s and an amplitude of 0.2 °C.

### 1.2.3 X-ray diffraction (PXRD)

Powder X-ray diffraction patterns were obtained by X'Pert Panalytical X-ray diffractometer (Philips, USA) using CuKα radiation, putting 40 mA of current and 45 kV of voltage. The recording spectral range was set at 5–50° with a measuring step (angular deviation between 2 consecutive points) of 0.0167° and an acquisition time of 100 s per point. In addition, the powder was rotated in its sample holder (1 s/revolution) during the acquisition of the results.

### 1.2.4 Scanning Electronic Microscopy (SEM)

SEM images were obtained using a scanning electron microscope HITACHI TM3030 Plus (HITACHI) with an acceleration voltage of 15 kV. Samples were fixed on support using a double-sided adhesive and covered with platinum using a high-resolution SEM coated spray Polaron SC7640 (Quorom Technologies, England).

### 1.2.5 Apparent solubility

Solubility measurements were performed following the standard shake flask method (Incubator Shaker SL 222, Solab). An excess mass of samples was added into 50 mL of purified water under magnetic agitation with 100 rpm at 37 ± 0.5 °C. Two mL of each sample was withdrawn, filtered through 0.22 μm cellulose acetate filter and immediately transferred to vial, at different time points: 30 min, 1h, 24h and 48 h. The concentration of PZQ in water was measured by HPLC system (Agilent 1100 Series) equipped with a UV-visible detector (with the same method described before). The experiments were carried out in duplicate.

### 1.2.6 Stability monitoring

To monitor the physical stability of the solid state of PZQ in the spray-dried powders, the samples were kept in glass vials protected from light and kept in a desiccator, which was stored under laboratory conditions (25 °C ± 2 °C and 60 % RH) during 5 months after production. DSC and PXRD analyses were undertaken over the storage period to check the solid state of the analysed samples.

## 2. RESULTS

### 2.1 Characterization of the spray-dried powders

#### 2.1.1. Determination of effective composition

HPLC measurements allowed to quantify the PZQ on the spray-dried samples, which were close to the theoretical values (Table 20).

To characterize the residual solvent content, the weight loss of SD samples at the end of the thermal analysis was measured, considering that the weight loss corresponded to solvent evaporation in the range 20 °C – 100 °C. The higher residual solvent in the samples SD 1 and SD 2 dried under milder conditions (dry method 1) was lower than 0.8 wt%.

Table 20. PZQ content in the samples produced by spray drying.

| ***Samples*** ***(n = 3)*** | ***Theoretical PZQ*** ***(wt%)*** | ***Real PZQ*** ***(wt%)*** ***(n = 2)*** |
|---|---|---|
| SD 1 | 50 | 50.8/51.8 |
| SD 2 | 70 | 69.8/69.3 |
| SD 3 | 50 | 50.9/49.6 |
| SD 4 | 70 | 70.2/67.1 |

#### 2.1.2. Powder X-Ray Diffraction (PXRD)

The X-ray diffraction pattern of the raw PZQ in Figure 49 shows well defined Bragg peaks, as already seen in the literature [10], [73], [74]. The most intense peaks were found at 2θ degrees of 6.2, 7.7, 11.5, 12, 12.5, 13.6, 14.6, 15.6, 15.8, 18.6. In the same figure, the diffraction pattern of the raw polymer (PVPVA) represents a single broad halo, characteristics of an amorphous material.

Still in Figure 49, PXRD patterns for the SD samples confirmed the transformation of the raw PZQ from crystalline to amorphous. In fact, for all produced

samples (SD 1, SD 2, SD 3 and SD 4), a broad halo with no diffraction signs is observed. Samples were produced in triplicate and all replicates presented the same PXRD patterns represented in Figure 52.

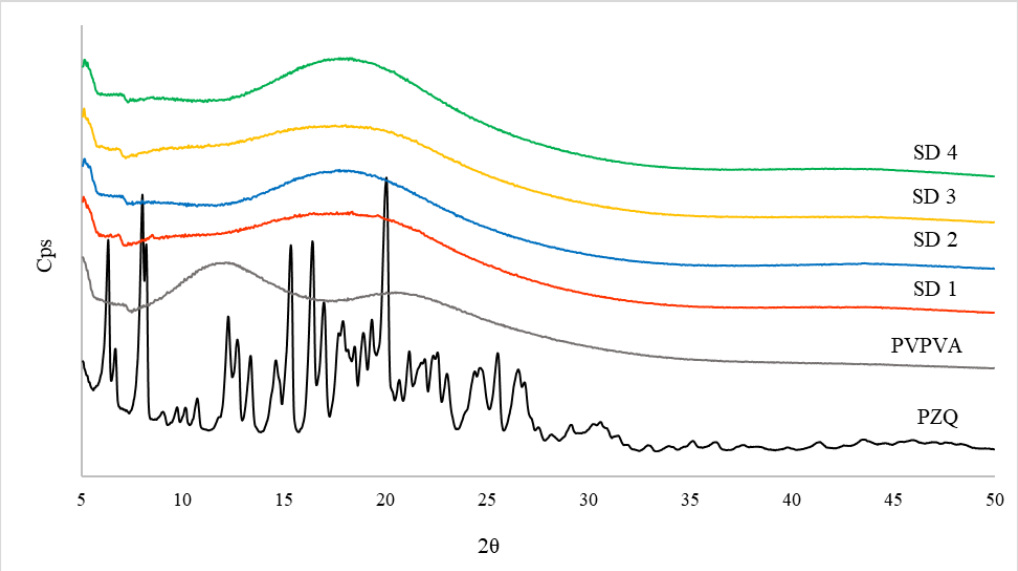


Figure 49. PXRD diffractograms for raw materials (PZQ and PVPVA) and spray-dried samples (SD 1, SD 2, SD 3, and SD 4).

### 2.1.3. Thermal analysis

Figures 50 and 51 show the DSC scans for the three replicates of all SD samples. The data from DSC curves are grouped in Table 21.

For the samples with 50 wt% PZQ: two values of $T_g$ were found for two of three replicates of the SD1 sample. Differently, the third replicate shows a single $T_g$ on 44.5 °C. For the SD3 sample, a single $T_g$ was detected for all replicates, with values in the range 45.6 to 59.9 °C.

For the samples with 70 wt% PZQ: A single $T_g$ of 37 °C was found for SD 2 sample, whereas for SD 4 sample, the $T_g$ failed in the range 29.7 to 34.1 °C.

Table 21. Glass transitions of SD samples obtained by reverse heat flow signal during the DSC analysis.

| ***Time*** | ***Batch*** | ***SD 1*** | | ***SD 2*** | | ***SD 3*** | | ***SD 4*** | |
|---|---|---|---|---|---|---|---|---|---|
| | | *Tg (°C)* | *ΔCP (J/g.°C)* | *Tg (°C)* | *ΔCP (J/g.°C)* | *Tg (°C)* | *ΔCP (J/g.°C)* | *Tg (°C)* | *ΔCP (J/g.°C)* |
| t0 - freshly produced | a | 56.58<br>108.23 | 0.30<br>0.87 | 41.88 | 0.35 | 45.55 | 0.30 | 34.12 | 0.38 |
| | b | 56.17<br>113.56 | 0.47<br>0.11 | 41.15 | 0.30 | 53.43 | 0.54 | 29.68 | 0.40 |
| | c | 44.49 | 0.45 | 37.01 | 0.37 | 59.88 | 0.88 | 33.76 | 0.36 |

The effect of the inlet drying temperature (referred as drying method) on the thermal profile of samples with 50 wt% PZQ can be analysed comparing Figures 50a (dry method 1) and Figure 50b (dry method 2). For samples with 70wt% PZQ, Figures 51a and 51b allow a similar analysis.

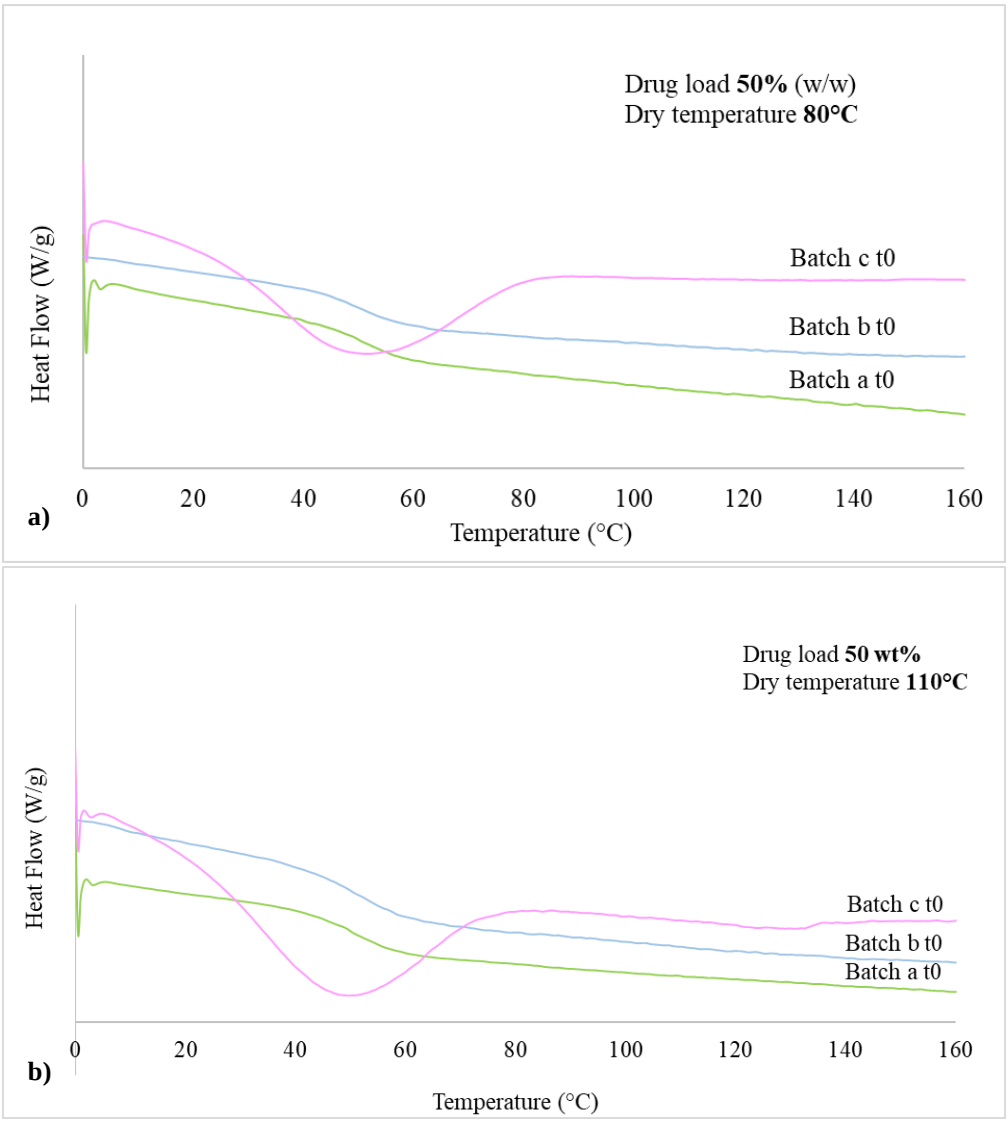


Figure 50. DSC curve for samples with 50 wt% PZQ (n = 3) generated at different drying temperatures: a) 80 °C, and b) 110 °C.

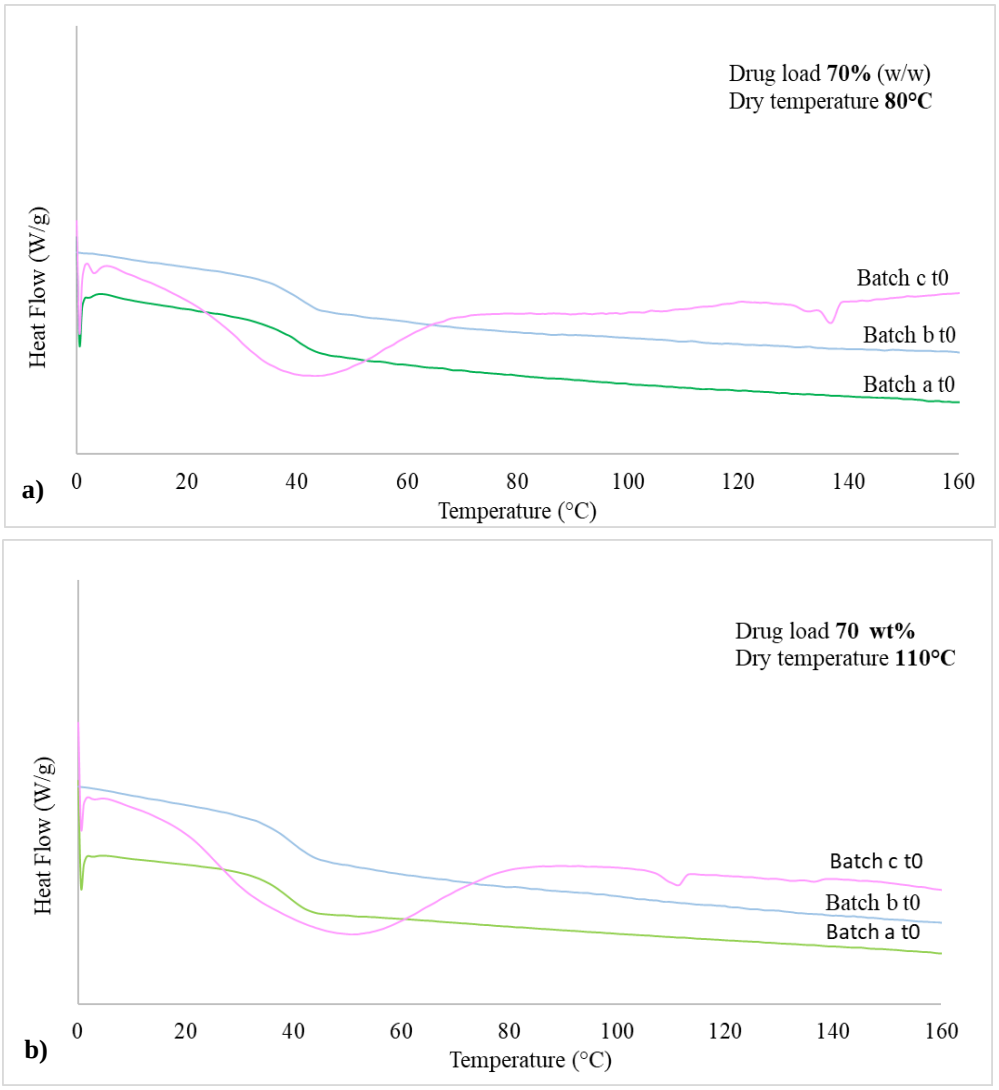


Figure 51 DSC curve for samples with 70 wt% PZQ (n = 3) generated at different drying temperatures: a) 80 °C, and b) 110 °C.

In some DSC curves of Figure 51, it can be observed the presence of endothermic events, which could correspond to melting transformations. The characteristic values are shown in Figure 52.

Considering that two of the replicates of SD 2 and SD 4 samples are amorphous without endothermic events, the differences in the solid state, detected in one of their triplicates, have evidenced that the final state of the spray-dried solid may undergo modifications during or immediately after the solid formation. It is important to remember that these samples contain around 70 wt% of PZQ which, if rendered amorphous during

the solid formation, need to stay amorphous within the polymeric matrix. Therefore, recrystallisation may take place if they are highly supersaturated. The higher PZQ concentration (70 wt%) in both samples (SD 2 and SD 4) could be the reason for the lack of repeatability of amorphous characteristics for the batches produced.

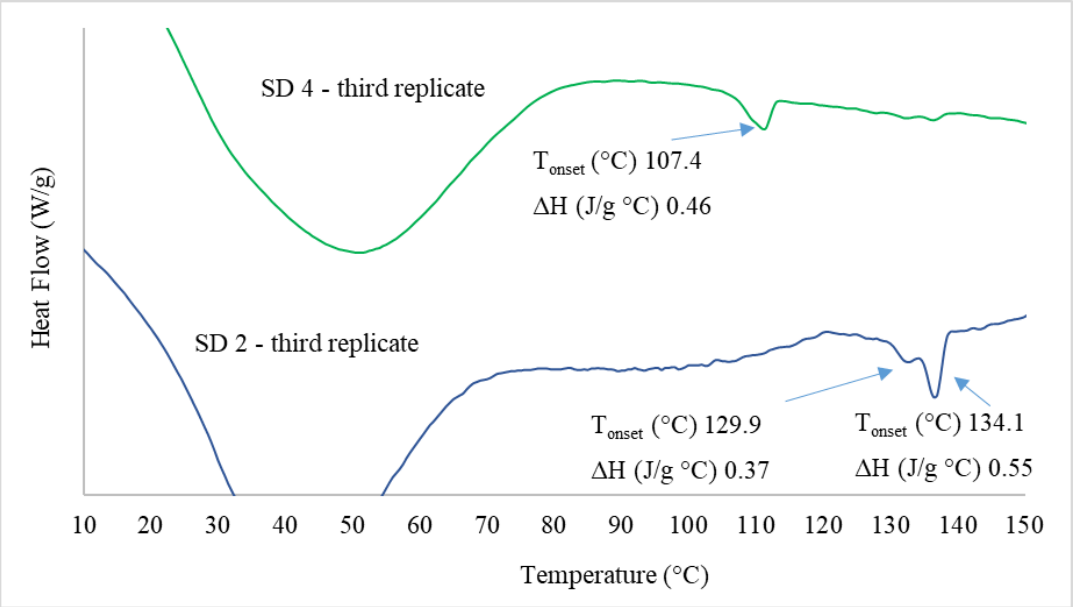


Figure 52. Magnification of DSC curves for SD 2 and SD 4 samples showing the endothermic events.

The endothermic events detected in these replicates did not correspond to the melting of the initial racemic molecule (around 137 °C). In fact, they could correspond to new polymorphic forms of PZQ recently described in the literature [30], [73] like the form B (melting temperature of 110 °C – 112 °C) or the form C (melting temperature of 106 °C). However, the broadness of the peaks prevents the clear identification of the polymorph form in the samples freshly produced. As these replicates (batch 'c' – Figure 51) were monitored for 3 and 5 months after production, this discussion will be continued later in the section dedicated to stability.

For purpose of comparison, the DSC scan of unprocessed PZQ reveals a first endotherm at peak at 137.78 °C, attributed to the melting of racemic form, in according with previous DSC measurements shown in Chapter 3 (item 4.3). Also, no dehydration event was observed in the TG curve, confirming its anhydrous nature. Regarding the polymer, the DSC thermogram confirms the absence of endothermic peaks due to melting, in according with describe in Chapter 3 (item 4.3). A variation of the baseline

starting 30 °C to ~110 °C is observed for PVPVA. This variation corresponds to the loss weight of the material and was confirmed by the TG analysis, as displayed in Figure 53b. Indeed, TG curves give information's related to the high degradation temperatures for PZQ and PVPVA (> 240 ºC and > 270 ºC, respectively). These results corroborate those reported in the literature [299][305].

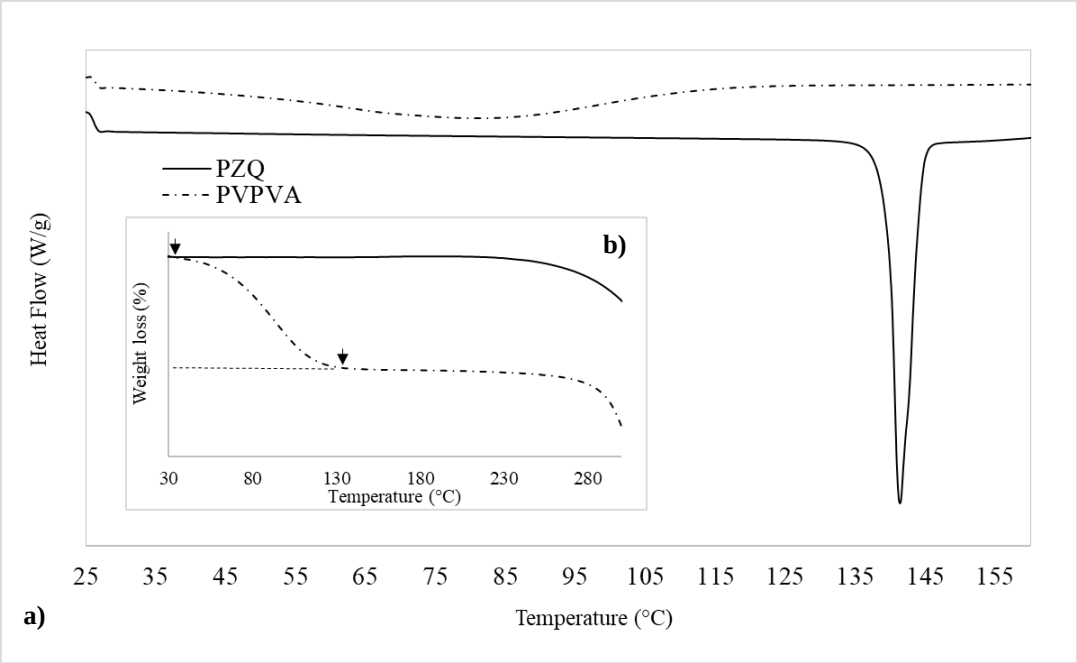


Figure 53. a) DSC curves and, b) TG curves of pure components - PZQ and PVPVA.

### 2.1.4 Scattering Electronic Microscopy (SEM)

SEM images of SD samples are presented in Figure 55. For comparison, the SEM images of the raw materials (PZQ and PVPVA) and their physical mixtures prepared in the same mass proportion of the SD samples are shown in Figure 54.

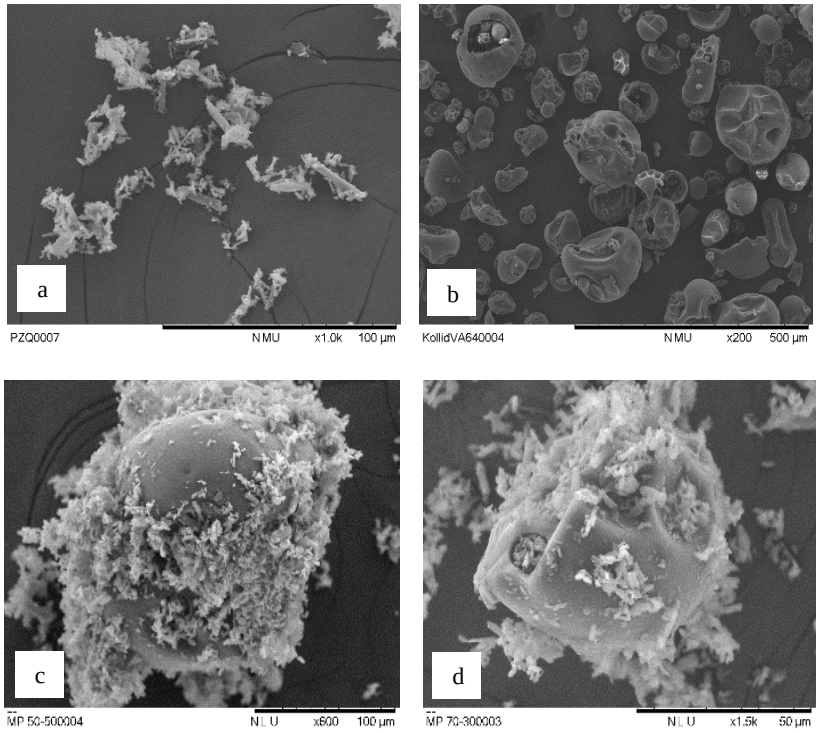


Figure 54. SEM images of raw materials and physical mixtures: a) PZQ; b) PVPVA; c) PM 50; d) PM 70.8

The raw PZQ is constituted of needle-shaped crystals (Figure 54a), while raw PVPVA particles are predominantly spherical (Figure 54b) and larger than those of raw PZQ. In the SEM images of PZQ and PVPVA physical mixtures with different mass proportions (Figures 54c and 54d), PZQ particles covered the PVPVA particle surfaces, which was not the case for SD spray-dried particles (Figures 58a to 58d). Figures 58a to 58d revealed the effect of two parameters on the microstructure morphologies of the SD powders, PZQ load and drying temperature.

The SD 1 powder (50 wt% PZQ, drying temperature of 80 °C) is constituted by spherical particles (Figure 55a). The SD 3 powder, that has a similar mass composition but is produced at higher drying temperature (100 °C), shows spherical particles partially sintered together (Figure 55c).

SD 2 and SD 4 spray-dried powders in Figures 55(b) and (d) correspond respectively to formulations dried at 80 °C and 100 °C. Their PZQ mass load is around 70 wt%. In both powders, particles with a less perfect spherical shape partially (also sintered together) were observed. Moreover, very fine needle-like particles are found at their surface and their presence became more apparent for SD 4 powder.

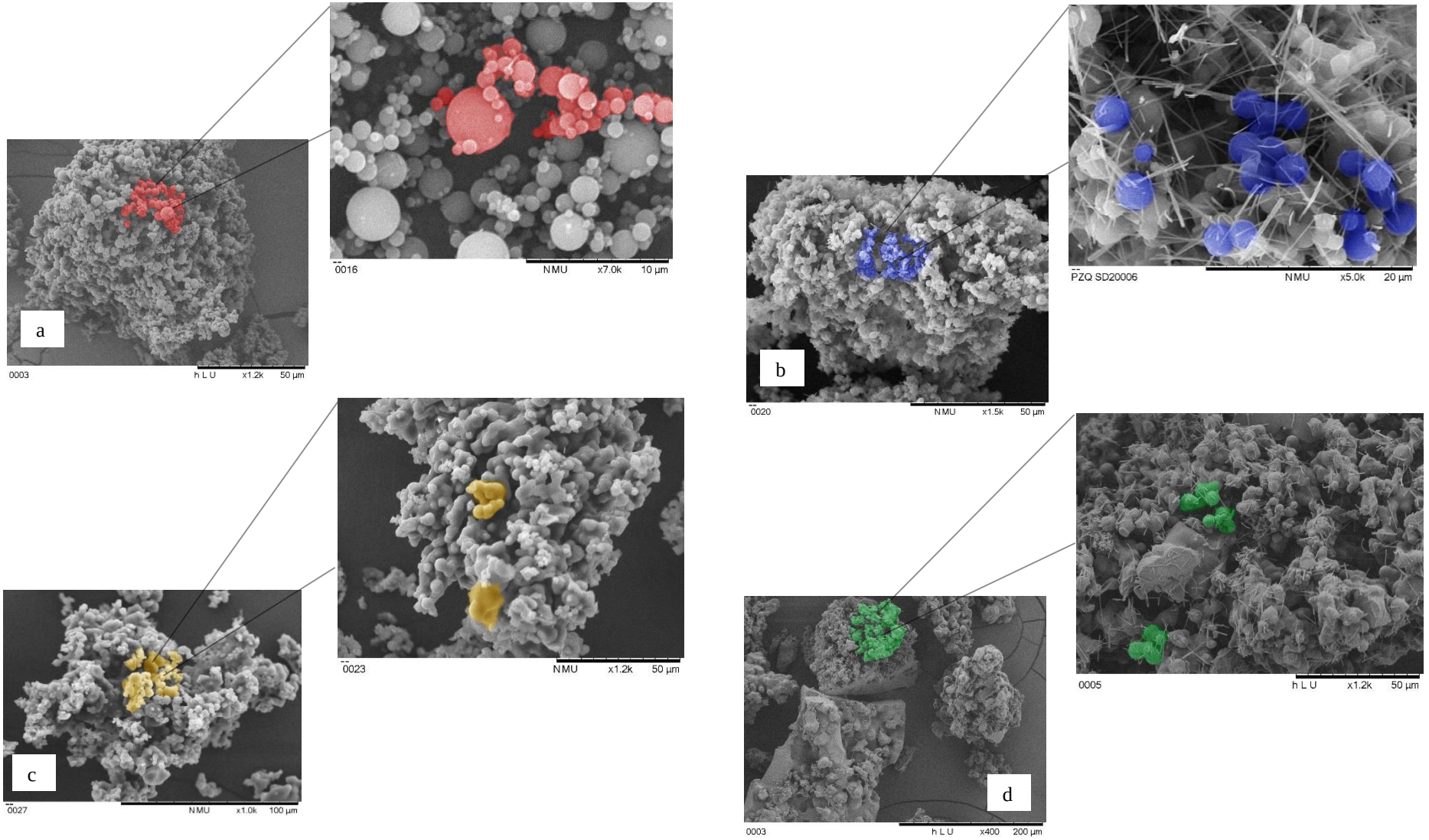


Figure 55. SEM images of SD samples: a) SD 1 with magnification 7000x; b) SD 2 with magnification 5000x; c) SD 3 with magnification 1200x and, d) SD 4 with magnification 1200x.

The differences in microstructure morphologies between SD samples are due to the combination of two different effects, the increase of the PZQ load in the formulation and the increase of the inlet gas drying temperature which affected the outlet drying temperature (see Table 1). As discussed before, SD powders are mostly amorphous, and their glass transition temperature is dependent on their PZQ load. The temperature reached by the solid powder during the spray drying process will strongly affect their physical stability and tendency for sintering and stuck, mainly if it is close to its glass transition temperature.

The physical characteristics of the powders were influenced by the process outlet temperature (48 ºC and 68 ºC) that was close to or even exceed the respective $T_g$, leading to the softening state and sintering effect between the particles.

The increase of PZQ concentration from 50 to 70 wt% is expected to lower $T_g$ on the amorphous mixture, increasing the tendency for sintering and stuck as observed in Figures 55(b) and 55(d). Another interesting characteristic evidenced in the same figures is the presence of needle-like particles on the surface of the larger partially sintered more spherical particles in SD 2 and SD 4 powders. They might correspond to PZQ particles, suggesting that there was a change in the morphology of the primary particles of PZQ initially used. As the raw PZQ was completely dissolved in ethanol before drying, these new particles were formed during drying or just after drying (recrystallization) considered the very high drug load (70 wt%) in the solid sample. They may correspond to the crystalline form identified in two replicates, as discussed before (item 2.1.3).

### 2.1.5 PZQ Water Solubility

In order to learn more about the SD samples, other properties were measured as the effect of the new solid state (amorphous or predominantly amorphous solid solutions) on the PZQ water solubility. For that, the solubilization of the SD samples in water at 37°C was investigated, in comparison to their corresponding compositions but as physical mixtures (PM 50, PM 70) and with raw PZQ as reference for solubility enhancement.

The solubilization process was monitored over time, at 0.5 h, 1 h, 24 h and 48 h, when the equilibrium concentration of PZQ in solution was reached. Data are given in Table 22 and represented in Figure 56 for the first point (0.5 h) and at the end of the experiment (48 h).

Table 22. PZQ water solubility (37 °C) for SD samples, in comparison to physical mixtures of corresponding compositions and raw API.

| ***Sample code*** | ***PZQ concentration (mg/mL)**** | | | |
|---|---|---|---|---|
| | ***0.5 h*** | ***1h*** | ***24h*** | ***48h*** |
| **PZQ** | 0.181 ± 0.02 | 0.189 ± 0.16 | 0.192 ± 0.03 | 0.204 ± 0.01 |
| **PM 50** | 0.217 ± 0.03 | 0.246 ± 0.00 | 0.206 ± 0.03 | 0.213 ± 0.01 |
| **SD 1** | 0.259 ± 0.10 | 0.252 ± 0.10 | 0.267 ± 0.04 | 0.263 ± 0.01 |
| **SD 3** | 0.312 ± 0.08 | 0.293 ± 0.05 | 0.284 ± 0.02 | 0.300 ± 0.03 |
| **PM 70** | 0.211 ± 0.01 | 0.215 ± 0.00 | 0.179 ± 0.01 | 0.210 ± 0.02 |
| **SD 2** | 0.283 ± 0.01 | 0.273 ± 0.03 | 0.274 ± 0.02 | 0.286 ± 0.00 |
| **SD 4** | 0.360 ± 0.01 | 0.331 ± 0.00 | 0.313 ± 0.01 | 0.269 ± 0.03 |

* Values represent the average and standard deviation, n = 2

From data, the concentration of PZQ[16] in solution was 0.181 ± 0.02 mg/mL in the first 30 minutes, reaching the equilibrium of 0.204 ± 0.01 mg/mL in 48 hours, a value that is in line with the literature data (Table 23) [157], [161], [304]. The same tendency of increased solubilization was verified for the physical mixtures of raw PZQ and the polymer (PM 50 and PM 70). The wetting agent effect of polymer, which favours PZQ solubilization in the first 30 min was observed, and it was directly proportional to the concentration of the polymer in the mixture. However, the equilibrium solubility reached from the physical mixtures is similar to the one obtained for raw PZQ, suggesting that the polymer in this formulation form exerts little or no solubility enhancing effect.

In contrast to raw PZQ and physical mixtures, Figure 56 shows that the SD samples improved the apparent solubility of PZQ. The maximum concentration of PZQ in solution was reached in the first 30 min for all SD samples, the highest being 0.360 ± 0.01 mg/mL for SD 4, which represents an increase of 47 %.

[16] This experiment was independent of Chapter 3. It means that the water solubility test for PZQ raw material was conducted simultaneously with the other samples presented here. The values of both experiments are comparable.

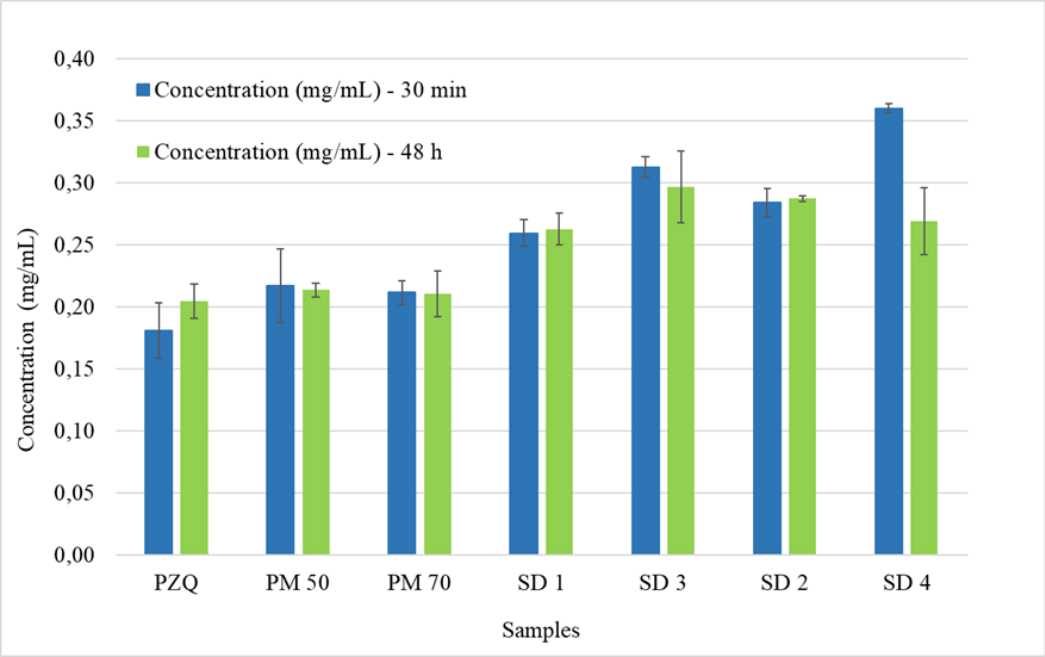


Figure 56. Solubility in water at 37 °C of raw praziquantel, physical mixtures (PM 50 and PM 70) and SD 1, SD 2, SD 3, and SD 4. Data are presented as the mean ± standard deviation (n=3).

SD 3 and SD 4 samples showed fast kinetics solubilization in 30 minutes compared to the other samples. However, SD 4 is also responsible for a higher decrease to 48 h. The 'spring effect' initially observed is related to the change from the crystalline form to the predominantly amorphous form of the drug in the SD samples. In fact, as already discussed in Chapter 2, a high-energy form of the drug in its amorphous state (the spring) provides the driving force to its solubilisation at a concentration greater than its equilibrium solubility level [306]. Nonetheless, amorphous forms are metastable structures and tend to migrate to their more stable form under conditions that can increase molecular mobility, for example, in the presence of water or temperature [186], [190], [192], which explains the tendency of reduction in the PZQ concentration in the medium measured at 48h. Still, although the decay, the apparent solubility is improved at least of 31% for SD4 sample. A 'parachute' effect (inhibition of the recrystallization expected with amorphous solid dispersions) in 48 h was observed for SD 1 and SD 2 samples, resulting in an improvement of 28 % and 41%, respectively, in the apparent solubility of PZQ.

### 2.1.6 Physical stability of the amorphous state

Finally, we have decided to verify the physical stability of the SD samples. For this purpose, they were stored in glass vials protected from light and kept in a desiccator at 25 °C and 60 % RH and reanalysed by DSC at 3 months and 5 months after production. Also, PXRD was performed after 3 months of aging under storage.

For all replicates, $T_g$ values initially detected by DSC in the samples freshly produced (t0) barely changed over time. As the evolution was quite similar, Figure 57 represents the $T_g$ data for one replicate of each SD sample at t0, t3 (after 3 months) and t5 (at the end of the experiment at 5 months). It should be noted that the only modification was seen for SD 1 sample for which two $T_g$ were identified in two replicates at t0. After 3 months of storage, only a single $T_g$ (54.35 °C) was identified in the sample near the first one detected before (56.58 °C). A reduction of this value was observed at t5 (43.76 °C). For SD 1 and SD 3, there was a greater decay of $T_g$ after 5 months when compared to samples SD 2 and SD 4.

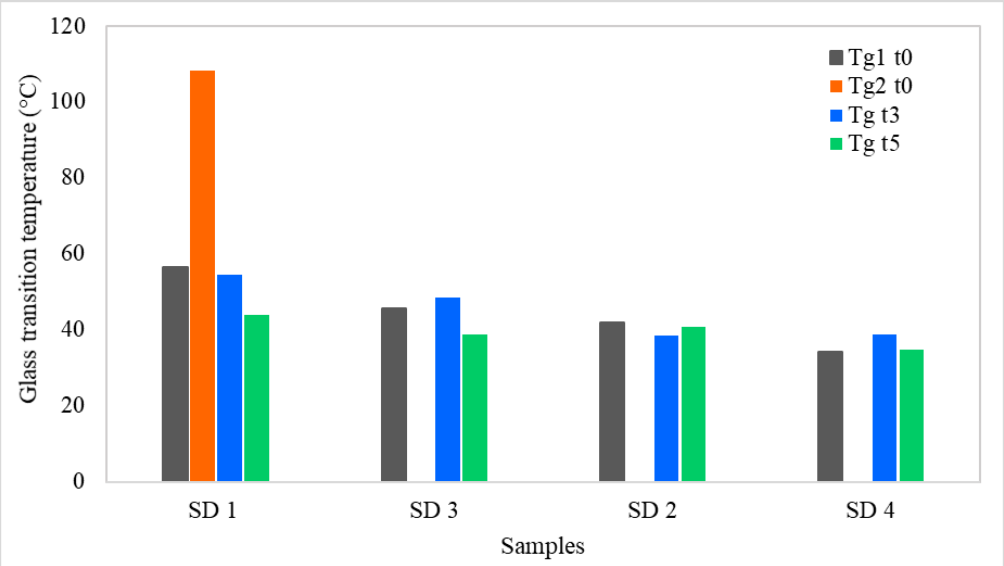


Figure 57. Monitoring the glass transition ($T_g$) of spray-dried binary systems (SD 1, SD 2, SD 3, and SD 4) at different times.

We consider that some values of $T_g$ are not high enough to guarantee the product's stability at room temperature, and, in these cases, small variations are sufficient to increase the molecular mobility of the system and cause drug recrystallization. This sensibility to temperature could explain the new endothermic event around 106.5 °C followed by 133 – 134 °C observed in the samples at t3 for samples with 50 wt% PZQ as

shown in Figure 58. It could be attributed to the recrystallization of the polymorphic form into racemic form.

Based on the recent literature on forms B and C of PZQ [75], we can hypothesize to interpret the observed transformations. Initially, there is a variation of the baseline related to residual ethanol evaporation, followed by the possible melting of form C (106 °C) and the recrystallization to the racemic commercial form (around 137 °C).

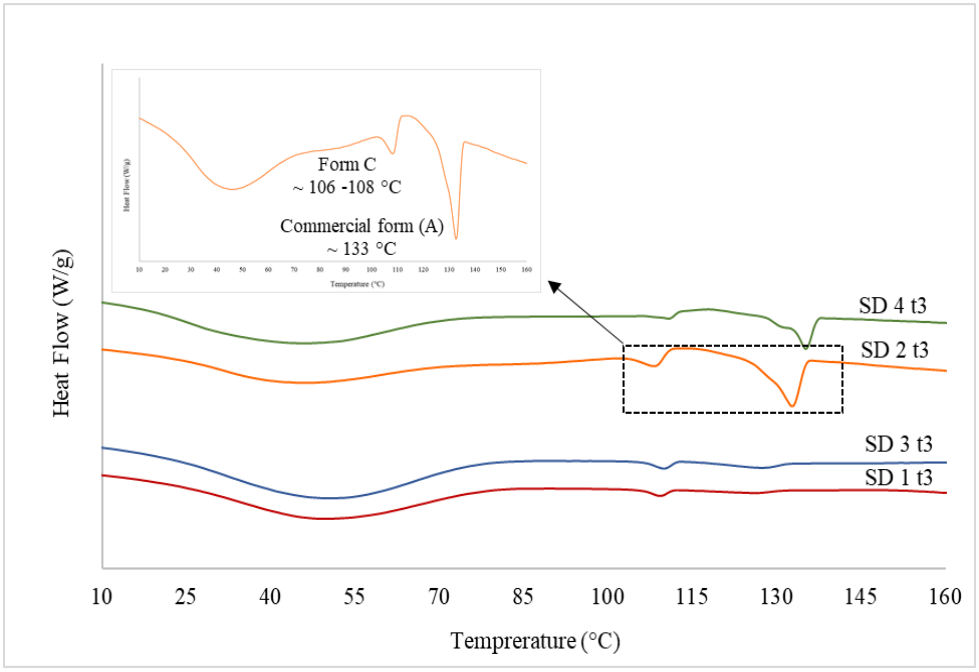


Figure 58. DSC thermograms for SD samples after 3 months of production (25 °C and 60 %RH).

XRPD analyses (Figure 59) confirmed the appearance of crystalline peaks during aging,

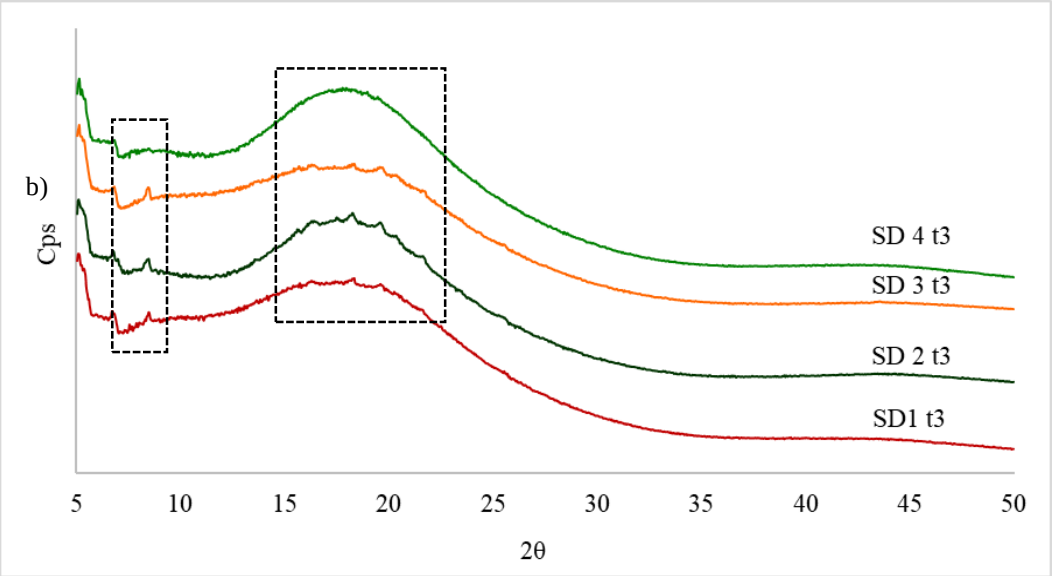


Figure 59. XRPD diffractograms for SD 1, SD 2, SD 3 and SD 4 after 3 months of production, stored at 25 °C and 60 % RH.

The main results from this part 1 are summarized now.

The spray drying technique is advantageous for obtaining amorphous systems as it is a fast procedure based on the drying of two compounds molecularly dispersed in a solution. It was demonstrated in this part of the Chapter that spray-dried amorphous binary mixtures of PZQ and PVPVA containing 50 and 70 wt% of PZQ could be generated by spray drying. Different techniques were applied to their characterization: DSC, PXRD, SEM, HPLC (for solubility and API content), besides monitoring of physical stability for 5 months.

The results from these analyses confirmed the predominantly amorphous state of the samples and, in some cases, a mixture of amorphous and a new polymorph (Form C or form B) recently identified in the literature and never reported for PZQ solid dispersions. For these samples, the confirmation of the PZQ polymorphic form (B or C) requires additional characterization to evaluate small amounts of crystalline material dispersed in a polymeric matrix such as X-ray pair distribution function (PDF), which has not been done here.

The physical evolution detected mainly after 3 to 5 months of aging under mild conditions, even if still not significant, reflects the behavior of an amorphous mixture supersaturated in the drug presenting a kinetic (and not thermodynamic) stability.

This study was undertaken to verify the feasibility for generating supersaturated solid solutions with PZQ. This material is required for the determination of the solubility of PZQ in PVPVA by means of a recrystallization method. Four samples were produced and after characterization, the SD1 sample was chosen for the recrystallization study that will detailed in the next part of this Chapter.

# PART 2 - DETERMINATION OF A TEMPERATURE-COMPOSITION PHASE DIAGRAM FOR THE BINARY PZQ-PVPVA

## 1. METHODS

### 1.1 Temperature-composition PZQ: PVPVA phase diagram

*First step – determination of the relation between $T_{gmix}$ and the binary composition*

The first step in determining the PZQ-PVPVA solubility curve was to determine $T_{gmix}$ for the binary mixture.

For PZQ-PVPVA mixture, $T_{gmix}$ was determined experimentally from mixtures prepared directly on the crucible, with different mass compositions. For DSC measurements, the experimental protocol is given in Table 2[17].

The analyses were performed by using a DSC Q200 with the base module and mDSC (TA instruments, USA). Nitrogen was used as the purging gas at 50 mL/min, the analysis was made in non-hermetic aluminium pans, indium standards were used for enthalpy and temperature calibration and an empty aluminium pan was used as a blank. As for mDSC, sapphire was used to calibrate in CP.

[17] Table 2 also regroups other DSC protocols employed in this study like that to reanalyse the raw materials (the first analysis presented in Chapter 2 was performed in another laboratory employing another DSC ecquipment) and the protocol used for the API-polymer solubility curve which is explained just after.

As already introduced in Chapter 2 (Section 6.1.2.1), one of the most popular equations for predicting glass transition temperatures of amorphous mixtures is the Gordon-Taylor (GT) equation [78], [88], [225]:

Equation 5

$$T_{gmix} = W_1 T_{g1} + K\, W_2 T_{g2} / W_1 + K\, W_2$$

where $T_{gmix}$ and $T_{g\,i}$ are respectively the glass transition temperature of the mixture and of the components, $W_i$ is the mass fraction of component $i$ and $K$ is an adjustable fitting parameter. By plotting experimental $T_g$ values as a function of the **glass** composition, one can usually apply the GT equation to determine the slope $K$, which subsequently can be used in $T_g$ predictions.

*Second step – determination of the solubility of PZQ in PVPVA (in the range 100-130°C)*

The second step was to determine the PZQ-PVPVA solubility from a supersaturated solid solution. To this end, one of the spray-dried powders generated in the first part of this study, with 50 wt% PZQ, was used. The sample was SD 1, batch "c" (method 1) with amorphous characteristic ($T_g$ 44.49 °C and $\Delta C_p$ 0.45 J/g.°C) described in "Part 1" of this Chapter and here named as SD 50% PZQ.

Figure 60 shows a typical DSC scan for the API-polymer solubility measured by recrystallization, which comprises four cycles of thermal analysis.

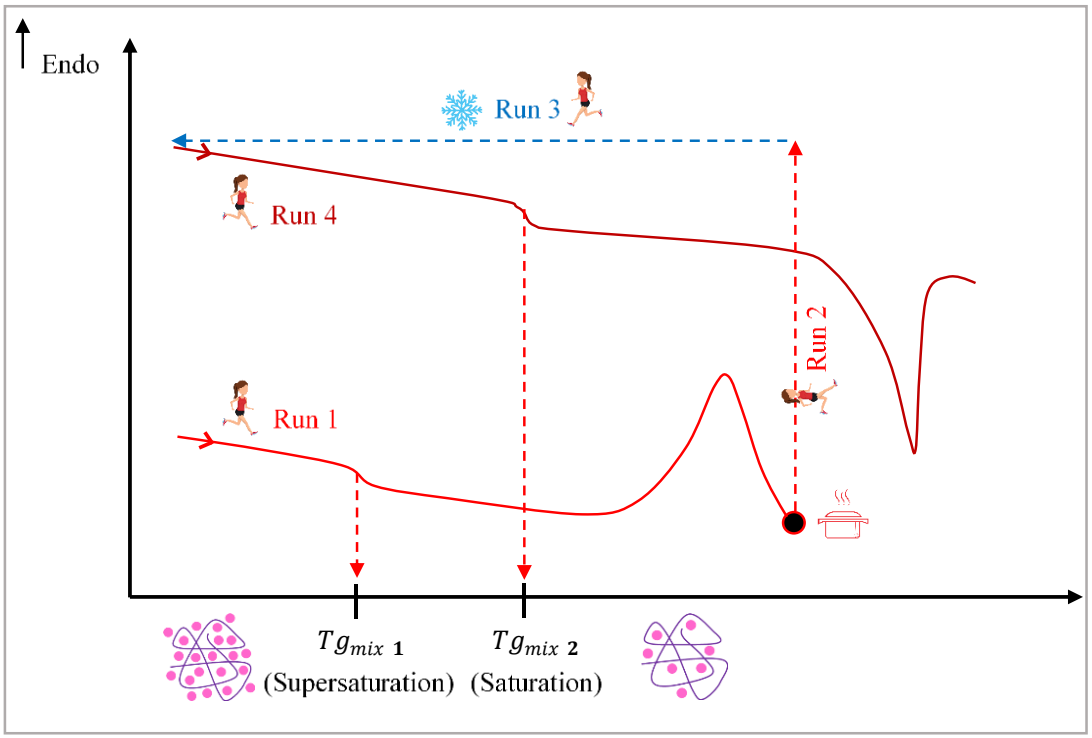


Figure 60. Recrystallization method by DSC where Run 1 - supersaturation heating (reveals the $Tg_{mix\ 1}$ of supersaturation system), Run 2 - isotherm, Run 3 - cooling and, Run 4 - saturation heating (reveals the $Tg_{mix\ 2}$ of saturation system).

The first cycle refers to the first heating step revealing the $T_{gmix\ 1}$ of the supersaturated binary system, followed by an exothermic phenomenon (recrystallization) **(run 1).**

The second cycle (referring to the isotherm) aims to reach the equilibrium state for the sample at a given annealing temperature **(run 2).**

In the third cycle, the sample is cooled down **(run 3).**

Finally, the fourth and last cycle corresponds to a second heat cycle that gives a new $T_{gmix\ 2}$ , corresponding to the API amount that still remains dispersed in the polymer at the annealing temperature **(run 4).**

For the recrystallization method, two factors are essential: annealing temperature and annealing time. The key relationship between annealing time and temperature is that a longer time is required to reach the equilibrium state for lower temperatures. This phenomenon is probably related to a slower demixing kinetics due to an insufficient molecular mobility, leading consequently to slower API diffusion in the polymer matrix [244].

Completing the DSC analysis, the new equilibrium concentration of API remaining dispersed in the polymer is calculated using the GT equation.

The experimental protocol used in this study was then the following:

The SD 50 % PZQ sample was loaded into the DSC analyser and heated at a rate of 2 °C/min up to the annealing temperature. The sample was annealed at different temperatures (100 °C to 130 °C) below the $T_m$ (melting point) of PZQ for 6 – 30 h, aiming to recrystallize the excess of PZQ in the mixture and to reach the equilibrium solubility (Table 23, method 2).

After annealing, the sample was cooled to 0 °C with a rate of 30 °C/min. Immediately after cooling, the second heating ramp was performed at a rate of 2 °C/min from 0 °C to 160 °C to obtain the value of $T_{gmix\,\mathbf{2}}$ (glass transition temperature) of the annealed material.

To determine the PZQ concentration corresponding to the new $T_{gmix\,\mathbf{2}}$ (annealed material), the GT equation was used.

Table 23. mDSC methods used to determine the experimental glass transitions of each physical mixture ($T_{gmix}$) and the API-polymer solubility curve by recrystallization

## 2. RESULTS

### 2.1. API-polymer solubility determination by recrystallization

*First step - determination of $T_{gmix}$ for PZQ-PVPVA amorphous binary mixtures*

From physical binary mixtures (prepared directly inside the DSC crucibles) it was possible to measure the glass transition temperatures $T_gmix$ with the reversing heat flow (RHF) mDSC data (second cycle of heating) (see Table 24 – method 1).

By plotting experimentally $T_{gmix}$ values as a function of the binary composition, the GT equation was used to determine the slope, k, which was subsequently used to identify, from the GT equation, the SD 50 % PZQ equilibrium composition associated to $T_{gmix\,2}$.

The experimental values used for k determination are done in Table 24. The best fitting was found for k equal to 0.2225. The GT curve is represented on Figure 61.

Table 24. Experimental glass transitions of physical mixtures (API:Polymer).

| $W_{PA}$ | *Experimental $T_{gmix}$ (ºC)*<br>*Molten physical mixtures and raw material* |
|---|---|
| 0 | 110.3 |
| 0.249 | 72.7 |
| 0.330 | 62.4 |
| 0.400 | 56.1 |
| 0.500 | 43.0 |
| 0.580 | 41.5 |
| 0.600 | 41.2 |
| 0.730 | 40.9 |
| 0.750 | 39.1 |
| 1 | 38.4 |

| *Method/samples analized* | *$T_{initial}$ (°C)* | *$T_{end}$ (°C)* | *Heating rate (°C/min)* | *Modulation temperature amplitude (°C)* | *Modulat. Period (s)* | *$T_{isotherm}$ (°C)* | *Time isotherm (h)* | *Cycle reference* |
|---|---|---|---|---|---|---|---|---|
| 1<br>(Raw materials and physical mixtures) | 0 | 180 | 2 | 0.2 | 40 | NA | NA | Heating 1 |
| | 180 | 180 | 0 | NA | NA | 170 | 0.017 | Isotherm |
| | 180 | 0 | 30 | NA | NA | NA | NA | Cooling |
| | 0 | 180 | 2 | 0.2 | 40 | NA | NA | Heating 2 |
| 2<br>(Amorphous solid solution - sample named SD 50 % PZQ | 0 | 120 | 2 | 0.2 | 40 | NA | NA | Heating 1 |
| | 120 | 120 | 0 | NA | NA | 100<br>110<br>120<br>130* | 6<br>10<br>20<br>30* | Isotherm |
| | 120 | 0 | 30 | NA | NA | NA | NA | Cooling |
| | 0 | 180 | 2 | 0.2 | 40 | NA | NA | Heating 2 |

*Variation of temperature and annealing time to evaluate SD 50% PZQ system.

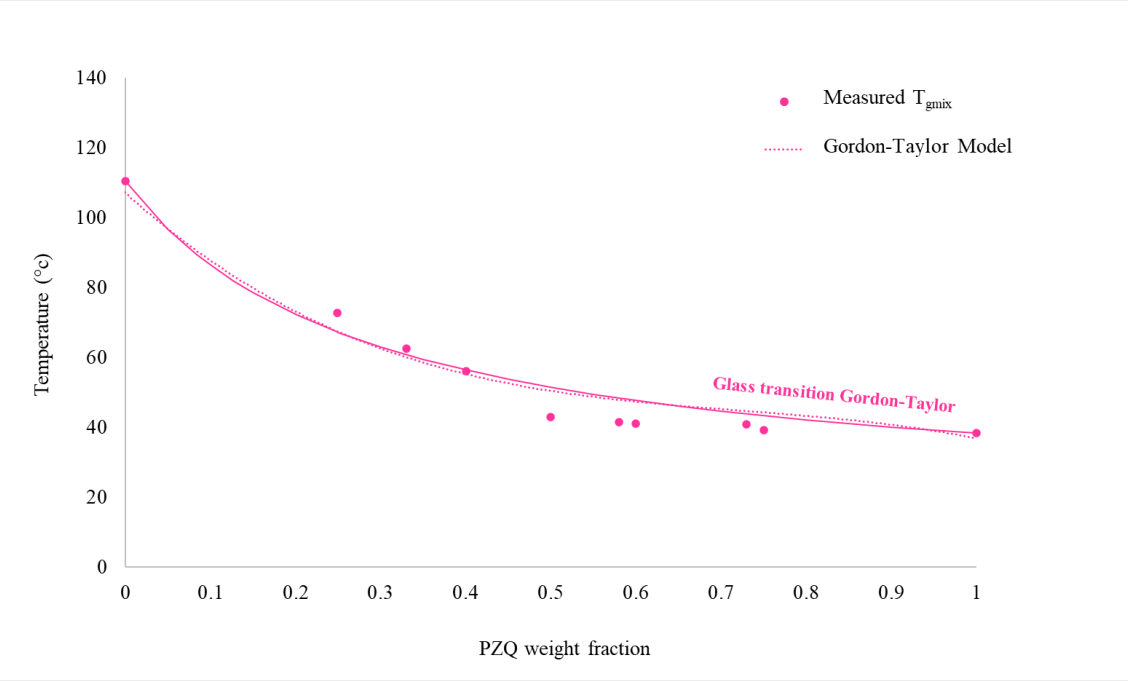


Figure 61. The Gordon Taylor equation adjusted from measured $Tg_{mix}$

*Second step – determination of the solubility of PZQ in PVPVA in the range 100-130°C*

The second step was to determine the PZQ-PVPVA solubility from the SD 50 t% PZQ.

The glass transition temperatures of ASD sample were determined by DSC (Table 24). A single and distinctive mixture glass transition temperature ($T_{gmix}$ ) in the reversing heat flow signals, indicated the formation of one-phase in the solid structure produced by spray-drying. PXRD also confirmed the results from DSC.

This sample was then annealed from 100 °C until 130 °C to promote the recrystallization of excess PZQ amount. In order to use a reasonable annealing time, the lower limit of temperature range (100°C) was chosen far enough above the glass transition (≈109 °C for pure polymer, 60.3°C for the binary mixture), the molecular mobility reducing strongly as we approach $T_{gmix}$ . The upper value of this range was chosen under the melting point of pure API ($T_{f\ PZQ}$ = 138 °C).

One example of the experimental recrystallization method is given here. When the SD 50 % PZQ sample undergoes an annealing from 10 h to 120 ºC, the $T_{gmix}$ goes from 44 ºC (run 1) followed by a recrystallization which starts at about 90 °C and is stopped at

the annealing temperature of 120 °C. In Run 2 (isotherm), the sample is kept at 120°C during 10 h. Here it is possible to understand why this step is considered crucial for the good execution of the method. At this point, when the recrystallization finishes, PZQ has the opportunity to reach equilibrium with the remaining excess of API into the sample.

After reaching equilibrium, the cooling step occurs, and then the second heating in the same conditions as the first (see Table 24, method 2). During this second heating, the $T_{gmix}$ was obtained at 60 ºC (run 4). After, the endothermic signal, related to the melting of the recrystallized material, can be visualized ($\Delta H_{fusion}$ 8.03 J / g) with heat flow signal.

After each annealing step (see method on Figure 60), the $T_{gmix\,2}$ detected in run 4 was associated to a new equilibrium concentration from the Gordon Taylor curve. Table 25 regroups the PZQ concentrations at equilibrium obtained for all annealing temperatures.

Table 25. Calculated equilibrium concentrations ( $W_{PA}$) from PZQ recrystallisation in spray-dried SD 50 % PZQ.

| ***Annealing temperature (ºC)*** | ***Annealing time (h)*** | $T^{g}_{mix2}$ ***(ºC) (run 4)*** | $W_{PZQ}$ |
|---|---|---|---|
| 100 | 10 | 77.6 | 0.16 |
| 100 | 20 | 75.9 | 0.17 |
| 110 | 10 | 70.1 | 0.22 |
| 110 | 20 | 73.4 | 0.19 |
| 110 | 30 | 72.6 | 0.20 |
| 120 | 10 | 60.3 | 0.34 |
| 130 | 6 | 59.3 | 0.50 |

A polynomial model gives the solubility curve of PZQ in PVPVA (Figure 62). Thanks to these plots, it is possible to identify regions of kinetic and thermodynamic stability. Praziquantel is practically insoluble in PVPVA at room temperature (25 °C). It means that a thermodynamic stability should be achieved at room temperature for API loads lower than ~ 2 %. In contrast, a high PZQ load SD with 50 % of PZQ might be phase separate and probably recrystallize at 25 °C.

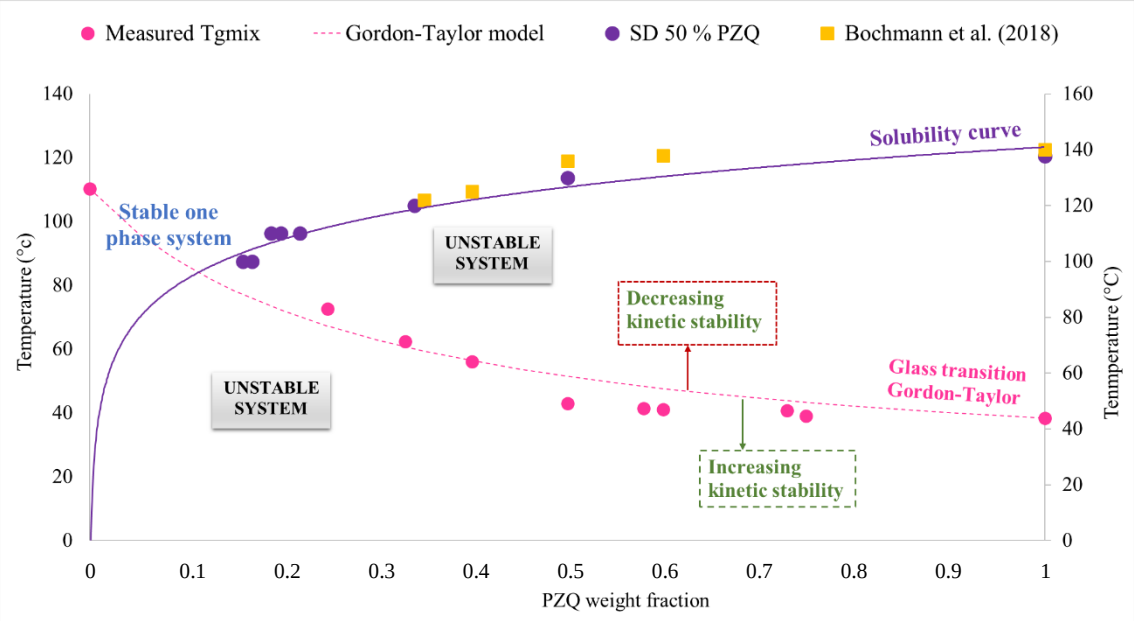


Figure 62. Composition-temperature phase diagram for the binary PZQ-PVPVA

*Comparison with PZQ-PVPVA solubility data obtained from a dissolution method*

Recently we have identified another study carried out in 2018 presenting a similar phase diagram for the binary PZQ-PVPVA (Kollidon® VA 64), constructed from a DSC method [56].This method was based on the dissolution of the API in the polymer following a DSC protocol developed in a previous work of the same authors [307]. The dissolution process was detected through DSC as an endothermic event. The melting temperature of the API/polymer solid mixture was determined as the temperature at which the dissolution of the API in the polymer was completed. Since this method is dynamic, the obtained temperature depends on the heating rate. A correlation between melting temperature and applied heating rate is necessary for the use of this method. From this correlation (found to be linear by the authors), the melting temperature for a API-polymer binary mixture of known composition was extrapolated to a heating rate of zero to obtain the equilibrium value (API solubility in the polymer).

This method was applied by Bochmann et al. [56] to determine the solubility of PZQ in the same polymer used in this thesis. The mentioned work has used the PZQ-PVPVA system as one of four systems evaluated (three other APIs) to correlate API solubility to the melt viscosity of amorphous solid dispersions. The aim was to propose a model-based melt viscosity in hot-melt extrusion numerical simulation.

The method we have employed is the recrystallization of a supersaturated solid solution. In this way, $T_{gmix\,2}$ is obtained from the residual crystalline material after annealing. Different annealing temperatures can provide specific $T_{gmix\,2}$ that, with a deviation fit model, the solubility curve can be established. Comparatively, the method used in this thesis presents a higher execution speed because regardless of the deviation adjustment model used, the process of obtaining the $T_{gmix\,2}$ is more practical, with only two heating cycles and one cooling.

Independently of the method used, the results described in the literature (plotted as orange points on Figure 62) have a good correlation with our data, which represent a greater number of points, thus generating a better relationship for solubility predictions with the mass fractions of the system at a given temperature.

## 3. CONCLUSIONS

API-polymer solubility and the glass transition temperature are the main factors that influence physical stability and performance behaviour. An API-polymer temperature-composition phase diagram is useful to predict the stability of amorphous binary-mixtures of different compositions under different temperature conditions.

The development of such phase diagram for the PZQ-PVPVA binary was one of the first objectives of this thesis to evaluate the risks of physical stability for amorphous solid dispersions with high content of PZQ (50wt% as primary ambition).

A demixing process characterizes the recrystallization of the API in a supersaturated API-Polymer solution up to reach the equilibrium concentration of the API at a given (annealing) temperature. Supersaturated amorphous systems could be generated by spray-drying and be widely characterized. The use of spray drying was proposed by our group in a previous PhD thesis as an alternative to determine API-polymer solubility from demixing, because it is a fast process (some seconds for sample production) compared to solvent casting or comilling which are very time-consuling (hours). We employed this preparation process for a second time. Its interest is confirmed from the comparison to the method used by other authors for the same binary (PZQ-PVPVA).

From our diagram, we could confirm that their physical stability against phase separation and recrystallization will be a great challenge. However, before stability risks, the previous question is related to the feasibility of producing amorphous solid dispersions containing 50 wt% PZQ by hot-melt extrusion technology.

We look at these questions in Chapter 5.

# CHAPTER 5 - BINARY AND TERNARY SYSTEMS OF PRAZIQUANTEL AMORPHOUS SOLID DISPERSIONS MANUFACTURED BY HOT MELT EXTRUSION

## 1. INTRODUCTION

This Chapter is dedicated to the development of amorphous solid dispersions of praziquantel, comprising binary (API and polymer) and ternary (API-polymer-surfactant) systems.

The binary and ternary systems were produced by hot-melt extrusion (HME) process.

The choice of HME as the manufacturing process was based on some of its advantages over other techniques: it is a continuous manufacturing process, does not require the use of solvents and can be transposed from the bench-scale to an industrial scale of production.

The Chapter is divided into four Sub-chapters:

*Sub-chapter 5.1* - has the main objective to present a binary PVPVA and PZQ amorphous solid dispersion. The theoretical PZQ load in the formulations was fixed at 50 wt%. The selected process parameters and the characteristics of the products obtained (solid state, apparent solubility, dissolution performance, stability) are presented and discussed.

*Sub-chapter 5.2* - is focused on the ternary amorphous solid dispersions (PVPVA, API, surfactant). Two surfactants, one liquid (monolaurate de sorbitan) and another in a powder form (sodium lauryl sulfate) were used, generating two different categories of ternary formulations. The main motivation for studying ternary formulations was to improve dissolution and solubility PZQ properties. The theoretical PZQ load in the formulations was also fixed at 50 wt%. The study described in this Sub-chapter was performed in a Pharma 11 Extruder (Thermo Scientific). The preparation method, the characteristics of the samples generated (solid state, apparent solubility, dissolution performance, stability) are presented and discussed. Batches of placebo formulations (without PZQ) were also produced and characterized.

*Sub-chapter 5.3* – is dedicated to the development of the same ternary systems of Sub-chapter 5.2 (theoretical PZQ load of 50 wt%), however, the samples were generated in another equipment, a Pharma 16 extruder (Thermo Scientific). Changing of HME extruder requested modifications in the preparation of the ternary mixture fed to the

extruder. Like for ternary ASDs generated before in Sub-chapter II, the preparation method, the characteristics of the samples generated are presented and discussed.

*Sub-chapter 5.4* - this last Sub-chapter is dedicated to new compositions of the ternary
formulations, in which the theoretical PZQ load was reduced to 35 wt%. The reasons for the load reduction will be presented and discussed. These new formulations are the ones that will be used in the production and evaluation of printlets (tablets obtained by 3D printing) explored in the Chapter 6.

To facilitate the lecture of the Chapter 5, Figure 63 gives a schematic representation of its Sub-chapters.

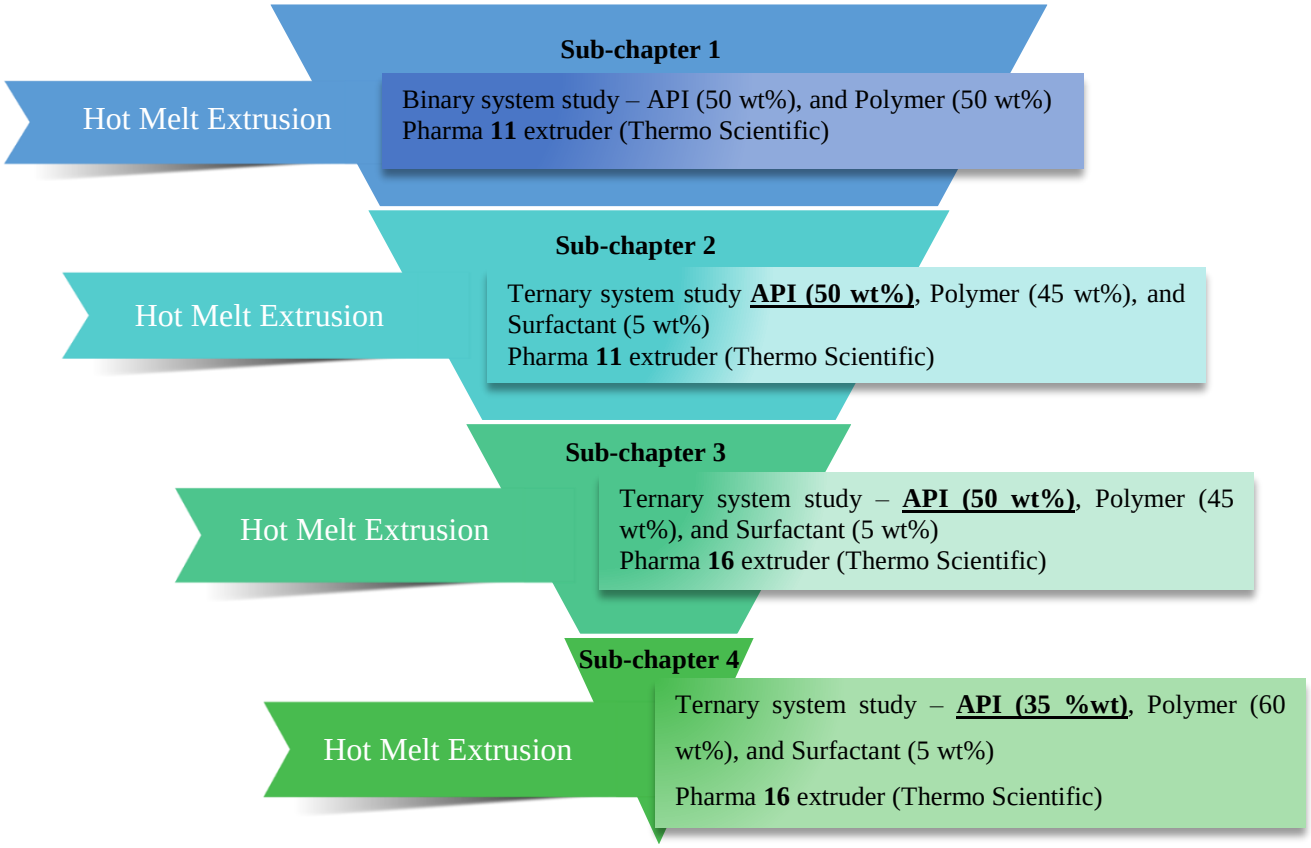


Figure 63. General view of the structure of chapter 5.

# SUB-CHAPTER 5.1 - PRAZIQUANTEL AMORPHOUS SOLID DISPERSIONS MANUFACTURED BY HME - BINARY SYSTEM (50 WT% PZQ) PHARMA 16 EXTRUDER

## 1. INTRODUCTION

This Sub-Chapter is dedicated to the binary amorphous solid dispersions (ASD) produced by hot-melt-extrusion (HME). The composition of these binary systems was fixed at the mass proportion of 1:1 for PZQ and PVPVA.

A co-rotating twin-screw extruder (pharma 16, Thermo-Fisher) was used for the HME process. The HME process parameters (speed and screw design, and feed rate) were adjusted in a first series of tests. Second, PZQ-PVPVA systems were produced at selected HME process conditions and the resulting HME extrudates were characterized with respect to their solid state (DSC, DRX, SEM) and performance behaviour (solubility, in-vitro dissolution).

The methodology used and the results obtained are presented and discussed in this Sub-Chapter.

## 2. METHODS

### 2.1 Binary ASD system prepared by HME (50 wt% PZQ)

The production of amorphous solid dispersions (ASD) containing praziquantel was performed using a twin-screw extruder (pharma 16, Thermo scientific™, Germany).

The twin-screw extruder comprises a pair of parallel **screws,** rotating inside a barrel with an 8-shaped cross-section (eight heating zones), two mixing zones and a screw diameter (D) of 16 mm and L/D ratio equal to 40 (L being the length of barrel) (Figure 64).

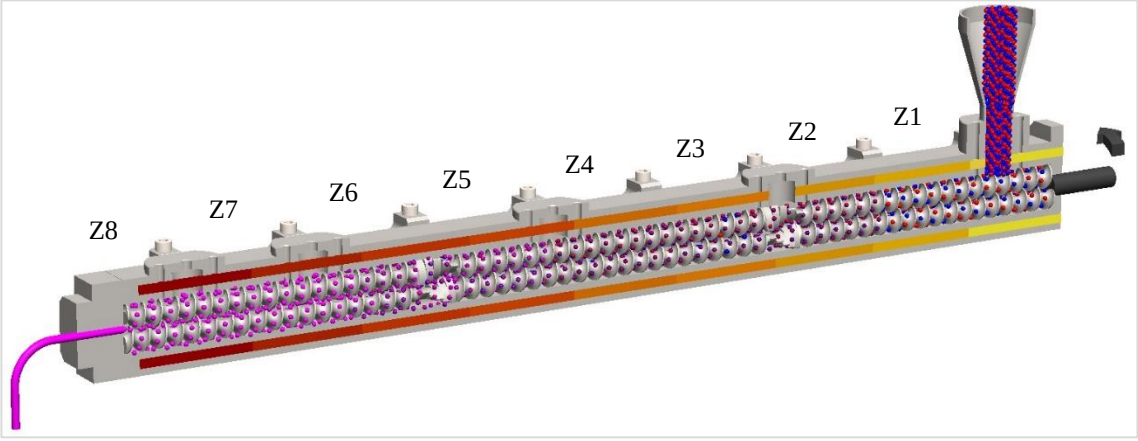


Figure 64. Schematic representation of extruder with 8-shaped cross-section heating zones. Source: Author.

Four auxiliary equipment was used in the production according to the needs of each formulation. They are: gravimetric feeder, peristaltic pump, and stirrer with heating, air cooling conveyor, and pelletizer. A general view of the equipment is shown in Figure 65. The adjustment of the equipment's settings was made on the control panel (touch screen).

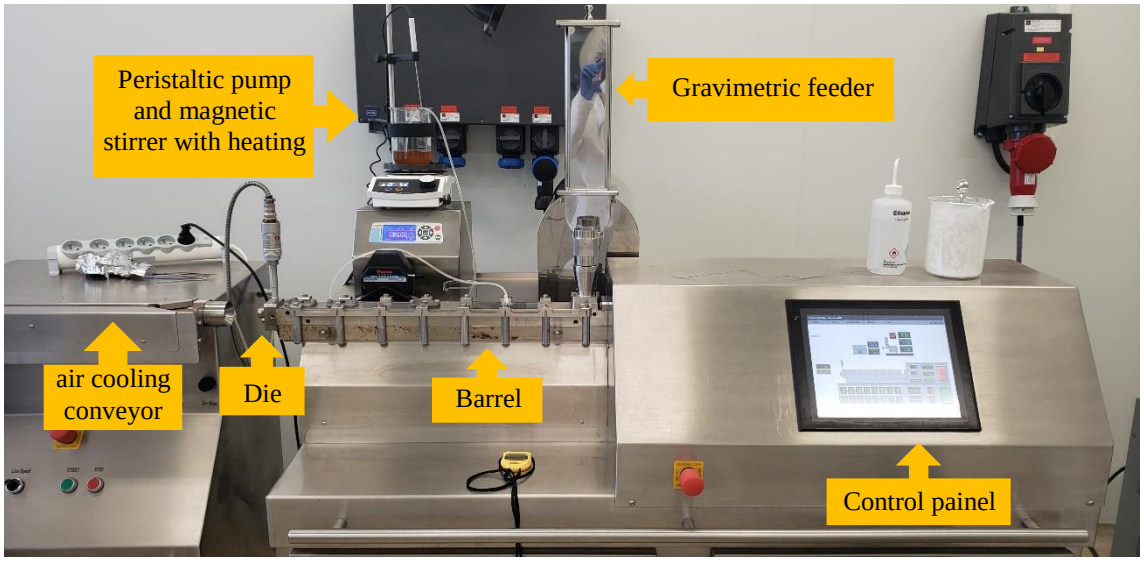


Figure 65. General view of the extruder (Thermo-Fisher pharma 16) and complementary equipment. Source: Author.

As introduced before (Chapter 2), the choice of the process parameters such as the temperature profile of the different zones, the screw speed, the thread configuration, and the material feed rate will impact the process feasibility and the quality of the extruded material [308][268][309].

The determination of the screw configuration is then an important step. In general, the three main types of elements are: conveying, kneading, or mixing, and reverse conveying (Table 26).

The main function of the conveying element is to flow the material along the screw [310]. However, different designs of these elements can change their characteristics. For example, the width of the step in conveying elements increases in the distributive and dispersed mixture per unit of mixing length, increasing conveying speed [311]. On the other hand, reverse conveying elements can be used. Usually, this strategy is applied to cause the backpressure and leaving the areas filled with API: Polymer, favouring the mixture [310]. Typically, the position of the reverse conveying elements is after the block

of kneading or mixing elements creating the resistance of the flow forward, causing an increase of the mixing efficiency, residence time, and shear (Figure 66) [272].

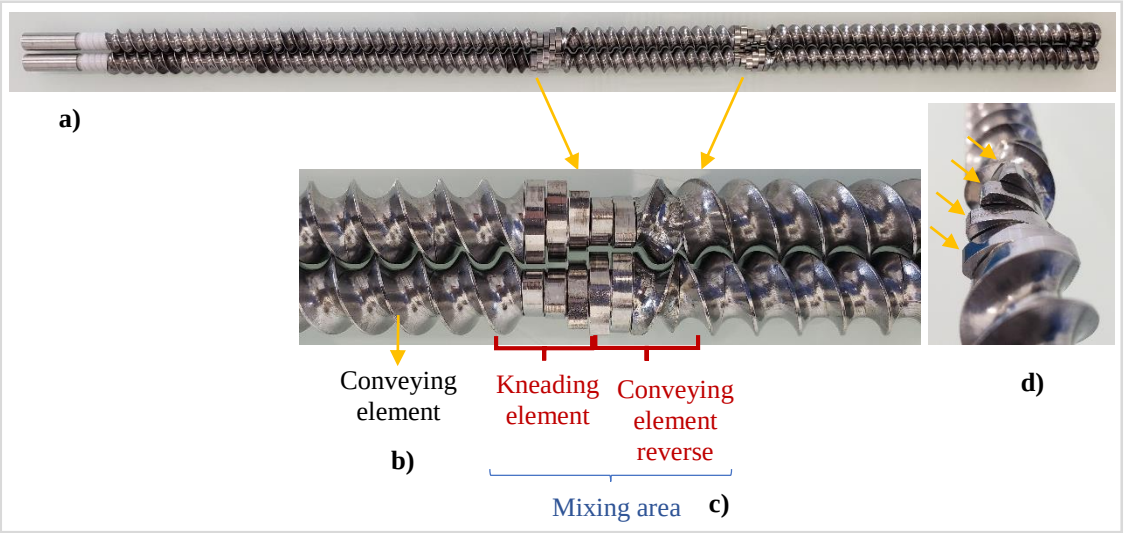


Figure 66. a) General screw view with element reverse, b) conveying element, c) Mixing area with kneading elements following the conveying element reverse and d) different angles with the kneading elements. Source: Author.

The kneading or mixing elements are designed with different offset angles between adjacent discs (Table 26). They are usually 30, 45, 60, and 90 º. The smaller displacement angles provide greater flow capacity (push the material), acting almost as a flow element. In this way, the kneading elements have the characteristic of controlling the residence time and pressure [310].

In this study, the rationale adopted to determine the screw design was:

a) a profile in which it had two mixing zones with a variation of the offset angles for conveying (smaller) and mixing (larger angles) (Table 27 - blue);
b) a profile with two points of conveying reverse elements positioned after the kneading zone (effective mixing) to extend the time of intense contact of constituents in the molten material (Table 27 - pink) [311].

Table 26.Screw elements used in this study.

| *Screw elements name* | *Screw elements* | *Symbol* | *Dimension* | *Application* |
|---|---|---|---|---|
| Conveying | 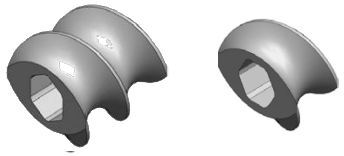 | C or ½ C | C: 16 mm width element<br>1½ C: 8 mm width element | Material conveying in feed, conveying, or mixing area<br>Presence only in mixing area to disperse or distribute the material |
| Kneading or Mixing |  | 0 or 90 ° (depending on the desired angle of inclination) | 1 element: 4 mm width | In mixing, dispersion and/or distribution area |

Table 27. Temperature and screw profile for screening tests with PZQ and PVPVA (1:1).

| *Parameter condition* | *Code* | *Temperature (°C)* | | | | | | | | | | | | |
|---|---|---|---|---|---|---|---|---|---|---|---|---|---|---|
| | | *Zone 2* | *Zone 3* | *Zone 4* | | | *Zone 5* | *Zone 6* | | | *Zone 7* | | *Zone 8* | *Die* |
| Temperature profile | ***T 1*** | 50 | 70 | 100 | | | 140 | 140 | | | 140 | | 100 | 90 |
| | T 2 | 50 | 70 | 100 | | | 140 | 140 | | | 140 | | 100 | 100 |
| Screw profile | RE | 5 C | 5 C | 0/90/0/90/0<br>30° | ½ C<br>***Reverse*** | ½ C | 1 C | 5 C | 0/90/0/90/0<br>30° | ½ C<br>***Reverse*** | ½ C | 3 C | 5 C | 3 C | ½ C<br>Fixe |
| | NRE | 5 C | 5 C | 0/90/0<br>90° | 0/0/0<br>60° | 0/90/0/90<br>30° | 2 C | 5 C | 0/90/0<br>90° | 0/0/0<br>60° | 0/90/0/90<br>30° | 1 C | 5 C | 3 C | 1/5 C<br>Fixe |

The extruder is connected to a central control, allowing the control of process parameters such as screw speed and temperature, and therefore pressure [272]. The process has to be conducted above the glass transition temperature ($T_g$) of the constituents but below its degradation temperature ($T_{deg}$). The API can be processed below or above its melting temperature ($T_m$) depending on the solubility capacity of the polymer [272].

In our studies, the temperature profile was established from the knowledge of the melting temperature of the crystalline component (PZQ). Process temperatures close to the PZQ melting temperature are expected to allow its miscibility with the polymer in the molten state. Table 27 presents the selected temperature profiles.

To produce the physical mixtures, a powder mixer (Turbula® T2F mixer) was used (Figure 67). This equipment is a reversible mixer whose operation is based on the combination of three movements: a translation, a rotation, and an inversion [312]. This combination leads to a three-dimensional movement. The device consists of a tank inserted and fixed in a mixing basket connected by two brackets with two axes of rotation. One of the two axes is a motor and drives the system at the chosen speed (Figure 67).

Figure 67. Turbula® T2F mixer (Willy A. Bachofen AG Switzerland). Source: [312] with permission.

The polymer PVPVA was dried overnight before use. Physical mixtures of PZQ and the polymer were premixed for 08 min (Turbula® T2F - 48 rpm) before feeding the twin-screw extruder as illustrated in Figure 68. A gravimetric feeder with a small dosing unit was used for feeding.

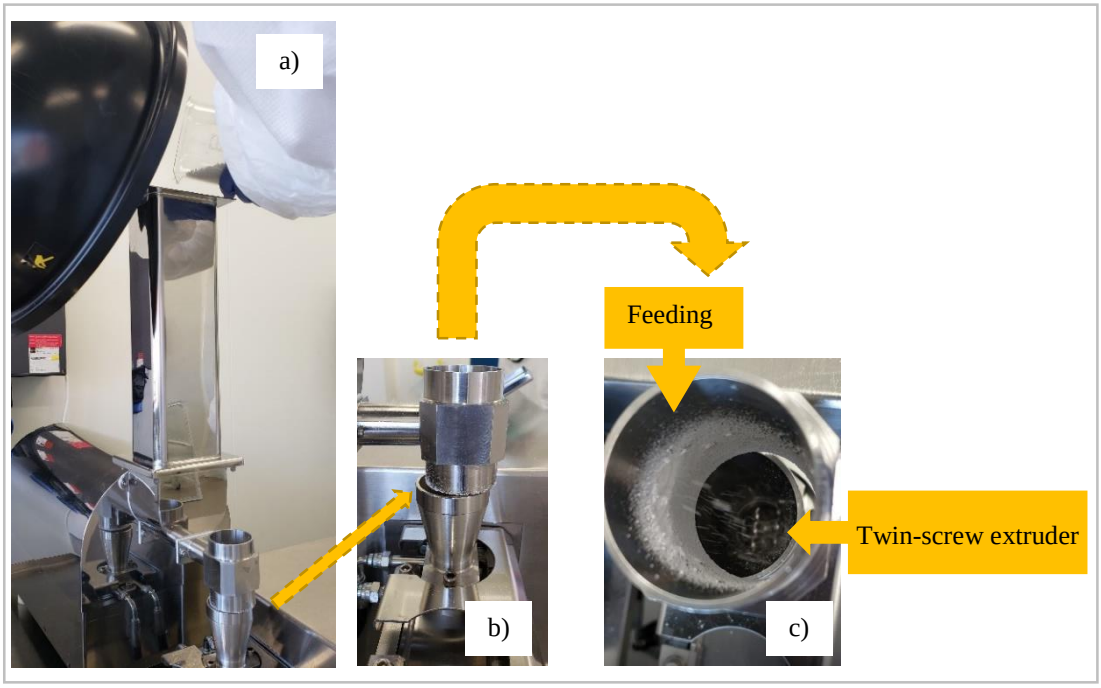


Figure 68. a) Gravimetric feeder; b) extruder feed hopper and, c) top view - mixing input into the extruder. Source: Author.

The extrudate comes out through the "die" and pass by the other two components in downstream processes: an air-cooling conveyor and a pelletizer (Figure 69). The first has the purpose of quickly cooling the freshly prepared extrudate, and the conveyor carries it to the second, the pelletizer.

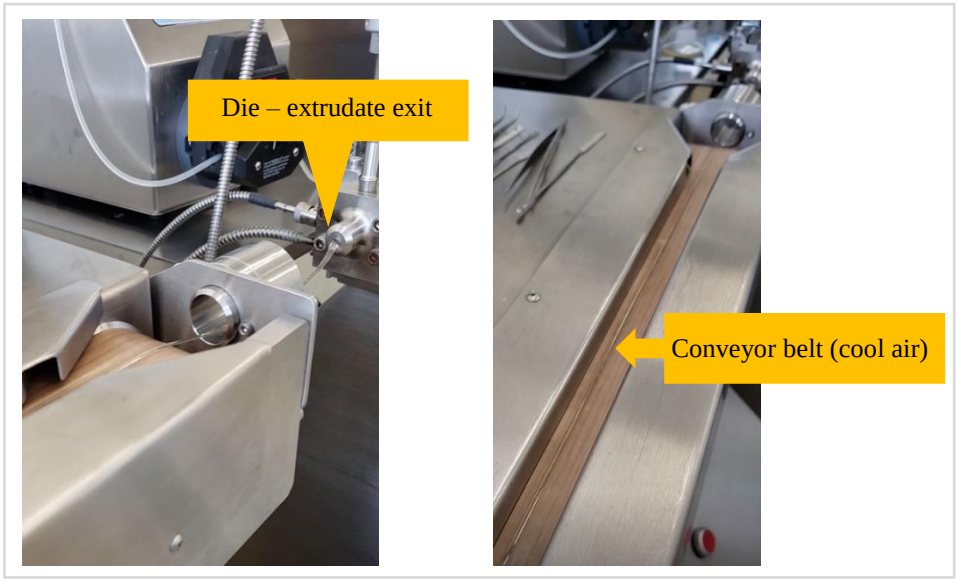


Figure 69. Air cooling conveyor belt (ThermoFisher Scientific).

At this point, the extrudate is broken up into small pieces and the pellet size can be adjusted according to the distance from the cutter (in the range 1.0 to 2.5 mm) (Figure 70).


Figure 70. Pelletizer (ThermoFisher Scientific).

The batches composed of PZQ and PVPVA in the mass proportion 1:1 prepared in this study are described in Table 28.

Table 28. Process operating conditions to produce PZQ: PVPVA systems.

| ***Sample code*** | ***Process operating conditions*** | | | | |
|---|---|---|---|---|---|
| | ***Rate Flow (kg/h)*** | ***Screw speed (rpm)*** | ***Temperature profile*** [+] | ***Screw profile*** [+] | ***Objective*** |
| HME 1 | 0.15 | 150 | T1 | NRE[*] | Parameter effect analysis |
| HME 2 | 0.15 | 300 | | | |
| HME 3 | 0.30 | 150 | | | |
| HME 4 | 0.15 | 150 | T1 | RE[**] | |
| HME 5 | 0.15 | 300 | | | |
| HME 6 | 0.30 | 150 | | | |
| HME 7 | 0.30 | 300 | | | |
| HME 8 | 0.50 | 300 | | | |
| HME 9 | 0.15 | 200 | T2 | | |
| HME 10 | 0.15 | 300 | T 1 | RE[**] | Repeatability test |
| HME 11 | 0.30 | 300 | | | |

[*] NRE = no reverse element, and [*]ER = reverse element.

[+] See details in Table 2.

## 2.2 Characterization of HME extrudates

HME extrudates were characterized by the techniques described previously in Chapter 5.1, that are powder X-ray diffraction (PXRD), scanning electron microscopy (SEM), differential scanning calorimetry (DSC), and water solubility.

The equipment and measurements protocols used for these analyses are the same described in Chapter 4 sections 1.2.2, 1.2.3, 1.2.4, and 1.2.5.

### 2.2.1 Dissolution profile

The experiments were carried out following the method described in Chapter 3 (item 3.1.9) to analyse praziquantel tablets from the American pharmacopeia [297].

For the HME extrudates produced here, an amount equivalent to 150 mg of PZQ was weighed in gelatine capsules (size 0). They were packed in a sinker to avoid the floating and adherence of the particulate materials in the dissolution medium. (Figure 71). The sinkers were added to the vats in the same way as adding tablets.

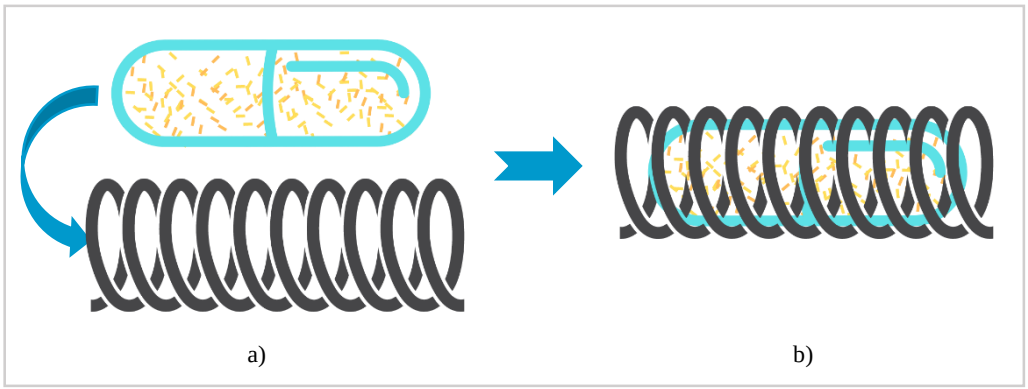


Figure 71. a) Capsules containing amorphous solid dispersions (pellets form) being inserted in the sinker and b) capsule inserted in the sinker, ready for addition to the dissolution vessel.

# 3. RESULTS

## 3.1 Extruder configuration

One of the factors that influence the efficiency of the extrusion process is the screw design [183] [313] [280].

Aiming to define the better screw design for the extrusion of a binary mixture with fixed composition (PZQ: PVPVA - 1:1), the first HME trials evidenced problems related to the powder flowability into the feeder.

Even with a gravimetric feeder, it was possible to visualize variations in the feed rate over the extrusion time. If the powder feed varied for a short time, and even within the limit set by the extruder, the result was a white and opaque product (Figure 72a), evidencing a non-homogeneous mixture. In some cases, the modification of operating conditions as the increase of the temperature in the zone of the barrel close to the exit orifice (die) shown in Figure 72b or the increase of the screw speed could improve the processability of the binary system.

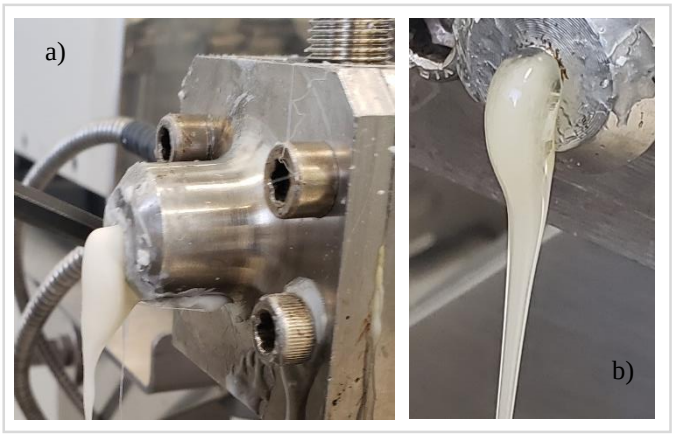


Figure 72. Opaque extrudate after interrupted feeding; b) extrudate after die temperature increase (change on visual aspect to semi-opaque)

However, the adequate selection of the screw elements should help reduce processability problems. To that purpose, different HME process configurations were investigated on the processability of the binary mixture (see Table 29). They are screw configuration (with and without the use of reverse elements), feed rate, and die temperature. Each of these parameters has a specific function during the extrusion process. At the same time, they all interact with each other to control the process as a whole [269]. The configuration with conveying and reverse elements was chosen because they generally result in better processability and production of homogeneous mixtures (transparent filaments). It is known that reverse elements may increase shear forces within the barrel in the mixing section and the residence time of the molten material in the

extruder [6]. Reverse elements were used in our screening configuration to generate back pressure and thus enhance the dispersive mixing by resisting forward flow as expected.

As shown in Table 29, the feed rate was also a parameter investigated in these trials. By impacting the residence time into the extruder, the feed rate may influence the quality of the mixture (homogeneity) and of its constituents (degradation). The lower the feed rate, the longer the residence time [269], [270].

From all HME trials performed with the extruder configurations presented in Table 29, 11 HME extrudates were produced and characterized with respect to their solid state (PDRX, DSC), physical aspect (SEM images) and product performance (PZQ solubility enhancement, dissolution behaviour). The analysis of these characteristics that are presented right after allowed us to select the better screw configuration for hot-melt extrusion of a binary system PZQ-PVPVA with 50 wt% PZQ.

### 3.2 Scattering Electronic Microscopy (SEM)

SEM images referring to six extruded samples (HME1 to HME7), and the powder mixed (before extrusion), are shown in Figure 73.

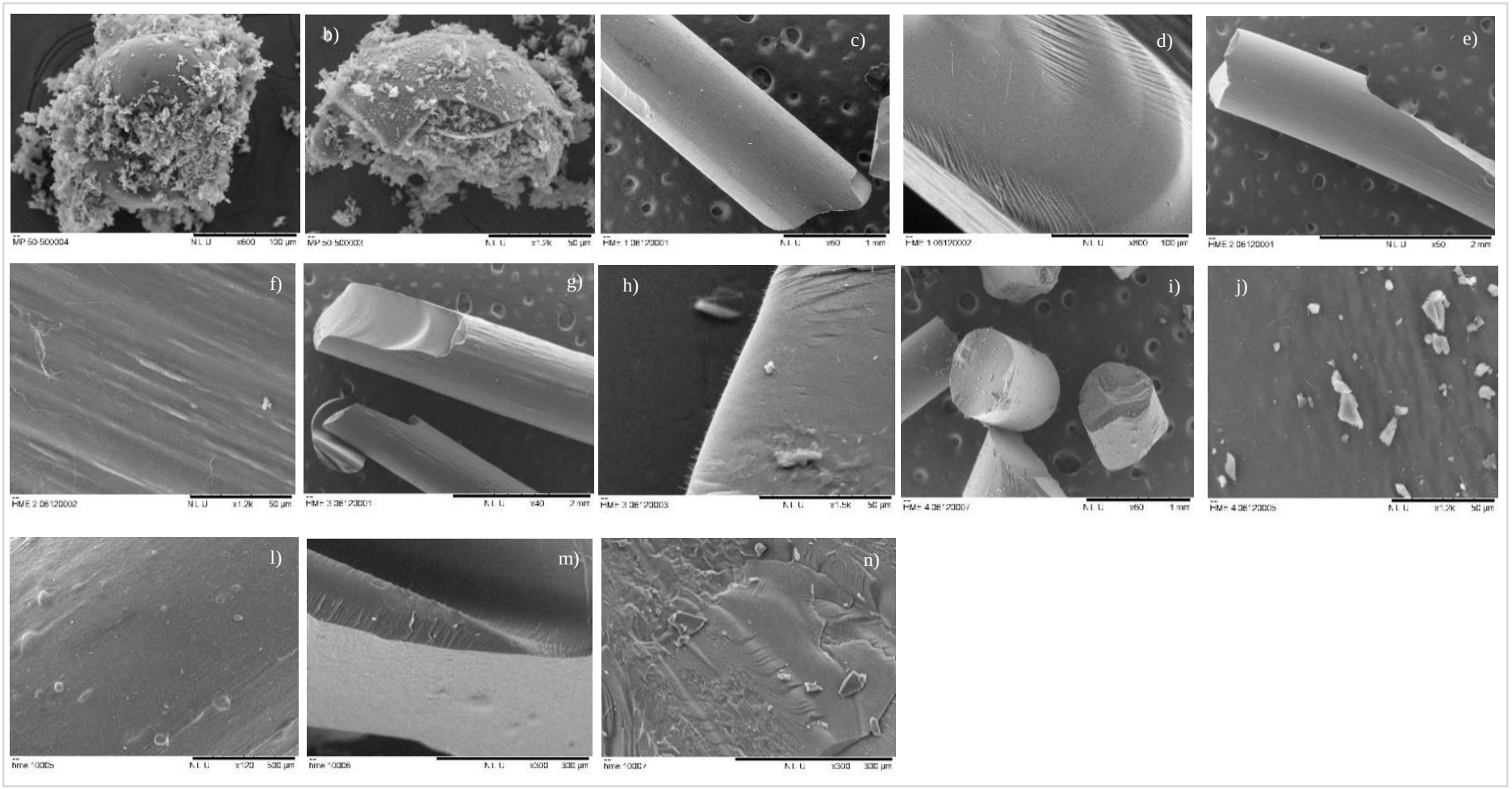


Figure 73. SEM images. a); b) physical mixture PZQ: PVPVA; c) and d) HME 1; e) and f) HME 2; g) and h) HME 3; i) and j) HME 4; l) HME 5; m) HME 6 and n) HME 7.

The SEM images of the physical mixtures were taken just after the mixing process in the Turbula® T2F mixer. The images on Figures 10a and 10b clearly show primary PZQ particles adhered to the spherical particles of the PVPVA polymer. No morphological change was identified between the components after the physical mixing procedure.

Regarding the HME extrudate samples, five different physical shapes can be observed in Figures 73c to 73n:

• HME 1 and HME 4: the presence of structures in the form of extremely fine needles (Figures 73c, 73d, 73i and 73j, respectively);

• HME2: the presence of thin structures, as agglomerated threads (Figure 73e and 73f);

• HME 3: the presence of thin structures, positioned vertically in the extrudates (Figure 73g and 73h);

• HME 5: absence of particles but presence of ripples in the spherical shape, that are probably related to the presence of bubbles in the extruded material (Figure 73l);

• HME 6 and HME7: absence of particles on the surface/core of the extrudates/pellets with evidence of irregular surface or structures arising from the pelletization (Figure 73m and 73n);

### 3.3 Powder X-ray diffraction (PXRD)

The results of PXRD are shown in Figure 74. All samples presented a broad halo characteristic of amorphous material. However, some diffractograms (HME1 and HME3 samples) exhibited very small diffraction **peaks which are rather characteristics of crystalline** than **amorphous** materials.

Here, it is important to note that the HME extrudates produced in the form of pellets were ground manually in a mortar with pistil to perform the PXRD analysis. The need to crush the HME pellets might have resulted in some crystallinity confirmed by the not-well-defined crystalline peaks observed in HME1 and HME 3 samples. As demonstrated in Chapter 3, a binary amorphous solid dispersion with 50 % PZQ in PVPVA is supersaturated at room conditions and a recrystallization could also be caused by milling in this way. On the other hand, the opposite is also true. Some crystalline structures can change their state under grinding. For this reason, techniques such as DSC are generally associated to PXRD for a more comprehensive analysis of amorphous solid dispersions.

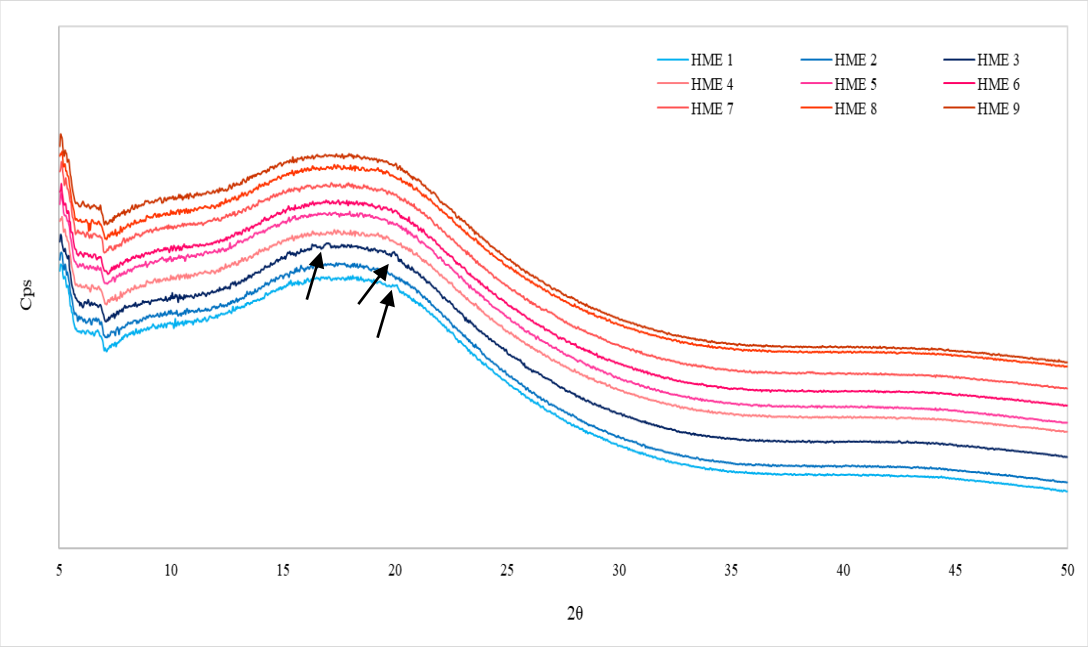


Figure 74. PXRD for samples produced for screening process parameters (arrow shows the very small signal diffraction for HME 1 and HME3 samples).

### 3.4 Differential scanning calorimetry (DSC)

The results obtained by DSC analysis for nine samples produced by HME are shown in Figure 75.

Six HME samples did not show endothermic events, corresponding to an amorphous state (Figure 75a). One of the extrudate samples (HME 4) showed two glass transitions ($T_{g1}$ = 48.24 ºC and $T_{g2}$ = 110.59 ºC), characteristic of a system constituted by two amorphous phases. Contrarily, three of them (HME1, HME3 and HM6) presented endothermic events related to melting transformations (Figure 75b), confirming for two of them (HM1 and HME3) the traces of crystallinity detected by PXRD.

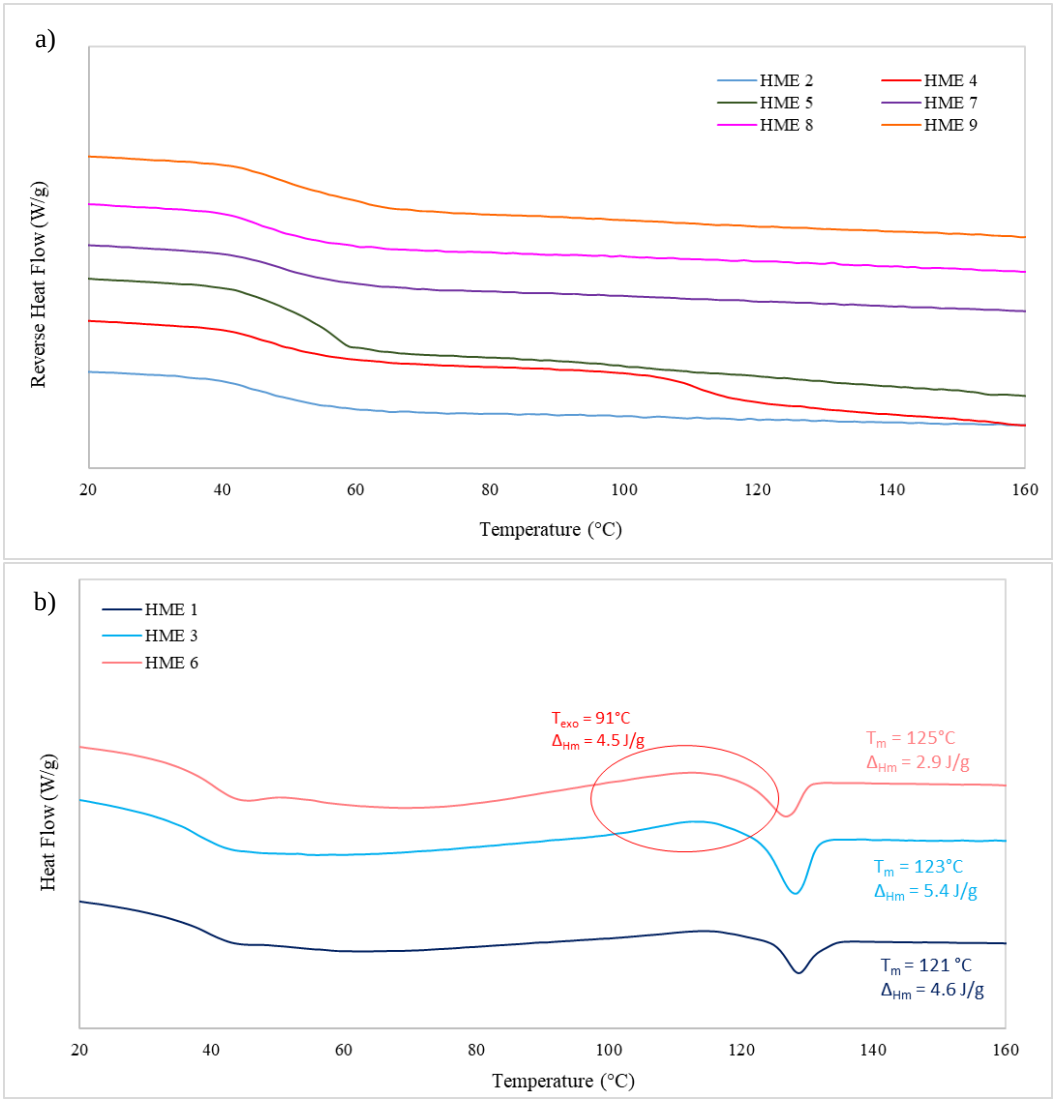


Figure 75. DSC curves. a) samples with amorphous characteristic; b) samples with crystalline diffraction peaks

Table 30 also presents the thermal characteristics from DSC analysis ($T_g$ and $T_m$).

A single $Tg$ was detected in eight samples, between 43.49 °C (HME 2) and 49.62 °C (HME 9). From the GT equation developed in Chap 4, for a binary system PZQ: PVPVA with 50 wt% PZQ, the estimated $Tg_{mix}$ is 4 3°C. The $Tg$ values measured for the HME samples were found to be dependent on the HME process conditions and screw profile. For some samples, the $Tg$ measured was very close to the GT value, but for others not so much. The variations could be related to mixture homogeneity or repeatability.

The visual aspect of the extrudates obtained for each of the nine conditions tested can be observed in Table 30. Differences are probably linked to the homogeneity of the

molten mixture that might have impacted the properties of the final solid dispersion as $Tg$.

For example, the higher $Tg$ (~ 57 °C) was found for the HME 5 sample, which was produced with only reverse elements (RE), and the lowest feed rate. The objective was to promote mixing with the use of "RE" and the longer residence time.

In contrast, the lowest $Tg$ (~ 45 °C) was found for the HME 8 sample, which was produced with the same RE, but with the highest feed rate (shorter residence time). Both HME 5 and HME 8 samples were produced with the same temperature profile (T1, see Table 29) in the extruder. These results evidenced, for a same screw elements design and temperature profile in the extruder, the effect of the residence time on the characteristics of the amorphous solid dispersion ($Tg$ in this case).

The screw design is another factor that influences the mixing efficiency of the extrusion process and a parameter commonly studied. For example, a study using nifedipine and hydroxypropylmethyl cellulose, demonstrated that the kneading elements impacted the alteration of the crystalline structure and the properties related to the dissolution of the produced solid dispersion [314]. Another study demonstrated that the position of the zones containing the kneading elements and the number of these elements does not influence the homogeneity and the drug release rate on the final extrudate product. However, one of these zones was essential to guarantee homogenous distribution [315]. From our first HME trials, the presence of reverse elements (RE) on the screw profile has been found to be essential for good mixing of the binary system under study.

Table 29. Summary of HME process conditions, thermal properties, and visual aspect for all HME extrudates generated from a binary PZQ: PVPVA 1:1.

| ***Sample name*** | ***Condition*** | | | | ***DSC result*** | | | | ***Visual aspect*** | ***Visual aspect and observations did during the production*** |
|---|---|---|---|---|---|---|---|---|---|---|
| | ***Rate Flow (kg/h)*** | ***Screw speed (rpm)*** | ***Temperature profile*** | ***Screw profile*** | ***$T_g$ (°C)*** | ***$T_{onset}$ (°C)*** | ***$T_{peak}$ (°C)*** | ***$\Delta H_m$ (J/g)*** | | |
| HME 1 | 0.15 | 150 | T1 | Zone 4 and 6 **without** RE | 45.59 | 125.32 | 128.82 | 2.916 |  | The flow was too slow for production. The filament thickness was not uniform, and it was smooth, brittle, and transparent with opacity points. |
| HME 2 | 0.15 | 300 | T1 | Zone 4 and 6 **without** RE | 43.49 | - | - | - | 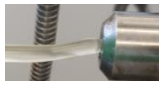 | similar to HME 1 and quite brittle |
| HME 3 | 0.3 | 150 | T1 | Zone 4 and 6 **without** RE | 48.41 | 123.51 | 128.3 | 5.426 |  | similar to HME 1 and 2 |
| HME 4 | 0.15 | 150 | T1 | Zone 4 and 6 **with** RE | $T_{g1}$ 48.24<br>$T_{g2}$ 110.59 | - | - | - |  | The flow was too slow for production. The filament was very thin and transparent. If the thickness, and the opacity increased |
| HME 5 | 0.15 | 300 | T1 | Zone 4 and 6 **with** RE | 57.12 | - | - | - |  | It started with an opaque aspect and became more transparent over time. |
| HME 6 | 0.3 | 150 | T1 | Zone 4 and 6 **with** RE | 45.97 | 120.91 | 126.8 | 0.358 |  | Opaque and formed a large volume of material at the "die" making it difficult to obtain and maintain the filament |
| HME 7 | 0.3 | 300 | T1 | Zone 4 and 6 **with** RE | 49.34 | - | - | - | 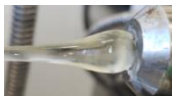 | It formed a "pear" at the exit of the filament. It was difficult to maintain the continuous filament shape. Always transparent. |
| HME 8 | 0.5 | 300 | T1 | Zone 4 and 6 **with** RE | 45.22 | - | - | - |  | Similar to HME 7 but with the white material as a coating at the "die" |
| HME 9 | 0.15 | 200 | T2 | Zone 4 and 6 **with** RE | 49.62 | - | - | - |  | Formation of "pear" at the exit. Transparent, but it was necessary to increase the temperature of the last zone to 100 °C after indication of "die" blocking. |

RE = reverse element on the screw profile

Finally, to verify the batch repeatability, two samples (HME 5 and HME 7) were reproduced. Table 30 presents the conditions of the two chosen samples.

Table 30. Summary of selected HME parameters.

| ***Test/Sample name*** | ***Condition*** | | | |
|---|---|---|---|---|
| | ***Rate Flow (kg/h)*** | ***Screw speed (rpm)*** | ***Temperature profile*** | ***Screw profile*** |
| HME 5 | 0.15 | 300 | (Z2) 50 °,70 °,100 °, 140° 140°,140°, 100 ° and 90 ° (die) | Zone 4 and 6 **with** RE |
| HME 7 | 0.30 | 300 | | |

Table 31 presents a comparison between replicates. The batches were successfully repeated, and the results were similar between them. Although the production of the extrudate with a 50 % drug load has a sensitivity to the process parameters, especially the feed rate, it was possible to obtain reproducible batches. However, the homogeneity of the mixture can influence the $Tg$ values.

Table 31. Summary of results obtained for the selected HME parameters.

| Step | Sample name | DSC result | | | | | PXRD |
|---|---|---|---|---|---|---|---|
| | | $T_g$ (°C) | ΔCp (J/g.°C) | $T_{onset}$ (°C) | $T_{peak}$ (°C) | $\Delta H_m$ (J/g) | |
| Parameter selection study | HME 5 | 57.12 | 0.62 | - | - | - | Amorphous |
| | HME 7 | 49.34 | 0.40 | - | - | - | Amorphous |
| Batch repeatability study | HME 10 | 51.16 | 0.32 | - | - | - | Amorphous |
| | HME 11 | 44.23 | 0.32 | - | - | - | Amorphous |
| PZQ (raw material) | | 39 | 0.36 | 131 | 138 | 95.72 | Crystalline |

## 3.5 Water solubility

Table 32 shows the evolution of the values of PZQ concentration in water (37°C) over 48 h.

Table 32. Solubility data (water at 37 °C) for all HME samples

| Samples | Solubility (mg/mL)* | | |
|---|---|---|---|
| | 1h | 24h | 48h |
| Raw PZQ | 0.138 ± 0.04 | 0.149 ± 0.02 | 0.136 ± 0.03 |
| Physical Mixture (1:1) | 0.190 ± 0.02 | 0.177 ± 0.03 | 0.146 ± 0.04 |
| HME 1 | 0.286 ± 0.02 | 0.221 ± 0.03 | 0.198 ± 0.04 |
| HME 2 | 0.291 ± 0.02 | 0.189 ± 0.01 | 0.191 ± 0.05 |
| HME 3 | 0.057 ± 0.01 | 0.222 ± 0.04 | 0.173 ± 0.06 |
| HME 4 | 0.142 ± 0.003 | 0.228 ± 0.04 | 0.161 ± 0.05 |
| HME 5 | 0.296 ± 0.02 | 0.215 ± 0.03 | 0.157 ± 0.07 |
| HME 6 | 0.307 ± 0.03 | 0.215 ± 0.05 | 0.191 ± 0.05 |
| HME 7 | 0.304 ± 0.03 | 0.266 ± 0.05 | 0.187 ± 0.05 |
| HME 8 | 0.154 ± 0.01 | 0.215 ± 0.04 | 0.172 ± 0.06 |
| HME 9 | 0.287 ± 0.03 | 0.189 ± 0.04 | 0.169 ± 0.05 |
| HME 10[1] | 0.257 ± 0.04 | 0.202 ± 0.05 | 0.197 ± 0.05 |
| HME 11[2] | 0.272 ± 0.02 | 0.203 ± 0.02 | 0.183 ± 0.04 |

* Values represent the mean of n =2 and SD. [1] replicate of HME5; [2] replicate of HME7

First, it can be seen from Table 33, that most HME extrudates showed a positive effect, increasing PZQ water solubility (37 °C) in comparison with raw PZQ, during a given period. The positive effect is lessened over time, as expected for amorphous solid dispersions. Except for HME samples 3, 4, and 8, all showed similar performance in increasing PZQ concentration in water in the first hour and subsequent decrease in the subsequent ones, sometimes an oscillatory variation (increase and decrease on measured concentration, corresponding to dissolution-recrystallization-dissolution events). Figure 76 represents graphically the same data grouped in Table 33 for better visualization of the mentioned solubilization behavior.

This kind of variation is typically found with amorphous solid dispersions for as efavirenz [184] and ritonavir [184], [316]. For example, with efavirenz (API) solid dispersion produced by spray drying, for which, an oscillatory variation in drug concentration was measured in the first two hours.

From our results, when comparing the ‘spring’ effect (the maximum measured concentration reached at 1h is taken for analysis here), we can see that the improvement in PZQ concentration reached more than 2-fold the equilibrium concentration (raw PZQ) for samples HME 5 and HME 7.

The HME 6 sample also presents a 2-fold increase in the PZQ concentration in the first hour compared to the API alone. However, the HME 6 sample presented an endothermic event, probably related to the fusion of the crystalline part of the system. We

can propose two hypotheses for this result: first, the crystalline phase is a polymorph of the PZQ that presents greater solubility in water than the racemic form; or the fraction used for the solubility experiments, although conducted in triplicate, did not have crystalline material (heterogeneity of the sample).

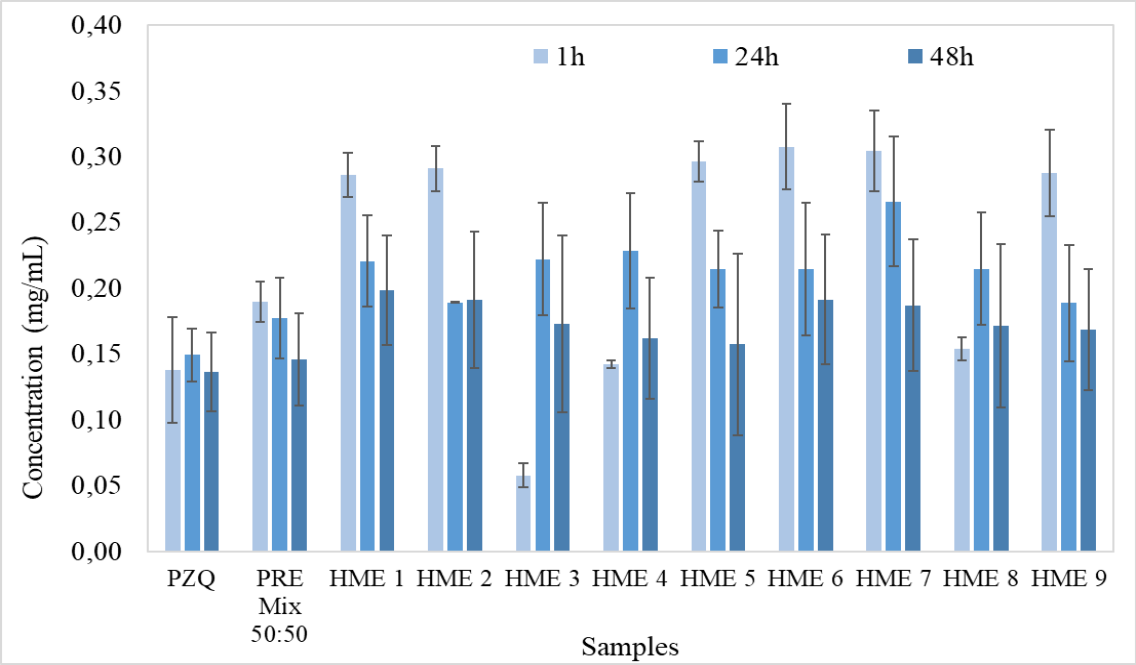


Figure 76. PZQ concentration measured in water (37 °C) from HME extrudates of PZQ and PVPVA (50%PZQ). Time points :1, 24 and 48h.

The HME 10 and HME 11 samples (replicates of HME 5 and HME7 respectively), showed similar performance in the solubility tests, confirming the reproducibility of HME samples' properties.

To briefly put things into context, different results obtained with PZQ amorphous solid dispersions already reported in the literature are discussed here.

Different studies that evaluated the increase in solubility for solid dispersions containing PZQ report success in reaching this objective, but none report monitoring over time and this phenomenon of solubility decay. For example, samples of PZQ and crospovidone produced by cryomilling (1: 1) showed about 3 times more solubility in water (at 20 °C, after 48 h) compared to the respective physical mixture and more than 4 times compared to raw API [179]. Another study evaluated the increase in solubility of solid dispersions obtained by the solvent evaporation method. The binary samples were prepared with different concentrations of PVP. It was concluded that the solubility

increased with the increasing proportion of PVP (better results for PZQ:PVP (3:1) prepared with water/ethanol show a solubility of 1.15 mg/mL, and PZQ: PVP prepared with ethanol show a solubility of 1.29 mg/mL, measured at 25°C after 72h) [65]. Another useful information from these studies concerned the maximum time for solubility studies, that should not exceed 48h due to the chemical degradation of PZQ at 72 h or more [10], [179].

Solid dispersions of praziquantel with starch glycolate [66] also showed an improvement on PZQ water solubility (25 °C, after 48 h) compared to their respective physical mixtures and raw API. The best results obtained with the highest proportion of starch glycolate (API: Polymer 1: 3) was around 1.2 mg/mL.

In our case, the experiments were conducted at 37 °C in water while most of the experiments described in the literature use 20 or 25 °C. At this time, the solubility maintenance effect was not achieved and we obtained an increase in solubility of 117 % and 111 % HME 7 and 5, respectively) when compared to the API in the first hour (spring effect).

### 3.6 Dissolution Profile

HME 10 and HME11 samples were the chosen extrudate products for dissolution tests that were carried in – HCl 0.1N with 0.2 wt% of SLS at 37 °C.

Figure 77 shows the dissolution curves obtained for both samples, taking the raw API as reference.

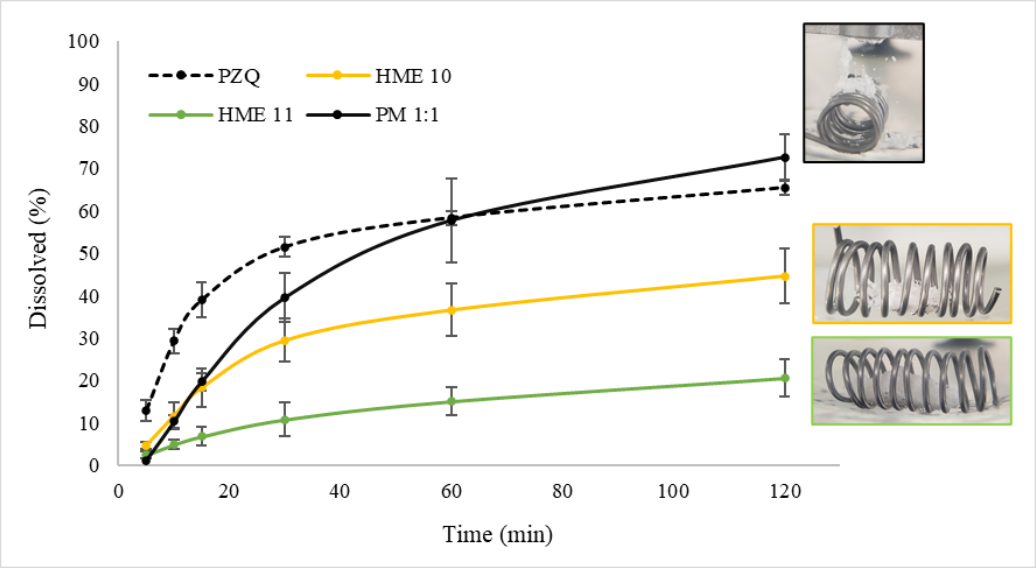


Figure 77 Dissolution profile for HME 10 and HME 11 samples.

Starting the analysis with the raw API, a dissolution of 65.4 % was reached at the end of the experiment (2 h). A similar dissolution profile was reported by Orlandi and collaborators [169] with about 57 wt% of racemic PZQ dissolved in 2 h, with the same conditions (medium HCl 0.1 with 0.2 wt% SLS).

Figure 77 shows that the dissolution profile from the physical mixture between PZQ and PVPVA revealed a retard effect of the polymer in the initial PZQ dissolution, but the final amount released remained almost the same. The same tendency is observed with the HME samples, however, with them, the drug dissolution was effectively retarded up the end of the experiment.

The interpretation of these data needs to consider some analytical factors that may have influenced the results. Initially, it could be seen some agglomeration between the pellets inside the capsule. That agglomeration was probably a limiting factor in the dissolution process because the free pellets would have a larger surface area in contact with the medium.

Still, the difference between the two samples (HME 10 and HME11) may be influenced by different particle sizes between the two amorphous solid dispersions. Although the pellets were produced by the same ‘pelletizing’ (to shape HME filaments into pellet form) process, after that, they are not sieved to guarantee a narrow range of particle sizes in the analysed samples. In the further studies on this thesis, samples with

different formats (powder and pellets) were evaluated as well the composition of the dissolution medium in view to identify the best discriminative conditions to compare dissolution profiles from different HME samples.

## 4. CONCLUSIONS

The study presented in the Part I of this Chapter aimed to verify the feasibility for producing binary amorphous solid of PZQ (50 wt%) and PVPVA (50 wt%) by hot-melt extrusion process.

A first series of HME trials was performed. It was soon realized that the high concentration of PZQ in the binary mixture make difficult the feed of the extruder and is a weak point for the processability of this composition. From the trials, it was demonstrated that the processability of this binary system was dependent on the adjustment of parameter as the residence time and the homogeneity of the molten mixture into the extruder. They can be varied by the adequate choice of operating parameters such as the feed rate, the screw design (conveying and mixing elements) and configuration (number and placement of screw elements).

Different HME extrudate samples were produced from these different extruder configurations and the characterization of these samples showed differences like:

- Thermal properties: they were predominantly amorphous, but the extruder configuration impacted their $T_g$, and even the presence of some crystallinity in some of them. This is an interesting finding because, as already seen in Chapter 4, a binary system with 50 wt% PZQ is falling in the region IV of the PZQ-PVPVA phase diagram at room conditions. Be or not partially amorphous can be the consequence of the sensitivity of the supersaturated samples to undergo recrystallization, depending on the homogeneity of the dispersed amorphous PZQ in the amorphous polymer, which could be influenced by the process conditions of their preparation.
- Desired characteristics of improved water solubility and dissolution: the typical behaviour of an amorphous product (spring effect) was evidenced during the solubilization in water. The parachute effect was not evaluated at this time. However, the dissolution kinetics was remarkably delayed, which needs to be improved. The dissolution methods were modified for the subsequent studies. The

other parameter studied was the composition of the amorphous solid dispersion, focused on the next Sub-chapters.

# SUB-CHAPTER 5.2 - PRAZIQUANTEL AMORPHOUS SOLID DISPERSIONS MANUFACTURED BY HME - TERNARY SYSTEM (40 AND 50 wt% PZQ) - PHARMA 11 EXTRUDER

## 1. INTRODUCTION

This subchapter presents the methodologies employed for preparing, manufacturing, and characterizing ternary solid dispersions containing PZQ by HME using a Pharma 11 extruder (Thermo Scientific).

Two formulations were prepared, both containing API, polymer, and surfactant. For one of them, a liquid surfactant (SPAN 20) was used, and for the other, a solid surfactant (SLS). Thus, two different ways of preparing the physical mixture to be used in the extruder feed were evaluated.

The main objectives of the study presented here are:

• Processability study of extruding physical mixtures with different characteristics.

• Characterization of solid-state, water solubility, in-vitro dissolution and physical stability.

• Evaluation of the in vitro and in vivo palatability

• In vivo pharmacokinetic profile of the ternary systems obtained.

For sake of clarity and to help the evaluation of results, the chapter 5.2 is divided in two parts:

- Part 1. Generation and physicochemical characterization of the extrudate ternary systems,

- Part 2. Taste masking and pharmacokinetics study.

# PART 1 - GENERATION AND PHYSICOCHEMICAL CHARACTERIZATION OF THE EXTRUDATE TERNARY SYSTEMS

## 1. METHODS

### 1.1 Ternary ASD system prepared by HME (40 and 50 wt% PZQ)

The production of solid amorphous dispersions containing praziquantel was performed using a Thermo-Fisher pharma 11 Extruder (Thermo scientific™, Germany) (Figure 78).

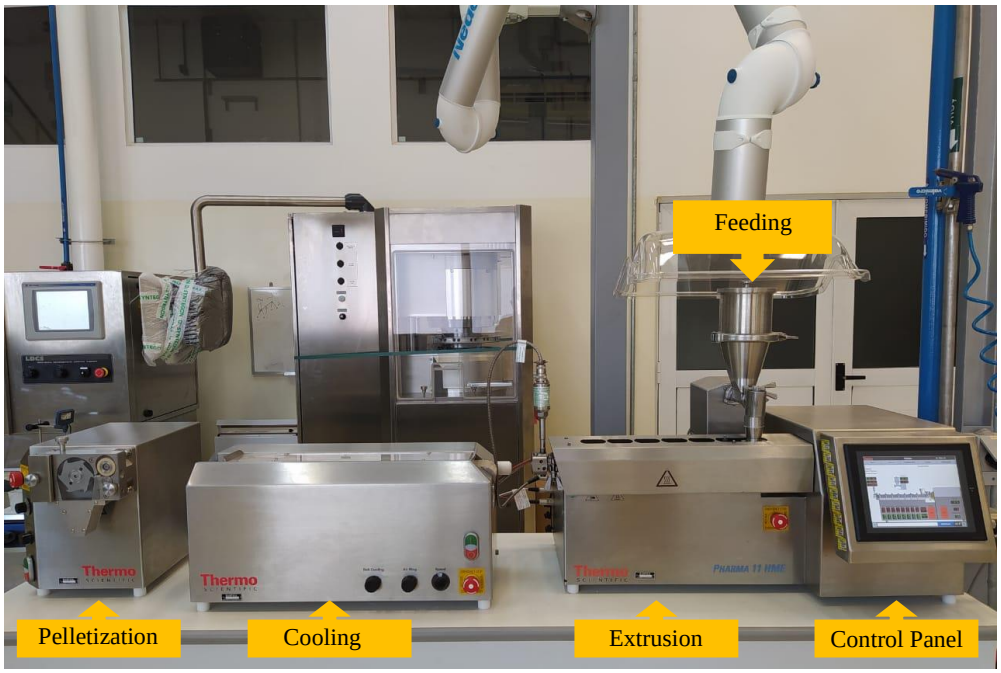


Figure 78. Extrusion system using Pharma 11 extruder.

The extruder was configured with a co-rotating twin-screw parallel with eight heating zones, two mixing zones and a screw diameter (D) of 11 mm. As in chapter 5.1, a gravimetric feeder, air cooling conveyor, and pelletizer were also used.

The composition of the formulations studied are shown in the Table 33.

The temperature profile and the twin-screw extruder profile used for each of the formulations produced is shown in Table 34.

Table 33. Composition used for manufacturing ternary system by HME.

| ***Ingredients*** | ***Formulation composition (wt%)*** | |
|---|---|---|
| | ***FEXT1*** | ***FEXT2*** |
| Praziquantel (PZQ) | 50 | 40 |
| Kollidon® VA64 (PVPVA) | 45 | 55 |
| Span (SPAN) | 5 | - |
| Kolliphor® SLS Fine (SLS) | - | 5 |

Table 34. Extrusion process parameters.

| ***Parameter condition*** | ***Code*** | ***Temperature (°C)*** | | | | | | | | | | | | | | |
|---|---|---|---|---|---|---|---|---|---|---|---|---|---|---|---|---|
| | | ***Zone 2*** | ***Zone 3*** | ***Zone 4*** | | | | ***Zone 5*** | ***Zone 6*** | | | | ***Zone 7*** | | ***Zone 8*** | ***Die*** |
| Temperature profile | ***T 1 FEXT 1*** | 50 | 80 | 120 | | | | 160 | 180 | | | | 160 | | 120 | 110 |
| | T 2 FEXT 2 | 50 | 80 | 120 | | | | 160 | 180 | | | | 160 | | 122 | 110 |
| | T3 Placebo | 50 | 80 | 120 | | | | 160 | 180 | | | | 160 | | 120 | 110 |
| | | | | | | | | | | | | | | | | |
| Screw profile | NRE | 5 C | 5 C | 0/90/0 90° | 0/0/0 60° | 0/90/0/90 30° | 2 C | 5 C | 0/90/0 90° | 0/0/0 60° | 0/90/0/90 30° | 1 C | 5 C | 3 C | 1/5 C Fixe | |

## 1.2 Preparation of the feeding material

Considering that the ternary systems had different surfactants in their composition, one solid (SLS) and the other liquid (SPAN 20), the preparation of the powdered mixtures for feeding the twin-screw extruder was specific por each ternary, depending on the type of surfactant used.

The FEXT 2 formulation, with the solid surfactant (SLS), correspond to a mixture of solid ingredients (PZQ, PVPVA, SLS). The preparation of the physical ternary mixture was quite simple and realized in plastic bags with manual homogenisation by the same operator for 3 minutes. A laboratory scale conical mill (Comil®) by Quadro® (Model U3 0125) shown in (Figure 79) was used to grind the ternary mixture. The material entered the mill through the hopper and a rotating impeller reduced the size of the material in the milling chamber. The rotational speed of the mill was set at 2200 rpm, and the sieve size used was 1575 mesh (1.5 mm). The milling operation was carried out for 5 min. The main objective of this procedure was to improve and standardize the homogeneity of the powder mixture since the constituents have different particle sizes.

Figure 79. Conical mill (Quadro® Comil® U3 0125) with the respective sieve size used.

A similar milling equipment was used in other subsequent studies in this thesis, at Rapsodee laboratory in France, where a part of the experimental work of this thesis was carried out. A similar equipment was more detailed in the Sub-chapter 5.4.

The preparation of the FEXT 1 formulation required additional steps on the preparation of the ternary mixture for feeding the twin-screw Pharma 11 extruder. As SPAN 20 is a liquid surfactant, the solution proposed was a wet granulation step followed by the drying of the granules.

First, PZQ was granulated with an ethanolic solution of PVPVA and the liquid surfactant was incorporated to the binary mixture during the granulation process.

For that, a high-speed granulator (Micromix Huttlin - Bosch®) was used. The equipment based on a mechanical impeller moves the powder while a liquid binder is applied into a moving powder bed. The addition of the liquid binder starts the formation of granules. The granulator also has a chopper that works to break larger agglomerates and facilitate uniform mixing [317], [318]. The following operating conditions were adjusted after preliminary tests: torque of 1.4 Nm, 10 % pump flow, chopper 1500 rpm, and impeller 100 rpm. The ‘binder’ solution was an alcoholic solution-of PVPVA at 20 wt%. This solution was prepared by dissolving 30 grams of PVPVA in 120 mL of ethanol under mechanical stirring (625 rpm) for 20 minutes. The surfactant SPAN 20 (previously warm in a water bath at 70°C) was then slowly poured during the granulation process (Figure 80).

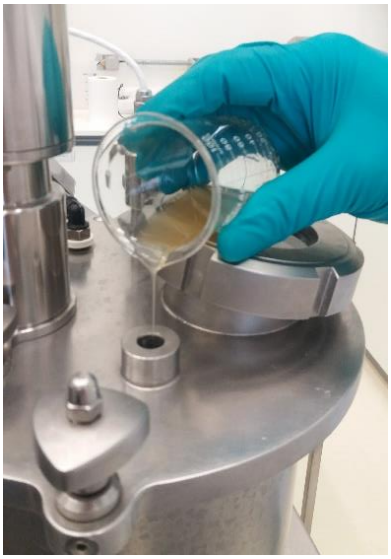

Figure 80. Slow addition of the surfactant SPAN 20 during granulation of PZQ by an ethanolic solution of PVPVA in a fluidized bed.

The granulated material was then transferred to the fluidized bed dryer (SOLIDLAB 1 – BOSCH®) (Figure 81). This equipment is used to reduce the moisture content of pharmaceutical powder and granules. It is works on a principle of fluidization of the feed materials. In fluidization process, hot air is introduced at high pressure through a perforated bed of moist solid particulate. The wet solids are lifted from the bottom and suspended in a stream of air (fluidized state). Heat transfer is accomplished by direct contact between the wet solid and hot gases. The vaporized liquid is carried away by the drying gasses.

During this step the material was kept fluidized by an air flow rate of 20 $m^3$/h at 22°C for 35 minutes. The air temperature was raised and kept at 40°C for 5 minutes, finalizing the drying operation for the granules.


Figure 81. Fluidized bed (Bosh®) for drying the FEXT 1 formulation after granulation.

Two batches were prepared using the same methodologies described above for each of the respective formulations, however, without the API. They corresponded to ‘placebo’ samples.

To produce the placebo samples for the mixture PVPVA and SPAN 20 (liquid surfactant), some adjustments on the operating conditions were made for the wet granulation. In fact, it was necessary to adjust the chopper to 3000 rpm and the impeller to 150 rpm. Likewise, the temperature profile for the placebo also needed to be adapted and is shown in Table 35.

The placebo referring to the FEXT 2 formulation was prepared as described before but without the API in the mixture.

### 1.3 Characterization of samples

Extruded were characterized as previously performed and described in Chapter 3 (powder X-ray Scattering diffraction (PXRD), differential scanning calorimetry (DSC), scanning electron microscopy (SEM), dissolution profile, and drug content). Other methods of physicochemical characterization (mass loss on drying, water content, taste masking and pharmacokinetic) were performed and are described in this section.

Placebo formulations were evaluated by TGA, DSC, PXRD and, SEM techniques.

The physical stability of the extrudate materials was investigated using the same procedure also described on Chapter 3 (section 3.1.10) and monitored with samples' characterization by DSC, TGA, PXRD, Stereomicroscopy, SEM.

A graphical summary of the techniques used for each ternary system is shown in Figure 82.

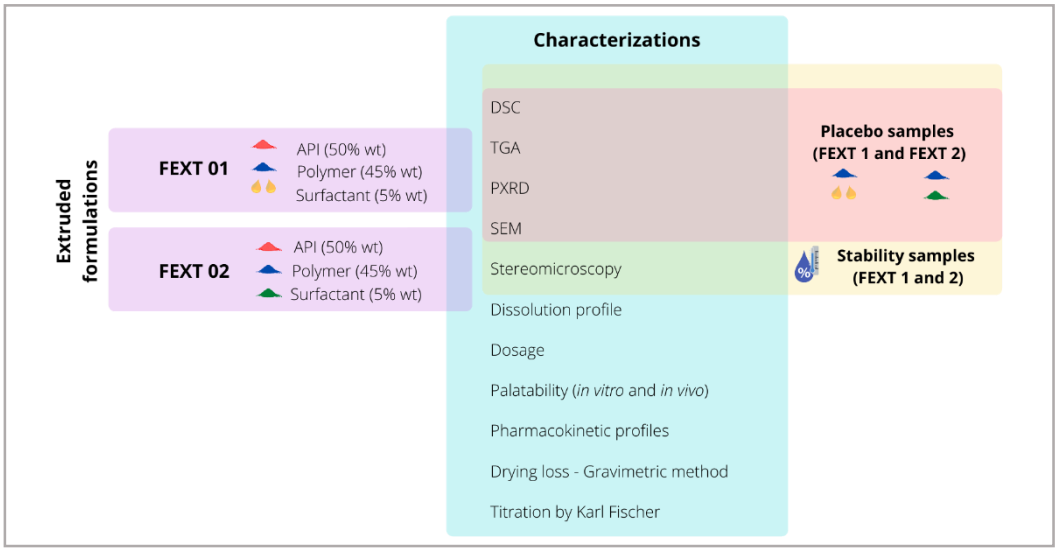


Figure 82. Schematic division of the characterizations carried out in this chapter according to the samples produced.

### 1.3.1 Determination of mass loss on drying

This analysis is used mainly in pharmaceutical laboratories to determine the total amount of volatiles on solid materials (i.e., water and residual solvents vaporized under the experimental conditions) [319]. It was carried out according to the method described in the Brazilian Pharmacopoeia [291]. In brief, 1 to 2 g of sample to be analysed were dried in a vacuum oven (5 mmHg) at 50 ºC to a constant weight.

### 1.3.2 Determination of water - Titration by Karl Fischer

Unlike loss on drying, the Karl Fischer titration titration is a moisture determination method specific for **water** [319]. It allows the quantification of the total water content on the sample (i.e., free moisture and water of crystallization). This test was carried out with both extrudate samples, FEXT 1 and FEXT 2, according to the Brazilian Pharmacopoeia [291]. Initially, enough methanol was transferred to the titration vessel, ensuring that the volume was sufficient to cover the electrodes (approximately 30 to 40 mL) and titrated with Karl Fisher's previously standardized solution up to the electrometric endpoint. This procedure was carried out so that all the moisture presents could be eliminated. The sample (about 200 mg) was then added to the titration vessel, mixed, and titrated with the Karl Fischer reagent to the end point.

## 2. RESULTS

### 2.1 API content and organic impurities

An initial identification test with a PZQ reference compound (SQR)[18] was performed by evaluating the peak retention time of the API (Table 35). After, the drug content for each formulation and the respective physical mixture (feeding the extruder) were analysed (Table 36).

Table 35. Identification test of PZQ.

| ***Sample*** | ***Retention time of principal peak (min)*** |
|---|---|
| SQR (for FEXT 1 analysis) | 2.74 |
| FEXT 1 | 2.75 |
| SQR (for FEXT 2 analysis) | 2.86 |
| FEXT 2 | 2.88 |

[18] An SQR sample was prepared for each formulation to make the injection and preparation as close as possible.

Table 36. PZQ content (extrudate samples and physical mixtures).

| *Sample* | *Measured drug content (wt%)* | *Theorical drug content (wt%)* |
|---|---|---|
| FEXT 1 Physical Mixture | 51.04 ± 0.87 | 50 |
| FEXT 1 | 46.52 ± 0.31 | |
| FEXT 2 Physical Mixture | 38.83 ± 0.88 | 40 |
| FEXT 2 | 34.03 ± 0.09 | |

Table 36 shows that the formulations FEXT 1 and FEXT 2 are characterized by a reduction in the PZQ content, in comparison to their respective physical mixtures (before HME processing). It is important remember that these materials were processed by HME and then ground.

Regarding the impurities, Table 37 gives information about the concentration of organic impurities for each extruded formulation (FEXT 1 and FEXT 2).

Table 37 Impurities of FEXT 1 and 2 samples.

| *Sample* | *Impurity* | *Impurity content (wt%)* |
|---|---|---|
| FEXT 1 Physical Mixture | A | 0.0040 ± 0.0001 |
| | B | 0.0476 ± 0.0009 |
| | C | 0.0038 ± 0.0009 |
| FEXT 2 Physical Mixture | A | 0.0036 ± 0.0001 |
| | B | 0.0494 ± 0.0023 |
| | C | 0.0078 ± 0.0034 |
| FEXT 1 | A | 0.3202 ± 0.0018 |
| | B | 0.0532 ± 0.0017 |
| | C | 0.0700 ± 0,0049 |
| FEXT 2 | A | 0.2962 ± 0.0152 |
| | B | 1.9827 ± 0.1370 |
| | C | 0.3470 ± 0.0116 |

First, by comparing the content of impurities associated to PZQ (impurities A, B and C) between the physical mixtures and the HME extrudates shown in Table 6, the impact, on the amount of these impurities, of the HME processing and the downstream step of milling, can be analysed.

What emerges from this analysis is an increase in impurities A and C in FEXT 1 and an increase of all impurities (A, B and C) in FEXT 2.

According to the American pharmacopoeia, the limit for each impurity of praziquantel (A, B and C) must be less than 0.2 wt %. However, this limitation is

described in the praziquantel monograph (API). The extrudate sample is not more a powder like API or a final product. It is considered an intermediate product.

### 2.2 Determination of mass loss on drying

The percentage of mass loss in drying is related to all volatile materials or decomposition products that may be present in the sample. The mass loss on drying from both studied formulations FEXT 1 FEXT 2 are very close, 0.7 and 0.6% (Table 38), respectively.

The American and Brazilian pharmacopoeia [53], [291], [297] determines that the acceptance criterion for weight loss trial is 0.5 %, however this value is related to the sample of the praziquantel tablet and API. Specific conditions for this type of "intermediate" material as the extrudate solid dispersions developed in this work are not established, and, even if used in a final formulation of PZQ, the results need to be re-evaluated according to the final dosage form and its storage conditions.

Table 38. Loss mass by drying method (50 ºC).

| *Sample* | *Mass loss (mg)* | *Loss (%)* |
|---|---|---|
| FEXT 1 | 0.00948 | 0.7 |
| FEXT 2 | 0.00912 | 0.6 |

### 2.3 Thermogravimetric analysis (TGA)

Following the sample procedure used for raw materials alone and already described (Chapter 3, item 3.1.2), these samples were stored at different environment conditions (RT[19] = room temperature; LT = long time stability, and AS = accelerate stability) for 15 days and reanalysed by TGA. Table 39 shows un up-take of moisture, dependent of the storage conditions and higher for FEXT 2 than FEXT 1.

[19] RT = between 15 and 30 ºC and max 60% RH, LT = 30 ± 2 ºC and 75 % RH, and AS = 40 ± 2 ºC and 75 % RH.

Table 39. Mass moisture variation after different storage conditions.

| *Sample* | *Δm (%) ** | | | |
|---|---|---|---|---|
| | ***RT t0*** | ***RT t15*** | ***LT t15*** | ***AS t15*** |
| FEXT 1 | 2.29 ± 0.02 | 3.20 ± 0,00 | 4,15 ± 0,00 | 4.76 ± 0,05 |
| FEXT 2 | 2.29 ± 0.01 | 4.42 ± 0,12 | 8.40 ± 0,10 | 9.71 ± 0,07 |

*SD = standard deviation (n=2)

## 2.4 Differential scanning calorimetry (standard DSC)

With standard DSC, temperature is always changed linearly, and the operator must specify the rate in degrees per minute (ºC/min). With a single heating rate, a single heat flow rate signal is produced, which is the sum of all heat flows occurring at any point in temperature or time. The operating principle of MDSC differs from standard DSC in that MDSC uses two simultaneous heating rates - a linear heating rate that provides information similar to standard DSC, and a sinusoidal or modulated heating rate that permits the simultaneous measurement of the sample's heat capacity. Creation of the sinusoidal temperature change requires the operator to select a modulation period (seconds) and modulation temperature amplitude (± ºC). Applying simultaneous heating rates (linear and modulated) provides further information on sample heat capacity or structure. MDSC is superior to standard DSC since it can separate kinetic events (e.g., a cold crystallization) from changes in heat capacity (e.g., a $T_g$).

MDSC was applied in the subsequent HME extrudates in this thesis, however, the thermal analyses performed for FEXT 1 and FEXT 2 were conducted with a standard DSC, which rendered difficult the identification of $T_g$ on these samples.

FEXT 1 and FEXT 2 were analysed just after production and after storage for 30 days under two different conditions: 30 °C/75 % RH and 40 °C/75 % RH. Their DSC curves are also shown in Figures 83 and 84, respectively.

Once freshly produced, both formulations did not show signs of presence of crystalline material (no melting point on the curves). Both remained unchanged for 30 days storage at room temperature.

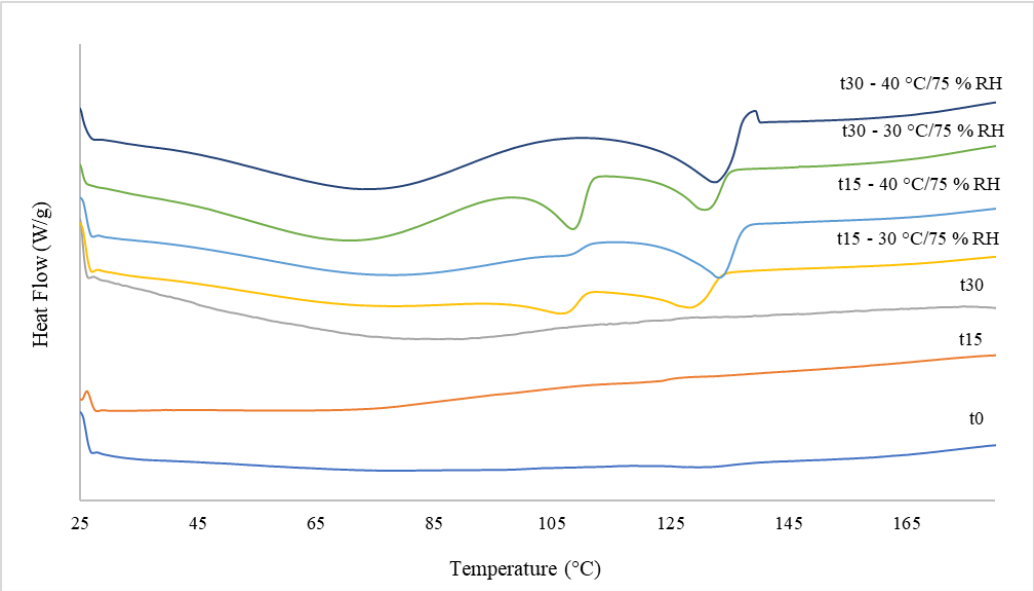


Figure 83. DSC curves for FEXT 1 under different storage conditions.

During storage under the other conditions (30 °C/75 % RH and 40 °C/75 % RH), an endothermic signal has appeared between 106 - 109 ºC followed by an exotherm and a second endothermic event in the range of 125 - 130 ºC. The recrystallisation process on the samples is evidenced. The first endothermic peak (106 - 109 ºC) could be associated with the recently published C form of the PZQ [4]. However, the second sign does not refer to PZQ forms B or commercial [5] [6].

For FEXT 2, during storage at 30 °C/75 % RH and 40 °C/75 % RH, an endothermic signal has appeared in the region of 125 ºC (Figure 84). The recrystallisation process is also observed, however the phase crystalline was not identified.

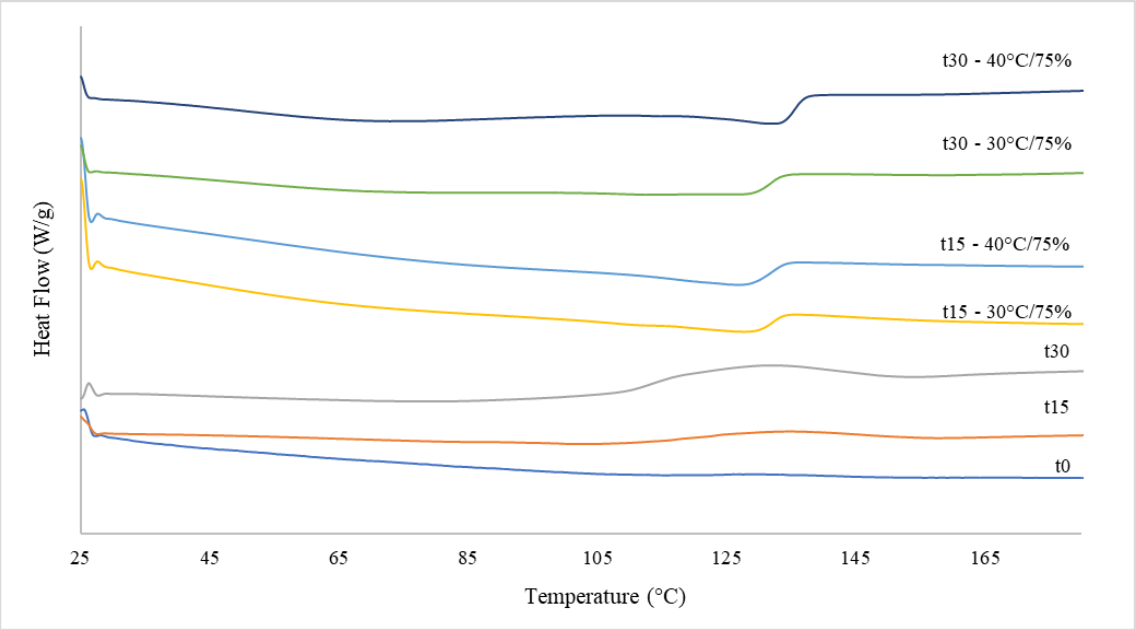


Figure 84. DSC curves for FEXT 2 under different storage conditions.

## 2.5 Powder X-Ray Diffraction (PXRD)

PXRD analyses were performed to help elucidate the solid state of PZQ in the HME extrudates. For that, the physical mixtures were also analysed.

Initially, PXRD was performed for the physical mixing of FEXT 1 sample after staying in the most stressful condition (AS t30) and immediately after the extrusion process (RT t0) (Figure 85). Naturally, the results report only the characteristic signs of pure PZQ and a slight change in the baseline due to the presence of the polymer (amorphous).

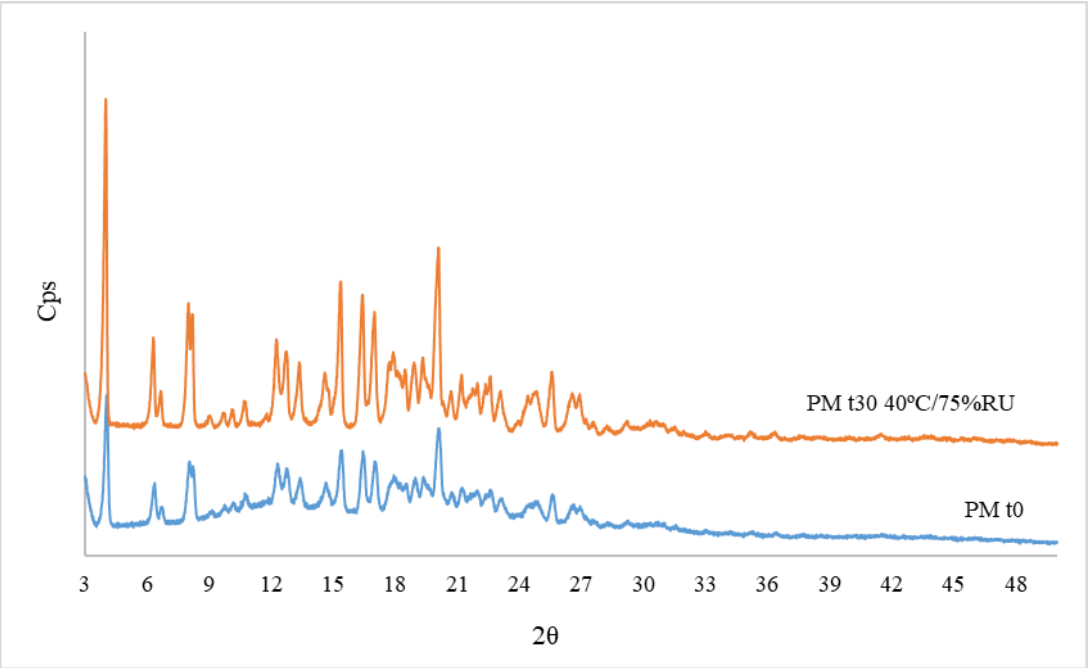


Figure 85. PXRD of the physical mixture corresponding to the composition of FEXT 1.

Figure 86 regroups all PXRD data for FEXT 1, freshly produced and during stability monitoring. The diffractograms corroborate the results obtained by DSC. The samples that were kept at room conditions did not present signs of crystallinity (no melting points), while those submitted to a climatic chamber already show signs of diffraction, confirming the presence of crystalline material resulted from a recrystallisation process on the samples during storage

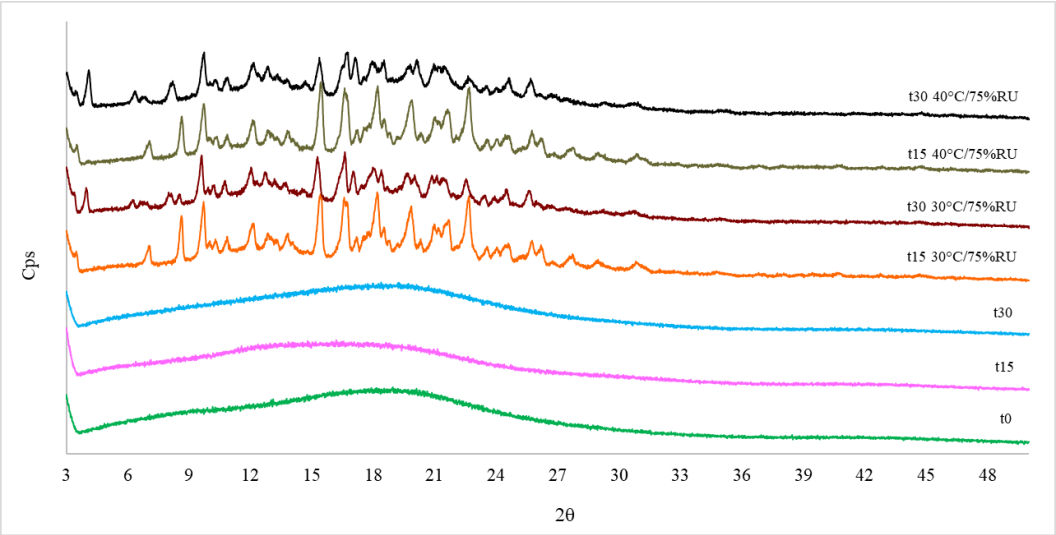


Figure 86. PXRD for FEXT 1, freshly produced and during stability monitoring.

However, the crystalline signals appeared in FEXT 1 cannot be attributed to the polymorphic forms of praziquantel reported in the literature. One explanation could be the low amount of crystalline material (low intensity of peaks) in presence of other materials, rendering difficult the data analysis.

To finish with FEXT 1, the placebo sample (extrudate) showed an amorphous characteristic, as expected by the presence of only PVPVA and SPAN (Figure 87).

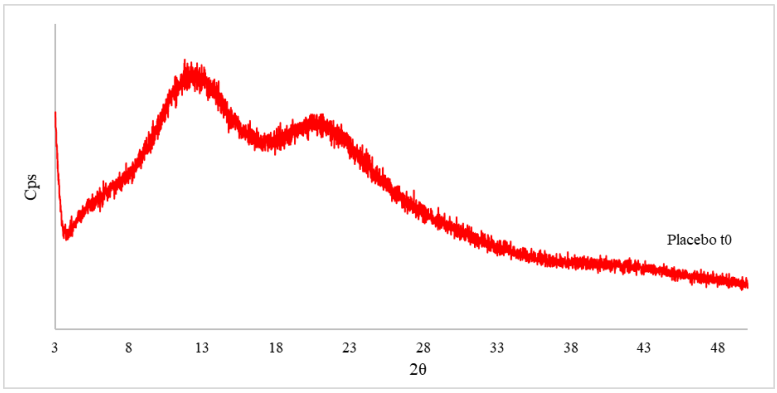


Figure 87. PXRD pattern of FEXT 1 placebo.

For the FEXT 2 sample, the same characterization was performed and, initially, the physical mixture presented the melting characteristic signs of the PZQ and the surfactant (SLS), also crystalline, and the same profile was observed for the physical mixture storage at 40°C/75%RH. (Figure 88).

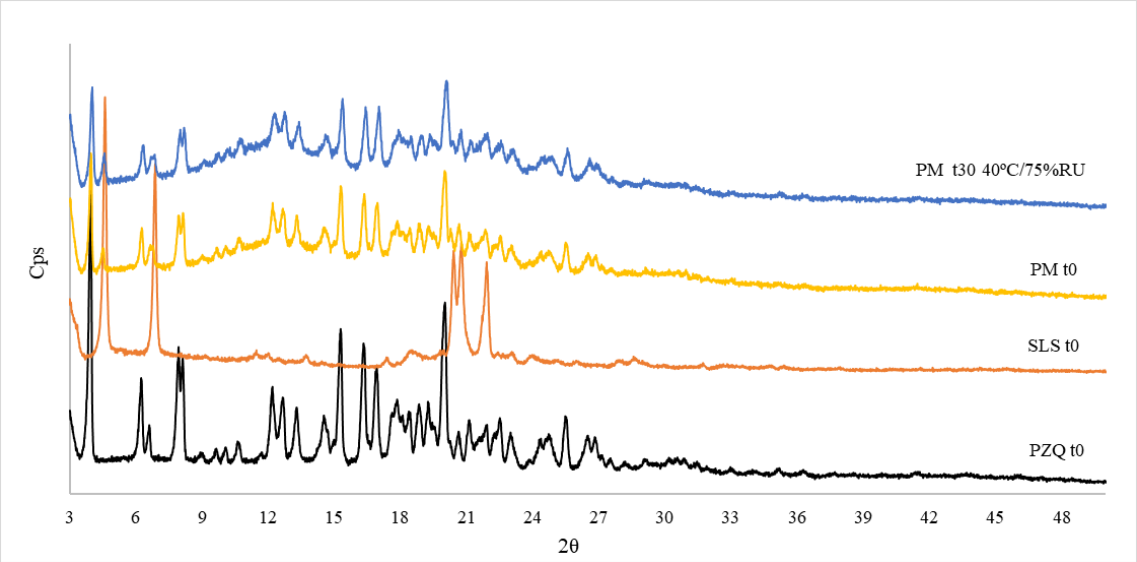


Figure 88. PXRD for FEXT 2 physical mixture.

Figure 89 regroups all PXRD data for FEXT 2, freshly produced and during stability monitoring. Contrarily to FEXT 1, the FEXT 2 samples that were kept at room conditions started to present signs of crystallinity after 15 days stored at room conditions. The DSC analysis did not detect the presence of crystalline material. Differently, for the FEXT 1 sample, the results of DSC and PXRD corroborate, and recrystallization was evidenced after 15 days, but only under stress conditions.

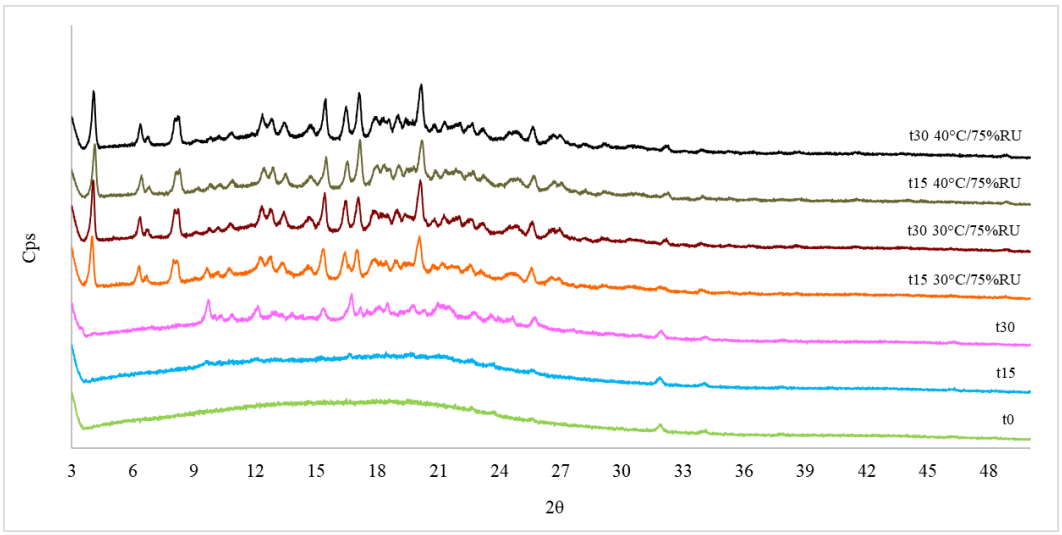


Figure 89. PXRD pattern for FEXT 2, freshly produced and under stability monitoring

Also, it is interesting to note that even after the extrusion process, the sample is characterized by small crystalline signals at 2θ 32 and 34 º, respectively. However, the

same diffractions can be seen for the placebo extrudate (Figure 90). Still, when these signs are compared to the physical mixture of the pure ingredients, they are not found. This means that, probably, something might happen in the physical structure between the materials (PVPVA and SLS) during the extrusion process.

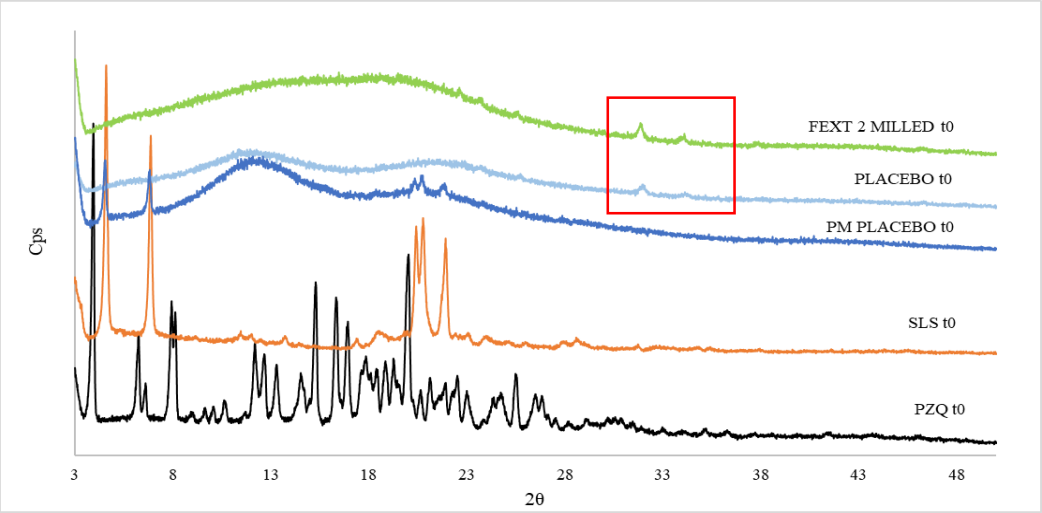


Figure 90. PXRD for placebo FEXT 2.

## 2.6 Scanning Electron Microscopy (SEM)

The milled extruded samples were evaluated right after processing and when storage under the different conditions of stability already presented (RT, LT, and AS).

Figures 91 and 92 show the SEM images obtained for the FEXT 1 and FEXT 2 extrudates obtained by samples submitted to the stability study.

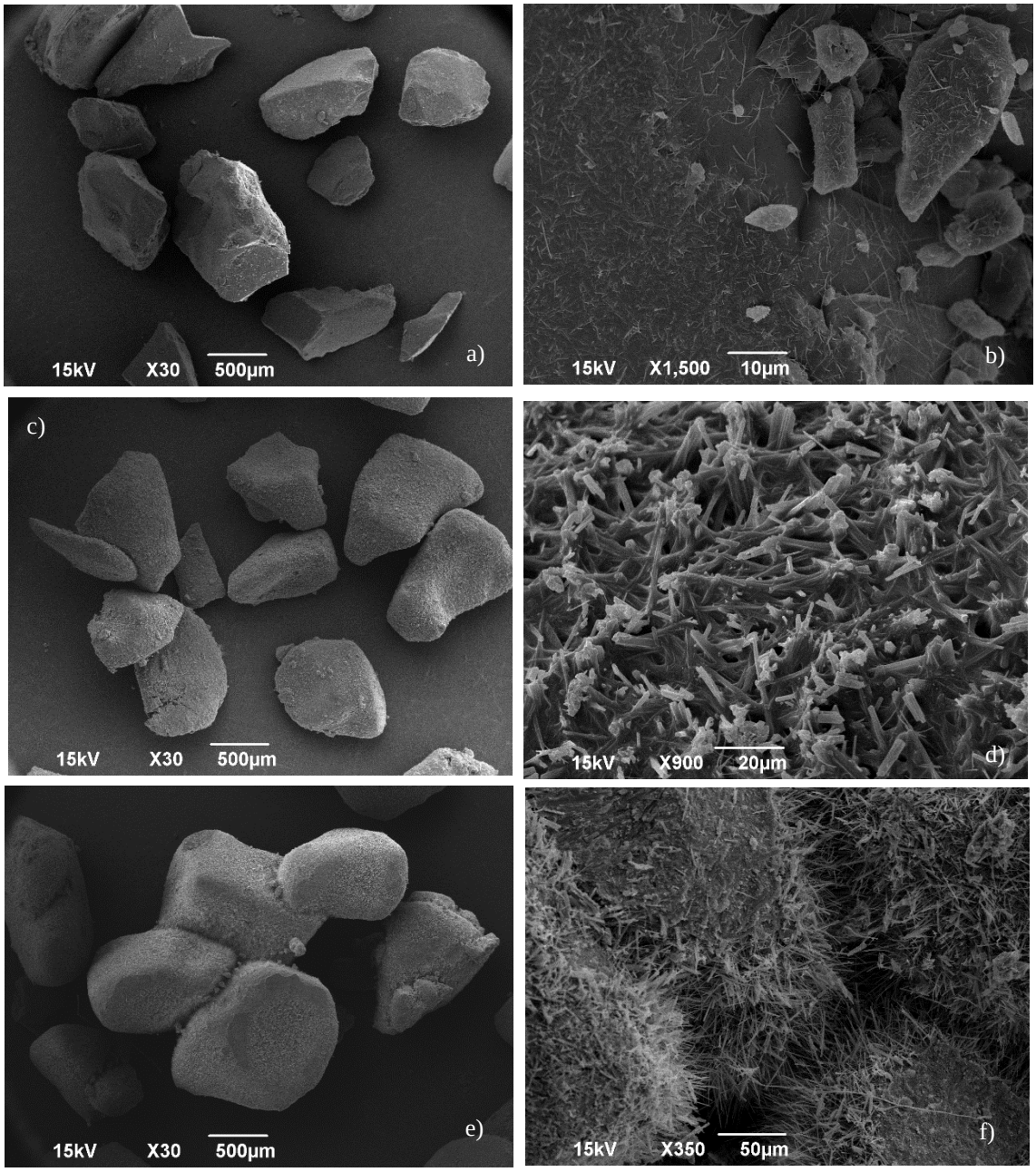


Figure 91. SEM images of FEXT 1 extrudate. a) RT; b) RT t15; c) RT t30, and d) LT t15; e) and f) AS t15.

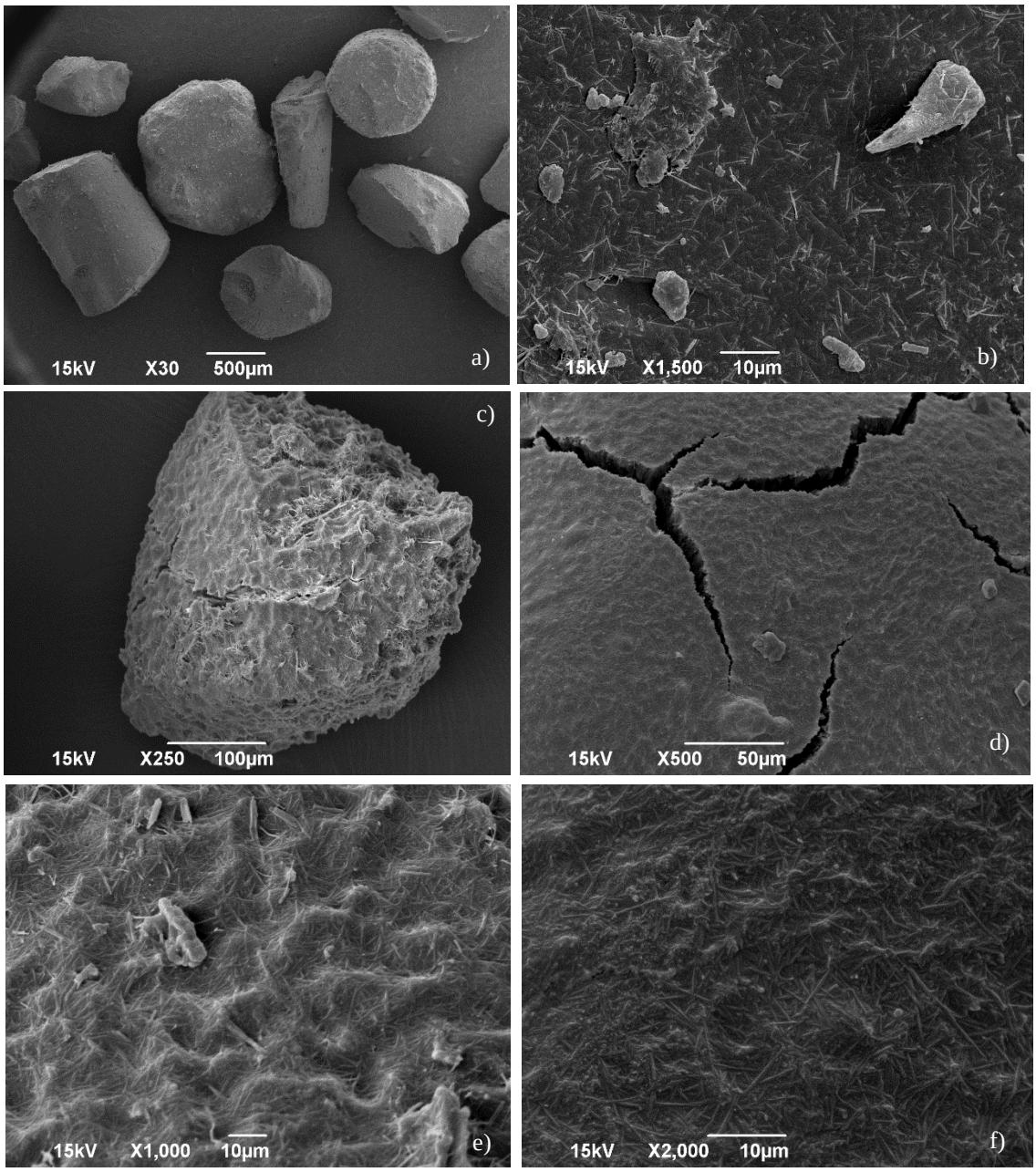


Figure 92. SEM imagen of FEXT 2 extrudate. a) RT; b) RT t15; c) RT t30, and d) LT t15; e) and f) AS t15.

For both extrudate formulations, fine needle-shaped particles can be seen on the surface of samples maintained at room temperature (Figures 91a and 92a). For higher temperature/RH conditions, it is possible to evidence particles with a columnar format similar to those identified for the raw API [300] (91d and 91d). Particles with a similar shape were found in a study that produced solid dispersions containing PZQ and PVP [65]. Different morphologies were identified depending on the variation in the composition of the solvent (ethanol and water) used to produce them. Samples produced

with PZQ and PVP (2: 1) using only ethanol for evaporation showed structures in the form of needles on the surface, like those obtained here (Figure 93).

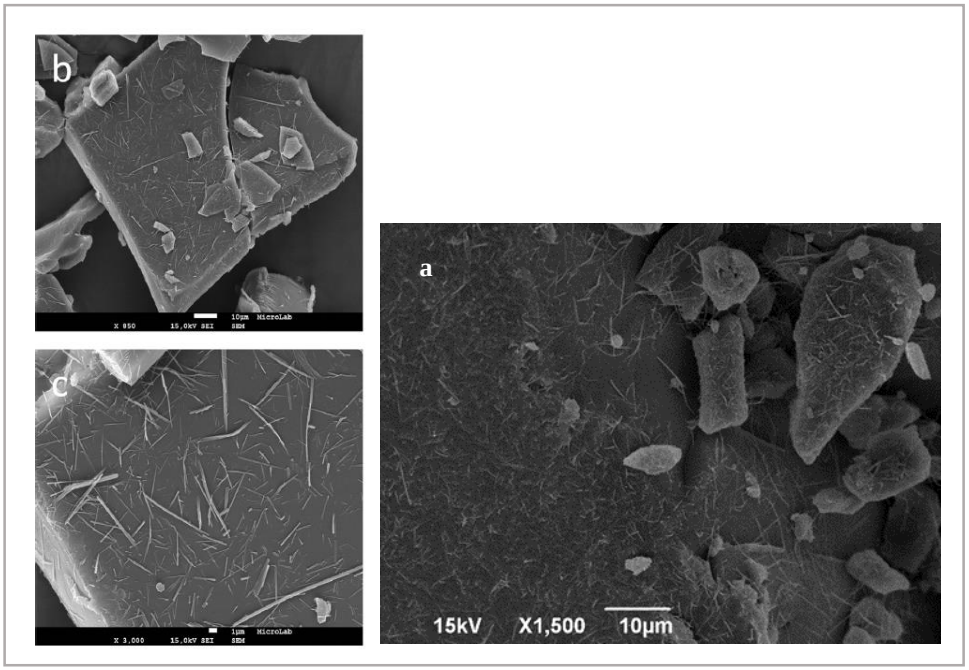


Figure 93. Comparison between solid dispersion obtained in this study by HME (PZQ: PVPVA - 1: 1) and solid dispersion obtained by solvent evaporation [14]. a) particle surface after RT t30- PZQ: PVPVA by HME and, b and c) PZQ: PVP (3: 1) - solvent evaporation (ethanol). Source: reprinted from [65] with permission.

As temperature and humidity increased during storage, the “growth” of the needles was clearly evidenced, and the FEXT 1 particles became agglomerate (Figures 15f and 15e). Although FEXT 2 also showed agglomeration of extruded material, the needles are found horizontally on the surface (Figures 11b, d, and f). Also, some “cracks” were identified in the extruded material (Figures 92c and 92d).

Samples of the placebo extrudate were not included in the stability study due to the absence of API. In this way, Figures 94 and 95 present the respective formulations after production. As expected, the surface of the material is smooth without the presence of particulate material. Only particles and deformations resulting from the pelletizing process are evident.

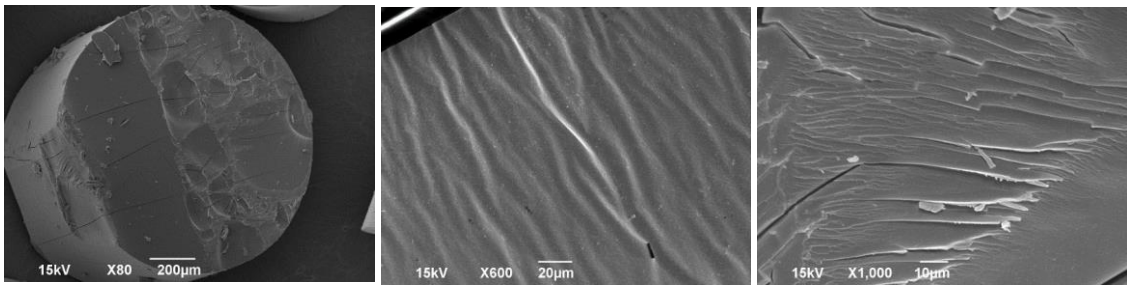


Figure 94. SEM imagens of Placebo FEXT 1.

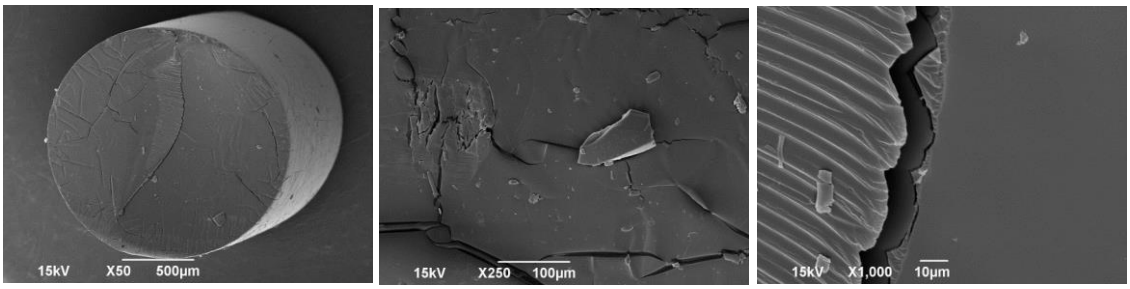


Figure 95. SEM imagens of Placebo FEXT 2.

## 2.7 Stereomicroscopy

Like SEM analysis, stereomicroscopy was applied to the materials after extrusion and during the stability studies to monitor morphological changes. Unlike SEM, this analysis aims to obtain macro information related to the aspect of extruded materials. Samples in pellet shape (before grinding) and milled were evaluated.

The images obtained by stereomicroscopy for the extruded material FEXT 1 (pellet), and its respective ground are presented in Figures 96 and 97. Changes on physical aspect were seen during stability monitoring.

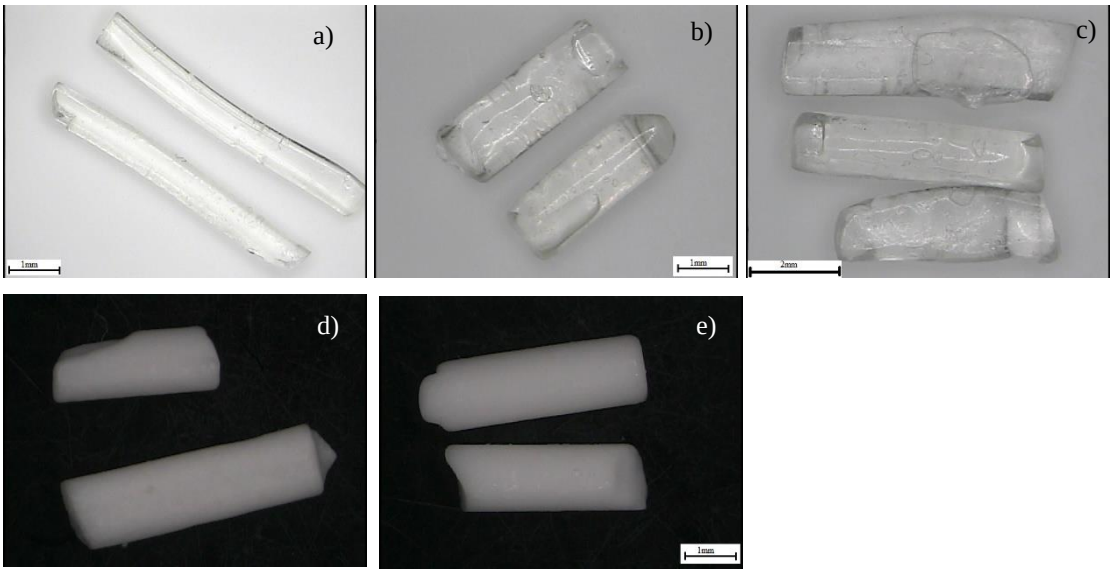


Figure 96. Images obtained by stereomicroscopy for extrudate FEXT 1. a) RT; b) RT t15; c) RT t30, and d) LT t15; e) and f) AS t15.

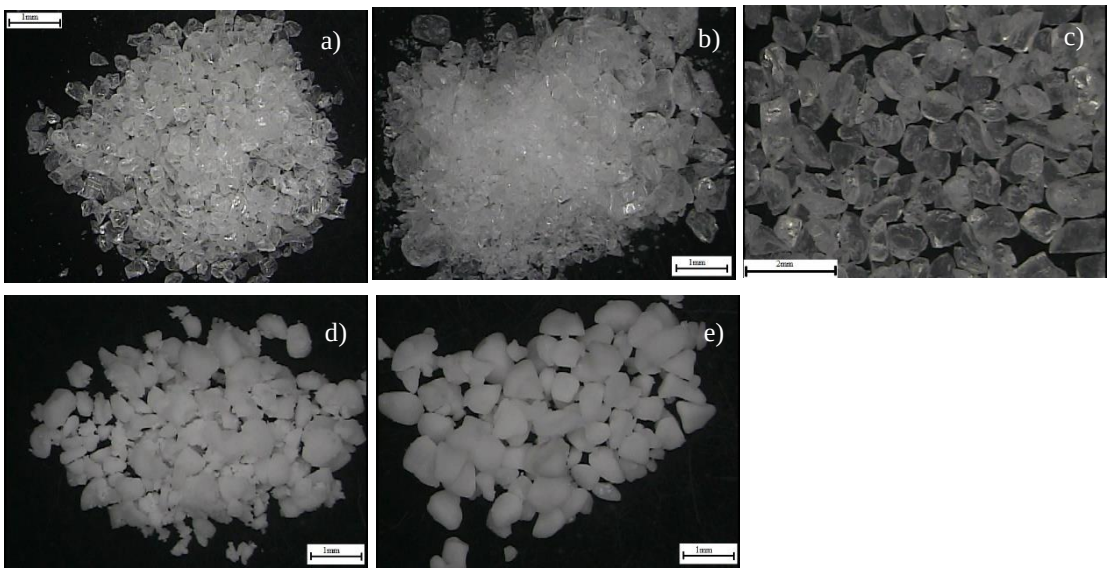


Figure 97. FEXT 1 milled. a) after extrusion. a) RT; b) RT t15; c) RT t30, and d) LT t15; e) and f) AS t15.

After 30 days at room temperature, it can see that the ground material has a more whitish colour when compared to the extruded material. This factor is probably related to the fact that the ground material has a larger surface area, favouring the uptake or water from the environment. For both cases, under higher humidity and temperature conditions, the material was completely opaque and brittle. This transformation was shown simultaneously, but to a lesser extent, in the material at the ambient condition.

As previously discussed, the FEXT 2 formulation exhibited the same aspect (Figures 98 and 99), and the colour change of the ground material was even more evident after 30 days on RT (Figure 98c) when compared to its respective extrudate (Figure 99c).

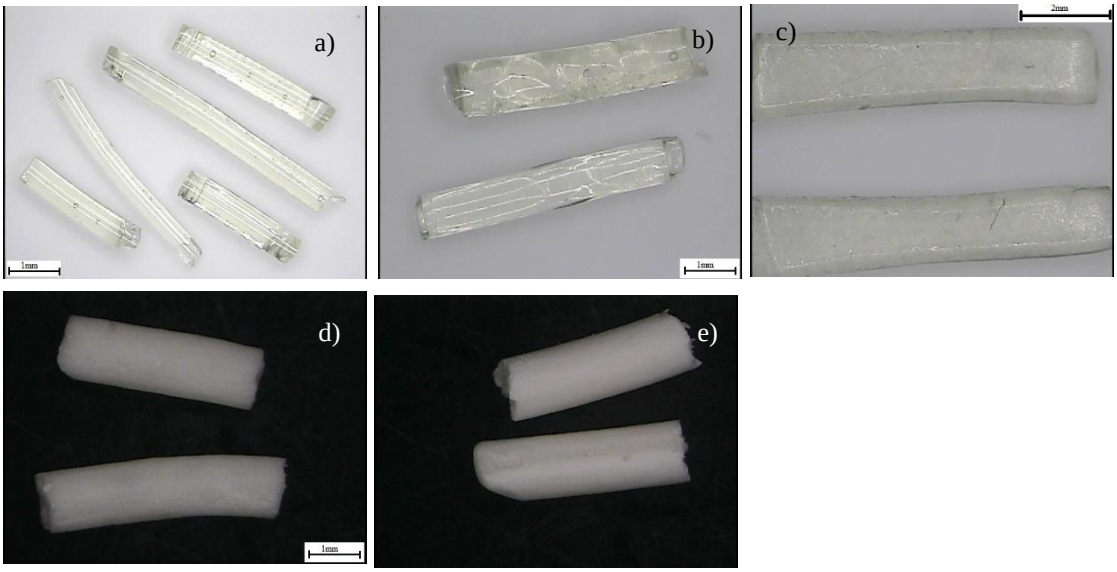


Figure 98. Images obtained by stereomicroscopy for extrudate FEXT 2. a) after extrusion; b) 15 days at RT; c) 30 days at RT; d) 15 days at 30ºC/75%RU; e) 15 days at 40ºC/75%RU.

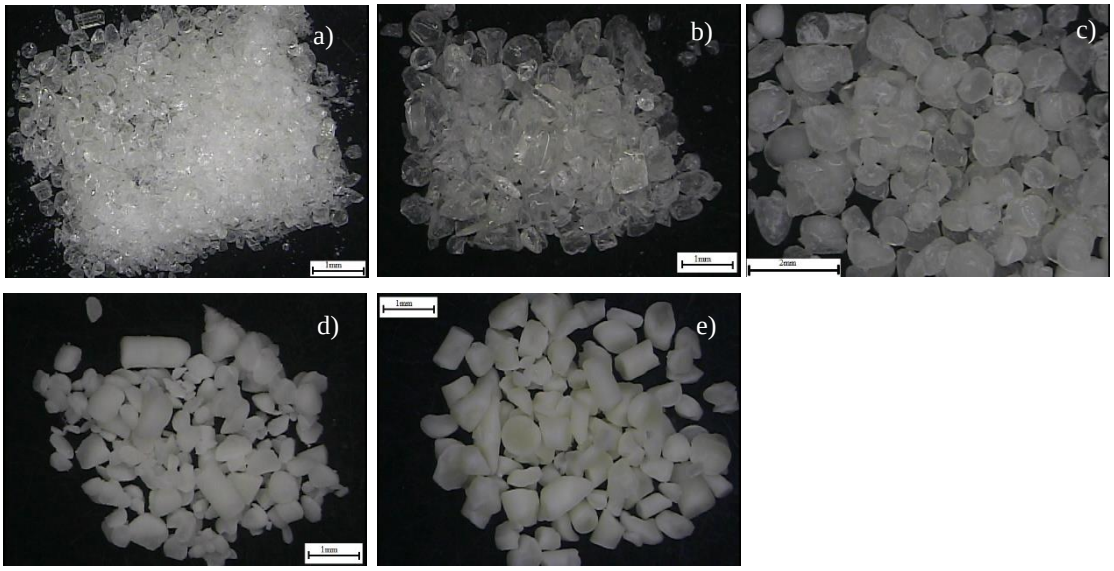


Figure 99. FEXT 2 milled. a) after extrusion; b) 15 days at RT; c) 30 days at RT; d) 15 days at 30ºC/75%RU and 15 days at 40ºC/75%RU.

## 2.8 PZQ-HME solubility in aqueous media

Measurements were carried out with both extrudate formulations to evaluate their capacity to improve the water solubility of the PZQ at 37°C (Table 40).

Table 40. Water solubility of FEXT 1 and 2.

| ***Solubility (mg/mL) at 37ºC*** | | | |
|---|---|---|---|
| | 1h | 24h | 48h |
| API | 0.138 ± 0.03 | 0.15 ± 0.01 | 0.136 ± 0.01 |
| FEXT 1 | 0.298 ± 0.03 | 0.228 ± 0.07 | 0.110 ± 0.01 |
| FEXT 2 | 0.479 ± 0.14 | 0.167 ± 0.003 | 0.219 ± 0.04 |

Both formulations showed an increase in the PZQ concentration in water (after 1 hour) compared to pure PZQ and FEXT 2 by more than two hundred percent. The measured solubility of pure PZQ is in accordance with the literature, as already presented in Chapter 4 (Section 4.2.2) [10]. For both samples, the apparent solubility decreases at the subsequent points, presenting a profile similar to that found for binary extrudates and solid dispersions of praziquantel produced by spray drying (Sub-chapters 5.2 and Chapter 4).The experiment should be performed again with more collect points for a better understanding of the evolution of the PZQ concentration in water during solubilization from the extrudate samples (these values can indicate recrystallization or degradation, for example).

## 2.9 Dissolution Profile

The dissolution profile was also evaluated and presented in Figure 100. Both (ground) FEXT 1 and 2 samples were analysed, reaching respectively 79 % and 90 % of PZQ release at the end of 2 hours.

Although both formulations present promising results for “intermediates” materials a difference can be evidenced between the dissolution profile of FEXT 1 and FEXT 2. The dissolution medium used followed the guidelines described in the American pharmacopeia [297] for the evaluation of PZQ tablets, and the composition is HCl 0.1N and 0.2 % (wt) of the surfactant (SLS). FEXT 2 has the same surfactant in its composition, and an assumption to elucidate the difference in the dissolution profile is related to this factor. LSS is an anionic surfactant, and molecule hydrophilic (with the sulfate group) that makes, soluble in water. Span™ 20 is a non-ionic surfactant, having no miscibility in water, causing the formulation containing it to dissolve more slowly.

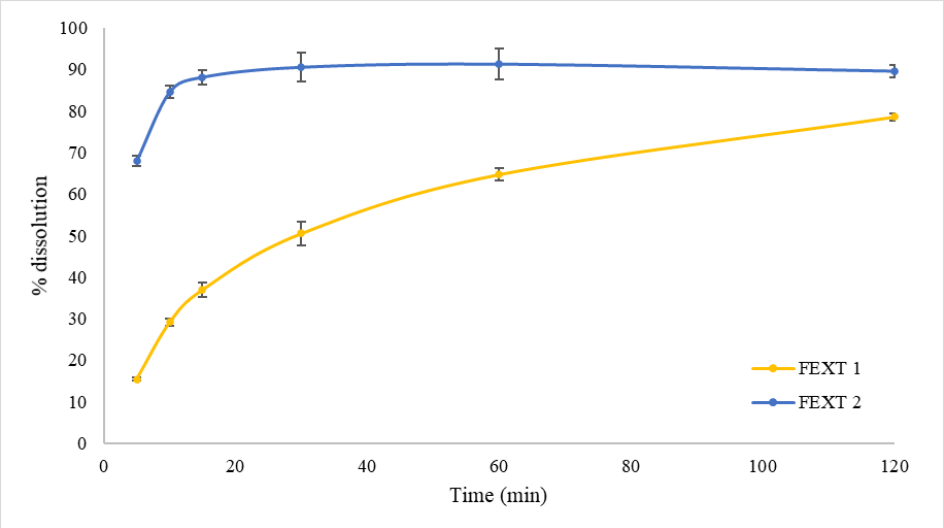


Figure 100. Dissolution profile for extrudate samples, FEXT 1 and FEXT 2.

Another factor influencing the dissolution rate is the granulometric size distribution of the extruded material added (by dispersion) in the dissolution tank. Although a precise evaluation of this characteristic has not been carried out, the samples used in this test have undergone a selection through the sieving tests, and both had a particle size in the range 210 to 300 µm. In addition, although FEXT 2 has a 10% less drug than FEXT 1, the mass used for the dissolution profile was based on the paediatric dose of PZQ (150 mg). Thus, the dissolution profile difference is related to the extrudate characteristics and not the different concentrations of the API in each formulation (FEXT 1 50 wt% and FEXT 2 40 wt%).

# PART 2 - TASTE MASKING AND PHARMACOKINETICS STUDY

## 1. METHODS

### 1.1 In vitro taste masking test by electronic tongue (e-tongue)

These analyses were carried out in collaboration with a Brazilian laboratory from USP – University of Sao Paulo in Brazil (Instituto de Física de São Carlos - IFSC), equipped with an e-tongue. Electronic tongue is a device simulating human sense of taste, that allows for the identification and classification of liquid samples regarding palatability [320].

The in vitro taste assessment was performed with an impedimetric electronic tongue comprised of an array with several units modified with nanostructured films. In this study, we used an array with 5 sensing units made with interdigitated gold electrodes coated layer-by-layer by alternating immersion of the electrodes into cationic and anionic layering solutions. The materials used to produce the multi-layer films were poly(ethyleneimine) (PEI), poly(styrene sulfonate) (PSS), poly(3,4-ethylene dioxythiophene): poly(styrene sulfonate) (PEDOT:PSS), poly(pyrrole) (PPy), poly(aniline) (PANI), chitosan (Chit) and tetrasulphonated nickel (II) phthalocyanine (NiTsPc). They were dissolved in ultrapure water from a Millipore Direct-Q5 system with a concentration of 0.5 g/l at pH 3 adjusted with HCl solution.

The architectures of the five sensing units were as follows: *i)* $(PEI/NiTsPc)_5$, *ii)* $(PANI/PSS)_5$, *iii)* $(PEI/PEDOT:PSS)_5$, *iv)* $(PEI/PPY)_5$ and *v)* $(Chit/PSS)_5$, where the number '5' means that all films had 5 bilayers (10). The capacitance data were collected with an impedance analyser (Solartron) in the frequency range from 1 Hz to 1 MHz, applying an a.c. voltage of 25 mV at room temperature. The electrical response of an array of 5 sensing units modified with conducting organic films was used to evaluate the taste characteristics of the formulations. The capacitance data were projected using the multidimensional projection technique referred to as Interactive Document Map (IDMAP), in the PEx-Sensors software [321]. The whole procedure is illustrated in Figure 101.

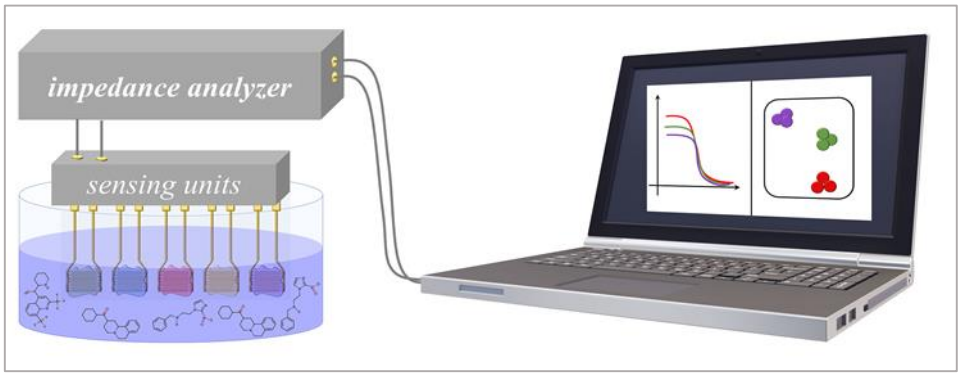


Figure 101. Schematic setup for in vitro taste experiment. An array of five sensing units were modified with (PEI/NiTsPc) 5, (PANI/PSS) 5, (PEI/PEDOT:PSS)5, (PEI/PPY) 5, and (Chit/PSS) 5 films.

The extrudate formulations FEXT 1 and FEXT 2 were analysed in the same concentration as the therapeutic dosage recommendation for paediatrics patients (150 mg). For each commercial tablet and the prepared dispersions were analysed in replicate (n = 3). For all analyses, 10 mL of water were used to disperse the samples.

### 1.2 In vivo taste masking by volume consumed

This method applied here is based on the evaluation of the palatability of a given sample according to the difference in the volume consumption of the sample by animals [116].

The animal's exposure is made under a controlled time. It is possible to predict taste palatability or hedonic impact (pleasant taste) because it was already described in the literature the similar behavioural pattern of human infants and rats and facial expression and certain taste-related behaviours (e.g., tongue protrusion) [116]. In this way, when exposing an animal to the test, the volume difference is measured, which is directly linked to the taste (the more consumed, the more palatable).

The in vivo taste assessment was performed on 42 adults female Wistar rats weighing between 300 - 350 g. All procedures were approved by the Animal Use Ethics Committee (CEUA) at Fluminense Federal University (UFF) Rio de Janeiro, Brazil (protocol number CEUA 4119060418 – Appendix I). They were housed alone in standard cages at 25± 2 °C and 50 % ± 10 % humidity under 12 light/12 h dark cycle. All training and testing occurred during the light phase of the cycle. Animals had free access to chow and water except for training and testing periods where a water-restriction schedule occurred. The experimental design consisted of two training and one testing days. Each

rat was water-deprived for 22 h before each session (training and testing) of 30 min to motivate the licking behaviour (response to thirst) but had access to food ad libitum. This method was adapted from the literature [68].

A system for recirculation of the solution/suspension samples was developed by our group for this study. The procedure adopted aims to maintain homogeneity of the dispersion taste during all experiments. The system was assembled using silicone tubes (8 mm ∅) and a recirculation pump (DC20C model, 4,5 W and flow rate 240 L/h) (Figure 102).

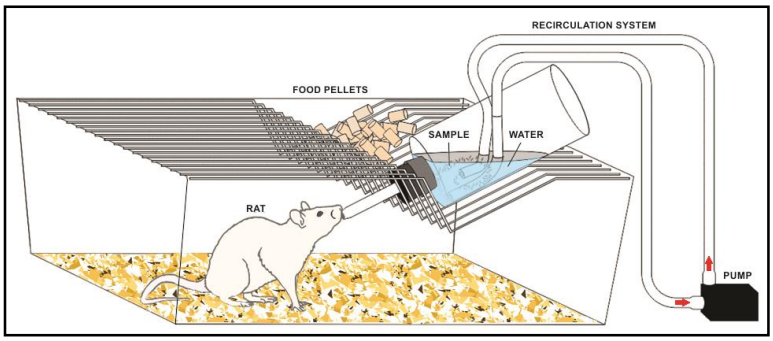


Figure 102. Representation of a rat exposed with a recirculation system.

The two initial days of the protocol were dedicated to training with water drinking bottle presenting 100 mL of purified water, and the system of recirculation was active all the time of the experiment. After each testing period, they received drinking water for one hour for rehydration.

At the third day, the animals were separated into 5 groups (n = 6) for receiving our FEXT 1, FEXT 2 formulations, their respective placebos, and water. The animals in each group were kept in separate cages. For each sample, the mass equivalent to the paediatric dose (150 mg) was dispersed in the bottle. The position of the silicone tubes was the same for all drinking bottles. Each dispersion was prepared immediately before the start of each experiment and the recirculation was kept active throughout the experiment. The taste of each sample was assessed by volumes of basal water consumption, commercial tablets and their placebos were measured and compared by statistical analysis to verify what there was a difference in the ingestion. Behavior visual responses, such as jaw smacking, oral grooming/paw wipe, retreating, and tail erection, were also observed and registered by taking pictures. Results of volume consumption

were analyzed by single factor ANOVA using JMP Statistical Discovery Software version 8.

## 1.3 Pharmacokinetic study

### 1.3.1 Animals

To carry out the efficacy tests, an animal study model was developed. 31 male and adult Wistar rats were selected, weighing between 350 and 500 g. The animals were supplied by the Oswaldo Cruz Foundation's Institute of Science and Technology in Biomodels (ICTB).

Animal experimentation and all its manipulation followed the Ethical Commission's principles on the Use of Animals (CEUA), under protocol L-009/2019 CEUA/IOC - Fiocruz (30/05/2019) (Appendix II).

The animals were kept animal house of the Oswaldo Cruz Institute (IOC), with free access for water and feed, being kept in a climate-controlled environment with a controlled temperature (Figure 103).

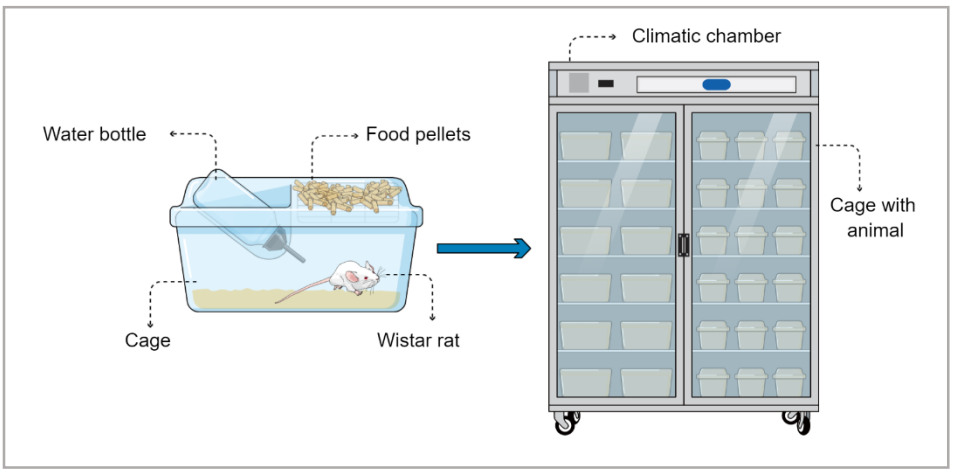


Figure 103. Representation of keeping animals in a bioterium during the acclimatization period.

On the experiment day, the rats were deprived of water and food for two hours before administering the test formulations.

### 1.3.2 Design of pharmacokinetic experiments

As it was a preliminary evaluation and considering the rational use of animals, it was decided to perform the experiment just with FEXT 1. This sample was selected based on the better palatability performance, higher API load, and less dissolution in the first minutes of analysis (which may favor the taste masking).

Four groups of formulations were then studied: Extruded placebo (vehicle); Blank (vehicle); Extruded FEXT 1 (extruded containing PZQ), and API (PZQ). All formulations were dispersed in the vehicle (solution of polyethylene glycol 400 (PEG 400) 60 wt% in water), except blank, which was the vehicle itself.

The number of animals for each group was defined through a sample space from a statistical calculation, where they were distributed, as shown in Figure 104.

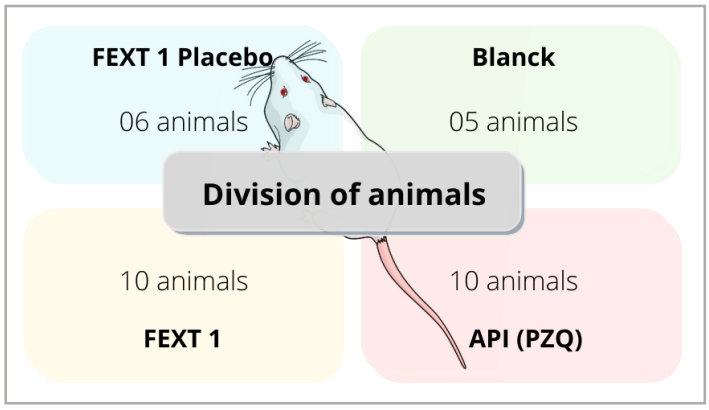


Figure 104. Animal groups for the study of pharmacokinetics.

The administration of the samples occurred orally using the gavage technique.

To determine the animal equivalent dose (AED), the bodyweight of the animal model and human and their body surface ($m^2$) were considered. For that, it is necessary to convert the dose from mg/kg to mg/$m^2$ using a constant, Km. This constant varies not only between species but also increases proportionally within each species [322], [323].

*1.3.2.1 Theorical considerations for the determination of AED*

***Determination of Km in animals*** [322]**:**

Rats and mice have K = 9 and humans weighing 70 kg, Km = 39.

Equation 6

$$\boldsymbol{Km} = \frac{10^2 * (peso)^{1/3}}{k}$$

*For rats, with an average weight of 300 grams: Km = 7.9*

***Determination of Animal Equivalent Dose (AED):***

The human dose to be used in the calculations is 50 mg/kg

Equation 7

$$\boldsymbol{AED}_{(\boldsymbol{mg/kg})} = human\ dose\ _{(mg/kg)} * \frac{Km\ human}{Km\ animal}$$

For the conversion of the human dose to RATS with an average weight of 300 grams: $\approx 262\ mg/kg$.

The equivalent animal dose refers only to the praziquantel API, it means that for the extruded formulation (50% PZQ API):

Equation 8

$$\boldsymbol{AED}_{\boldsymbol{FEXT\ 1\ (mg/kg)}} = \boldsymbol{AED}_{\boldsymbol{PZQ\ API\ (mg/kg)}} * 2$$

According to this, the AED is around $524\ mg/kg$.

All rats were weighed in order to adjust the dose schedule for each animal. 12 blood samples were collected from each animal at the intervals: 00:00 (pre-dose), 00:05 min; 00:10, 00:20 min, 00:30 min, 00:40 min, 00:50 min, 01:00 h, 01h:30 min, 02h:00 h, 04:00 h, 06:00 h. The blood samples were centrifuged (15000 rpm for 5 min at 10 ºC) to obtain the plasma fraction, and it was stored in a freezer at -70 °C.

The collected material was sent to SEFAR/FIOCRUZ, the laboratory responsible for plasma quantification and PZQ determination using the high-performance liquid chromatography technique coupled to mass spectrometry (HPLC-MS/MS) by electrospray ionization.

The methodology used for this step is represented in Figure 105.

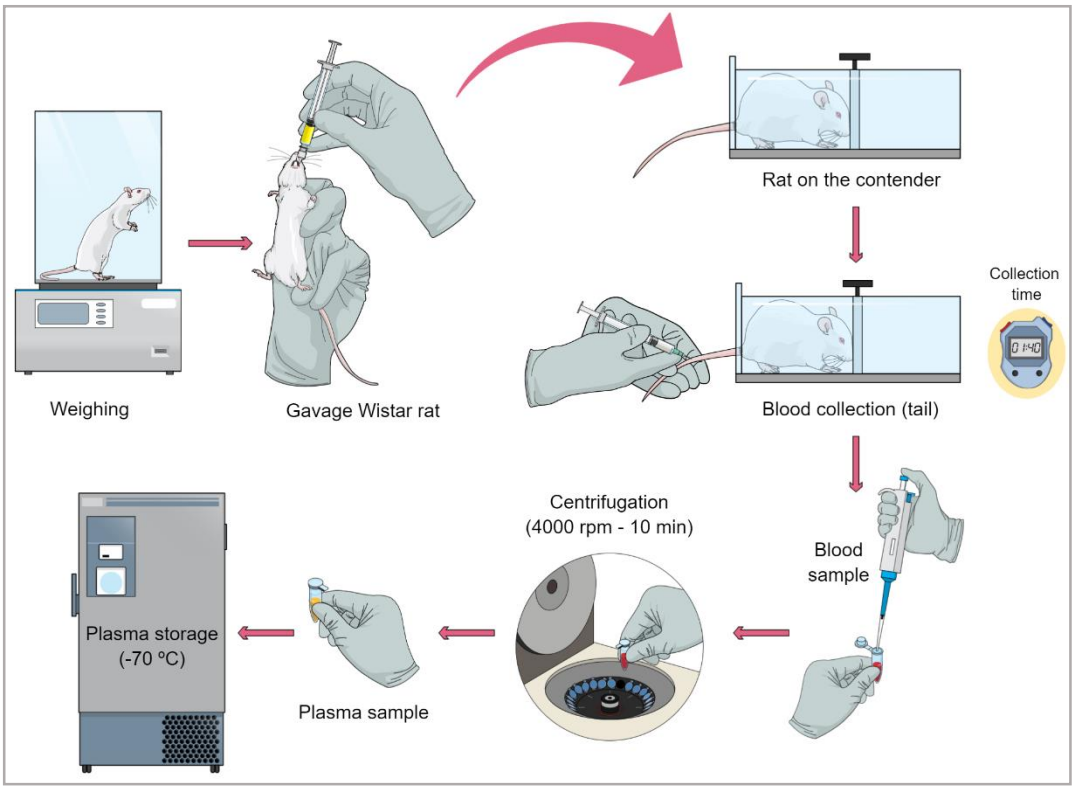


Figure 105. Gaving and taking plasma samples for the pharmacokinetics study.

To guarantee the reliability of the results obtained from animal samples, it was essential to develop and optimize a validated bioanalytical method according to the guidelines recommended by ANVISA, present in Brazilian resolution RDC n. 27 [324]. Tests of stability, precision and accuracy, matrix, and residual effect were performed.

*1.3.2.2 Bioanalytical method*

Analyses were performed with Nexera XRTM HPLC (Shimadzu, Kyoto, Japan) coupled to a Qtrap 4500 linear ion trap quadrupole mass spectrometer (Ab Sciex, Franingham, MA, USA). Chromatographic separation was carried out using a Zorbax C18 column (4.6 × 150 mm, 5 µm) (Merck KGaA, Darmstadt, Germany), using the isocratic method. The mobile phase used was a mixture of methanol (and an aqueous solution containing 0.1 wt% of formic acid (70:30, v/v) at a flow rate of 0.800 mL/min. The autosampler and column oven temperatures were equal to 10 ºC and 40 ºC, respectively. Sample injection volumes of 10 µL were used.

The mass spectrometer was operated with electrospray ionization (ESI) in the positive mode. Nitrogen was used as the nebulizer and auxiliary gas. Important operation parameters were: (i) source temperature of 650 ºC, (ii) curtain gas at 30 psi, (iii) nebulizer gas (GS1) at 65 psi and (iv) heater gas (GS2) at 50 psi. Collision-activated dissociation (CAD) gas was high. The ion spray voltage was equal to 5500 V, while the entrance potential (EP) was equal to 10 V. Quantification was carried out using multiple reaction monitoring (MRM). The MRM transitions selected were m/z 312.89 > 203.10 for PZQ and m/z 284.68 > 193.20 for Diazepam (DZP).

Four standards were used in this work, PZQ reference standard, Diazepam internal standard (IS), as well caffeine and Nicotine Bitartrate Dihydrate as possible interfering.

The stock solution of PZQ (1 mg/mL) and DZP (IS) (1 mg/mL) were prepared by dissolving the accurately weighed in methanol/ water (50:50, v/v). The calibration standards and quality controls solutions were prepared from the stock solution in methanol/ water (50:50, v/v) at the concentrations: 100.00, 300.00, 600.00, 1200.00, 3000.00, 6000.00, 12000.00 and 15000.00 ng/mL. Low, medium, high and dilution quality controls were prepared at 300.00, 6000.00, 12000.00 and 120000.00 ng/ mL, respectively. For the analysis, spiked plasma at dilution quality control (120000.00 ng/ mL) was 10-fold diluted with blank plasma to 12000.00 ng/ mL. The IS working solution was prepared in methanol/ water (50:50, v/v) at 5000.00 ng/ mL.

An aliquot of 25 µL of rat plasma was dispensed into a microtube. Then, 25 µL of IS working solution was added and the extraction was 1.50 mL of tertmethy buthyl ether. After mixing in automatic shakers for 5 minutes, samples were submitted to centrifugation at 19.90 g at 10 ºC at 5 minutes. The organic phase was transferred to a clean microtube (300 µL) and evaporated under nitrogen flow. The sample was reconstituted in 1.50 mL of the mobile phase (methanol/ 0.1% formic acid in water – 70:30 v/v). The sample was transferred to a vial and 10 µL were injected into the HPLC-MS/MS system for analysis.

*1.3.2.3 Pharmacokinetic data analysis*

Non-compartmental analyses were performed with the Phoenix WinNonlin software (version 6.3, Pharsight, St. Louis, MO, USA). The pharmacokinetic (PK) parameters determined were the maximum concentration ($C_{max}$), time to achieve maximum concentration ($T_{max}$), area under the curve (AUC0-t and AUC 0−∞), the

terminal elimination rate constant (Ke) and the terminal elimination halflife (T½). Parameters $C_{max}$ and Tmax were extracted directly from the plasma concentration (Cp) versus time curve, AUC 0−t was calculated with a linear trapezoidal method, AUC0−∞ was calculated by combining AUC0−tlast with Ctlast/Ke, Ke was obtained by calculating the slope of the decay phase from the graph of ln (Cp) versus time and T½ was calculated using the equation: T½ = 0.693/ Ke. Outliers were detected with the Dixon and Chauvente tests.

## 2. RESULTS

### 2.1 Taste masking

#### 2.1.1 In vitro taste masking (e-tongue)

A positive effect on taste masking for PZQ is expected with the extrudate solid dispersions studied in this thesis. It is true that the literature has already reported promising results on HME solid dispersions with different APIs such as efavirenz [325], griseofulvin [326], caffeine [326], verapamil hydrochloride [327], ibuprofen [281], and paracetamol [328]. One of these works [329] is cited as example. It appears be the first that demonstrated the use HME solid dispersions of verapamil HCl for taste masking using two polymers, Eudragit L100 and L100 55. The results were very promising confirming a good taste masking for extrudates with high drug loads (neutral taste for 50 wt% of API and slightly bitter taste for 70 wt% API). However, the taste-masking ability might be dependent on the right combination of the excipients (polymers and others), the API load and the extrusion parameters.

Starting the palatability studies of our extrudate samples produced in this time of the thesis, in-vitro taste masking data of FEXT 1 and FEXT 2 samples and their respective placebos, PZQ commercial tablet as well the correspondent placebo were obtained by using an electronic tongue with impedance analyser.

The results are shown in Figure 106, coded by different colours. The number of balls represents the replicates for each sample. The distance between replicate can indicate variability of sample homogeneity. Finally, the palatability can be predicted by the distance between the group of balls from the water. The water taste is considered

neutral. If a sample is situated next to water, a good palatability could be expected from it.

In summary, from the in-vitro palatability test performed with an e-tongue, the better palatability was found for FEXT 1. For remembering FEXT 1 is composed by (PZQ 50 wt%: PVPVA 45 wt%: SPAN 20 5 wt%).

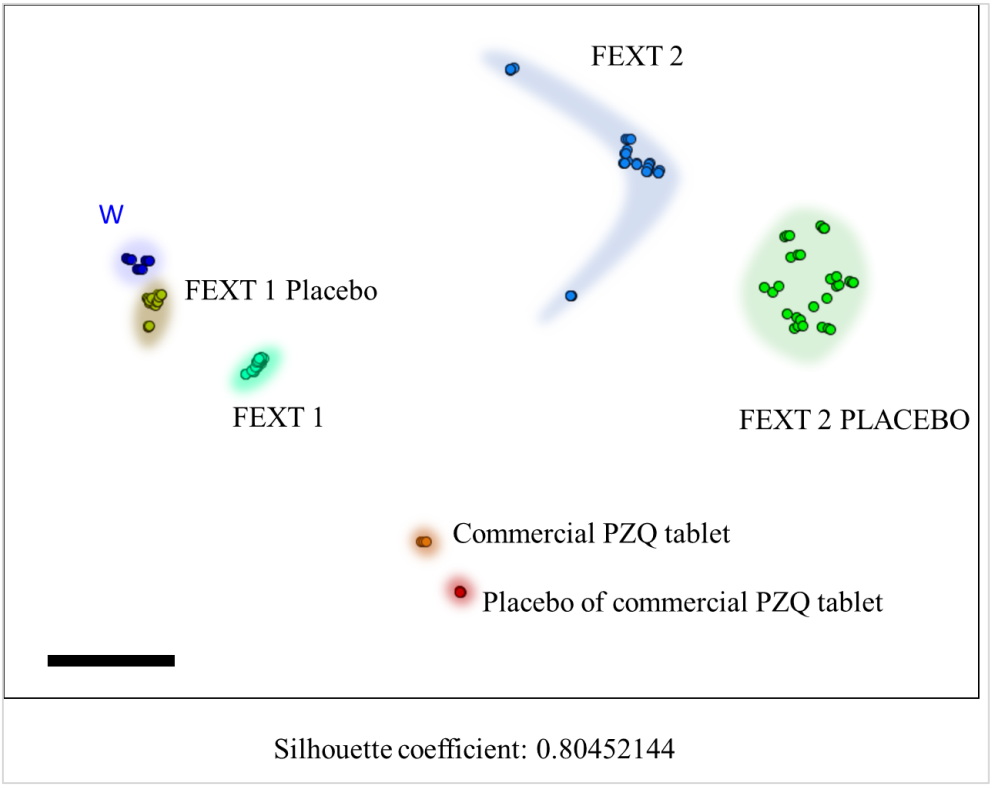


Figure 106. IDMAP plot for FEXT 1, 2, commercial PZQ tablet and their respective placebos (n=3).

Regarding the e-tongue test, a French electronic language (α Astree) is one of the two types of equipment available on the market for this purpose [121]. The sensors respond in the form of an electric potential (measured by an ion-selective field-effect-transistor, ISFET) that is generated across the membrane of individual sensors due to the taste quality of the formulation or test sample [134]. However, a limitation for this type of sensor is non-ionic molecules that generate very low conductivity signals such as praziquantel, ibuprofen, and caffeine [68]. This barrier was overcame using an electronic language developed by partners of the research group where our samples were analysed. The sensitivity improvement of the technique was obtained thanks to changes in the surface of the electrodes using nanomaterials [121]. This alteration permitted analysing

molecules like praziquantel. Machado et al. [134] has already successfully been demonstrated the evaluation of the taste mask of PZQ with microencapsulated products.

### 2.1.2 In vivo taste masking by volume consumed

In a study published in 2017, PZQ was encapsulated with maltodextrin and cyclodextrins. The palatability was evaluated by in vivo (aversion test in rats) and in vitro (electronic language TS-5000Z - Insent - Japan). The in vivo method used in the mentioned study, although using animals, is considered the gold standard for assessing taste masking of drugs in development. The researchers established a very important data through this experiment, that is the taste threshold for praziquantel (0.03 mg / mL) in vivo. From this data, in vitro methods can estimate a correlation with the perception of taste in vivo.

The results are shown in Figure 107 that displays the difference on volume consumption for each 'treatment' (sample tested). These data indicated a tendency towards aversion of the commercial PZQ tablet and the FEXT 2 extrudate (below the zero lines). This result agrees with the animal's behaviour observed, since they lie in the water trough and remain retracted at the bottom of the cage for the rest of the experiment (Figure 108). For placebo samples, the animals behaved normally, indicating that the perception of taste was acceptable. Likewise, the results for FEXT 1 were statistically similar to those for water and placebos. The bitterness profile detected by the e-tongue (in vitro palatability tests) are in accordance with those found here in the in vivo tests.

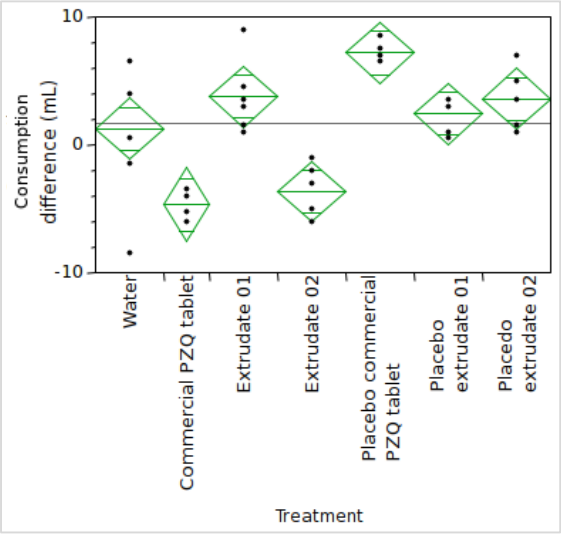


Figure 107. In vivo palatability test. (A) ANOVA (single factor 95%) for the samples.


Figure 108. Observation of rat's behaviour. a and b) drinking with neutral mouth movements (similar behaviour for water, placebos and FEXT 2); c and d) after taste FEXT 1 and commercial PZQ solutions, the rat tries to get it out of his mouth - oral grooming/paw wipe and retreating during the entire exposure time.

## 2.2 Pharmacokinetic study (PK)

### 2.2.1 Bioanalytical validation method

Bioanalytical methods refer to the identification and quantification of analytes in various biological matrices (e.g., blood, plasma, urine, and saliva) [323]. The high quality of bioanalytical methods is critical because it confers reliability, traceability, standardization of steps (e.g., sample collection, storage, and preparation) [302], [330]. All of these factors contribute to decision-making in pharmacokinetic studies that can result in an impact on the patient's health [330].

The results obtained in the validation of the methodology are presented in summary form in Table 41. The intra-day and inter-day precision RSD % did not exceed 8.48 % at any QC concentration levels. Since both intra-day and inter-day precision were below 15 % and accuracy was within ± 15%, the stability studies were also satisfactory, thus the proposed bioanalytical method could be regarded as precise and accurate according the current Brazilian guide for bioanalytical validation [324].

Table 41. Summary of precision and accuracy assay (intra-day and inter-day) for PZQ in rat plasma.

| ***Precision accuracy of control*** | | | | | | | | | | | | |
|---|---|---|---|---|---|---|---|---|---|---|---|---|
| ***Nominal concetration (n=8)*** | ***Intra-day*** | | | | | | | | | ***Inter-day*** | | |
| | ***Day 1*** | | | ***Day 2*** | | | ***Day 3*** | | | ***Overall*** | | |
| | Mean | RSD (%) | Accuracy (%) | Mean | RSD (%) | Accuracy (%) | Mean | RSD (%) | Accuracy (%) | Mean | RSD (%) | Accuracy (%) |
| 100 ng/mL | 103.71 | 4.69 | 103.71 | 88.64 | 5.79 | 88.64 | 82.22 | 5.67 | 82.22 | 91.52 | 8.48 | 91.52 |
| 300 ng/mL | 299.33 | 2.57 | 99.78 | 266.33 | 3.48 | 88.78 | 277.44 | 2.29 | 92.48 | 281.03 | 6.32 | 93.68 |
| 6000 ng/mL | 6207.41 | 3.43 | 103.46 | 5905.64 | 1.80 | 98.43 | 6056.05 | 3.86 | 100.93 | 6056.37 | -0.94 | 100.94 |
| 12000 ng/mL | 12554.33 | 4.89 | 104.62 | 12207.59 | 2.56 | 101.73 | 12125.17 | 0.80 | 101.04 | 12295.70 | -2.46 | 102.46 |
| 12000 ng/mL | 11798.45 | 1.91 | 98.32 | 12579.25 | 3.42 | 104.83 | 12015.84 | 1.53 | 100.13 | 12131.18 | -1.09 | 101.09 |

Table 42. Stability during storage.

| ***Stability during storage in different conditions (n=8)*** | | | | | | | | | |
|---|---|---|---|---|---|---|---|---|---|
| ***Nominal concentration (n=8)*** | ***Stability at room temperature*** | | | ***Stability at 10 °C in the autosampler*** | | | ***Stability of three freeze-thaw*** | | |
| | 05h:02min | | | 26h:45min | | | 08 cycles | | |
| | Mean | CV (%) | RSD (%) | Mean | CV (%) | RSD (%) | Mean | CV (%) | RSD (%) |
| 300 ng/mL | 308.11 | 2.04 | 2.70 | 323.79 | 3.61 | 7.93 | 283.56 | 1.90 | -5.48 |
| 12000 ng/mL | 12227.46 | 1.16 | 1.90 | 13062.56 | 2.97 | 8.85 | 11104.02 | 4.85 | -7.47 |

The results of the long-term stability of the sample into a biological matrix are shown in Table 42. For all determined conditions, the results are within limits established by legislation (CV% <15%) [324]. In addition, the long-term stability test demonstrated that the sample showed no signs of degradation of the analyte after 237 days. Thus, all samples analysed in this study (140 days) are within the stability time evaluated in the method validation protocol.

### 2.2.2 Pharmacokinetic profile

Pharmacokinetic studies were performed to determine the absorption, bioavailability and elimination profile of praziquantel administered in milled extrudate (FEXT 1) after single oral doses (50 mg/Kg) and to compare with the raw PZQ profile. After outlier detection, one animal from the FEXT 1 group and three animals from the PZQ group were excluded, according to criteria established by the Grubbs test. Then, the pharmacokinetic parameters were calculated with six placebo animals (extrudate placebo without PZQ) (n = 6), five animals in control group (n = 5), nine animals in FEXT 1 group (n = 9) and seven animals in API group (n = 7). PZQ in rat plasma was observed from 5 mins until 6 h after oral administration in FEXT 1 and PZQ groups. In the control group, PZQ was not detected in any of the analysed times, demonstrating that the vehicle used (water with 60 % PEG 400) was free of the drug, PEG 400 did not interfere with the analytical setup and there was no cross-contamination during sample preparation and analysis.

The absorption speed of FEXT 1 was 4.5 times higher ($T_{max}$: p = 0.006) than the API (mean $T_{max}$ was 13 min and 59 min, respectively). The API guarantees a good characterization of the absorption phase over time with 4 quantifiable points before $C_{max}$. Unlike the FEXT 1 formulation, which has only one point up to its $C_{max}$. This reveals an improvement point for the protocol design. According to this fast speed of the extruded material (spring effect), more collection points must be performed (1 point) in this initial phase of absorption (before 10 min). Although the statistical results do not allow a difference between the $C_{max}$ of FEXT 1 and API (p = 0.053), the average values of this parameter indicate that FEXT 1 has twice the maximum API concentration. In the literature, this $C_{max}$ value for praziquantel is variable, mainly depending on the composition of the formulation used, the experimental model, and the dosage. For example, poly (methyl methacrylate) (PMMA) nanoparticles loaded with PZQ (PZQ-NP) and obtained by sintering showed $C_{max}$ and AUC 3 times less than the API raw material (60 mg/Kg) in rats [180]. Another study that evaluated the pharmacokinetics of lipid nanoparticles loaded with PZQ demonstrated that it significantly increases bioavailability compared to the

praziquantel tablet [331]. However, this previous study evaluated intramuscular administration (5 mg/kg) in dogs.

The phase of elimination of the PZQ was significantly greater than the FEXT 1 ($p << 0.05$), where the $T_{1/2}$ was approximately three times greater with the time of 196.21 min and 64.33 min, respectively. If we consider that both samples (FEXT 1 and API) were prepared with the same vehicle and same concentration, a hypothesis that could explain the slow elimination of the API is the crystalline state. Differently of the extrudate in supersaturated amorphous form (or mostly amorphous) that has a spring absorption effect demonstrated by $C_{max}$. This profile has already been described for solid amorphous PZQ dispersions using a mixture of two surfactants (PZQ: PEG 4000: Poloxamer 188; 1: 3.75: 1.25) [332]. $C_{max}$ (173 ± 34 µg/L) was obtained in 1h. However, it should be noted that the experiment was carried out in dogs, and the number of animals was very limited (n = 3). The absence of parachute effect from FEXT 1 may be related to the recrystallization of the PZQ in the lumen. And the next question could be: why does FEXT 1, supposedly recrystallized, not maintain the same absorption level as PZQ? Three main assumptions could be made:

a) the amount of recrystallized material is too small to maintain the same level;

b) it is unknown if the recrystallization process would be associated with the same crystalline form as the raw material;

c) the recrystallized material is still in a polymeric system, resulting in a solubilization disadvantage compared to API in its free form. Another question that could be asked is: why is the FEXT 1 elimination time much longer than the API? The assumption that could explain this phenomenon is related to the first hypothesis described above. The recrystallized material is in small amount. So, first the PZQ was quickly absorbed due to the amorphous structure, but as the system is supersaturated, a small amount recrystallizes. The elimination is proportional to the absorption.

The results of ASC0-t showed no statistical difference between FEXT 1 and PZQ, indicating that the extent of absorption can be considered similar for both. The flattening of the concentration curve as a function of the time observed for API compared to the FEXT 1 and the possible similarity between the observed absorption extension values (ASC0-t) seem to reinforce the discussion above.

It is important to say that although the mean ASC0-inf values showed a statistically significant difference between the groups ($p = 0.005$; 95% CI [-6.65 x 105; -1.43 x 105]), this data can be considered fragile in the function of another possibility to improve the experimental protocol. An adequate collection schedule should include a period of not less than three half-

lives of the substance to be dosed (this interval should be between 3-5 $T_{1/2}$) [302], [323]. The maximum interval for collecting blood samples for the PZQ dosage adopted in the present study was 360 min (6 hours). Therefore, five and a half times the calculated half-life for the PZQ after administration of the preparation FEXT 1 (mean $T_{1/2}$ of 64.33 min). However, only approximately twice the half-life was calculated for the PZQ after administering the preparation "PZQ" (mean $T_{1/2}$ of 196.21 min). An extended schedule for this case with a minimum of 10 hours should be necessary. The values presented must be corrected by the bioavailability factor (F) provided by the preparations, which is unknown for this study. The bioavailability factor must be calculated in a comparative test with an intravenous administration.

Figure 109 shows the profiles of the average concentration of PZQ as a function of time after removing outlier animals. Table 43 presents the descriptive statistics of the pharmacokinetics parameters observed for FEXT 1 and the API, respectively, after removing the outlier animals.

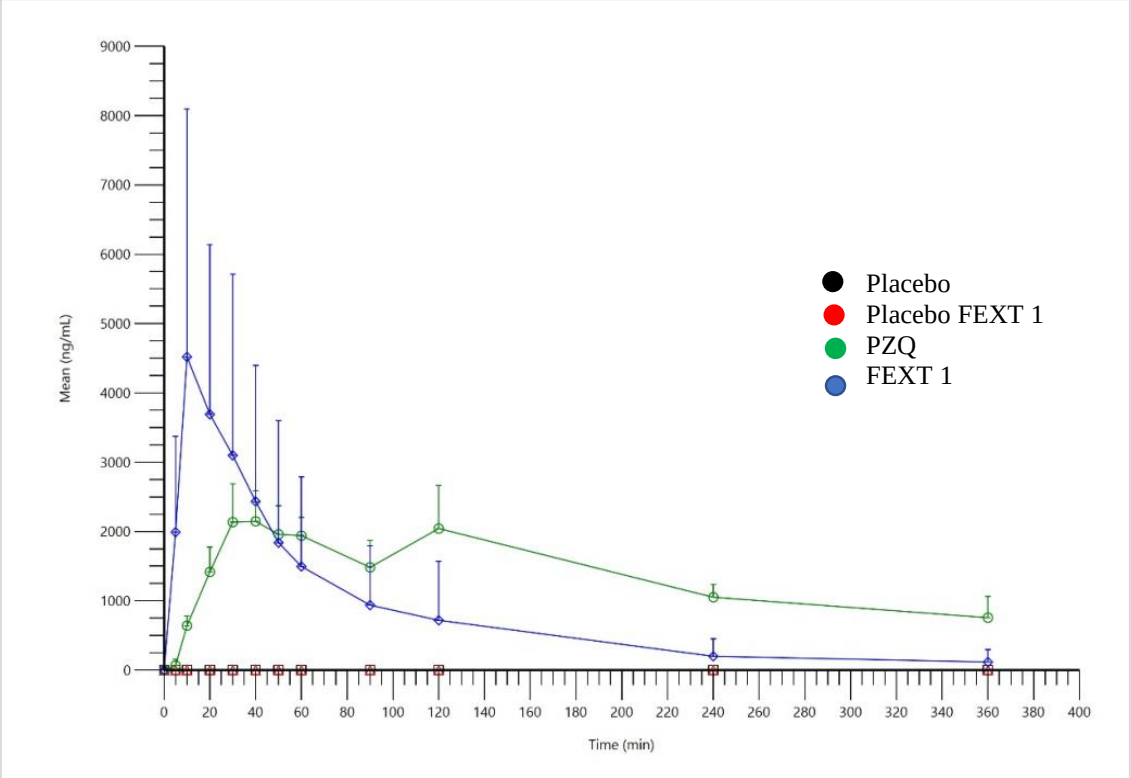


Figure 109. Comparative profile of mean plasma concentrations of PZQ as a function of time for each preparation administered (arithmetic mean + standard deviation). After removing the outlier animals.

Table 43. Non-compartimental pharmacokinetic parameter of PZQ in rat plasma after oral administration of FEXT 1 (n=9) and PZQ (n=6).

| ***Group*** | ***Pharmacokinetic parameters*** | | | | |
|---|---|---|---|---|---|
| | ***$C_{max}$ (ng/mL)*** | ***$T_{max}$ (min)*** | ***$ASC_{0-t}$ (min*ng/mL)*** | ***Ke (1/min)*** | ***$T_{1/2}$ (min)*** |
| FEXT 1 | 5407.43 ± 3515.07 | 13 ± 8 | 292876.47 ± 249299.25 | 0.0149 ± 0.0085 | 64.33 ± 44.15 |
| PZQ | 2574.97 ± 284.08 | 59 ± 42 | 490022.03 ± 56502.12 | 0.0038 ± 0.0010 | 196.21 ± 58.07 |

Although the extruded material has achieved increased solubility, the PZQ efficacy does not depend on the maximum API concentration but rather on the extension ratio over time when the parasites are exposed to the limit concentration of the drug [178], [333], [334]. Some authors have already shown that dividing the total dose administered in 3 times almost doubled the effectiveness compared to administering a single oral dose [333]. Thus, the improvement in the controlled release of the API in the extruded system is necessary.

Analysing the data obtained for the API raw material, it is possible to see a considerable variation in main pharmacokinetic parameters compared with similar protocols in the literature (e.g., $C_{max}$ 554.23 µg/L, whereas in our study, it was 2754 µg/L). For example, Malhado et al. [180] used the same animal model, administration method (gavage), and PZQ (commercial form) raw material. The main differences were in the dispersion vehicle used (aqueous solution containing 2 % of Cremophor E), in the administered dose (60 mg/Kg), and the calculation of the administered mass (simple human dose/Kg relation for the animal's weight). Even though the authors administered a 10 mg higher dose, the $C_{max}$ value is almost 5 times higher.

This evidence may be related to the fact that, as described in item 1.3.2.1 of this Chapter, the calculation of mass administered to animals took into account critical physiological parameters described in the literature (e.g., body area, metabolism, animal model) for the correlation of human dose versus animal [322], [323].

## 3. CONCLUSIONS

The knowledge developed in this chapter was fundamental because:

- It was possible to check the stability of the ternary systems looking for and, through them, the importance of determining the solubility of the API in the polymer during the early-stage development.

- It was possible to evaluate for the first time the in vitro (and tongue) and in vivo (volume consumed) palatability of solid amorphous dispersions produced by HME containing 50 wt% PZQ. The promising results of taste masking corroborate with literature on the application of the HME technique to overcome the bitterness of drugs.

- Although the information is still not ideal, it was possible to verify the increase in bioavailability found by the production of the amorphous solid dispersion with the ternary composition: PZQ (50 wt%), PVPVA (45 wt%) and SPAN 20 (5 wt%).

- It was possible to identify two potential improvement points for pharmacokinetic protocols to evaluate the bioavailability of ASD, which are first the increase in the number of collection points before 10 minutes to prove the initial phase of PZQ ASD absorption and second the extension of the PK study to at least 10 hours to meet the requirements considered for drugs with API-like half-life.

The subsequent steps of the work turned toward improvements on the studied formulations, FEXT 1 and FEXT 2, more specifically on the quality of the extruded formulations and knowledge of their characteristics.

It was possible to identify the most suitable HME process conditions for obtaining solid amorphous dispersions that resulted in a significant increase in kinetic solubility when compared to the starting API. However, through the screening of the HME process parameters initiated in this phase of the work, it could be verified that a load of 50 wt% PZQ in the ternary system is challenging in balancing the processability and the necessary characteristics of the solid dispersion.

# SUB-CHAPTER 5.3 - PRAZIQUANTEL AMORPHOUS SOLID DISPERSIONS MANUFACTURED BY HME - TERNARY SYSTEM (50 wt% PZQ) PHARMA 16 EXTRUDER

## 1. INRTODUCTION

This Sub-chapter presents new results for ternary solid dispersions of same composition that those described in the previous Sub-chapter. This time the production was performed in an extruder with larger capacity (Pharma 16, Thermofisher), the same used to produce the binary amorphous solid dispersions (Chapter 5.1).

Contrarily to the procedure described in Chapter 5.2, for the ternary systems containing the liquid surfactant (span20), it was directly fed into the extruder. This modification aimed to simplify the production process by eliminating the granulation step previously described. It required some preliminary investigations on the liquid feed realized by a peristaltic pump (feed rate, insertion zone in the barrel). Then, two batches were produced for each of the two formulations, as schematically illustrated in Figure 110.

The HME extrudate samples obtained were shaped in two different physical forms: first as pellets (size around 1mm), and secondly, the pellets were milled to produce a powdered sample. Both forms were characterized, and the methods used and the results obtained are presented in this Sub-chapter.

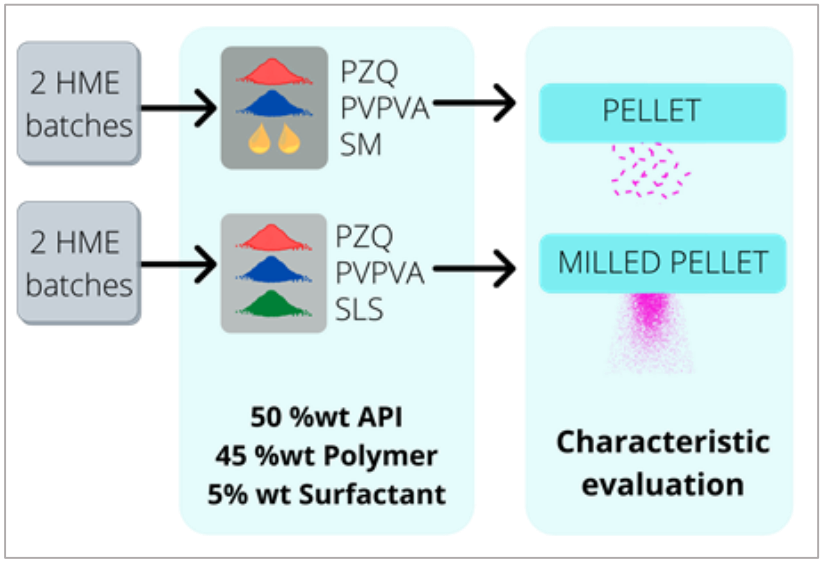


Figure 110. Schematic representation of the batches produced and presented in this sub-chapter.

## 2. METHODS

### 2.1 Ternary ASD system prepared by HME (50 wt% PZQ)

Two formulations were produced, with the same qualitative composition described in the previous Sub-chapter. The concentration of 50 wt% PZQ was maintained for both formulations, regardless of the surfactant.

The formulations were made in duplicate in a different period. Table 44 shows the formulations produced and the respective compositions.

Table 44. HME extrudate samples produced and the respective compositions.

| ***Samples*** | ***Composition (wt%)*** | | | |
|---|---|---|---|---|
| | ***PZQ*** | ***PVPVA*** | ***SLS*** | ***SPAN20*** |
| HME 14 and HME 23 | 50 | 45 | 5 | |
| HME 16 and HME 24 | | | | 5 |

Two formulations were produced in an extruder from the same manufacturer (Thermo Scientific) but with a larger model (Pharma 16). Pharma 11 extruder used in the previous study presented in Chapter 5.2 is a bench-scale equipment, while Pharma 16 is a pilot one [1]. The difference between the extruders lies mainly in the size and production capacity (Table 45).

Table 45. Features of Pharma 11 and Pharma 16 extruders (ThermoFisher Scientific) [1].

| ***Equipment*** | ***Barrel Diameter (mm)*** | ***Barrel Lenght (mm)*** | ***Screw lenght (mm)*** | ***Achievable output (kg/h)*** |
|---|---|---|---|---|
| Pharma 11 | 11 | 40 | 440 | 0.02 - 2.5 |
| Pharma 16 | 16 | 40 | 640 | 0.2 - 5 |

The temperature profile of the formulation containing SPAN 20 was kept the same[20] used for the binary mixture and described in Chapter 5.1. In contrast, for the formulation containing the SLS surfactant (powder), the temperature profile was adjusted according to the SLS melting characteristics (around 200 °C).

[20] The extruder was fed with the binary mixture and the SPAN 20 was added into the barrel during extrusion.

The best screw profile selected from the hot-melt extrusion of the binary formulations (Chapter 5.1) was used for this study.

The powder flow rate and the screw speed were adjusted according to the characteristics of the mixture to ensure good processability.

The extrusion parameters can be seen in Table 46.

Table 46. Extrusion conditions for the ternary system (50 % PZQ) using Pharma 16 extruder.

| ***Sample Code*** | ***Composition*** | ***Conditions*** | | | | | ***Observation*** |
|---|---|---|---|---|---|---|---|
| | | ***Powder Rate Flow (kg/h)*** | ***Screw speed (rpm)*** | ***Liquid Rate Flow (mL/min)*** | ***Temperature profile*** | ***Screw profile*** | |
| HME 14 | 50 % API / 45 % KOL / SPAN 5 % | 0.25 | 300 | 0.23 | (Z1) 50°, 70°,100°, 140°, 140°,140°, 100° and 90° (die) | Zone 4 and 6 **without** RE | - |
| HME 16 | 50 % API / 45 % KOL / SLS 5 % | 0.15 | 300 | NA* | (Z1) 50°, 100°,140°, 180°, 180°,180°, 130° and 105° (die) | | - |
| HME 23 | 50 % API / 45 % KOL / SPAN 5 % | 0.3 | 150 | 0.23 | (Z1) 50°, 70°,100°, 140°, 140°,140°, 100° and 90° (die) | | samples were cryomilled after extrusion |
| HME 24 | 50% API / 45% KOL / SLS 5% | 0.15 | 150 | NA* | (Z1) 50°, 100°,140°, 180°, 180°,180°, 130° and 105° (die) | | |

* NA = not applicable

For formulations (HME 14 and HME 23), in which the surfactant was a powder (SLS), preparation was carried out by physical mixing the components in the Turbula® T2F mixer (08 min, 46 tr/min rotation speed).

For formulations (HME 16 and HME 24), where the surfactant was liquid (SPAN 20), it was added using a peristaltic pump directly in the extruder. Unlike what was previously presented, there was no need to carry out the wet granulation step to incorporate the surfactant into the powder mixture of PZQ and VPVA. This step is discussed in detail in this Sub-chapter.

### 2.1.1 Addition of a liquid surfactant

The first steps were to calibrate the peristaltic pump for liquid feeding and define the zone in the extruder for addition of the surfactant into the molten material during extrusion.

The calibration was based on the flow rate of the peristaltic pump as a function of the feed flow rate of the powder mixture and the desired final surfactant concentration in the formulation. To this end, the following relationship was used (Equation 6):

Equation 9

$$FR_{pump} g/h \; = \; ([\%Surf] \; x \; [FR_{mix} \; g/h]) \; / \; [\%API] \; x \; [\%Pol]$$

Where $FR_{pump}$ is the pump flow rate and $(FR_{mix})$ is the flow rate of the molten material on the extruder with a respective composition of API ($\%API$), polymer ($\%Pol$), and surfactant ($\%Surf$).

## 2.2 Cryomilling process

As one of our objectives was to produce an amorphous solid dispersion by HME aiming its use in a pharmaceutical formulation, we decided to reduce the granulometry of the pellets produced. For that, and considering the amorphous nature of the extruded material, the milling of the pellets was performed by cryomilling. In short, cryomilling is a process to reduce the particle size mainly used for thermolabile materials. It can be carried out first by freezing the materials to be ground in liquid nitrogen or milling under cryogenic conditions (in the presence of liquid nitrogen) [335].

The equipment available in the laboratory (6775 Freezer/Mill® (SPEX SamplePre, LLC) and used in this work is shown in Figure 111. The pellets were added up to half of the sample holder (Figure 82Figure 111b) and inserted into the equipment that already contained the appropriate liquid nitrogen level for the procedure (Figure 82c). At the end of the experiment, the sample holder was accommodated on the support (Figure 82d) for removing the lid and removing the sample. The method parameters were previously adjusted, and the sample was pre-cooled for 4 minutes, rate 5, 2 cycles of 1 minute and 30 seconds each (minimum equipment time). After cryomilling, the samples were placed in plastic test tubes with a screw cap, parafilm, and aluminium for light protection and kept in a desiccator under laboratory conditions (25 °C and 60 % RH).

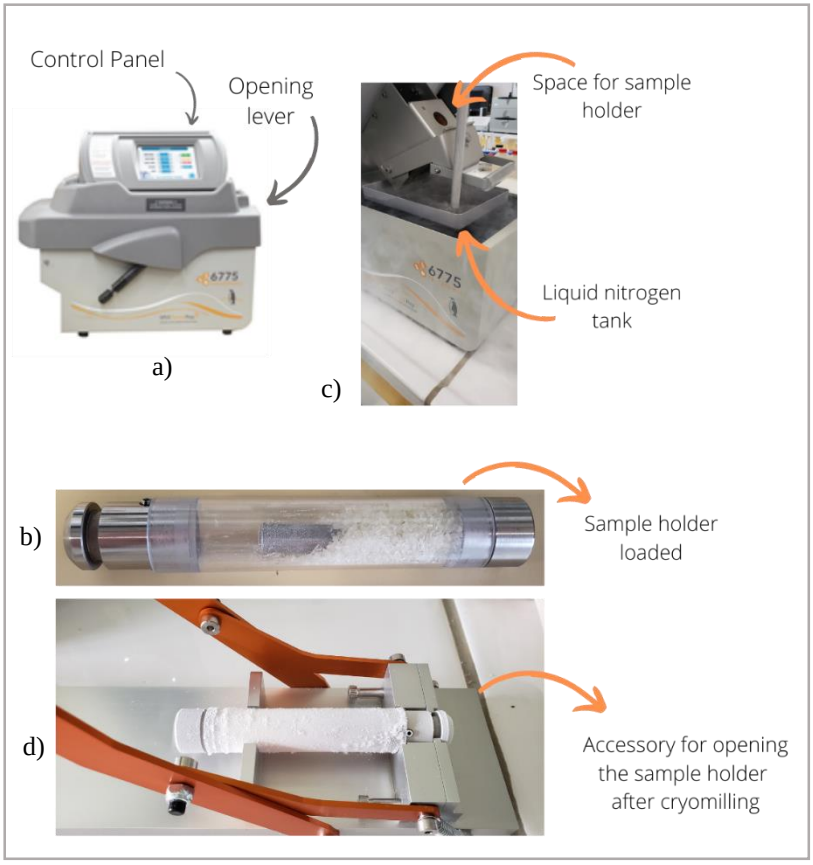


Figure 111. a) Cryomilling equipment; b) sample holder loaded; c) open equipment ready for insertion of the sample holder and d) sample holder after cryomilling in a specific accessory to perform the opening. Source: Author.

Samples HME 23 and HME 24 were cryomilled, while HME 14 and HME 16 samples were kept in the form of pellets (Figure 112).

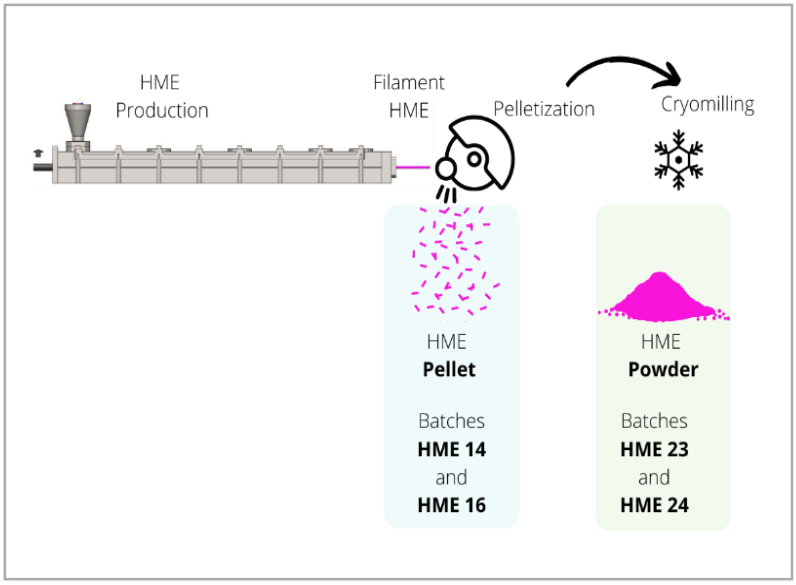


Figure 112. General view of production process described in this chapter.

Pellet samples were placed in opaque plastic flasks with a screw cap, parafilm and kept in a desiccator under laboratory conditions (25 °C and 60 % RH).

## 2.3 Characterization of PZQ-ASD

DSC, PXRD, Optical microscopy, and SEM were used to characterize the solid state of the HME samples produced. Likewise, other characteristics were also evaluated (water solubility, drug content, and in vitro dissolution profile).

All the characterization methods (except optical microscopy) used in this Sub-chapter have been described previously (see Chapter 5.1).

### 2.3.1 Optical microscopy

Images were obtained using a Leca EZ4 HD ® microscope with an integrated high-definition digital camera, set to 8x magnification. These images were then edited with the Leica LAS EZ software program. For calibration purposes, an image (obtained under the same conditions) of a standard slide containing a straight 1cm segment, with 100 divisions, was employed.

# 3. RESULTS

## 3.1 Ternary ASD system prepared by HME (50 wt% PZQ)

### 3.1.1 Addition and determination of the liquid surfactant feeding zone

For a HME extrudate with the desired composition (50 wt% PZQ, 45 wt% PVPVA and 5 wt% SPAN20), the following mass flow rates had to be adjusted (Equation 6):

For 250 g/h of powdered mixture PZQ-PVPVA, the mass flow rate for SPAN 20 was 13.16 g/h (0.24 mL/min), whereas

For 300 g/h of powdered mixture PZQ-PVPVA, the mass flow rate for SPAN 20 was 15.79 g/h (0.27 mL/min).

The calibration results for the peristaltic pump are shown in Table 47.

Table 47. Calibration pump for directly addition of surfactant (SPAN 20) on the extruder.

| ***Tube diameter (mm)*** | ***Theorical flow rate (mL/min)*** | ***Calibration time (sec)*** | ***Recovered mass (g)*** | ***Density of surfactant (g/ml)*** | ***Recovered volume (ml)*** | ***Real Flow rate (ml/min)*** |
|---|---|---|---|---|---|---|
| **24** | $FR_{max}$ 1,37mL/min | | | | | |
| **16** | $FR_{max}$ 0,19mL/min | | | | | |
| **16** | 0.20 | 600 | 2.5 | 1.032 | 2.42 | 0.24 |
| **16** | 0.23 | 300 | 1.4 | 1.032 | 1.36 | 0.27 |

The surfactant was initially fed int the extruder after the first mixing zone. However, in this region, as the powder mixture has not yet been fully melted, the introduction of a liquid caused adherence of the powder to the surface of the surfactant droplet. Consequently, in that open region of the extruder, it was formed an ‘agglomerate’ that no longer had the same temperature as the internal part (close to the screw), making it difficult to maintain a continuous liquid (surfactant) feeding (Figure 113Figure 113).

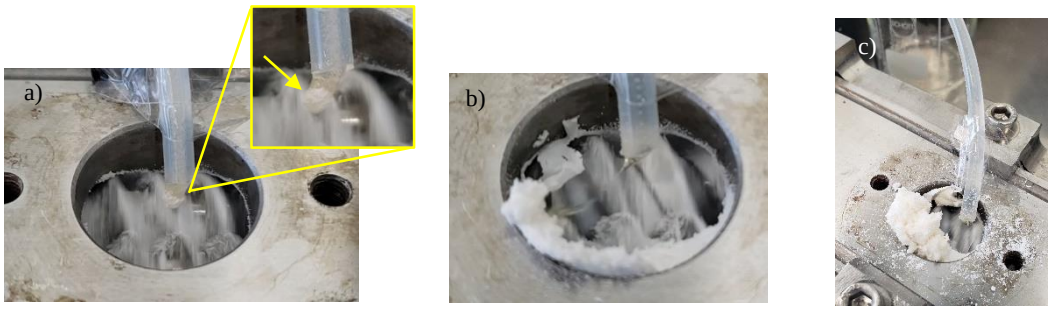


Figure 113. Addition of the liquid surfactant directly in the extruder after the first mixing zone. a) Adhesion of the powder to the surfactant drop; b) Formation of an 'agglomerate' that begins to be lost and, c) large amount of product lost after a few minutes of extrusion.

The change in the liquid surfactant feeding point to the back of the second mixing zone (Figure 114) caused the liquid to be completely incorporated into the melted mixture that passes through the thread in this region. This ensured the homogeneity of the surfactant concentration in the extruded material obtained.

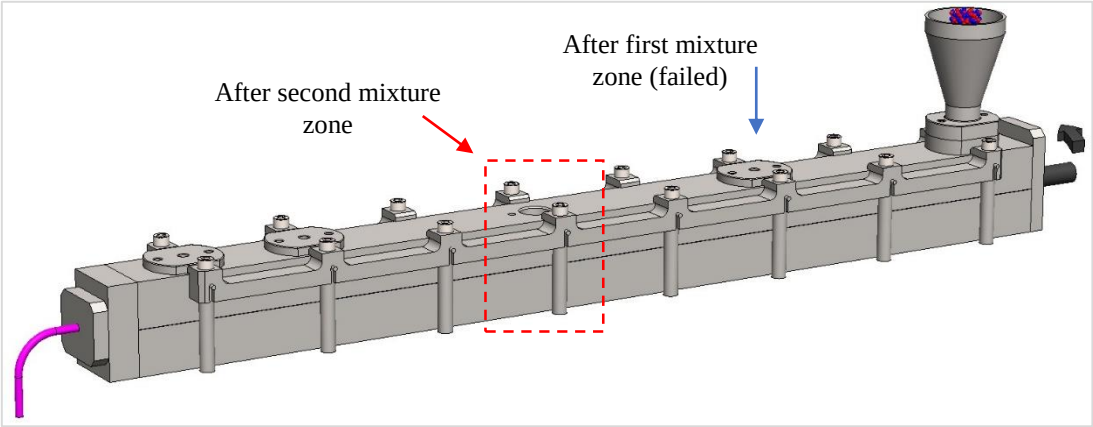


Figure 114. Schematic view of the point to addition the liquid surfactant (after the second mixing zone). Source: Author.

Also, a specific extruder accessory was finally necessary for feeding liquids during the process in order to reduce the opening and to decrease the variation of temperature and humidity in the product (Figure 115).

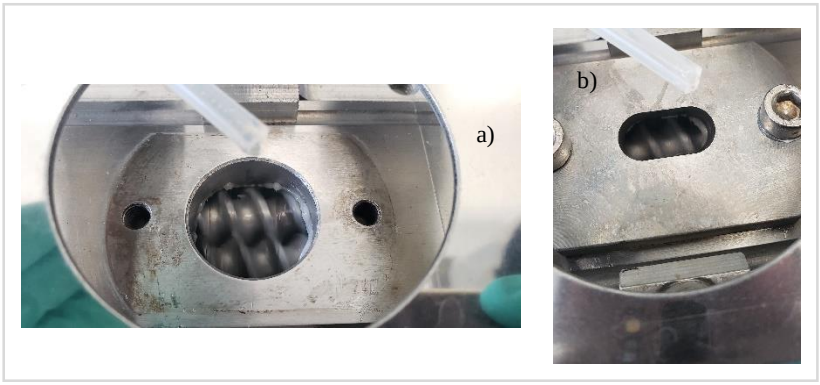


Figure 115. Surfactant addition zone (after the second mixing zone). a) without orifice reduction accessory and, b) with accessory - entry restricted to the surfactant drop.

After developing the conditions for continuous processing of the two ternary systems in Pharma 16 extruder, with the adequate addition of the surfactant regardless of its solid or liquid nature, four HME extrudate samples were produced.

## 3.2 Characterization of PZQ - ternary ASDs

### 3.2.1 PZQ dosage in the HME extrudates

The real content of PZQ in the HME samples, measured by HPLC (method described in Chapter 3, item 3.1.1) is given in Table 48.

Table 48. Dosage result for physical mixture and extrudate samples (HME 23 and 24).

| ***Samples*** | ***Theoretical drug content (wt%)*** | ***Measured drug content (wt%)*** |
|---|---|---|
| PM HME 23 | 50% | NM* |
| HME 23 | 50% | 51.74 % ± 0.2 |
| PM HME 24 | 50% | 47.38 % ± 0.1 |
| HME 24 | 50% | 43.15 % ± 0.2 |
| API | 100% | 100.58 % ± 0.2 |

*NM = not measured; PM = physical mixture

Comparing with the theoretical load (50 wt%), the PZQ content in the HME sample is in according to the theoretical value, while lower values were found for the other samples, even the physical mixtures.

### 3.2.2 Scattering Electronic Microscopy (SEM)

SEM images of HME extrudates can be visualized in Figure 116 (pellets) and 117 (cryomilled pellets).

In Figure 116, the images show the dense structure of the extrudates, and it is possible to observe the presence of thin filaments on the surface of some of them.

After cryomilling, Figure 117 allowed us to find the physical characteristics of a milled powder, with a particle size distribution in the micrometric range. Small particles appear to be adhered to the larger ones. The thin filaments observed in the surface of some pellets can be seen in some milled particles too, as shown in Figure 117c and 117f.

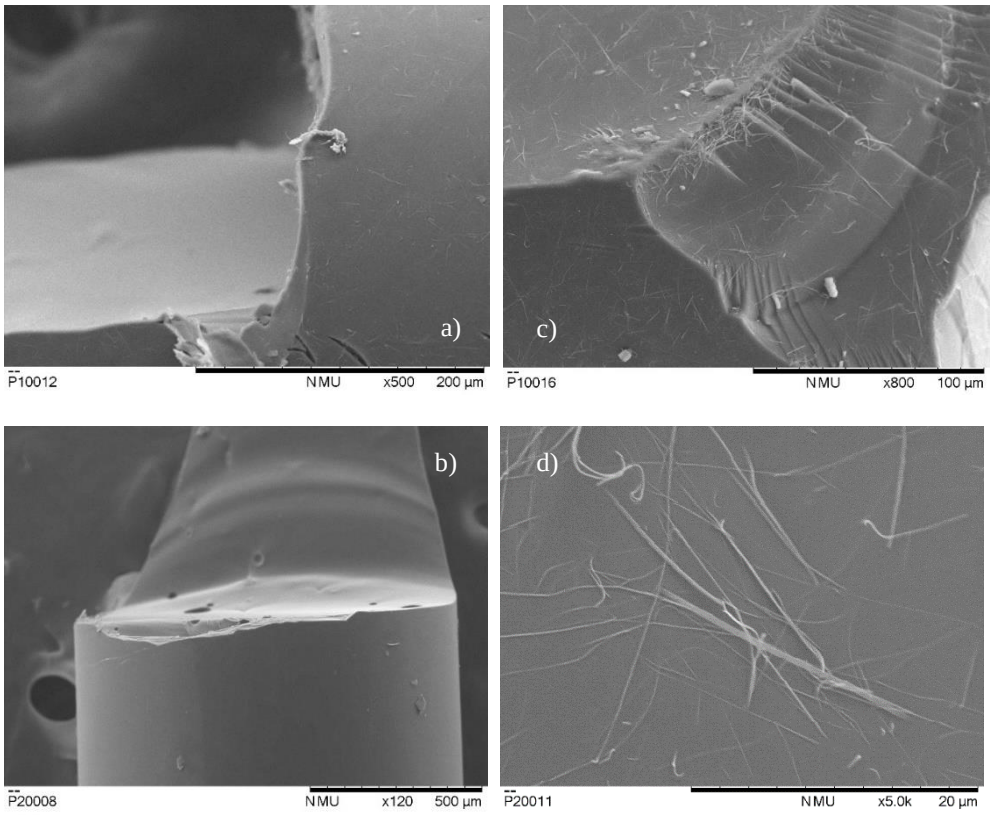


Figure 116. SEM images of HME ternary extrudate filaments shaped as pellets. a) HME 14, b) HME 23, c) HME 16, and d) HME 24 samples.

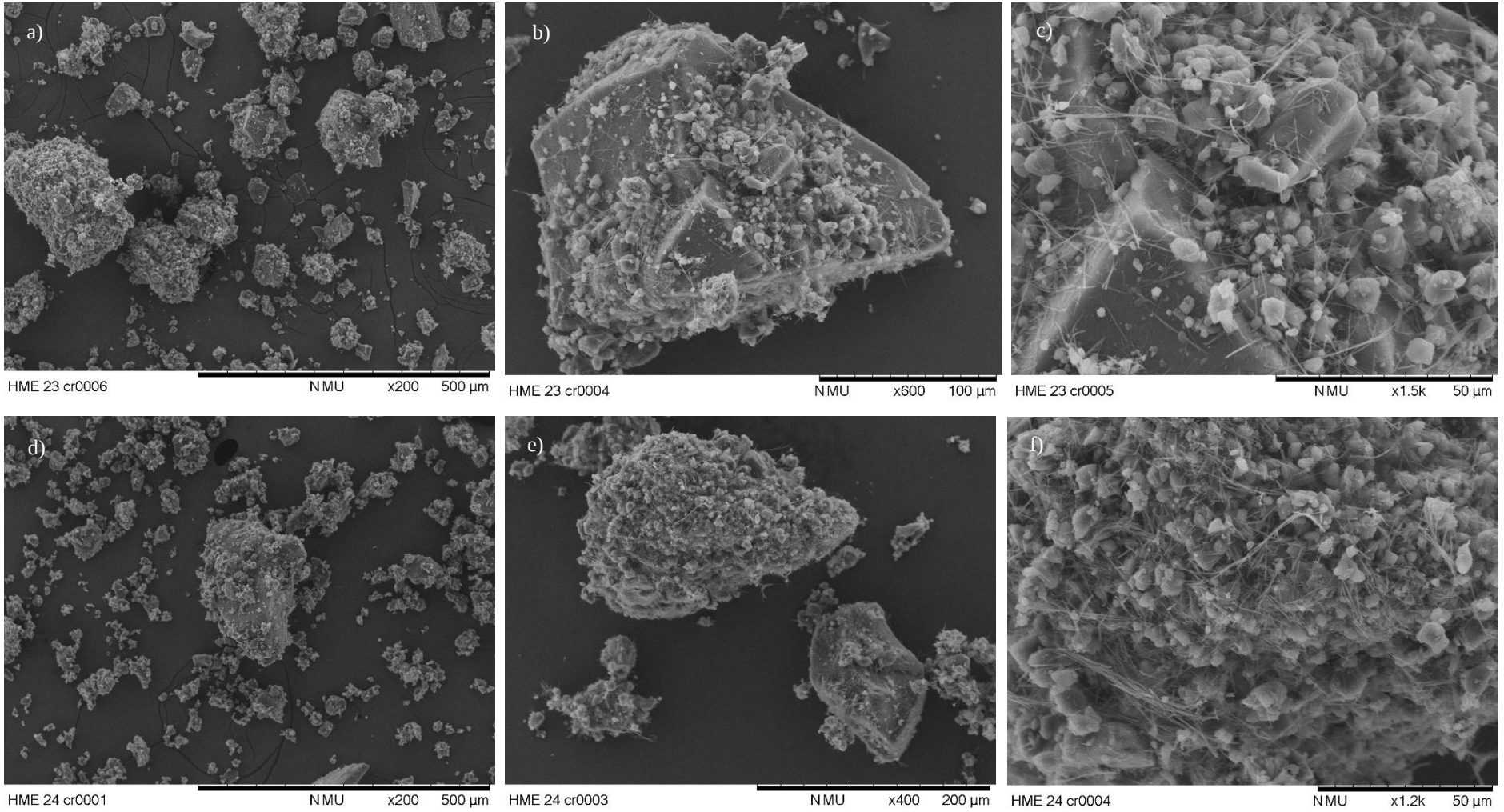


Figure 117. SEM images of HME ternary extrudate filaments shaped as pellets and then cryomilled. a - c) HME 23; d- f) HME 24 samples.

In an attempt to understand to what could correspond the thin filaments, observed in some pellets and even in cryomilled HME powders, a SEM image published by Zanolla and collaborators [30] is shown in Figure 118. It corresponds to the polymorph B of PZQ, produced by milling in a vibrational mill in that work, and described by them as "agglomerates of long and very thin whiskers". DCS analysis could perhaps identify the presence of form B in our HME extrudates, and this is discussed later in this Chapter.

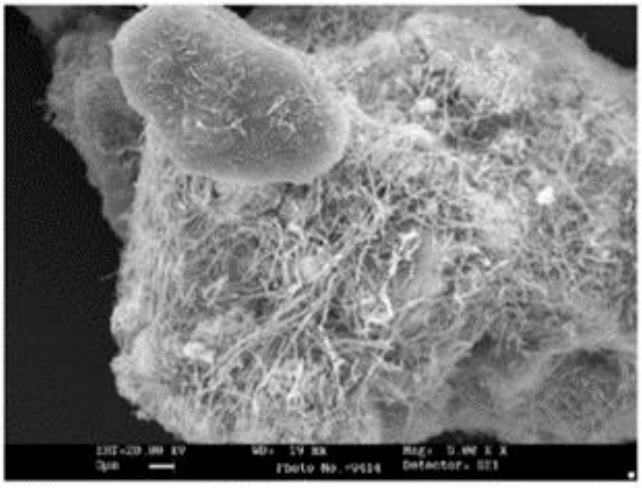

Figure 118. SEM image of PZQ form B. Reuse from [30] with permission.

### 3.2.3 Differential scanning calorimetry (DSC)

Figure 119 displays the DSC curves obtained for the ternary systems produced with both surfactants, SLS and SPAN 20. Surprisingly, they did not correspond to typical DSC thermograms for completely amorphous materials. In all DSC curves, endothermic events can be observed, probably due to melting transformations. For formulations containing SLS (Figure 119b), an exothermic signal is visualized before the endotherm.

The thermal data corresponding to these curves are grouped in Table 49.

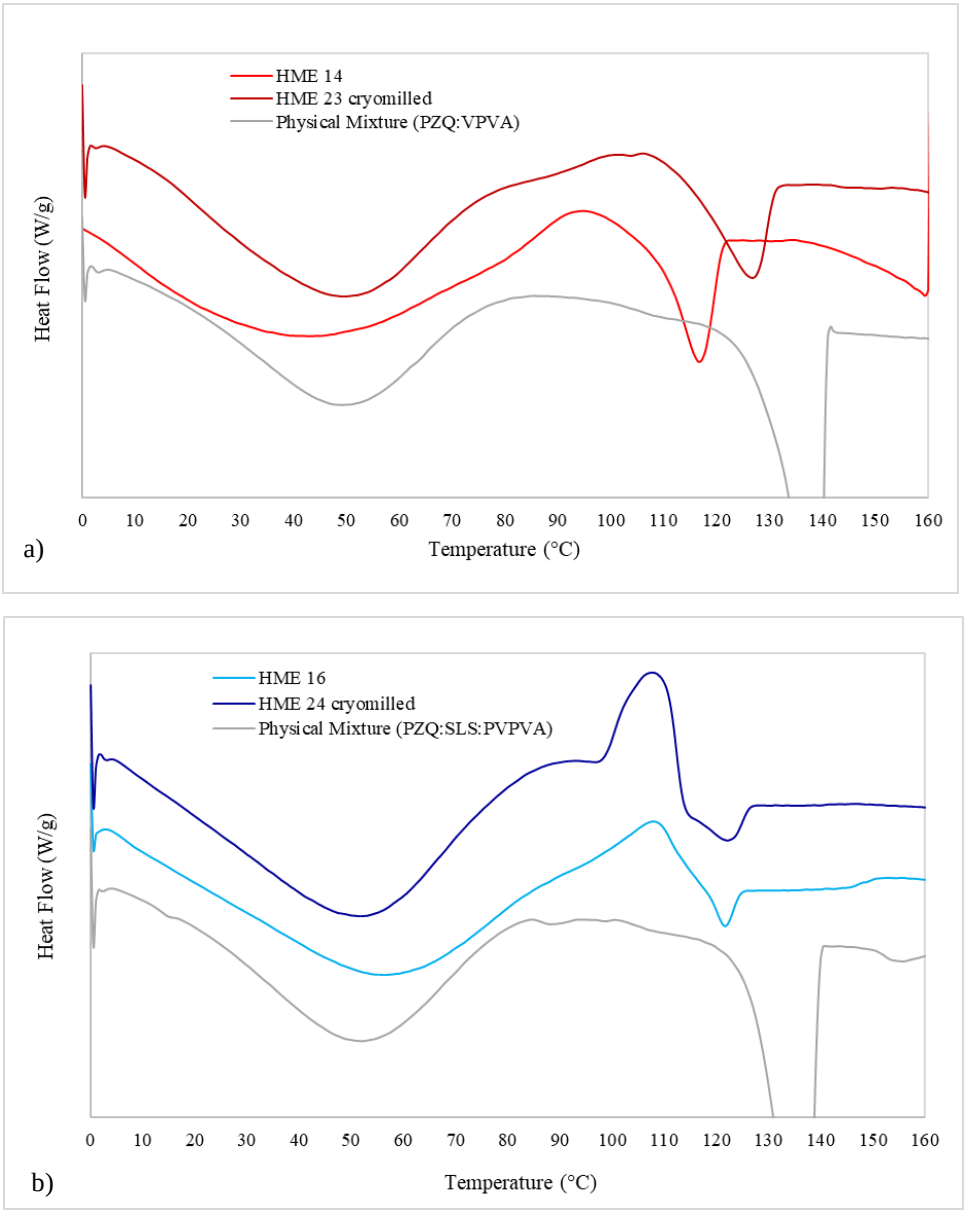


Figure 119. DSC curves of HME ternary extrudates and their respective physical mixtures. a) samples containing SPAN 20 surfactant (HME 14 and HME 23), and b) samples containing SLS surfactant (HME 16 and HME 24).

Table 49. Thermal characteristics of ternary HME samples (50 wt% PZQ).

| *Sample* | $Tm_{onset}$ *(°C)* | *Tpeak (°C)* | $\Delta H_m$ *(J/g)* | $T_g$ *(°C)* | *ΔCp J/g.°C* | *Observations* |
|---|---|---|---|---|---|---|
| PM (SPAN 20)* | 135.93 | 138.63 | 51.18 | 110.49 | 0.06 | Powder |
| HME 14 | 118.13 | 125.74 | 11.13 | 25.13 | 0.32 | Pellets |
| HME 16 | 117.92 | 121.57 | 2.165 | 13.18 | 0.34 | |
| PM (SLS) | 128.69 | 136.82 | 41.49 | 106.9 | 0.14 | Powder |
| HME 23 | 115.31 | 126.6 | 11.87 | 26.17 | 0.42 | Cryomilled |
| HME 24 | 115.91 | 122.2 | 2.435 | 13.80 | 0.35 | |

* PM (SPAN 20) corresponds to a mixture made without the surfactant (added directly to the extruder).

In comparison to the binary system (PZQ and PVPVA), the reduction of $T_g$ due to the presence of SLS or SPAN 20 was evidenced (Table 5). On the other hand, the cryomillling did not result in changes on $T_g$ for both HME ternary samples. In addition, samples with SPAN 20 presented lower $T_g$ than those formulated with SLS.

The other values of temperature in Table 50, corresponding to the endothermic signals in the DSC curves (Figure 119a and 119b), are probably related to the fusion of the API. The crystalline racemic PZQ used in this thesis has a characteristic melting point of $T_{onset}$ 138 ºC and $T_{peak}$139.4 ºC (presented in Chapter 3). The physical mixtures of both formulations also showed a corresponding racemic PZQ melting $T_{peak}$ around 137 ºC.

However, the values in Table 49 are lower (118°C for HME 14 and HME 16 and 115 °C for HME 23 and HME 24). The melting point of an API can be reduced in presence of a miscible polymer [336]. For PZQ, a lowering from 140 °C to 133 °C was already reported during hot-melt extrusion of PZQ (PZQ –33 wt%)with Eudragit EPO [118]. The lower $T_m$ found here could rather correspond to the melting of the form B of PZQ recently described and characterized by melting at 110 °C.

The melting temperatures (115 °C-118 °C) closer to the melting of the polymorph B (110 °C), the morphology of the thin filaments detected in the surface of samples presented in section (3.2.2) that was very similar to the morphology attributed to form B in the literature [10], let us suppose that the HME ternary samples presented here are characterized by an amorphous and a crystalline fraction (polymorph B?) which could be formed by recrystallization during or after hot-melt extrusion.

The low values of $T_g$ showed in Table 50 could perhaps explain the presence of crystallinity in the samples. Once freshly extruded, they were cooled to the room temperature, that is close (or higher) their $T_g$. As we already know, a binary mixture with PVPVA and 50 wt% PZQ is supersaturated in PZQ and kinetically (and not thermodynamically) stable at room conditions. The lowering of $T_g$ with the presence of 5 wt% of surfactant can contribute to their physical evolution to more stable (crystalline) API forms.

### 3.2.4 Powder X-ray diffraction (PXRD)

As mentioned earlier, PXRD analyses were performed only for cryomilled HME samples, for two main reasons: the final material of interest is in the powder form. The PXRD analysis of pellets would be carried out with grinding (manual with mortar and pistil), adding another variable (potential amorphization on surface) that could influence the data interpretation.

The PXRD diffractograms are shown in Figure 1200. The differences between the diffractograms of HME ternary extrudates (predominantly amorphous) and their respective physical mixtures (crystalline materials) are clear. However, small crystalline peaks are also observed in the broad halo for the sample HME 24 cryomilled. Some of these diffraction signals (around 32°) have also been observed in HME placebo extrudates containing only SLS and PVPVA presented in the Sub-chapter 5.2. These diffraction signals might be related to the structural organization of the excipients during the extrusion process.

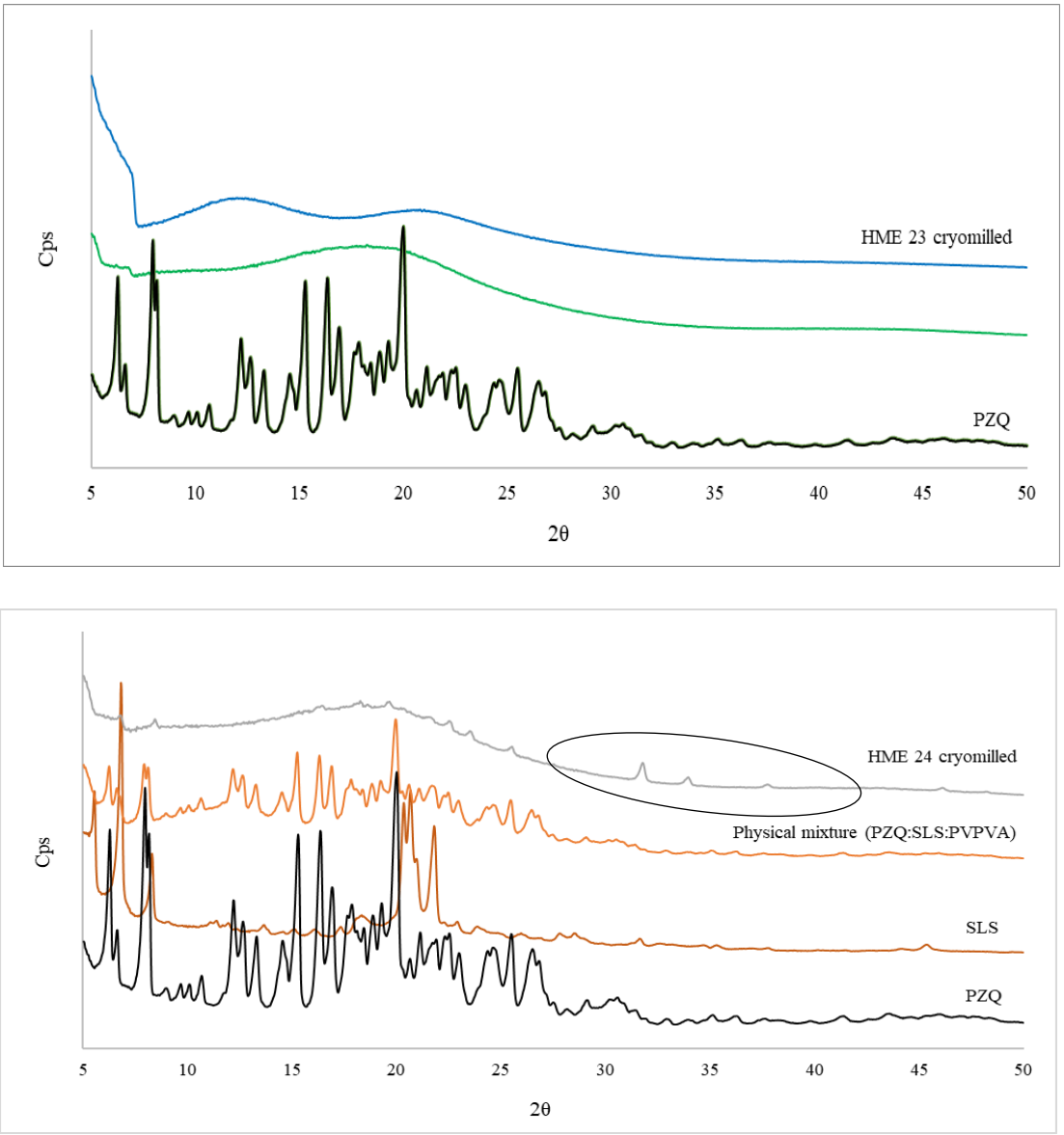


Figure 120. PXRD diffractograms. a) raw materials (PZQ, SLS, and PVPVA), binary and ternary physical mixture (PZQ: PVPVA and PZQ: PVPVA: SLS), and extrudate HME 23 and HME 24 (PZQ:SPAN 20:PVPVA and PZQ:SLS:PVPVA) cryomilled.

No signs of crystallinity or residual crystallinity were detected on the X-ray diffraction pattern for HME ternary with SPAN 20, contrarily to that found on DSC thermograms.

A published work [337] studying a HME binary amorphous solid dispersion with another API (felodipine, 30 wt%) and the same polymer used here (PVPVA) can be mentioned as example of similar findings. The x-ray diffraction pattern revealed an amorphous characteristic for the sample, while DSC analysis showed an endothermic event in the API melting region, demonstrating the presence of an API crystalline form

in the solid dispersion. In fact, by transmission electron microscopy, the crystalline phase was found to correspond to felodipine nanocrystals. The analysis of PXDR with powders was considered limiting to demonstrate the difference between a completely amorphous material and an amorphous material with small and fine crystals (<10 nm). The imitation of PXRD technique as exemplified by this example might explain the differences between DSC and PXRD results.

### 3.2.5 Water solubility

The solubility experiments in water were conducted according to the method described in Chapter 3 (item 3.1.8).

However, the physical mixture corresponding to the HME 23 pellets, using a liquid surfactant (SPAN 20), was not produced due to the technical difficulties in the preparation of a homogeneous mixture. Only the physical mixture of HME 24 pellets was thus used in these experiments.

Figure 121 regroups all values of PZQ concentration measured in water at 37°C at 1h, 24h and 48h for HME 23 and HM24 ternary extrudate samples in the form of pellets.

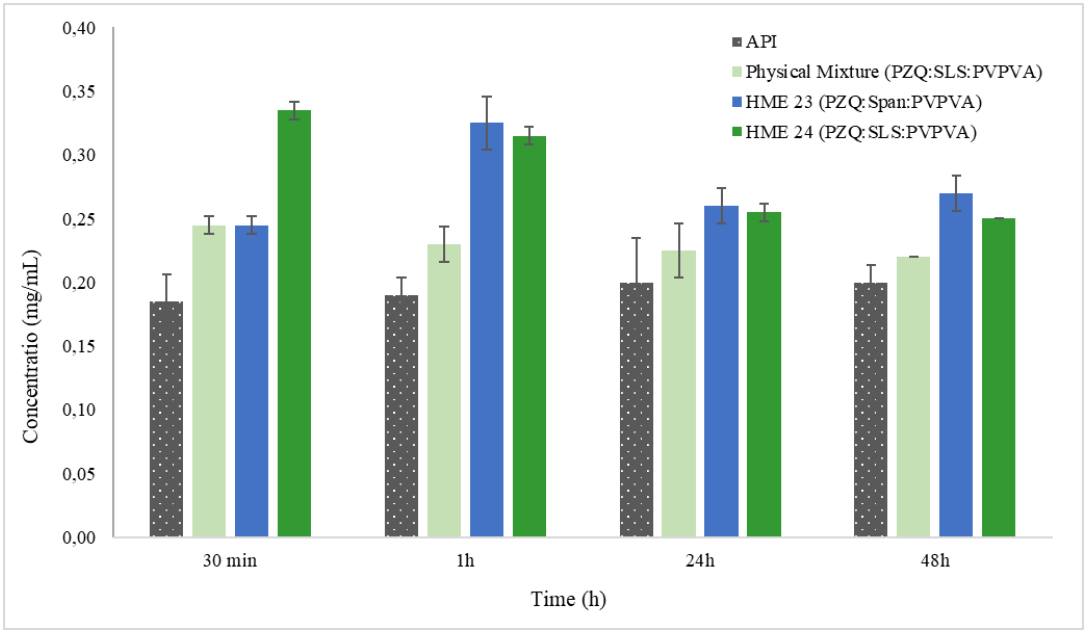


Figure 121. Variation of the PZQ concentration in water at 37°C from different samples: HME 23 and HME 24 pellets, its respective physical mixture and raw PZQ.

*For HME 24 pellets (ternary system 50% PZQ and with SLS as surfactant):*

- The highest PZQ concentration (0.335 mg/mL) was reached in 30 min, decaying over time up to 0.255 mg/mL at 24h, after what it remained practically constant up to the end of the experiment (0.250 mg/mL at 48h).
- The corresponding physical mixtures PM also increased the water solubility of PZQ to a constant value of approximately 0.233 mg/mL, that remained lesser than the PZQ concentration reached with the corresponding HME ternary pellets.

*For HME 23 pellets (ternary system 50% PZQ with Span 20 as surfactant):*

- The highest PZQ concentration was reached in 60 min (0.325 mg/mL), decaying later up to the same level of concentration maintained with HME 24 pellets.

Comparing HME 23 and HM24 pellets regarding their capacity to improve the apparent solubility of PZQ in water, HME24 pellets can lead faster to an equivalent supersaturation in water.

Figure 122 regroups the apparent solubility data obtained with the two ternary systems which were just presented, and the data obtained with the binary system (without surfactant) presented before in the Sub-chapter 5.1. All samples have the same physical characteristics (pellets) and similar dimensions (1mm in size), as illustrated in Figure 123 for HME 23.

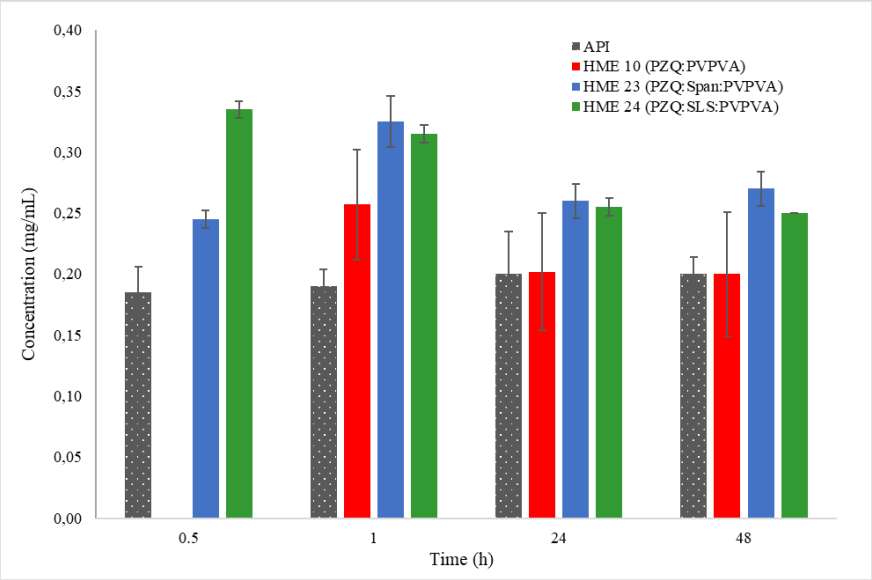


Figure 122. Comparison between binary (HME 10) and ternary systems (HME 23, HME 24). Raw PZQ is the reference.

Figure 123. Optical microscopy for HME 23 (before mill) a) part of an extrudate and pellets, and b) pellets. Both microphotographs have a scale that refers to 2 mm.

Although the PZQ concentration in water was not measured at 30 min for the binary system, at 60 min the concentration reached with the binary was lesser than those reached with both ternary ones. Until the end of the experiment the beneficial effect of the ternary systems was observed.

### 3.2.6 Dissolution profile

Although the main interest is the extruded powder material, the respective pellets were also evaluated for the dissolution profile.

Figure 124 displays the dissolution curves obtained for all ternary systems (HME 23 and HME 24), as pellets and powder (cryomilled). An unexpected very slow dissolution was demonstrated in all cases.

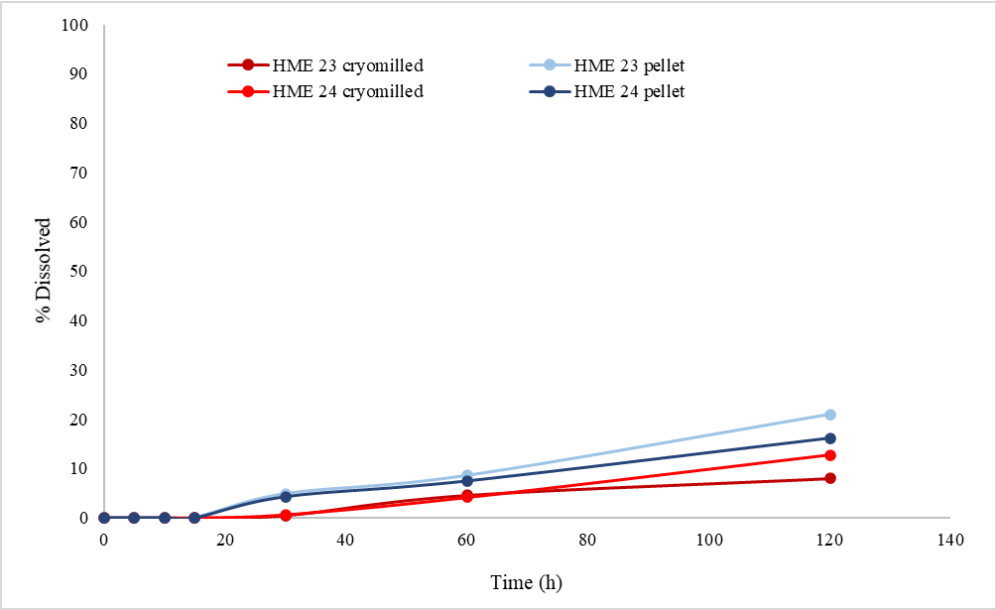


Figure 124. Dissolution curves for all HME ternary systems (HME23 and HME 24), as pellets and powder (cryomilled). Experiments conducted in 37 ºC ± 0.5 ºC and HCl 0.1N with 0.2% of SLS in the medium.

The dissolution test was thus considered unsuccessful owing to a lack of adequate dispersion of the pellets and powders from the capsules that resulted in the formation of insoluble agglomerates remaining undissolved until the end of the experiment. They can be visualized in Figure 125. Although the cryomilling process was not efficient (also in terms of operation), additional particle size distribution analyses could be performed to better understand the phenomenon visualized in this dissolution test.


Figure 125. Visual aspects of HME 23 and HME 24 residual after dissolution test.

## 4. CONCLUSIONS

After the generation of binary systems constituted by PZQ and PVPVA with 50 wt% PZQ (Sub-chapter 5.1), the feasibility to generate ternary systems (adding a surfactant to the binary) was also demonstrated in the large model of extruder used in this thesis, the Pharma 16. The use of two different surfactants was validate in the process, one solid (SLS) and directly incorporated into the solid mixture of PZQ and PVPVA before feeding to the extruder, the other liquid (span 20) added to the molten mixture during extrusion. For the later, The HME operating conditions were modified to allow the continuous manufacturing with the addition of the liquid surfactant.

Two new samples were generated (HME 23 and HME 24), which were used as pellets and as powder (obtained from cryomilling of the pellets).

According to DRX and DSC analysis, these ternary samples were predominantly amorphous, however all they presented some crystallinity.

Their capability to improve the apparent PZQ water solubility was demonstrated, representing an increase of 71 % for HME 23 (SPAN 20) and 66 % for HME 24 (SLS) in the first hour when compared to the API alone at the same time. HME 24 reached higher value faster (81% increase in 30 min when compared to the API).

Finally, the better capacity of the ternary systems to increase the apparent solubility of PZQ in water could be demonstrated in comparison to that of the binary system (without surfactant in the solid product).

Although the apparent solubility has increased with the use of the surfactant, the decrease in $T_g$ might be one of the major causes contributing to a partial solid state transformation of the amorphous API (recrystallisation to form B?) in the solid dispersions. Aiming to improve the physical stability of the ternary systems, a reformulation was proposed concerning a reduction of the PZQ load in these systems. New samples were produced with the following composition: 35 wt% PZQ, 45 wt% PVPVA and 5 wt% surfactant (SPAN 20 or SLS). They are the subject of the next Sub-chapter 5.4.

# SUB-CHAPTER 5.4 - PRAZIQUANTEL AMORPHOUS SOLID DISPERSIONS MANUFACTURED BY HME - TERNARY SYSTEM (35 wt% PZQ) - PHARMA 16 EXTRUDER

## 1. INTRODUCTION

One of the main objectives of this thesis is to develop an amorphous solid dispersion of praziquantel with a high drug concentration to be used in the formulation of paediatric medicines. For children, the dosage is adjustable to the child body weight by administering in sets of 150 mg. As already explained, an ASD containing 50 wt% PZQ could be adequate for designing a PZQ dose close to 150 mg to children. This load was the target in the PZQ-ASD formulations studied so far.

As outlined earlier in the Chapter 4, a phase diagram was constructed from experimental data related to the solubility of PZQ in the polymer of our choice, PVPVA, and on another side, from the glass transition temperature variation of the binary mixtures as a function of composition and temperature. From this pre-formulation tool, it was evident that the challenge to produce an amorphous solid dispersion with acceptable physical stability was substantial. Even if the feasibility for producing binary and ternary solid dispersions containing 50 wt% of PZQ by HME process was proved by the studies presented until this point of the manuscript, it appeared interesting to investigate a new formulation with a lower PZQ load (35 wt%) in the ternary configuration (PZQ-PVPVA-surfactant), aiming to create a more favourable condition to preserve its physical stability.

This Sub-chapter is focused on the development of a new formulation of ASD. The composition was fixed at 35 wt% PZQ, 60 wt% PVPVA and 5 wt% Surfactant (SLS or SPAN 20).

Two formulations (differencing on the type of surfactant used) were produced in duplicate (on different days). As a powdered material is the preferential physical form for a subsequent development of a pharmaceutical product from PZQ-ASD, samples of the two formulations were ground, this time not by cryomilling as performed before (chap 5.3) but by using a milling process industrially applicable.

The new HME samples generated were characterized as the last ones presented in Chapter 5.3. However, a new evaluation method was introduced regarding the taste masking capacity of the formulations. For this purpose, a collaboration has been established with a laboratory in England (School of Pharmacy - SoP, UCL - University College London) where these experiments were performed. The method used was developed by this laboratory. The principle is to simulate an oral cavity with an evaluation of API release in the function of time.

The different activities of this part of the thesis are presented in the Sub-chapter following the schematic procedure shown in Figure 126.

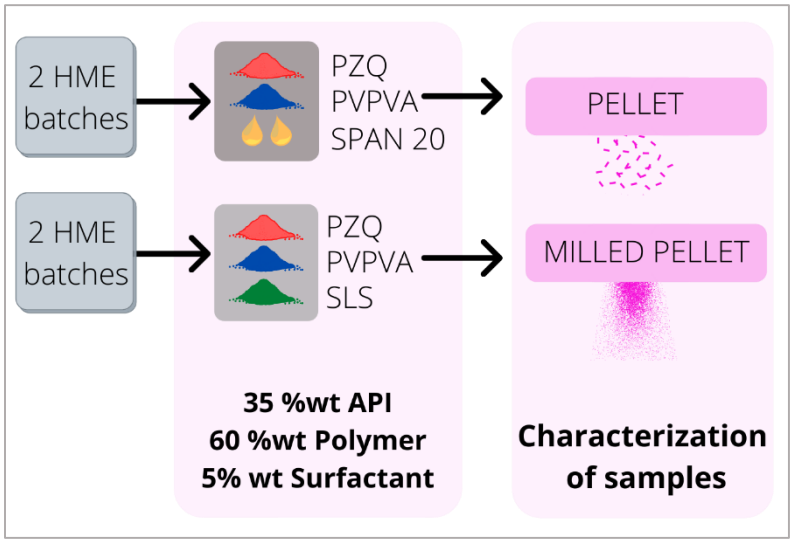


Figure 126. Schematic procedure of chapter 5.4. Source: Author.

## 2. METHODS

### 2.1 Ternary ASD systems prepared by HME (35 wt% PZQ)

Pharma 16 (Thermo Fisher), the twin-screw extruder used in a previous investigation (binary system, see Chapter 5.1), was used in the study presented here. This equipment was described earlier in chap 5.1 (item 2.1).

The composition of the new formulations studied here are given in Table 51.

Table 50. Ternary ASD composition.

| ***Sample code*** | ***Composition (wt%)*** | | | |
|---|---|---|---|---|
| | ***PZQ*** | ***PVPVA*** | ***SLS*** | ***SPAN 20*** |
| HME 25* and HME 27 | 35 | 60 | 5 | - |
| HME 26* and HME 28 | | | - | 5 |

*Produced in replicate (n=2), at different periods

The HME process parameters used to produce the samples coded HME 25 an HME 26 are grouped in Table 51.

Table 51. HME process parameters for production of ternary systems with 35 wt% PZQ.

| ***Samples*** | ***Extrusion parameters*** | | | | |
|---|---|---|---|---|---|
| | ***Powder Rate Flow (kg/h)*** | ***Screw speed (rpm)*** | ***Liquid Rate Flow (mL/min)*** | ***Temperature profile*** | ***Screw profile*** |
| HME 25 and HME 27 | 0.25 | 300 | 0,23 | (Z1) 50°, 70°,100°, 140°, 140°,140°, 110° and 100° (die) | Zone 4 and 6 **with** RE** |
| HME 26 and HME 28 | 0.3 | 300 | NA* | (Z1) 50°, 100°,140°, 180°, 180°,180°, 130° and 105° (die) | |

* NA = not aplicable

** RE = reverse element

Regarding the surfactant addition, the same methodology developed in Chapter 5.3 (item 2.1.1) to produce ternary systems with 50 wt% PZQ was also applied. In brief, the solid surfactant (SLS) was directly incorporated into the solid mixture of PZQ and

PVPVA before feeding to the extruder, while the other surfactant, which is a liquid (SPAN 20), was added to the molten mixture during extrusion.

## 2.2 Generation of a placebo formulation (without PZQ)

To get more information about the thermal properties of a homogeneous (amorphous) mixture between PVPVA and the surfactants, we have decided to prepare placebo samples, whose compositions are shown in Table 52. The same HME process conditions used to produce the samples are given in Table 53. They are essentially identical to those used in the generation of ASD ternary systems with PZQ, with some adjustments.

Table 52. Placebo formulations and respective compositions.

| ***Samples*** | ***Composition (wt%)*** | | | |
|---|---|---|---|---|
| | ***PZQ*** | ***PVPVA*** | ***SLS*** | ***SPAN 20*** |
| Placebo HME 25 | - | 95 | 5 | - |
| Placebo HME 26 | | | - | 5 |

Table 53. Extrusion parameters for production of placebo HME formulations.

| ***Formulation*** | ***Flow rate - Peristaltic pump (mL/min)*** | ***Flow Rate powder/mixture (kg/h)*** | ***Screw speed*** | ***Temperatur profile*** | ***Visual aspect*** |
|---|---|---|---|---|---|
| PVPVA and SPAN 20 | 0.48 | 0.27 | 300 | (Z1) 30°, 50°,110°, 130°, 150°,150°, 150° and 150° (die) |  |
| PVPVA and SLS | NA | 0.3 | 300 | (Z1) 50°, 100°,140°, 180°, 180°,180°, 130° and 105° (die) |  |

* NA = not applicable

## 2.3 Extrudate milling process

The powder form can be the most appropriate for subsequent steps of use in pharmaceutical paediatric formulations. For this reason, the HME extrudates are produced and characterized in both forms: as pellets, and as powders (after milling).

This procedure is commonly adopted for HME materials to reduce the largest pellets and, subsequently, obtain greater homogeneity in the granulometry of the powder [338].

In the previous study with HME ASD ternary systems with 50 wt% PZQ, powder was produced from a cryomilling of pellets. It was performed in a bench laboratory equipment. In this point of the work, another milling process, industrially applicable, was used. The mill used is a Quadro® Comil H5 High Energy Mill (Figure 127). The equipment operates by impeller rotates and it forces the material through the holes in the screen, reducing the size of the particles. The important step is the choice of the size of the role screen.

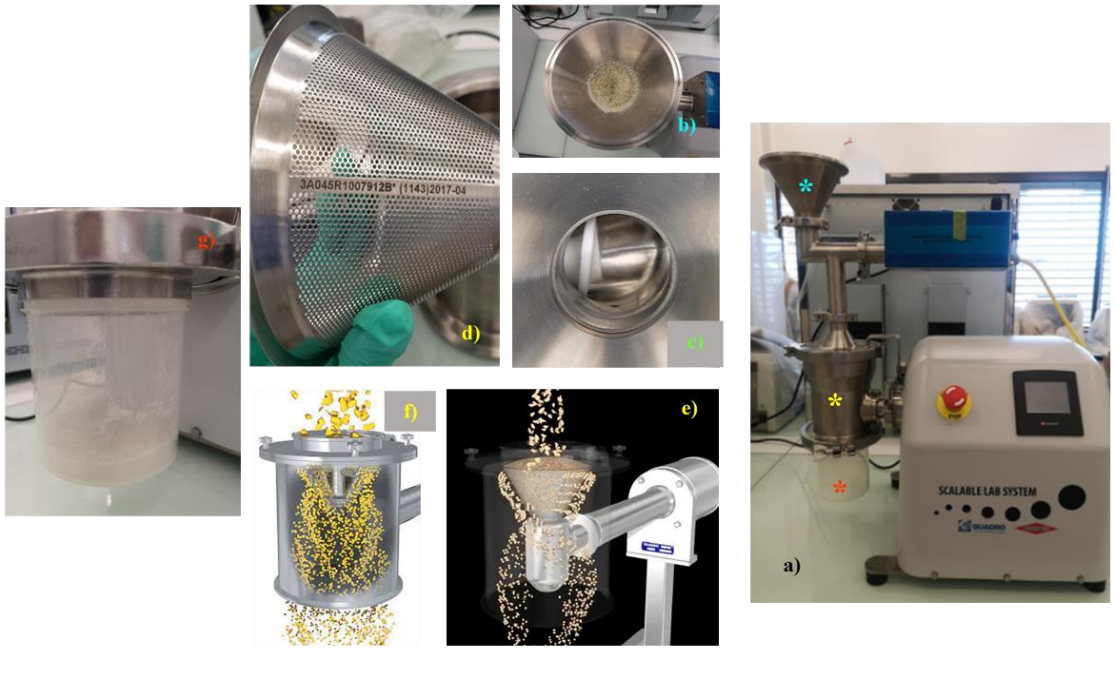


Figure 127. a) General view of Quadro® Comill with HE High energy Mill, b) material feed, c) feed screw, d) grinder, e, and f) different view of particle grinding, and g) collector. Source: Author and from [349].

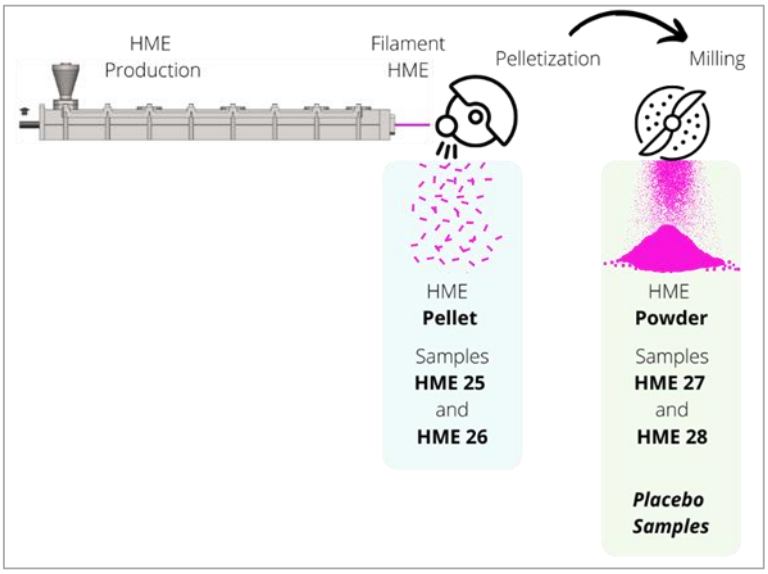


Figure 128. Schematic view of the process to obtain pellet shape and powder for the samples produced in this step. Source: Author.

## 2.4 Characterization of ASDs

As described in the previous Chapter 5.3, solid-state characterizations of ternary ASDs with 35 wt% PZQ were performed by DSC, XRD, SEM, and optical microscopy. The same methods used previously to evaluate water solubility and drug content were applied. Additionally, the extruded material was evaluated for taste masking using a method described by Keeley et al. [80].

The dissolution method used to evaluate the ASD ternary with higher drug load (50 wt%) in Chapter 5.3 was modified here, because it was found unsatisfactory for dissolution kinetics evaluation.

The main modifications were:

- Evaluation of the dissolution medium composition with the remotion of the surfactant.

It should be remembered that the pharmacopeial method [297] contain 0.2 wt% of SLS.

- Addition of the sample (power or pellet) directly into the dissolution vessel.

The previous studies have been carried out with the samples into a capsule. This method caused an incomplete dissolution of the extrudate by retaining the sample and forming a unique mass.

Regardless of these changes, the procedure of collecting samples, HPLC, calibration curve, and the mass amount (equivalent to 150 mg of PZQ) were maintained.

### 2.4.1 In vitro taste masking by buccal dissolution evaluation

Taste masking prediction of the ternary systems produced by HME with 35 wt% PZQ were analysed by an in vitro method using a system consisting of a magnetic stirrer and heating monitoring, a peristaltic pump and the oral dissolution column (Figure 129) [80].

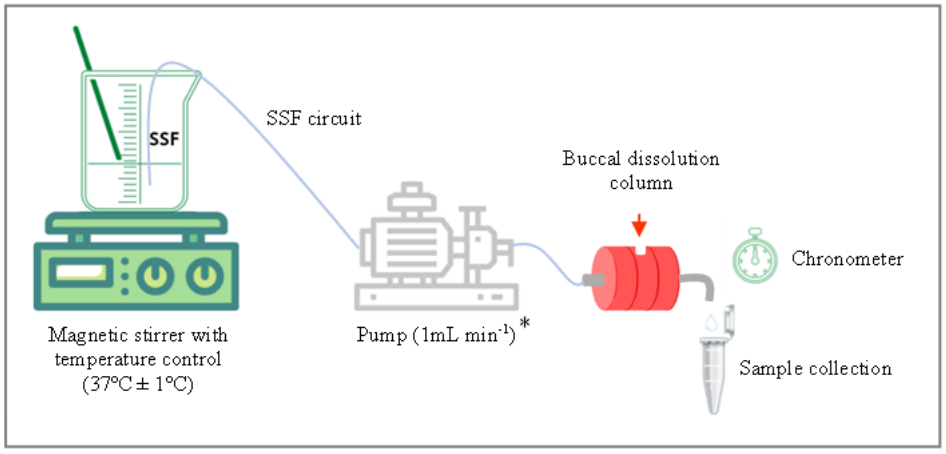


Figure 129. Flow diagram representing the biorelevant buccal dissolution test to evaluate taste masking. (*calculated internal volume of the column). Source: Author.

The simulated salivary fluid (SSF) (Table 54) [339] was kept in agitation and constant temperature of 37 °C ± 1 ºC and pumped to the buccal dissolution column using a peristaltic pump at the rate of 1 mL.min $^{-1}$.

Table 54. Composition of SSF [339].

| ***Composition of SSF*** | |
|---|---|
| ***Compound*** | ***Concentration g/L*** |
| Sodium chloride | 8.00 |
| Potassium phosphate monobasic | 0.19 |
| Sodium phosphate dibasic | 2.38 |
| pH 6.8 | |

The sample (precisely weighed to give 150 mg PZQ) was added to the centre and top of the column. The other two adjacent parts are threaded. A system composed of wire mesh discs was placed either side of the column for particles retention. After inserting the material to be analyse in the column lumen (where the medium SSF constantly flows at 1 mL.min$^{-1}$), sampling was taken at 60, 120, 180, 240, 300, 360, 420, 480, 540 and 600 seconds and filtered through a 0.22 µm membrane (cellulose acetate). The final solution was immediately analyzed by HPLC (Agilent Technologies 1200 series) with an ultraviolet (UV) detector a column Kinetex 5 µm C18 100 Å (150×4.60 mm). The mobile phase was comprised of methanol and water (60:40 V/V), the flow rate was 1.5 mL/min, injection volume was 10 µL and absorbance readings were conducted at fixed wavelength of 210 nm. The HPLC method was the sample described to USP for PZQ [53]. Quantification was carried out using a fresh stock solution prepared each time before

starting the analysis. PZQ standard solution was prepared with the same method described for dissolution test for PZQ tablets by USP [297], with adaptation (change of the dissolution medium). For this test, SSF was used. A calibration curve was prepared using 9 points in the range 0.01 mg/mL to 1 mg/mL. Each point on the calibration curve was prepared in duplicate.

## 3. RESULTS

### 3.1 Characterization of ternary ASD system produced by HME (35 wt% PZQ)

#### 3.1.1 PZQ dosage in the HME extrudates

The drug content in the HME extrudates and respective physical mixtures are given in Table 55. They are close to the theoretical values, confirming that no drug loss occurred during the extrusion process.

Table 55. PZQ content

| ***Samples*** | ***Theoretical drug content (wt%)*** | ***Measured drug content (wt %)*** |
|---|---|---|
| PM - PVPVA/SLS/PZQ | 35 | 34.35 ± 3.13 |
| PM - PVPVA/SPAN/PZQ | 35 | 35.15 ± 2.51 |
| HME 28 | 35 | 34.84 ± 1.01 |
| HME 27 | 35 | 33.25 ± 1.75 |
| API | 100 | 100.58 ± 0.2 |

#### 3.1.2 Differential scanning calorimetry (DSC)

The DSC curves for the four new HME samples are shown in Figure 130.

Firstly, in all DSC curves, variations in the baseline are displayed up to approximately 100 °C. They are probably related to the loss of water from the samples.

The DSC curves for HME 25 (pellet) and HME 27 (powder) as well as those for HME 26 (pellet) and HME 28 (powder) did not show endothermic peak characteristic of the fusion of crystalline PZQ. However, for the latter, an exothermic variation in the

baseline between 112 and 114 ºC was observed (Figure 130b), that cannot yet be explained.

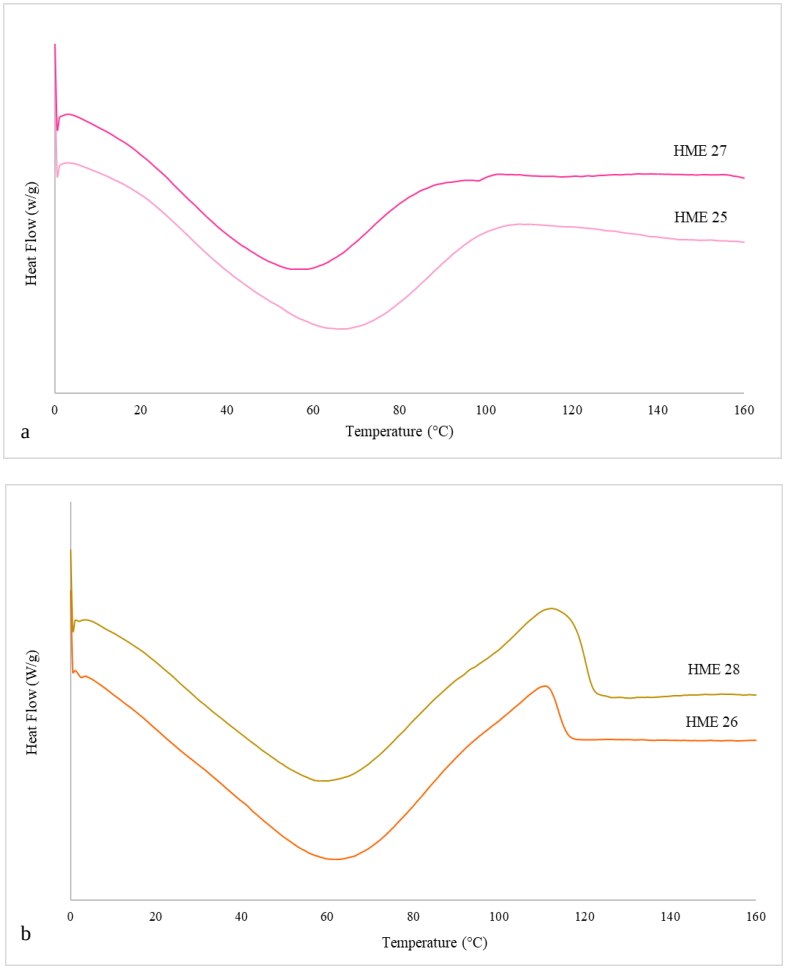


Figure 130. DSC curves for pellets a) HME 25 and HME 27 (with SPAN 20), and for milled powders b) HME 26 and HME 28 (with SLS).

Only the samples HME 27 and HME 28 could be analyzed by mDSC. The mDSC data are grouped on Table 56 with other ones taken from Chapter 5.3. A comparison between $T_g mix$ of equivalent ternary systems (same surfactant) and different API content is thus possible:

As expected, the decrease of PZQ load from 43% to 32% led to an increase in $T_g$ from 13.80 °C to 29.67 °C, in formulations with SPAN 20 as third component. The decrease of PZQ load from 51 % to 33.8 % had the same effect on $T_g$,which was 26.2 °C and 27.6 °C in formulations with SLS.

Table 56 DSC data for ternary HME samples with different PZQ content.

| *Sample* | $Tm_{onset}$ *(°C)* | $\Delta H_m$ *(J/g)* | $T_g$ *(°C)* | *ΔCp J/g.°C* | *Observations* | *Measured PZQ load (wt%)* |
|---|---|---|---|---|---|---|
| HME 17 | - | - | 49.34 | 0.40 | binary | NM |
| HME 23 | 117.92 | 2.165 | 13.18 | 0.34 | ternary with SPAN 20 | 51.74% ± 0.2 |
| HME 24 | 115.91 | 2.435 | 13.80 | 0.35 | ternary with SLS | 43.15% ± 0.2 |
| HME 27 | - | - | 29.67 | 0.27 | ternary with SPAN 20 | 34.84 ± 1.01 |
| HME 28 | - | - | 27.60 | 0.38 | ternary with SLS | 33.25 ± 1.75 |

NM = not measured

### 1.1.1 Powder X-ray diffraction (PXRD)

Similarly, as presented previously, XRD diffractograms are shown in Figure 131a and Figure 131b for HME 25 and HME 27 (with SPAN 20) in the first and HME 26 and HME 28 (with SLS) in the second. Still, the results obtained for placebos and raw crystalline materials are presented in both figures.

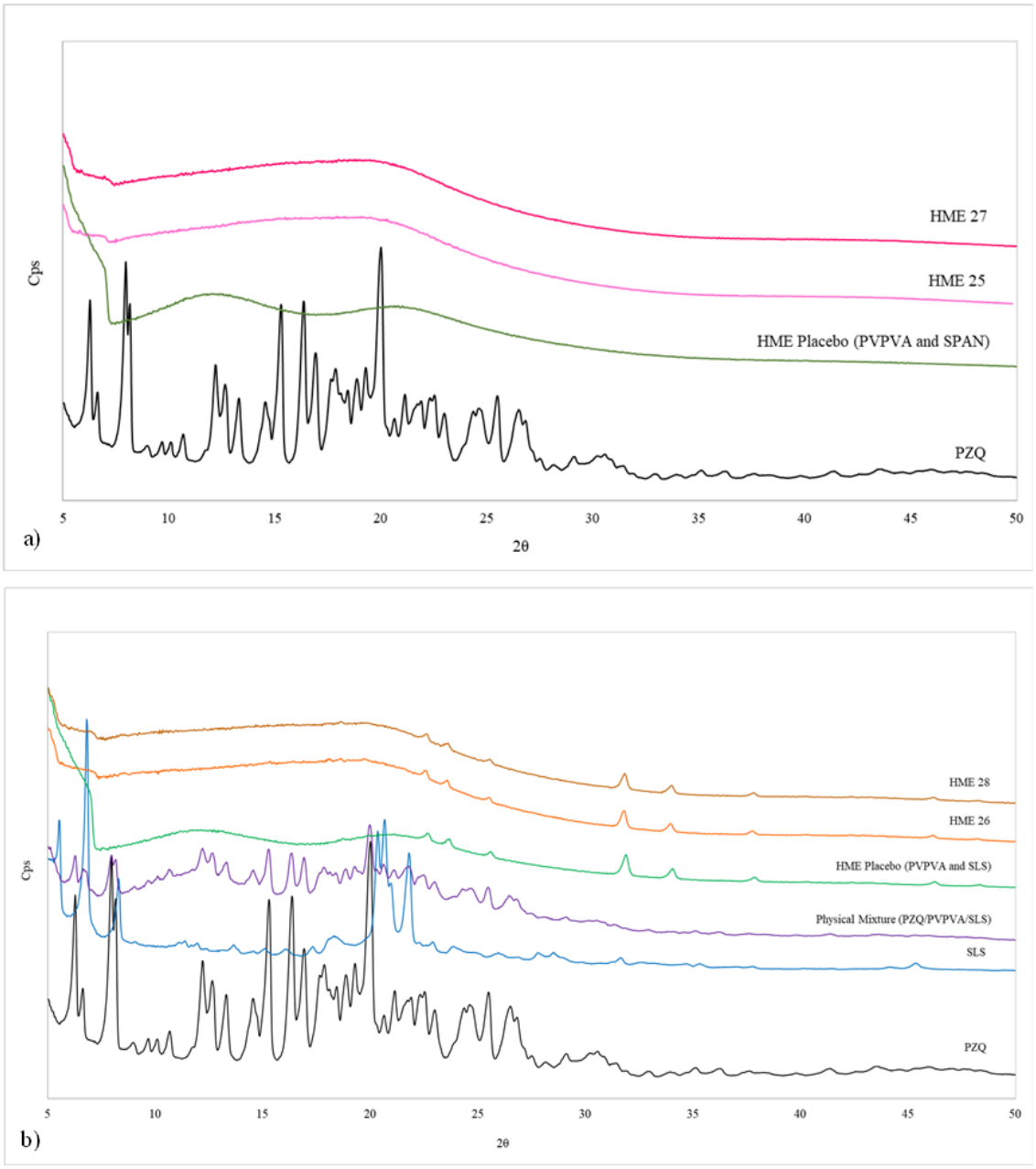


Figure 131. PXRD diffractograms for a) HME 25 and HME 27 (with SPAN 20) and the corresponding placebos, and b) HME 26 and HME 28 (with SLS), and corresponding physical mixture and placebo. Crystalline raw materials as given as references.

The PXRD results for batches HME 25 and HME27 (with SPAN 20) show a characteristic halo of amorphous material. Likewise, the respective placebo shows the same profile.

In contrast, the XRD diffraction patterns for batches HME 27 and HME 28 show small diffraction peaks. However, the same peaks are also observed in the absence of PZQ (in the placebos). Comparatively, they were not found in raw PZQ and SLS. These peaks were already observed in similar HME placebo extrudates presented in Chapter 5.2, as well as in HME 24 (cryomilled) discussed in Chapter 5.3. Considering that they were

not present in the raw materials (PVPVA and SLS) and have appeared in the HME extrudates, they might be related to some structural change on the excipients during the extrusion process.

### 1.1.2 Scanning Electron Microscopy (SEM)

As previously mentioned, HME 27 and 28 samples were ground after extrusion, while HME 25 and 26 samples were kept as pellets.

The images deal with pellets and powders (batches are duplicated). Thus, Figure 132 shows the images obtained for samples HME 25 and HME 26 as pellets, while Figure 133 shows the images of samples HME 27 and HME 28 as powders (after pellet grinding).

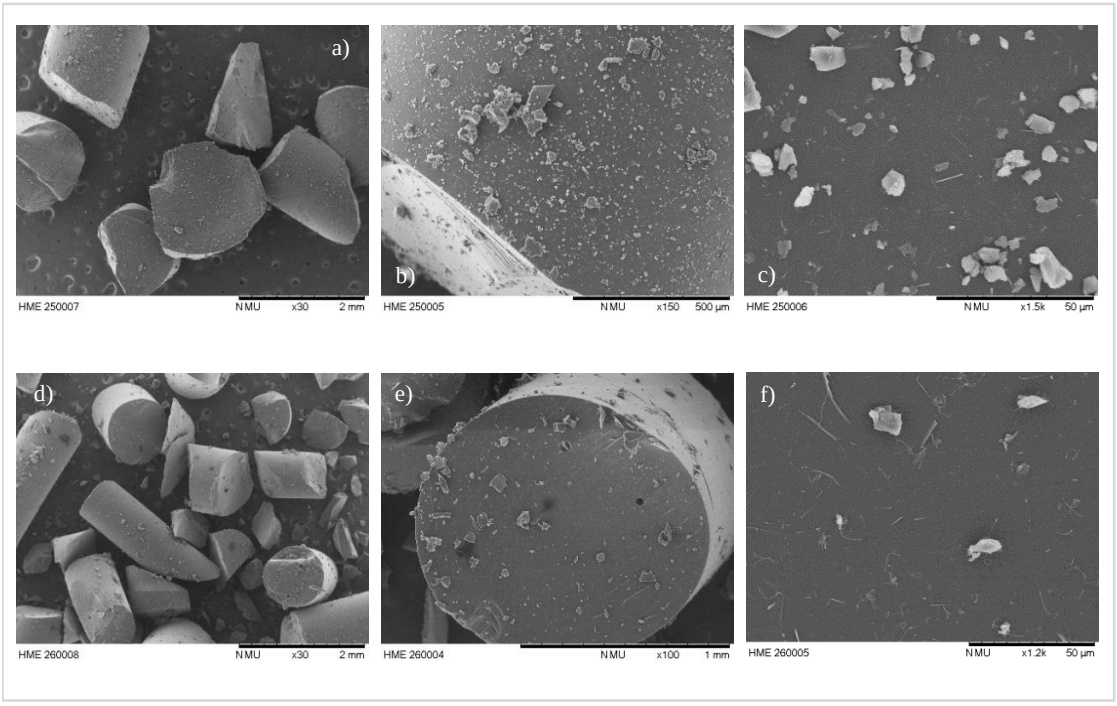


Figure 132. SEM images obtained for pellets: HME 25 (a-c) and HME 26 (d-f).

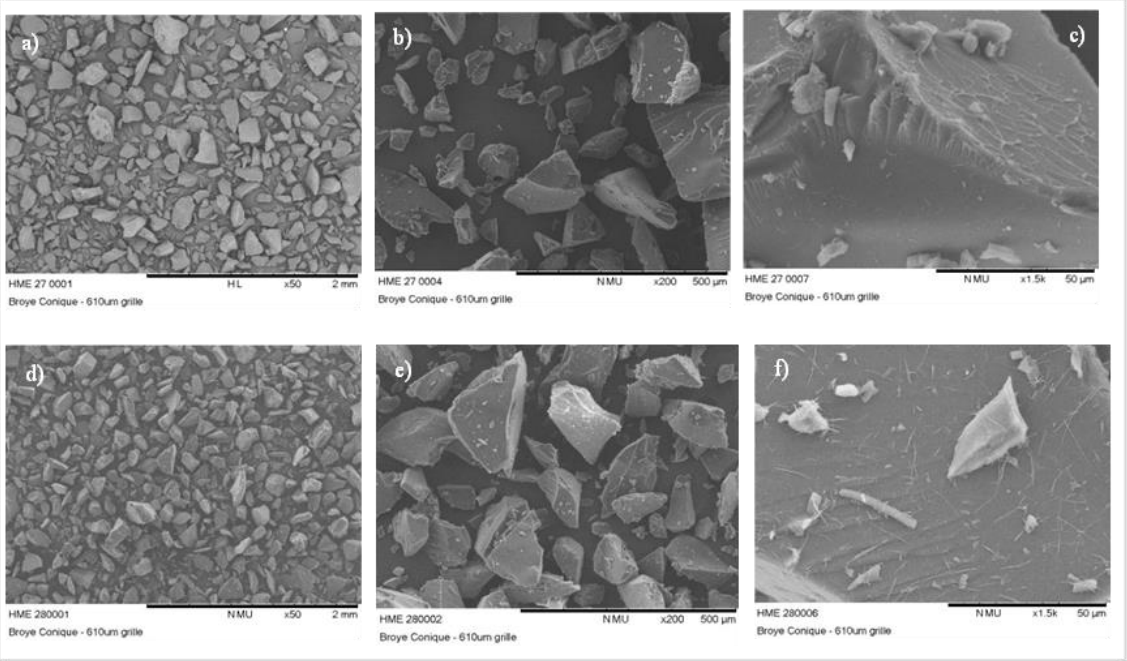


Figure 133. SEM images obtained for powders: HME 27 (a-c) and HME 28 (d-f).

Similarly, as previously presented, both pellets and primary particles generated by milling have very fine structures on the surface resembling to ‘needles’. They are found in very low amount on the surface of the samples. As discussed in Sub-chapter 5.3, similar morphology has been attributed to the polymorph B of praziquantel [10]. However, no signs of crystallinity were detected in the samples.

### 3.1.3 Optical Microscopy

This analysis was carried out in order to evaluate the physical aspect and transparency characteristics of the extrudates produced. The images obtained by optical microscopy, for both formulations in pellet shape, are shown in Figure 134.

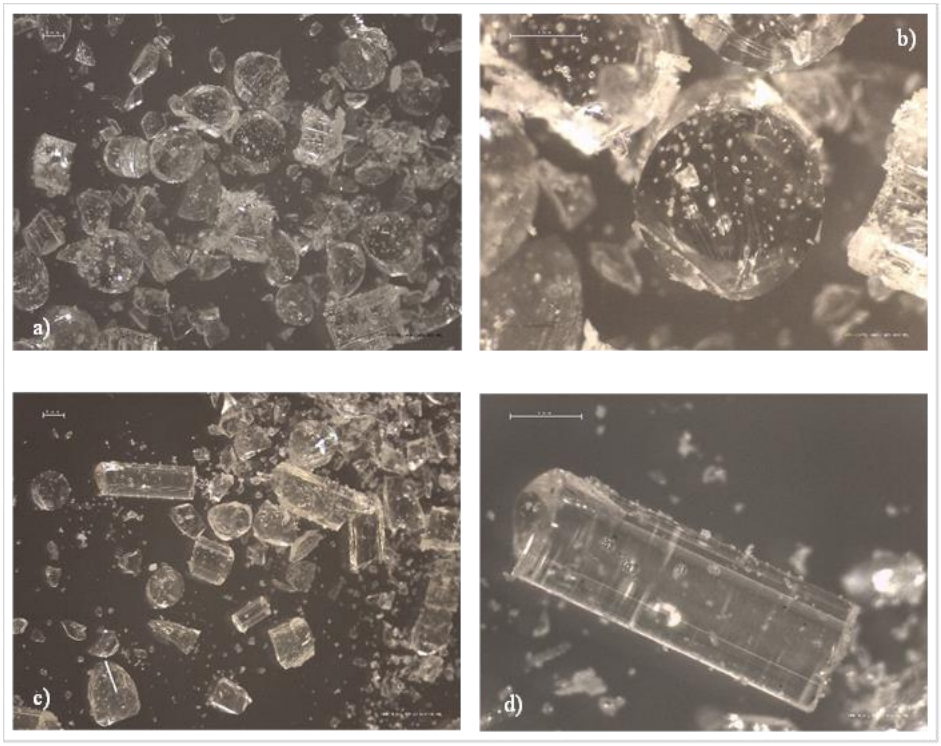


Figure 134. Optical microscopy images for HME 27 (a-b) and HME 28 (c-d). Scale: 2 mm (b and d) and 0.5 mm (a and c).

The images obtained by this technique are interesting because they allow visualizing in detail the physical aspect of the HME filaments and final shaped forms. Both formulations were translucent and included air bubbles are visible. A difference in colour between the two ternary systems is also evident (Figure 135). It can be due to the difference in composition between them (type of surfactant). Although yellow, the formulation containing SLS has a translucent aspect, characteristic of amorphous homogeneous mixture (to be confirmed by other techniques as DSC and PXRD analysis).

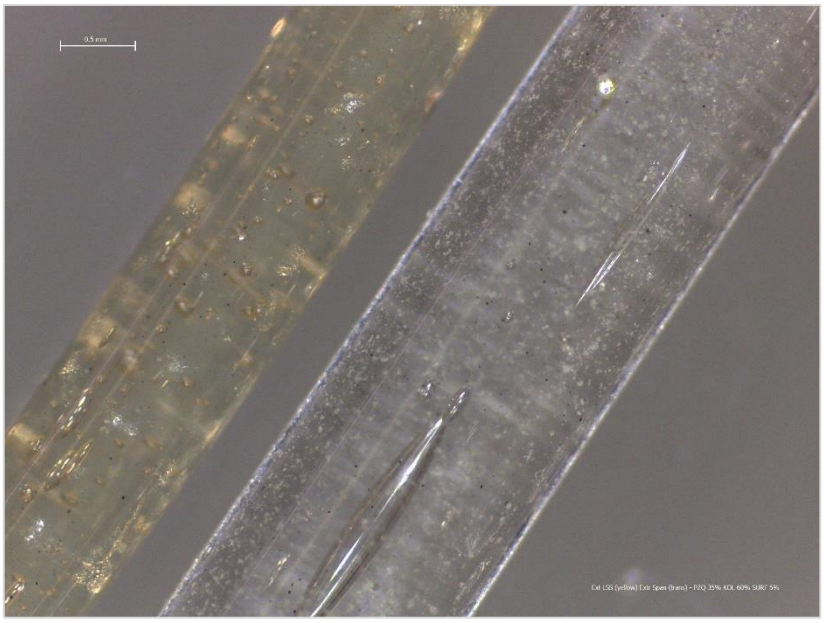

Figure 135. Optical microphotography showing the color difference between the two HME ternary studied (left side HME 28/26 (with SLS) and right side HME 25/27 (with SPAN). Scale 0.5 mm.

Similarly, the analysis of the ground HME ternary samples was carried out, and, although qualitatively, a micrometric size range of the particles was confirmed. The images are shown in Figure 136.

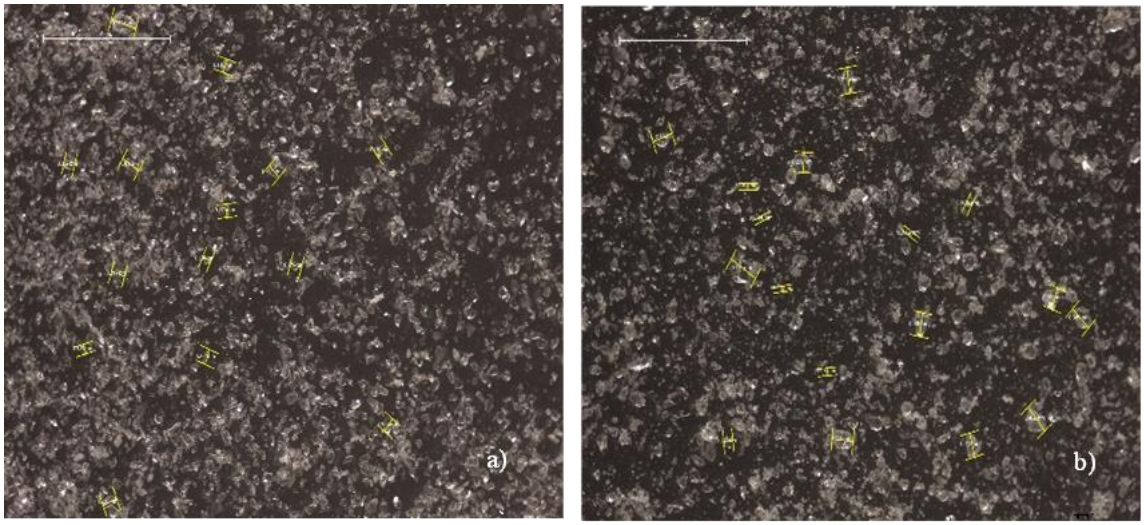


Figure 136. Optical microscopy images for a) HME 2, and b) and HME 28 milled. Scale: 2 mm.

Figure 137 displays the microphotographs for the HME placebo samples.

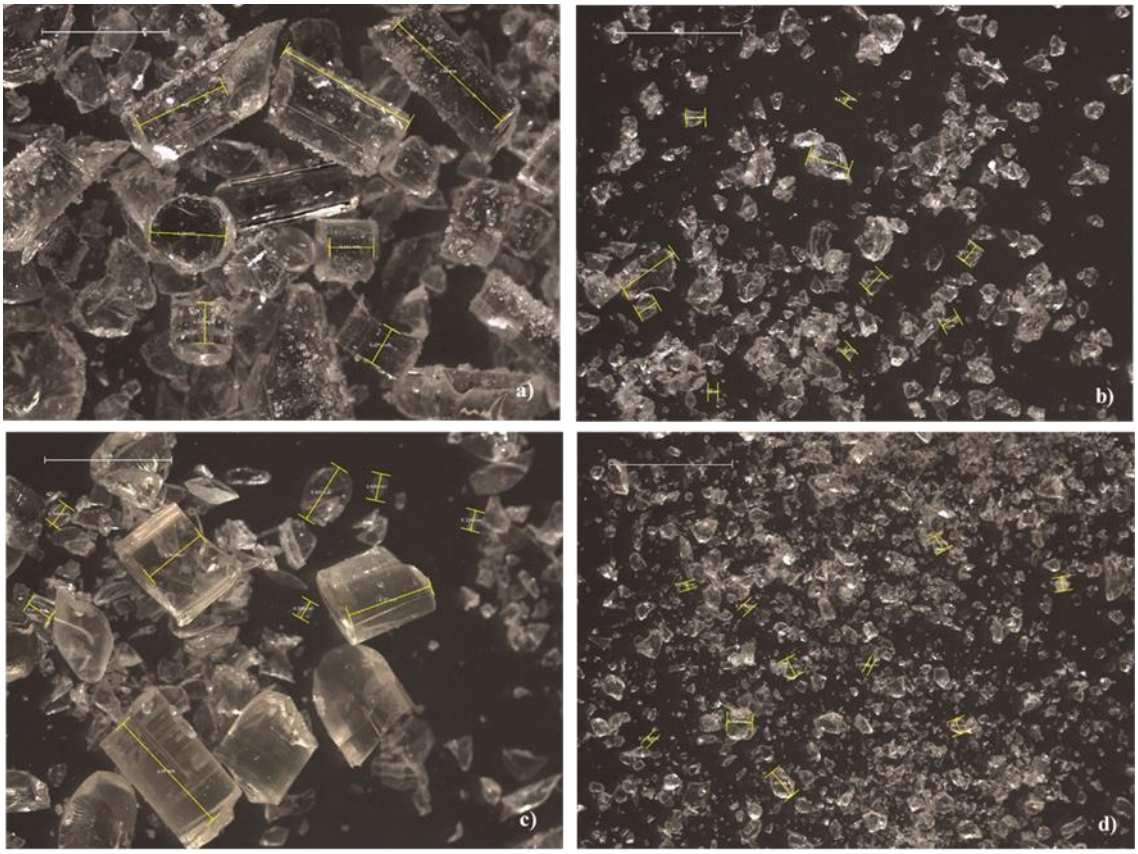


Figure 137. Photomicrographs for HME placebo samples. a and c) unmilled, HME SPAN 20 and HME SLS, respectively and, b and d) milled HME SPAN 20 and HME SLS, respectively. All images refer to a 2 mm scale.

Figure 138 represents the difference in colour shown for the placebo samples (HME 27 and HME 28). Both follow the same colour trend for extrudates containing PZQ (yellowish to HME 28 and transparent to HME 27).

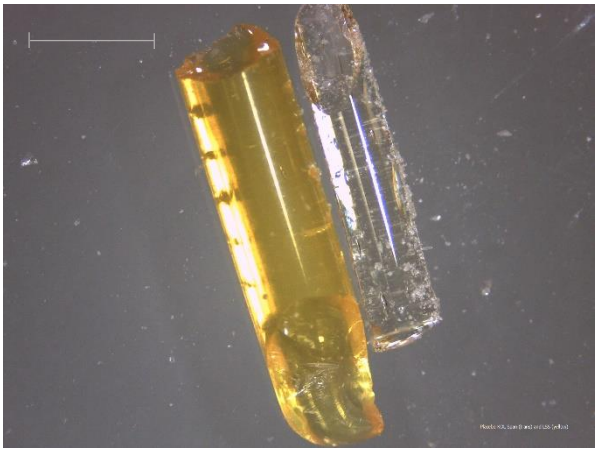

Figure 138. Optical microphotography showing the color difference between the two HME placebo (left and yellow – HME 28 and right and transparent HME 27). Scale 2 mm.

Unfortunately, it was not possible to perform particle size distribution analysis of the samples produced.

### 3.1.4 Water solubility

The water solubility experiments were performed for a sample of each formulation HME 27 (with SPAN 20) and HME 28 (with SLS). Although HME 27 and HME 28 samples referred as 'powders' were used, this experiment was carried out using them as pellets because the grinding process had not yet been carried out at this time of the study. The raw API was also analysed as reference.

The comparative variation of the PZQ concentration in water through time for both samples can be visualized in Figure 139.

*For HME 27 pellets (ternary system 50% PZQ, SPAN 20 as surfactant):*

- The highest PZQ concentration (0.343 mg/mL) was reached in 60 min, decaying over time up to 0.278 mg/mL at 24h, after what it is remained practically constant up to the end of the experiment (0.275 mg/mL at 48h, representing a 25% drop when compared to the value obtained in 1 hour).

*For HME 28 pellets (ternary system 50% PZQ, SLS as surfactant):*

- The highest PZQ concentration was reached also in 60 min (0.319 mg/mL), decaying after up to 0.252 mg/mL (26% less than the value obtained in one hour).

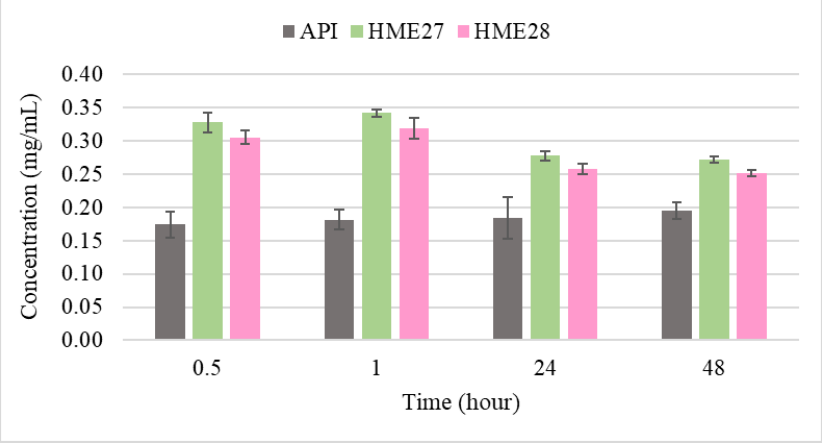


Figure 139. PZQ Concentration in water at 37°C released from different pellets: a) HME 27 and b) HME 28 Raw PZQ is the reference.

Figure 140 gives a comparative view on the capacity of the different ternary systems studied to improve the apparent solubility of PZQ in water at 37 °C. The parameters investigated were the composition (type of surfactant used as third component) and the PZQ load (two levels).

In summary, with ~35 wt% PZQ in the ternary systems, the two surfactants presented similar performance in terms of water solubility improvement), the best ones always in the first hour due to solubilization of a supersaturated solid state of the drug. With increased PZQ load (~50 wt%), the higher concentration was reached 30 min later when for 35 wt% it was reached in 30 min. Otherwise, the water solubility improvement is not the discriminating factor between them.

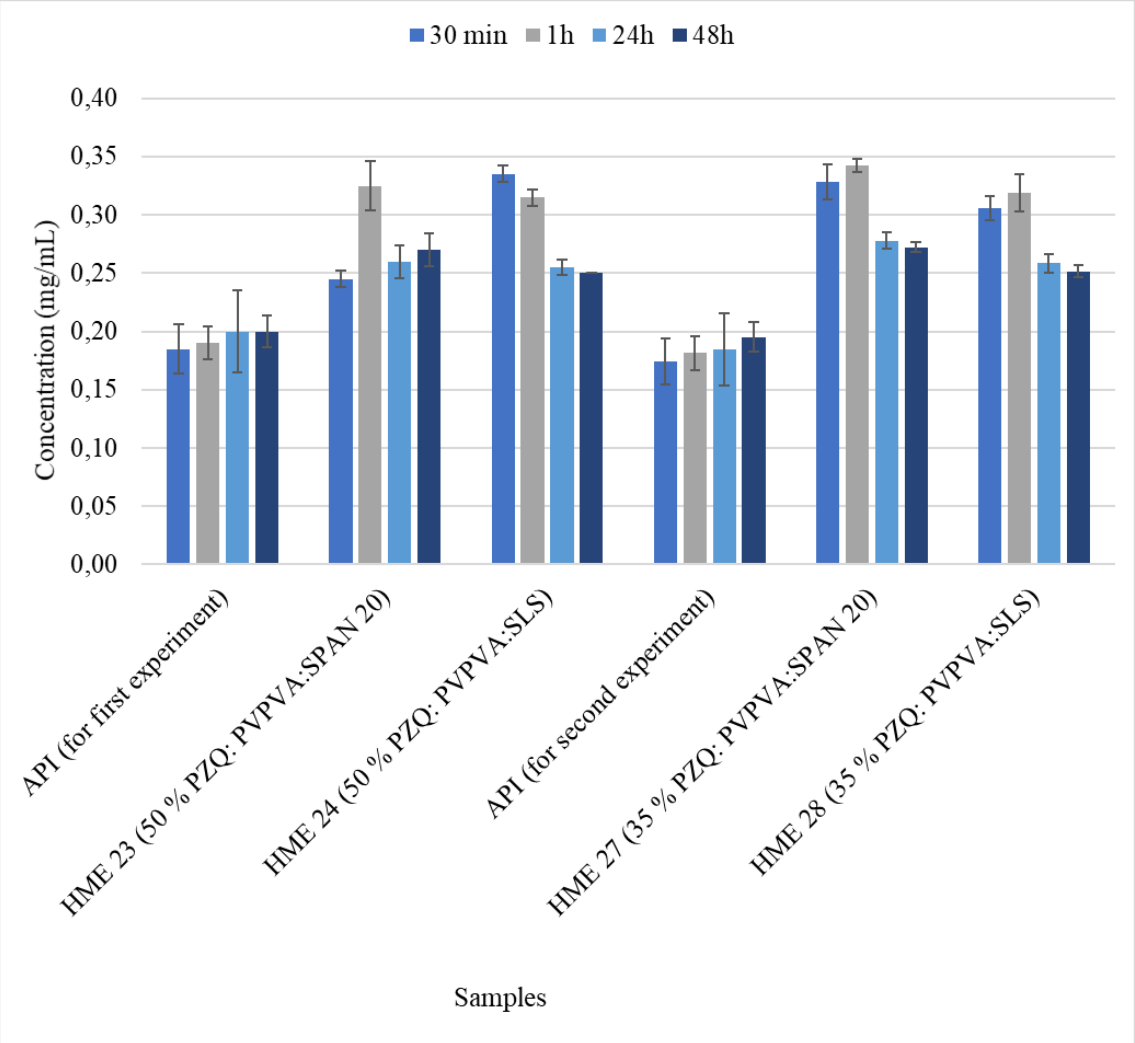


Figure 140. Comparative dynamic solubility study, grouping HME ternary samples developed in chapters 5.3 and 5.4. For 30 min: HME 27 (0.328 mg/mL), HME 28 (0.305 mg/mL), and API (0.185 mg/mL and 0.174 mg/mL). For 60 min: HME 23 (0.325 mg/mL), HME 24 (0.315 mg/mL, and API (0.190 mg/mL and 0.180 mg/mL).

Turning back to the analysis of the graphic represented in Figure 139, the decrease of the PZQ concentration in the medium corresponds well to the diminution of the spring effect of amorphous solids during dissolution. We have tried to analyse the solid phase remaining in the medium at the end of the experiment (48h) with the HME 27 sample. The final suspension was filtered and analysed by DSC. The DSC thermogram is represented in Figure 141. Interestingly, a sequence of endothermic events occurs, indicating that the remaining solid phase might be the product of dissolution-recrystallization steps which could explain the different endothermic events. Some values could correspond perhaps to metastable polymorphs (form C, $T_m$ at 106.8 ºC [73], form B 110.3 ºC [10]). However, this subject had not always been sufficiently investigated.

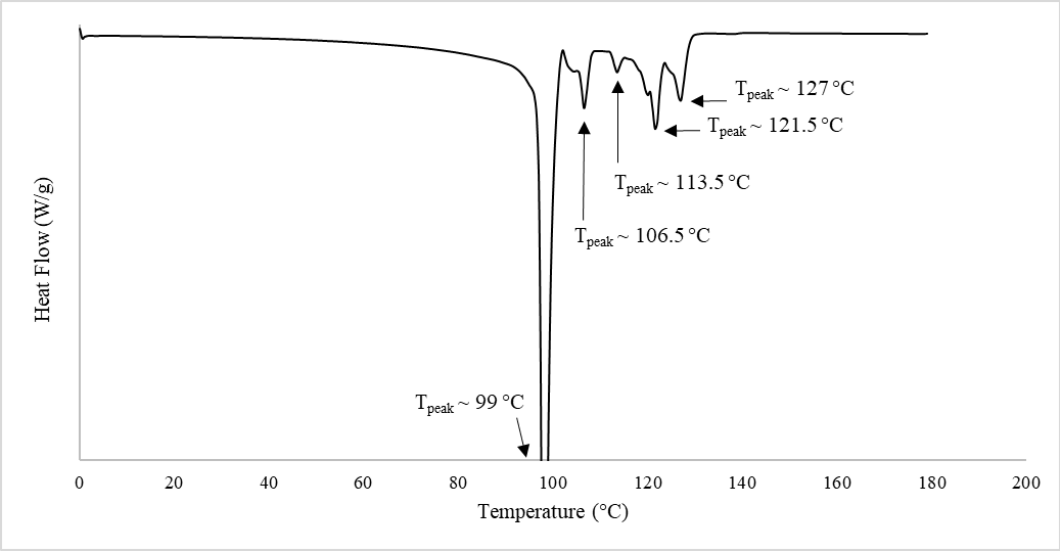


Figure 141. DSC scan for the remaining solid in suspension after the water solubility experiment (37°C) for sample HME 27.

### 3.1.5 Dissolution studies

The dissolution profile was evaluated for the HME 27 and HME 28 samples in two physical forms: pellet and powder. As described above, particle size distribution analyses should be further explored to understand the dissolution profile results better. However, for comparative purposes, the results are evaluated in this chapter in the form of pellets (about 1 mm) and powder (less than 500 µm) with approximate dimensions obtained by optical microscopy (see 3.1.5).

The dissolution profile method described in Chapter 5.3 was slightly modified regarding the addition of the sample in the medium (by adding the equivalent to the dose studied directly in the dissolution vessel).

Usually, the experiments reveal dissolution dependence on the surfactant concentration, that influences solid's wettability. Aiming to eliminate the wettability (and perhaps solubilizing effect) of the surfactant, the dissolution kinetics were studied in two different media:

- 0.1N HCl with 0.2 wt% of SLS (described in the Sub-chapter 5.3), which corresponds to the pharmacopeial method [297];
- 0.1N HCl without surfactant.

The dissolution profiles for the HME 27 sample in the medium with and without surfactant are shown respectively in Figure 142a and 142b. The remarkable effect of the presence of SLS in the medium is observed comparing the release profile for the raw PZQ in Figures 113a and 113b, for which wettability is important for dissolution. The presence of the surfactant has less impact on the PZQ release from the ternary amorphous solid dispersion.

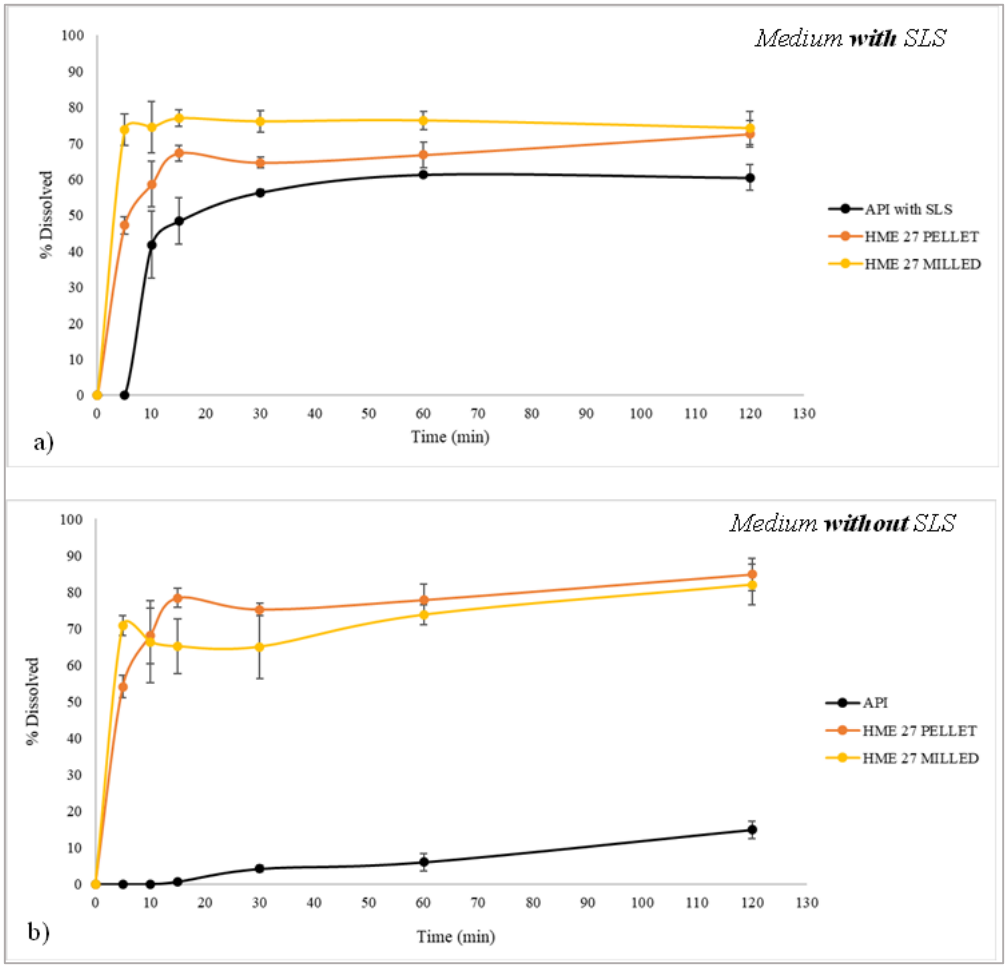


Figure 142. Dissolution profile for sample HME 27 (powder and pellets) on a) pharmacopeial medium (with SLS 0.2%) and b) without SLS in the medium. For both the medium was HCl 0.1N at 37 ºC ± 1ºC.

Likewise, Figure 143a and 143b show the dissolution profiles for the HME 28 sample, for purpose of comparison in this case also the effect of the physical form (pellets and powder). The powder form of HME 28 showed a reduced dissolution compared to the pellets in the medium with surfactant, but the performance remained comparable.

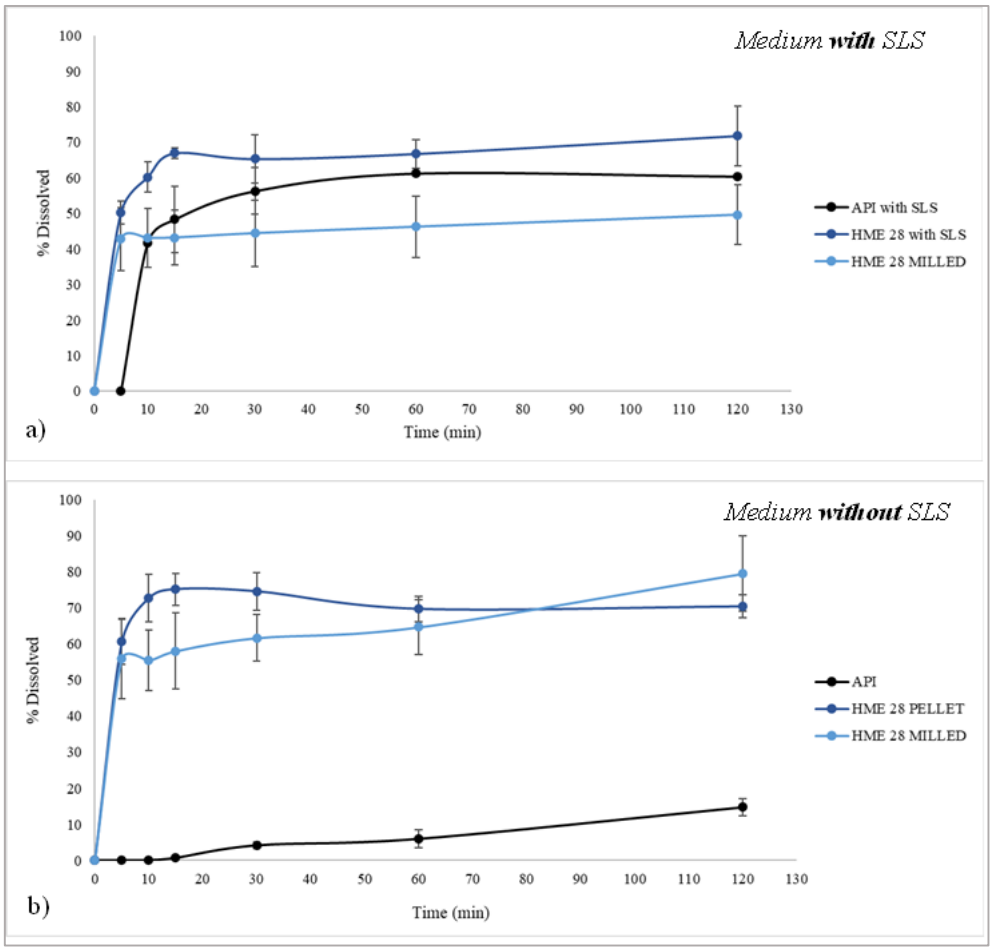


Figure 143. Dissolution profile for sample HME 28 (powder and pellet) on a) pharmacopeial medium (with SLS 0.2%) and b) without SLS in the medium. For both the medium was HCl 0.1N at 37 ºC ± 1ºC.

### 3.1.6 In vitro buccal dissolution test to predict the palatability

The taste masking test was applied to samples containing 35 wt% PZQ load, as powder and pellets. As mentioned before, a recent study, that sought to achieve taste masking of PZQ, evaluated the production of solid dispersions of PZQ and Eudragit® EPO: Glyceryl monostearate (1:0.3 w/w) containing 27.8 % and 43.5 % PZQ (provided a delayed release of the API below 0.01 mg/ml after 1 min) [118]. On this occasion, the author aimed to generate a product partially crystalline to minimize the increase in dissolution caused by the amorphous state and, consequently, the amount of PZQ in the oral cavity in the first contact with the taste buds. Thus, the idea was to increase solubility/dissolution, even if not as much as possible, and to achieve the masking of the bitter taste of PZQ. The results showed that one of their samples had masking capacity, and this characteristic was proportional to the API concentration. This example showed that a major cause for the worst performance of another tested sample was the smaller

particle size resulting in greater dissolution and taste perception. The masking experiments were carried out in an animal model using the BATA method [117]. Additionally, the acceptability limits of the rat for PZQ were evaluated by different concentrations. Solutions with different concentrations of PZQ were prepared and offered to the animals in a very short and predetermined time. The taste evaluation is measured according to the number of licks. That means that the lower the number of licks, the less acceptable the product is. In this way, it is possible to estimate the concentrations: completely tolerable, well tolerable, tolerable, not tolerable/aversive and, highly aversive/highly not tolerable. The limits found for the PZQ are shown in Table 57.

Table 57. Relation of PZQ taste threshold determined in vivo using BATA model for Munster et al. [68]

| ***Classification*** | ***PZQ concentration (mg/mL)*** |
|---|---|
| Fully tolerated | 0.005 to 0.01 |
| Well tolerated | 0.03 |
| Tolerated | 0.05 |
| Aversive/untolerated | 0.1 and 0.2 |

The BATA evaluation model was previously tested with nine different APIs with different degrees of aversiveness and its result compared to the respective data obtained from the human panel (gold standard) [80], [119], [125]. The results demonstrated an extensive correlation between animals (rats) and humans for 8 of the tested API models. The data from this correlation indicate that the BATA model can be used as a screening tool for medicines in the early development stage, helpful in predicting the human taste response.

With these data, predicting an in vivo taste evaluation with the extrudate samples produced in this thesis is possible. Using the dissolution method that mimics the oral cavity (2 mL of SSF), the concentrations released from the API as a function of time were obtained. In this way, HME 27 and HME 28 were evaluated as well as the relation of taste with their physical form (pellets or powder).

The results are shown in Figure 144. For both formulations, the pellets are considered very tolerable/tolerable in the first minute. The taste perception with the powders can be explained as did in the example we have just described, that is the fast dissolution of smaller particles [118]. Figure 145 shows the remaining solids in the in

vitro buccal dissolution apparatus, where the physical differences between samples can be visualized.


Figure 144. PZQ release as a function of both type of shape (powder and pellet) for extrudate samples a) HME 27 and b) HME 28. The taste thresholds are represented as black and pink dashed lines.

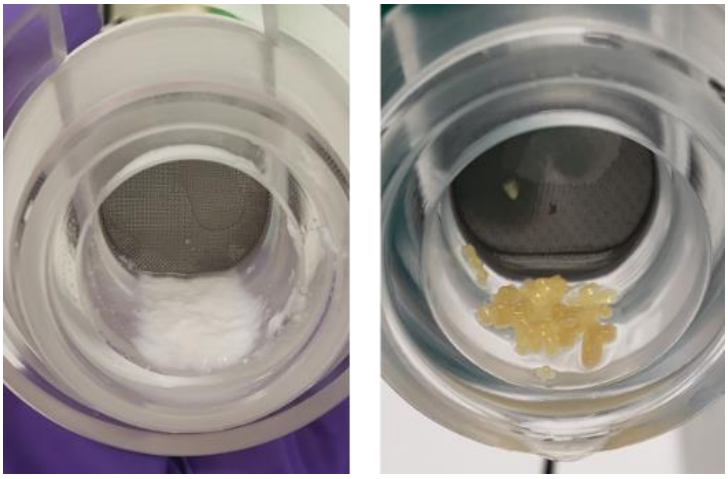

Figure 145. Residual sample of HME pellet and HME powder after in vitro buccal dissolution taste to predict palatability.

Still, to better understand the taste masking profile of the samples produced, the pellets made by extrusion and described in Sub-chapter 5.3 containing 50% drug load were evaluated. In a comparative way between the concentrations of API in the extrudates, the results are presented in Figure 146.

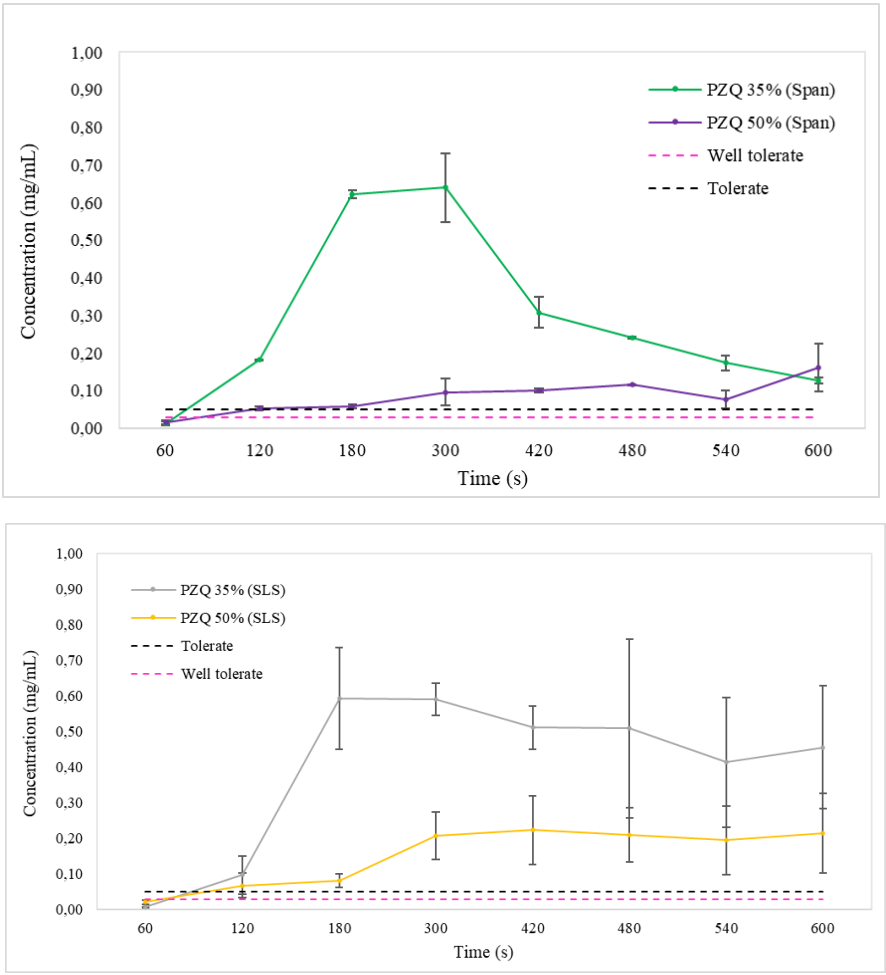


Figure 146. PZQ release as a function of both API load for extrudate samples a) HME 27 and HME 23 (Sub-chapter 5.3), and b) HME 28 and HME 24 (Sub-chapter 5.3). The taste thresholds are represented as black and pink dashed lines.

Surprisingly, the results for HME containing 50 wt% drug showed a better profile in terms of release and taste. However, it is necessary to make some considerations in the interpretation of this result. As discussed in Sub-chapter 5.3, samples with 50 wt% are highly supersaturated and already presented traces of crystallinity just after production. Also, they were previously produced and oldest at the time of this analysis. An aging/recrystallization effect would contribute to a lower release.

Although the results are promising, these evaluation results of taste masking need to be confirmed in vivo.

## 4. CONCLUSIONS

Aiming to develop amorphous solid dispersions of praziquantel with a high drug concentration, we have started with 50 wt% PZQ and studied their production first in Brazil (FIOCRUZ) with a twin-screw extruder Pharma 11 and then in France (Centre Rapsodee) with a twin-screw extruder Pharma 16 with large production capacity.

The ternary systems of our interest (PZQ-PVPVA-surfactant) loaded with 50%PZQ produced in the Pharma 16 showed confirmed capacity to improve PZQ concentration in water (apparent solubility) during an appropriate period (1h). However, they are highly supersaturated and evidenced traces of crystallinity and instability.

This sub-chapter thus focused on the production of new ternary with 35 wt% PZQ, 60 wt% PVPVA and 5 wt% Surfactant (SLS or SPAN 20).

The reduction of the PZQ load in the ternary extrudates resulted in a complete amorphization of the mixture and elimination of crystallinity.

Unlike the samples presented in the Chapter 5.3, HME 27 (with SPAN 20) and HME 28 (with SLS) were produced using a conical mill (Quadro® Comil®). Changing the grinding methodology represented an advance in the process because it is most common on the industrial scale. Also, the dissolution method, considered inadequate for analysis of our extrudates, was improved by changing the operating procedure (addition of samples in the dissolution vessels; identification of a more discriminating medium for comparative study, without surfactant).

Both studied new ternary showed the typical behaviour of amorphous solid dispersion during solubilization characterized by an initial spring effect followed by the decay of the API concentration in solution. Both have proved their capacity to increase the apparent solubility of PZQ in the first one hour (90 % and 76 % higher than the equilibrium solubility of PZQ for HME 27 and HME 28, respectively). The reached concentrations are higher than those from the ternary samples with similar composition (API-polymer-surfactant) and higher PZQ load (50 %) presented in chapter 5.3.

As expected, pellet extruded products showed better performance in taste masking (in vitro method) compared to the respective milled ones. Both formulations (HME 27 and 28) were considered "well-tolerated" up to one minute in contact with the SSF medium. This result is promising for two main reasons: a) the formulations evaluated did not contain the addition of excipients with a function of taste improvement as sweeteners.

Also, the final formulation can still be improved (with excipients like edulcorates), and b) One minute time is reasonable time for the medication to remain in the oral cavity.

Although we still need to deepen the characterization of the formulations presented in this chapter (such as particle size distribution by other analysis methods such as laser granulometry), they it could be promising to develop prototypes of paediatric drugs based on praziquantel. The formulations presented here showed positive prospects for overcoming two of the three main formulation challenges with this API.

# CHAPTER 6 - 3D PRINTING TO OVERCOME PRAZIQUANTEL PAEDIATRIC FORMULATION CHALLENGES

## 1. INTRODUCTION

As discussed in Chapter 2, the use of 3D printing in the production of medicines has some interesting advantages over the techniques commonly used in the pharmaceutical industry.

The first advantage concerns the possibility of customizing the dose and composition of drugs produced by 3D printing. The second advantage is related to the fact that 3D printers, given their characteristics (ease of transport, installation, and operation), can be used in places of difficult access and inadequate structure that are the focus of neglected diseases. In this sense, it is possible to imagine 3D printers in field hospitals or primary care clinics in more remote regions.

These exciting advantages had motivated the study presented in this Chapter which was focused on the investigation of the use of innovative 3D printing technology to overcome the main challenges to formulate PZQ for paediatric patients widely discussed in the previous Chapters (low drug solubility, bad taste, need of high and variable drug doses).

In this study, direct powder extrusion 3D printing was used to prepare PZQ-ASD as paediatric printlets (3D printed tablets). The suitability of different powdered materials to directly feed the 3D printer was investigated. The powdered materials tested were physical mixtures of crystalline drug and polymer and pellets and powder forms obtained from ASD-HME filaments. The characteristics of the resulting 3D printlets were evaluated with special focus on drug dissolution profiles, effectiveness of taste masking and physical stability and are presented and discussed in this Chapter.

The study presented in the Chapter 6 was carried out in collaboration with:

- Professor Alvaro Goyanes, School of Pharmacy, University College of London (UCL) and FabRX, London.
- Professor Catherine Tuleu, School of Pharmacy, University College of London (UCL).

Figure 147 show the schematic of the HME and FDM 3D printing process used in this Chapter.

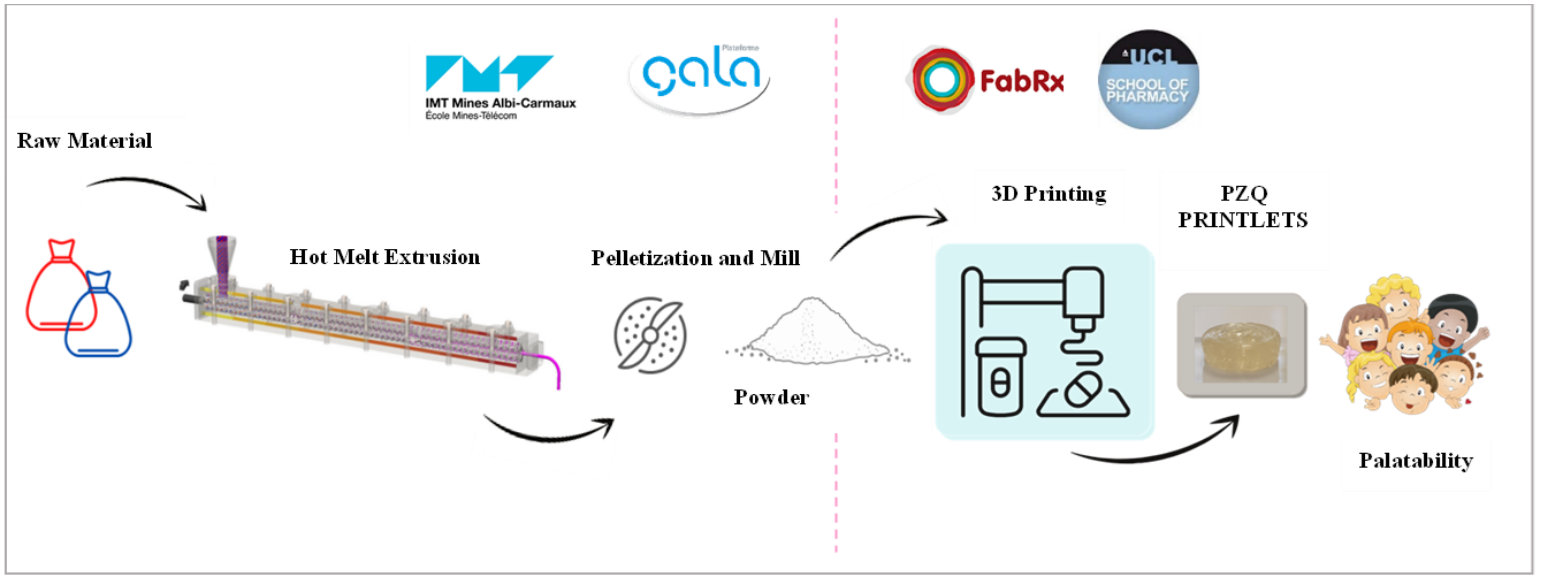


Figure 147. Printlets production as part of this thesis. Source: Author

## 2. METHODS

### 2.1 Preparation of the powdered materials

As already said, direct powder extrusion 3D printing (DPE 3D printing) was used to prepare 3D printed tablets from powdered materials.

Different powdered materials were tested in the DPE 3D printing: physical mixture of crystalline PZQ and polymer (PM), pellets produced by HME in a twin-screw extruder (Pharma 16, Thermofisher) and powder obtained by milling the HME-pellets. The mass composition of the powdered materials is given in Table 58.

Table 58. Feedstocks used for printlets production.

| Formulation code | Composition (% w/w) | | | | Print Parameters | | |
|---|---|---|---|---|---|---|---|
| | PZQ | PVPVA | SLS | Span | Extruder temperature (°C) | Flow rate* (%) | Feed rate * (%) |
| **Physical mixtures (PM)** | | | | | | | |
| PM 50 | 50 | 50 | - | - | 145 - 170 | 100 - 140 | 100 |
| PM 35 | 35 | 65 | - | - | 145 - 170 | 100 - 140 | 100 |
| PM 35 SLS | 35 | 60 | 5 | - | 140 - 200 | 100 - 140 | 100 |
| **Pellet (P) and milled powder (M) obtained by HME filaments produced in a twin-screw extruder** | | | | | | | |
| P 50 | 50 | 50 | - | - | 140 | 90 | 100 |
| M 50 | 50 | 50 | - | - | 135 | 75 | 100 |
| M 35 Span | 35 | 60 | - | 5 | 130 | 75 | 100 |
| M 35 SLS | 35 | 60 | 5 | - | 130 | 75 | 100 |

*The flow rate is given as a percentage relative to the calibrated value of its full scale

The physical mixtures (PM 50, PM 35, and PM 35 SLS) were prepared in a Turbula® T2F mixer (96 rpm, 8 min). The equipment used and the experimental protocol were described before (Sub-chapter 5.2).

As already described in Sub-chapters 5.3 and 5.4, HME filaments were generated using the Thermo-Fisher pharma 16 Extruder (Thermo scientific ™, Germany) presented in Sub-chapter 5.2 (1.1). The heating extrusion zones were determined for each of the formulations according to their specific characteristics. The HME filaments were cut in pellets of 1 mm size. Part of the binary formulation was used as pellets (P 50), and part was milled (M 50). The two ternary formulations (M 35 Span, M 35 SLS) were milled (M 35 Span and M 35 SLS). The milling process was carried out using Quadro Comil H5

High Energy Mill (Fitzpatrick® Quadro®) with 8000 rpm for speed mill and a sieve with 610 µm of size. The samples were protected from light and kept in a desiccator for conservation.

The three formulations of PZQ processed by hot-melt extrusion (HME) contained 50 or 35 wt% PZQ, in the presence (or not) of surfactants. As already explained in Sub-chapter 5.4, the addition of the surfactants (Span or SLS) in the formulations had as main objective to increase the dissolution of the solid dispersions (SD) produced by HME. This investigation was conducted with the formulations containing 35 wt% of PZQ. The respective placebo formulations were produced (M Placebo Span and M Placebo SLS) to check the printer's cleanliness by contaminating the batches with PZQ.

## 2.2 3D Printing

The prepared mixtures, pellets or milled extrudates were added to the hopper of a M3DIMAKER™ pharmaceutical 3D printer (FabRx, London, UK) with a direct powder extruder nozzle [156]. AutoCAD 2014 (Autodesk Inc., USA) was used to design the templates of the printlets, which were then exported as a stereolithography (.stl) file into the 3D printer software (Repetier host Version 2.1.3, Germany). The selected 3D geometry was a cylindrical printlet (10 mm diameter × 3.6 mm height). The printer settings in the Repetier Host software were as follows: Feed 2100 steps/mm, infill 100%, high resolution with brim, without raft, extruding (20 mm/s), speed while travelling (90 mm/s), number of shells (2) and layer height (0.20 mm). The flow rate, extruder temperature and feed rate were determined according to each formulation (Table 1).

The 3D printer used (FabRx, UK) is specifically designed with a direct single-screw powder extruder and a nozzle diameter of 0.8 mm. Its design is based on a single-screw HME with rotation speed (and hence extrusion) controlled by the 3D printer software (Repetier-Host V 2.1.3, Germany). Furthermore, the extruder nozzle moves in three dimensions to create the objects in a layer-by-layer fashion (Figure 148).

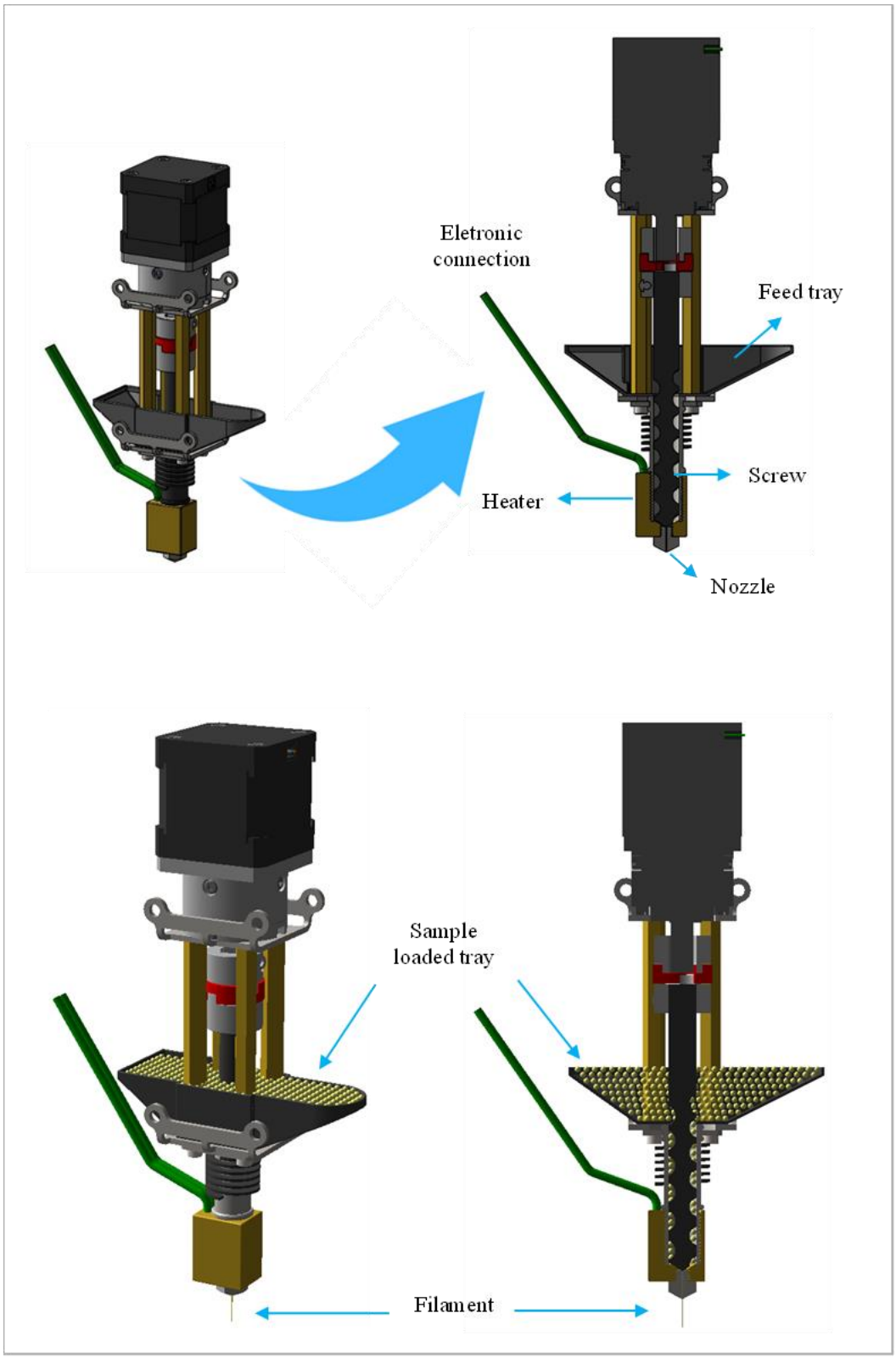


Figure 148. Design of the single-screw powder extruder FabRX 3D printer used in this thesis.

After printing each formulation, the extruder was removed from the printing platform and the screw was dismounted and washed to avoid cross-contamination between different formulations.

## 2.3 Printlet characterisation

Microphotographs were obtained by SEM and optical microscopy. The methods used were described in Sub-chapters 5.3, item 2.3.1.

### 2.3.1 Dimensions

The physical dimensions of the printlets were measured using a digital Vernier caliper and a Sartorius Entris 124-1S analytical balance to determine the mass of each printlet.

### 2.3.2 X-ray diffraction (XRD)

Discs of 20 mm diameter × 2 mm height made from the same formulations of the printlets were 3D printed and analysed. X'Pert Panalytical X-ray diffractometer (Philips, USA) using CuKα radiation, putting 40 mA of current and 45 kV of voltage was used. The recording spectral range was set at 7-50° with a measuring step (angular deviation between 2 consecutive points) of 0.0167° and an acquisition time of 100 s per point. Also, the disc was rotated in its sample holder (1 revolution/s) during the results acquisition. Disc printing was performed only for feeding with HME-extrudate powder. X-ray powder diffraction (PXRD) was performed for the raw and extruded materials ground using the same method.

### 2.3.3 Differential Scanning Calorimetry (DSC)

The analysis was performed by using a DSC Q200 with the base module and mDSC (TA instruments, USA) and the conditions were the same that described before (Chapter 4 item 1.2.2).

For analysis, the printlets were broken with a spatula and two analyzes of each unit were performed: one with part of the edge and another with the interior part (Figure 149).

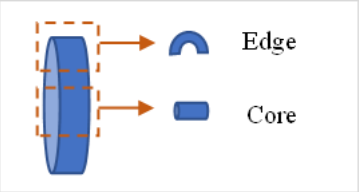


Figure 149. Schematic representation of the printlet samples used for DSC analysis.

### 2.3.4 Raman Microscopy

Raman mapping was performed using a Raman confocal microscope 300R Alpha (Witec, Germany), equipped with a laser at a wavelength of 532 nm and the analyses were conducted at room temperature. Samples were analysed by a 50x objective on the surface and deep mapping (8x8 μm PVPVA, 5x5 PZQ and 10x10 and 10x20 P and M printlets) was applied to predict drug and polymer distribution.

### 2.3.5 Determination of drug loading

A printlet of each formulation was placed in a volumetric flask phase mobile (50 mL) under ultrasound for 5 minutes until complete dissolution (n = 2). Samples of the solutions were then filtered through 0.22 μm PTFE filter (Millipore Ltd., Ireland) and the concentration of drug was determined with HPLC system (Agilent 1100 Series) equipped with a UV-visible detector, by the same method detailed before (item 3.1.1, Chapter 3).

### 2.3.6 Dissolution test

Dissolution of printlets was monitored using a dissolution rate test type II apparatus (DT 60 ERWEKA, Germany). The method was described before on the Chapter 3 (3.1.9).

Three printlets of each formulation were analyzed with manually addition to the cube.

### 2.3.7 Assessment of Taste Masking Efficiency Using a Novel Biorelevant Buccal Dissolution

The in vitro method described by Keeley et al. [80] was used to predict the taste of PZQ released from the milled extrudates and printlets in a simulated buccal environment.

The simulated salivary fluid (SSF) (Sodium chloride−8 g/L; Potassium phosphate monobasic−0.19 g/L; Sodium phosphate dibasic−2.38 g/L; pH 7.4) [339] kept under magnetic stirring at 37 ° C ± 1 ° C, was pumped through the 'buccal dissolution column' using a peristaltic pump at a rate of 1 mL/min, corresponding to an average adult normal total simulated saliva flow range. The other two adjacent parts were composed of wire mesh discs, placed either side of the column. After inserting the sample in the centre of the column lumen, from the top, aliquots were collected at 60, 120, 180, 240, 300, 360, 420, 480, 540, and 600 s, filtered through a 0.22 um membrane, and PZQ analysed by HPLC. Tests were conducted in triplicate. Data are reported throughout as mean ± standard deviation using Microsoft Excel (Microsoft Corp., Redmond, WA, USA) software (version 2016 MSO).

The PZQ taste-concentration profile was previously determined with the rat brief access taste aversion (BATA) model [114]. It was found that the half maximal inhibitory concentration (IC50) was 0.06 mg/mL, and the taste threshold was 0.03 mg/mL. The classification proposed by Mohamed-Ahmed et al. [114] was used to classify levels of PZQ released at different time points as fully tolerated, well tolerated, tolerated, aversive/untolerated, or highly aversive/highly untolerated, and predict taste masking efficiency of the different formulations.

### 2.3.8 Stability study

The stability study was performed with a Memmert HPP260eco (Germany) and the conditions are described in Table 59.

Table 59. Stability study conditions.

| ***Stability study conditions*** | |
|---|---|
| Temperature (°C) | 25 |
| Humidity (%) | 60 |
| Points of analysis | 1 and 3 month |

The stability study was designed to monitor only physical changes in the printlets produced. Therefore, the formulations submitted to the study were analyzed by DSC and XRDP.

The printlets were packaged in amber glass bottles with a plastic screw cap and seal for DSC analysis. For each point of the stability study, a single bottle, containing one printlet inside, was prepared. The bottles ready for the study are shown in Figure 150.


Figure 150. Flasks used for packaging printlets during the stability study.

For XRD analysis, discs were used instead of printlets, and they were subjected to the same conditions of humidity, temperature, and storage time. However, due to the lack of sufficient quantity, the same disk was analyzed during all successive time points. Another necessary adjustment was the use of transparent glass bottles with a plastic screw cap. It was made according to the diameter of the bottle opening. Aluminium was used to protect the bottle and reduce the difference between light from the amber bottles used for printlets. The prepared bottles are shown in Figure 151.

Figure 151. Flasks used for packaging printed discs during the stability study.

# 3. RESULTS

## 3.1 Physical characteristics of printlets

### 3.1.1 From physical mixtures

The physical mixture of PZQ and KOL (PM 50) was directly added to the hopper of the 3D printer extruder, the feeding material hampered the printing process and led to unsatisfactory final products (Figure 152). Different mass feed rates and screw speed parameters were tested, but none produced printlets with satisfactory visual quality or enough material. The poor flow of the mixture and electrostatic forces caused high variation in the feeding during printing, making it impossible a continuous and homogeneous flow of material through the screw.

Figure 152. Aspect of the PZQ printlets obtained by directly feeding the physical mixture of praziquantel and PVPVA (1: 1) into the hopper of the 3D printer extruder.

A similar and unsatisfactory behaviour was verified when another physical mixture of PZQ (PM 35 SLS) was directly added to the hopper of the 3D printer extruder. These results showed that, for 3D printing with direct powdered material feeding, powder characteristics capable of providing fluidity and homogeneity are essential to a regular flow through the extruder. Without adding additional excipients to improve the flow properties of physical mixtures, it was not possible to obtain printlets with good quality from both PZQ formulations.

For the third tested formulation (PM 35 Span), printing experiments were not possible since the mixture could not be prepared with the same conditions used for HME extrusion (addition of the liquid surfactant directly in the extruder).

### 3.1.2 From pellets and powders produced from HME-filaments

The main objective of printing using HME-filaments cut into pellets was to improve powdered properties like mixing homogeneity and flowability compared to a physical mixture of same composition being directly fed to the extruder of the printer. Although it was possible to print with this type of material, the pellets' flow into the printer has not improved significantly. This barrier is probably related to the size of these particles (around 1 mm) and the lack of homogeneity in these particulate materials' morphology. The printing of the printlets using the sample P 50 was possible, however, with a limited number of printlets since the cleaning of the screw was necessary practically to each unit produced. For this reason, only DSC analysis was performed for this sample to verify the thermal properties after printing and during the stability period.

In contrast, milled materials provided a continuous flow, and the printing process took place more easily. However, it was evidenced that the feed rate was impacted for the drug load in the system. The samples in the powder form with a load of 35% PZQ (M 35) showed greater ease of continuous printing than the sample containing 50% load of PZQ (M 50). For this reason, even the powder formulation containing 50% drug load (M 50) presented limitations in the quantity of units produced. Because of this, SEM and palatability analyses were not performed. Even with these limitations, the characterizations present in this work are an important step as they demonstrate the possibility to print with material containing high drug load from HME.

The images obtained by optical microscopy of PZQ printlets are shown in Figure 153). The difference between the printlets colours is related to the composition of each one. The HME-filaments containing surfactant (M 35 Span and M 35 SLS) have a yellow appearance, with the most intense coloration for M 35 SLS. This characteristic was maintained for the respective printlets produced with the M 35 Span and M 35 SLS formulations. Another aspect that can be identified in optical microscopy is the greater opacity of the printlet containing 50 wt% PZQ load (M 50) compared to the others having 35 wt% drug load. When comparing the M 35 Span and M 35 SLS printlets to the respective placebos, it was evidenced that the presence of PZQ resulted in less transparency. However, all printlets presented good physical aspect, quite smooth and with a shiny appearance.

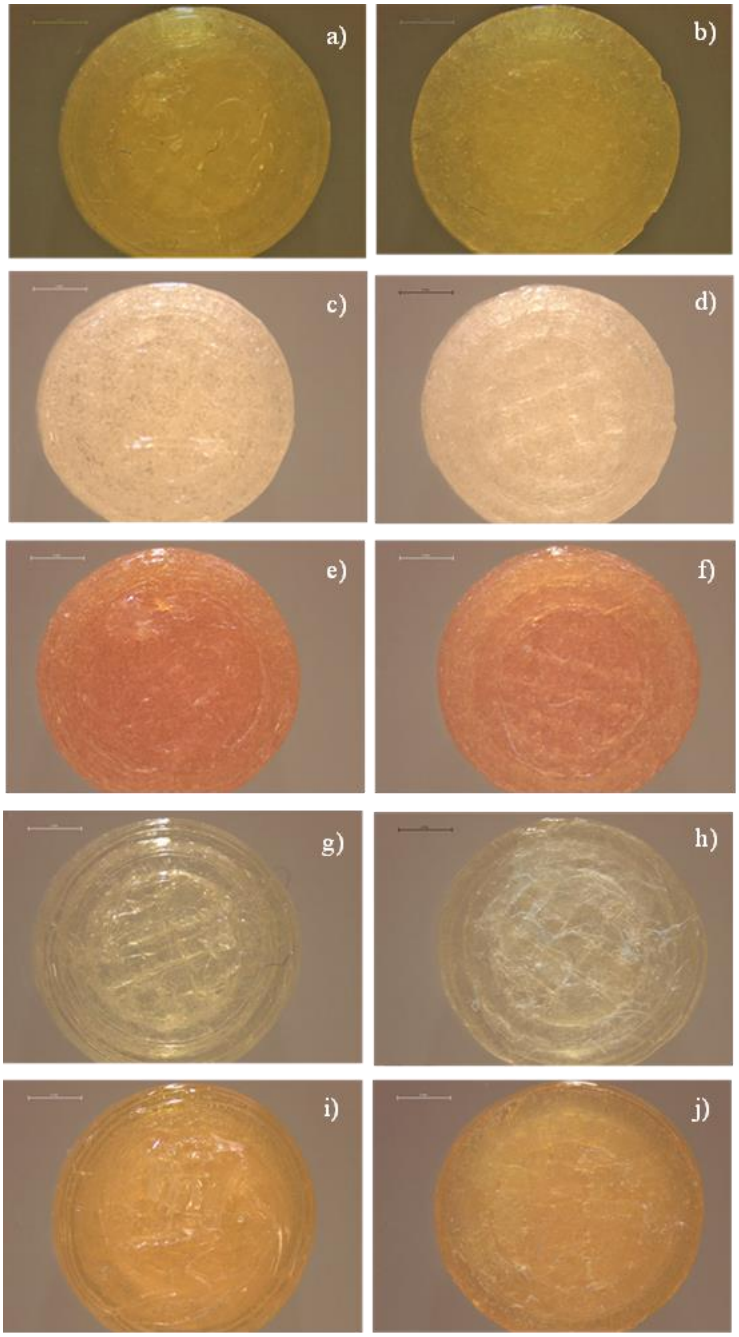


Figure 153. Top and bottom image of printlets obtained with: a - b) PM 50, c - d) M 35 Span, e – f) M ASD 35 SLS, g- h) M Placebo Span and, i – j) M Placebo SLS.

SEM cross-section images of some PZQ printlets (M 35 Span and M 35 SLS) are shown in Figure 154. They show a dense and homogeneous inner matrix, in which some small holes can be observed. They are probably formed from air bubbles entrapped during the printing process. The images also provide a clear view of the layers formed by the layer-by-layer deposition of material during printing.

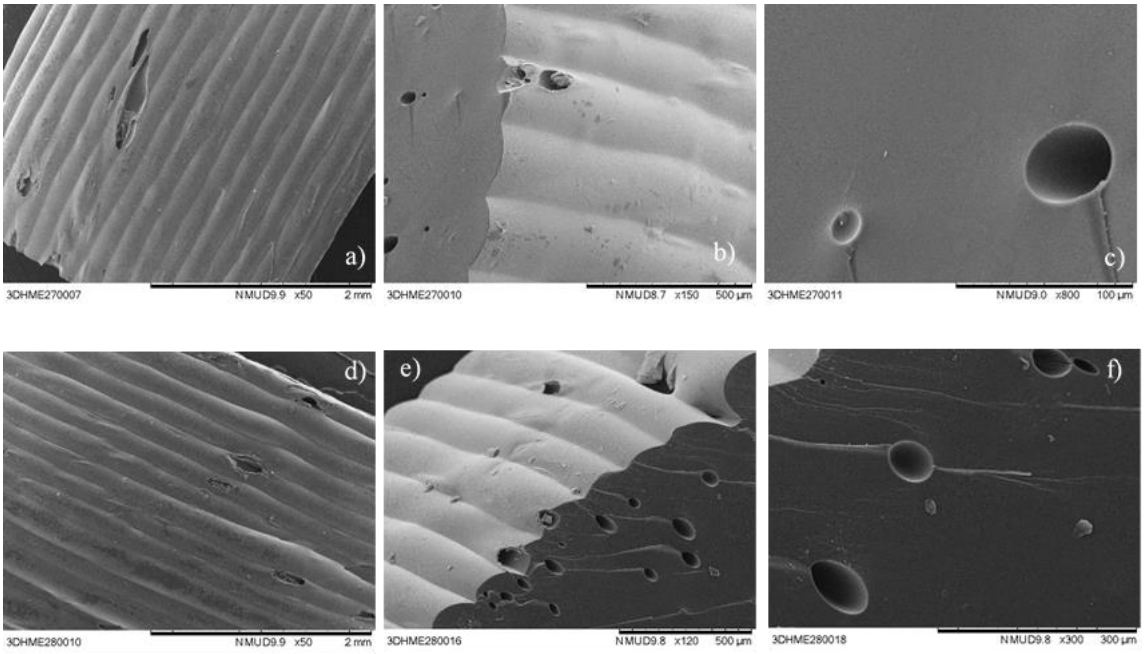


Figure 154. SEM images of printlets: a – c) obtained with M 35 Span and, d – f) obtained with M 35 SLS.

All printlets were designed for the following dimensions: 10 mm diameter and 3.6 mm height. The measured printlet dimension, weight and PZQ load is given in Table 3.

M 50 and P 50 printlets showed higher mass variation (0.298 and 0.270, respectively), probably due to differences in feed flow. PZQ content was determined only for M 50 printlet according to the number of units available and was close to the theoretical content value (48.4 %), showing that the dose is around 150 mg.

The formulations M 35 with surfactants (Span and SLS) showed a homogeneous flow during feeding in the printer and good uniformity in the physical dimensions (Table 60). Before print, the milled HME-filaments, M 35 Span and M 35 SLS, contained 34.84 wt% and 33.25 wt% of PZQ, respectively. After printing, the values remained similar for both formulations (35.02 % and 33.54 %, respectively), corresponding to a dosage of the tablet of approximately 100 mg.

One of the most discussed approaches for applying 3D printing of medicines is adjusting the dose using the manipulation of the sizes, structure, or format of the tablets.

As an initial stage in developing a paediatric pharmaceutical formulation, characteristics such as pharmacokinetics and pharmacodynamics, potential routes of administration, toxicity relationship, and taste preferences should be evaluated due to the children's age [66]. In general, it can be said that from birth to around 16 or 18 years old, individuals are considered paediatric patients [75]. However, let's analyse this age group.

It is easy to see significant differences in the physiological development of the body and the need for personalized development for different stages of childhood [66]. The 3D printing approach can promote different designs for new dosage forms with specific pharmacokinetic characteristics.

Tabela 60. Printlets characteristics.

| ***Printlets Formulation*** | ***Measured characteristics of printlets*** | | |
|---|---|---|---|
| | ***Weight (mg)*** | ***Diameter (mm)*** | ***Height (mm)*** |
| P 50* | 0.270 ± 0.02 | 9.720 ± 0.22 | 3.579 ± 0.05 |
| M 50* | 0.298 ± 0.01 | 9.810 ± 0.16 | 3.554 ± 0.14 |
| M 35 Span** | 0.297 ± 0.02 | 9.982 ± 0.25 | 3.507 ± 0.09 |
| M 35 SLS** | 0.290 ± 0,04 | 9.841 ± 0.22 | 3.591 ± 0.11 |

* Values represent the standard deviation, n = 8 and ** n= 18.

Placebo printlets were also analyzed for drug dosage to check for the possibility of contamination of printer parts. For all placebo printlets, the presence of PZQ was not identified, thus indicating that cleaning the printer between one batch and another was effective, and there was no contamination.

The printed discs for XRD analysis also showed good uniformity of dimensional characteristics, and the results are shown in Table 61.

Table 61. Characteristics of the discs printlets.

| ***Formulation*** | ***Measured characteristics**** | | |
|---|---|---|---|
| | ***Weight (mg)*** | ***Diameter (mm)*** | ***Height (mm)*** |
| Disc M 35 Span | 0.621 ± 0.04 | 20.01 ± 0.25 | 1.79 ± 0.01 |
| Disc M 35 SLS | 0.596 ± 0.01 | 19.85 ± 0.07 | 1.79 ± 0.01 |
| Printlet M 50 | 0.656 ± 0.04 | 20.05 ± 0.07 | 1.85 ± 0.02 |

* Values represent the standard deviation, n = 2

The visual aspect of the obtained printlets is shown in Figure 155.

Figure 155. Visual aspect of disc, on left printlet M 35 Span and right side printlet M 35 SLS.

### 3.2 Physicochemical characterizations

DSC, XRD, and Raman mapping were used to characterize the solid state of printlets.

DSC thermograms confirms the crystalline nature of the raw drug (melting point at 137.78 °C and enthalpy of 95.72 J/g), and the amorphous state of the polymer PVPVA (Figure 157), as reported in the literature [73], [75], [340], [341] and already discussed in the previous Chapters. Although an endothermic event was observed in the HME powdered material and mainly after milling (data not shown), its low intensity allows us to conclude that P 50 and M 50 powdered materials were predominantly amorphous before printing.

These physical characteristics are maintained after printing for both formulations where the P 50 remained amorphous while the DSC thermogram of M 50 printlet shows an endothermic signal visualized in the range of 120 - 122 °C with $\Delta H_{fusion}$ 2.15 J/g, indicating that M 50 printlet became slightly crystalline. However, the crystallinity is similar to that evidenced in the material before printing and cannot be attributed to the presence of the started PZQ ($T_m$ ~ 136 ºC) or one of the polymorphs of PZQ, B or C, for which the melting temperatures described in the literature are different (around 106 ºC and 112 ºC, respectively) [30], [73], [75]. The endothermic event shown in Figure 10 would be, rather, related to the effect of the polymer on lowering the melting temperature of the drug in the mixture. Figure 156 also shows the homogeneity of the printlets without differences on their thermal characteristics measured on the core and on the bord.

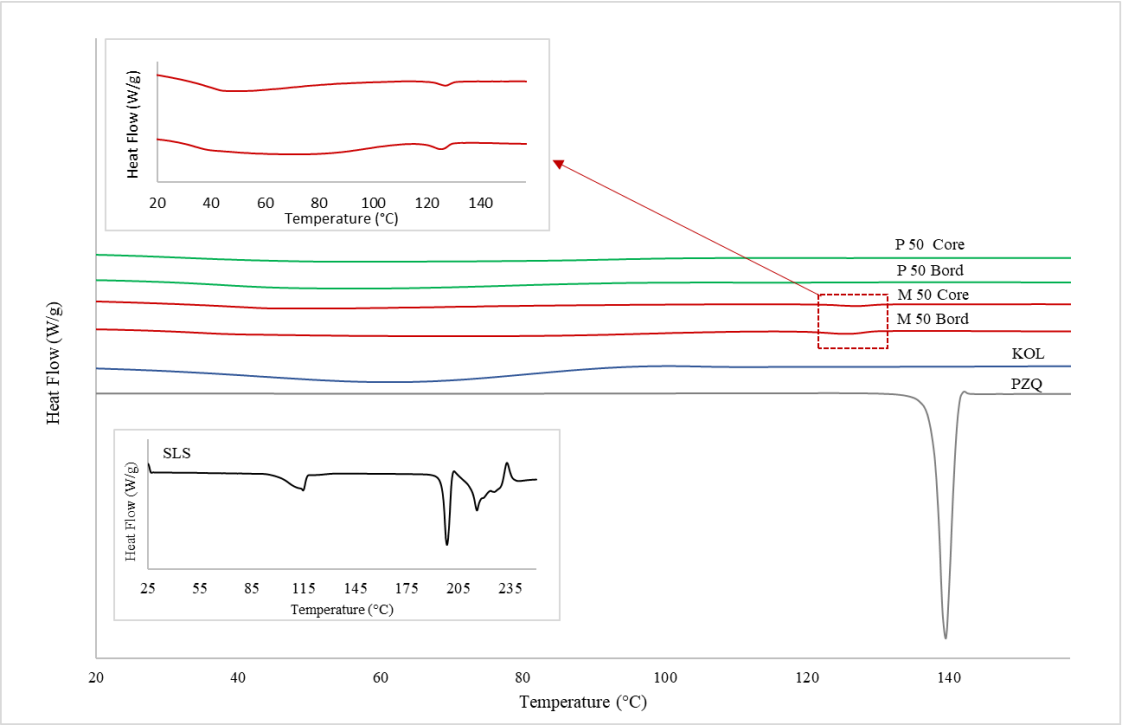


Figure 156. DSC thermograms for P 50 and M 50 printlets, performed in two different parts of each unit (core and bord).

Although M 50 printlets presented a mixture of crystalline and amorphous material, it was verified that, over 3 months of storage under controlled conditions (25 °C, 60 % RH), the endothermic melting event detected after production remained unchanged (data no show), indicating no evolution of the solid structure exposed to the mentioned environmental conditions.

Figure 157 displays DSC thermograms for printlets containing 35 wt% of PZQ, formulated with surfactants (Span or SLS). The amorphous nature of M 35 Span and M 35 SLS materials before printing was confirmed, with no evidence of crystalline PZQ due to the absence of melting event and the presence of a single glass transition ($T_{g\ M\ 35\ SPAN}$ 33 °C and $\Delta C_p$ 0.37 J/g.°C; $T_{g\ M\ 35\ SLS}$ 25 °C and $\Delta C_p$ 0.36 J/g.°C, respectively). The amorphous pattern after printing (M 35 Span and M 35 SLS printlets) remained unchanged and no evolution was detected by DSC analysis after 3 months of storage at 25 °C, 60 % RH.

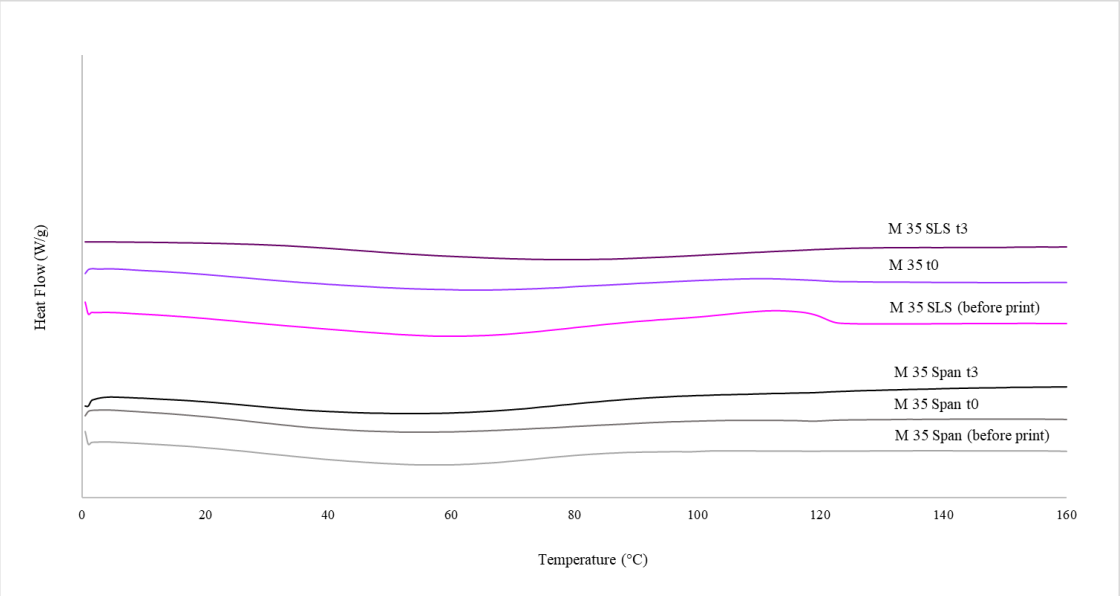


Figure 157. DSC thermograms for M 35 Span and M 35 SLS powdered materials (before print) and their respective printlets performed with freshly samples and after 3 months at 25 °C/60 % RH.

XRD diffractograms of all raw, powdered, and printed materials are grouped in Figure 158.

The crystalline nature of the raw PZQ, SLS and its physical mix with the polymer (PVPVA) are confirmed by the sharp peaks, in line with the data already described in the literature for the commercial racemic molecule [25], [30]. Likewise, the polymer (PVPVA) also presents a characteristic halo of amorphous material.

The amorphous nature of powdered materials (M 35 Span and M 35 SLS) and their respective printlets previously found in the DSC analysis was also confirmed by XRD diffractograms. However, M 35 SLS printlet was the only material presenting some diffraction signals indicating the presence of crystalline material. It could be verified during this study that these signals are also identified in absence of the drug in a placebo formulation (see Figure 158), being related to some structural change on the surfactant (SLS), which was not further investigated here.

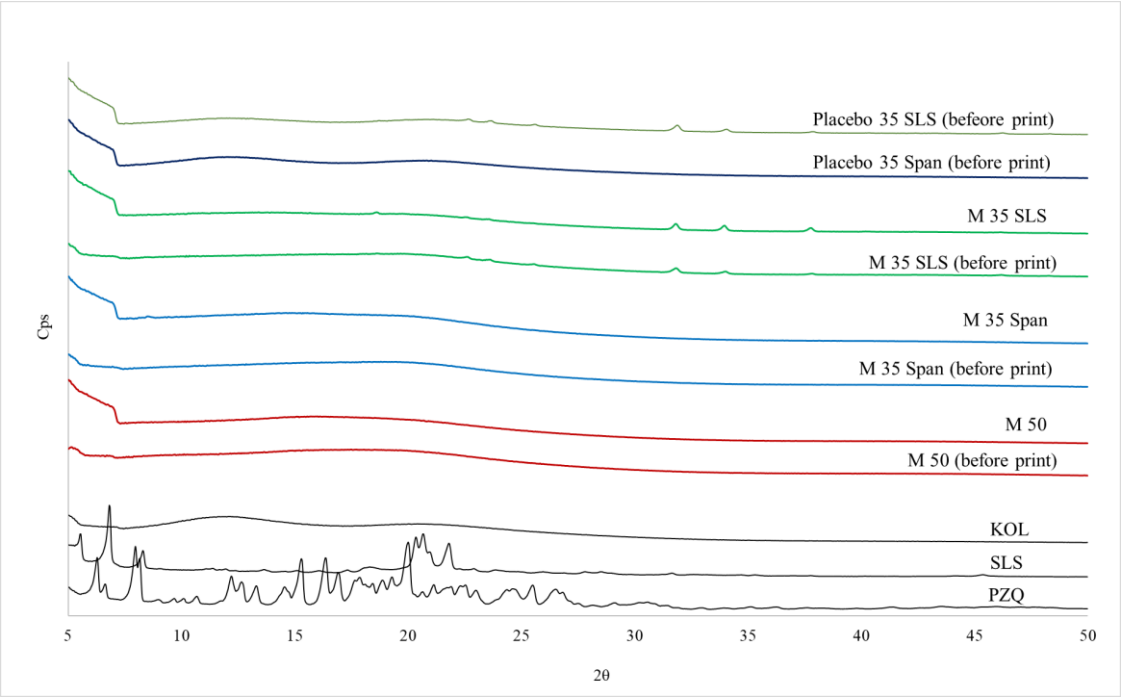


Figure 158. XRD diffractograms for raw materials (PZQ, KOL and SLS), ASDs (M 50, M 35 SLS and M 35 Span) and their respective 3D disc.

Raman microscopy was performed to provide information about the distribution of PZQ in the printlets. Figure 159 shows Raman spectra for PZQ and KOL and their respective characteristic signs (1054, 1451, 2866, 3061 cm-1 and 749, 862, 1740, 2940 cm-1, respectively).

The results showed the presence of PZQ in M 35 SLS and M 50 printlets (2879, 2873 and 3068, 3071 $cm^{-1}$), but it is not possible to detect Raman characteristic peaks of the surfactant (SLS), probably due to the small proportion used (5 wt%) (Figure 159).

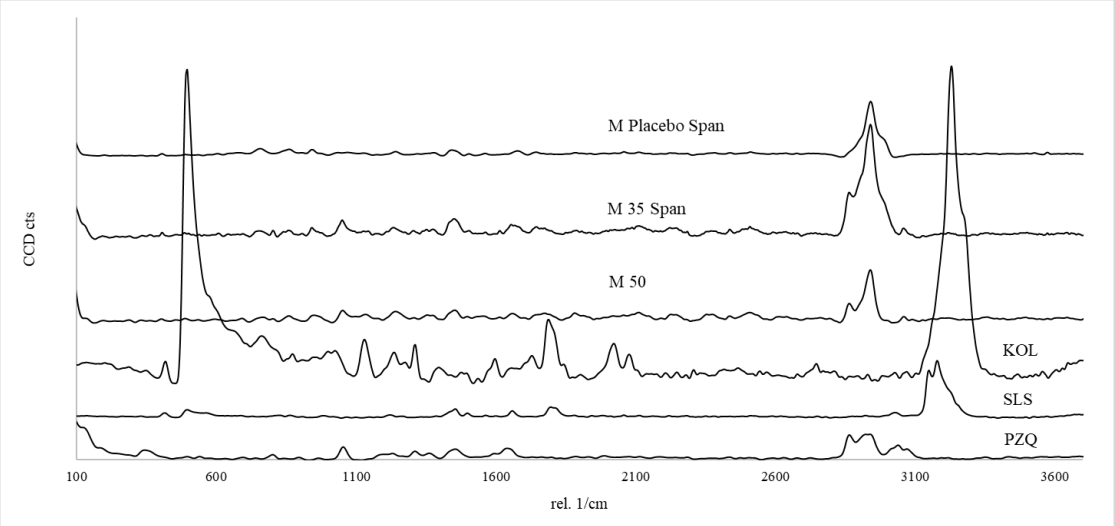


Figure 159. Raman mapping for raw materials (PZQ, KOL and SLS) and printlets (M 50, M 35 Span and M Placebo Span).

3D images (Figure 161) obtained from the integration of PZQ and PVPVA peaks revealed each material's distribution in the analysis area (Figure 160a and 160b). It is possible to visualize the graphs with different colour intensities that reflect the distribution of PZQ concentration. Areas that appear in light yellow indicate high absorbance (high concentration of drug). The darker the colour is (black), the lower concentration of drug it represents [342]. Thus, these colour variations can map the homogeneity and the concentration of the dispersed drug on the screened printlet area showing that for all printed samples there is a good distribution of PZQ in the polymer.

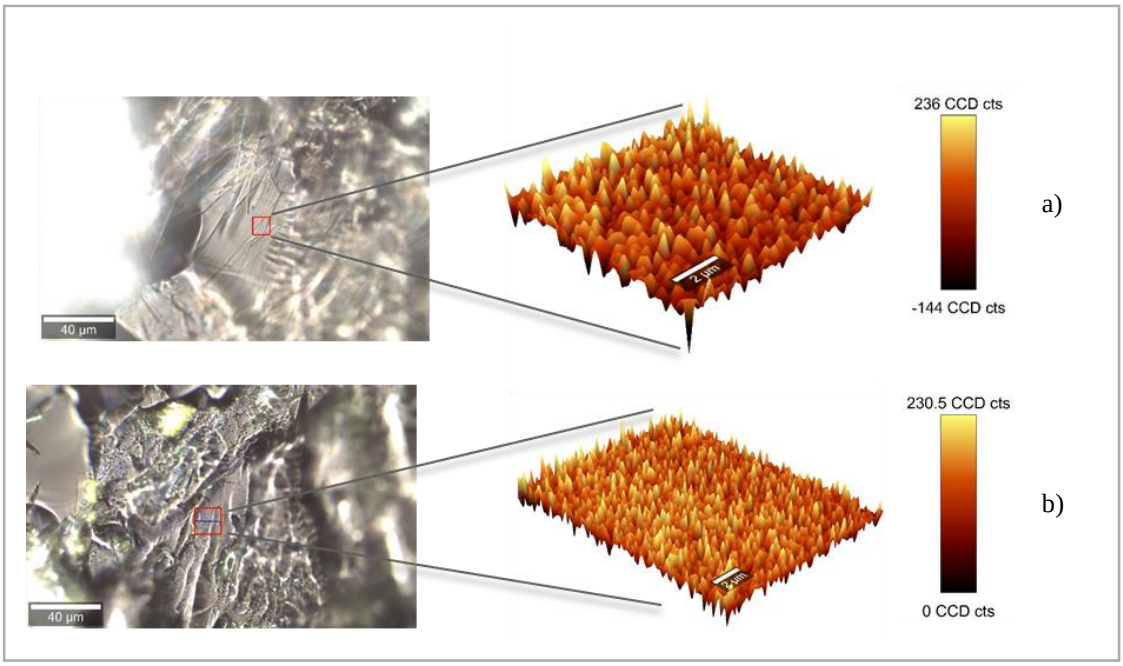


Figure 160. Raman mapping 3D for: a) M 50 printlet with area 10x10 microns, and b) M 35 Span printlet with area 15x15 microns.

For the M 35 SLS printlet, several analyses were performed, with two lasers (532 and 785 nm), different integration times and laser intensities. In all these analyses, the fluorescence phenomena remain important for the perimeter of Raman images. Therefore, it was impossible to obtain a spectrum on this sample, certainly, because of the printlet colour.

### 3.3 Dissolution profiles

The dissolution profiles of M 50, M 35 Span, and M 35 SLS printlets show a greater than four-fold increase in drug release after 2 h compared to PZQ alone (Figure 161). It is important to mention that all printlets were printed directly with powdered materials obtained from HME extrudates without the addition of other excipients that could improve properties such as flowability, dissolution, disintegration, and taste masking. This proves that 3DP can be a highly valuable technology for producing personalised pharmaceutical dosage forms to improve physical and sensory properties necessary for a large variety of medicines. The combination of HME and 3DP techniques could be useful to overcome challenges in the formulation development of BCS class II drugs with low solubility, which represent more than 70% of new drug candidates in the pipeline [88].

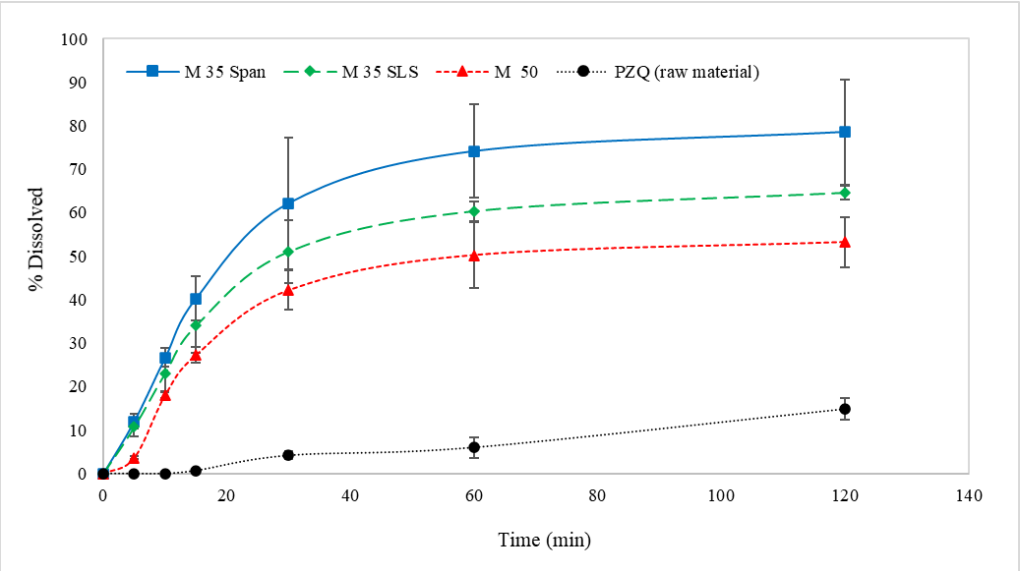


Figure 161. In vitro dissolution profile of PZQ (raw material) and printlets (M 50, M 35 Span and M 35 SLS) using HCl 0.1N medium with 0.2 % w/w of SLS at 37°C.

### 3.4 In vitro taste masking test

Considering that the highest concentration of 50 wt% would be more sensitive to recrystallization, M 35 Span and M 35 SLS printlets were chosen to be evaluated for palatability using an in vitro method described by Keeley et al. [80]. This method evaluates the drug release profile in a spine system that mimics the oral cavity with artificial saliva.

M 35 Span and M 35 SLS powdered materials (before print) present about 0.2 to 0.3 mg/mL PZQ in the medium in the first minute of the experiment (Figure 162a). The dashed lines indicate the tolerability thresholds about the taste of the PZQ previously determined in a study that evaluated different concentrations of the raw drug in an in vivo model (BATA) [68]. This means that when ingesting a particulate material produced, for example, being a powder formulation for dispersion, probably the bitter taste of the PZQ would quickly be noticeable in the mouth.

Also, according to Münster and collaborators [68], the $IC_{50}$ determined for PZQ during BATA was 0.06 mg/ml. Figure 162b presents the results obtained for the printlets. It is possible to better visualize the difference when comparing to the extrudates previously produced by HME. Both printlets (M 35 Span and M 35 SLS) are below the

threshold of good PZQ tolerability, suggesting that the formulations are also promising in taste masking and palatability.

The bespoke flowthrough oral dissolution apparatus was used in a previous study to evaluate chlorphenamine maleate incorporated in sugar spheres coated with different technologies and components [80]. In this study, the apparatus showed real results on different formulations' taste masking capacity, showing a good correlation with the BATA (rodent model) and human panel methods.

In the case of PZQ, this in vitro taste assessment is a very useful tool to screen formulations and evaluate printlets in early-stage formulation development. The method is simple to execute, relatively inexpensive, and can guide development decisions so that animal experimentation can be reduced as only one taste profiling of the drug is needed. However, although the preliminary results of the printlets are encouraging, there is still the possibility of improving the final formulation with additional excipients to further favour taste masking.

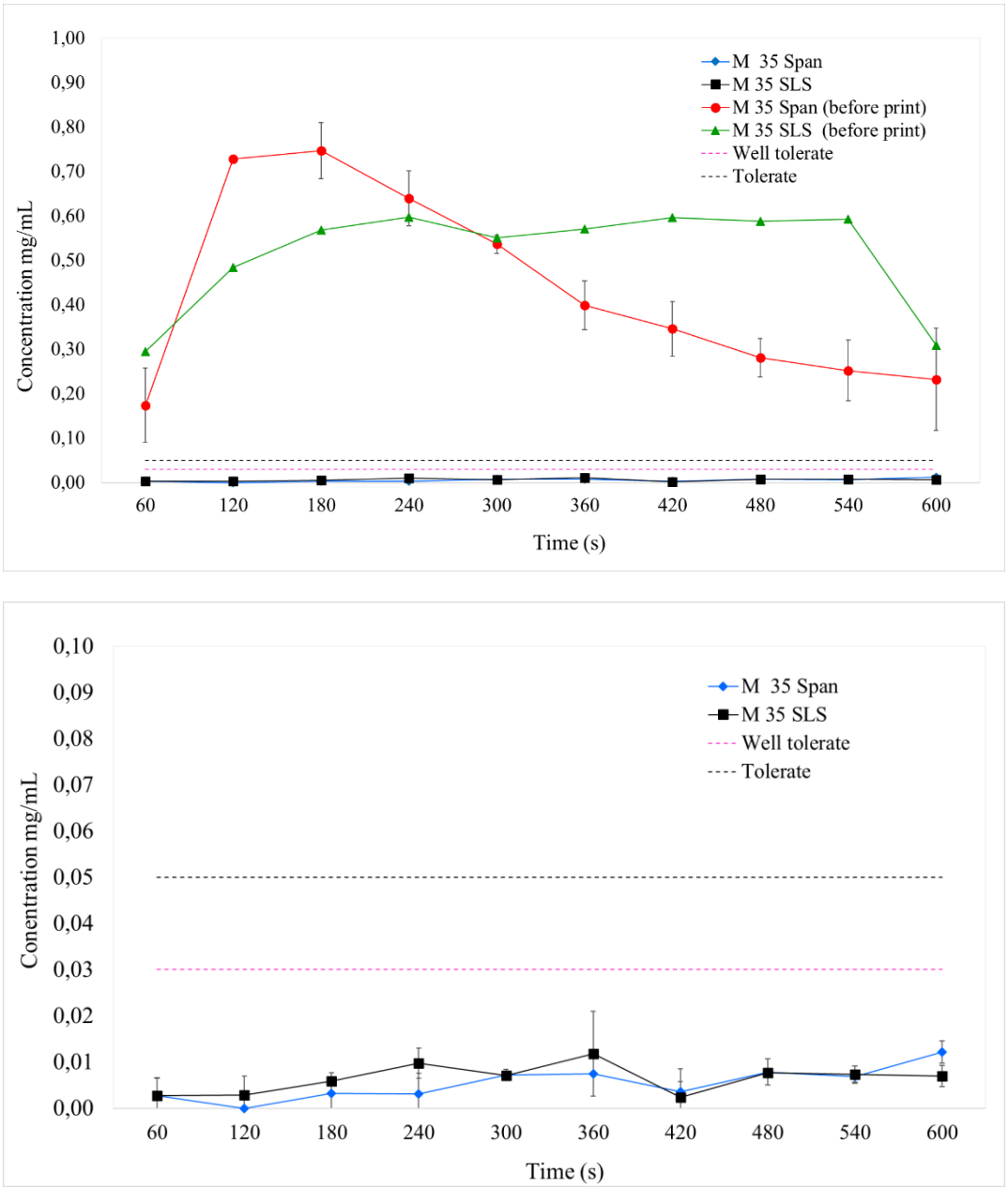


Figure 162. a) PZQ release (mean ± SD) for M 35 Span and M 35 SLS materials (before print) and their respective printlets and, b) detail of the 3D printed formulations. The taste thresholds are represented as pink and purple dotted line.

## 4. CONCLUSIONS

For the first time, 3D printed tablets containing 35 and 50 wt% praziquantel (PZQ) were successfully produced by direct powder extrusion (DPE) 3DP from HME extrudates (in pellet and powder form), reducing the dependence on the strict mechanical properties of HME filaments for FDM 3DP.

Printlets with adequate dimensional characteristics and two different doses (~150 and 100 mg) were produced. In vitro dissolution studies showed a greater than four-fold increase in PZQ from the printlets when compared to pure PZQ, most likely due to the predominantly amorphous solid state of PZQ after printing. In addition to the improved performance in the dissolution studies, in vitro taste masking results revealed that the formulations would be within acceptable taste thresholds (tolerated and well tolerated), with enhanced features for paediatric patients.

Most of the paediatric users of PZQ are found in developing countries, with a large variation in the children's weight due to the poor dietary conditions, showing a wide range of physiological and pharmacokinetic characteristics within a heterogeneous age group. Due to the absence of an appropriate paediatric formulation, treatment of schistosomiasis patients involves the breaking or crushing of a standard adult tablet to achieve the required dose of 40 mg/kg [343]–[345] .

The printlets in this work were developed with a focus on paediatric patients, and although the drug loading still requires optimisation, promising results with amorphous systems have been obtained in taste masking and possible dose reduction compared to what is currently available [68], [346]. The results from this work demonstrate the unique potential of 3DP in customising PZQ medicines from amorphous systems, specifically for paediatric patients.

# CHAPTER 7 - GENERAL CONCLUSION AND PERSPECTIVES

# 1. GENERAL CONCLUSION AND PERSPECTIVES

Neglected tropical diseases affect more than 1.4 billion people worldwide, with children making a significant proportion. The second most frequent is schistosomiasis disease and affects around 28 million preschool-age children.

Praziquantel is the reference medicine for schistosomiasis treatment according to WHO, but there is no appropriate paediatric formulation available in the market.

This thesis aimed to contribute with alternatives to address an important public health problem that is schistosomiasis, through the development of a praziquantel formulation based on ASDs to improve both physicochemical (low solubility) and sensory (bitter) API characteristics, and personalizing dosage for children.

***The first challenge is to improve the water solubility of praziquantel.***

New formulations were proposed here, associating praziquantel to Poly (Vinyl Pyrrolidone/Vinyl Acetate) (PVP/VA) in a binary mixture, or both with a surfactant to compose a ternary mixture.

Hot-melt extrusion (HME) was the process used. Amorphous solid dispersion could be generated from binary and ternary mixtures in different twin-screw extruders (Pharma 11 and Pharma 16, Thermo Fisher).

The ternary formulations varied on the type of the surfactant used and API load (35%, 40% and 50 wt%). The two surfactants used were: 1. SLS, a solid surfactant used directly in the physical mixture prepared for extrusion; 2. SPAN 20, a liquid surfactant added to the solid mixture of PZQ and PVPVA in two ways: wet granulation before extrusion and direct addition to the molten material during extrusion).

*Regarding the praziquantel solubility in water:*

All ternary and binary extrudate forms proved to increase the apparent solubility, evidencing the solubilization behaviour of amorphous solid dispersions (produced totally or predominantly amorphous) with a spring effect on drug concentration observed mainly between the initial 30 and 60 min of the experiments in water at 37 °C.

More specifically, the apparent solubility could be increased 70 % to 90 % more than the equilibrium concentration in this medium.

Regarding the dissolution kinetics, it was also improved by these new ASDs, for example, 90 % of drug release in 1 h for the ternary formulation containing SPAN 20 as

a surfactant and 35 wt% of API (pharma 16), compared with the (crystalline) API alone. However, it is essential to mention that the characterization regarding particle sizes of the studied formulations needs to be improved to allow a better comparative analysis of their dissolution profiles and the effect of this parameter (particle size) on this kinetics.

This same formulation was used to carry out pharmacokinetic experiments on animals. Although the ASD pharmacokinetic assessment protocol will require some improvements, the results are promising and demonstrate that ASD approach (and the composition proposed) might be an alternative to overcoming the PZQ solubility challenge.

This issue was addressed, it remained another challenge that is the physical stability of these systems requiring high drug loads as those of interest here.

One of the main parameters affecting the physical stability of an ASD is the drug solubility in the carrier, because this value determines the maximal drug load without a risk of phase separation and recrystallization. In the thesis, a composition-temperature phase diagram Praziquantel - PVPVA was established. The determination of API-polymer solubility was performed from a supersaturated solid solution produced by spray drying. A recrystallization (thermal) method based on demixing was then applied. The diagram was built and through these data, it is possible to know if the binary system is above or below its saturation at a given temperature. With the valuable assistance of this diagram, new compositions that could make the system more stable could be tested.

Unexpectedly, in some batches of spray-dried powders produced in this study, traces of crystalline forms of PZQ were found, which are different from the initial racemic form. They might correspond to one of these polymorphic forms of PZQ recently reported. It is an interesting finding because, to the best of our knowledge, it was the first time that the new polymorphic forms of praziquantel are supposed to be formed from the recrystallization of an amorphous form.

***The second challenge is to mask the bitter taste of praziquantel.***

The unpleasant taste of praziquantel is also a problem when administering adult medicine to children. Unpleasant taste is crucial for adherence to paediatric treatment and, consequently, for effectiveness.

Extruded formulations (pellets) and printlets obtained positive results in all three forms of tests performed (in vivo, oral cavity dissolution, and electronic tongue), related to masking the bitter taste of praziquantel for both API load (50 and 35 wt%).

In vivo taste masking showed that a ternary formulation (FEXT 1) was better acceptable for rats than the commercial praziquantel tablets. This result was according to the in vitro test performed with electronic tongue.

Electronic tongue tested two extrudate formulations: FEXT 1 and FEXT 2. The first one showed better results indicating that the taste was better than the commercial PZQ tablets and FEXT 2. From the in vivo experiment, it was possible to demonstrate that the adaptation of the methodology using solution recirculation pumps is feasible and makes sure that the animal is always exposed to a homogeneous solution/suspension of the sample tested.

It is important to highlight that the electronic tongue sensors were adapted to determine the impedance, overcoming the limiting factor presented by currently commercialized equipment that does not allow the identification of taste for molecules with low conductivity characteristics such as praziquantel.

Oral cavity dissolution showed that the printlets obtained from two ternary formulations (both with 35 wt% of praziquantel) are considered well tolerable until the end of the experiment (600 seconds). The two formulations tested (pellets), and from which printlets were generated, have demonstrated better taste masking capacity in 1 minute of contact with artificial saliva, remaining below the well tolerable limit. Surprisingly, this same result was observed for pellets of different concentrations (35 and 50 wt%).

It is important to highlight that all taste masking tests in this thesis were performed with intermediate materials (extruded) and printlets as testing materials. There was no addition of excipients with taste-enhancing functionality (e.g., sweeteners, flavours). In this way, increments on pharmaceutical formulation can still be explored to optimize a medicine specifically designed for children.

***The third challenge for paediatric praziquantel is the need of accurate dose adjustment.***

As an alternative to overcome the challenge of adjusting the doses of a paediatric medicine based on PZQ for children, the use of 3D printing technology (FDM) with direct feeding of particulate material was proposed.

The prototypes produced at this stage of the study showed that 3D printing can be a viable tool for customizing doses since the design of the drug can be precisely adjusted.

In this thesis, we could demonstrate the possibility of obtaining two different doses (100 and 150 mg) using the ternary formulations obtained by HME. The printlets containing 35 wt% of API load and SPAN 20 as surfactant showed the best dissolution performance (81 % in 2 h). However, as previously mentioned, printlets were produced only with the extruded material, without the addition of taste masking or disintegrating agents. For the next steps, these formulations can be further improved both, in taste masking, and in increasing dissolution.

A major result was also obtained concerning the printability of particulate materials using this 3D printing technology that has a direct feed. It was not possible to directly print the physical mixtures containing 50% or 35% of API (with or without surfactant in the formulation), contrary to the previously existing literature. For this specific API, the use of previously processed materials represented better processability due to the change in physical characteristics such as less electrostatic charges and better flow. However, for PZQ, in addition to these characteristics, the amorphization obtained by HME is essential to address the first challenge described above, increasing solubility. Still, it was demonstrated that the use of pellets of extruded materials resulted in printlets, but the printing process showed little processability (need for constant cleaning of the printer). Amorphous solid dispersions produced by HME and shaped as powders seems to be the better technical solution for production of printlets of praziquantel for paediatric medicines by 3D printing technology (FDM) with direct feeding of solid material.

Nowadays, 3D printing technology i**s** beginning to be seen as promising for developing pharmaceutical products, and legislation, especially regarding the quality assessment of this type of product, needs to accompany this evolution. In this thesis, routine tests were presented to assess the quality of printlets, such as dissolution and content. However, it is essential to determine the need for specific tests and procedures to monitor the quality of these new products emerging on the market from 3D printing.

Although 3D printing has been presented as a strategy and with promising results, other paths can be followed to obtain a final pharmaceutical form suitable for paediatric patients. According to our results and the outcome of the discussions on the theme, there is still a need to optimize the amorphous solid dispersions produced here by hot melt extrusion, especially to achieve stability characteristics. The coating could be an additional step to test for improving their physical stability against exposition to environmental conditions. In this sense, a few experiments were performed during this thesis (not presented in the manuscript) from which the interest of this technical

improvement was demonstrated. Coated amorphous solid dispersions could create an opening for another pharmaceutical form that is their use in the form of a sachet.

.

# CHAPTER 8 - BIBLIOGRAPHY

[1] O. MONDIALE and D. LA SANTÉ, “Schistosomiasis : number of people treated worldwide in 2014 Schistosomiase : nombre de personnes traitées dans le monde en 2014,” *Wkly. Epidemiol. Rec.*, vol. 30, no. 5, pp. 25–31, 2015.

[2] M. L. Nelwan, “Schistosomiasis: Life Cycle, Diagnosis, and Control,” *Curr. Ther. Res. - Clin. Exp.*, vol. 91, no. 24, pp. 5–9, 2019, doi: 10.1016/j.curtheres.2019.06.001.

[3] E. Y. Li, D. Gurarie, N. C. Lo, X. Zhu, and C. H. King, “Improving public health control of schistosomiasis with a modified WHO strategy : a model-based comparison study,” *Lancet Glob. Heal.*, vol. 7, no. 10, pp. e1414–e1422, 2019, doi: 10.1016/S2214-109X(19)30346-8.

[4] L. B. da Fonseca, “DESENVOLVIMENTO DE NANOPARTÍCULAS POLIMÉRICAS CONTENDO PRAZIQUANTEL PARA O TRATAMENTO DA ESQUISTOSSOMOSE,” Universidade Federal do Rio de Janeiro, 2012.

[5] H. Wang *et al.*, “Metabolic profiling of praziquantel enantiomers,” vol. 90, pp. 166–178, 2014.

[6] P. T. Loverde, “Digenetic Trematodes,” in *Schistosomiasis*, R. T. Fried, Ed. Springer, 2019.

[7] D. P. Mcmanus, D. W. Dunne, M. Sacko, N. Zhou, and B. J. Vennervald, “Schistosomiasis,” *Nat. Rev. Dis. Prim.*, pp. 1–19, 2018, doi: 10.1038/s41572-018-0013-8.

[8] J. P. Soldati, “Dose maior é sinônimo de eficácia ?,” *Inf. IOC. Inst. Oswaldo Cruz/Fiocruz* -, p. 2012, 2011.

[9] R. Trastullo, L. S. Dolci, N. Passerini, and B. Albertini, “Development of flexible and dispersible oral formulations containing praziquantel for potential schistosomiasis treatment of pre-school age children,” *Int. J. Pharm.*, vol. 495, no. 1, pp. 536–550, 2015, doi: 10.1016/j.ijpharm.2015.09.019.

[10] D. Zanolla *et al.*, “A new soluble and bioactive polymorph of praziquantel,” *Eur. J. Pharm. Biopharm.*, vol. 127, no. January, pp. 19–28, 2018, doi: 10.1016/j.ejpb.2018.01.018.

[11] A. A. L. Carvalho, A. C. Mafud, P. L. S. Pinto, Y. P. Mascarenhas, and J. De

Moraes, “Schistosomicidal effect of the anti-inflammatory drug diclofenac and its structural correlation with praziquantel,” *Int. J. Antimicrob. Agents*, vol. 44, no. 4, pp. 372–374, 2014, doi: 10.1016/j.ijantimicag.2014.06.018.

[12] Alan Lane de Melo and P. M. Z. Coelho, *Parasitologia Humana - Leishmaniose Visceral Americana*. 2007.

[13] Ministério da Saúde, *Guide to Health Surveillance*. 2019.

[14] M. da S. BRASIL, “MANSONI Diretrizes Técnicas Diretrizes técnicas,” 2014.

[15] K. E. R. Silva, R. M. F. Silva, S. P. M. Costa, L. A. Rolim, M. do C. A. Lima, and P. J. Rolim-Neto, “Alternativas terapêuticas no combate à Esquistossomose Mansônica,” *Rev. Ciencias Farm. Basica e Apl.*, vol. 33, no. 1, pp. 9–16, 2012.

[16] C. V. V. Rollemberg *et al.*, “Aspectos epidemiológicos e distribuição geográfica da esquistossomose e geo-helmintos, no Estado de Sergipe, de acordo com os dados do Programa de Controle da Esquistossomose,” *Rev. Soc. Bras. Med. Trop.*, vol. 44, no. 1, pp. 91–96, 2011, doi: 10.1590/s0037-86822011000100020.

[17] M. L. A. Ferrari, P. M. Z. Coelho, C. M. F. Antunes, C. A. P. Tavares, and A. S. Da Cunha, “Efficacy of oxamniquine and praziquantel in the treatment of Schistosoma mansoni infection: A controlled trial,” *Bull. World Health Organ.*, vol. 81, no. 3, pp. 190–196, 2003, doi: 10.1590/S0042-96862003000300009.

[18] R. E. Zaparoli, “2011 Sorocaba / SP,” 2011.

[19] 2013. Pernambuco. Secretaria Estadual de Saúde. Secretaria Executiva de Vigilância em Saúde. Programa de Enfretamento das Doenças Negligenciadas no Estado de Pernambuco SANAR – 2011 / 2014 / Secretaria Estadual de Saúde. Secretaria Executiva de Vigilância em Sa, “SANAR. Programa de enfrentamento às doenças negligenciadas.”

[20] L. B. Da Fonseca *et al.*, “Desenvolvimento de um medicamento brasileiro nanoencapsulado para o tratamento da esquistossomose,” *Vigilância Sanitária em Debate*, vol. 1, no. 4, pp. 85–91, 2013, doi: 10.3395/vd.v1i4.111pt.

[21] J. Zwang and P. L. Olliaro, “Clinical Efficacy and Tolerability of Praziquantel for Intestinal and Urinary Schistosomiasis—A Meta-analysis of Comparative and Non-comparative Clinical Trials,” *PLoS Negl. Trop. Dis.*, vol. 8, no. 11, 2014, doi: 10.1371/journal.pntd.0003286.

[22] N. Katz and P. M. Z. Coelho, “Clinical therapy of schistosomiasis mansoni: The Brazilian contribution,” *Acta Trop.*, vol. 108, no. 2–3, pp. 72–78, 2008, doi: 10.1016/j.actatropica.2008.05.006.

[23] V. B. R. da Silva, B. R. K. L. Campos, J. F. de Oliveira, J. L. Decout, and M. do Carmo Alves de Lima, “Medicinal chemistry of antischistosomal drugs: Praziquantel and oxamniquine,” *Bioorganic Med. Chem.*, vol. 25, no. 13, pp. 3259–3277, 2017, doi: 10.1016/j.bmc.2017.04.031.

[24] M. R. Carvalho Garbi Novaes, J. P. de Souza, and H. Clemente de Araújo, “Anthelmintic praziquantel synthesis from glycine,” *Quim. Nova*, no. 1, pp. 5–10, 1999.

[25] A. Borrego-Sánchez *et al.*, “Conformational polymorphic changes in the crystal structure of the chiral antiparasitic drug praziquantel and interactions with calcium carbonate,” *Eur. J. Pharm. Biopharm.*, vol. 132, no. July, pp. 180–191, 2018, doi: 10.1016/j.ejpb.2018.09.028.

[26] F. C. Lombardo, V. Pasche, G. Panic, Y. Endriss, and J. Keiser, “Life cycle maintenance and drug-sensitivity assays for early drug discovery in Schistosoma mansoni,” *Nat. Protoc.*, vol. 14, no. 2, pp. 461–481, 2019, doi: 10.1038/s41596-018-0101-y.

[27] S. K. Park *et al.*, “The anthelmintic drug praziquantel activates a schistosome transient receptor potential channel,” *J. Biol. Chem.*, vol. 294, no. 49, pp. 18873–18880, 2019, doi: 10.1074/jbc.AC119.011093.

[28] WHO, “WHO Model Lists of Essential Medicines - Praziquantel,” 2021.

[29] C. S. Ferreira Marques *et al.*, “Solid dispersion of praziquantel enhanced solubility and improve the efficacy of the schistosomiasis treatment,” *J. Drug Deliv. Sci. Technol.*, vol. 45, no. December 2017, pp. 124–134, 2018, doi: 10.1016/j.jddst.2018.03.009.

[30] D. Zanolla *et al.*, “A new soluble and bioactive polymorph of praziquantel,” *Eur. J. Pharm. Biopharm.*, vol. 127, no. August 2017, pp. 19–28, 2018, doi: 10.1016/j.ejpb.2018.01.018.

[31] D. Cioli, L. Pica-mattoccia, A. Basso, and A. Guidi, “Schistosomiasis control : praziquantel forever ?,” *Mol. Biochem. Parasitol.*, vol. 195, no. 1, pp. 23–29, 2014,

doi: 10.1016/j.molbiopara.2014.06.002.

[32] A. M. de L. A. B. E. de A. B. E. de O. L. S. de C. Barros, *Re lação Na cional de Me dicamentos Essenciais Re lação Na cional de Me dicamentos Essenciais*. 2020.

[33] J. C. Espinosa-Lara *et al.*, "Cocrystals of active pharmaceutical ingredients - Praziquantel in combination with oxalic, malonic, succinic, maleic, fumaric, glutaric, adipic, and pimelic acids," *Cryst. Growth Des.*, vol. 13, no. 1, pp. 169–185, 2013, doi: 10.1021/cg301314w.

[34] A. Borrego-Sánchez, C. Viseras, C. Aguzzi, and C. I. Sainz-Díaz, "Molecular and crystal structure of praziquantel. Spectroscopic properties and crystal polymorphism," *Eur. J. Pharm. Sci.*, vol. 92, pp. 266–275, 2016, doi: 10.1016/j.ejps.2016.04.023.

[35] WHO, "International strategies for tropical disease treatments - Experiences with praziquantel," 1998.

[36] WHO, "Schistosomiasis in children_ a major public health problem," pp. 1–3, 2017, [Online]. Available: https://www.pediatricpraziquantelconsortium.org/schistosomiasis.

[37] M. Cugovčan, J. Jablan, J. Lovrić, D. Cinčić, N. Galić, and M. Jug, "Biopharmaceutical characterization of praziquantel cocrystals and cyclodextrin complexes prepared by grinding," *J. Pharm. Biomed. Anal.*, vol. 137, pp. 42–53, 2017, doi: 10.1016/j.jpba.2017.01.025.

[38] M. J. Doenhoff, D. Cioli, and J. Utzinger, "Praziquantel: Mechanisms of action, resistance and new derivatives for schistosomiasis," *Curr. Opin. Infect. Dis.*, vol. 21, no. 6, pp. 659–667, 2008, doi: 10.1097/QCO.0b013e328318978f.

[39] W. Wu, W. Wang, and Y. X. Huang, "New insight into praziquantel against various developmental stages of schistosomes," *Parasitol. Res.*, vol. 109, no. 6, pp. 1501–1507, 2011, doi: 10.1007/s00436-011-2670-3.

[40] F. C. Lombardo, B. Perissutti, and J. Keiser, "Activity and pharmacokinetics of a praziquantel crystalline polymorph in the Schistosoma mansoni mouse model," *Eur. J. Pharm. Biopharm.*, vol. 142, no. June, pp. 240–246, 2019, doi: 10.1016/j.ejpb.2019.06.029.

[41] J. Kovač, M. Vargas, and J. Keiser, "In vitro and in vivo activity of R- and S-

praziquantel enantiomers and the main human metabolite trans-4-hydroxy-praziquantel against Schistosoma haematobium," *Parasites and Vectors*, vol. 10, no. 1, pp. 3–7, 2017, doi: 10.1186/s13071-017-2293-3.

[42] T. Meyer, H. Sekljic, S. Fuchs, H. Bothe, D. Schollmeyer, and C. Miculka, "Taste, a new incentive to switch to (R)-praziquantel in schistosomiasis treatment," *PLoS Negl. Trop. Dis.*, vol. 3, no. 1, pp. 3–7, 2009, doi: 10.1371/journal.pntd.0000357.

[43] D. Zhang, H. Wang, J. Ji, L. Nie, and D. Sun, "A quantification method for determination of racemate praziquantel and R-enantiomer in rat plasma for comparison of their pharmacokinetics," *J. Chromatogr. B*, vol. 1048, pp. 64–69, 2017, doi: 10.1016/j.jchromb.2017.02.013.

[44] I. Meister *et al.*, "Activity of praziquantel enantiomers and main metabolites against Schistosoma mansoni," *Antimicrob. Agents Chemother.*, vol. 58, no. 9, pp. 5466–5472, 2014, doi: 10.1128/AAC.02741-14.

[45] W. M. Bagchus, D. Bezuidenhout, E. Harrison-moench, E. Kourany-lefoll, and P. Wolna, "Relative Bioavailability of Orally Dispersible Tablet Formulations of Levo- - and Racemic Praziquantel : Two Phase I Studies," no. December 2018, pp. 66–76, 2019, doi: 10.1111/cts.12601.

[46] G. Z. Id and F. Mutapi, "Drug metabolism and pharmacokinetics of praziquantel : A review of variable drug exposure during schistosomiasis treatment in human hosts and experimental models," pp. 1–26, 2020, doi: 10.1371/journal.pntd.0008649.

[47] ANVISA, "Consulta Medicamentos ANVISA - Praziquantel," 2020.

[48] Merck, "Bula Cisticid 500mg Merck."

[49] F.- Fiocruz, "Praziquantel - DMG-FAR-PRO-PRZ-001-2017," in *Memento Terapeutico*, 2017, pp. 1–9.

[50] A. Garba *et al.*, "Acta Tropica Schistosomiasis in infants and preschool-aged children : Infection in a single Schistosoma haematobium and a mixed S . haematobium – S . mansoni foci of Niger," vol. 115, no. May 2001, pp. 212–219, 2010, doi: 10.1016/j.actatropica.2010.03.005.

[51] M. Woelfle, J. Seerden, J. De Gooijer, K. Pouwer, P. Olliaro, and H. Matthew, "Resolution of Praziquantel," vol. 5, no. 9, pp. 1–7, 2013, doi:

10.1371/journal.pntd.0001260.

[52] S. Botros, N. El-lakkany, S. H. Seif, A. Sabra, and M. Ibrahim, “Experimental Parasitology Comparative efficacy and bioavailability of different praziquantel brands,” *Exp. Parasitol.*, vol. 127, no. 2, pp. 515–521, 2011, doi: 10.1016/j.exppara.2010.10.019.

[53] The United States Pharmaceutical Convention., “USP43 Praziquantel API,” p. 3649, 2020.

[54] ANVISA, “Farmacopeia Brasileira Volume II – Monografias Insumos Farmacêuticos e Especialidades,” *Farm. Bras.*, vol. 2, pp. 1–1504, 2019.

[55] U. S. N. L. of Medicine, “ChemIDplus Advanced - Chemical information - Praziquantel,” 2021.

[56] E. S. Bochmann, A. Gryczke, and K. G. Wagner, “Validation of Model-Based Melt Viscosity in Hot-Melt Extrusion Numerical Simulation,” pp. 9–12, 2018, doi: 10.3390/pharmaceutics10030132.

[57] U. S. P. Convention, “Promoting the Quality of Medicines (PQM). Product Information Report: Praziquantel,” Rockville, Maryland., 2019.

[58] N. Passerini, B. Albertini, B. Perissutti, and L. Rodriguez, “Evaluation of melt granulation and ultrasonic spray congealing as techniques to enhance the dissolution of praziquantel,” *Int. J. Pharm.*, vol. 318, no. 1–2, pp. 92–102, 2006, doi: 10.1016/j.ijpharm.2006.03.028.

[59] D. Zanolla *et al.*, “Milling and comilling Praziquantel at cryogenic and room temperatures: Assessment of the process-induced effects on drug properties,” *J. Pharm. Biomed. Anal.*, vol. 153, pp. 82–89, 2018, doi: 10.1016/j.jpba.2018.02.018.

[60] B. Albertini *et al.*, “Combining mechanochemistry and spray congealing for new praziquantel pediatric formulations in schistosomiasis treatment,” *Int. J. Mol. Sci.*, vol. 20, no. 5, 2019, doi: 10.3390/ijms20051233.

[61] M. Münster, C. Schoch, C. Schmidt, and J. Breitkreutz, “Multiparticulate system combining taste masking and immediate release properties for the aversive compound praziquantel,” *Eur. J. Pharm. Sci.*, vol. 109, no. August, pp. 446–454, 2017, doi: 10.1016/j.ejps.2017.08.034.

[62] P. Olliaro, P. Delgado-romero, and J. Keiser, “The little we know about the pharmacokinetics and pharmacodynamics of praziquantel ( racemate and R - enantiomer ),” no. January, pp. 863–870, 2014, doi: 10.1093/jac/dkt491.

[63] P. R. Dametto, A. C. Dametto, L. Polese, C. A. Ribeiro, M. Chorilli, and O. de Freitas, “Development and physicochemical characterization of solid dispersions containing praziquantel for the treatment of schistosomiasis,” *J. Therm. Anal. Calorim.*, vol. 127, no. 2, pp. 1693–1706, 2017, doi: 10.1007/s10973-016-5759-1.

[64] PUBCHEM, “Praziquantel - Chemical and Physical Properties,” 2019.

[65] E. D. Costa *et al.*, “Unexpected solvent impact in the crystallinity of praziquantel/poly(vinylpyrrolidone) formulations. A solubility, DSC and solid-state NMR study,” *Int. J. Pharm.*, vol. 511, no. 2, pp. 983–993, 2016, doi: 10.1016/j.ijpharm.2016.08.009.

[66] M. V. Chaud *et al.*, “Development and evaluation of praziquantel solid dispersions in sodium starch glycolate,” *Trop. J. Pharm. Res.*, vol. 12, no. 2, pp. 163–168, 2013, doi: 10.4314/tjpr.v12i2.5.

[67] S. K. El-arini and H. Leuenberger, “Dissolution properties of praziquantel – PVP systems,” pp. 89–94, 1998.

[68] M. Münster *et al.*, “Comparative in vitro and in vivo taste assessment of liquid praziquantel formulations,” *Int. J. Pharm.*, vol. 529, no. 1–2, pp. 310–318, 2017, doi: 10.1016/j.ijpharm.2017.06.084.

[69] A. Gaggero *et al.*, “Co-grinding with surfactants as a new approach to enhance in vitro dissolution of praziquantel,” *J. Pharm. Biomed. Anal.*, vol. 189, 2020, doi: 10.1016/j.jpba.2020.113494.

[70] S. K. El-Arini, D. Giron, and H. Leuenberger, “Solubility properties of racemic praziquantel and its enantiomers,” *Pharm. Dev. Technol.*, vol. 3, no. 4, pp. 557–564, 1998, doi: 10.3109/10837459809028638.

[71] K.-K. and C. B. C. Yue Liu, Xin Wang, “Investigation of the phase diagrams of chiral praziquantel,” *Chirality*, vol. 18, pp. 259–264, 2006, doi: 10.1002/chir.

[72] A. Cedillo-Cruz, M. I. Aguilar, M. Flores-Alamo, F. Palomares-Alonso, and H. Jung-Cook, “A straightforward and efficient synthesis of praziquantel enantiomers and their 4′-hydroxy derivatives,” *Tetrahedron Asymmetry*, vol. 25, no. 2, pp. 133–

140, 2014, doi: 10.1016/j.tetasy.2013.11.004.

[73] D. Zanolla *et al.*, “Exploring mechanochemical parameters using a DoE approach: Crystal structure solution from synchrotron XRPD and characterization of a new praziquantel polymorph,” *Eur. J. Pharm. Sci.*, vol. 140, no. October, p. 105084, 2019, doi: 10.1016/j.ejps.2019.105084.

[74] D. Salazar-Rojas, R. M. Maggio, and T. S. Kaufman, “Preparation and characterization of a new solid form of praziquantel, an essential anthelmintic drug. Praziquantel racemic monohydrate,” *Eur. J. Pharm. Sci.*, vol. 146, no. December 2019, p. 105267, 2020, doi: 10.1016/j.ejps.2020.105267.

[75] D. Zanolla *et al.*, “Mechanochemical formation of racemic praziquantel hemihydrate with improved biopharmaceutical properties,” *Pharmaceutics*, vol. 12, no. 3, pp. 1–22, 2020.

[76] G. L. Amidon, H. Lennernäs, V. P. Shah, and J. R. Crison, “A Theoretical Basis for a Biopharmaceutic Drug Classification: The Correlation of in Vitro Drug Product Dissolution and in Vivo Bioavailability,” *Pharmaceutical Research: An Official Journal of the American Association of Pharmaceutical Scientists*, vol. 12, no. 3. pp. 413–420, 1995, doi: 10.1023/A:1016212804288.

[77] A. Charalabidis, M. Sfouni, C. Bergström, and P. Macheras, “The Biopharmaceutics Classification System (BCS) and the Biopharmaceutics Drug Disposition Classification System (BDDCS): Beyond guidelines,” *Int. J. Pharm.*, vol. 566, no. April, pp. 264–281, 2019, doi: 10.1016/j.ijpharm.2019.05.041.

[78] S. Baghel, H. Cathcart, and N. J. O. Reilly, “Polymeric Amorphous Solid Dispersions : A Review of Amorphization , Crystallization , Stabilization , Solid-State Characterization , and Aqueous Solubilization of Biopharmaceutical Classi fi cation System Class II Drugs,” *J. Pharm. Sci.*, 2016, doi: 10.1016/j.xphs.2015.10.008.

[79] K. Göke *et al.*, “European Journal of Pharmaceutics and Biopharmaceutics Novel strategies for the formulation and processing of poorly water- soluble drugs,” *Eur. J. Pharm. Biopharm.*, vol. 126, pp. 40–56, 2018, doi: 10.1016/j.ejpb.2017.05.008.

[80] A. Keeley *et al.*, “In Vitro Dissolution Model Can Predict the in Vivo Taste Masking Performance of Coated Multiparticulates,” *Mol. Pharm.*, vol. 16, no. 5,

pp. 2095–2105, 2019, doi: 10.1021/acs.molpharmaceut.9b00060.

[81] X. Nsabagasani *et al.*, “The ‘child size medicines’ concept: Policy provisions in Uganda,” *J. Pharm. Policy Pract.*, vol. 8, no. 1, pp. 1–9, 2015, doi: 10.1186/s40545-015-0025-7.

[82] V. Klingmann *et al.*, “Acceptability of an orodispersible film compared to syrup in neonates and infants: A randomized controlled trial,” *Eur. J. Pharm. Biopharm.*, vol. 151, no. December 2019, pp. 239–245, 2020, doi: 10.1016/j.ejpb.2020.03.018.

[83] European Commission, “State of Paediatric Medicines in the EU: 10 years of the EU Paediatric Regulation,” *DG Heal. Consum.*, pp. 1–17, 2017.

[84] V. Ivanovska, C. M. A. Rademaker, L. Van Dijk, and A. K. Mantel-Teeuwisse, “Pediatric drug formulations: A review of challenges and progress,” *Pediatrics*, vol. 134, no. 2, pp. 361–372, 2014, doi: 10.1542/peds.2013-3225.

[85] K. Vithani and D. Douroumis, “Hot-melt extruded lipidic pellets for pediatric applications : An investigation of the e ff ects and stability on drug dissolution,” *J. Drug Deliv. Sci. Technol.*, vol. 49, no. August 2018, pp. 43–49, 2019, doi: 10.1016/j.jddst.2018.10.033.

[86] R. Ternik *et al.*, “Assessment of swallowability and palatability of oral dosage forms in children: Report from an M-CERSI pediatric formulation workshop,” *Int. J. Pharm.*, vol. 536, no. 2, pp. 570–581, 2018, doi: 10.1016/j.ijpharm.2017.08.088.

[87] L. Freerks, J. Sommerfeldt, P. C. Löper, and S. Klein, “Safe, swallowable and palatable paediatric mini-tablet formulations for a WHO model list of essential medicines for children compound – A promising starting point for future PUMA applications,” *Eur. J. Pharm. Biopharm.*, vol. 156, no. August, pp. 11–19, 2020, doi: 10.1016/j.ejpb.2020.08.014.

[88] N. Mendonsa *et al.*, “Manufacturing strategies to develop amorphous solid dispersions: An overview,” *J. Drug Deliv. Sci. Technol.*, vol. 55, no. December 2019, p. 101459, 2020, doi: 10.1016/j.jddst.2019.101459.

[89] G. C. Bazzo, B. R. Pezzini, and H. K. Stulzer, “Eutectic mixtures as an approach to enhance solubility , dissolution rate and oral bioavailability of poorly water-soluble drugs,” *Int. J. Pharm.*, vol. 588, no. May, p. 119741, 2020, doi: 10.1016/j.ijpharm.2020.119741.

[90] A. Batra, D. Desai, and A. T. M. Serajuddin, “Conversion of α-lactose monohydrate to anhydrous form with superior tabletability by twin-screw extrusion at elevated temperature,” *Int. J. Pharm.*, vol. 588, no. July, p. 119790, 2020, doi: 10.1016/j.ijpharm.2020.119790.

[91] S. Jacob and A. B. Nair, “Cyclodextrin complexes : Perspective from drug delivery and formulation,” no. May, pp. 201–217, 2018, doi: 10.1002/ddr.21452.

[92] A. Ramrao, T. Id, and J. N. Yadav, “A Review on Solid Dispersion and Carriers Used Therein for Solubility Enhancement of Poorly Water Soluble Drugs,” *Tabriz Univ. Med. Sci.*, vol. 10, no. 3, pp. 359–369, 2020, doi: 10.34172/apb.2020.044.

[93] J. Keiser, H. Sayed, M. El-ghanam, H. Sabry, S. Anani, and A. El-wakeel, “Efficacy and Safety of Artemether in the Treatment of Chronic Fascioliasis in Egypt : Exploratory Phase-2 Trials,” vol. 5, no. 9, 2011, doi: 10.1371/journal.pntd.0001285.

[94] S. E. Gerrard, J. Walsh, N. Bowers, S. Salunke, and S. Hershenson, “Innovations in Pediatric Drug Formulations and Administration Technologies for Low Resource Settings,” 2019.

[95] W. H. O. E. Committee, W. H. O. M. List, E. Medicines, W. H. O. M. List, and E. Medicines, “THE SELECTION AND USE OF ESSENTIAL MEDICINES Report of the WHO Expert Committee , 2009 ( including the 16th WHO Model List of Essential Medicines and the 2nd WHO Model List of Essential Medicines for Children ),” 2009.

[96] W. H. O. E. Committee, W. H. O. M. List, E. Medicines, M. List, and E. Medicines, “The Selection and Use of Essential Medicines,” 2017.

[97] B. Group, “BNF for Children. The essencial resource for clinical use of medicines in children,” UK.

[98] V. Anand, M. Kataria, V. Kukkar, V. Saharan, and P. K. Choudhury, “The latest trends in the taste assessment of pharmaceuticals,” *Drug Discov. Today*, vol. 12, no. 5–6, pp. 257–265, 2007, doi: 10.1016/j.drudis.2007.01.010.

[99] P. Kozarewicz, “Regulatory perspectives on acceptability testing of dosage forms in children,” *Int. J. Pharm.*, vol. 469, no. 2, pp. 245–248, 2014, doi: 10.1016/j.ijpharm.2014.03.057.

[100] European Medicines Agency (EMA), “Guideline on pharmaceutical development of medicines for paediatric use,” *European Medicines Agency*, vol. rev 2. London, UK, pp. 1–24, 2013, [Online]. Available: https://www.ema.europa.eu/en/documents/scientific-guideline/guideline-pharmaceutical-development-medicines-paediatric-use_en.pdf.

[101] M. Moreira and M. Sarraguça, “How can oral paediatric formulations be improved? A challenge for the XXI century,” *Int. J. Pharm.*, vol. 590, no. July, p. 119905, 2020, doi: 10.1016/j.ijpharm.2020.119905.

[102] F. Rodieux, M. Wilbaux, J. N. Van Den Anker, and M. Pfister, “Effect of Kidney Function on Drug Kinetics and Dosing in Neonates , Infants , and Children,” *Clin. Pharmacokinet.*, 2015, doi: 10.1007/s40262-015-0298-7.

[103] J. T. Coulibaly, G. Panic, K. D. Silué, J. Kovač, J. Hattendorf, and J. Keiser, “Efficacy and safety of praziquantel in preschool-aged and school-aged children infected with Schistosoma mansoni: a randomised controlled, parallel-group, dose-ranging, phase 2 trial,” *Lancet Glob. Heal.*, vol. 5, no. 7, pp. e688–e698, 2017, doi: 10.1016/S2214-109X(17)30187-0.

[104] M. K. Freeman, W. White, and M. Iranikhah, “Tablet Splitting: A Review of Weight and Content Uniformity,” *Consult. Pharm. may*, vol. 27, no. 5, pp. 341–352, 2012.

[105] J.-P. R. & M. P. Charlotte Verrue, Els Mehuys, Koen Boussery, “Tablet-splitting : a common yet not so innocent practice,” *J. Adv. Nurs.*, vol. 67, no. 1, pp. 26–32, 2010, doi: 10.1111/j.1365-2648.2010.05477.x.

[106] H. R. Devantier *et al.*, “Quantitative assessment of TRPM5-dependent oral aversiveness of pharmaceuticals using a mouse brief-access taste aversion assay,” *Behav. Pharmacol.*, vol. 19, no. 7, pp. 673–682, 2008, doi: 10.1097/FBP.0b013e3283123cd6.

[107] S. M. Hanning, F. L. Lopez, I. C. K. Wong, T. B. Ernest, C. Tuleu, and M. Orlu Gul, “Patient centric formulations for paediatrics and geriatrics: Similarities and differences,” *Int. J. Pharm.*, vol. 512, no. 2, pp. 355–359, 2016, doi: 10.1016/j.ijpharm.2016.03.017.

[108] E. Grossi, F. Pace, and R. Stockbrugger, “Human nutrition from the

gastroenterologist's perspective: Lessons from expo milano 2015," *Hum. Nutr. From Gastroenterol. Perspect. Lessons From Expo Milano 2015*, pp. 1–213, 2016, doi: 10.1007/978-3-319-30361-1.

[109] J. Walsh *et al.*, "Playing hide and seek with poorly tasting paediatric medicines : Do not forget the excipients ☆," *Adv. Drug Deliv. Rev.*, vol. 73, pp. 14–33, 2014, doi: 10.1016/j.addr.2014.02.012.

[110] C. S. Mennella JA, Spector AC, Reed DR, "Bad taste of medicines," *Clin Ther*, vol. 35, no. 8, pp. 1225–1246, 2013, doi: 10.1016/j.clinthera.2013.06.007.The.

[111] R. Ternik *et al.*, "Assessment of swallowability and palatability of oral dosage forms in children: Report from an M-CERSI pediatric formulation workshop," *Int. J. Pharm.*, vol. 536, no. 2, pp. 570–581, 2018, doi: 10.1016/j.ijpharm.2017.08.088.

[112] A. A. Lee and C. Owyang, *Sugars, sweet taste receptors, and brain responses*. Elsevier Inc., 2019.

[113] R. Bala, S. badjatya, and R. Madaan, "Strategies practiced to perk up oral palatability and acceptance of bitter drugs," *J. Drug Deliv. Sci. Technol.*, vol. 56, no. February, p. 101580, 2020, doi: 10.1016/j.jddst.2020.101580.

[114] A. H. A. Mohamed-Ahmed, J. Soto, T. Ernest, and C. Tuleu, "Non-human tools for the evaluation of bitter taste in the design and development of medicines: A systematic review," *Drug Discov. Today*, vol. 21, no. 7, pp. 1170–1180, 2016, doi: 10.1016/j.drudis.2016.05.014.

[115] C. P. Milne and J. B. Bruss, "The economics of pediatric formulation development for off-patent drugs," *Clin. Ther.*, vol. 30, no. 11, pp. 2133–2145, 2008, doi: 10.1016/j.clinthera.2008.11.019.

[116] R. V. Tiwari, A. N. Polk, H. Patil, X. Ye, M. B. Pimparade, and M. A. Repka, "Rat Palatability Study for Taste Assessment of Caffeine Citrate Formulation Prepared via Hot-Melt Extrusion Technology," *AAPS PharmSciTech*, vol. 18, no. 2, pp. 341–348, 2017, doi: 10.1208/s12249-015-0447-1.

[117] A. V Keating, J. Soto, C. Tuleu, C. Forbes, M. Zhao, and D. Q. M. Craig, "Solid state characterisation and taste masking ef fi ciency evaluation of polymer based extrudates of isoniazid for paediatric administration," *Int. J. Pharm.*, vol. 536, no. 2, pp. 536–546, 2018, doi: 10.1016/j.ijpharm.2017.07.008.

[118] M. Münster, “Paediatric drug development for praziquantel,” 2018.

[119] J. Soto *et al.*, “Rats can predict aversiveness of Active Pharmaceutical Ingredients,” *Eur. J. Pharm. Biopharm.*, vol. 133, no. August, pp. 77–84, 2018, doi: 10.1016/j.ejpb.2018.09.027.

[120] S. D.-B. Gesine Winzenburg∗, “Industry perspective on palatability testing in children—Two case studies,” *Tech. Res. Dev. Novartis Pharma AG, Basel CH 4056, Switz.*, vol. 2012, no. 435, pp. 131–151, 2012.

[121] A. Riul, C. A. R. Dantas, C. M. Miyazaki, and O. N. Oliveira, “Recent advances in electronic tongues,” *Analyst*, vol. 135, no. 10, pp. 2481–2495, 2010, doi: 10.1039/c0an00292e.

[122] K. C. Berridge, “Measuring hedonic impact in animals and infants: Microstructure of affective taste reactivity patterns,” *Neurosci. Biobehav. Rev.*, vol. 24, no. 2, pp. 173–198, 2000, doi: 10.1016/S0149-7634(99)00072-X.

[123] S. Gittings, N. Turnbull, C. J. Roberts, and P. Gershkovich, “Dissolution methodology for taste masked oral dosage forms,” *J. Control. Release*, vol. 173, no. 1, pp. 32–42, 2014, doi: 10.1016/j.jconrel.2013.10.030.

[124] D. H. Choi, N. A. Kim, T. S. Nam, S. Lee, and S. H. Jeong, “Evaluation of taste-masking effects of pharmaceutical sweeteners with an electronic tongue system,” *Drug Dev. Ind. Pharm.*, vol. 40, no. 3, pp. 308–317, 2014, doi: 10.3109/03639045.2012.758636.

[125] M. Maniruzzaman, J. S. Boateng, M. Bonnefille, A. Aranyos, J. C. Mitchell, and D. Douroumis, “Taste masking of paracetamol by hot-melt extrusion: An in vitro and in vivo evaluation,” *Eur. J. Pharm. Biopharm.*, vol. 80, no. 2, pp. 433–442, 2012, doi: 10.1016/j.ejpb.2011.10.019.

[126] M. Guhmann, M. Preis, F. Gerber, N. Pöllinger, J. Breitkreutz, and W. Weitschies, “Development of oral taste masked diclofenac formulations using a taste sensing system,” *Int. J. Pharm.*, vol. 438, no. 1–2, pp. 81–90, 2012, doi: 10.1016/j.ijpharm.2012.08.047.

[127] G. A. Campbell *et al.*, “Evaluating the taste masking effectiveness of various flavors in a stable formulated pediatric suspension and solution using the Astree trade; electronic tongue,” *Powder Technol.*, vol. 224, pp. 109–123, 2012, doi:

10.1016/j.powtec.2012.02.038.

[128] H. Nakamura, S. Uchida, T. Sugiura, and N. Namiki, “The prediction of the palatability of orally disintegrating tablets by an electronic gustatory system,” *Int. J. Pharm.*, vol. 493, no. 1–2, pp. 305–312, 2015, doi: 10.1016/j.ijpharm.2015.07.056.

[129] Y. Deng, L. Shen, Y. Yang, and J. Shen, “Development of nanoparticle-based orodispersible palatable pediatric formulations,” *Int. J. Pharm.*, vol. 596, no. January, p. 120206, 2021, doi: 10.1016/j.ijpharm.2021.120206.

[130] M. Wesoły, M. Zabadaj, A. Amelian, K. Winnicka, W. Wróblewski, and P. Ciosek, “Tasting cetirizine-based microspheres with an electronic tongue,” *Sensors Actuators, B Chem.*, vol. 238, pp. 1190–1198, 2017, doi: 10.1016/j.snb.2016.06.147.

[131] K. Woertz, C. Tissen, P. Kleinebudde, and J. Breitkreutz, “A comparative study on two electronic tongues for pharmaceutical formulation development,” *J. Pharm. Biomed. Anal.*, vol. 55, no. 2, pp. 272–281, 2011, doi: 10.1016/j.jpba.2011.02.002.

[132] J. B. KATHARINA WOERTZ, CORINNA TISSEN, PETER KLEINEBUDDE, “Development of a Taste-Masked Generic Ibuprofen Suspension: Top-Down Approach Guided by Electronic Tongue Measurements,” *J. Pharm. Sci.*, vol. 100, no. 10, pp. 4460–4470, 2011, doi: DOI 10.1002/jps.22629.

[133] L. I. Immohr *et al.*, “Early pediatric formulation development with new chemical entities: Opportunities of e-tongue besides human taste assessment,” *Int. J. Pharm.*, vol. 530, no. 1–2, pp. 201–212, 2017, doi: 10.1016/j.ijpharm.2017.07.069.

[134] J. C. Machado *et al.*, “Efficient praziquantel encapsulation into polymer microcapsules and taste masking evaluation using an electronic tongue,” *Bull. Chem. Soc. Jpn.*, vol. 91, no. 6, pp. 865–874, 2018, doi: 10.1246/bcsj.20180005.

[135] M. Pein, M. Preis, C. Eckert, and F. E. Kiene, “Taste-masking assessment of solid oral dosage forms – A critical review,” *Int. J. Pharm.*, vol. 465, no. 1–2, pp. 239–254, 2014, doi: 10.1016/j.ijpharm.2014.01.036.

[136] M. W. J. Dodds, D. A. Johnson, and C. Yeh, “Health benefits of saliva : a review,” pp. 223–233, 2005, doi: 10.1016/j.jdent.2004.10.009.

[137] S. T. Prajapati, P. B. Patel, and C. N. Patel, “Formulation and evaluation of

sublingual tablets containing Sumatriptan succinate," vol. 2, no. 3, 2012, doi: 10.4103/2230-973X.104400.

[138] A. Lura, G. Tardy, and P. Kleinebudde, "Tableting of mini-tablets in comparison with conventionally sized tablets : A comparison of tableting properties and tablet dimensions," vol. 2, no. November, 2020, doi: 10.1016/j.ijpx.2020.100061.

[139] V. Tumuluri, *Pharmaceutical mini - tablets : a*. Elsevier Inc., 2020.

[140] V. Klingmann *et al.*, "Favorable Acceptance of Mini-Tablets Compared with Syrup: A Randomized Controlled Trial in Infants and Preschool Children," pp. 1728–1733, 2013, doi: 10.1016/j.jpeds.2013.07.014.

[141] A. Tsiligiannis, M. Sfouni, R. Nalda-molina, and A. Dokoumetzidis, "European Journal of Pharmaceutical Sciences Optimization of a paediatric fixed dose combination mini-tablet and dosing regimen for the first line treatment of tuberculosis," *Eur. J. Pharm. Sci.*, vol. 138, no. June, p. 105016, 2019, doi: 10.1016/j.ejps.2019.105016.

[142] T. Huong, H. Thi, S. Lha, S. Pinto, and M. Flament, "Feasability of a new process to produce fast disintegrating pellets as novel multiparticulate dosage form for pediatric use," vol. 496, pp. 842–849, 2015.

[143] S. Kayuni *et al.*, "A systematic review with epidemiological update of male genital schistosomiasis (MGS): A call for integrated case management across the health system in sub-Saharan Africa," *Parasite Epidemiol. Control*, vol. 4, p. e00077, 2019, doi: 10.1016/j.parepi.2018.e00077.

[144] T. Sangnim and K. Huanbutta, "Journal of Drug Delivery Science and Technology Development and evaluation of taste-masked paracetamol chewable tablets using a polymer and / or wax dispersion technique," *J. Drug Deliv. Sci. Technol.*, vol. 54, no. August, p. 101361, 2019, doi: 10.1016/j.jddst.2019.101361.

[145] G. G. Pereira, S. Figueiredo, and A. I. Fernandes, "Polymer Selection for Hot-Melt Extrusion Coupled to Fused Deposition Modelling in Pharmaceutics," 2020.

[146] T. Tagami, E. Ito, R. Kida, K. Hirose, T. Noda, and T. Ozeki, "3D printing of gummy drug formulations composed of gelatin and an HPMC-based hydrogel for pediatric use," *Int. J. Pharm.*, vol. 594, no. September 2020, p. 120118, 2021, doi: 10.1016/j.ijpharm.2020.120118.

[147] M. Elbadawi, B. Muñiz, F. K. H. Gavins, J. Jie, and S. Gaisford, “M3DISEEN : A novel machine learning approach for predicting the 3D printability of medicines,” *Int. J. Pharm.*, vol. 590, no. September, p. 119837, 2020, doi: 10.1016/j.ijpharm.2020.119837.

[148] G. Chen, Y. Xu, P. Chi, L. Kwok, and L. Kang, “Pharmaceutical Applications of 3D Printing,” *Addit. Manuf.*, vol. 34, no. November 2019, p. 101209, 2020, doi: 10.1016/j.addma.2020.101209.

[149] G. Chen, Y. Xu, P. Chi, L. Kwok, and L. Kang, “Pharmaceutical Applications of 3D Printing,” *Addit. Manuf.*, vol. 34, no. April, p. 101209, 2020, doi: 10.1016/j.addma.2020.101209.

[150] B. Shaqour, A. Samaro, B. Verleije, K. Beyers, and C. Vervaet, “Production of Drug Delivery Systems Using Fused Filament Fabrication : A Systematic Review,” pp. 1–16, 2020.

[151] A. Melocchi *et al.*, “A Graphical Review on the Escalation of Fused Deposition Modeling ( FDM ) 3D Printing in the Pharmaceutical Field,” *J. Pharm. Sci.*, vol. 109, no. 10, pp. 2943–2957, 2020, doi: 10.1016/j.xphs.2020.07.011.

[152] A. Goyanes, A. B. M. Buanz, A. W. Basit, and S. Gaisford, “Fused- fi lament 3D printing ( 3DP ) for fabrication of tablets,” vol. 476, pp. 88–92, 2014, doi: 10.1016/j.ijpharm.2014.09.044.

[153] A. Ghanizadeh Tabriz *et al.*, “3D printed bilayer tablet with dual controlled drug release for tuberculosis treatment,” *Int. J. Pharm.*, vol. 593, no. November 2020, p. 120147, 2021, doi: 10.1016/j.ijpharm.2020.120147.

[154] A. Goyanes, P. Robles, A. Buanz, A. W. Basit, and S. Gaisford, “Effect of geometry on drug release from 3D printed tablets,” *Int. J. Pharm.*, vol. 494, no. 2, pp. 657–663, 2015, doi: 10.1016/j.ijpharm.2015.04.069.

[155] K. Shi, J. P. Salvage, M. Maniruzzaman, and A. Nokhodchi, “Role of release modifiers to modulate drug release from fused deposition modelling ( FDM ) 3D printed tablets,” *Int. J. Pharm.*, vol. 597, no. January, p. 120315, 2021, doi: 10.1016/j.ijpharm.2021.120315.

[156] A. Goyanes, N. Allahham, S. J. Trenfield, E. Stoyanov, S. Gaisford, and A. W. Basit, “Direct powder extrusion 3D printing: Fabrication of drug products using a

novel single-step process," *Int. J. Pharm.*, vol. 567, no. May, 2019, doi: 10.1016/j.ijpharm.2019.118471.

[157] M. A. Gonzalez, M. V. Ramírez Rigo, and N. L. Gonzalez Vidal, "Praziquantel systems with improved dissolution rate obtained by high pressure homogenization," *Mater. Sci. Eng. C*, vol. 93, no. September 2017, pp. 28–35, 2018, doi: 10.1016/j.msec.2018.07.050.

[158] S. G. Rodrigues, I. Chaves, N. Ferreira, S. De Melo, and M. B. De Jesus, "Computational analysis and physico-chemical characterization of an inclusion compound between praziquantel and methyl- β -cyclodextrin for use as an alternative in the treatment of s ... Computational analysis and physico-chemical characterization of an i," *J. Incl. Phenom.*, no. May, 2011, doi: 10.1007/s10847-010-9852-y.

[159] G. Becket, L. J. Schep, and M. Yee, "Improvement of the in vitro dissolution of praziquantel by complexation with a - , b - and g -cyclodextrins," vol. 179, pp. 65–71, 1999.

[160] W. W. Shuyu Xie, Baoliang Pan, Zhou, Baoxin shi, Zhuangzhi Zhang Xu, Zhang Ming, "Solid lipid nanoparticle suspension enhanced the therapeutic efficacy of praziquantel against tapeworm," *Int. J. Nanomedicine*, pp. 2367–2374, 2011.

[161] L. N. Andrade *et al.*, "Praziquantel-loaded solid lipid nanoparticles: Production, physicochemical characterization, release profile, cytotoxicity and in vitro activity against Schistosoma mansoni," *J. Drug Deliv. Sci. Technol.*, vol. 58, no. June 2019, p. 101784, 2020, doi: 10.1016/j.jddst.2020.101784.

[162] G. C. Bazzo, G. Tambosi, E. C. Brüske, and M. Zétola, "Evaluation of enhanced aqueous solubility of praziquantel incorporated in poly (3- hydroxybutyrate) and Eudragit® E microspheres," *Acta Sci.*, pp. 91–96, 2013, doi: 10.4025/actascihealthsci.v35i1.10673.

[163] R. M. Mainardes, M. Palmira, D. Gremião, and R. C. Evangelista, "Thermoanalytical study of praziquantel-loaded PLGA nanoparticles," vol. 42, 2006.

[164] L. B. Da Fonseca *et al.*, "Development of a brazilian nanoencapsulated drug for schistosomiasis treatment," *Vigilância Sanitária em Debate*, vol. 1, no. 4, pp. 4–

10, 2013, doi: 10.3395/vd.v1i4.111en.

[165] Lorena Menezes Vieira, “ENCAPSULAMENTO IN SITU DE PRAZIQUANTEL NA POLIMERIZAÇÃO EM SUSPENSÃO DO METACRILATO DE METILA PARA A PRODUÇÃO DE SISTEMAS DE LIBERAÇÃO CONTROLADA,” UNIVERSIDADE FEDERAL DO RIO DE JANEIRO COMO, 2014.

[166] J. B. Alves, T. Franckini Paiva, V. M. Salim, H. Conceição Ferraz, and J. C. Pinto, “ In situ encapsulation of praziquantel through methyl methacrylate/diethylaminoethyl methacrylate and MMA / DMAEMA miniemulsion copolymerizations in presence of distinct ionic surfactants ,” *SPE Polym.*, vol. 2, no. 2, pp. 110–121, 2021, doi: 10.1002/pls2.10037.

[167] S. T. and S. T. Paloma de la Torre, “Preparation, dissolution and characterization of praziquantel solid dispersions,” *Chem. Pharm. Bull*, vol. 47, no. 11, pp. 1629–1633, 1999, [Online]. Available: http://www.mendeley.com/research/geology-volcanic-history-eruptive-style-yakedake-volcano-group-central-japan/.

[168] A. Borrego-s *et al.*, “Ground Calcium Carbonate as a Low Cost and Biosafety Excipient for Solubility and Dissolution Improvement of Praziquantel,” 2019.

[169] S. Orlandi, J. Priotti, H. P. Diogo, D. Leonardi, C. J. Salomon, and T. G. Nunes, “Structural Elucidation of Poloxamer 237 and Poloxamer 237 / Praziquantel Solid Dispersions : Impact of Poly ( Vinylpyrrolidone ) over Drug Recrystallization and Dissolution Research Article Structural Elucidation of Poloxamer 237 and Poloxamer 237 / Prazi,” no. January, 2018, doi: 10.1208/s12249-017-0946-3.

[170] B. Om, S. Amruta, D. Shashikant, P. Rohini, R. Vinita, and K. Priyanka, “Design and statistical optimisation of praziquantel tablets by using solid dispersion approach,” no. June, pp. 83–92, 2015, doi: 10.4103/0973-8398.154689.

[171] M. V. Chaud *et al.*, “Solid dispersions with hydrogenated castor oil increase solubility , dissolution rate and intestinal absorption of praziquantel,” vol. 46, 2010.

[172] F. C. Cunha, “Separation of praziquantel enantiomers using simulated moving bed chromatographic unit with performance designed for semipreparative applications,” no. March, pp. 9–13, 2019, doi: 10.1002/chir.23084.

[173] X. Wang, S. Du, R. Zhang, X. Jia, T. Yang, and X. Zhang, “Drug-drug cocrystals :

Opportunities and challenges," *Asian J. Pharm. Sci.*, no. xxxx, 2020, doi: 10.1016/j.ajps.2020.06.004.

[174] R. Thakuria, A. Delori, W. Jones, M. P. Lipert, L. Roy, and N. Rodríguez-hornedo, "Pharmaceutical cocrystals and poorly soluble drugs," *Int. J. Pharm.*, vol. 453, no. 1, pp. 101–125, 2013, doi: 10.1016/j.ijpharm.2012.10.043.

[175] C. Jacobs, O. Kayser, and R. H. Muller, "Nanosuspensions as particulate drug formulations in therapy Rationale for development and what we can expect for the future," vol. 47, pp. 3–19, 2001.

[176] V. Chikhalia *et al.*, "The effect of crystal morphology and mill type on milling induced crystal disorder," vol. 7, pp. 19–26, 2005, doi: 10.1016/j.ejps.2005.08.013.

[177] E. C. Arrúa, M. J. G. Ferreira, C. J. Salomon, and T. G. Nunes, "Elucidating the guest-host interactions and complex formation of praziquantel and cyclodextrin derivatives by 13 C and 15 N solid-state NMR spectroscopy," *Int. J. Pharm.*, vol. 496, no. 2, pp. 812–821, 2015, doi: 10.1016/j.ijpharm.2015.11.026.

[178] S. Xie *et al.*, "Formulation, characterization and pharmacokinetics of praziquantel-loaded hydrogenated castor oil solid lipid nanoparticles," *Nanomedicine*, vol. 5, pp. 693–701, 2010.

[179] B. Perissutti *et al.*, "An explorative analysis of process and formulation variables affecting comilling in a vibrational mill : The case of praziquantel," *Int. J. Pharm.*, vol. 533, no. 2, pp. 402–412, 2017, doi: 10.1016/j.ijpharm.2017.05.053.

[180] M. Malhado *et al.*, "Journal of Pharmaceutical and Biomedical Analysis Preclinical pharmacokinetic evaluation of praziquantel loaded in poly ( methyl methacrylate ) nanoparticle using a HPLC – MS / MS," vol. 117, pp. 405–412, 2016, doi: 10.1016/j.jpba.2015.09.023.

[181] B. Kumari and H. Bishnoi, "Review Article SOLID DISPERSION : ITS TYPES AND MECHANISM OF J ournal of P harma R esearch," no. March, 2019, doi: 10.5281/zenodo.2594669.

[182] A. Kapourani, E. Vardaka, K. Katopodis, and K. Kachrimanis, "Crystallization tendency of APIs possessing di ff erent thermal and glass related properties in amorphous solid dispersions," *Int. J. Pharm.*, vol. 579, no. February, p. 119149, 2020, doi: 10.1016/j.ijpharm.2020.119149.

[183] S. Shah, S. Maddineni, J. Lu, and M. A. Repka, “Melt extrusion with poorly soluble drugs,” *Int. J. Pharm.*, vol. 453, no. 1, pp. 233–252, 2013, doi: 10.1016/j.ijpharm.2012.11.001.

[184] B. L. de A. Costa, “Generation of high drug loading amorphous solid dispersions by different manufacturing processes,” 2017.

[185] H. Veith, F. Wiechert, C. Luebbert, and G. Sadowski, “Combining crystalline and polymeric excipients in API solid dispersions – Opportunity or risk ?,” *Eur. J. Pharm. Biopharm.*, vol. 158, no. September 2020, pp. 323–335, 2021, doi: 10.1016/j.ejpb.2020.11.025.

[186] A. Newman, *Rational Design for Amorphous Solid Dispersions*. Elsevier Inc., 2017.

[187] P. Pandi, R. Bulusu, N. Kommineni, W. Khan, and M. Singh, “Amorphous solid dispersions: An update for preparation, characterization, mechanism on bioavailability, stability, regulatory considerations and marketed products,” *Int. J. Pharm.*, vol. 586, no. June, p. 119560, 2020, doi: 10.1016/j.ijpharm.2020.119560.

[188] P. Kanaujia, P. Poovizhi, W. K. Ng, and R. B. H. Tan, “Amorphous formulations for dissolution and bioavailability enhancement of poorly soluble APIs,” *Powder Technol.*, vol. 285, pp. 2–15, 2015, doi: 10.1016/j.powtec.2015.05.012.

[189] K. Kogermann *et al.*, “Dissolution testing of amorphous solid dispersions,” *Int. J. Pharm.*, vol. 444, no. 1–2, pp. 40–46, 2013, doi: 10.1016/j.ijpharm.2013.01.042.

[190] M. Tobyn *et al.*, “Amorphous Drug – PVP Dispersions : Application of Theoretical , Thermal and Spectroscopic Analytical Techniques to the Study of a Molecule With Intermolecular Bonds in Both the Crystalline and Pure Amorphous State,” *J. Am. Pharm. Assoc.*, vol. 98, no. 9, pp. 3456–3468, 2009, doi: 10.1002/jps.21738.

[191] M. Savolainen *et al.*, “Better understanding of dissolution behaviour of amorphous drugs by in situ solid-state analysis using Raman spectroscopy,” *Eur. J. Pharm. Biopharm.*, vol. 71, no. 1, pp. 71–79, 2009, doi: 10.1016/j.ejpb.2008.06.001.

[192] P. J. Skrdla, P. D. Floyd, and P. C. D. Orco, “The amorphous state : first-principles derivation of the Gordon – Taylor equation for direct prediction of the glass transition temperature of mixtures ; glass formers ; physical basis of the ‘“ Rule of 2 / 3 ,”” ” *Phys. Chem. Chem. Phys.*, vol. 19, pp. 20523–20532, 2017, doi:

10.1039/C7CP04124A.

[193] O. Jennotte, N. Koch, A. Lechanteur, and B. Evrard, “Three-dimensional printing technology as a promising tool in bioavailability enhancement of poorly water-soluble molecules : A review,” *Int. J. Pharm.*, vol. 580, no. December 2019, p. 119200, 2020, doi: 10.1016/j.ijpharm.2020.119200.

[194] M. Hanada, S. V Jermain, X. Lu, Y. Su, and R. O. Williams, “Predicting physical stability of ternary amorphous solid dispersions using speci fi c mechanical energy in a hot melt extrusion process ☆,” *Int. J. Pharm.*, vol. 548, no. 1, pp. 571–585, 2018, doi: 10.1016/j.ijpharm.2018.07.029.

[195] S. Xu and W. Dai, “Drug precipitation inhibitors in supersaturable formulations,” *Int. J. Pharm.*, vol. 453, no. 1, pp. 36–43, 2013, doi: 10.1016/j.ijpharm.2013.05.013.

[196] K. Kachrimanis and I. Nikolakakis, “Polymers as Formulation Excipients for Hot-Melt Extrusion Processing of Pharmaceuticals,” in *Handbook of Polymers for Pharmaceutical Technologies*, vol. 2, 2015, pp. 121–149.

[197] P. J. Skrdla, P. D. Floyd, and P. C. D. Orco, “Predicting the solubility enhancement of amorphous drugs and related phenomena using basic thermodynamic principles and semi-empirical kinetic models,” *Int. J. Pharm.*, vol. 567, no. July, p. 118465, 2019, doi: 10.1016/j.ijpharm.2019.118465.

[198] B. C. Hancock and M. Parks, “What is the True Solubility Advantage for Amorphous Pharmaceuticals ?,” vol. 17, no. 4, 2000.

[199] R. Han *et al.*, “Insight into the Dissolution Molecular Mechanism of Ternary Solid Dispersions by Combined Experiments and Molecular Simulations,” *AAPS PharmSciTech*, vol. 20, no. 7, pp. 10–20, 2019, doi: 10.1208/s12249-019-1486-9.

[200] S. Huang, C. Mao, R. O. W. Iii, and C. Yang, “Solubility Advantage ( and Disadvantage ) of Pharmaceutical Amorphous Solid Dispersions,” *J. Pharm. Sci.*, pp. 1–13, 2016, doi: 10.1016/j.xphs.2016.08.017.

[201] A. Alhayali, “In Vitro Solubility and Supersaturation Behavior of Supersaturating Drug Delivery Systems,” Luleå University of Technology May.

[202] A. Schittny, “Mechanisms of increased bioavailability through amorphous solid dispersions : a review,” vol. 27, no. 1, pp. 110–127, 2020, doi:

10.1080/10717544.2019.1704940.

[203] G. Zogra and A. Newman, “Interrelationships Between Structure and the Properties of Amorphous Solids of Pharmaceutical Interest,” vol. 106, pp. 5–27, 2017, doi: 10.1016/j.xphs.2016.05.001.

[204] T. Pas, S. Verbert, B. Appeltans, and G. Van Den Mooter, “The influence of crushing amorphous solid dispersion dosage forms on the in-vitro dissolution kinetics,” *Int. J. Pharm.*, vol. 573, no. November 2019, p. 118884, 2020, doi: 10.1016/j.ijpharm.2019.118884.

[205] R. B. Chavan, S. Rathi, V. G. S. S. Jyothi, and N. R. Shastri, “Cellulose based polymers in development of amorphous solid dispersions,” *Asian J. Pharm. Sci.*, vol. 14, no. 3, pp. 248–264, 2019, doi: 10.1016/j.ajps.2018.09.003.

[206] A. R. Nair *et al.*, “Review Article Overview of Extensively Employed Polymeric Carriers in Solid Dispersion Technology,” 2020, doi: 10.1208/s12249-020-01849-z.

[207] T. D. Vaibhav Sihorkara, *The role of polymers and excipients in developing amorphous solid dispersions: An industrial perspective*. Elsevier Inc., 2020.

[208] S. B. Teja, S. P. Patil, G. Shete, S. Patel, and A. K. Bansal, “Drug-excipient behavior in polymeric amorphous solid dispersions .,” vol. 4, no. September, pp. 70–94, 2013.

[209] K. Lehmkemper, S. O. Kyerematen, O. Heinzerling, M. Degenhardt, and G. Sadowski, “Long-Term Physical Stability of PVP- and PVPVA-Amorphous Solid Dispersions,” 2017, doi: 10.1021/acs.molpharmaceut.6b00763.

[210] D. Feng *et al.*, “Polymer – Surfactant System Based Amorphous Solid Dispersion : Precipitation Inhibition and Bioavailability Enhancement of Itraconazole,” no. 1, pp. 1–15, 2018, doi: 10.3390/pharmaceutics10020053.

[211] H. J. Jung *et al.*, “Improved oral absorption of tacrolimus by a solid dispersion with hypromellose and sodium lauryl sulfate,” *Int. J. Biol. Macromol.*, vol. 83, pp. 282–287, 2016, doi: 10.1016/j.ijbiomac.2015.11.063.

[212] J. Chen, J. D. Ormes, J. D. Higgins, and L. S. Taylor, “Impact of Surfactants on the Crystallization of Aqueous Suspensions of Celecoxib Amorphous Solid Dispersion Spray Dried Particles,” 2015, doi: 10.1021/mp5006245.

[213] D. Hoon *et al.*, “Improved oral absorption of dutasteride via Soluplus 1 -based supersaturable self-emulsifying drug delivery system ( S-SEDDS ),” vol. 478, pp. 341–347, 2015.

[214] S. P. Chaudhari and R. P. Dugar, “Application of surfactants in solid dispersion technology for improving solubility of poorly water soluble drugs Journal of Drug Delivery Science and Technology Application of surfactants in solid dispersion technology for improving solubility of poorly w,” *J. Drug Deliv. Sci. Technol.*, vol. 41, no. February 2018, pp. 68–77, 2017, doi: 10.1016/j.jddst.2017.06.010.

[215] W. Zhang, S. S. Hate, D. J. Russell, H. H. Hou, and K. Nagapudi, “Impact of Surfactant and Surfactant-Polymer Interaction on Desupersaturation of Clotrimazole,” *J. Pharm. Sci.*, vol. 108, no. 10, pp. 3262–3271, 2019, doi: 10.1016/j.xphs.2019.05.035.

[216] A. Schittny, S. Philipp-bauer, P. Detampel, J. Huwyler, and M. Puchkov, “Mechanistic insights into e ff ect of surfactants on oral bioavailability of amorphous solid dispersions,” *J. Control. Release*, vol. 320, no. August 2019, pp. 214–225, 2020, doi: 10.1016/j.jconrel.2020.01.031.

[217] R. C. Rowe, P. J. Sheskey, and S. C. Owen, *Handbook of Pharmaceutical Excipients*, 5th ed. London: Pharmaceutical Pres, 2006.

[218] C. Viet and P. C. Cho, “Application of D -α-tocopheryl polyethylene glycol 1000 succinate ( TPGS ) in transdermal and topical drug delivery systems ( TDDS ),” *J. Pharm. Investig.*, vol. 0, no. 0, p. 0, 2017, doi: 10.1007/s40005-016-0300-x.

[219] D. Hurley, M. Davis, G. M. Walker, J. G. Lyons, and C. L. Higginbotham, “The E ff ect of Cooling on the Degree of Crystallinity , Solid-State Properties , and Dissolution Rate of Multi-Component Hot-Melt Extruded Solid Dispersions,” no. 2004, 2020.

[220] Y. A. and M. S. François Hallouarda, Lyes Mehennic, Malika Lahiani-Skibaa, “Solid Dispersions for Oral Administration : An Overview of the Methods for their Preparation Solid Dispersions for Oral Administration : An Overview of the Methods for their Preparation,” *Curr. Pharm. Des.*, vol. 22, no. August, pp. 1–17, 2016, doi: 10.2174/138161282266616072.

[221] J. Knapik-kowalczuk, K. Chmiel, J. Pacułt, and K. Bialek, “Enhancement of the

Physical Stability of Amorphous Sildenafil in a Binary Mixture , with either a Plasticizing or Antiplasticizing Compound," pp. 23–28, 2020.

[222] A. Prudic, T. Kleetz, M. Korf, Y. Ji, and G. Sadowski, "In fl uence of Copolymer Composition on the Phase Behavior of Solid Dispersions," 2014.

[223] K. Deboyace and P. L. D. Wildfong, "The Application of Modeling and Prediction to the Formation and Stability of Amorphous Solid Dispersions," *J. Pharm. Sci.*, vol. 107, no. 1, pp. 57–74, 2018, doi: 10.1016/j.xphs.2017.03.029.

[224] J. L. Calahan and F. Alvarez-nunez, "Characterization of Amorphous Solid Dispersions of AMG 517 in HPMC-AS and Crystallization using Isothermal Microcalorimetry By," 2011.

[225] M. F. Simões, R. M. A. Pinto, and S. Simões, "Hot-melt extrusion in the pharmaceutical industry : toward filing a new drug application," *Drug Discov. Today*, vol. 00, no. 00, 2019, doi: 10.1016/j.drudis.2019.05.013.

[226] F. C. Campbell, "Thermodynamics and Phase Diagrams," pp. 41–72, 2012.

[227] D. Jeli, "Thermal Stability of Amorphous Solid Dispersions," 2021.

[228] W. F. WEI LIU, , YU LIU, JIAOQI HUANG, ZHONGQUAN LIN, XUANCHENG PAN, XIAOJUN ZENG, MARC LAMY DE LA CHAPELLE, YANG ZHANG, "Identification and investigation of the vibrational properties of crystalline and co- amorphous drugs with Raman and terahertz spectroscopy," vol. 10, no. 8, pp. 4290–4304, 2019, doi: 10.1364/BOE.10.004290.

[229] D. G. Dastidar and G. Chakrabarti, *Thermoresponsive Drug Delivery Systems, Characterization and Application*. Elsevier Inc., 2019.

[230] Y. Peng, D. D. Dussan, and R. Narain, *Thermal, mechanical, and electrical properties*. 2020.

[231] N. R. Jadhav, V. L. Gaikwad, K. J. Nair, and H. M. Kadam, "Glass transition temperature : Basics and application in pharmaceutical sector," no. June, 2009, doi: 10.4103/0973-8398.55043.

[232] C. Wu and J. W. Mcginity, "Influence of Ibuprofen as a Solid-State Plasticizer in Eudragit ® RS 30 D on the Physicochemical Properties of Coated Beads," vol. 2, no. 4, 2001.

[233] J. A. Baird and L. S. Taylor, “Evaluation of amorphous solid dispersion properties using thermal analysis techniques ☆,” vol. 64, pp. 396–421, 2012, doi: 10.1016/j.addr.2011.07.009.

[234] V. Corrtelius T. Moynihan,” Allan J. Easteal, James Wilder, “Dependence of the glass transition temperature on heating and cooling rate,” vol. 7, no. 26, 1974, doi: 10.1021/j100619a008.

[235] A. H. L. K. C.-L. HSU, D.R. HELDMAN, T.A. TAYLOR and ABSTRACT:, “Influence of Cooling Rate on Glass Transition Temperature of Sucrose Solutions and Rice Starch Gel,” vol. 68, no. 6, pp. 1–6, 2003.

[236] A. Newman and G. Zografi, “Commentary Commentary : Considerations in the Measurement of Glass Transition Temperatures of Pharmaceutical Amorphous Solids,” pp. 1–13, 2020, doi: 10.1208/s12249-019-1562-1.

[237] S. Janssens and G. Van Den Mooter, “Review : physical chemistry of solid dispersions,” pp. 1571–1586, 2009, doi: 10.1211/jpp/61.12.0001.

[238] P. G. Royall, D. Q. M. Craig, and C. Doherty, “Characterisation of moisture uptake effects on the glass transitional behaviour of an amorphous drug using modulated temperature DSC,” vol. 192, pp. 39–46, 1999.

[239] R. Tanaka, Y. Hattori, Y. Horie, H. Kamada, and T. Nagato, “Characterization of Amorphous Solid Dispersion of Pharmaceutical Compound with pH-Dependent Solubility Prepared by Continuous-Spray Granulator,” doi: 10.3390/pharmaceutics11040159.

[240] M. Latreche, “Maîtrise de la stabilité physique des alliages moléculaires amorphes pour optimiser l’efficacité des médicaments,” L’Université de Lille, 2019.

[241] S. Dedroog, T. Pas, B. Vergauwen, C. Huygens, and G. Van Den Mooter, “Analysis Solid-state analysis of amorphous solid dispersions : Why DSC and XRPD may not be regarded as stand-alone techniques,” *J. Pharm. Biomed. Anal.*, vol. 178, p. 112937, 2020, doi: 10.1016/j.jpba.2019.112937.

[242] H. A. Schneider, “The Gordon-Taylor equation . Additivity and interaction in compatible polymer blends,” vol. 1955, pp. 1941–1955, 1988.

[243] M. M. Knopp *et al.*, “A Promising New Method to Estimate Drug-Polymer Solubility at Room Temperature,” vol. 105, pp. 2621–2624, 2016, doi:

10.1016/j.xphs.2016.02.017.

[244] B. L. A. Costa, M. Sauceau, S. Del Confetto, R. Sescousse, and M. I. Ré, “Determination of drug-polymer solubility from supersaturated spray-dried amorphous solid dispersions : A case study with Efavirenz and Soluplus ®,” *Eur. J. Pharm. Biopharm.*, vol. 142, no. July 2018, pp. 300–306, 2019, doi: 10.1016/j.ejpb.2019.06.028.

[245] A. Karagianni, “Co-Amorphous Solid Dispersions for Solubility and Absorption Improvement of Drugs : Composition , Preparation , Characterization and Formulations for Oral Delivery,” 2018, doi: 10.3390/pharmaceutics10030098.

[246] and M. D. Aurélien Mahieu, Jean-François Willart,* Emeline Dudognon, Florence Danède, “A New Protocol To Determine the Solubility of Drugs into Polymer Matrixes,” *Mol. Pharm.*, 2013.

[247] Y. E. Sun, J. Tao, G. G. Z. Zhang, and L. Yu, “Solubilities of Crystalline Drugs in Polymers : An Improved Analytical Method and Comparison of Solubilities of Indomethacin and Nifedipine in PVP , PVP / VA , and PVAc,” *J. Pharm. Sci.*, vol. 99, no. 9, pp. 4023–4031, 2010, doi: 10.1002/jps.22251.

[248] Z. Yang, K. Nollenberger, J. Albers, and S. Qi, “Molecular Implications of Drug − Polymer Solubility in Understanding the Destabilization of Solid Dispersions by Milling,” 2014.

[249] E. Sawicki, “Solid dispersions in oncology : a solution to solubility-limited oral drug absorption,” Universiteit Utrecht, 2017.

[250] N. Boersen, T. Lee, and H. Hui, *Toxicology Studies*. Elsevier Inc., 2013.

[251] A. Newman, *Pharmaceutical amorphous solid dispersion*. New Jersey, 2015.

[252] A. W. M. Navnit Shah, Harpreet Sandhu, Duk Soon Choi Hitesh Chokshi, *Amorphous Solid Dispersions Theory and Practice*. London: Springer NewYork Heidelberg Dordrecht London, 2014.

[253] D. D. Sun, H. Wen, and L. S. Taylor, “Non-Sink Dissolution Conditions for Predicting Product Quality and In Vivo Performance of Supersaturating Drug Delivery Systems,” *J. Pharm. Sci.*, vol. 105, no. 9, pp. 2477–2488, 2016, doi: 10.1016/j.xphs.2016.03.024.

[254] K. Sugita and N. Takata, “Dose-Dependent Solubility – Permeability Interplay for Poorly Soluble Drugs under Non-Sink Conditions,” pp. 297–307, 2021.

[255] S. Petralito *et al.*, “Apparent Solubility and Dissolution Profile at Non-Sink Conditions as Quality Improvement Tools,” 2010.

[256] M. Descamps and J. F. Willart, “Perspectives on the amorphisation / milling relationship in pharmaceutical materials ☆,” *Adv. Drug Deliv. Rev.*, vol. 100, pp. 51–66, 2016, doi: 10.1016/j.addr.2016.01.011.

[257] M. Descamps, A. Aumelas, S. Desprez, and J. F. Willart, “The amorphous state of pharmaceuticals obtained or transformed by milling : Sub-Tg features and rejuvenation,” vol. 407, pp. 72–80, 2015, doi: 10.1016/j.jnoncrysol.2014.08.055.

[258] M. Descamps, J. F. Willart, E. Dudognon, and V. Caron, “Transformation of Pharmaceutical Compounds upon Milling and Comilling : The Role of T g,” vol. 96, no. 5, pp. 1398–1407, 2007, doi: 10.1002/jps.

[259] S. Dedroog, C. Huygens, and G. Van Den Mooter, “Chemically identical but physically different : A comparison of spray drying , hot melt extrusion and cryo-milling for the formulation of high drug loaded amorphous solid dispersions of naproxen,” *Eur. J. Pharm. Biopharm.*, vol. 135, no. November 2018, pp. 1–12, 2019, doi: 10.1016/j.ejpb.2018.12.002.

[260] M. Latreche, J. Willart, M. Guerain, H. Alain, and F. Dan, “Using Milling to Explore Physical States : The Amorphous and Polymorphic Forms of Sulindac,” vol. 108, pp. 2635–2642, 2019, doi: 10.1016/j.xphs.2019.03.017.

[261] B. Wang *et al.*, “A critical review of spray-dried amorphous pharmaceuticals : Synthesis , analysis and application,” *Int. J. Pharm.*, vol. 594, no. October 2020, p. 120165, 2021, doi: 10.1016/j.ijpharm.2020.120165.

[262] M. Ré, “Formulating Drug Delivery Systems by Spray Drying,” *Dry. Technol. An Int. J.*, vol. 24, no. 4, pp. 433–446, 2007, doi: 10.1080/07373930600611877.

[263] A. Paudel, Z. A. Worku, J. Meeus, S. Guns, and G. Van Den Mooter, “Manufacturing of solid dispersions of poorly water soluble drugs by spray drying : Formulation and process considerations,” *Int. J. Pharm.*, vol. 453, no. 1, pp. 253–284, 2013, doi: 10.1016/j.ijpharm.2012.07.015.

[264] D. S. / M. Y. / D. Isadiartuti1, “Ternary solid dispersion to improve solubility and

dissolution of meloxicam Abstract :," *J. Basic Clin. Physiol. Pharmacol. 2019; 20190244*, pp. 1–8, 2019, doi: 10.1515/jbcpp-2019-0244.

[265] C. C. C. Teixeira *et al.*, "Microparticles Containing Curcumin Solid Dispersion : Stability , Bioavailability and Anti-Inflammatory Activity," vol. 17, no. 2, pp. 252–261, 2016, doi: 10.1208/s12249-015-0337-6.

[266] K. Wlodarski and F. Zhang, "Synergistic Effect of Polyvinyl Alcohol and Copovidone in Itraconazole Amorphous Solid Dispersions," no. 1, 2018.

[267] M. Maniruzzaman, D. Douroumis, J. S., and M. J., "Hot-Melt Extrusion (HME): From Process to Pharmaceutical Applications," *Recent Adv. Nov. Drug Carr. Syst.*, pp. 3–16, 2012, doi: 10.5772/51582.

[268] R. Thakkar, R. Thakkar, A. Pillai, E. A. Ashour, and M. A. Repka, "Systematic screening of pharmaceutical polymers for hot melt extrusion processing: a comprehensive review," *Int. J. Pharm.*, vol. 576, no. October 2019, p. 118989, 2020, doi: 10.1016/j.ijpharm.2019.118989.

[269] A. Alshetaili, S. M. Alshahrani, B. K. Almutairy, and M. A. Repka, "Hot Melt Extrusion Processing Parameters Optimization," pp. 1–14, 2020.

[270] H. Patil, R. V Tiwari, and M. A. Repka, "Hot-Melt Extrusion : from Theory to Application in Pharmaceutical Formulation," 2015, doi: 10.1208/s12249-015-0360-7.

[271] S. Narala, D. Nyavanandi, P. Srinivasan, P. Mandati, and S. Bandari, "Pharmaceutical Co-crystals , Salts , and Co-amorphous Systems : A novel opportunity of hot-melt extrusion," *J. Drug Deliv. Sci. Technol.*, vol. 61, no. November 2020, p. 102209, 2021, doi: 10.1016/j.jddst.2020.102209.

[272] J. Thiry, F. Krier, and B. Evrard, "A review of pharmaceutical extrusion : Critical process parameters and," *Int. J. Pharm.*, vol. 479, no. 1, pp. 227–240, 2015, doi: 10.1016/j.ijpharm.2014.12.036.

[273] L. Saerens *et al.*, "In-line NIR spectroscopy for the understanding of polymer – drug interaction during pharmaceutical hot-melt extrusion," *Eur. J. Pharm. Biopharm.*, vol. 81, no. 1, pp. 230–237, 2012, doi: 10.1016/j.ejpb.2012.01.001.

[274] N. Follonier, E. Doelker, and E. T. Cole, "controlled release Various ways of modulating the release of diltiazem hydrochloride from hot-melt extruded

sustained release pellets prepared using polymeric materials," vol. 36, pp. 243–250, 1995.

[275] A. Gryczke, S. Schminke, M. Maniruzzaman, J. Beck, and D. Douroumis, "Colloids and Surfaces B : Biointerfaces Development and evaluation of orally disintegrating tablets ( ODTs ) containing Ibuprofen granules prepared by hot melt extrusion," *Colloids Surfaces B Biointerfaces*, vol. 86, no. 2, pp. 275–284, 2011, doi: 10.1016/j.colsurfb.2011.04.007.

[276] V. W. Yeung and I. C. K. Wong, "R ESEARCH ARTICLE," pp. 399–402, 2005.

[277] A. S. Alshetaili, J. Morott, S. Shah, and V. Kulkarni, "Mefenamic acid taste-masked oral disintegrating tablets with enhanced solubility via molecular interaction produced by hot melt extrusion technology," pp. 18–27, 2016, doi: 10.1016/j.jddst.2015.03.003.Mefenamic.

[278] L. F. B. Malaquias *et al.*, "Hot Melt Extrudates Formulated Using Design Space: One Simple Process for Both Palatability and Dissolution Rate Improvement," *J. Pharm. Sci.*, vol. 107, no. 1, pp. 286–296, 2018, doi: 10.1016/j.xphs.2017.08.014.

[279] R. Censi and M. R. Gigliobianco, "Hot Melt Extrusion : Highlighting Physicochemical Factors to Be Investigated While Designing and Optimizing a Hot Melt Extrusion Process," 2018, doi: 10.3390/pharmaceutics10030089.

[280] A. Butreddy, S. Bandari, and M. A. Repka, "Quality-by-design in hot melt extrusion based amorphous solid dispersions: An industrial perspective on product development," *Eur. J. Pharm. Sci.*, vol. 158, no. November 2020, p. 105655, 2020, doi: 10.1016/j.ejps.2020.105655.

[281] M. Maniruzzaman, J. S. Boateng, M. J. Snowden, and D. Douroumis, "A Review of Hot-Melt Extrusion : Process Technology to Pharmaceutical Products," vol. 2012, 2012, doi: 10.5402/2012/436763.

[282] S. V Jermain, C. Brough, and R. O. Williams, "Amorphous solid dispersions and nanocrystal technologies for poorly water- soluble drug delivery – An update," *Int. J. Pharm.*, vol. 535, no. 1–2, pp. 379–392, 2018, doi: 10.1016/j.ijpharm.2017.10.051.

[283] X. Ma and R. O. W. Iii, "Characterization of amorphous solid dispersions : An update," *J. Drug Deliv. Sci. Technol.*, vol. 50, no. November 2018, pp. 113–124,

2019, doi: 10.1016/j.jddst.2019.01.017.

[284] Y. L. N. T. R. L. J. Q. W. Wu, “Understanding the Relationship between Wettability and Dissolution of Solid Dispersion,” 2014, doi: 10.1016/j.ijpharm.2014.02.004.

[285] J. Thiry *et al.*, “Continuous production of itraconazole-based solid dispersions by hot melt extrusion : Preformulation , optimization and design space determination,” *Int. J. Pharm.*, vol. 515, no. 1–2, pp. 114–124, 2016, doi: 10.1016/j.ijpharm.2016.10.003.

[286] M. M. Crowley *et al.*, “Pharmaceutical Applications of Hot-Melt Extrusion : Part I Pharmaceutical Applications of Hot-Melt Extrusion : Part I,” vol. 9045, 2008, doi: 10.1080/03639040701498759.

[287] M. A. Azad, D. Olawuni, G. Kimbell, A. Z. Badruddoza, S. Hossain, and T. Sultana, *Polymers for Extrusion-Based 3D Printing of Pharmaceuticals : A Holistic Materials – Process Perspective*. .

[288] A. Goyanes, U. Det-Amornrat, J. Wang, A. W. Basit, and S. Gaisford, “3D scanning and 3D printing as innovative technologies for fabricating personalized topical drug delivery systems,” *J. Control. Release*, vol. 234, pp. 41–48, 2016, doi: 10.1016/j.jconrel.2016.05.034.

[289] A. G. Iria Seoane-Viaño, Patricija Januskaite, Carmen Alvarez-Lorenzo, Abdul W. Basit, “Semi-solid extrusion 3D printing in drug delivery and biomedicine: Personalised solutions for healthcare challenges,” *J. Control. Release*, 2021, doi: 10.1016/j.jconrel.2021.02.027.

[290] A. Goyanes *et al.*, “Automated therapy preparation of isoleucine formulations using 3D printing for the treatment of MSUD : First single-centre , prospective , crossover study in patients,” *Int. J. Pharm.*, vol. 567, no. June, p. 118497, 2019, doi: 10.1016/j.ijpharm.2019.118497.

[291] Brasil and Agência Nacional de Vigilância Sanitária, “Farmacopeia Brasileira,” *Farm. Bras.*, vol. 1, p. 874, 2019.

[292] BASF, “kOLLIDON VA 64 Technical Informations,” no. June 2008, pp. 1–16, 2011.

[293] BASF, “Kolliphor ® SLS Kolliphor ® SLS Fine,” no. 119863, pp. 1–6, 2012.

[294] A. Venkateshaiah, V. V. T. Padil, and M. Nagalakshmaiah, “Microscopic Techniques for the Analysis of Micro and Nanostructures of Biopolymers and Their Derivatives.”

[295] International Organization for Standardization, “International Organization for Standardization. 13320 2009,” 2009.

[296] The United States Pharmaceutical Convention., “<429> Light diffraction measurement of particle size,” *Suppl. to USP 43*, vol. 43, no. 4, p. 6697, 2020.

[297] The United States Pharmaceutical Convention., “USP43 Praziquantel Tablets,” vol. 43, p. 3650, 2020.

[298] J. Sha *et al.*, “Solid-liquid phase equilibrium of praziquantel in eleven pure solvents: Determination, model correlation, solvent effect, molecular simulation and thermodynamic analysis,” *J. Chem. Thermodyn.*, no. xxxx, 2020, doi: 10.1016/j.jct.2020.106327.

[299] S. S. Gupta, N. Solanki, and A. T. M. Serajuddin, “Investigation of Thermal and Viscoelastic Properties of Polymers Relevant to Hot Melt Extrusion, IV: Affinisol™ HPMC HME Polymers,” *AAPS PharmSciTech*, vol. 17, no. 1, pp. 148–157, 2016, doi: 10.1208/s12249-015-0426-6.

[300] The United States Pharmaceutical Convention., “⟨ 776 ⟩ optical microscopy,” *Suppl. to USP 43*, vol. 43, p. 6998, 2020.

[301] T. Templeman, S. Sengupta, N. Maman, E. Bar-or, and M. Shandalov, “Oriented Attachment: A Path to Columnar Morphology in Chemical Bath Deposited PbSe Thin Films,” 2018, doi: 10.1021/acs.cgd.7b01771.

[302] D. Colegiada *et al.*, “Ministério da Saúde RESOLUÇÃO - RDC Nº 37, DE 3 DE AGOSTO DE 2011,” 2011.

[303] U. S. D. of H. and H. Services and F. and D. Administration, “Waiver of In Vivo Bioavailability and Bioequivalence Studies for Immediate-Release Solid Oral Dosage Forms Based on a Biopharmaceutics Classification System Guidance for Industry,” 2017.

[304] K. Yamasaki, K. Taguchi, K. Nishi, M. Otagiri, and H. Seo, “Enhanced dissolution and oral bioavailability of praziquantel by emulsification with human serum albumin followed by spray drying,” *Eur. J. Pharm. Sci.*, vol. 139, no. September,

p. 105064, 2019, doi: 10.1016/j.ejps.2019.105064.

[305] M. Karl and K. Kolter, “Suitability of Plasticized Polymers for Hot Melt Extrusion,” *Excipients Act. Pharma*, vol. 24, no. Table 1, pp. 2–6, 2010.

[306] Y. Chen *et al.*, “Initial Drug Dissolution from Amorphous Solid Dispersions Controlled by Polymer Dissolution and Drug-Polymer Interaction,” *Pharm. Res.*, 2016, doi: 10.1007/s11095-016-1969-2.

[307] A. Prudic, Y. Ji, and G. Sadowski, “Thermodynamic Phase Behavior of API/Polymer Solid Dispersions,” 2014.

[308] T. R. Hörmann *et al.*, “Sensitivity of a continuous hot-melt extrusion and strand pelletization line to control actions and composition variation,” *Int. J. Pharm.*, vol. 566, no. February, pp. 239–253, 2019, doi: 10.1016/j.ijpharm.2019.05.046.

[309] H. G. Moradiya, M. T. Islam, N. Scoutaris, S. A. Halsey, B. Z. Chowdhry, and D. Douroumis, “Continuous Manufacturing of High Quality Pharmaceutical Cocrystals Integrated with Process Analytical Tools for In-Line Process Control,” *Cryst. Growth Des.*, vol. 16, no. 6, pp. 3425–3434, 2016, doi: 10.1021/acs.cgd.6b00402.

[310] F. Z. Tongzhou Liu, Nada Kittikunakorn, Yi Zhang, “Mechanisms of twin screw melt granulation Tongzhou,” *J. Drug Deliv. Sci. Technol.*, vol. 61, no. August 2020, p. 102150, 2021, doi: 10.1016/j.jddst.2020.102150.

[311] B. Mayoral, G. Garrett, and T. McNally, “Influence of screw profile employed during melt mixing on the micro-scale dispersion of MWCNTs in poly(propylene),” *Macromol. Mater. Eng.*, vol. 299, no. 6, pp. 748–756, 2014, doi: 10.1002/mame.201300172.

[312] M. Marigo, D. L. Cairns, M. Davies, A. Ingram, and E. H. Stitt, “Developing mechanistic understanding of granular behaviour in complex moving geometry using the Discrete Element Method Part B : Investigation of fl ow and mixing in the Turbula ® mixer,” *Powder Technol.*, vol. 212, no. 1, pp. 17–24, 2011, doi: 10.1016/j.powtec.2011.04.009.

[313] C. S. Yee, “The Development of PVP-based Solid Dispersions using Hot Melt Extrusion for the Preparation of Immediate Release Formulations,” vol. 9, no. November, 2014.

[314] K. Nakamichi, T. Nakano, H. Yasuura, S. Izumi, and Y. Kawashima, “The role of the kneading paddle and the effects of screw revolution speed and water content on the preparation of solid dispersions using a twin-screw extruder,” *Int. J. Pharm.*, vol. 241, no. 2, pp. 203–211, 2002, doi: 10.1016/S0378-5173(02)00134-5.

[315] E. Verhoeven, T. R. M. De Beer, G. Van den Mooter, J. P. Remon, and C. Vervaet, “Influence of formulation and process parameters on the release characteristics of ethylcellulose sustained-release mini-matrices produced by hot-melt extrusion,” *Eur. J. Pharm. Biopharm.*, vol. 69, no. 1, pp. 312–319, 2008, doi: 10.1016/j.ejpb.2007.10.007.

[316] N. Siriwannakij, T. Heimbach, and A. T. M. Serajuddin, “Aqueous Dissolution and Dispersion Behavior of Polyvinylpyrrolidone Vinyl Acetate-based Amorphous Solid Dispersion of Ritonavir Prepared by Hot-Melt Extrusion with and without Added Surfactants,” *J. Pharm. Sci.*, pp. 1–15, 2020, doi: 10.1016/j.xphs.2020.08.007.

[317] L. Briens and R. Logan, “The Effect of the Chopper on Granules from Wet High-Shear Granulation Using a PMA-1 Granulator,” vol. 12, no. 4, pp. 1358–1365, 2011, doi: 10.1208/s12249-011-9703-1.

[318] J. Dun and C. C. Sun, *Structures and Properties of Granules Prepared By High Shear Wet Granulation*. Elsevier Inc., 2019.

[319] R. Nogueira *et al.*, “Determination of Volatiles in Pharmaceutical Certified Reference Materials,” vol. 23, no. 9, pp. 1636–1646, 2012.

[320] M. Ja, A. Kuty, K. Sollohub, H. Wosicka, K. Cal, and P. Ciosek, “Bioelectrochemistry Electronic tongue for the detection of taste-masking microencapsulation of active pharmaceutical substances,” vol. 80, pp. 94–98, 2010, doi: 10.1016/j.bioelechem.2010.08.006.

[321] F. V. Paulovich, M. L. Moraes, R. M. Maki, M. Ferreira, O. N. Oliveira, and M. C. F. De Oliveira, “Information visualization techniques for sensing and biosensing,” *Analyst*, vol. 136, no. 7, pp. 1344–1350, Mar. 2011, doi: 10.1039/c0an00822b.

[322] S. J. Anroop B. Nair, “A simple practice guide for dose conversion between animals and human,” *J. Basic Clin. Pharm.* |, vol. 7, pp. 27–31, 2016, doi:

10.4103/0976-0105.177703.

[323] FDA, “Bioanalytical Method Validation Guidance for Industry Bioanalytical Method Validation Guidance for Industry,” no. May, 2018.

[324] ANVISA, *RESOLUÇÃO - RDC Nº 27 , DE 17 DE MAIO DE 2012*. 2012.

[325] A. Noorjahan, B. Amrita, and S. Kavita, “In vivo evaluation of taste masking for developed chewable and orodispersible tablets in humans and rats,” *Pharm. Dev. Technol.*, vol. 19, no. 3, pp. 290–295, 2014, doi: 10.3109/10837450.2013.778870.

[326] A. Juluri *et al.*, “Taste Masking of Griseofulvin and Caffeine Anhydrous Using Kleptose Linecaps DE17 by Hot Melt Extrusion,” vol. 17, no. 1, 2016, doi: 10.1208/s12249-015-0374-1.

[327] D. K. Tan, D. A. Davisjr, D. A. Miller, R. O. Williamsiii, and A. Nokhodchi, “Innovations in Thermal Processing : Hot-Melt Extrusion and KinetiSol ® Dispersing,” 2020, doi: 10.1208/s12249-020-01854-2.

[328] X. Zheng, F. Wu, Y. Hong, L. Shen, X. Lin, and Y. Feng, “Developments in Taste-Masking Techniques for Traditional Chinese Medicines,” pp. 1–22, 2018, doi: 10.3390/pharmaceutics10030157.

[329] M. Maniruzzaman, J. S. Boateng, B. Z. Chowdhry, M. J. Snowden, and D. Douroumis, “A review on the taste masking of bitter APIs: hot-melt extrusion (HME) evaluation,” vol. 9045, pp. 1–12, 2013, doi: 10.3109/03639045.2013.804833.

[330] M. Kaza, M. Kara, K. Kosicka, A. Siemi, and P. J. Rudzki, “Journal of Pharmaceutical and Biomedical Analysis Bioanalytical method validation : new FDA guidance vs . EMA guideline . Better or worse ?,” vol. 165, pp. 381–385, 2019, doi: 10.1016/j.jpba.2018.12.030.

[331] L. Yang, Y. Geng, H. Li, Y. Zhang, J. You, and Y. Chang, “Enhancement the oral bioavailability of praziquantel by incorporation into solid lipid nanoparticles,” vol. 64, pp. 3–6, 2009, doi: 10.1691/ph.2009.8140.

[332] Y. Liu *et al.*, “Dissolution and oral bioavailability enhancement of praziquantel by solid dispersions,” 2018.

[333] H. Jung, R. Medina, N. Castro, T. Corona, I. Nacional, and D. Neurologia,

"Pharmacokinetic Study of Praziquantel Administered Alone and in Combination with Cimetidine in a Single-Day Therapeutic Regimen," vol. 41, no. 6, pp. 1256–1259, 1997.

[334] R. G. and P. Andrews, "Praziquantel, a New Broad-spectrum Antischistosomal Agent," *Parasitenkunde*, vol. 150, pp. 129–150, 1977.

[335] Z. Hui, A. Kumar, P. Wan, and S. Heng, "ScienceDirect Overview of milling techniques for improving the solubility of poorly water-soluble drugs," *Asian J. Pharm. Sci.*, vol. 10, no. 4, pp. 255–274, 2015, doi: 10.1016/j.ajps.2014.12.006.

[336] M. M. Knopp *et al.*, "Comparative Study of Di ff erent Methods for the Prediction of Drug − Polymer Solubility," 2015, doi: 10.1021/acs.molpharmaceut.5b00423.

[337] S. Mark *et al.*, "Characterization of Amorphous Solid Dispersions and Identi fi cation of Low Levels of Crystallinity by Transmission Electron Microscopy," 2021, doi: 10.1021/acs.molpharmaceut.0c00918.

[338] A. Agrawal *et al.*, "Development of Tablet Formulation of Amorphous Solid Dispersions Prepared by Hot Melt Extrusion Using Quality by Design Approach," vol. 17, no. 1, pp. 214–232, 2016, doi: 10.1208/s12249-015-0472-0.

[339] M. R. C. Marques and M. Almukainzi, "Simulated Biological Fluids with Possible Application in Dissolution Testing," no. March 2015, pp. 14–28, 2011, doi: 10.14227/DT180311P15.

[340] J. N. Pawar *et al.*, "Development of amorphous dispersions of artemether with hydrophilic polymers via spray drying: Physicochemical and in silico studies," *Asian J. Pharm. Sci.*, vol. 11, no. 3, pp. 385–395, 2016, doi: 10.1016/j.ajps.2015.08.012.

[341] S. S. Gupta, A. Meena, T. Parikh, and A. T. M. Serajuddin, "Investigation of thermal and viscoelastic properties of polymers relevant to hot melt extrusion - I: Polyvinylpyrrolidone and related polymers," *J. Excipients Food Chem.*, vol. 5, no. 1, pp. 32–45, 2014.

[342] Á. A. N. de Lima, "Avaliação dos aspectos físico-químicos do antichagásico Benznidazol, diferentes sistemas carreadores e formas farmacêuticas, através de técnicas analíticas e de imagens," Universidade Federal de Pernambuco, 2012.

[343] World Health Organization, "Report of a meeting to review the results of studies

on the treatment of schistosomiasis in preschool-age children," GENEVA, SWITZERLAND, 2010. [Online]. Available: https://apps.who.int/iris/bitstream/handle/10665/44639/9789241501880_eng.pdf?sequence=1.

[344] P. L. Olliaro *et al.*, "Efficacy and safety of single 40 mg/kg oral praziquantel in the treatment of schistosomiasis in preschool-age versus school-age children: An individual participant data meta-analysis," *PLoS Negl. Trop. Dis.*, vol. 14, no. 6, pp. 1–23, 2020, doi: 10.1371/journal.pntd.0008277.

[345] J. T. Coulibaly *et al.*, "Efficacy and safety of ascending doses of praziquantel against Schistosoma haematobium infection in preschool-aged and school-aged children: A single-blind randomised controlled trial," *BMC Med.*, vol. 16, no. 1, pp. 1–10, 2018, doi: 10.1186/s12916-018-1066-y.

[346] J. Boniatti *et al.*, "Taste evaluation of three different commercial tablets for paediatric patients for neglected tropical diseases," in *Poster presented on European Paediatric Formulation initiative (EUPFI)*, 2019, vol. 5, p. 2019.

[347] S. Qi, J. Nasereddin, and F. Alqahtani, "Personalized Polypills Produced by Fused Deposition Modeling 3D Printing," 2019.

[348] T. Information, "Technical Information Soluplus ®," no. September 2015, pp. 1–14, 2019.

[349] F. H. M. La, "Quadro Comil Scalable Lab System ™." p. 10, 2020.

[1] O. MONDIALE and D. LA SANTÉ, "Schistosomiasis : number of people treated worldwide in 2014 Schistosomiase : nombre de personnes traitées dans le monde en 2014," *Wkly. Epidemiol. Rec.*, vol. 30, no. 5, pp. 25–31, 2015.

[2] M. L. Nelwan, "Schistosomiasis: Life Cycle, Diagnosis, and Control," *Curr. Ther. Res. - Clin. Exp.*, vol. 91, no. 24, pp. 5–9, 2019, doi: 10.1016/j.curtheres.2019.06.001.

[3] E. Y. Li, D. Gurarie, N. C. Lo, X. Zhu, and C. H. King, "Improving public health control of schistosomiasis with a modified WHO strategy : a model-based comparison study," *Lancet Glob. Heal.*, vol. 7, no. 10, pp. e1414–e1422, 2019, doi: 10.1016/S2214-109X(19)30346-8.

[4] L. B. da Fonseca, “DESENVOLVIMENTO DE NANOPARTÍCULAS POLIMÉRICAS CONTENDO PRAZIQUANTEL PARA O TRATAMENTO DA ESQUISTOSSOMOSE,” Universidade Federal do Rio de Janeiro, 2012.

[5] H. Wang *et al.*, “Metabolic profiling of praziquantel enantiomers,” vol. 90, pp. 166–178, 2014.

[6] P. T. Loverde, “Digenetic Trematodes,” in *Schistosomiasis*, R. T. Fried, Ed. Springer, 2019.

[7] D. P. Mcmanus, D. W. Dunne, M. Sacko, N. Zhou, and B. J. Vennervald, “Schistosomiasis,” *Nat. Rev. Dis. Prim.*, pp. 1–19, 2018, doi: 10.1038/s41572-018-0013-8.

[8] J. P. Soldati, “Dose maior é sinônimo de eficácia ?,” *Inf. IOC. Inst. Oswaldo Cruz/Fiocruz* -, p. 2012, 2011.

[9] R. Trastullo, L. S. Dolci, N. Passerini, and B. Albertini, “Development of flexible and dispersible oral formulations containing praziquantel for potential schistosomiasis treatment of pre-school age children,” *Int. J. Pharm.*, vol. 495, no. 1, pp. 536–550, 2015, doi: 10.1016/j.ijpharm.2015.09.019.

[10] D. Zanolla *et al.*, “A new soluble and bioactive polymorph of praziquantel,” *Eur. J. Pharm. Biopharm.*, vol. 127, no. January, pp. 19–28, 2018, doi: 10.1016/j.ejpb.2018.01.018.

[11] A. A. L. Carvalho, A. C. Mafud, P. L. S. Pinto, Y. P. Mascarenhas, and J. De Moraes, “Schistosomicidal effect of the anti-inflammatory drug diclofenac and its structural correlation with praziquantel,” *Int. J. Antimicrob. Agents*, vol. 44, no. 4, pp. 372–374, 2014, doi: 10.1016/j.ijantimicag.2014.06.018.

[12] Alan Lane de Melo and P. M. Z. Coelho, *Parasitologia Humana - Leishmaniose Visceral Americana*. 2007.

[13] Ministério da Saúde, *Guide to Health Surveillance*. 2019.

[14] M. da S. BRASIL, “MANSONI Diretrizes Técnicas Diretrizes técnicas,” 2014.

[15] K. E. R. Silva, R. M. F. Silva, S. P. M. Costa, L. A. Rolim, M. do C. A. Lima, and P. J. Rolim-Neto, “Alternativas terapêuticas no combate à Esquistossomose Mansônica,” *Rev. Ciencias Farm. Basica e Apl.*, vol. 33, no. 1, pp. 9–16, 2012.

[16] C. V. V. Rollemberg *et al.*, “Aspectos epidemiológicos e distribuição geográfica da esquistossomose e geo-helmintos, no Estado de Sergipe, de acordo com os dados do Programa de Controle da Esquistossomose,” *Rev. Soc. Bras. Med. Trop.*, vol. 44, no. 1, pp. 91–96, 2011, doi: 10.1590/s0037-86822011000100020.

[17] M. L. A. Ferrari, P. M. Z. Coelho, C. M. F. Antunes, C. A. P. Tavares, and A. S. Da Cunha, “Efficacy of oxamniquine and praziquantel in the treatment of Schistosoma mansoni infection: A controlled trial,” *Bull. World Health Organ.*, vol. 81, no. 3, pp. 190–196, 2003, doi: 10.1590/S0042-96862003000300009.

[18] R. E. Zaparoli, “2011 Sorocaba / SP,” 2011.

[19] 2013. Pernambuco. Secretaria Estadual de Saúde. Secretaria Executiva de Vigilância em Saúde. Programa de Enfretamento das Doenças Negligenciadas no Estado de Pernambuco SANAR – 2011 / 2014 / Secretaria Estadual de Saúde. Secretaria Executiva de Vigilância em Sa, “SANAR. Programa de enfrentamento às doenças negligenciadas.”

[20] L. B. Da Fonseca *et al.*, “Desenvolvimento de um medicamento brasileiro nanoencapsulado para o tratamento da esquistossomose,” *Vigilância Sanitária em Debate*, vol. 1, no. 4, pp. 85–91, 2013, doi: 10.3395/vd.v1i4.111pt.

[21] J. Zwang and P. L. Olliaro, “Clinical Efficacy and Tolerability of Praziquantel for Intestinal and Urinary Schistosomiasis—A Meta-analysis of Comparative and Non-comparative Clinical Trials,” *PLoS Negl. Trop. Dis.*, vol. 8, no. 11, 2014, doi: 10.1371/journal.pntd.0003286.

[22] N. Katz and P. M. Z. Coelho, “Clinical therapy of schistosomiasis mansoni: The Brazilian contribution,” *Acta Trop.*, vol. 108, no. 2–3, pp. 72–78, 2008, doi: 10.1016/j.actatropica.2008.05.006.

[23] V. B. R. da Silva, B. R. K. L. Campos, J. F. de Oliveira, J. L. Decout, and M. do Carmo Alves de Lima, “Medicinal chemistry of antischistosomal drugs: Praziquantel and oxamniquine,” *Bioorganic Med. Chem.*, vol. 25, no. 13, pp. 3259–3277, 2017, doi: 10.1016/j.bmc.2017.04.031.

[24] M. R. Carvalho Garbi Novaes, J. P. de Souza, and H. Clemente de Araújo, “Anthelmintic praziquantel synthesis from glycine,” *Quim. Nova*, no. 1, pp. 5–10, 1999.

[25] A. Borrego-Sánchez *et al.*, “Conformational polymorphic changes in the crystal structure of the chiral antiparasitic drug praziquantel and interactions with calcium carbonate,” *Eur. J. Pharm. Biopharm.*, vol. 132, no. July, pp. 180–191, 2018, doi: 10.1016/j.ejpb.2018.09.028.

[26] F. C. Lombardo, V. Pasche, G. Panic, Y. Endriss, and J. Keiser, “Life cycle maintenance and drug-sensitivity assays for early drug discovery in Schistosoma mansoni,” *Nat. Protoc.*, vol. 14, no. 2, pp. 461–481, 2019, doi: 10.1038/s41596-

018-0101-y.

[27] S. K. Park *et al.*, “The anthelmintic drug praziquantel activates a schistosome transient receptor potential channel,” *J. Biol. Chem.*, vol. 294, no. 49, pp. 18873–18880, 2019, doi: 10.1074/jbc.AC119.011093.

[28] WHO, “WHO Model Lists of Essential Medicines - Praziquantel,” 2021.

[29] C. S. Ferreira Marques *et al.*, “Solid dispersion of praziquantel enhanced solubility and improve the efficacy of the schistosomiasis treatment,” *J. Drug Deliv. Sci. Technol.*, vol. 45, no. December 2017, pp. 124–134, 2018, doi: 10.1016/j.jddst.2018.03.009.

[30] D. Zanolla *et al.*, “A new soluble and bioactive polymorph of praziquantel,” *Eur. J. Pharm. Biopharm.*, vol. 127, no. August 2017, pp. 19–28, 2018, doi: 10.1016/j.ejpb.2018.01.018.

[31] D. Cioli, L. Pica-mattoccia, A. Basso, and A. Guidi, “Schistosomiasis control : praziquantel forever ?,” *Mol. Biochem. Parasitol.*, vol. 195, no. 1, pp. 23–29, 2014, doi: 10.1016/j.molbiopara.2014.06.002.

[32] A. M. de L. A. B. E. de A. B. E. de O. L. S. de C. Barros, *Re lação Na cional de Me dicamentos Essenciais Re lação Na cional de Me dicamentos Essenciais*. 2020.

[33] J. C. Espinosa-Lara *et al.*, “Cocrystals of active pharmaceutical ingredients - Praziquantel in combination with oxalic, malonic, succinic, maleic, fumaric, glutaric, adipic, and pimelic acids,” *Cryst. Growth Des.*, vol. 13, no. 1, pp. 169–185, 2013, doi: 10.1021/cg301314w.

[34] A. Borrego-Sánchez, C. Viseras, C. Aguzzi, and C. I. Sainz-Díaz, “Molecular and crystal structure of praziquantel. Spectroscopic properties and crystal polymorphism,” *Eur. J. Pharm. Sci.*, vol. 92, pp. 266–275, 2016, doi: 10.1016/j.ejps.2016.04.023.

[35] WHO, “International strategies for tropical disease treatments - Experiences with praziquantel,” 1998.

[36] WHO, “Schistosomiasis in children_ a major public health problem,” pp. 1–3, 2017, [Online]. Available: https://www.pediatricpraziquantelconsortium.org/schistosomiasis.

[37] M. Cugovčan, J. Jablan, J. Lovrić, D. Cinčić, N. Galić, and M. Jug, “Biopharmaceutical characterization of praziquantel cocrystals and cyclodextrin complexes prepared by grinding,” *J. Pharm. Biomed. Anal.*, vol. 137, pp. 42–53, 2017, doi: 10.1016/j.jpba.2017.01.025.

[38] M. J. Doenhoff, D. Cioli, and J. Utzinger, “Praziquantel: Mechanisms of action, resistance and new derivatives for schistosomiasis,” *Curr. Opin. Infect. Dis.*, vol. 21, no. 6, pp. 659–667, 2008, doi: 10.1097/QCO.0b013e328318978f.

[39] W. Wu, W. Wang, and Y. X. Huang, “New insight into praziquantel against various developmental stages of schistosomes,” *Parasitol. Res.*, vol. 109, no. 6, pp. 1501–1507, 2011, doi: 10.1007/s00436-011-2670-3.

[40] F. C. Lombardo, B. Perissutti, and J. Keiser, “Activity and pharmacokinetics of a praziquantel crystalline polymorph in the Schistosoma mansoni mouse model,” *Eur. J. Pharm. Biopharm.*, vol. 142, no. June, pp. 240–246, 2019, doi: 10.1016/j.ejpb.2019.06.029.

[41] J. Kovač, M. Vargas, and J. Keiser, “In vitro and in vivo activity of R- and S-praziquantel enantiomers and the main human metabolite trans-4-hydroxy-praziquantel against Schistosoma haematobium,” *Parasites and Vectors*, vol. 10, no. 1, pp. 3–7, 2017, doi: 10.1186/s13071-017-2293-3.

[42] T. Meyer, H. Sekljic, S. Fuchs, H. Bothe, D. Schollmeyer, and C. Miculka, “Taste, a new incentive to switch to (R)-praziquantel in schistosomiasis treatment,” *PLoS Negl. Trop. Dis.*, vol. 3, no. 1, pp. 3–7, 2009, doi: 10.1371/journal.pntd.0000357.

[43] D. Zhang, H. Wang, J. Ji, L. Nie, and D. Sun, “A quantification method for determination of racemate praziquantel and R-enantiomer in rat plasma for comparison of their pharmacokinetics,” *J. Chromatogr. B*, vol. 1048, pp. 64–69, 2017, doi: 10.1016/j.jchromb.2017.02.013.

[44] I. Meister *et al.*, “Activity of praziquantel enantiomers and main metabolites against Schistosoma mansoni,” *Antimicrob. Agents Chemother.*, vol. 58, no. 9, pp. 5466–5472, 2014, doi: 10.1128/AAC.02741-14.

[45] W. M. Bagchus, D. Bezuidenhout, E. Harrison-moench, E. Kourany-lefoll, and P. Wolna, “Relative Bioavailability of Orally Dispersible Tablet Formulations of Levo- - and Racemic Praziquantel : Two Phase I Studies,” no. December 2018, pp. 66–76, 2019, doi: 10.1111/cts.12601.

[46] G. Z. Id and F. Mutapi, “Drug metabolism and pharmacokinetics of praziquantel : A review of variable drug exposure during schistosomiasis treatment in human hosts and experimental models,” pp. 1–26, 2020, doi: 10.1371/journal.pntd.0008649.

[47] ANVISA, “Consulta Medicamentos ANVISA - Praziquantel,” 2020.

[48] Merck, “Bula Cisticid 500mg Merck.”

[49] F.- Fiocruz, “Praziquantel - DMG-FAR-PRO-PRZ-001-2017,” in *Memento Terapeutico*, 2017, pp. 1–9.

[50] A. Garba *et al.*, “Acta Tropica Schistosomiasis in infants and preschool-aged children : Infection in a single Schistosoma haematobium and a mixed S . haematobium – S . mansoni foci of Niger,” vol. 115, no. May 2001, pp. 212–219, 2010, doi: 10.1016/j.actatropica.2010.03.005.

[51] M. Woelfle, J. Seerden, J. De Gooijer, K. Pouwer, P. Olliaro, and H. Matthew, “Resolution of Praziquantel,” vol. 5, no. 9, pp. 1–7, 2013, doi: 10.1371/journal.pntd.0001260.

[52] S. Botros, N. El-lakkany, S. H. Seif, A. Sabra, and M. Ibrahim, “Experimental Parasitology Comparative efficacy and bioavailability of different praziquantel brands,” *Exp. Parasitol.*, vol. 127, no. 2, pp. 515–521, 2011, doi: 10.1016/j.exppara.2010.10.019.

[53] The United States Pharmaceutical Convention., “USP43 Praziquantel API,” p. 3649, 2020.

[54] ANVISA, “Farmacopeia Brasileira Volume II – Monografias Insumos Farmacêuticos e Especialidades,” *Farm. Bras.*, vol. 2, pp. 1–1504, 2019.

[55] U. S. N. L. of Medicine, “ChemIDplus Advanced - Chemical information - Praziquantel,” 2021.

[56] E. S. Bochmann, A. Gryczke, and K. G. Wagner, “Validation of Model-Based Melt Viscosity in Hot-Melt Extrusion Numerical Simulation,” pp. 9–12, 2018, doi: 10.3390/pharmaceutics10030132.

[57] U. S. P. Convention, “Promoting the Quality of Medicines (PQM). Product Information Report: Praziquantel,” Rockville, Maryland., 2019.

[58] N. Passerini, B. Albertini, B. Perissutti, and L. Rodriguez, “Evaluation of melt granulation and ultrasonic spray congealing as techniques to enhance the dissolution of praziquantel,” *Int. J. Pharm.*, vol. 318, no. 1–2, pp. 92–102, 2006, doi: 10.1016/j.ijpharm.2006.03.028.

[59] D. Zanolla *et al.*, “Milling and comilling Praziquantel at cryogenic and room temperatures: Assessment of the process-induced effects on drug properties,” *J. Pharm. Biomed. Anal.*, vol. 153, pp. 82–89, 2018, doi: 10.1016/j.jpba.2018.02.018.

[60] B. Albertini *et al.*, “Combining mechanochemistry and spray congealing for new praziquantel pediatric formulations in schistosomiasis treatment,” *Int. J. Mol. Sci.*, vol. 20, no. 5, 2019, doi: 10.3390/ijms20051233.

[61] M. Münster, C. Schoch, C. Schmidt, and J. Breitkreutz, “Multiparticulate system combining taste masking and immediate release properties for the aversive compound praziquantel,” *Eur. J. Pharm. Sci.*, vol. 109, no. August, pp. 446–454, 2017, doi: 10.1016/j.ejps.2017.08.034.

[62] P. Olliaro, P. Delgado-romero, and J. Keiser, “The little we know about the pharmacokinetics and pharmacodynamics of praziquantel ( racemate and R - enantiomer ),” no. January, pp. 863–870, 2014, doi: 10.1093/jac/dkt491.

[63] P. R. Dametto, A. C. Dametto, L. Polese, C. A. Ribeiro, M. Chorilli, and O. de Freitas, “Development and physicochemical characterization of solid dispersions containing praziquantel for the treatment of schistosomiasis,” *J. Therm. Anal. Calorim.*, vol. 127, no. 2, pp. 1693–1706, 2017, doi: 10.1007/s10973-016-5759-1.

[64] PUBCHEM, “Praziquantel - Chemical and Physical Properties,” 2019.

[65] E. D. Costa *et al.*, “Unexpected solvent impact in the crystallinity of praziquantel/poly(vinylpyrrolidone) formulations. A solubility, DSC and solid-state NMR study,” *Int. J. Pharm.*, vol. 511, no. 2, pp. 983–993, 2016, doi: 10.1016/j.ijpharm.2016.08.009.

[66] M. V. Chaud *et al.*, “Development and evaluation of praziquantel solid dispersions in sodium starch glycolate,” *Trop. J. Pharm. Res.*, vol. 12, no. 2, pp. 163–168, 2013, doi: 10.4314/tjpr.v12i2.5.

[67] S. K. El-arini and H. Leuenberger, “Dissolution properties of praziquantel – PVP systems,” pp. 89–94, 1998.

[68] M. Münster *et al.*, “Comparative in vitro and in vivo taste assessment of liquid praziquantel formulations,” *Int. J. Pharm.*, vol. 529, no. 1–2, pp. 310–318, 2017, doi: 10.1016/j.ijpharm.2017.06.084.

[69] A. Gaggero *et al.*, “Co-grinding with surfactants as a new approach to enhance in vitro dissolution of praziquantel,” *J. Pharm. Biomed. Anal.*, vol. 189, 2020, doi: 10.1016/j.jpba.2020.113494.

[70] S. K. El-Arini, D. Giron, and H. Leuenberger, “Solubility properties of racemic praziquantel and its enantiomers,” *Pharm. Dev. Technol.*, vol. 3, no. 4, pp. 557–564, 1998, doi: 10.3109/10837459809028638.

[71] K.-K. and C. B. C. Yue Liu, Xin Wang, “Investigation of the phase diagrams of chiral praziquantel,” *Chirality*, vol. 18, pp. 259–264, 2006, doi: 10.1002/chir.

[72] A. Cedillo-Cruz, M. I. Aguilar, M. Flores-Alamo, F. Palomares-Alonso, and H. Jung-Cook, “A straightforward and efficient synthesis of praziquantel enantiomers

and their 4′-hydroxy derivatives," *Tetrahedron Asymmetry*, vol. 25, no. 2, pp. 133–140, 2014, doi: 10.1016/j.tetasy.2013.11.004.

[73] D. Zanolla *et al.*, "Exploring mechanochemical parameters using a DoE approach: Crystal structure solution from synchrotron XRPD and characterization of a new praziquantel polymorph," *Eur. J. Pharm. Sci.*, vol. 140, no. October, p. 105084, 2019, doi: 10.1016/j.ejps.2019.105084.

[74] D. Salazar-Rojas, R. M. Maggio, and T. S. Kaufman, "Preparation and characterization of a new solid form of praziquantel, an essential anthelmintic drug. Praziquantel racemic monohydrate," *Eur. J. Pharm. Sci.*, vol. 146, no. December 2019, p. 105267, 2020, doi: 10.1016/j.ejps.2020.105267.

[75] D. Zanolla *et al.*, "Mechanochemical formation of racemic praziquantel hemihydrate with improved biopharmaceutical properties," *Pharmaceutics*, vol. 12, no. 3, pp. 1–22, 2020.

[76] G. L. Amidon, H. Lennernäs, V. P. Shah, and J. R. Crison, "A Theoretical Basis for a Biopharmaceutic Drug Classification: The Correlation of in Vitro Drug Product Dissolution and in Vivo Bioavailability," *Pharmaceutical Research: An Official Journal of the American Association of Pharmaceutical Scientists*, vol. 12, no. 3. pp. 413–420, 1995, doi: 10.1023/A:1016212804288.

[77] A. Charalabidis, M. Sfouni, C. Bergström, and P. Macheras, "The Biopharmaceutics Classification System (BCS) and the Biopharmaceutics Drug Disposition Classification System (BDDCS): Beyond guidelines," *Int. J. Pharm.*, vol. 566, no. April, pp. 264–281, 2019, doi: 10.1016/j.ijpharm.2019.05.041.

[78] S. Baghel, H. Cathcart, and N. J. O. Reilly, "Polymeric Amorphous Solid Dispersions : A Review of Amorphization , Crystallization , Stabilization , Solid-State Characterization , and Aqueous Solubilization of Biopharmaceutical Classi fi cation System Class II Drugs," *J. Pharm. Sci.*, 2016, doi: 10.1016/j.xphs.2015.10.008.

[79] K. Göke *et al.*, "European Journal of Pharmaceutics and Biopharmaceutics Novel strategies for the formulation and processing of poorly water- soluble drugs," *Eur. J. Pharm. Biopharm.*, vol. 126, pp. 40–56, 2018, doi: 10.1016/j.ejpb.2017.05.008.

[80] A. Keeley *et al.*, "In Vitro Dissolution Model Can Predict the in Vivo Taste Masking Performance of Coated Multiparticulates," *Mol. Pharm.*, vol. 16, no. 5, pp. 2095–2105, 2019, doi: 10.1021/acs.molpharmaceut.9b00060.

[81] X. Nsabagasani *et al.*, "The 'child size medicines' concept: Policy provisions in

Uganda," *J. Pharm. Policy Pract.*, vol. 8, no. 1, pp. 1–9, 2015, doi: 10.1186/s40545-015-0025-7.

[82] V. Klingmann *et al.*, "Acceptability of an orodispersible film compared to syrup in neonates and infants: A randomized controlled trial," *Eur. J. Pharm. Biopharm.*, vol. 151, no. December 2019, pp. 239–245, 2020, doi: 10.1016/j.ejpb.2020.03.018.

[83] European Commission, "State of Paediatric Medicines in the EU: 10 years of the EU Paediatric Regulation," *DG Heal. Consum.*, pp. 1–17, 2017.

[84] V. Ivanovska, C. M. A. Rademaker, L. Van Dijk, and A. K. Mantel-Teeuwisse, "Pediatric drug formulations: A review of challenges and progress," *Pediatrics*, vol. 134, no. 2, pp. 361–372, 2014, doi: 10.1542/peds.2013-3225.

[85] K. Vithani and D. Douroumis, "Hot-melt extruded lipidic pellets for pediatric applications : An investigation of the e ff ects and stability on drug dissolution," *J. Drug Deliv. Sci. Technol.*, vol. 49, no. August 2018, pp. 43–49, 2019, doi: 10.1016/j.jddst.2018.10.033.

[86] R. Ternik *et al.*, "Assessment of swallowability and palatability of oral dosage forms in children: Report from an M-CERSI pediatric formulation workshop," *Int. J. Pharm.*, vol. 536, no. 2, pp. 570–581, 2018, doi: 10.1016/j.ijpharm.2017.08.088.

[87] L. Freerks, J. Sommerfeldt, P. C. Löper, and S. Klein, "Safe, swallowable and palatable paediatric mini-tablet formulations for a WHO model list of essential medicines for children compound – A promising starting point for future PUMA applications," *Eur. J. Pharm. Biopharm.*, vol. 156, no. August, pp. 11–19, 2020, doi: 10.1016/j.ejpb.2020.08.014.

[88] N. Mendonsa *et al.*, "Manufacturing strategies to develop amorphous solid dispersions: An overview," *J. Drug Deliv. Sci. Technol.*, vol. 55, no. December 2019, p. 101459, 2020, doi: 10.1016/j.jddst.2019.101459.

[89] G. C. Bazzo, B. R. Pezzini, and H. K. Stulzer, "Eutectic mixtures as an approach to enhance solubility , dissolution rate and oral bioavailability of poorly water-soluble drugs," *Int. J. Pharm.*, vol. 588, no. May, p. 119741, 2020, doi: 10.1016/j.ijpharm.2020.119741.

[90] A. Batra, D. Desai, and A. T. M. Serajuddin, "Conversion of α-lactose monohydrate to anhydrous form with superior tabletability by twin-screw extrusion at elevated temperature," *Int. J. Pharm.*, vol. 588, no. July, p. 119790, 2020, doi: 10.1016/j.ijpharm.2020.119790.

[91] S. Jacob and A. B. Nair, "Cyclodextrin complexes : Perspective from drug delivery

and formulation," no. May, pp. 201–217, 2018, doi: 10.1002/ddr.21452.

[92] A. Ramrao, T. Id, and J. N. Yadav, "A Review on Solid Dispersion and Carriers Used Therein for Solubility Enhancement of Poorly Water Soluble Drugs," *Tabriz Univ. Med. Sci.*, vol. 10, no. 3, pp. 359–369, 2020, doi: 10.34172/apb.2020.044.

[93] J. Keiser, H. Sayed, M. El-ghanam, H. Sabry, S. Anani, and A. El-wakeel, "Efficacy and Safety of Artemether in the Treatment of Chronic Fascioliasis in Egypt : Exploratory Phase-2 Trials," vol. 5, no. 9, 2011, doi: 10.1371/journal.pntd.0001285.

[94] S. E. Gerrard, J. Walsh, N. Bowers, S. Salunke, and S. Hershenson, "Innovations in Pediatric Drug Formulations and Administration Technologies for Low Resource Settings," 2019.

[95] W. H. O. E. Committee, W. H. O. M. List, E. Medicines, W. H. O. M. List, and E. Medicines, "THE SELECTION AND USE OF ESSENTIAL MEDICINES Report of the WHO Expert Committee , 2009 ( including the 16th WHO Model List of Essential Medicines and the 2nd WHO Model List of Essential Medicines for Children )," 2009.

[96] W. H. O. E. Committee, W. H. O. M. List, E. Medicines, M. List, and E. Medicines, "The Selection and Use of Essential Medicines," 2017.

[97] B. Group, "BNF for Children. The essencial resource for clinical use of medicines in children," UK.

[98] V. Anand, M. Kataria, V. Kukkar, V. Saharan, and P. K. Choudhury, "The latest trends in the taste assessment of pharmaceuticals," *Drug Discov. Today*, vol. 12, no. 5–6, pp. 257–265, 2007, doi: 10.1016/j.drudis.2007.01.010.

[99] P. Kozarewicz, "Regulatory perspectives on acceptability testing of dosage forms in children," *Int. J. Pharm.*, vol. 469, no. 2, pp. 245–248, 2014, doi: 10.1016/j.ijpharm.2014.03.057.

[100] European Medicines Agency (EMA), "Guideline on pharmaceutical development of medicines for paediatric use," *European Medicines Agency*, vol. rev 2. London, UK, pp. 1–24, 2013, [Online]. Available: https://www.ema.europa.eu/en/documents/scientific-guideline/guideline-pharmaceutical-development-medicines-paediatric-use_en.pdf.

[101] M. Moreira and M. Sarraguça, "How can oral paediatric formulations be improved? A challenge for the XXI century," *Int. J. Pharm.*, vol. 590, no. July, p. 119905, 2020, doi: 10.1016/j.ijpharm.2020.119905.

[102] F. Rodieux, M. Wilbaux, J. N. Van Den Anker, and M. Pfister, “Effect of Kidney Function on Drug Kinetics and Dosing in Neonates , Infants , and Children,” *Clin. Pharmacokinet.*, 2015, doi: 10.1007/s40262-015-0298-7.

[103] J. T. Coulibaly, G. Panic, K. D. Silué, J. Kovač, J. Hattendorf, and J. Keiser, “Efficacy and safety of praziquantel in preschool-aged and school-aged children infected with Schistosoma mansoni: a randomised controlled, parallel-group, dose-ranging, phase 2 trial,” *Lancet Glob. Heal.*, vol. 5, no. 7, pp. e688–e698, 2017, doi: 10.1016/S2214-109X(17)30187-0.

[104] M. K. Freeman, W. White, and M. Iranikhah, “Tablet Splitting: A Review of Weight and Content Uniformity,” *Consult. Pharm. may*, vol. 27, no. 5, pp. 341–352, 2012.

[105] J.-P. R. & M. P. Charlotte Verrue, Els Mehuys, Koen Boussery, “Tablet-splitting : a common yet not so innocent practice,” *J. Adv. Nurs.*, vol. 67, no. 1, pp. 26–32, 2010, doi: 10.1111/j.1365-2648.2010.05477.x.

[106] H. R. Devantier *et al.*, “Quantitative assessment of TRPM5-dependent oral aversiveness of pharmaceuticals using a mouse brief-access taste aversion assay,” *Behav. Pharmacol.*, vol. 19, no. 7, pp. 673–682, 2008, doi: 10.1097/FBP.0b013e3283123cd6.

[107] S. M. Hanning, F. L. Lopez, I. C. K. Wong, T. B. Ernest, C. Tuleu, and M. Orlu Gul, “Patient centric formulations for paediatrics and geriatrics: Similarities and differences,” *Int. J. Pharm.*, vol. 512, no. 2, pp. 355–359, 2016, doi: 10.1016/j.ijpharm.2016.03.017.

[108] E. Grossi, F. Pace, and R. Stockbrugger, “Human nutrition from the gastroenterologist’s perspective: Lessons from expo milano 2015,” *Hum. Nutr. From Gastroenterol. Perspect. Lessons From Expo Milano 2015*, pp. 1–213, 2016, doi: 10.1007/978-3-319-30361-1.

[109] J. Walsh *et al.*, “Playing hide and seek with poorly tasting paediatric medicines : Do not forget the excipients ☆,” *Adv. Drug Deliv. Rev.*, vol. 73, pp. 14–33, 2014, doi: 10.1016/j.addr.2014.02.012.

[110] C. S. Mennella JA, Spector AC, Reed DR, “Bad taste of medicines,” *Clin Ther*, vol. 35, no. 8, pp. 1225–1246, 2013, doi: 10.1016/j.clinthera.2013.06.007.The.

[111] R. Ternik *et al.*, “Assessment of swallowability and palatability of oral dosage forms in children: Report from an M-CERSI pediatric formulation workshop,” *Int. J. Pharm.*, vol. 536, no. 2, pp. 570–581, 2018, doi: 10.1016/j.ijpharm.2017.08.088.

[112] A. A. Lee and C. Owyang, *Sugars, sweet taste receptors, and brain responses*. Elsevier Inc., 2019.

[113] R. Bala, S. badjatya, and R. Madaan, "Strategies practiced to perk up oral palatability and acceptance of bitter drugs," *J. Drug Deliv. Sci. Technol.*, vol. 56, no. February, p. 101580, 2020, doi: 10.1016/j.jddst.2020.101580.

[114] A. H. A. Mohamed-Ahmed, J. Soto, T. Ernest, and C. Tuleu, "Non-human tools for the evaluation of bitter taste in the design and development of medicines: A systematic review," *Drug Discov. Today*, vol. 21, no. 7, pp. 1170–1180, 2016, doi: 10.1016/j.drudis.2016.05.014.

[115] C. P. Milne and J. B. Bruss, "The economics of pediatric formulation development for off-patent drugs," *Clin. Ther.*, vol. 30, no. 11, pp. 2133–2145, 2008, doi: 10.1016/j.clinthera.2008.11.019.

[116] R. V. Tiwari, A. N. Polk, H. Patil, X. Ye, M. B. Pimparade, and M. A. Repka, "Rat Palatability Study for Taste Assessment of Caffeine Citrate Formulation Prepared via Hot-Melt Extrusion Technology," *AAPS PharmSciTech*, vol. 18, no. 2, pp. 341–348, 2017, doi: 10.1208/s12249-015-0447-1.

[117] A. V Keating, J. Soto, C. Tuleu, C. Forbes, M. Zhao, and D. Q. M. Craig, "Solid state characterisation and taste masking ef fi ciency evaluation of polymer based extrudates of isoniazid for paediatric administration," *Int. J. Pharm.*, vol. 536, no. 2, pp. 536–546, 2018, doi: 10.1016/j.ijpharm.2017.07.008.

[118] M. Münster, "Paediatric drug development for praziquantel," 2018.

[119] J. Soto *et al.*, "Rats can predict aversiveness of Active Pharmaceutical Ingredients," *Eur. J. Pharm. Biopharm.*, vol. 133, no. August, pp. 77–84, 2018, doi: 10.1016/j.ejpb.2018.09.027.

[120] S. D.-B. Gesine Winzenburg∗, "Industry perspective on palatability testing in children—Two case studies," *Tech. Res. Dev. Novartis Pharma AG, Basel CH 4056, Switz.*, vol. 2012, no. 435, pp. 131–151, 2012.

[121] A. Riul, C. A. R. Dantas, C. M. Miyazaki, and O. N. Oliveira, "Recent advances in electronic tongues," *Analyst*, vol. 135, no. 10, pp. 2481–2495, 2010, doi: 10.1039/c0an00292e.

[122] K. C. Berridge, "Measuring hedonic impact in animals and infants: Microstructure of affective taste reactivity patterns," *Neurosci. Biobehav. Rev.*, vol. 24, no. 2, pp. 173–198, 2000, doi: 10.1016/S0149-7634(99)00072-X.

[123] S. Gittings, N. Turnbull, C. J. Roberts, and P. Gershkovich, "Dissolution

methodology for taste masked oral dosage forms," *J. Control. Release*, vol. 173, no. 1, pp. 32–42, 2014, doi: 10.1016/j.jconrel.2013.10.030.

[124] D. H. Choi, N. A. Kim, T. S. Nam, S. Lee, and S. H. Jeong, "Evaluation of taste-masking effects of pharmaceutical sweeteners with an electronic tongue system," *Drug Dev. Ind. Pharm.*, vol. 40, no. 3, pp. 308–317, 2014, doi: 10.3109/03639045.2012.758636.

[125] M. Maniruzzaman, J. S. Boateng, M. Bonnefille, A. Aranyos, J. C. Mitchell, and D. Douroumis, "Taste masking of paracetamol by hot-melt extrusion: An in vitro and in vivo evaluation," *Eur. J. Pharm. Biopharm.*, vol. 80, no. 2, pp. 433–442, 2012, doi: 10.1016/j.ejpb.2011.10.019.

[126] M. Guhmann, M. Preis, F. Gerber, N. Pöllinger, J. Breitkreutz, and W. Weitschies, "Development of oral taste masked diclofenac formulations using a taste sensing system," *Int. J. Pharm.*, vol. 438, no. 1–2, pp. 81–90, 2012, doi: 10.1016/j.ijpharm.2012.08.047.

[127] G. A. Campbell *et al.*, "Evaluating the taste masking effectiveness of various flavors in a stable formulated pediatric suspension and solution using the Astree trade; electronic tongue," *Powder Technol.*, vol. 224, pp. 109–123, 2012, doi: 10.1016/j.powtec.2012.02.038.

[128] H. Nakamura, S. Uchida, T. Sugiura, and N. Namiki, "The prediction of the palatability of orally disintegrating tablets by an electronic gustatory system," *Int. J. Pharm.*, vol. 493, no. 1–2, pp. 305–312, 2015, doi: 10.1016/j.ijpharm.2015.07.056.

[129] Y. Deng, L. Shen, Y. Yang, and J. Shen, "Development of nanoparticle-based orodispersible palatable pediatric formulations," *Int. J. Pharm.*, vol. 596, no. January, p. 120206, 2021, doi: 10.1016/j.ijpharm.2021.120206.

[130] M. Wesoły, M. Zabadaj, A. Amelian, K. Winnicka, W. Wróblewski, and P. Ciosek, "Tasting cetirizine-based microspheres with an electronic tongue," *Sensors Actuators, B Chem.*, vol. 238, pp. 1190–1198, 2017, doi: 10.1016/j.snb.2016.06.147.

[131] K. Woertz, C. Tissen, P. Kleinebudde, and J. Breitkreutz, "A comparative study on two electronic tongues for pharmaceutical formulation development," *J. Pharm. Biomed. Anal.*, vol. 55, no. 2, pp. 272–281, 2011, doi: 10.1016/j.jpba.2011.02.002.

[132] J. B. KATHARINA WOERTZ, CORINNA TISSEN, PETER KLEINEBUDDE, "Development of a Taste-Masked Generic Ibuprofen Suspension: Top-Down

Approach Guided by Electronic Tongue Measurements," *J. Pharm. Sci.*, vol. 100, no. 10, pp. 4460–4470, 2011, doi: DOI 10.1002/jps.22629.

[133] L. I. Immohr *et al.*, "Early pediatric formulation development with new chemical entities: Opportunities of e-tongue besides human taste assessment," *Int. J. Pharm.*, vol. 530, no. 1–2, pp. 201–212, 2017, doi: 10.1016/j.ijpharm.2017.07.069.

[134] J. C. Machado *et al.*, "Efficient praziquantel encapsulation into polymer microcapsules and taste masking evaluation using an electronic tongue," *Bull. Chem. Soc. Jpn.*, vol. 91, no. 6, pp. 865–874, 2018, doi: 10.1246/bcsj.20180005.

[135] M. Pein, M. Preis, C. Eckert, and F. E. Kiene, "Taste-masking assessment of solid oral dosage forms – A critical review," *Int. J. Pharm.*, vol. 465, no. 1–2, pp. 239–254, 2014, doi: 10.1016/j.ijpharm.2014.01.036.

[136] M. W. J. Dodds, D. A. Johnson, and C. Yeh, "Health benefits of saliva : a review," pp. 223–233, 2005, doi: 10.1016/j.jdent.2004.10.009.

[137] S. T. Prajapati, P. B. Patel, and C. N. Patel, "Formulation and evaluation of sublingual tablets containing Sumatriptan succinate," vol. 2, no. 3, 2012, doi: 10.4103/2230-973X.104400.

[138] A. Lura, G. Tardy, and P. Kleinebudde, "Tableting of mini-tablets in comparison with conventionally sized tablets : A comparison of tableting properties and tablet dimensions," vol. 2, no. November, 2020, doi: 10.1016/j.ijpx.2020.100061.

[139] V. Tumuluri, *Pharmaceutical mini - tablets : a*. Elsevier Inc., 2020.

[140] V. Klingmann *et al.*, "Favorable Acceptance of Mini-Tablets Compared with Syrup: A Randomized Controlled Trial in Infants and Preschool Children," pp. 1728–1733, 2013, doi: 10.1016/j.jpeds.2013.07.014.

[141] A. Tsiligiannis, M. Sfouni, R. Nalda-molina, and A. Dokoumetzidis, "European Journal of Pharmaceutical Sciences Optimization of a paediatric fixed dose combination mini-tablet and dosing regimen for the first line treatment of tuberculosis," *Eur. J. Pharm. Sci.*, vol. 138, no. June, p. 105016, 2019, doi: 10.1016/j.ejps.2019.105016.

[142] T. Huong, H. Thi, S. Lha, S. Pinto, and M. Flament, "Feasability of a new process to produce fast disintegrating pellets as novel multiparticulate dosage form for pediatric use," vol. 496, pp. 842–849, 2015.

[143] S. Kayuni *et al.*, "A systematic review with epidemiological update of male genital schistosomiasis (MGS): A call for integrated case management across the health system in sub-Saharan Africa," *Parasite Epidemiol. Control*, vol. 4, p. e00077,

2019, doi: 10.1016/j.parepi.2018.e00077.

[144] T. Sangnim and K. Huanbutta, “Journal of Drug Delivery Science and Technology Development and evaluation of taste-masked paracetamol chewable tablets using a polymer and / or wax dispersion technique,” *J. Drug Deliv. Sci. Technol.*, vol. 54, no. August, p. 101361, 2019, doi: 10.1016/j.jddst.2019.101361.

[145] G. G. Pereira, S. Figueiredo, and A. I. Fernandes, “Polymer Selection for Hot-Melt Extrusion Coupled to Fused Deposition Modelling in Pharmaceutics,” 2020.

[146] T. Tagami, E. Ito, R. Kida, K. Hirose, T. Noda, and T. Ozeki, “3D printing of gummy drug formulations composed of gelatin and an HPMC-based hydrogel for pediatric use,” *Int. J. Pharm.*, vol. 594, no. September 2020, p. 120118, 2021, doi: 10.1016/j.ijpharm.2020.120118.

[147] M. Elbadawi, B. Muñiz, F. K. H. Gavins, J. Jie, and S. Gaisford, “M3DISEEN : A novel machine learning approach for predicting the 3D printability of medicines,” *Int. J. Pharm.*, vol. 590, no. September, p. 119837, 2020, doi: 10.1016/j.ijpharm.2020.119837.

[148] G. Chen, Y. Xu, P. Chi, L. Kwok, and L. Kang, “Pharmaceutical Applications of 3D Printing,” *Addit. Manuf.*, vol. 34, no. November 2019, p. 101209, 2020, doi: 10.1016/j.addma.2020.101209.

[149] G. Chen, Y. Xu, P. Chi, L. Kwok, and L. Kang, “Pharmaceutical Applications of 3D Printing,” *Addit. Manuf.*, vol. 34, no. April, p. 101209, 2020, doi: 10.1016/j.addma.2020.101209.

[150] B. Shaqour, A. Samaro, B. Verleije, K. Beyers, and C. Vervaet, “Production of Drug Delivery Systems Using Fused Filament Fabrication : A Systematic Review,” pp. 1–16, 2020.

[151] A. Melocchi *et al.*, “A Graphical Review on the Escalation of Fused Deposition Modeling ( FDM ) 3D Printing in the Pharmaceutical Field,” *J. Pharm. Sci.*, vol. 109, no. 10, pp. 2943–2957, 2020, doi: 10.1016/j.xphs.2020.07.011.

[152] A. Goyanes, A. B. M. Buanz, A. W. Basit, and S. Gaisford, “Fused- fi lament 3D printing ( 3DP ) for fabrication of tablets,” vol. 476, pp. 88–92, 2014, doi: 10.1016/j.ijpharm.2014.09.044.

[153] A. Ghanizadeh Tabriz *et al.*, “3D printed bilayer tablet with dual controlled drug release for tuberculosis treatment,” *Int. J. Pharm.*, vol. 593, no. November 2020, p. 120147, 2021, doi: 10.1016/j.ijpharm.2020.120147.

[154] A. Goyanes, P. Robles, A. Buanz, A. W. Basit, and S. Gaisford, “Effect of

geometry on drug release from 3D printed tablets," *Int. J. Pharm.*, vol. 494, no. 2, pp. 657–663, 2015, doi: 10.1016/j.ijpharm.2015.04.069.

[155] K. Shi, J. P. Salvage, M. Maniruzzaman, and A. Nokhodchi, "Role of release modifiers to modulate drug release from fused deposition modelling ( FDM ) 3D printed tablets," *Int. J. Pharm.*, vol. 597, no. January, p. 120315, 2021, doi: 10.1016/j.ijpharm.2021.120315.

[156] A. Goyanes, N. Allahham, S. J. Trenfield, E. Stoyanov, S. Gaisford, and A. W. Basit, "Direct powder extrusion 3D printing: Fabrication of drug products using a novel single-step process," *Int. J. Pharm.*, vol. 567, no. May, 2019, doi: 10.1016/j.ijpharm.2019.118471.

[157] M. A. Gonzalez, M. V. Ramírez Rigo, and N. L. Gonzalez Vidal, "Praziquantel systems with improved dissolution rate obtained by high pressure homogenization," *Mater. Sci. Eng. C*, vol. 93, no. September 2017, pp. 28–35, 2018, doi: 10.1016/j.msec.2018.07.050.

[158] S. G. Rodrigues, I. Chaves, N. Ferreira, S. De Melo, and M. B. De Jesus, "Computational analysis and physico-chemical characterization of an inclusion compound between praziquantel and methyl- β -cyclodextrin for use as an alternative in the treatment of s ... Computational analysis and physico-chemical characterization of an i," *J. Incl. Phenom.*, no. May, 2011, doi: 10.1007/s10847-010-9852-y.

[159] G. Becket, L. J. Schep, and M. Yee, "Improvement of the in vitro dissolution of praziquantel by complexation with a - , b - and g -cyclodextrins," vol. 179, pp. 65–71, 1999.

[160] W. W. Shuyu Xie, Baoliang Pan, Zhou, Baoxin shi, Zhuangzhi Zhang Xu, Zhang Ming, "Solid lipid nanoparticle suspension enhanced the therapeutic efficacy of praziquantel against tapeworm," *Int. J. Nanomedicine*, pp. 2367–2374, 2011.

[161] L. N. Andrade *et al.*, "Praziquantel-loaded solid lipid nanoparticles: Production, physicochemical characterization, release profile, cytotoxicity and in vitro activity against Schistosoma mansoni," *J. Drug Deliv. Sci. Technol.*, vol. 58, no. June 2019, p. 101784, 2020, doi: 10.1016/j.jddst.2020.101784.

[162] G. C. Bazzo, G. Tambosi, E. C. Brüske, and M. Zétola, "Evaluation of enhanced aqueous solubility of praziquantel incorporated in poly (3- hydroxybutyrate) and Eudragit® E microspheres," *Acta Sci.*, pp. 91–96, 2013, doi: 10.4025/actascihealthsci.v35i1.10673.

[163] R. M. Mainardes, M. Palmira, D. Gremião, and R. C. Evangelista, “Thermoanalytical study of praziquantel-loaded PLGA nanoparticles,” vol. 42, 2006.

[164] L. B. Da Fonseca *et al.*, “Development of a brazilian nanoencapsulated drug for schistosomiasis treatment,” *Vigilância Sanitária em Debate*, vol. 1, no. 4, pp. 4–10, 2013, doi: 10.3395/vd.v1i4.111en.

[165] Lorena Menezes Vieira, “ENCAPSULAMENTO IN SITU DE PRAZIQUANTEL NA POLIMERIZAÇÃO EM SUSPENSÃO DO METACRILATO DE METILA PARA A PRODUÇÃO DE SISTEMAS DE LIBERAÇÃO CONTROLADA,” UNIVERSIDADE FEDERAL DO RIO DE JANEIRO COMO, 2014.

[166] J. B. Alves, T. Franckini Paiva, V. M. Salim, H. Conceição Ferraz, and J. C. Pinto, “ In situ encapsulation of praziquantel through methyl methacrylate/diethylaminoethyl methacrylate and MMA / DMAEMA miniemulsion copolymerizations in presence of distinct ionic surfactants ,” *SPE Polym.*, vol. 2, no. 2, pp. 110–121, 2021, doi: 10.1002/pls2.10037.

[167] S. T. and S. T. Paloma de la Torre, “Preparation, dissolution and characterization of praziquantel solid dispersions,” *Chem. Pharm. Bull*, vol. 47, no. 11, pp. 1629–1633, 1999, [Online]. Available: http://www.mendeley.com/research/geology-volcanic-history-eruptive-style-yakedake-volcano-group-central-japan/.

[168] A. Borrego-s *et al.*, “Ground Calcium Carbonate as a Low Cost and Biosafety Excipient for Solubility and Dissolution Improvement of Praziquantel,” 2019.

[169] S. Orlandi, J. Priotti, H. P. Diogo, D. Leonardi, C. J. Salomon, and T. G. Nunes, “Structural Elucidation of Poloxamer 237 and Poloxamer 237 / Praziquantel Solid Dispersions : Impact of Poly ( Vinylpyrrolidone ) over Drug Recrystallization and Dissolution Research Article Structural Elucidation of Poloxamer 237 and Poloxamer 237 / Prazi,” no. January, 2018, doi: 10.1208/s12249-017-0946-3.

[170] B. Om, S. Amruta, D. Shashikant, P. Rohini, R. Vinita, and K. Priyanka, “Design and statistical optimisation of praziquantel tablets by using solid dispersion approach,” no. June, pp. 83–92, 2015, doi: 10.4103/0973-8398.154689.

[171] M. V. Chaud *et al.*, “Solid dispersions with hydrogenated castor oil increase solubility , dissolution rate and intestinal absorption of praziquantel,” vol. 46, 2010.

[172] F. C. Cunha, “Separation of praziquantel enantiomers using simulated moving bed chromatographic unit with performance designed for semipreparative

applications," no. March, pp. 9–13, 2019, doi: 10.1002/chir.23084.

[173] X. Wang, S. Du, R. Zhang, X. Jia, T. Yang, and X. Zhang, "Drug-drug cocrystals : Opportunities and challenges," *Asian J. Pharm. Sci.*, no. xxxx, 2020, doi: 10.1016/j.ajps.2020.06.004.

[174] R. Thakuria, A. Delori, W. Jones, M. P. Lipert, L. Roy, and N. Rodríguez-hornedo, "Pharmaceutical cocrystals and poorly soluble drugs," *Int. J. Pharm.*, vol. 453, no. 1, pp. 101–125, 2013, doi: 10.1016/j.ijpharm.2012.10.043.

[175] C. Jacobs, O. Kayser, and R. H. Muller, "Nanosuspensions as particulate drug formulations in therapy Rationale for development and what we can expect for the future," vol. 47, pp. 3–19, 2001.

[176] V. Chikhalia *et al.*, "The effect of crystal morphology and mill type on milling induced crystal disorder," vol. 7, pp. 19–26, 2005, doi: 10.1016/j.ejps.2005.08.013.

[177] E. C. Arrúa, M. J. G. Ferreira, C. J. Salomon, and T. G. Nunes, "Elucidating the guest-host interactions and complex formation of praziquantel and cyclodextrin derivatives by 13 C and 15 N solid-state NMR spectroscopy," *Int. J. Pharm.*, vol. 496, no. 2, pp. 812–821, 2015, doi: 10.1016/j.ijpharm.2015.11.026.

[178] S. Xie *et al.*, "Formulation, characterization and pharmacokinetics of praziquantel-loaded hydrogenated castor oil solid lipid nanoparticles," *Nanomedicine*, vol. 5, pp. 693–701, 2010.

[179] B. Perissutti *et al.*, "An explorative analysis of process and formulation variables affecting comilling in a vibrational mill : The case of praziquantel," *Int. J. Pharm.*, vol. 533, no. 2, pp. 402–412, 2017, doi: 10.1016/j.ijpharm.2017.05.053.

[180] M. Malhado *et al.*, "Journal of Pharmaceutical and Biomedical Analysis Preclinical pharmacokinetic evaluation of praziquantel loaded in poly ( methyl methacrylate ) nanoparticle using a HPLC – MS / MS," vol. 117, pp. 405–412, 2016, doi: 10.1016/j.jpba.2015.09.023.

[181] B. Kumari and H. Bishnoi, "Review Article SOLID DISPERSION : ITS TYPES AND MECHANISM OF J ournal of P harma R esearch," no. March, 2019, doi: 10.5281/zenodo.2594669.

[182] A. Kapourani, E. Vardaka, K. Katopodis, and K. Kachrimanis, "Crystallization tendency of APIs possessing di ff erent thermal and glass related properties in amorphous solid dispersions," *Int. J. Pharm.*, vol. 579, no. February, p. 119149, 2020, doi: 10.1016/j.ijpharm.2020.119149.

[183] S. Shah, S. Maddineni, J. Lu, and M. A. Repka, "Melt extrusion with poorly soluble

drugs," *Int. J. Pharm.*, vol. 453, no. 1, pp. 233–252, 2013, doi: 10.1016/j.ijpharm.2012.11.001.

[184] B. L. de A. Costa, "Generation of high drug loading amorphous solid dispersions by different manufacturing processes," 2017.

[185] H. Veith, F. Wiechert, C. Luebbert, and G. Sadowski, "Combining crystalline and polymeric excipients in API solid dispersions – Opportunity or risk ?," *Eur. J. Pharm. Biopharm.*, vol. 158, no. September 2020, pp. 323–335, 2021, doi: 10.1016/j.ejpb.2020.11.025.

[186] A. Newman, *Rational Design for Amorphous Solid Dispersions*. Elsevier Inc., 2017.

[187] P. Pandi, R. Bulusu, N. Kommineni, W. Khan, and M. Singh, "Amorphous solid dispersions: An update for preparation, characterization, mechanism on bioavailability, stability, regulatory considerations and marketed products," *Int. J. Pharm.*, vol. 586, no. June, p. 119560, 2020, doi: 10.1016/j.ijpharm.2020.119560.

[188] P. Kanaujia, P. Poovizhi, W. K. Ng, and R. B. H. Tan, "Amorphous formulations for dissolution and bioavailability enhancement of poorly soluble APIs," *Powder Technol.*, vol. 285, pp. 2–15, 2015, doi: 10.1016/j.powtec.2015.05.012.

[189] K. Kogermann *et al.*, "Dissolution testing of amorphous solid dispersions," *Int. J. Pharm.*, vol. 444, no. 1–2, pp. 40–46, 2013, doi: 10.1016/j.ijpharm.2013.01.042.

[190] M. Tobyn *et al.*, "Amorphous Drug – PVP Dispersions : Application of Theoretical , Thermal and Spectroscopic Analytical Techniques to the Study of a Molecule With Intermolecular Bonds in Both the Crystalline and Pure Amorphous State," *J. Am. Pharm. Assoc.*, vol. 98, no. 9, pp. 3456–3468, 2009, doi: 10.1002/jps.21738.

[191] M. Savolainen *et al.*, "Better understanding of dissolution behaviour of amorphous drugs by in situ solid-state analysis using Raman spectroscopy," *Eur. J. Pharm. Biopharm.*, vol. 71, no. 1, pp. 71–79, 2009, doi: 10.1016/j.ejpb.2008.06.001.

[192] P. J. Skrdla, P. D. Floyd, and P. C. D. Orco, "The amorphous state : first-principles derivation of the Gordon – Taylor equation for direct prediction of the glass transition temperature of mixtures ; glass formers ; physical basis of the '" Rule of 2 / 3 ,"'" *Phys. Chem. Chem. Phys.*, vol. 19, pp. 20523–20532, 2017, doi: 10.1039/C7CP04124A.

[193] O. Jennotte, N. Koch, A. Lechanteur, and B. Evrard, "Three-dimensional printing technology as a promising tool in bioavailability enhancement of poorly water-soluble molecules : A review," *Int. J. Pharm.*, vol. 580, no. December 2019, p.

119200, 2020, doi: 10.1016/j.ijpharm.2020.119200.

[194] M. Hanada, S. V Jermain, X. Lu, Y. Su, and R. O. Williams, “Predicting physical stability of ternary amorphous solid dispersions using speci fi c mechanical energy in a hot melt extrusion process ☆,” *Int. J. Pharm.*, vol. 548, no. 1, pp. 571–585, 2018, doi: 10.1016/j.ijpharm.2018.07.029.

[195] S. Xu and W. Dai, “Drug precipitation inhibitors in supersaturable formulations,” *Int. J. Pharm.*, vol. 453, no. 1, pp. 36–43, 2013, doi: 10.1016/j.ijpharm.2013.05.013.

[196] K. Kachrimanis and I. Nikolakakis, “Polymers as Formulation Excipients for Hot-Melt Extrusion Processing of Pharmaceuticals,” in *Handbook of Polymers for Pharmaceutical Technologies*, vol. 2, 2015, pp. 121–149.

[197] P. J. Skrdla, P. D. Floyd, and P. C. D. Orco, “Predicting the solubility enhancement of amorphous drugs and related phenomena using basic thermodynamic principles and semi-empirical kinetic models,” *Int. J. Pharm.*, vol. 567, no. July, p. 118465, 2019, doi: 10.1016/j.ijpharm.2019.118465.

[198] B. C. Hancock and M. Parks, “What is the True Solubility Advantage for Amorphous Pharmaceuticals ?,” vol. 17, no. 4, 2000.

[199] R. Han *et al.*, “Insight into the Dissolution Molecular Mechanism of Ternary Solid Dispersions by Combined Experiments and Molecular Simulations,” *AAPS PharmSciTech*, vol. 20, no. 7, pp. 10–20, 2019, doi: 10.1208/s12249-019-1486-9.

[200] S. Huang, C. Mao, R. O. W. Iii, and C. Yang, “Solubility Advantage ( and Disadvantage ) of Pharmaceutical Amorphous Solid Dispersions,” *J. Pharm. Sci.*, pp. 1–13, 2016, doi: 10.1016/j.xphs.2016.08.017.

[201] A. Alhayali, “In Vitro Solubility and Supersaturation Behavior of Supersaturating Drug Delivery Systems,” Luleå University of Technology May.

[202] A. Schittny, “Mechanisms of increased bioavailability through amorphous solid dispersions : a review,” vol. 27, no. 1, pp. 110–127, 2020, doi: 10.1080/10717544.2019.1704940.

[203] G. Zogra and A. Newman, “Interrelationships Between Structure and the Properties of Amorphous Solids of Pharmaceutical Interest,” vol. 106, pp. 5–27, 2017, doi: 10.1016/j.xphs.2016.05.001.

[204] T. Pas, S. Verbert, B. Appeltans, and G. Van Den Mooter, “The influence of crushing amorphous solid dispersion dosage forms on the in-vitro dissolution kinetics,” *Int. J. Pharm.*, vol. 573, no. November 2019, p. 118884, 2020, doi:

10.1016/j.ijpharm.2019.118884.

[205] R. B. Chavan, S. Rathi, V. G. S. S. Jyothi, and N. R. Shastri, “Cellulose based polymers in development of amorphous solid dispersions,” *Asian J. Pharm. Sci.*, vol. 14, no. 3, pp. 248–264, 2019, doi: 10.1016/j.ajps.2018.09.003.

[206] A. R. Nair *et al.*, “Review Article Overview of Extensively Employed Polymeric Carriers in Solid Dispersion Technology,” 2020, doi: 10.1208/s12249-020-01849-z.

[207] T. D. Vaibhav Sihorkara, *The role of polymers and excipients in developing amorphous solid dispersions: An industrial perspective*. Elsevier Inc., 2020.

[208] S. B. Teja, S. P. Patil, G. Shete, S. Patel, and A. K. Bansal, “Drug-excipient behavior in polymeric amorphous solid dispersions .,” vol. 4, no. September, pp. 70–94, 2013.

[209] K. Lehmkemper, S. O. Kyerematen, O. Heinzerling, M. Degenhardt, and G. Sadowski, “Long-Term Physical Stability of PVP- and PVPVA-Amorphous Solid Dispersions,” 2017, doi: 10.1021/acs.molpharmaceut.6b00763.

[210] D. Feng *et al.*, “Polymer – Surfactant System Based Amorphous Solid Dispersion : Precipitation Inhibition and Bioavailability Enhancement of Itraconazole,” no. 1, pp. 1–15, 2018, doi: 10.3390/pharmaceutics10020053.

[211] H. J. Jung *et al.*, “Improved oral absorption of tacrolimus by a solid dispersion with hypromellose and sodium lauryl sulfate,” *Int. J. Biol. Macromol.*, vol. 83, pp. 282–287, 2016, doi: 10.1016/j.ijbiomac.2015.11.063.

[212] J. Chen, J. D. Ormes, J. D. Higgins, and L. S. Taylor, “Impact of Surfactants on the Crystallization of Aqueous Suspensions of Celecoxib Amorphous Solid Dispersion Spray Dried Particles,” 2015, doi: 10.1021/mp5006245.

[213] D. Hoon *et al.*, “Improved oral absorption of dutasteride via Soluplus 1 -based supersaturable self-emulsifying drug delivery system ( S-SEDDS ),” vol. 478, pp. 341–347, 2015.

[214] S. P. Chaudhari and R. P. Dugar, “Application of surfactants in solid dispersion technology for improving solubility of poorly water soluble drugs Journal of Drug Delivery Science and Technology Application of surfactants in solid dispersion technology for improving solubility of poorly w,” *J. Drug Deliv. Sci. Technol.*, vol. 41, no. February 2018, pp. 68–77, 2017, doi: 10.1016/j.jddst.2017.06.010.

[215] W. Zhang, S. S. Hate, D. J. Russell, H. H. Hou, and K. Nagapudi, “Impact of Surfactant and Surfactant-Polymer Interaction on Desupersaturation of

Clotrimazole," *J. Pharm. Sci.*, vol. 108, no. 10, pp. 3262–3271, 2019, doi: 10.1016/j.xphs.2019.05.035.

[216] A. Schittny, S. Philipp-bauer, P. Detampel, J. Huwyler, and M. Puchkov, "Mechanistic insights into e ff ect of surfactants on oral bioavailability of amorphous solid dispersions," *J. Control. Release*, vol. 320, no. August 2019, pp. 214–225, 2020, doi: 10.1016/j.jconrel.2020.01.031.

[217] R. C. Rowe, P. J. Sheskey, and S. C. Owen, *Handbook of Pharmaceutical Excipients*, 5th ed. London: Pharmaceutical Pres, 2006.

[218] C. Viet and P. C. Cho, "Application of D -α-tocopheryl polyethylene glycol 1000 succinate ( TPGS ) in transdermal and topical drug delivery systems ( TDDS )," *J. Pharm. Investig.*, vol. 0, no. 0, p. 0, 2017, doi: 10.1007/s40005-016-0300-x.

[219] D. Hurley, M. Davis, G. M. Walker, J. G. Lyons, and C. L. Higginbotham, "The E ff ect of Cooling on the Degree of Crystallinity , Solid-State Properties , and Dissolution Rate of Multi-Component Hot-Melt Extruded Solid Dispersions," no. 2004, 2020.

[220] Y. A. and M. S. François Hallouarda, Lyes Mehennic, Malika Lahiani-Skibaa, "Solid Dispersions for Oral Administration : An Overview of the Methods for their Preparation Solid Dispersions for Oral Administration : An Overview of the Methods for their Preparation," *Curr. Pharm. Des.*, vol. 22, no. August, pp. 1–17, 2016, doi: 10.2174/1381612822666160 72.

[221] J. Knapik-kowalczuk, K. Chmiel, J. Pacułt, and K. Bialek, "Enhancement of the Physical Stability of Amorphous Sildenafil in a Binary Mixture , with either a Plasticizing or Antiplasticizing Compound," pp. 23–28, 2020.

[222] A. Prudic, T. Kleetz, M. Korf, Y. Ji, and G. Sadowski, "In fl uence of Copolymer Composition on the Phase Behavior of Solid Dispersions," 2014.

[223] K. Deboyace and P. L. D. Wildfong, "The Application of Modeling and Prediction to the Formation and Stability of Amorphous Solid Dispersions," *J. Pharm. Sci.*, vol. 107, no. 1, pp. 57–74, 2018, doi: 10.1016/j.xphs.2017.03.029.

[224] J. L. Calahan and F. Alvarez-nunez, "Characterization of Amorphous Solid Dispersions of AMG 517 in HPMC-AS and Crystallization using Isothermal Microcalorimetry By," 2011.

[225] M. F. Simões, R. M. A. Pinto, and S. Simões, "Hot-melt extrusion in the pharmaceutical industry : toward filing a new drug application," *Drug Discov. Today*, vol. 00, no. 00, 2019, doi: 10.1016/j.drudis.2019.05.013.

[226] F. C. Campbell, “Thermodynamics and Phase Diagrams,” pp. 41–72, 2012.

[227] D. Jeli, “Thermal Stability of Amorphous Solid Dispersions,” 2021.

[228] W. F. WEI LIU, , YU LIU, JIAOQI HUANG, ZHONGQUAN LIN, XUANCHENG PAN, XIAOJUN ZENG, MARC LAMY DE LA CHAPELLE, YANG ZHANG, “Identification and investigation of the vibrational properties of crystalline and co- amorphous drugs with Raman and terahertz spectroscopy,” vol. 10, no. 8, pp. 4290–4304, 2019, doi: 10.1364/BOE.10.004290.

[229] D. G. Dastidar and G. Chakrabarti, *Thermoresponsive Drug Delivery Systems, Characterization and Application*. Elsevier Inc., 2019.

[230] Y. Peng, D. D. Dussan, and R. Narain, *Thermal, mechanical, and electrical properties*. 2020.

[231] N. R. Jadhav, V. L. Gaikwad, K. J. Nair, and H. M. Kadam, “Glass transition temperature : Basics and application in pharmaceutical sector,” no. June, 2009, doi: 10.4103/0973-8398.55043.

[232] C. Wu and J. W. Mcginity, “Influence of Ibuprofen as a Solid-State Plasticizer in Eudragit ® RS 30 D on the Physicochemical Properties of Coated Beads,” vol. 2, no. 4, 2001.

[233] J. A. Baird and L. S. Taylor, “Evaluation of amorphous solid dispersion properties using thermal analysis techniques ☆,” vol. 64, pp. 396–421, 2012, doi: 10.1016/j.addr.2011.07.009.

[234] V. Corrtelius T. Moynihan,” Allan J. Easteal, James Wilder, “Dependence of the glass transition temperature on heating and cooling rate,” vol. 7, no. 26, 1974, doi: 10.1021/j100619a008.

[235] A. H. L. K. C.-L. HSU, D.R. HELDMAN, T.A. TAYLOR and ABSTRACT:, “Influence of Cooling Rate on Glass Transition Temperature of Sucrose Solutions and Rice Starch Gel,” vol. 68, no. 6, pp. 1–6, 2003.

[236] A. Newman and G. Zografi, “Commentary Commentary : Considerations in the Measurement of Glass Transition Temperatures of Pharmaceutical Amorphous Solids,” pp. 1–13, 2020, doi: 10.1208/s12249-019-1562-1.

[237] S. Janssens and G. Van Den Mooter, “Review : physical chemistry of solid dispersions,” pp. 1571–1586, 2009, doi: 10.1211/jpp/61.12.0001.

[238] P. G. Royall, D. Q. M. Craig, and C. Doherty, “Characterisation of moisture uptake effects on the glass transitional behaviour of an amorphous drug using modulated temperature DSC,” vol. 192, pp. 39–46, 1999.

[239] R. Tanaka, Y. Hattori, Y. Horie, H. Kamada, and T. Nagato, “Characterization of Amorphous Solid Dispersion of Pharmaceutical Compound with pH-Dependent Solubility Prepared by Continuous-Spray Granulator,” doi: 10.3390/pharmaceutics11040159.

[240] M. Latreche, “Maîtrise de la stabilité physique des alliages moléculaires amorphes pour optimiser l’efficacité des médicaments,” L’Université de Lille, 2019.

[241] S. Dedroog, T. Pas, B. Vergauwen, C. Huygens, and G. Van Den Mooter, “Analysis Solid-state analysis of amorphous solid dispersions : Why DSC and XRPD may not be regarded as stand-alone techniques,” *J. Pharm. Biomed. Anal.*, vol. 178, p. 112937, 2020, doi: 10.1016/j.jpba.2019.112937.

[242] H. A. Schneider, “The Gordon-Taylor equation . Additivity and interaction in compatible polymer blends,” vol. 1955, pp. 1941–1955, 1988.

[243] M. M. Knopp *et al.*, “A Promising New Method to Estimate Drug-Polymer Solubility at Room Temperature,” vol. 105, pp. 2621–2624, 2016, doi: 10.1016/j.xphs.2016.02.017.

[244] B. L. A. Costa, M. Sauceau, S. Del Confetto, R. Sescousse, and M. I. Ré, “Determination of drug-polymer solubility from supersaturated spray-dried amorphous solid dispersions : A case study with Efavirenz and Soluplus ®,” *Eur. J. Pharm. Biopharm.*, vol. 142, no. July 2018, pp. 300–306, 2019, doi: 10.1016/j.ejpb.2019.06.028.

[245] A. Karagianni, “Co-Amorphous Solid Dispersions for Solubility and Absorption Improvement of Drugs : Composition , Preparation , Characterization and Formulations for Oral Delivery,” 2018, doi: 10.3390/pharmaceutics10030098.

[246] and M. D. Aurélien Mahieu, Jean-François Willart,* Emeline Dudognon, Florence Danède, “A New Protocol To Determine the Solubility of Drugs into Polymer Matrixes,” *Mol. Pharm.*, 2013.

[247] Y. E. Sun, J. Tao, G. G. Z. Zhang, and L. Yu, “Solubilities of Crystalline Drugs in Polymers : An Improved Analytical Method and Comparison of Solubilities of Indomethacin and Nifedipine in PVP , PVP / VA , and PVAc,” *J. Pharm. Sci.*, vol. 99, no. 9, pp. 4023–4031, 2010, doi: 10.1002/jps.22251.

[248] Z. Yang, K. Nollenberger, J. Albers, and S. Qi, “Molecular Implications of Drug − Polymer Solubility in Understanding the Destabilization of Solid Dispersions by Milling,” 2014.

[249] E. Sawicki, “Solid dispersions in oncology : a solution to solubility-limited oral

drug absorption," Universiteit Utrecht, 2017.

[250] N. Boersen, T. Lee, and H. Hui, *Toxicology Studies*. Elsevier Inc., 2013.

[251] A. Newman, *Pharmaceutical amorphous solid dispersion*. New Jersey, 2015.

[252] A. W. M. Navnit Shah, Harpreet Sandhu, Duk Soon Choi Hitesh Chokshi, *Amorphous Solid Dispersions Theory and Practice*. London: Springer NewYork Heidelberg Dordrecht London, 2014.

[253] D. D. Sun, H. Wen, and L. S. Taylor, "Non-Sink Dissolution Conditions for Predicting Product Quality and In Vivo Performance of Supersaturating Drug Delivery Systems," *J. Pharm. Sci.*, vol. 105, no. 9, pp. 2477–2488, 2016, doi: 10.1016/j.xphs.2016.03.024.

[254] K. Sugita and N. Takata, "Dose-Dependent Solubility – Permeability Interplay for Poorly Soluble Drugs under Non-Sink Conditions," pp. 297–307, 2021.

[255] S. Petralito *et al.*, "Apparent Solubility and Dissolution Profile at Non-Sink Conditions as Quality Improvement Tools," 2010.

[256] M. Descamps and J. F. Willart, "Perspectives on the amorphisation / milling relationship in pharmaceutical materials ☆," *Adv. Drug Deliv. Rev.*, vol. 100, pp. 51–66, 2016, doi: 10.1016/j.addr.2016.01.011.

[257] M. Descamps, A. Aumelas, S. Desprez, and J. F. Willart, "The amorphous state of pharmaceuticals obtained or transformed by milling : Sub-Tg features and rejuvenation," vol. 407, pp. 72–80, 2015, doi: 10.1016/j.jnoncrysol.2014.08.055.

[258] M. Descamps, J. F. Willart, E. Dudognon, and V. Caron, "Transformation of Pharmaceutical Compounds upon Milling and Comilling : The Role of T g," vol. 96, no. 5, pp. 1398–1407, 2007, doi: 10.1002/jps.

[259] S. Dedroog, C. Huygens, and G. Van Den Mooter, "Chemically identical but physically different : A comparison of spray drying , hot melt extrusion and cryo-milling for the formulation of high drug loaded amorphous solid dispersions of naproxen," *Eur. J. Pharm. Biopharm.*, vol. 135, no. November 2018, pp. 1–12, 2019, doi: 10.1016/j.ejpb.2018.12.002.

[260] M. Latreche, J. Willart, M. Guerain, H. Alain, and F. Dan, "Using Milling to Explore Physical States : The Amorphous and Polymorphic Forms of Sulindac," vol. 108, pp. 2635–2642, 2019, doi: 10.1016/j.xphs.2019.03.017.

[261] B. Wang *et al.*, "A critical review of spray-dried amorphous pharmaceuticals : Synthesis , analysis and application," *Int. J. Pharm.*, vol. 594, no. October 2020, p. 120165, 2021, doi: 10.1016/j.ijpharm.2020.120165.

[262] M. Ré, “Formulating Drug Delivery Systems by Spray Drying,” *Dry. Technol. An Int. J.*, vol. 24, no. 4, pp. 433–446, 2007, doi: 10.1080/07373930600611877.

[263] A. Paudel, Z. A. Worku, J. Meeus, S. Guns, and G. Van Den Mooter, “Manufacturing of solid dispersions of poorly water soluble drugs by spray drying : Formulation and process considerations,” *Int. J. Pharm.*, vol. 453, no. 1, pp. 253–284, 2013, doi: 10.1016/j.ijpharm.2012.07.015.

[264] D. S. / M. Y. / D. Isadiartuti1, “Ternary solid dispersion to improve solubility and dissolution of meloxicam Abstract :,” *J. Basic Clin. Physiol. Pharmacol. 2019; 20190244*, pp. 1–8, 2019, doi: 10.1515/jbcpp-2019-0244.

[265] C. C. C. Teixeira *et al.*, “Microparticles Containing Curcumin Solid Dispersion : Stability , Bioavailability and Anti-Inflammatory Activity,” vol. 17, no. 2, pp. 252–261, 2016, doi: 10.1208/s12249-015-0337-6.

[266] K. Wlodarski and F. Zhang, “Synergistic Effect of Polyvinyl Alcohol and Copovidone in Itraconazole Amorphous Solid Dispersions,” no. 1, 2018.

[267] M. Maniruzzaman, D. Douroumis, J. S., and M. J., “Hot-Melt Extrusion (HME): From Process to Pharmaceutical Applications,” *Recent Adv. Nov. Drug Carr. Syst.*, pp. 3–16, 2012, doi: 10.5772/51582.

[268] R. Thakkar, R. Thakkar, A. Pillai, E. A. Ashour, and M. A. Repka, “Systematic screening of pharmaceutical polymers for hot melt extrusion processing: a comprehensive review,” *Int. J. Pharm.*, vol. 576, no. October 2019, p. 118989, 2020, doi: 10.1016/j.ijpharm.2019.118989.

[269] A. Alshetaili, S. M. Alshahrani, B. K. Almutairy, and M. A. Repka, “Hot Melt Extrusion Processing Parameters Optimization,” pp. 1–14, 2020.

[270] H. Patil, R. V Tiwari, and M. A. Repka, “Hot-Melt Extrusion : from Theory to Application in Pharmaceutical Formulation,” 2015, doi: 10.1208/s12249-015-0360-7.

[271] S. Narala, D. Nyavanandi, P. Srinivasan, P. Mandati, and S. Bandari, “Pharmaceutical Co-crystals , Salts , and Co-amorphous Systems : A novel opportunity of hot-melt extrusion,” *J. Drug Deliv. Sci. Technol.*, vol. 61, no. November 2020, p. 102209, 2021, doi: 10.1016/j.jddst.2020.102209.

[272] J. Thiry, F. Krier, and B. Evrard, “A review of pharmaceutical extrusion : Critical process parameters and,” *Int. J. Pharm.*, vol. 479, no. 1, pp. 227–240, 2015, doi: 10.1016/j.ijpharm.2014.12.036.

[273] L. Saerens *et al.*, “In-line NIR spectroscopy for the understanding of polymer –

drug interaction during pharmaceutical hot-melt extrusion," *Eur. J. Pharm. Biopharm.*, vol. 81, no. 1, pp. 230–237, 2012, doi: 10.1016/j.ejpb.2012.01.001.

[274] N. Follonier, E. Doelker, and E. T. Cole, "controlled release Various ways of modulating the release of diltiazem hydrochloride from hot-melt extruded sustained release pellets prepared using polymeric materials," vol. 36, pp. 243–250, 1995.

[275] A. Gryczke, S. Schminke, M. Maniruzzaman, J. Beck, and D. Douroumis, "Colloids and Surfaces B : Biointerfaces Development and evaluation of orally disintegrating tablets ( ODTs ) containing Ibuprofen granules prepared by hot melt extrusion," *Colloids Surfaces B Biointerfaces*, vol. 86, no. 2, pp. 275–284, 2011, doi: 10.1016/j.colsurfb.2011.04.007.

[276] V. W. Yeung and I. C. K. Wong, "R ESEARCH ARTICLE," pp. 399–402, 2005.

[277] A. S. Alshetaili, J. Morott, S. Shah, and V. Kulkarni, "Mefenamic acid taste-masked oral disintegrating tablets with enhanced solubility via molecular interaction produced by hot melt extrusion technology," pp. 18–27, 2016, doi: 10.1016/j.jddst.2015.03.003.Mefenamic.

[278] L. F. B. Malaquias *et al.*, "Hot Melt Extrudates Formulated Using Design Space: One Simple Process for Both Palatability and Dissolution Rate Improvement," *J. Pharm. Sci.*, vol. 107, no. 1, pp. 286–296, 2018, doi: 10.1016/j.xphs.2017.08.014.

[279] R. Censi and M. R. Gigliobianco, "Hot Melt Extrusion : Highlighting Physicochemical Factors to Be Investigated While Designing and Optimizing a Hot Melt Extrusion Process," 2018, doi: 10.3390/pharmaceutics10030089.

[280] A. Butreddy, S. Bandari, and M. A. Repka, "Quality-by-design in hot melt extrusion based amorphous solid dispersions: An industrial perspective on product development," *Eur. J. Pharm. Sci.*, vol. 158, no. November 2020, p. 105655, 2020, doi: 10.1016/j.ejps.2020.105655.

[281] M. Maniruzzaman, J. S. Boateng, M. J. Snowden, and D. Douroumis, "A Review of Hot-Melt Extrusion : Process Technology to Pharmaceutical Products," vol. 2012, 2012, doi: 10.5402/2012/436763.

[282] S. V Jermain, C. Brough, and R. O. Williams, "Amorphous solid dispersions and nanocrystal technologies for poorly water- soluble drug delivery – An update," *Int. J. Pharm.*, vol. 535, no. 1–2, pp. 379–392, 2018, doi: 10.1016/j.ijpharm.2017.10.051.

[283] X. Ma and R. O. W. Iii, "Characterization of amorphous solid dispersions : An

update," *J. Drug Deliv. Sci. Technol.*, vol. 50, no. November 2018, pp. 113–124, 2019, doi: 10.1016/j.jddst.2019.01.017.

[284] Y. L. N. T. R. L. J. Q. W. Wu, "Understanding the Relationship between Wettability and Dissolution of Solid Dispersion," 2014, doi: 10.1016/j.ijpharm.2014.02.004.

[285] J. Thiry *et al.*, "Continuous production of itraconazole-based solid dispersions by hot melt extrusion : Preformulation , optimization and design space determination," *Int. J. Pharm.*, vol. 515, no. 1–2, pp. 114–124, 2016, doi: 10.1016/j.ijpharm.2016.10.003.

[286] M. M. Crowley *et al.*, "Pharmaceutical Applications of Hot-Melt Extrusion : Part I Pharmaceutical Applications of Hot-Melt Extrusion : Part I," vol. 9045, 2008, doi: 10.1080/03639040701498759.

[287] M. A. Azad, D. Olawuni, G. Kimbell, A. Z. Badruddoza, S. Hossain, and T. Sultana, *Polymers for Extrusion-Based 3D Printing of Pharmaceuticals : A Holistic Materials – Process Perspective*. .

[288] A. Goyanes, U. Det-Amornrat, J. Wang, A. W. Basit, and S. Gaisford, "3D scanning and 3D printing as innovative technologies for fabricating personalized topical drug delivery systems," *J. Control. Release*, vol. 234, pp. 41–48, 2016, doi: 10.1016/j.jconrel.2016.05.034.

[289] A. G. Iria Seoane-Viaño, Patricija Januskaite, Carmen Alvarez-Lorenzo, Abdul W. Basit, "Semi-solid extrusion 3D printing in drug delivery and biomedicine: Personalised solutions for healthcare challenges," *J. Control. Release*, 2021, doi: 10.1016/j.jconrel.2021.02.027.

[290] A. Goyanes *et al.*, "Automated therapy preparation of isoleucine formulations using 3D printing for the treatment of MSUD : First single-centre , prospective , crossover study in patients," *Int. J. Pharm.*, vol. 567, no. June, p. 118497, 2019, doi: 10.1016/j.ijpharm.2019.118497.

[291] Brasil and Agência Nacional de Vigilância Sanitária, "Farmacopeia Brasileira," *Farm. Bras.*, vol. 1, p. 874, 2019.

[292] BASF, "kOLLIDON VA 64 Technical Informations," no. June 2008, pp. 1–16, 2011.

[293] BASF, "Kolliphor ® SLS Kolliphor ® SLS Fine," no. 119863, pp. 1–6, 2012.

[294] A. Venkateshaiah, V. V. T. Padil, and M. Nagalakshmaiah, "Microscopic Techniques for the Analysis of Micro and Nanostructures of Biopolymers and

Their Derivatives."

[295] International Organization for Standardization, "International Organization for Standardization. 13320 2009," 2009.

[296] The United States Pharmaceutical Convention., "<429> Light diffraction measurement of particle size," *Suppl. to USP 43*, vol. 43, no. 4, p. 6697, 2020.

[297] The United States Pharmaceutical Convention., "USP43 Praziquantel Tablets," vol. 43, p. 3650, 2020.

[298] J. Sha *et al.*, "Solid-liquid phase equilibrium of praziquantel in eleven pure solvents: Determination, model correlation, solvent effect, molecular simulation and thermodynamic analysis," *J. Chem. Thermodyn.*, no. xxxx, 2020, doi: 10.1016/j.jct.2020.106327.

[299] S. S. Gupta, N. Solanki, and A. T. M. Serajuddin, "Investigation of Thermal and Viscoelastic Properties of Polymers Relevant to Hot Melt Extrusion, IV: Affinisol™ HPMC HME Polymers," *AAPS PharmSciTech*, vol. 17, no. 1, pp. 148–157, 2016, doi: 10.1208/s12249-015-0426-6.

[300] The United States Pharmaceutical Convention., "⟨ 776 ⟩ optical microscopy," *Suppl. to USP 43*, vol. 43, p. 6998, 2020.

[301] T. Templeman, S. Sengupta, N. Maman, E. Bar-or, and M. Shandalov, "Oriented Attachment: A Path to Columnar Morphology in Chemical Bath Deposited PbSe Thin Films," 2018, doi: 10.1021/acs.cgd.7b01771.

[302] D. Colegiada *et al.*, "Ministério da Saúde RESOLUÇÃO - RDC Nº 37, DE 3 DE AGOSTO DE 2011," 2011.

[303] U. S. D. of H. and H. Services and F. and D. Administration, "Waiver of In Vivo Bioavailability and Bioequivalence Studies for Immediate-Release Solid Oral Dosage Forms Based on a Biopharmaceutics Classification System Guidance for Industry," 2017.

[304] K. Yamasaki, K. Taguchi, K. Nishi, M. Otagiri, and H. Seo, "Enhanced dissolution and oral bioavailability of praziquantel by emulsification with human serum albumin followed by spray drying," *Eur. J. Pharm. Sci.*, vol. 139, no. September, p. 105064, 2019, doi: 10.1016/j.ejps.2019.105064.

[305] M. Karl and K. Kolter, "Suitability of Plasticized Polymers for Hot Melt Extrusion," *Excipients Act. Pharma*, vol. 24, no. Table 1, pp. 2–6, 2010.

[306] Y. Chen *et al.*, "Initial Drug Dissolution from Amorphous Solid Dispersions Controlled by Polymer Dissolution and Drug-Polymer Interaction," *Pharm. Res.*,

2016, doi: 10.1007/s11095-016-1969-2.

[307] A. Prudic, Y. Ji, and G. Sadowski, “Thermodynamic Phase Behavior of API/Polymer Solid Dispersions,” 2014.

[308] T. R. Hörmann *et al.*, “Sensitivity of a continuous hot-melt extrusion and strand pelletization line to control actions and composition variation,” *Int. J. Pharm.*, vol. 566, no. February, pp. 239–253, 2019, doi: 10.1016/j.ijpharm.2019.05.046.

[309] H. G. Moradiya, M. T. Islam, N. Scoutaris, S. A. Halsey, B. Z. Chowdhry, and D. Douroumis, “Continuous Manufacturing of High Quality Pharmaceutical Cocrystals Integrated with Process Analytical Tools for In-Line Process Control,” *Cryst. Growth Des.*, vol. 16, no. 6, pp. 3425–3434, 2016, doi: 10.1021/acs.cgd.6b00402.

[310] F. Z. Tongzhou Liu, Nada Kittikunakorn, Yi Zhang, “Mechanisms of twin screw melt granulation Tongzhou,” *J. Drug Deliv. Sci. Technol.*, vol. 61, no. August 2020, p. 102150, 2021, doi: 10.1016/j.jddst.2020.102150.

[311] B. Mayoral, G. Garrett, and T. McNally, “Influence of screw profile employed during melt mixing on the micro-scale dispersion of MWCNTs in poly(propylene),” *Macromol. Mater. Eng.*, vol. 299, no. 6, pp. 748–756, 2014, doi: 10.1002/mame.201300172.

[312] M. Marigo, D. L. Cairns, M. Davies, A. Ingram, and E. H. Stitt, “Developing mechanistic understanding of granular behaviour in complex moving geometry using the Discrete Element Method Part B : Investigation of fl ow and mixing in the Turbula ® mixer,” *Powder Technol.*, vol. 212, no. 1, pp. 17–24, 2011, doi: 10.1016/j.powtec.2011.04.009.

[313] C. S. Yee, “The Development of PVP-based Solid Dispersions using Hot Melt Extrusion for the Preparation of Immediate Release Formulations,” vol. 9, no. November, 2014.

[314] K. Nakamichi, T. Nakano, H. Yasuura, S. Izumi, and Y. Kawashima, “The role of the kneading paddle and the effects of screw revolution speed and water content on the preparation of solid dispersions using a twin-screw extruder,” *Int. J. Pharm.*, vol. 241, no. 2, pp. 203–211, 2002, doi: 10.1016/S0378-5173(02)00134-5.

[315] E. Verhoeven, T. R. M. De Beer, G. Van den Mooter, J. P. Remon, and C. Vervaet, “Influence of formulation and process parameters on the release characteristics of ethylcellulose sustained-release mini-matrices produced by hot-melt extrusion,” *Eur. J. Pharm. Biopharm.*, vol. 69, no. 1, pp. 312–319, 2008, doi:

10.1016/j.ejpb.2007.10.007.

[316] N. Siriwannakij, T. Heimbach, and A. T. M. Serajuddin, “Aqueous Dissolution and Dispersion Behavior of Polyvinylpyrrolidone Vinyl Acetate-based Amorphous Solid Dispersion of Ritonavir Prepared by Hot-Melt Extrusion with and without Added Surfactants,” *J. Pharm. Sci.*, pp. 1–15, 2020, doi: 10.1016/j.xphs.2020.08.007.

[317] L. Briens and R. Logan, “The Effect of the Chopper on Granules from Wet High-Shear Granulation Using a PMA-1 Granulator,” vol. 12, no. 4, pp. 1358–1365, 2011, doi: 10.1208/s12249-011-9703-1.

[318] J. Dun and C. C. Sun, *Structures and Properties of Granules Prepared By High Shear Wet Granulation*. Elsevier Inc., 2019.

[319] R. Nogueira *et al.*, “Determination of Volatiles in Pharmaceutical Certified Reference Materials,” vol. 23, no. 9, pp. 1636–1646, 2012.

[320] M. Ja, A. Kuty, K. Sollohub, H. Wosicka, K. Cal, and P. Ciosek, “Bioelectrochemistry Electronic tongue for the detection of taste-masking microencapsulation of active pharmaceutical substances,” vol. 80, pp. 94–98, 2010, doi: 10.1016/j.bioelechem.2010.08.006.

[321] F. V. Paulovich, M. L. Moraes, R. M. Maki, M. Ferreira, O. N. Oliveira, and M. C. F. De Oliveira, “Information visualization techniques for sensing and biosensing,” *Analyst*, vol. 136, no. 7, pp. 1344–1350, Mar. 2011, doi: 10.1039/c0an00822b.

[322] S. J. Anroop B. Nair, “A simple practice guide for dose conversion between animals and human,” *J. Basic Clin. Pharm.* |, vol. 7, pp. 27–31, 2016, doi: 10.4103/0976-0105.177703.

[323] FDA, “Bioanalytical Method Validation Guidance for Industry Bioanalytical Method Validation Guidance for Industry,” no. May, 2018.

[324] ANVISA, *RESOLUÇÃO - RDC Nº 27 , DE 17 DE MAIO DE 2012*. 2012.

[325] A. Noorjahan, B. Amrita, and S. Kavita, “In vivo evaluation of taste masking for developed chewable and orodispersible tablets in humans and rats,” *Pharm. Dev. Technol.*, vol. 19, no. 3, pp. 290–295, 2014, doi: 10.3109/10837450.2013.778870.

[326] A. Juluri *et al.*, “Taste Masking of Griseofulvin and Caffeine Anhydrous Using Kleptose Linecaps DE17 by Hot Melt Extrusion,” vol. 17, no. 1, 2016, doi: 10.1208/s12249-015-0374-1.

[327] D. K. Tan, D. A. Davisjr, D. A. Miller, R. O. Williamsiii, and A. Nokhodchi,

"Innovations in Thermal Processing : Hot-Melt Extrusion and KinetiSol ® Dispersing," 2020, doi: 10.1208/s12249-020-01854-2.

[328] X. Zheng, F. Wu, Y. Hong, L. Shen, X. Lin, and Y. Feng, "Developments in Taste-Masking Techniques for Traditional Chinese Medicines," pp. 1–22, 2018, doi: 10.3390/pharmaceutics10030157.

[329] M. Maniruzzaman, J. S. Boateng, B. Z. Chowdhry, M. J. Snowden, and D. Douroumis, "A review on the taste masking of bitter APIs: hot-melt extrusion (HME) evaluation," vol. 9045, pp. 1–12, 2013, doi: 10.3109/03639045.2013.804833.

[330] M. Kaza, M. Kara, K. Kosicka, A. Siemi, and P. J. Rudzki, "Journal of Pharmaceutical and Biomedical Analysis Bioanalytical method validation : new FDA guidance vs . EMA guideline . Better or worse ?," vol. 165, pp. 381–385, 2019, doi: 10.1016/j.jpba.2018.12.030.

[331] L. Yang, Y. Geng, H. Li, Y. Zhang, J. You, and Y. Chang, "Enhancement the oral bioavailability of praziquantel by incorporation into solid lipid nanoparticles," vol. 64, pp. 3–6, 2009, doi: 10.1691/ph.2009.8140.

[332] Y. Liu *et al.*, "Dissolution and oral bioavailability enhancement of praziquantel by solid dispersions," 2018.

[333] H. Jung, R. Medina, N. Castro, T. Corona, I. Nacional, and D. Neurologia, "Pharmacokinetic Study of Praziquantel Administered Alone and in Combination with Cimetidine in a Single-Day Therapeutic Regimen," vol. 41, no. 6, pp. 1256–1259, 1997.

[334] R. G. and P. Andrews, "Praziquantel, a New Broad-spectrum Antischistosomal Agent," *Parasitenkunde*, vol. 150, pp. 129–150, 1977.

[335] Z. Hui, A. Kumar, P. Wan, and S. Heng, "ScienceDirect Overview of milling techniques for improving the solubility of poorly water-soluble drugs," *Asian J. Pharm. Sci.*, vol. 10, no. 4, pp. 255–274, 2015, doi: 10.1016/j.ajps.2014.12.006.

[336] M. M. Knopp *et al.*, "Comparative Study of Di ff erent Methods for the Prediction of Drug − Polymer Solubility," 2015, doi: 10.1021/acs.molpharmaceut.5b00423.

[337] S. Mark *et al.*, "Characterization of Amorphous Solid Dispersions and Identi fi cation of Low Levels of Crystallinity by Transmission Electron Microscopy," 2021, doi: 10.1021/acs.molpharmaceut.0c00918.

[338] A. Agrawal *et al.*, "Development of Tablet Formulation of Amorphous Solid Dispersions Prepared by Hot Melt Extrusion Using Quality by Design Approach,"

vol. 17, no. 1, pp. 214–232, 2016, doi: 10.1208/s12249-015-0472-0.

[339] M. R. C. Marques and M. Almukainzi, “Simulated Biological Fluids with Possible Application in Dissolution Testing,” no. March 2015, pp. 14–28, 2011, doi: 10.14227/DT180311P15.

[340] J. N. Pawar *et al.*, “Development of amorphous dispersions of artemether with hydrophilic polymers via spray drying: Physicochemical and in silico studies,” *Asian J. Pharm. Sci.*, vol. 11, no. 3, pp. 385–395, 2016, doi: 10.1016/j.ajps.2015.08.012.

[341] S. S. Gupta, A. Meena, T. Parikh, and A. T. M. Serajuddin, “Investigation of thermal and viscoelastic properties of polymers relevant to hot melt extrusion - I: Polyvinylpyrrolidone and related polymers,” *J. Excipients Food Chem.*, vol. 5, no. 1, pp. 32–45, 2014.

[342] Á. A. N. de Lima, “Avaliação dos aspectos físico-químicos do antichagásico Benznidazol, diferentes sistemas carreadores e formas farmacêuticas, através de técnicas analíticas e de imagens,” Universidade Federal de Pernambuco, 2012.

[343] World Health Organization, “Report of a meeting to review the results of studies on the treatment of schistosomiasis in preschool-age children,” GENEVA, SWITZERLAND, 2010. [Online]. Available: https://apps.who.int/iris/bitstream/handle/10665/44639/9789241501880_eng.pdf?sequence=1.

[344] P. L. Olliaro *et al.*, “Efficacy and safety of single 40 mg/kg oral praziquantel in the treatment of schistosomiasis in preschool-age versus school-age children: An individual participant data meta-analysis,” *PLoS Negl. Trop. Dis.*, vol. 14, no. 6, pp. 1–23, 2020, doi: 10.1371/journal.pntd.0008277.

[345] J. T. Coulibaly *et al.*, “Efficacy and safety of ascending doses of praziquantel against Schistosoma haematobium infection in preschool-aged and school-aged children: A single-blind randomised controlled trial,” *BMC Med.*, vol. 16, no. 1, pp. 1–10, 2018, doi: 10.1186/s12916-018-1066-y.

[346] J. Boniatti *et al.*, “Taste evaluation of three different commercial tablets for paediatric patients for neglected tropical diseases,” in *Poster presented on European Paediatric Formulation initiative (EUPFI)*, 2019, vol. 5, p. 2019.

[347] S. Qi, J. Nasereddin, and F. Alqahtani, “Personalized Polypills Produced by Fused Deposition Modeling 3D Printing,” 2019.

[348] T. Information, “Technical Information Soluplus ®,” no. September 2015, pp. 1–

14, 2019.

[349] F. H. M. La, “Quadro Comil Scalable Lab System ™.” p. 10, 2020.

# CHAPTER 9 - RESUME ETENDU EN FRANÇAIS

Les maladies tropicales négligées (MTN) touchent plus de 1,4 milliard de personnes dans le monde, dont une proportion importante d'enfants [1]-[3]. La deuxième maladie la plus fréquente est la schistosomiase et touche environ 28 millions d'enfants en âge préscolaire (5 à 14 ans) [1]-[6]. Il s'agit d'une maladie causée par des vers parasites, correspondant à des helminthes de la classe Trematoda, de la famille Schistossomatidae et du genre Schistosoma [1]. Les parasites à l'origine de la schistosomiase vivent dans certains types d'escargots d'eau douce. La forme infectieuse du parasite, appelée cercaire, émerge de l'escargot dans l'eau. Les personnes peuvent être infectées lorsque leur peau entre en contact avec de l'eau douce contaminée. À l'échelle mondiale, on estime qu'elle touche plus de 250 millions de personnes dans 78 pays du monde et qu'elle est responsable de quelque 280 000 décès chaque année [6]. Le praziquantel (PZQ) est le médicament de référence dans le traitement de la schistosomiase selon l'Organisation Mondiale de la Santé (OMS), pour des raisons telles que sa grande efficacité, sa faible toxicité et son faible coût. Tous ces facteurs font du praziquantel le seul médicament commercialisé pour le traitement de la schistosomiase, pour laquelle il n'existe aucun vaccin.

En ce qui concerne le PZQ, il n'y a toujours pas de médicament pédiatrique approprié disponible sur le marché. Actuellement, le traitement des enfants est réalisé en adaptant le médicament pour adultes, en divisant ou en écrasant les comprimés [9]. Pour les enfants, la posologie est adaptée au poids corporel de l'enfant en administrant des doses de 150 mg (1/4 de comprimé) [9], [10]. Cette pratique conduit clairement à une faible adhésion au traitement car elle met en évidence le mauvais goût du médicament. De plus, des facteurs tels que la grande variabilité corporelle et la division des comprimés en parties homogènes nuisent à l'efficacité du médicament [11].

L'OMS recommande vivement aux fabricants d'anthelminthiques responsables des programmes de santé publique destinés aux enfants d'âge préscolaire de développer des formulations appropriées [95]-[97]. L'OMS [98] présente une classification en 5 bandes pour le groupe de patients pédiatriques : a) nouveau-nés, prématurés, allaitants ; b) nouveau-nés de zéro à 28 jours ; c) bébés et enfants de 28 jours à 23 mois ; d) enfants de 2 à 12 ans et ; e) adolescents de 12 à 16/18 ans.

L'obtention d'une formulation de PZQ pédiatrique devrait alors répondre à trois questions principales :

a) augmenter la solubilité et la dissolution de la PZQ, ce qui devrait permettre de réduire la dose de médicament à administrer, d'augmenter l'efficacité de l'absorption et de réduire les effets secondaires et les coûts liés au processus de production,

b) optimiser les formulations avec différents dosages pour permettre une administration correcte de la dose en fonction du poids des enfants, ce qui contribue à l'efficacité du traitement,

c) masquer le goût amer de la molécule PZQ pour permettre aux patients pédiatriques d'accepter le médicament PZQ et d'adhérer au traitement de la schistosomiase.

Dans ce contexte, cette thèse a eu pour objectif le développement d'une formulation de PZQ (l'IPA) à usage pédiatrique pour répondre aux trois questions ci-dessus.

**Le premier défi était d'améliorer la solubilité du praziquantel dans l'eau.**

Le praziquantel (PZQ) est un dérivé de l'imidazole, chimiquement connu sous le nom de (+)-2cyclohexylcarbonyl-1,2,3,6,7,11b-hexahydro-4H-pyrazine[2,1 a]isoquilonin-4-one. Certaines caractéristiques physicochimiques du PZQ sont présentées dans le Tableau 1.

Tableau 62. Résumé des caractéristiques physicochimiques du Praziquantel.

| **PZQ – caractéristiques physicochimiques** | | **Références** |
|---|---|---|
| Poids moléculaire | 312.4 g/mol | [53]–[57] |
| Point de fusion | 136-144 ºC | [53]–[58] |
| Température de transition vitreuse | 35.9 -37.7 ºC | [56], [59] |
| Solubilité dans l'eau | 0.14 mg/mL (20 ºC) | [30], [60] |
| | 0.22 mg/mL (25 ºC) | [61] |
| | 0.40 mg/mL (25 ºC) | [4], [57], [62]–[66] |
| | 0.28 mg/mL (37 ºC) | [67] |
| Solubilité dans l'eau | 63 - 97 mg/mL | [57] |
| pKa | 19.38 | [57] |
| LogP | 2.42 | [57] |
| Seuil de perception du goût | 0.03 mg/mL | [68] |

Chimiquement, le PZQ est une substance hydrophobe et chirale (position 11b), obtenue principalement à partir d'un mélange racémique (mélange 1:1 d'énantiomères) (Figure 5). La résolution optique a prouvé que l'activité anthelminthique est principalement due à l'énantiomère R-(-) (L-PZQ ou (-)-PZQ ou R-PZQ) tandis que l'énantiomère S-(+) (D-PZQ ou (+)-PZQ ou S-PZQ) est inactif, présentant une toxicité plus élevée et étant le principal responsable du goût amer du praziquantel. Les isomères ont également des caractéristiques physico-chimiques différentes, telles que la solubilité

(R-PZQ 1,91 mmol/L, S-PZQ 1,64 mmol/L et Rac-PZQ 0. 92 mmol/L) et la température de fusion (R-PZQ T_onset 109,4 ºC, T_peak 122,3 ºC et, ΔH 77,3 J/g ; S-PZQ T_onset 109,7, T_peak 112,6 ºC et ΔH 78,2 J/g) [70].

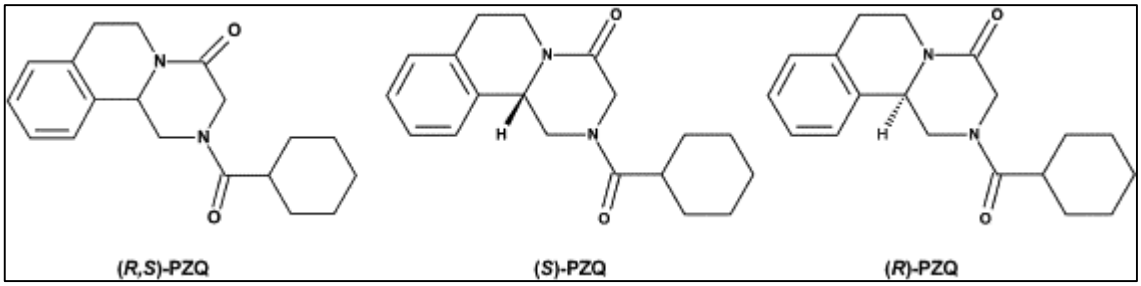


Figure 163. Structure chimique du praziquantel a) (R,S)-praziquantel (racémique), b) (S)-praziquantel et, c) (R)-praziquantel (réutilisation de [5] avec permission).

Les travaux de cette thèse ont porté sur le développement de dispersions solides amorphes de (R,S)-praziquantel (racémique) pour améliorer les caractéristiques physico-chimiques (faible solubilité dans l'eau) et sensorielles (goût amer) de ce principe actif pharmaceutique.

Les dispersions solides amorphes (DSA, ASD en anglais) sont une approche de formulation de plus en plus importante pour améliorer la vitesse de dissolution et la solubilité apparente de composés peu solubles dans l'eau comme le PZQ. Les DSA sont largement connues pour leur définition : une molécule d'intérêt pharmaceutique amorphe dispersée dans une phase amorphe qui comprend un polymère, un mélange de polymères ou un mélange de polymères et de tensioactifs.

Le procédé utilisé est l'extrusion à chaud (HME). Il s'agit d'un procédé de fabrication (thermo)mécanique par lequel un matériau fondu est contraint de traverser une filière au travers de laquelle il est poussé. Dans les extrudeuses à vis, le matériau fondu (mélange de matières premières) est acheminé dans le fourreau de la machine par une (mono) ou deux (bi) vis sans fin jusqu'à la filière au travers de laquelle il est poussé. Un extrudat est formé en continu sous la forme de jonc qui peut être alors mis en forme (pellets ou poudre de différentes granulométries) en fonction de l'opération de post-traitement utilisée, notamment le broyage. Pendant le processus d'extrusion à l'état fondu, la dissolution des molécules actives dans la matrice polymère est accélérée sous l'effet du cisaillement et de la chaleur. Les différents paramètres du procédé comme la configuration (profil) et la vitesse de la vis, le débit d'alimentation et le profil de température sont généralement variés lors d'une étude afin d'influencer sur l'extrudabilité et la stabilité du produit extrudé.

La figure 27 illustre la représentation du processus HME avec les extrudeuses à double vis utilisées dans cette thèse.

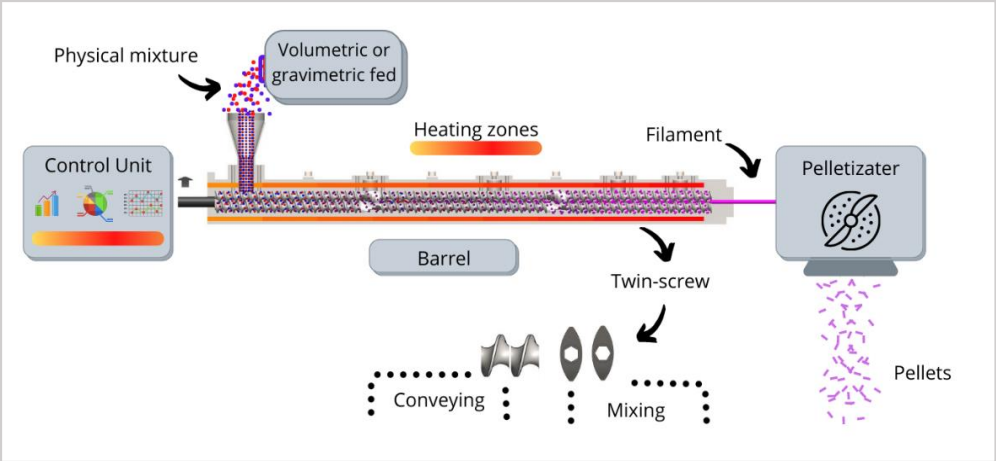


Figure 27. Représentation du processus HME. Source : Auteur.

De nouvelles formulations de DSA ont été proposées associant le PZQ au poly (vinyl pyrrolidone/vinyl acetate) (PVP/VA) dans un mélange binaire, ou les deux avec un tensioactif pour composer un mélange ternaire. Elles ont pu être générées à l'aide de deux extrudeuses à double vis (Pharma 11 et Pharma 16, Thermo Fisher).

Les systèmes ternaires varient en fonction du type de tensioactif utilisé et de la teneur en PZQ (35 %, 40 % et 50 % en masse). Les deux tensioactifs utilisés sont les suivants : a) SLS, un tensioactif solide utilisé directement dans le mélange physique préparé pour l'extrusion ; b) SPAN 20, un tensioactif liquide introduit dans le mélange PZQ/PVPVA de deux façons (granulation humide avant l'extrusion ou ajout direct au matériau fondu pendant l'extrusion).

*En ce qui concerne la solubilité du praziquantel dans l'eau :*

Toutes les formes d'extrudat ternaires et binaires se sont avérées capables d'améliorer la solubilité apparente, mettant en évidence le comportement de solubilisation des dispersions solides (amorphes ou majoritairement amorphes) avec un effet de ressort (*spring* en anglais) sur la concentration du PZQ dans l'eau à 37 °C principalement dans les premiers 60 min (Figure 147). Plus précisément, la solubilité apparente a pu être augmentée de 70 % à 90 % de plus que la concentration à l'équilibre dans ce milieu.

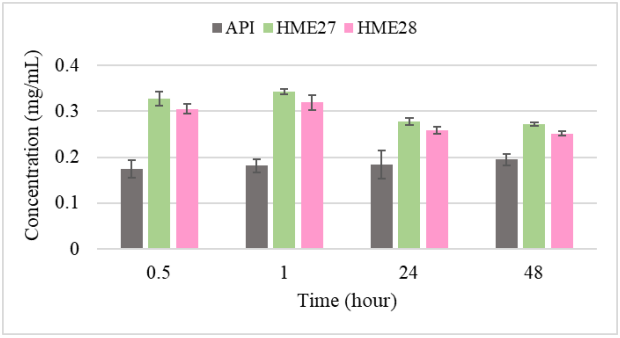


Figure 164. Concentration de PZQ dans l'eau à 37°C libéré de différents extrudats coupés en pellets (~1 mm) : PZQ brut, HME 27 (PZQ:Kollidon® VA 64 : SLS) et, HME 28 (PZQ:Kollidon® VA 64 : SPAN).

En ce qui concerne la cinétique de dissolution, elle a également été améliorée par ces nouveaux DSA, par exemple, 90 % de libération du PZQ en 1 h pour la formulation ternaire contenant SPAN 20 comme agent tensioactif et 35 % en masse de PZQ (extrudeuse bi-vis pharma 16, Thermofisher), par rapport à la molécule (cristalline) de départ. Cette même formulation a été utilisée pour réaliser des expériences pharmacocinétiques sur des animaux. Bien que le protocole d'évaluation pharmacocinétique des DSA nécessite quelques améliorations, les résultats sont prometteurs et démontrent que l'approche DSA (et la composition proposée) pourrait être une alternative pour surmonter le défi de la solubilité du PZQ (Figure 109).

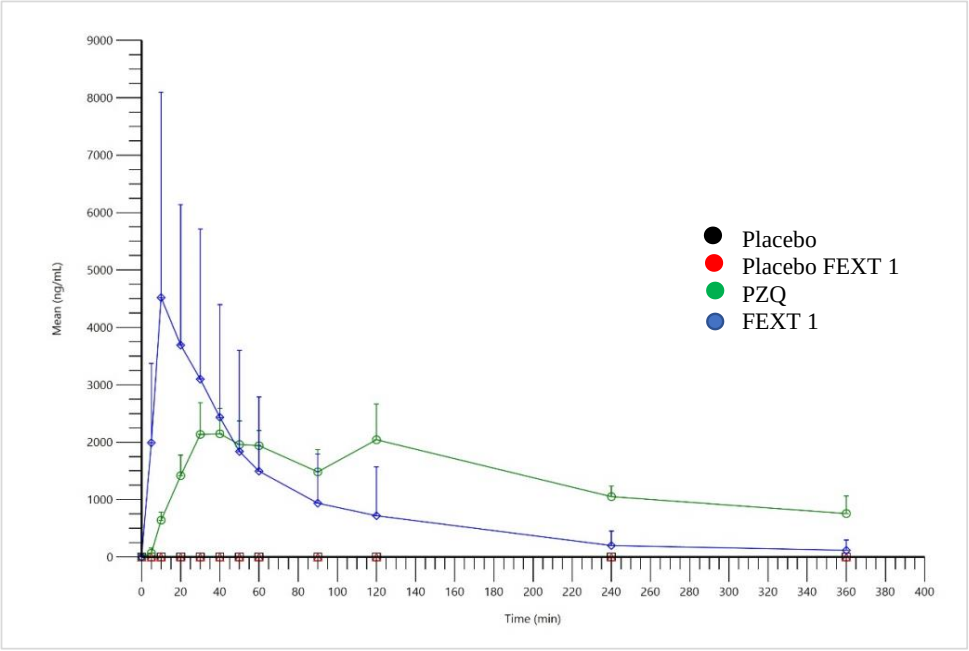


Figure 165. Profil comparatif des concentrations plasmatiques moyennes de PZQ en fonction du temps pour chaque préparation administrée (moyenne arithmétique + écart-type). Après élimination des animaux aberrants.

Cette question d'amélioration de la pharmacocinétique étant traitée, il restait un autre défi qui est la stabilité physique de ces systèmes. Afin de développer rationnellement des DSA fortement chargés en PZQ, une des premières études de cette thèse s'est concentrée sur la construction d'un diagramme de phases PZQ-PVPVA.

Le diagramme de phases présenté dans la Figure 62 a été construit à partir d'une étude thermique de la recristallisation d'une DSA sursaturé (50% PZQ en masse) généré par séchage par pulvérisation. À notre connaissance, il s'agit de la première étude rapportant un diagramme de phases pour ce système binaire.

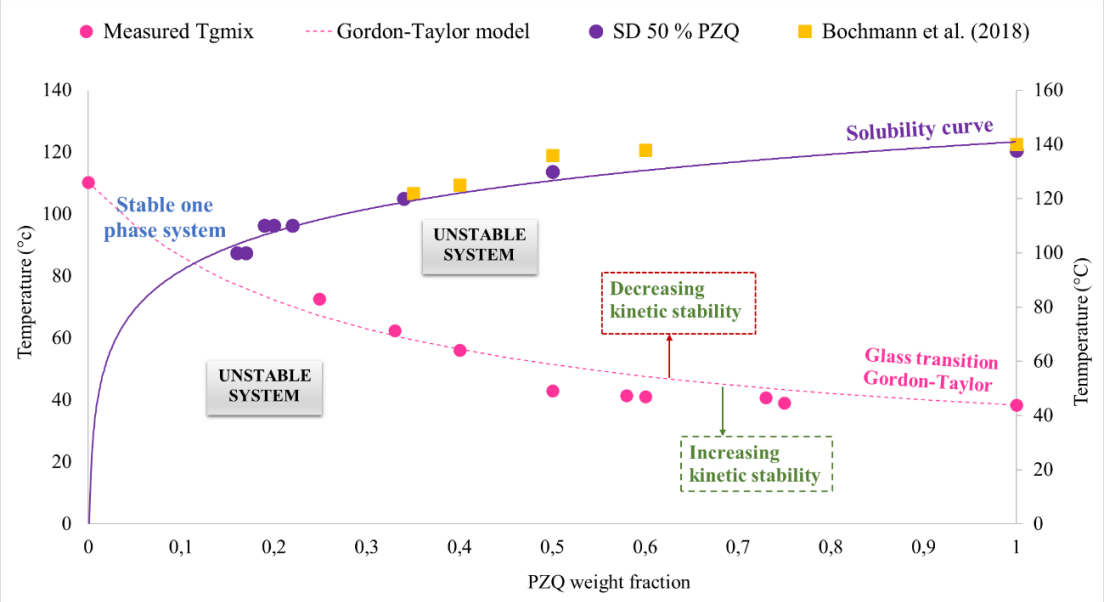


Figure 166. Diagramme de phases composition-température pour le binaire PZQ-PVPVA.

De manière inattendue, dans certains lots de poudres séchées par pulvérisation produits dans cette étude, des traces de formes cristallines de PZQ ont été trouvées, qui sont différentes de la forme racémique initiale. Elles pourraient correspondre à l'une de ces formes polymorphes de PZQ récemment rapportées. Il s'agit d'une découverte intéressante car, à notre connaissance, c'est la première fois que les nouvelles formes polymorphes du praziquantel sont supposées se former à partir de la recristallisation d'une forme amorphe.

**Le deuxième défi pour le praziquantel pédiatrique est l'ajustement précis des doses.**

Comme alternative pour surmonter le défi de l'ajustement des doses d'un médicament pédiatrique à base de PZQ pour les enfants, l'utilisation de la technologie d'impression 3D (FDM) avec alimentation directe d'un matériau particulaire a été proposée. La faisabilité d'impression 3D de comprimés directement à partir de différents matériaux granulaires (poudres, pellets..) a été étudiée. Les matériaux testés étaient des mélanges physiques des cristaux de PZQ de départ et de polymère, ainsi que des pellets et poudres (extrudats broyés) produits a partir de filaments DSA obtenus par extrusion à chaud (*HME* en anglais). Les caractéristiques des imprimés 3D résultants ont été évaluées, surtout les profils de dissolution du médicament, l'efficacité du masquage du goût et la stabilité physique. Cette étude a été réalisée en collaboration avec le professeur Alvaro Goyanes, de la faculté de pharmacie de l'University College of London (UCL) et de FabRX, Londres, et le professeur Catherine Tuleu, de la faculté de pharmacie de l'University College of London (UCL).

L'imprimante utilisée est une imprimante 3D pharmaceutique M3DIMAKER™ (FabRx, Londres, Royaume-Uni) [156]. Cette imprimante a été conçue par FabRx avec une extrudeuse à vis unique en amont de l'impression dont la vitesse de rotation (et donc l'extrusion) est contrôlée par le logiciel de l'imprimante 3D (Repetier-Host V 2.1.3, Allemagne). L'extrudeuse est alimentée par une trémie qui permet l'alimentation d'un matériau granulaire (poudre, pellets..). La sortie de l'extrudeuse (une buse de 0,8 mm de diamètre) se déplace en trois dimensions pour créer les objets couche par couche avec le matériau fondu. Le débit, la température de l'extrudeuse et la vitesse d'alimentation ont été déterminés pour chaque matériau utilisé. AutoCAD 2014 (Autodesk Inc., États-Unis) a été utilisé pour concevoir les gabarits des empreintes, qui ont ensuite été exportés sous forme de fichier de stéréolithographie (.stl) dans le logiciel de l'imprimante 3D. La géométrie 3D sélectionnée est une empreinte cylindrique (10 mm de diamètre × 3,6 mm de hauteur).

Nous avons ainsi pu démontrer la faisabilité de la production des comprimés imprimés (appelés simplement imprimés) avec une empreinte cylindrique et deux doses différentes (100 et 150 mg) (Figure 167) en utilisant une DSA ternaire obtenue préalablement par HME avant impression 3D.

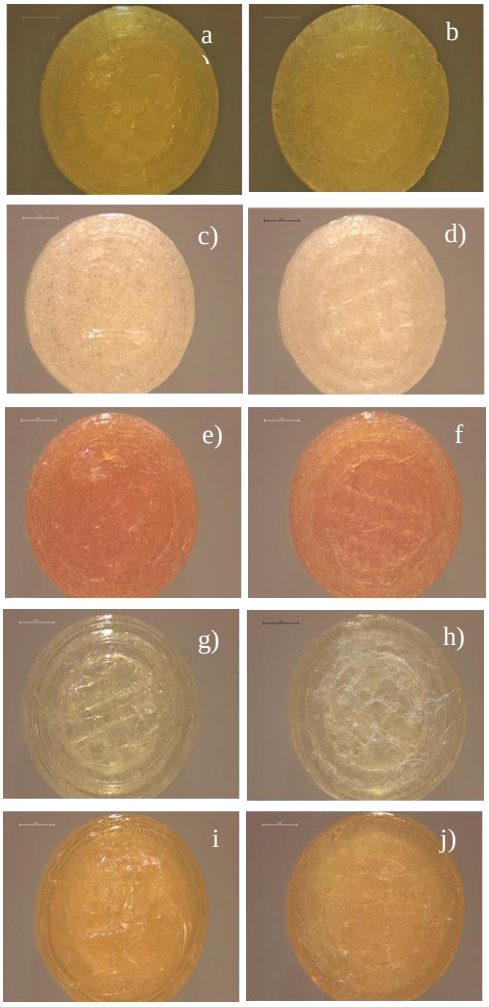


Figure 168. Image supérieure et inférieure d'empreintes obtenues avec : a - b) PM 50, c - d) M 35 Span, e - f) M ASD 35 SLS, g - h) M Placebo Span et, i - j) M Placebo SLS.

Les imprimés contenant 35 % en masse de PZQ et SPAN 20 comme tensioactif ont montré la meilleure performance de dissolution (81 % en 2 h) (Figure 175).

Un résultat majeur concerne l'imprimabilité des matériaux particulaires en utilisant une technologie d'impression 3D qui dispose d'une alimentation directe de poudre. Il n'a pas été possible d'imprimer directement les mélanges physiques contenant 50% ou 35% de PZQ (avec ou sans tensioactif dans la formulation), contrairement à d'autres matériaux testés par FaBRx (données obtenues avec d'autres principes actifs). Pour notre principe actif spécifique, l'utilisation des DSA a été une étape indispensable pour assurer l'amorphisation du PZQ (relever le premier défi décrit ci-dessus, c'est-à-dire l'amélioration de la solubilité) en plus d'un changement des caractéristiques physiques de la poudre (diminution des charges électrostatiques et meilleur écoulement).

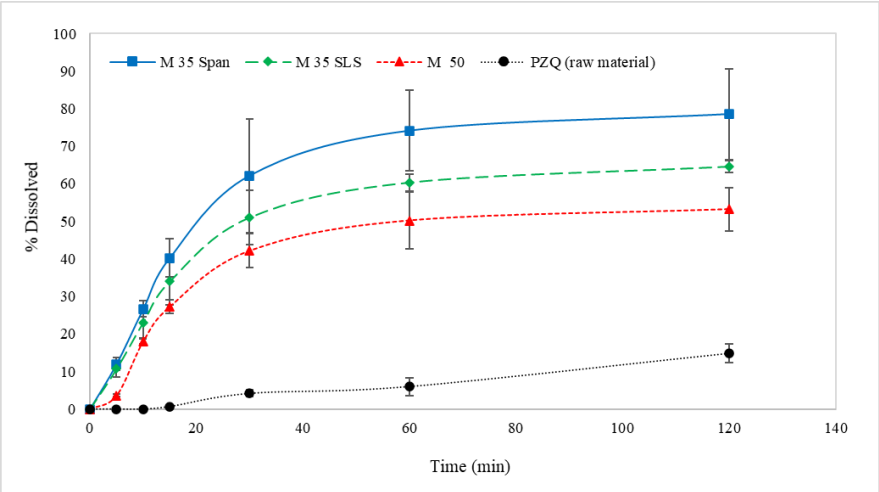


Figure 169. Profil de dissolution in vitro de PZQ (matière première) et des imprimés (M 50, M 35 Span et M 35 SLS) en utilisant un milieu HCl 0,1N avec 0.2 % p/p de SLS a 37°C.

En conclusion, les prototypes produits dans cette étude ont montré que l'impression 3D peut être un outil viable pour la personnalisation des doses de praziquantel pour les médicaments pédiatriques puisque la conception du médicament peut être ajustée avec précision.

**Le troisième défi consiste à masquer le goût amer du praziquantel.**

Un goût désagréable est crucial pour l'adhésion au traitement pédiatrique et, par conséquent, pour l'efficacité. Les formulations extrudées (pellets) et les imprimés ont montré des résultats positifs dans les trois types de tests réalisés (in vivo, dissolution dans la cavité buccale et langue électronique), en ce qui concerne le masquage du goût amer du praziquantel pour les deux charges API (50 et 35 % en masse).

La langue électronique a permis de tester deux formulations de DSA : la première a donné des meilleurs résultats, indiquant que le goût était meilleur que celui des comprimés commerciaux de PZQ et de FEXT 2 (Figure 106). Il est important de souligner que les capteurs électroniques de la langue ont été adaptés pour déterminer l'impédance, surmontant ainsi le facteur limitant présenté par les équipements actuellement commercialisés qui ne permettent pas l'identification du goût pour les molécules ayant des caractéristiques de faible conductivité comme le praziquantel.

Le masquage du goût in vivo a montré qu'une formulation ternaire (FEXT 1) était mieux acceptée par les rats que les comprimés commerciaux de PZQ (Figure 107). Ce résultat est conforme au test in vitro réalisé avec la langue électronique. L'expérience in

vivo a permis de démontrer que l'adaptation de la méthodologie en utilisant des pompes de recirculation de la solution est réalisable et garantit que l'animal est toujours exposé à une solution/suspension homogène de l'échantillon testé.

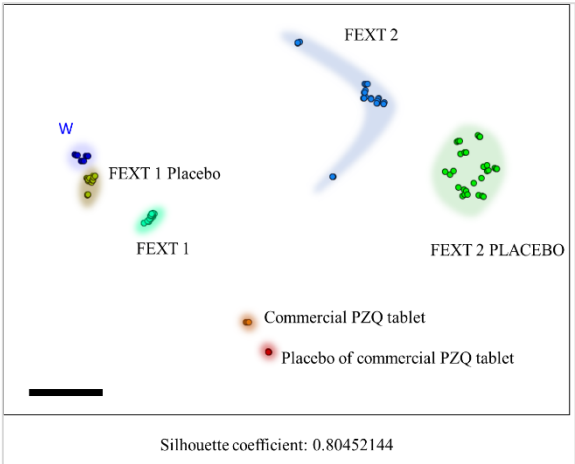


Figure 171. Tracé IDMAP pour FEXT 1, 2, comprimé commercial PZQ et leurs placebos respectifs (n=3).

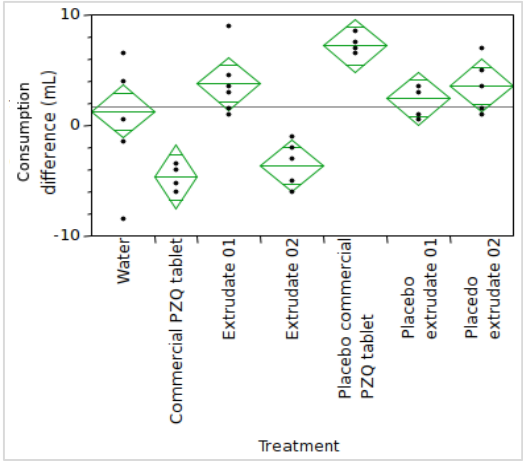


Figure 170. Test de palatabilité in vivo. (A) ANOVA (facteur unique 95%) pour les échantillons.

La dissolution dans la cavité buccale a montré que les imprimés obtenus a partir de deux DSA ternaires (tous deux avec 35 % de PZQ) sont considérés comme bien tolérables jusqu'à la fin de l'expérience (600 secondes). Les deux DSA ternaires testées (et à partir desquelles les imprimés 3D ont été générés) ont démontré une meilleure capacité de masquage du goût en 1 minute de contact avec de la salive artificielle, restant en dessous de la limite bien tolérable (Figure 176),. De manière surprenante, ce même résultat a été observé pour des pellets de concentrations différentes (35 et 50 % PZQ).

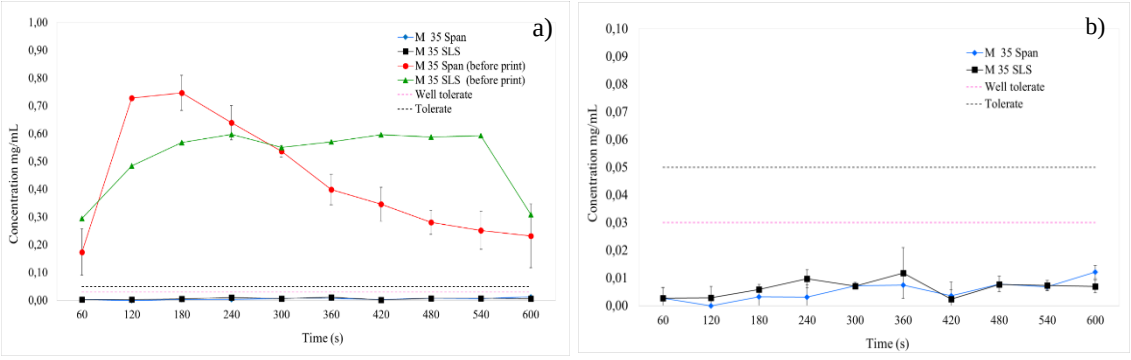


Figure 172. a) Profil de libération de PZQ (moyenne ± SD) pour les matériaux M 35 Span et M 35 SLS (avant impression) et leurs imprimés respectifs et, b) détail des formulations imprimées en 3D. Les seuils de goût sont représentés par des lignes pointillées roses et violettes.

Il est important de souligner que tous les tests de masquage du goût dans cette thèse ont été réalisés avec des matériaux intermédiaires (extrudés) et des imprimés 3D comme matériaux d'essai. Il n'y a pas eu d'ajout d'excipients ayant une fonctionnalité d'amélioration du goût (par exemple, des édulcorants, des arômes). De cette façon, les incréments sur la formulation pharmaceutique peuvent encore être explorés pour optimiser un médicament contenant du PZQ spécifiquement conçu pour les enfants.

# CHAPTER 10 - PUBLISHED WORK

### *Publications in international journals*

- ✓ Janine Boniatti[1]; Marcelo R R Tappin[1]; Rafaela G da S Teixeira[2]; Tamires de A V Gandos[1,2]; Luis P S Rios[2]; Izabelle A M Ferreira[2]; Karina C Oliveira[2]; Sabrina Calil-Elias[2]; Aila K M Santana[3], Laís B da Fonseca[1]; Flavio M Shimizu[4,5]; Olívia Carr[4]; Osvaldo N. Oliveira Jr.[4]; Fabio M L Dantas[6]; Fabio C. Amendoeira[1]; Alessandra L Viçosa[1]. **In vivo and in vitro taste assessment of drugs for neglected tropical diseases and paediatric patients.** Received: 24 March 2021; accepted: 14 October 2021. AAPS PharmSciTech (2022) 23:22 Vol (0123456789) DOI: 10.1208/s12249-021-02162-z.

- ✓ Janine Boniatti, L.B. Fonseca, A.L. Viçosa, F.C. Amendoeira, A. W. Basit, P. Januskaite, A. Goyanes, M. I. Ré. **Direct Powder Extrusion 3D Printing of Praziquantel to Overcome Neglected Disease Formulation Challenges in Paediatric Populations.** Received: 29 June 2021 Accepted: 18 July 2021 Published: 21 July 2021. Pharmaceutics 2021, 13, 1114. https://doi.org/10.3390/pharmaceutics13081114.

### *Publications in preparation*

- ✓ Janine Boniatti, S.P. Lacerda, L.B. Fonseca, A.L. Viçosa, F.C. Amendoeira, M. I. Ré. **Overcoming solubility challenges for praziquantel with high-drug load solid dispersions produced by spray drying**.

- ✓ Janine Boniatti, S. Delconfetto, R. Sescousse, M. Sauceau, M. I. Ré. **Determination of praziquantel-PVPVA solubility from a thermal study of recrystallization of a supersaturated solid solution.**

### *Publications in International Conferences/Seminar*

- ✓ Janine Boniatti, L.B. Fonseca, A.L. Viçosa, F.C. Amendoeira, A. W. Basit, P. Januskaite, A. Goyanes, M. I. Ré. **Direct Powder Extrusion 3D printing for neglected disease to overcome Praziquantel formulation challenges. EUPFI 2021. Best poster/oral presentation award.**

- ✓ Janine Boniatti1; Marcelo R R Tappin1; Rafaela G da S Teixeira2; Tamires de A V Gandos1,2; Luis P S Rios2; Izabelle A M Ferreira2; Karina C Oliveira2; Sabrina Calil-Elias2; Aila K M Santana3, Laís B da Fonseca1; Flavio M Shimizu4,5; Olívia Carr4; Osvaldo N. Oliveira Jr.4; Fabio M L Dantas6; Fabio C. Amendoeira1; Alessandra L Viçosa1. **Taste evaluation of three commercial tablets for paediatric patients for neglected tropical diseases. EUPFI 2019. Best poster presentation award.**

- ✓ Janine Boniatti1; Marcelo R R Tappin1; Rafaela G da S Teixeira2; Sabrina Calil-Elias2; Laís B da Fonseca1, Thiago F Guimarães1; Flavio M Shimizu3; Osvaldo N Oliveira Jr4; Fabio M L Dantas5; Alessandra L Viçosa1. **Extrudate materials via hot melt extrusion mask the bitter taste of drugs used for neglected tropical diseases**. 12th PBP World Meeting. 2021.

- ✓ Boniatti, J.; Viçosa, L. A.; Amendoeira, F.; Fonseca, B. L.; Ré, M.-I. **Amorphous Solid Solution by Hot Melt Extrusion: development for a paediatric drug formulation for neglected diseases.** Seminar How to accelerate your pharmaceutical developments based on the solid dispersion strategy. International Seminar Gala-Merck.

# CHAPTER 11 - APPENDIX

# APPENDIX 1

Universidade Federal Fluminense

ceua
Comitê de Ética no Uso de Animais

## CERTIFICADO

Certificamos que a proposta intitulada " AVALIAÇÃO DA PALATABILIDADE DE MEDICAMENTOS PEDIÁTRICOS PARA DOENÇAS NEGLIGENCIADAS ", protocolada sob o CEUA nº 4119060418 (ID 000095), sob a responsabilidade de **Sabrina Calil Elias** *e equipe; RAFAELA GOMES; Luciana Ferrazani; Alessandra Viçosa* - que envolve a produção, manutenção e/ou utilização de animais pertencentes ao filo Chordata, subfilo Vertebrata (exceto o homem), para fins de pesquisa científica ou ensino - está de acordo com os preceitos da Lei 11.794 de 8 de outubro de 2008, com o Decreto 6.899 de 15 de julho de 2009, bem como com as normas editadas pelo Conselho Nacional de Controle da Experimentação Animal (CONCEA), e foi **aprovada** pela Comissão de Ética no Uso de Animais da Universidade Federal Fluminense (CEUA/UFF) na reunião de 14/06/2018.

We certify that the proposal ""EVALUATION OF PALATABILITY OF PEDIATRIC MEDICINES FOR NEGLIGENCED DISEASES"", utilizing 30 Heterogenics rats (30 females), protocol number CEUA 4119060418 (ID 000095), under the responsibility of **Sabrina Calil Elias** *and team; RAFAELA GOMES; Luciana Ferrazani; Alessandra Viçosa* - which involves the production, maintenance and/or use of animals belonging to the phylum Chordata, subphylum Vertebrata (except human beings), for scientific research purposes or teaching - is in accordance with Law 11.794 of October 8, 2008, Decree 6899 of July 15, 2009, as well as with the rules issued by the National Council for Control of Animal Experimentation (CONCEA), and was **approved** by the Ethic Committee on Animal Use of the Federal University Fluminense (CEUA/UFF) in the meeting of 06/14/2018.

Finalidade da Proposta: Pesquisa (Acadêmica)

Vigência da Proposta: de 06/2018 a 05/2019 Área: Farmacia

| | | | | | | | |
|---|---|---|---|---|---|---|---|
| Origem: | Biotério Central | | | | | | |
| Espécie: | Ratos heterogênicos | sexo: | Fêmeas | idade: | 3 a 5 meses | N: | 30 |
| Linhagem: | Rattus novergicus albinus | | | Peso: | 200 a 350 g | | |

Local do experimento: Laboratório de Farmacologia da Faculdade de Farmácia

Niteroi, 05 de fevereiro de 2019

Profa. Dra. Mônica Diuana Calasans Maia
Coordenadora da Comissão de Ética no Uso de Animais
Universidade Federal Fluminense

Dr. Fabio Otero Ascoli
Vice-Coordenador da Comissão de Ética no Uso de Animais
Universidade Federal Fluminense

# APPENDIX 2

Ministério da Saúde
Fundação Oswaldo Cruz
Instituto Oswaldo Cruz
Comissão de Ética no Uso de Animais - CEUA/IOC

IOC Instituto Oswaldo Cruz

## LICENÇA L-009/2019

Certificamos que o protocolo (CEUA/IOC-007/2019), intitulado, "Avaliação terapêutica e farmacocinética de um novo medicamento contendo praziquantel para o tratamento da Esquistossomose mansônica", sob a responsabilidade de **CLÉLIA CHRISTINA MELLO SILVA ALMEIDA DA COSTA** atende ao disposto na Lei 11794/08, que dispõe sobre o uso científico no uso de animais, inclusive, aos princípios da Sociedade Brasileira de Ciência em Animais de Laboratório (SBCAL). A referida licença não exime a observância das Leis e demais exigências legais na vasta legislação nacional.

Esta licença tem validade até 30/04/2023 e inclui o uso total de:

**Camundongo (*Mus musculus*), linhagem**

Swiss Webster - 420 animais fêmeas de 4-5 semanas – origem ICTB

***Rattus Norvegicus***

Wistar -180 animais machos de entre 12 e 17 semanas – origem – ICTB

Observação: Esta licença não substitui outras licenças necessárias, como Certificado de Qualidade em Biossegurança para animais geneticamente modificados, certificado do IBAMA para captura de animais silvestres ou outros.

Rio de Janeiro, 30 de maio de 2019.

Cecília J. G. de Almeida

Cecília Jacques Gonçalves de Almeida
**Coordenadora da CEUA/Instituto Oswaldo Cruz**
**Fundação Oswaldo Cruz**

Cecília Jacques G. de Almeida
Coordenadora da CEUA - IOC
IOC - FIOCRUZ
Mat. SIAPE: 1635407-0

# APPENDIX 3

| *USE LICENSES* | | | |
|---|---|---|---|
| ***License Number*** | ***Journal*** | ***Title*** | ***Authors*** |
| 5062820970919 | Journal of Drug Delivery Science and Technology | Solid dispersion of praziquantel enhanced solubility and improvethe efficacy of the schistosomiasis treatment | Carine Santana Ferreira Marques,Polyana Rezende,Luciana N.Andrade,Tiago M.F. Mendes,Silmara M. Allegretti,CristianeBani,Marco Vinicius Chaud,Mônica Batista de Almeida,Eliana B.Souto,Luiz Pereira da Costa,Patrícia Severino |
| 5067790284403 | Powder Technology | Developing mechanistic understanding of granular behaviour incomplex moving geometry using the Discrete Element MethodPart B: Investigation of flow and mixing in the Turbula® mixer | M. Marigo,D.L. Cairns,M. Davies,A. Ingram,E.H. Stitt |
| 5062750322927 | Biochemical Pharmacology | Metabolic profiling of praziquantel enantiomers | Haina Wang,Zhong-Ze Fang,Yang Zheng,Kun Zhou,ChangyanHu,Kristopher W. Krausz,Dequn Sun,Jeffrey R. Idle,Frank J.Gonzalez |
| 5062750543004 | European Journal of Pharmaceutics and Biopharmaceutics | A new soluble and bioactive polymorph of praziquantel | Debora Zanolla,Beatrice Perissutti,Nadia Passerini,Michele R.Chierotti,Dritan Hasa,Dario Voinovich,Lara Gigli,NicolaDemitri,Silvano Geremia,Jennifer Keiser,Paolo CerreiaVioglio,Beatrice Albertini |
| 5062701319600 | European Journal of Pharmaceutical Sciences | Exploring mechanochemical parameters using a DoE approach:Crystal structure solution from synchrotron XRPD andcharacterization of a new praziquantel polymorph | Debora Zanolla,Beatrice Perissutti,Paolo Cerreia Vioglio,MicheleR. Chierotti,Lara Gigli,Nicola Demitri,Nadia Passerini,BeatriceAlbertini,Erica Franceschinis,Jennifer Keiser,Dario Voinovich |